AD NUMBER
ADB013904
LIMITATION CHANGES
TO: **Approved for public release; distribution is unlimited.**
FROM: **Distribution authorized to U.S. Gov't. agencies only; Test and Evaluation; DEC 1973. Other requests shall be referred to Air Force Flight Dynamics Laboratory, Attn: FEE, Wright-Paterson AFB, OH 45433.**
AUTHORITY
AFFDL ltr, 27 Dec 1977

AFFDL-TR-76-9

ADB013904

ELECTRONIC EQUIPMENT COLD PLATES

ENVIRONMENTAL CONTROL BRANCH
VEHICLE EQUIPMENT DIVISION

D D C
OCT 7 1976

APRIL 1976

TECHNICAL REPORT AFFDL-TR-76-9

AD No. ___
DDC FILE COPY

Distribution limited to U.S. Government agencies only; test and evaluation; statement applied December 1973. Other request for this document must be referred to the Air Force Flight Dynamics Laboratory (FEE), Wright-Patterson Air Force Base, Ohio 45433.

AIR FORCE FLIGHT DYNAMICS LABORATORY
AIR FORCE SYSTEMS COMMAND
WRIGHT-PATTERSON AIR FORCE BASE, OHIO 45433

NOTICE

When Government drawings, specifications, or other data are used for any purpose other than in connection with a definitely related Government procurement operation, the United States Government thereby incurs no responsibility nor any obligation whatsoever; and the fact that the government may have formulated, furnished, or in any way supplied the said drawings, specifications, or other data is not to be regarded by implication or otherwise as in any manner licensing the holder or any other person or corporation, or conveying any rights or permission to manufacture, use, or sell any patented invention that may in any way be related thereto.

This technical report has been reviewed and is approved for publication.

Carl J. Feldmanis

CARL J. FELDMANIS
Project Engineer

Duane A. Baker

DUANE A. BAKER, Lt Col, USAF
Actg. Chief, Vehicle Equipment Division
AF Flight Dynamics Laboratory

Copies of this report should not be returned unless return is required by security considerations, contractual obligations, or notice on a specific document.

UNCLASSIFIED

SECURITY CLASSIFICATION OF THIS PAGE (When Data Entered)

REPORT DOCUMENTATION PAGE

READ INSTRUCTIONS BEFORE COMPLETING FORM

1. REPORT NUMBER: 14 AFFDL-TR-76-9
2. GOVT ACCESSION NO.
3. RECIPIENT'S CATALOG NUMBER
4. TITLE (and Subtitle): 6 ELECTRONIC EQUIPMENT COLD PLATES.
5. TYPE OF REPORT & PERIOD COVERED: 9 Final report for period Jun 1975 – Apr 1976.
6. PERFORMING ORG. REPORT NUMBER
7. AUTHOR(s): 10 Carl J. Feldmanis
8. CONTRACT OR GRANT NUMBER(s)
9. PERFORMING ORGANIZATION NAME AND ADDRESS: Air Force Flight Dynamics Laboratory, Wright-Patterson Air Force Base, Ohio 45433
10. PROGRAM ELEMENT, PROJECT, TASK AREA & WORK UNIT NUMBERS: 16 AF-6146 02 24 17 614602
11. CONTROLLING OFFICE NAME AND ADDRESS: Same as item 9
12. REPORT DATE: 11 Apr 76
13. NUMBER OF PAGES: 12 45p.
14. MONITORING AGENCY NAME & ADDRESS (if different from Controlling Office): Same as item 9
15. SECURITY CLASS. (of this report): UNCLASSIFIED
15a. DECLASSIFICATION DOWNGRADING SCHEDULE
16. DISTRIBUTION STATEMENT (of this Report)

Distribution limited to U.S. Government agencies only; test and evaluation; statement applied 1973. Other requests for this document must be referred to the Air Force Flight Dynamics Laboratory (FEE), Wright-Patterson Air Force Base, Ohio, 45433.

17. DISTRIBUTION STATEMENT (of the abstract entered in Block 20, if different from Report): Same as item 16
18. SUPPLEMENTARY NOTES

19. KEY WORDS (Continue on reverse side if necessary and identify by block number)

Electronic Equipment Cooling
Cold Plates
Heat Pipes

20. ABSTRACT (Continue on reverse side if necessary and identify by block number)

Experimental and analytical work have been performed to investigate capabilities and thermal performance characteristics of cold plates for electronic equipment cooling. The effort includes air-cooled cold plates, liquid-cooled cold plates, and cold plates provided with heat pipes. Different designs were selected for each of the three categories and thermal tests at different coolant flow and equipment power dissipation rates performed. It has been shown that large amounts of equipment waste heat can be removed by this cooling — over

DD FORM 1 JAN 73 1473 EDITION OF 1 NOV 65 IS OBSOLETE

UNCLASSIFIED

SECURITY CLASSIFICATION OF THIS PAGE (When Data Entered)

012 070

20. technique, and thermal performance accurately predicted, particularly with computer-aided analysis.

FOREWORD

This report was prepared by C. J. Feldmanis of the Environmental Control Branch, Vehicle Equipment Division, Air Force Flight Dynamics Laboratory, Wright-Patterson Air Force Base, Ohio. The study was conducted under Project 6146, "Environmental Control Systems for Military Aircraft."

The report describes the program conducted during the period from June 1975 to April 1976. It contains the results of experimental and analytical work on electronic equipment air- and liquid-cooled cold plates, and cold plates provided with heat pipes.

TABLE OF CONTENTS

SECTION		PAGE
I	INTRODUCTION	1
II	THERMAL REQUIREMENTS OF ELECTRONIC EQUIPMENT	3
III	ELECTRONIC EQUIPMENT MOUNTING	5
IV	HEAT REMOVAL CONCEPTS AND HEAT TRANSFER FROM ELECTRONIC DEVICES	12
V	CONVECTION HEAT TRANSFER	15
	a. Heat Transfer Fluids	23
VI	CONDUCTION HEAT TRANSFER	32
	a. Interface Thermal Conductance	32
VII	HEAT TRANSFER FROM FINNED SURFACES	51
	a. Efficiency of Finned Extended Surfaces	72
VIII	RADIATION HEAT TRANSFER	77
IX	HEAT STORAGE	81
	a. Application of Heat of Fusion Materials	81
	b. Application of Evaporative Coolants	86
X	APPLICATIONS OF HEAT PIPES	89
	a. Design Principles of Heat Pipes	90
	b. Radial Heat Flux Limitations	95
	c. Constant Temperature Heat Pipe	98
XI	THERMAL ANALYSIS TECHNIQUES	102
	a. Finite Differences	102
	b. Application of Computer Techniques	105
XII	GENERAL THERMAL CONTROL SYSTEMS AND THEIR REQUIREMENTS	120
XIII	FLOW DISTRIBUTION IN MANIFOLDS	123
XIV	THE COLD PLATE	127

TABLE OF CONTENTS (CONT'D)

SECTION		PAGE
XV	DESCRIPTION OF TEST EQUIPMENT AND APPARATUS	132
	a. Liquid-Cooled Cold Plates	132
	1. Liquid-Cooled Cold Plate No. 1	132
	2. Liquid-Cooled Cold Plate No. 2	155
	3. Liquid-Cooled Cold Plate No. 3	169
	4. Thermal Performance Comparison of Liquid-Cooled Cold Plates	179
	5. Sample Calculations	183
	b. Air-Cooled Cold Plates	188
	1. Types of Cold Plates Tested	188
	2. Manifold Configurations	188
	(1) Air-Cooled Cold Plate No. 1	189
	(2) Air-Cooled Cold Plate No. 2	214
	(3) Air-Cooled Cold Plate No. 3	235
	(4) Air-Cooled Cold Plate No. 4	260
	(5) Air-Cooled Cold Plate No. 5	267
	(6) Air-Cooled Cold Plate No. 6	284
	3. Thermal Performance Comparison of Air-Cooled Cold Plates	295
	4. Sample Calculations of Air-Cooled Cold Plates	307
	(1) Cold Plates Without Finned Surfaces	307
	(2) Cold Plates with Finned Surfaces	314
	(3) Sample Calculations for Determining Heat Transfer Coefficients from Experimental Data	321
	c. Cold Plates Provided with Heat Pipes	338
	1. Cold Plates Provided with Conventional Heat Pipes	339
	(1) Heat-Pipe Cold Plate No. 1	339
	(2) Heat-Pipe Cold Plate No. 2	339
	(3) Heat-Pipe Cold Plate No. 3	347
	2. Cold Plates Provided with Heat Pipes and Phase Change Materials	355
	(1) Heat-Pipe Cold Plate No. 1	355
	(2) Heat-Pipe Cold Plate No. 2	358
	(3) Heat-Pipe Cold Plate No. 3	362

TABLE OF CONTENTS (CONCLUDED)

SECTION		PAGE
	3. Cold Plates Provided with Variable Conduction Heat Pipes	362
	(1) Variable-Conductance Heat-Pipe Cold Plate No. 1	362
	(2) Variable-Conductance Heat-Pipe Cold Plate No. 2	366
	(3) Variable-Conductance Heat-Pipe Cold Plate No. 3	374
	4. Circuit Card Heat Pipe	379
	5. Thermal Performance Characteristics of Cold Plates Provided with Heat Pipes	387
APPENDIX A	TEST DATA	
REFERENCES		

LIST OF ILLUSTRATIONS

FIGURE		PAGE
1	Component Mounting on Heat Sink	8
2	Junction Temperature Rise vs Time as a Function of Pulse Width and Duty Cycle	11
3	Flow Over a Flat Plate	18
4	Heat-Transfer Figure of Merit (Ref 18)	28
5	Comparison of Gaseous Coolants on the Basis of Pumping Power and Heat Transfer (Ref 19)	29
6	Comparison of Liquid Coolants on the Basis of Pumping Power and Heat Transfer (Ref 19)	30
7	Composite Wall	33
8	Heat Flow Across the Interface	34
9	Ratio of Average Surface Irregularity to RMS Surface Roughness vs RMS Surface Roughness	37
10	$n\bar{a}$ vs Contact Pressure	38
11	Stress Distribution in a Bolted Joint	39
12	Lieb's Interface Stress Distribution Parameters	40
13	Bolted Joint	41
14	Resistance Network of a Joint	44
15	Resistance Network of a Joint and Plates	44
16	Radial Heat Flow in a Disk	45
17	Section of a Cold Plate with Flux Plot	46
18	Resistance Network	48
19	Division of Plate at Concentrated Heat Loads	48
20	Longitudinal Fin of Rectangular Profile	51
21	Temperature Distribution Along a Fin	56
22	Radial Fin of Rectangular Profile	57

LIST OF ILLUSTRATIONS (CONT'D)

FIGURE		PAGE
23	Efficiency of Longitudinal Fins of Rectangular Profile	58
24	Temperature Excess Ratio of Longitudinal Fins of Rectangular Profile	59
25	Section of Radial Fin	61
26	Efficiency of Radial Fins of Rectangular Profile	64
27	Temperature Excess Ratio of Radial Fins of Rectangular Profile	65
28	Circular Ring Sector	66
29	Cold Plates with Finned Surfaces	69
30	Melting of a Solid with Arbitrary Heat Flux	84
31	Heat-Pipe Schematic	89
32	Constant-Temperature Heat Pipe	99
33	Heat Transfer in a Rod	102
34	Heat Flow Through a Plain Wall	106
35	R-C Network of a Longitudinal Fin	108
36	Circular Fin with Rectangular Cross Section	110
37	Air-Cooled Cold Plate	112
38	R-C Network of Air-Cooled Cold Plate Section and Air Stream	113
39	R-C Network of an Air-Cooled Cold Plate	115
40	Section of a Cold Plate	116
41	Liquid-Cooled Cold Plate	117
42	Manifold with Discharge Openings	123
43	Possible Manifold Arrangements for a Tube Bank	126
44	Outline of a Cold Plate and Its Temperature Profile	129
45	Liquid-Cooled Cold Plate No. 1	133

LIST OF ILLUSTRATIONS (CONT'D)

FIGURE		PAGE
46	Transistor Mounting on Liquid-Cooled Cold Plate No. 1	132
47	R-C Network of Liquid-Cooled Cold Plate No. 1	135
48	R-C Network of Mounting Bracket for Liquid-Cooled Cold Plate No. 1	136
49	R-C Network of Coolant Flow Passage for Liquid-Cooled Cold Plate No. 1	137
50	Temperature Distribution of Liquid-Cooled Cold Plate No. 1 (Effects of Convection Heat-Transfer Coefficient)	140
51	Temperature Distribution of Liquid-Cooled Cold Plate No. 1 at Test Condition Nos. 1, 2, and 3 (TC 17-25)	143
52	Temperature Distribution of Liquid-Cooled Cold Plate No. 1 at Test Condition Nos. 1, 2, and 3 (TC 32-35)	144
53	Temperature Distribution of Liquid-Cooled Cold Plate No. 1 at Test Condition Nos. 4 thru 6	145
54	Temperature Distribution of Liquid-Cooled Cold Plate No. 1 at Test Condition Nos. 7 thru 9	146
55	Component Case Temperature vs Coolant Flow Rate for Liquid-Cooled Cold Plate No. 1	147
56	Component Temperature Changes Caused by Heat-Load Changes	151
57	Component Temperature Changes Caused by Turning Electrical Power On and Off	152
58	Simplified R-C Network of Liquid-Cooled Cold Plate No. 1 (Preliminary)	153
59	Analytical and Experimental Temperature Distributions for Liquid-Cooled Cold Plate No. 1	154
60	Liquid-Cooled Cold Plate No. 2	156
61	R-C Network of Liquid-Cooled Cold Plate No. 2	157
62	R-C Network of Coolant Flow Passages for Liquid-Cooled Cold Plate No. 2	158
63	Temperature Distribution of Liquid-Cooled Cold Plate No. 2 at Test Condition Nos. 1 thru 3	161

LIST OF ILLUSTRATIONS (CONT'D)

FIGURE		PAGE
64	Temperature Distribution of Liquid-Cooled Cold Plate No. 2 at Test Condition Nos. 4 thru 6	162
65	Temperature Distribution of Liquid-Cooled Cold Plate No. 2 at Test Condition Nos. 7 thru 9	163
66	Component Case Temperature vs Coolant Flow Rate for Liquid-Cooled Cold Plate No. 2	164
67	Case Temperature of Transistors vs Electrical Power Dissipation Rate for Liquid-Cooled Cold Plate No. 2	165
68	Thermal Resistance of Transistor #1 Mounting Joint vs Stud Torque (without Mounting Washer)	167
69	Thermal Resistance of Transistor #1 Mounting Joint vs Stud Torque (with Mounting Washer)	168
70	Liquid-Cooled Cold Plate No. 3	170
71	Transistor Mounting on Liquid-Cooled Cold Plate No. 3	169
72	R-C Network of Liquid-Cooled Cold Plate No. 3	171
73	R-C Network of Coolant Flow Passage for Liquid-Cooled Cold Plate No. 3 (Only One Section Shown)	172
74	Temperature Distribution of Liquid-Cooled Cold Plate No. 3 at Test Condition Nos. 1 thru 3	175
75	Temperature Distribution of Liquid-Cooled Cold Plate No. 3 at Test Condition Nos. 10 thru 12	176
76	Component Case Temperature vs Coolant Flow Rate for Liquid-Cooled Cold Plate No. 3	177
77	Component Case Temperature vs Electrical Power Dissipation for Liquid-Cooled Cold Plate No. 3	178
78	Case Temperature of Transistor #2 vs Electrical Power Dissipation (Effects of Washer Thickness)	180
79	Case Temperature of Transistor #2 vs Electrical Power Dissipation (Effects of Stud Torque)	181
80	Thermal Resistance of Transistor #2 Mounting Joint vs Thickness of Mica Washer	182

LIST OF ILLUSTRATIONS (CONT'D)

FIGURE		PAGE
81	Air-Cooled Cold Plate No. 1	190
82	Air-Cooled Cold Plate No. 1 with Manifold Configuration #1	191
83	Variation of Temperature Difference	192
84	Temperature Distribution of Air-Cooled Cold Plate No. 1 (Manifold #1) at Test Condition Nos. 1 thru 4	195
85	Temperature Distribution of Air-Cooled Cold Plate No. 1 (Manifold #1) at Test Condition Nos. 8 thru 10	196
86	Temperature Distribution of Air-Cooled Cold Plate No. 1 (Manifold #1) Showing Comparison Between Experimental and Analytical Data	197
87	Temperature Distribution of Air-Cooled Cold Plate No. 1 (Manifold #1) Showing Comparison Between Experimental and Analytical Data	200
88	Temperature Distribution of Air-Cooled Cold Plate No. 1 (Manifold #1) at Test Condition Nos. 5 thru 7	201
89	Case Temperature of Transistor No. 3 vs Cooling Air Flow Rate for Air-Cooled Cold Plate No. 1 (Manifold #1)	202
90	Air-Cooled Cold Plate No. 1 with Manifold Configuration #2	204
91	Temperature Distribution of Air-Cooled Cold Plate No. 1 (Manifold #2) at Test Condition Nos. 1 thru 4	205
92	Air-Cooled Cold Plate No. 1 with Manifold Configuration #3	206
93	Temperature Distribution of Air-Cooled Cold Plate No. 1 (Manifold #3) at Test Condition Nos. 1 thru 4	208
94	Temperature Distribution of Air-Cooled Cold Plate No. 1 (Manifold #3) at Test Condition Nos. 5 thru 7	209
95	Experimentally Determined Nusselt Numbers of Cold Plate No. 1 - Comparison of Three Different Manifold Configurations	210
96	R-C Network of Air-Cooled Cold Plate No. 1	215

LIST OF ILLUSTRATIONS (CONT'D)

FIGURE		PAGE
97	Air-Cooled Cold Plate No. 2	216
98	Air-Cooled Cold Plate No. 2 with Manifold Configuration #1	217
99	Temperature Distribution of Cold Plate No. 2 (Manifold #1) at Test Condition Nos. 1 thru 3 (TC 16-21)	219
100	Temperature Distribution of Cold Plate No. 2 (Manifold #1) at Test Condition Nos. 1 thru 3 (TC 8-15)	219
101	Temperature Distribution of Cold Plate No. 2 (Manifold #1) at Test Condition Nos. 1 thru 3 (TC 10-25)	220
102	Temperature Distribution of Cold Plate No. 2 (Manifold #1) at Test Condition Nos. 4 thru 6 (TC 16-21)	221
103	Temperature Distribution of Cold Plate No. 2 (Manifold #1) at Test Condition Nos. 4 thru 6 (TC 14-25)	221
104	Predicted Temperature Distribution of Cold Plate No. 2 (Manifold #1) at Different Heat-Transfer Coefficients	223
105	Air-Cooled Cold Plate No. 2 with Manifold Configuration #2	224
106	Temperature Distribution of Air-Cooled Cold Plate No. 2 (Manifold #2) at Test Condition Nos. 1 thru 3 (TC 11-24)	226
107	Temperature Distribution of Air-Cooled Cold Plate No. 2 (Manifold #2) at Test Condition Nos. 1 thru 3 (TC 3-25)	226
108	Air-Cooled Cold Plate No. 2 with Manifold Configuration #3	227
109	Temperature Distribution of Air-Cooled Cold Plate No. 2 (Manifold #3) at Test Condition Nos. 1 thru 3 (TC 8-15)	228
110	Temperature Distribution of Air-Cooled Cold Plate No. 2 (Manifold #3) at Test Condition Nos. 1 thru 3 (TC 16-21)	228
111	Temperature Distribution of Air-Cooled Cold Plate No. 2 (Manifold #3) at Test Condition Nos. 4 thru 6	229
112	Air-Cooled Cold Plate No. 2 with Manifold Configuration #4	231
113	Temperature Distribution of Air-Cooled Cold Plate No. 2 (Manifold #4) at Test Condition Nos. 1 thru 3 (TC 16-21)	232

LIST OF ILLUSTRATIONS (CONT'D)

FIGURE		PAGE
114	Temperature Distribution of Air-Cooled Cold Plate No. 2 (Manifold #4) at Test Condition Nos. 1 thru 3 (TC 8-15)	232
115	Gasket Slots	233
116	Temperature Distribution of Air-Cooled Cold Plate No. 2 (Manifold #3 with Tapered Slot) at Test Condition Nos. 1 and 2	234
117	Temperature Distribution of Air-Cooled Cold Plate No. 2 (Manifold #4 with Tapered Slot) at Test Condition Nos. 1 and 2	234
118	Experimentally Determined Nusselt Numbers vs Reynolds Numbers of Air-Cooled Cold Plate No. 2	236
119	Air-Cooled Cold Plate No. 3	237
120	Air-Cooled Cold Plate No. 3 with Manifold Configuration #1	238
121	Temperature Distribution of Air-Cooled Cold Plate No. 3 (Manifold #1) at Test Condition Nos. 1 thru 4	239
122	Temperature Distribution of Air-Cooled Cold Plate No. 3 (Manifold #1) at Test Condition Nos. 1 thru 5	240
123	Temperature Distribution of Air-Cooled Cold Plate No. 3 (Manifold #1) at Test Condition Nos. 1 thru 5	241
124	Case Temperature of Transistors vs Cooling Air Flow Rate for Air-Cooled Cold Plate No. 3 (Manifold #1)	243
125	Temperature Distribution of Air-Cooled Cold Plate No. 3 (Manifold #1) at Different Thicknesses of Cover Plate	244
126	Temperature Distribution of Air-Cooled Cold Plate No. 3 (Manifold #1) at Different Heat-Transfer Coefficients	245
127	Case Temperature of Transistor #2 vs Electrical Power Dissipation Rate (Cold Plate No. 3, Manifold #1)	246
128	Air-Cooled Cold Plate No. 3 with Manifold Configuration #2	248
129	Temperature Distribution of Air-Cooled Cold Plate No. 3 (Manifold #2) at Test Condition Nos. 1 thru 5	249

LIST OF ILLUSTRATIONS (CONT'D)

FIGURE		PAGE
130	Air-Cooled Cold Plate No. 3 with Manifold Configuration #2a	251
131	Temperature Distribution of Air-Cooled Cold Plate No. 3 (Manifold #2a) at Test Condition Nos. 1 thru 5	252
132	Air-Cooled Cold Plate No. 3 with Manifold Configuration #3	254
133	Temperature Distribution of Air-Cooled Cold Plate No. 3 (Manifold #3) at Test Condition Nos. 1 thru 5	256
134	Temperature Distribution of Air-Cooled Cold Plate No. 3 (Manifold #3) at Test Condition Nos. 6 thru 8	257
135	Temperature of Transistor #2 vs Cooling Air Flow Rate Comparison among Manifold Configurations Cold Plate No. 3	258
136	Experimentally Determined Nusselt Numbers vs Reynolds Numbers of Air-Cooled Cold Plate No. 3	259
137	Air-Cooled Cold Plate No. 4	261
138	Temperature Distribution of Air-Cooled Cold Plate No. 4 at Test Condition Nos. 1 thru 4 (TC 16-21)	262
139	Temperature Distribution of Air-Cooled Cold Plate No. 4 at Test Condition Nos. 1 thru 4 (TC 9-23)	263
140	Temperature Distribution of Air-Cooled Cold Plate No. 4 at Test Condition Nos. 4 thru 6	265
141	Case Temperature of Transistors vs Cooling Air Flow Rate for Air-Cooled Cold Plate No. 4	266
142	Air-Cooled Cold Plate No. 5	268
143	Air-Cooled Cold Plate No. 5 with Manifold Configuration #1	269
144	Mounting of Transistor on Bracket	267
145	Temperature Distribution of Air-Cooled Cold Plate No. 5 (Manifold #1) at Test Condition Nos. 1 thru 3	271
146	Case Temperature of Transistors vs Cooling Air Flow Rate for Air-Cooled Cold Plate No. 5 (Manifold #1)	272
147	Case Temperature of Transistors vs Electrical Power Dissipation Rates for Air-Cooled Cold Plate No. 5 (Manifold #1)	274

LIST OF ILLUSTRATIONS (CONT'D)

FIGURE		PAGE
148	Air-Cooled Cold Plate No. 5 with Manifold Configuration #2	275
149	Temperature Distribution of Air-Cooled Cold Plate No. 5 (Manifold #2) at Test Condition Nos. 1 thru 3	277
150	Air-Cooled Cold Plate No. 5 with Manifold Configuration #3	278
151	Temperature Distribution of Air-Cooled Cold Plate No. 5 (Manifold #3) at Test Condition Nos. 1 thru 3	279
152	Temperature Distribution of Air-Cooled Cold Plate No. 5 (Manifold #3) at Test Condition No. 4	280
153	Air-Cooled Cold Plate No. 5 with Manifold Configuration #4	282
154	Temperature Distribution of Air-Cooled Cold Plate No. 5 (Manifold #4) at Test Condition Nos. 1 thru 3	283
155	Experimentally Determined Nusselt Numbers vs Reynolds Numbers of Cold Plate No. 5 at the Different Manifold Configurations	285
156	Air-Cooled Cold Plate No. 6	286
157	Air-Cooled Cold Plate No. 6 with Manifold Configuration #1	288
158	Temperature Distribution of Air-Cooled Cold Plate No. 6 (Manifold #1) at Test Condition Nos. 1 thru 3 (TC 13-17)	289
159	Temperature Distribution of Air-Cooled Cold Plate No. 6 (Manifold #1) at Test Condition Nos. 1 thru 3 (TC 11-19)	290
160	Temperature Distribution of Cold Plate No. 6 (Manifold #1) at Test Condition Nos. 1 thru 3 (TC 7-17)	291
161	Case Temperature of Transistors vs Cooling Air Flow Rate for Cold Plate No. 6 (Manifold #1)	293
162	Air-Cooled Cold Plate No. 6 with Manifold Configuration #4	294
163	Temperature Distribution of Air-Cooled Cold Plate No. 6 (Manifold #4) at Test Condition Nos. 1 thru 3 (TC 13-17)	296

LIST OF ILLUSTRATIONS (CONT'D)

FIGURE		PAGE
164	Temperature Distribution of Air-Cooled Cold Plate No. 6 (Manifold #4) at Test Condition Nos. 1 thru 3 (TC 6-11)	297
165	Temperature Distribution of Cold Plate No. 6 (Manifold #4) at Test Condition Nos. 1 thru 3 (TC 7-17)	298
166	Experimentally Determined Convection Heat-Transfer Coefficients vs Reynolds Numbers (Comparison Among Cold Plate Nos. 1 thru 3)	299
167	Experimentally Determined Nusselt Numbers vs Reynolds Numbers (Comparison Among Cold Plate Nos. 1 thru 3)	301
168	Convection Resistance vs Cooling Air Flow Rate (Comparison Among Cold Plate Nos. 1 thru 3)	302
169	Experimentally Determined Convection Heat-Transfer Coefficients vs Reynolds Numbers (Comparison Between Cold Plate Nos. 1 and 5)	304
170	Convection Resistance vs Cooling Air Flow Rate (Comparison Among Cold Plate Nos. 1, 2, 3, and 5)	305
171	Case Temperature of Transistor #3 vs Cooling Air Flow Rate	306
172	Cold-Plate Effectiveness vs Cooling Air Flow Rate	320
173	Temperature Distribution of Cold Plate No. 1 with Manifold Configuration #1	324
174	Section of Sample Cold Plate	331
175	Heat-Pipe Cold Plate No. 1	340
176	Temperature Changes of Heat-Pipe Cold Plate No. 1 vs Electrical Power Input Rates	341
177	Cold Plate No. 1 with Attached Components	342
178	Temperature Distribution of Heat-Pipe Cold Plate No. 1 Under Coolant Flow and No-Flow Conditions	343
179	Heat-Pipe Cold Plate No. 2	344
180	Section A-A of Cold Plate	345
181	Section B-B of Cold Plate	345
182	Temperature Distribution of Heat-Pipe Cold Plate No. 2	346

LIST OF ILLUSTRATIONS (CONT'D)

FIGURE		PAGE
183	Temperature Distribution from Component Mounting Base to Coolant for Cold Plate No. 2	348
184	Heat-Pipe Cold Plate No. 3	349
185	Section A-A of Heat-Pipe Cold Plate No. 6	350
186	Section B-B of Heat-Pipe Cold Plate No. 6	351
187	Resistance Network of Evaporator Section	347
188	Temperature Distribution from Transistor to Coolant for Heat-Pipe Cold Plate No. 3	353
189	Temperature Distribution from Transistor to Coolant for Heat-Pipe Cold Plate No. 3	354
190	Heat-Pipe Cold Plate No. 1 with High Thermal Capacity	356
191	Temperature Changes vs Time of Heat-Pipe Cold Plate No. 1 at Different Test Conditions	357
192	Heat-Pipe Cold Plate No. 2 with High Thermal Capacity	359
193	Resistor Circuit Diagram	360
194	Temperature Changes of Resistor and Heat-Pipe Cold Plate No. 2 vs Time After Coolant Shut-Off	361
195	Heat-Pipe Cold Plate No. 3 with High Thermal Capacity	363
196	Temperature Changes of Resistor and Heat-Pipe Cold Plate No. 3 vs Time After Coolant Shut-Off	364
197	Variable Conductance Heat-Pipe Cold Plate No. 1	365
198	Temperature Distribution of Variable-Conductance Heat-Pipe Cold Plate No. 1 (Coolant Inlet Temperature 55°F)	367
199	Temperature Distribution of Variable-Conductance Heat-Pipe Cold Plate No. 1 (Coolant Inlet Temperature 72°F)	368
200	Temperature Changes of Variable-Conductance Heat-Pipe Cold Plate No. 1 vs Electrical Power Input Rates	369
201	Variable-Conductance Heat-Pipe Cold Plate No. 2	370

LIST OF ILLUSTRATIONS (CONCLUDED)

FIGURE		PAGE
202	Inert Gas Bellows	371
203	Wick Details	372
204	Transistor and Thermocouple Locations	373
205	Transistor Mounting Detail	375
206	Temperature Changes of Variable-Conductance Heat-Pipe Cold Plate No. 2 and Transistor Q17 vs Coolant Inlet Temperature	376
207	Case Temperature Changes of Transistor Q17 vs Electrical Power Dissipation Rate	377
208	Thermocouple, Transistor and Diode Locations on Variable-Conductance Heat-Pipe Cold Plate No. 3	378
209	Temperature Changes of Variable-Conductance Heat-Pipe Cold Plate No. 3 and Transistor vs Coolant Inlet Temperature	380
210	Temperature Changes of Variable-Conductance Heat-Pipe Cold Plate No. 3 and Transistor Q21 vs Electrical Power Dissipation Rate	381
211	Case Temperature of Transistors Q1 and Q2 vs Electrical Power Dissipation Rate	382
212	Circuit-Card Heat-Pipe	384
213	Circuit-Card Heat-Pipe with Hybrid Circuit Packages	385
214	Wedge Clamp	386
215	Temperature Distribution of Circuit Card	383

LIST OF TABLES

TABLE		PAGE
1	Typical Thermal Resistance of Bonded Joints (Ref 1)	7
2	Thermal Conductivity of Electrical Insulation Materials (Ref 1)	7
3	Interface Resistance (Case to Sink) for Typical Semiconductor Cases (Ref 5)	9
4	Relative Heat Transfer Coefficients of Gases in Forced Convection at Equal Fan Horsepower	24
5	Thermal Properties of Coolants (Ref 17)	27
6	Heat of Fusion Materials and Their Properties	87
7	Evaporative Coolant Properties	88
8	Test Conditions of Liquid-Cooled Cold Plate No. 1	142
9	Thermal Resistances of Transistor Mounting Joints	148
10	Thermal Resistances of Resistor Mounting Joints	149
11	Computed Transistor Junction Temperatures	150
12	Test Conditions of Liquid-Cooled Cold Plate No. 2	160
13	Thermal Resistances of Transistor Mounting Joints (Cold Plate No. 2)	159
14	Thermal Resistances of Resistor Mounting Joints (Cold Plate No. 2)	166
15	Test Conditions of Liquid-Cooled Cold Plate No. 3	174
16	Thermal Performance Comparison of Liquid-Cooled Cold Plates	183
17	Test Conditions of Air-Cooled Cold Plate No. 1, Manifold Configuration #1	194
18	Test Conditions of Air-Cooled Cold Plate No. 1, Manifold Configuration #2	203
19	Test Conditions of Air-Cooled Cold Plate No. 1, Manifold Configuration #3	207

LIST OF TABLES (CONT'D)

TABLE		PAGE
20	Experimentally Determined Heat-Transfer Coefficients and Nusselt Numbers of Air-Cooled Cold Plate No. 1	213
21	Test Conditions of Air-Cooled Cold Plate No. 2, Manifold Configuration #1	218
22	Test Conditions of Air-Cooled Cold Plate No. 2, Manifold Configuration #2	225
23	Test Conditions of Air-Cooled Cold Plate No. 2, Manifold Configuration #3	230
24	Test Conditions of Air-Cooled Cold Plate No. 2, Manifold Configuration #4	230
25	Test Conditions of Air-Cooled Cold Plate No. 3, Manifold Configuration #1	242
26	Test Conditions of Air-Cooled Cold Plate No. 3, Manifold Configuration #2	250
27	Test Conditions of Air-Cooled Cold Plate No. 3, Manifold Configuration #2a	253
28	Test Conditions of Air-Cooled Cold Plate No. 3, Manifold Configuration #3	255
29	Test Conditions of Air-Cooled Cold Plate No.4	264
30	Test Conditions of Air-Cooled Cold Plate No. 5, Manifold Configuration #1	270
31	Test Conditions of Air-Cooled Cold Plate No. 5, Manifold Configuration #2	273
32	Test Conditions of Air-Cooled Cold Plate No. 5, Manifold Configuration #3	276
33	Test Conditions of Air-Cooled Cold Plate No. 5, Manifold Configuration #4	281
34	Test Conditions of Air-Cooled Cold Plate No. 6, Manifold Configuration #1	287
35	Test Conditions of Air-Cooled Cold Plate No. 6, Manifold Configuration #4	292

LIST OF TABLES (CONT'D)

TABLE		PAGE
A-1	Test Data of Liquid-Cooled Cold Plate No. 1	A-1
A-2	Test Data of Liquid-Cooled Cold Plate No. 2	A-5
A-3	Test Data of Liquid-Cooled Cold Plate No. 3	A-9
A-4	Test Data of Air-Cooled Cold Plate No. 1, Manifold Configuration #1	A-12
A-5	Test Data of Air-Cooled Cold Plate No. 1, Manifold Configuration #2	A-15
A-6	Test Data of Air-Cooled Cold Plate No. 1, Manifold Configuration #3	A-16
A-7	Test Data of Air-Cooled Cold Plate No. 2, Manifold Configuration #1	A-18
A-8	Test Data of Air-Cooled Cold Plate No. 2, Manifold Configuration #2	A-20
A-9	Test Data of Air-Cooled Cold Plate No. 2, Manifold Configuration #3	A-22
A-10	Test Data of Air-Cooled Cold Plate No. 2, Manifold Configuration #4	A-24
A-11	Test Data of Air-Cooled Cold Plate No. 2	A-25
A-12	Test Data of Air-Cooled Cold Plate No. 3, Manifold Configuration #1	A-26
A-13	Test Data of Air-Cooled Cold Plate No. 3, Manifold Configuration #2	A-29
A-14	Test Data of Air-Cooled Cold Plate No. 3, Manifold Configuration #2a	A-30
A-15	Test Data of Air-Cooled Cold Plate No. 3, Manifold Configuration #3	A-31
A-16	Test Data of Air-Cooled Cold Plate No. 4	A-33
A-17	Test Data of Air-Cooled Cold Plate No. 5, Manifold Configuration #1	A-35
A-18	Test Data of Air-Cooled Cold Plate No. 5, Manifold Configuration #2	A-37

LIST OF TABLES (CONCLUDED)

TABLE		PAGE
A-19	Test Data of Air-Cooled Cold Plate No. 5, Manifold Configuration #3	A-38
A-20	Test Data of Air-Cooled Cold Plate No. 5, Manifold Configuration #4	A-39
A-21	Test Data of Air-Cooled Cold Plate No. 6, Manifold Configuration #1	A-40
A-22	Test Data of Air-Cooled Cold Plate No. 6, Manifold Configuration #4	A-41

SYMBOLS

A	area, ft^2
C	thermal conductance, Btu/hr °F
C	heat capacity, Btu/°F
c_p	specific heat, Btu/lb °F
D, d	diameter, ft
D_h	hydraulic diameter, ft
F	force, lb
G	mass velocity, lb/hr ft^2
g	acceleration due to gravity, ft/hr^2, or ft/sec^2
g_c	universal gravitational constant, ft. $lb_m/lb_f hr^2$
H	heat of fusion, Btu/lb
h	heat transfer coefficient, Btu/hr ft^2°F
K	thermal conductance, Btu/hr °F
k	thermal conductivity, Btu/hr ft^2 °F/ft
L, l	length, ft
P	electric power dissipation, watts
P	pressure, psf, or psi
ΔP	pressure differential, psf, or psi
Q, q	rate of heat transfer, Btu/hr, or Btu/sec
R	thermal resistance, hr °F/Btu, or °C/watt
r	radius, ft
T	temperature, °R
t	temperature, °F
t_a	environment temperature, °F
t_c	case temperature, °F

SYMBOLS (CONCLUDED)

t_j	junction temperature, °F
t_s	heat sink temperature, °F
Δt	temperature differential, °F
U	flow velocity, ft/sec, or ft/hr
V	volume, ft^3
W	weight, lb
$\dot{w}$	mass flow rate, lb/hr
Nu	Nusselt number
Pr	Prandtl number
Re	Reynolds number
ρ	density, lb/ft^3
μ	absolute viscosity, lb/ft hr
ν	kinematic viscosity, ft^2/hr
η	fin effectiveness
δ	fin thickness, ft
δ	gap thickness, ft
ϵ	hemispherical emittance
ϵ	porosity
σ	stefan - Boltzmann constant, Btu/hr ft^2 $°R^4$
σ	stress, psi
σ	surface tension, lb/ft
τ	time, hr, or sec
$\Delta\tau$	time increment, hr
α	slope or angle, degrees
θ	contact angle, degrees
μ	Poissons ratio

ABSTRACT

Because of the thermal and packaging requirements of latest avionics equipment, cold plates are becoming the most predominant cooling devices. The primary advantages of their application are ease of repair and part replacement; removal of highly concentrated heat loads; a heat conduction path which can be tailored to fit the particular thermal requirement; and, in the case of air cooling, critical electronic components can be protected from moisture, dust, and other contaminants which may be contained in the cooling air.

Regardless of how cold plates have been used in avionics equipment cooling, little information can be found in the open literature about their capabilities and thermal performance characteristics. To overcome this deficiency and provide guidance in the application of cold plates to electronic equipment cooling, information obtained from contractual and in-house studies has been collected and is presented in this report. The information covers liquid-cooled cold plates, air-cooled cold plates, and cold plates with heat pipes.

Experimental liquid-cooled cold plates of three different designs have been fabricated and tested, and correlation between analytical and experimental data made. It has been shown that accurate thermal performance prediction can be achieved, particularly with computer-aided analysis, if proper thermal resistance values are provided. Highly concentrated heat loads can be removed by liquid-cooled cold plates, and their thermal performance accurately predicted.

The air-cooled cold plates tested can be divided into two general categories: (1) cold plates with plain airflow channels (without finned or extended surfaces) and (2) cold plates with compact heat exchanger cores. Each of the two categories represented three different aspect ratios and was tested with three or four different manifold configurations. The test results revealed that standard textbook equations, developed for fully-established velocity and temperature profiles, cannot be used in predicting heat-transfer coefficients of actual cold plates. Particularly large differences between analytically and experimentally determined heat-transfer coefficients can be observed with the cold plates having flow channels without extended surfaces. Heat-transfer coefficients computed from the standard textbook equations were significantly lower than those obtained from actual experimental data. The differences were particularly large at the lower Reynolds numbers. Heat-transfer coefficients of cold plates equipped with standard heat exchanger cores, for which heat transfer data were available, could be accurately predicted.

The test results further revealed that both geometry of the airflow channel and manifold configuration had effects upon heat transfer and flow distribution of the cold plates. The effects, however, were

ABSTRACT (CONCLUDED)

more significant for the cold plates without extended surfaces, particularly for the ones of larger hydraulic diameters. Neither the heat-transfer coefficients nor flow distribution were significantly affected by the manifold configurations of the cold plates equipped with compact heat exchanger cores.

Close temperature control of cold plates can be achieved by the use of variable-conductance heat pipes. Thermal cycling caused by heat load changes or heat-sink temperature changes can be significantly reduced by the application of heat-pipe technology. Uniform temperature mounting surfaces, often a requirement in microelectronic circuit design, can be conveniently provided by using heat pipes. However, high dynamic forces, experienced in advanced aircraft, will impose limitations on the application of heat pipes to avionics equipment cooling.

Although the data presented in this report will not provide answers to all problems and conditions occurring in cold-plate design, parameters affecting heat transfer and flow distribution have been identified and their effects upon the thermal performance of cold plates determined. Electronic equipment standardization, presently under consideration, should lead to standardization of cooling devices and systems. This condition will simplify design of the thermal control system and provide the cooling required for equipment reliability and improved performance characteristics.

SECTION I

INTRODUCTION

Advanced aircraft rely more and more on avionics; consequently, performance of the aircraft is becoming closely related to that of the electronic equipment. The electronic systems are growing in complexity and compactness, particularly with the development of semiconductor devices and resulting microcircuit applications. Although microminiaturized circuitry dissipates less total power, the power density (watts per unit volume) is frequently much higher than that of conventional circuitry. Heat fluxes at the component and package level have increased by an order of magnitude, causing difficulties in removing the waste heat. It is known from experience that operating temperature is a major factor in electronics reliability, and failure rates are related to temperature. Operation of devices and circuitry at elevated temperatures usually requires derating (operation at less than design capacity) to satisfy reliability goals.

In addition to stresses induced by high temperatures, stresses are also caused by thermal cycling. Because of thermal cycling, failure rate increases of approximately an order of magnitude have been reported. Furthermore, most transistor circuits in present use require temperature stabilizing circuits in order to permit operation over a desired temperature range. Also, memory units require a relatively narrow temperature range for proper performance.

There are three basic thermal conditions to consider to improve component reliability: (1) temperature level, (2) thermal cycling, and (3) temperature uniformity. Heat removal and thermal control, therefore, are the result of careful design of the entire thermal control system and the establishment of low temperature gradients between the heat sink and the temperature sensitive parts and circuitry. Selection of the proper cooling technique to satisfy all the thermal requirements is difficult, and consideration should be given to many particular conditions.

In electronic equipment cooling, generally all of the three basic heat transfer modes (i.e., conduction, convection and radiation) are taking part in heat dissipation. The relative importance of each mode depends upon the thermal requirements of the equipment; the available heat sinks; and other considerations like weight, volume, and cost. Natural convection and radiation modes of heat transfer are used in the cooling of low-power-density equipment. For electronic equipment of high packaging densities and heat dissipation rates, forced convection or evaporative cooling techniques must be considered. Forced convection cooling can be divided into direct and indirect cooling techniques. While in the direct cooling systems the electronic components and/or circuitry are directly exposed to the cooling fluid, in the indirect cooling systems the coolant does not come in direct contact with the equipment.

Indirect cooling, considered under this effort, has the following advantages over immersion or direct fluid cooling: (1) easier accessibility for maintenance, (2) smaller amount of coolant (liquid) within the system, (3) less sealing problems, (4) simpler and lighter cooling system, and (5) the ability to use coolants with better thermal properties. This cooling technique is known as the "cold plate" principle. In this cooling technique, the electronic equipment is mounted to cold plates through which the coolant is circulated. Depending on the heat loads and thermal requirements, liquids or gases can be used as the heat transport fluids.

Although cold plates have been used in electronic equipment thermal control, very limited information can be found in the open literature about capabilities and thermal performance characteristics of such plates. This effort, therefore, will be mainly oriented towards collection and presentation of available data, including some analytical and experimental work in areas where information was not available. Included will be performance characteristics of liquid-cooled cold plates, air-cooled cold plates, and cold plates provided with heat pipes. In order to establish confidence in the analytical procedures and discover deficiencies, the analytically predicted thermal performance of the cold plates will be compared with actual test data.

The cold plates shown in this report are generally of experimental nature, and might not present the best possible design features and performance characteristics. They present, however, the general thermal capabilities of the different cold plates tested, and allow determination of parameters affecting heat transfer and flow distribution. The extensive experimental work also provided information about problem areas which need further exploration and development work.

SECTION II

THERMAL REQUIREMENTS OF ELECTRONIC EQUIPMENT

Effective heat transfer and removal is essential to the achievement of long life, high reliability and performance of electronic equipment. Operating temperature is a major factor in electronic equipment reliability, and failure rates are commonly related to the junction temperature. Although electronic equipment reliability is affected by other environments, field experience indicates that a significant number of failures arise from temperature effects. To minimize the failure rate and achieve successful operation of electronic equipment, low, stable temperatures are required.

It is recognized that thermal design is as important as circuit design because temperature effects can determine the life of electronic parts and circuitry. Heat degrades bulk characteristics and has a degenerative runaway effect on junction characteristics. To protect against this, current limiting fuses, temperature compensating circuitry, temperature sensitive bypass diodes, etc. are necessary for proper equipment operation and reliability. Temperature effects can be generally outlined as follows: (1) chemical changes which cause corrosion and diffusion; (2) physical changes, including changes in calibration, insulation damage, and weakening of leads and bonds; and (3) electrical changes which cause drift of component characteristics, electrical noise, and spontaneous switching of logic circuits. There is a maximum temperature at which the ability to tune the circuit becomes extremely difficult because of thermal noise and rapidly changing device characteristics. Furthermore, the trend toward faster logic circuitry requires closer spacing of components to reduce the delay in signal transmission. Besides electrical problems, closely-spaced components cause serious thermal problems. Thus, the closer spacing of components means that more power must be dissipated per unit area. It can generally be stated that circuit temperature sensitivity is increased with circuit complexity.

Semiconductors include such components as transistors, diodes, integrated circuits, rectifiers, etc. All of these components are temperature limited, depending on the type of electrical junction construction and the basic semiconductor material forming the device. Most semiconductors are made of germanium or silicon material. Maximum junction temperatures for germanium devices are quoted as high as 110°C, and for silicon devices 200°C. The actual operating temperatures, however, because of circuit performance requirements and reliability specifications, dictate much lower junction temperatures. In many instances a 125°C junction or silicon chip temperature is set as a typical conservative upper limit for reliable operation of present-day microelectronics. This limit is also enforced for equipment to be installed in aircraft presently under development. Silicon junction temperatures in space flight and computer equipment are often specified in the range from 70°C to 80°C. Reference 1 points out that silicon

devices operated at 300°C will age 10,000 times faster than the same devices at 125°C. The effect of a 200°C temperature, compared to one at 125°C, is aging at a rate 170 times faster.

In addition to the stresses induced by high temperatures, additional stresses are caused by thermal cycling. Studies performed by the Navy (NADC) reveal that temperature cycling has significant effect upon the reliability of electronic equipment. References 2 and 3 indicate that temperature-cycled part life may be six to seven times less than similar parts operated under constant temperature conditions. Cracked insulator cases and open circuits between the devices and leads are common failure modes caused by thermal cycling or shock. Hermetic seals, particularly the soft-solder type, are affected by high surface temperatures and temperature cycling. A successful cooling system for electronic components, therefore, not only facilitates operation at some reduced temperature, but must also moderate thermal cycling resulting from variations in power dissipation and/or heat-sink temperature changes.

Another important thermal requirement is temperature uniformity. Uniform cooling is important in circuits that have components in parallel as differences in temperature can cause unequal power loading of the components. Uniform cooling is also important in circuits where distortion of signal or calibration changes may be caused by differences in temperature. Uniform cooling has become increasingly important as electronic speeds have increased. Packaging density must be significantly increased for very high-speed logic circuitry. It is important to the circuit designer that the entire cold plate or circuit board is at a uniform temperature because component layout based on thermal considerations can be eliminated.

Reference 4 points out that thermal design of microelectronics must satisfy the following two general requirements: (1) provisions must be made to limit temperature variations within an electronic system to certain maximum and minimum, and (2) temperature variations from point-to-point within a system must be kept to a minimum. These requirements must be satisfied for optimum performance and reliability of the electronic system.

The most temperature-sensitive types of military avionic equipment are computation, communication, multimode radar antennas, electronic countermeasures receivers, and navigation equipment. The design point of the cooling system for this equipment is generally specified as 100°C maximum for extended normal operation.

In summary, there are three basic thermal conditions to consider to insure electronic equipment reliability and performance: (1) temperature level, (2) temperature cycling, and (3) temperature uniformity. In designing a thermal control system for avionics equipment, all of these requirements must be satisfied as closely as possible.

SECTION III

ELECTRONIC EQUIPMENT MOUNTING

Semiconductor devices are widely used in present-day avionic systems. Many of the high-power devices are designed for stud or flange mounting and are provided with a flat surface to insure good thermal contact with the heat sink. A good conduction path between heat-producing components and the heat-sink surface is essential for efficient heat removal. A thin air gap or film can cause large temperature differentials between the electronic component and the heat sink. The mating surfaces should be machined flat; protected with noncorrosive film finishes; and for best heat transfer results, application of silicone greases to eliminate the air gap is highly recommended.

Some transistors are fabricated with their case electrically connected to one of the transistor elements. Such transistors require insulating washers, and the thermal resistance from the case to the heat sink includes also the insulation thermal resistance, which may be quite significant. There may be other thermal interfaces in the heat-transfer path, such as between circuit-card thermal-mounting plates and the card slots or between modular assemblies, and the cold plates to which they are bolted.

Parameters that control the thermal resistance across metal surfaces include flatness; surface finish; hardness, as well as thermal conductivity of the mating surfaces; and the interstitial fluid and pressure between the mating surfaces. It is recommended that to assure low interface thermal resistance, mating surfaces should be flat to within 0.001 inch, and surfaces should be finished to a tolerance of 63 microinches or less. All paint and other impurities should be removed completely by a treatment with #000 fine steel wool and silicone oil. If the interface is not properly prepared, the thermal resistance may become excessive and make the heat transfer capability of a good heat sink worthless. Thermal resistance from the mounting surface of the device to the ultimate heat sink must be tailored to satisfy the maximum allowable temperature requirements.

The heat conduction away from a heat-producing electronic device is enhanced by using large conductor cross sections, obtaining good joint contact (by having very smooth surfaces under high pressure exerted by the fasteners), and using minimum thickness of electrical insulators. It should be pointed out that black surfaces enhance radiative heat transfer.

Integrated circuits may be cooled by conduction as well as by convection heat transfer to ensure low temperatures. The simplest method of achieving conductive cooling is to bond integrated circuits to a conductive layer which is connected to a heat sink.

Either electrically conductive (soft solder or conductive cements) or non-conductive (plastics or ceramic cements) bonding materials may be used, depending upon whether isolation is required. The component shape, bonding technique, bond strength, and removal requirements, as well as thermal conductivity, all enter into the choice of bonding agent.

Reference 5 points out that the bond should be as thin as possible and cover the entire bonding surface of the component. When a thick bond is required for electrical insulation, appropriate size glass beads may be included in the adhesive to support the component at the proper distance during bonding. When additional insulation is required, a ceramic spacer may be bonded between the component and heat sink. The thermal resistance of the bond will depend on the bond thickness, joint surface area, and thermal conductivity of the bonding material. Table 1 (Ref 5) presents typical thermal resistance values for bonded joints. Table 2 (Ref 5) presents thermal conductivity of typical electrical insulation materials.

Reference 6 points out that some electronic parts are specified in terms of external surface temperatures at given locations, and the internal thermal resistances from these surfaces to the most temperature sensitive internal elements are given. Other electronic parts are, in general, rated individually for certain performance at specified ambient temperatures. The ambient temperature for a part is the temperature of the surrounding medium in which the part must operate. Ambient temperatures, however, do not have much meaning with densely-packed electronic systems. The maximum safe temperatures must be calculated, based on the part stress analysis, and must be consistent with the required equipment reliability and the failure rate assigned to each part.

The internal thermal resistance of a solid-state device is expressed in degrees Centigrade per watt (or also per milliwatt). In accordance with Reference 7, the lowest internal thermal resistance is about 0.5°C/watt. Low-power transistors, however, have internal resistances between forty and two thousand times larger, i.e., 20°C/watt to 1000°C/watt (or 1°C/mw). It can be seen that regardless of the low power dissipation rates, case temperatures of the devices must be kept low. The thermal resistance from the case by radiation and natural convection is usually very high, and the primary mode of heat transfer in cooling semiconductor devices is metallic conduction. Reference 7 also indicates that a power transistor which could dissipate 70 watts when mounted on an infinite heat sink at 25°C had a maximum power dissipation of approximately 2 watts when mounted in free air. Under the same conditions, the smaller, lower-power devices had convection-radiation thermal resistances ranging up to 500°C/watt.

Electronic equipment manufacturers furnish mounting hardware for the several types of cases and publish the effective thermal interface resistance between the case and the heat sink, usually for stated torque or contact pressure. The contact resistance varies with the surface

Table 1. Typical Thermal Resistance of Bonded Joints (Ref 1)

BOND MATERIAL	THERMAL CONDUCTIVITY (watt/°C in)	TYPICAL BOND THICKNESS (inch)	THERMAL RESISTANCE (°C/watt in^2)
Soft Solder	1.6	0.005	0.003
Epoxy Resin	0.005	0.005	1
Aluminum Oxide Filled Epoxy Resin	0.025	0.005	0.2
Aerobic Contact Cement	0.005	0.001	0.2

Table 2. Thermal Conductivity of Electrical Insulation Materials (Ref 1)

INSULATION MATERIAL	THERMAL CONDUCTIVITY (watt/°C in)
BeO Beryllium	4.0
Al_2O_3 Aluminum	0.65
Mica	0.0013
Fiberglass Epoxy Laminate	0.1

flatness and the torque applied to tighten the bolts. These variations can be greatly reduced by applying silicone compounds to the mating surfaces. These compounds are grease-like silicone material filled with heat-conductive metal oxide.

If the electronic component must be electrically isolated from the heat sink, insulating washers made of Teflon, anodized aluminum, mica, and beryllium oxide must be used. The choice of washer material depends on fragility, ease of assembly, cost, and manufacturing methods. Flexible materials such as Teflon and mica partly compensate for surface imperfections. However, the heat-sink surface should always be reasonably flat and smooth. Beryllium oxide is brittle and anodized aluminum is hard so that very flat mounting surfaces are required for these materials. Table 3 of Reference 5 presents case-to-sink thermal resistances for typical semiconductor cases.

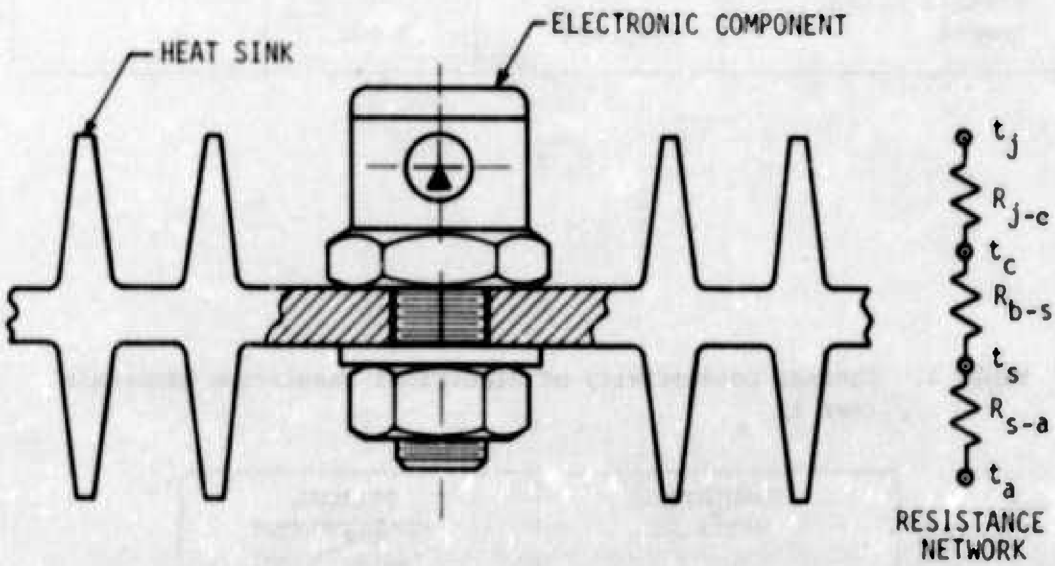

Figure 1. Component Mounting on Heat Sink

Consider an ordinary air-cooled heat sink with a power dissipating device mounted on it as shown on Figure 1. Heat generated by the device flows mainly to the base of the device. From the base it flows across the mounting joint into the heat sink, then to the surrounding air. The total thermal resistance, R_t, can be expressed as follows:

$$R_t = R_{j-a} = R_{j-c} + R_{c-s} + R_{s-a} \quad (1)$$

Table 3. Interface Resistance (Case to Sink) for Typical Semiconductor Cases (Ref 5)

TYPICAL JEDEC CASE				TO-3, -41	TO-36	TO-66	TO-59, -60 DO-4	TO-48	TO-51 DO-5	TO-63	
CONTACT AREA in^2				0.86	0.75	0.38	0.11	0.18	0.30	0.52	0.66
STUD SIZE in				-	#10	-	#10	1/4	1/4	5/16	1/2
HEX SIZE in				-	-	-	7/16	9/16	11/16	7/8	1-1/16
INTERFACE		CONTACT RESISTANCE ($^{\circ}C$ in^2/watt)		CONTACT RESISTANCE ($^{\circ}C$/watt)							
Metal to Metal	Dry	High	0.55	0.64	0.73	1.4	5.0	3.0	1.8	1.0	0.83
		Mean	0.4	0.46	0.53	1.0	3.6	2.2	1.3	0.77	0.60
		Low	0.14	0.16	0.19	0.37	1.3	.78	.47	0.27	0.21
	Silicone Grease	High	0.36	0.42	0.48	0.95	3.2	2.0	1.2	0.70	0.55
		Mean	0.2	0.23	0.27	0.53	1.8	1.1	0.67	0.38	0.30
		Low	0.075	0.09	0.10	0.20	0.69	0.42	0.25	0.15	0.12
	Thermal Compound	High	0.17	0.20	0.23	0.45	1.5	0.95	0.56	0.33	0.26
		Mean	0.1	0.12	0.13	0.26	0.90	0.55	0.33	0.19	0.15
		Low	0.05	0.06	0.07	0.13	0.45	0.28	0.17	0.10	0.08
Indium 0.005 thick	Dry	High	0.09	0.10	0.12	0.24	0.82	0.55	0.33	0.19	0.13
		Mean	0.07	0.08	0.09	0.18	0.64	0.39	0.23	0.13	0.11
		Low	0.05	0.06	0.07	0.13	0.45	0.28	0.17	0.10	0.08
Mica 0.002 to 0.003 thick	Dry	High	1.75	2.0	2.3	4.6	16.0	9.7	5.8	3.3	2.6
		Mean	1.2	1.4	1.6	3.2	11.0	6.7	4.0	2.3	1.3
		Low	0.60	0.70	0.80	1.6	5.5	3.3	2.0	1.2	0.91
	Silicone Grease	High	1.0	1.1	1.3	2.6	9.1	5.5	3.3	1.9	1.5
		Mean	0.6	0.70	0.80	1.6	5.5	3.3	2.0	1.2	0.91
		Low	0.3	0.35	0.40	0.79	2.7	1.7	1.0	0.58	0.45
BeO 0.020 to 0.062 thick	Dry		0.31	0.36	0.41	0.82	2.8	1.7	1.0	0.60	0.47
	Indium Foil Washers		0.14	0.16	0.19	0.37	1.3	0.78	0.47	0.27	0.21
	Filled Epoxy		0.11	0.13	0.15	0.29	1.0	0.61	0.37	0.21	0.17

where R_{j-c} = thermal resistance from junction to mounting base

R_{c-s} = thermal resistance from component mounting base to heat sink (interface thermal resistance)

R_{s-a} = thermal resistance between the heat sink and the ambient air.

Actually, the heat sink will also have a certain resistance to heat flow and will cause a temperature drop. However, because of the large cross-sectional area and high thermal conductance of the material, this resistance is usually neglected. When the thermal resistances are known, or they may be measured, the junction temperature can be determined from the following expression:

$$t_j = t_a + P\left(R_{j-c} + R_{c-s} + R_{s-a}\right) \quad (2)$$

where P is the electric power dissipation in watts.

If the base temperature of the device is known, the junction temperature can be determined as follows:

$$t_j = t_c + PR_{j-c} \quad (3)$$

For determining the heat transfer rate and temperature gradients within a cooling device, two general conditions of the heat generating component must be distinguished: (1) continuous wave and (2) pulsed operation. In continuous wave operation, a steady-state heat transfer analysis can be used on the component. In pulsed operation, the junction temperature of the component varies with time. The average junction temperature is proportional to the duty cycle, while the maximum and minimum junction temperatures are a function of both the duty cycle and pulse length. The pulse width, τ, is interrelated by the expression

$$\tau = \frac{d}{PRF} \quad (4)$$

where d is the duty cycle and PRF is the pulse repetition frequency. The duty cycle multiplied by the peak module output yields the average power output of the module. Figure 2 shows pulsed operation of an electronic component.

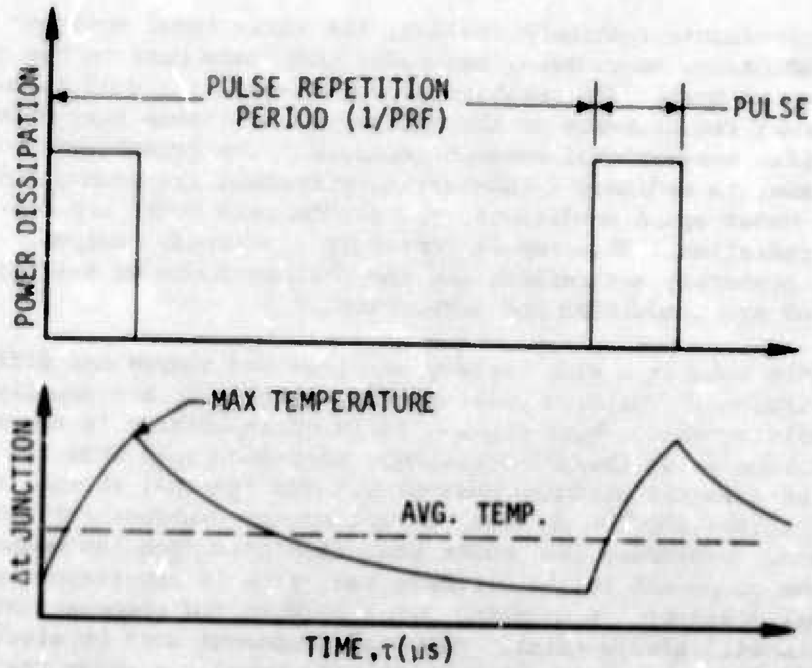

Figure 2. Junction Temperature Rise vs Time as a Function of Pulse Width and Duty Cycle

SECTION IV

HEAT REMOVAL CONCEPTS AND HEAT TRANSFER FROM ELECTRONIC DEVICES

In all electronic equipment cooling, the three basic modes of heat transfer (conduction, convection, and radiation) take part in the dissipation of waste heat. The relative importance of each mode depends upon the thermal requirements of the equipment, available heat sinks, and the specific heat-removal concept employed. The predominant modes of heat transfer in ordinary (planetary) environment are conduction and convection. Under space conditions, the predominant modes are conduction and radiation. This report considers electronic equipment operation in planetary environment and the primary modes of heat transfer considered are conduction and convection.

Components come in a wide variety of sizes and shapes and different mounting provisions. The high power density components are usually designed for bolting to the heat sinks. It is of importance in thermal design to provide a low thermal-resistance heat-flow path from the heat dissipating part to the ultimate heat sink. The internal thermal resistance of the part (junction to case) is set by the manufacturer and cannot be changed. Providing the proper heat-flow path from the mounting surface of the component to the ultimate heat sink is the responsibility of the thermal designer. A mounting joint between the component(s) and the cold plate will always exist. When the component must be electrically isolated from the plate, this joint will usually provide the largest thermal resistance in the heat-flow path. At the joint between two surfaces, there is a variable thermal resistance which depends on the contact pressure, the contact area, the material, and the surface finish and flatness. More detailed discussions about joint thermal resistances follow. When components are mounted on circuit cards, a thermal interface occurs between the cards and the card slots.

Forced convection (liquid or gas) cooling systems can be basically classified as either direct or indirect. In a direct system, the coolant is in direct contact with the electronic components. Heat is transferred directly from the heat-producing parts to the coolant. Forced convection in this case is the primary mode of heat transfer from the part. In the indirect system, the coolant does not come in direct contact with the electronic components. Heat is removed from the electronic components by conduction to the plate or chassis and from there by convection to the circulating coolant. For electronic systems having low or medium heat-dissipation rates, air cooling, because of its availability, provides simple, cheap, and effective cooling. Both direct and indirect air cooling have been extensively used. However, since air often contains large amounts of moisture and dust, there is a tendency and sometimes the requirement to employ indirect air cooling by the application of cold plates or chassis.

Reference 8 gives the following guidance in selecting an electronic-equipment cooling method: (1) when the power dissipation density is less than 0.25 watts/in^2, and with ambient pressure of one atmosphere and temperature of 25°C, natural cooling (free convection, conduction, and radiation) can be used; (2) for power densities between 0.25 and 2 watts/in^2, forced air cooling should be used; and (3) if the power density is over 2 watts/in^2, indirect cooling should be used with metallic conduction paths from the heat sources to the liquid coolant.

Individual solid-state devices have such small areas that natural convection and radiation from them are relatively ineffective. To provide sufficient cooling, these devices must be provided with extended surfaces of high thermal conductance. Thermal conductance must be considered as the simplest means of heat distribution that can be effectively applied to cooling of solid-state devices. High-power devices in general have large, flat-mounting surfaces with provisions for attachment to a heat sink.

To accomplish effective thermal design of any electronic device or part, information about its allowable maximum temperature, heat dissipation rate, and internal and external thermal resistances must be known. For standard semiconductors, the overall junction-to-case thermal resistance, R_{j-c}, is given by the manufacturer. The resistance, however, might be given directly or it can be calculated from basic rating data

$$R_{j-c} = \frac{t_{jmax} - t_c}{q} \tag{5}$$

For example, if $t_{jmax} = 200°C$ at $q = 0$ watts

and at $t_c = 25°C$, $q = 100$ watts;

then, $R_{j-c} = \frac{200-25}{100} = 1.75°C/\text{watt}$.

On the other hand, when thermal resistance is known, the case temperature of the device can be determined from the following expression:

$$t_{c(\text{max. allow})} = t_{jmax} - q\left(R_{j-c}\right) \tag{6}$$

For example, if a transistor with R_{j-c} = 1.75°C/watt dissipates 50 watts; then, the maximum allowable case temperature will be

$$t_{c(\text{max. allow})} = 200-50\ (1.75) = 112.5°C$$

Most of the high-power components are designed for bolting to a heat sink. The thermal resistance from the case to the heat sink includes the joint thermal resistance and insulation thermal resistance if an insulator is used. Insertion of soft materials and application of silicone grease at mounting surfaces will replace air and reduce the need for perfectly flat and smooth surfaces. The thermal interface in the heat-flow path from the component case to the heat sink is a significant parameter in the analysis of conduction cooling of electronic devices. For a more complex joint, it is almost always necessary to make the evaluation experimentally or search for a similar situation in the literature.

SECTION V

CONVECTION HEAT TRANSFER

Although many excellent handbooks and technical papers have been written about convection heat transfer, it is felt that a short summary of this important mode of heat transfer will be of benefit to the thermal designer. Investigators in heat-transfer experimental work often discover that large differences can occur between predicted and actual test results. Furthermore, most of the developed equations pertain to circular tubes, flat plates, and rectangular ducts of rather small aspect ratios. Little information is available about flow passages encountered in the design of cold plates, particularly air-cooled cold plates.

The simplest possible case occurs when the velocity and temperature profiles are fully developed, i.e., the heated section is located far from the tube or duct entrance. Also, only two general boundary conditions are considered, one at a constant surface temperature and the other at a constant heat rate per unit of tube length. Such ideal conditions will occur very seldom in actual heat-transfer equipment design, thus causing differences in predictions. It must also be noted that heat-transfer coefficients for flow inside tubes are not the same as for flow over external surfaces and ducts of different cross sections and aspect ratios. At an entrance of a tube or duct, the heat-transfer coefficient has a high value. This value reduces as the distance is increased from the entrance. Reference 9 points out that developed solutions are excellent approximations for fluids whose Prandtl numbers are high relative to one. For example, if the Prandtl number is greater than 5, the velocity profile leads the temperature profile sufficiently so that a solution based on a fully-developed velocity profile will apply for conditions without hydrodynamic starting length. For fluids with Prandtl number less than one, the temperature profile develops more rapidly than the velocity profile and the developed solutions do not apply. There is another item of consideration: any fitting close to the test section that would cause turbulence or produce swirl flow would also increase the heat-transfer coefficient.

In a fluid flow through a duct or tube, two general flow regimes can be realized: (1) laminar or streamline flow and (2) turbulent flow. Below Reynolds numbers of 2300, the fluid flow is considered as laminar, and above 10,000 the flow normally will be turbulent. Results between the two values are difficult to predict; the literature must be consulted for specific information. Reference 10 points out that, for turbulent flow, the thermal entry length is much shorter than for a laminar flow. Harnett et al (Ref 10) present information on the hydrodynamic entrance region for laminar flow in rectangular tubes. It was found that the entrance configuration had little effect on the hydrodynamic entry length for Reynolds numbers below 2000, but had a large effect above the value of 2000. Hartnett used the following expression:

$$\frac{x}{D_h} = C \cdot Re \tag{7}$$

where C is approximately 0.033 for an aspect ratio of 10 to 1, 0.046 for an aspect ratio of 5 to 1, and 0.057 for an aspect ratio of 1:1. It can be seen that the aspect ratio has effect upon the entrance length. The lower aspect ratio ducts require greater length for the establishment of fully-developed flow. It is important to note that the critical Reynolds number is affected by the entrance manifold configuration. This also has been found from experiments performed under this study. Levy et al (Ref 10) found that, for a rectangular duct with an aspect ratio of 25 to 1, the combined thermal and hydraulic entry length to diameter ratio was 55 to 65 diameters, in contrast to circular tube values on the order of 15 diameters. The reference also notes that at high Reynolds numbers (approximately Re = 24000), the flow does not become fully developed, even at an L/D_h ratio of 114. Numerous experiments with flow in noncircular ducts prove that thermal entry regions are much longer than those in circular tubes.

It should be further noted that for duct shapes with sharp corners, the local heat-transfer coefficient varies around the periphery of the duct and approaches zero at the corners. Assumption is also generally made that the heat-transfer coefficient is constant along the length of the fin. Some investigators, however, have shown that this is not true for all conditions. Reference 10 indicates that the local heat-transfer coefficient around the tube wall can vary from 0.1 of the average value to over 2 times the average value. The assumption of a constant heat-transfer coefficient along the length of the fin can be made only under conditions when the fins are highly effective (temperature is almost uniform and equal to the plate temperature).

The basic equation for convection heat transfer is

$$Q = hA \left(t_w - t_f\right) \tag{8}$$

on the heat flux per unit area of the wall

$$Q/A = h \left(t_w - t_f\right) \tag{8a}$$

where t_w is the wall temperature, t_f is the cooling fluid temperature, and h is defined as the heat-transfer rate divided by the temperature difference causing the heat transfer. Since the heat flux is often variable over the surface area, the heat-transfer coefficient also varies over the surface. The local value of h, therefore, can be expressed as follows:

$$h_x = \frac{q_x}{t_w - t_f} \tag{9}$$

The forced-convection heat-transfer coefficients depend on flow regimes and can vary within a very wide range; for example, with gases, h can range from approximately 2 to 50 Btu/hr ft^2 °F.

In order to correlate experimental data, the well known Nusselt expression can be used:

$$Nu = C\,(Re)^m\,(Pr)^n \tag{10}$$

$$Nu = \frac{hD}{k} \text{ is the Nusselt number} \tag{11}$$

$$Re = \frac{DU\rho}{\mu} \text{ is the Reynolds number} \tag{12}$$

$$Pr = \frac{C_p\mu}{k} \text{ is the Prandtl number} \tag{13}$$

C is a dimensionless constant; m and n are exponents the values of which depend on the configuration and the degree of turbulence of the coolant flow. Different values of C and n have also been found for heating and cooling of liquids in tubes. Experiments have shown that the Nusselt expression is applicable for all fluids, whether in the liquid or gaseous state.

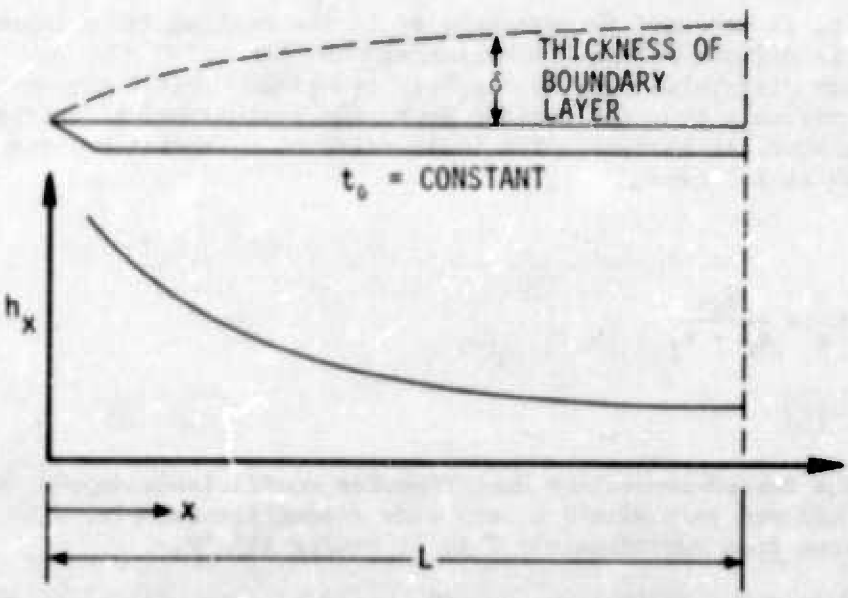

Figure 3. Flow Over a Flat Plate

Consider first the simplest case: flow over a flat plate as shown in Figure 3. Under laminar flow conditions, Reference 11 gives the following expression for the local heat-transfer coefficient:

$$h_x = 0.332\, k\, (Pr)^{1/3} \sqrt{\frac{U_\infty}{\nu \cdot x}} \tag{14}$$

or

$$Nu_x = h_x \frac{x}{k} = 0.332\, (Pr)^{1/3} \sqrt{\frac{U_\infty x}{\nu}} \tag{15}$$

and the average heat-transfer coefficient is

$$h = \frac{1}{L} \int_0^L h_x dx = 0.664\ k(Pr)^{1/3} \sqrt{\frac{U_\infty}{\nu L}} \tag{16}$$

$$h = 2\ h_x$$

$$Nu = 0.664\ (Re)^{1/2}\ (Pr)^{1/3} \tag{17}$$

All the results are valid for Pr greater than 0.5 and uniform temperature of the plate.

For laminar flow inside smooth tubes, under fully-developed velocity and temperature profiles and constant heat rate, Reference 9 gives the following expression:

$$Nu = \frac{hD}{k} = 4.364 \tag{11}$$

and for constant surface temperature

$$Nu = \frac{hD}{k} = 3.658$$

Sieder and Tate (Ref 12) suggest the following empirical equation for both cooling and heating of viscous liquids at laminar flow:

$$Nu = 1.86 \left(Re \cdot Pr \cdot \frac{D}{L}\right)^{1/3} \left(\frac{\mu}{\mu_w}\right)^{0.14} \tag{18}$$

The fluid properties should be evaluated at the arithmetic mean bulk temperature where μ_w is the absolute viscosity at surface temperature.

For moderate temperature differences between the wall and coolant, the term $(\mu/\mu_w)^{0.14}$ approaches unity, and

$$Nu = 1.86 \left(Re \cdot Pr \cdot \frac{D}{L}\right)^{1/3} \tag{18a}$$

Reference 13 recommends the following empirical expression developed by Hausen:

$$Nu = 3.65 + \frac{0.0668\ (D/L)\ Re \cdot Pr}{1 + 0.04\ [(D/L)\ Re \cdot Pr]^{2/3}} \tag{19}$$

The equation gives the average Nusselt number for uniform wall temperature and fully-developed flow.

For the transition region (Reynolds numbers from 2100 to 10,000) the Nusselt type equation based on the work of Hausen is:

$$Nu = 0.116 \left[(Re)^{2/3} - 125\right] (Pr)^{1/3} \left(\frac{\mu}{\mu_w}\right)^{0.14} \left[1 + \left(\frac{D}{L}\right)^{2/3}\right] \tag{20}$$

Although laminar flow has advantages as far as pressure drop, acoustic noise, and power reuqirements are concerned, turbulent flow is desired because of much higher heat-transfer coefficients. This is particularly true for air cooling. For air cooling, Reference 14 recommends Reynolds numbers within the range from 2000 to 4000 and higher. The upper limit of Reynolds number is dictated by pressure drop, power requirements, and acoustic noise.

One of the earliest equations used for fully-developed turbulent flow in a smooth tube is the so called Dittus - Boelter equation, modified and recommended by McAdams as follows:

$$Nu = 0.023\ (Re)^{0.8}\ (Pr)^{0.4} \tag{21}$$

The equation was based on experimental data covering the Prandtl number range from 0.7 to 120, Reynolds numbers from 10,000 to 120,000, and L/D greater than 60. This equation is also used for Re greater than 2300.

For shorter channels where the entrance effects must be considered

$$Nu = 0.036\ (Re)^{0.8}\ (Pr)^{.3}\ (D/L)^{0.055} \tag{22}$$

For a large temperature difference between the fluid and wall, Reference 11 suggests the following equation to correlate experimental data:

$$Nu = 0.020\ (Re)^{0.8}\ (Pr)^{0.4} \tag{23}$$

This equation is valid for Re greater than 10,000 and t_w/t_f up to 3.55.

In the entrance region of round tubes where the flow is developing, the measured experimental magnitudes of h are much greater than in the fully-developed flow region. For correlating data, McAdams suggests the following expression:

$$\frac{h_m}{h_\infty} = 1 + \frac{C}{(L/D)^n} \tag{24}$$

In the Re range of 26,000 to 56,000, experimental data for air with a bell-mouthed entrance was correlated with C = 1.4 and n = 1. With Re greater than 10,000, the entrance effects are limited to the region of L/D less than 20. In addition, the entrance effect varies with the type of entrance, sharp-edged entrance, bell-mouthed entrance, etc.

For rectangular tubes and ducts the Nusselt number is defined as:

$$Nu = \frac{D_h\, h}{k} \tag{25}$$

where

$$D_h = 4 \frac{\text{Flow area}}{\text{Perimeter}} , \text{ (hydraulic diameter)}$$

The transition Reynolds number $(UD_h\rho/\mu)$ is found to be approximately 2300, the same as for circular ducts. Reference 9 presents values of Nusselt numbers for ducts of various cross sections and aspect ratios for fully-developed velocity and temperature profiles.

It can be generally assumed that for square, rectangular, and other shapes which are not drastically different from circular tubes, the developed equations can be used if the diameter, D, is replaced by the equivalent or hydraulic diameter, D_h. In accordance with Reference 9, for such passages, the velocity and temperature profiles can be assumed to be developed within a distance of L/D = 30 from the entrance. Passages of complicated shape or with high aspect ratios require special relations. For duct shapes with sharp corners (squares or rectangulars), the local heat-transfer coefficient varies around the periphery and approaches zero at the corners. It has also been found that a significant difference in heat-transfer coefficients occurs between the heated and unheated duct walls. This condition is shown and discussed in more detail in Section X. Reference 15 points out that for practical applications the assumption of a uniform heat-transfer coefficient is unrealistic. The reference presents the following expression for the heat-transfer coefficient expressed as a function of the distance x from the fin base:

$$h_x = (\gamma + 1)\, h_{ave} \left(\frac{x}{b}\right)^{\gamma} \qquad (26)$$

with linear increase in h, $\gamma = 1$

with parabolic increase in h, $\gamma = 2$

Information about the nonuniform heat-transfer coefficients along extended surfaces, however, is limited.

Generally, in heat-transfer equipment, high air velocity can cause objectionable noise, depending on the plate and fin or tube and fin arrangement. If objectionable noise develops, its effect can be reduced with sound absorbers. Increased air velocity increases the heat-transfer coefficient, but also increases the required blower power. It is generally recommended that heat exchangers be designed for a maximum air velocity of 800 to 900 ft/min, unless stringent

space requirements outweigh the objections mentioned above. Turbulent, rather than laminar, air flow is desired because turbulence results in a thinner boundary layer and reduced thermal resistance to heat flow.

The general equations presented in heat-transfer text and handbooks have rigorous applications only when a hydrodynamic starting length is provided so that the velocity profile is fully developed before heat transfer starts. Such conditions, however, are rarely encountered in actual heat-transfer equipment. The standard solutions are, however, excellent approximations for fluids whose Prandtl numbers are high relative to one (1). Reference 9 gives the following expression for determining distance for fully-developed flow:

$$\frac{x}{D}_{\text{Fully dev.}} = 0.05\ (Re)\ (Pr) \tag{27}$$

Furthermore, the literature covers two general boundary conditions: (1) a constant heat rate per unit of tube or duct length and (2) a constant surface temperature. The constant heat-rate Nusselt number is always greater than the constant surface-temperature Nusselt number. However, neither of the above conditions occurs in actual electronic-equipment cooling apparatus, particularly in cold plates.

a. Heat Transfer Fluids

Both liquids and gases are extensively used in cooling of electronic equipment. Because of their better thermophysical properties, liquid coolants are generally used for high packaging densities and high heat-generation rates. For equipment of low-power generation rates and packaging densities, air is one of the most desirable coolants because of its availability, low cost, safety, and dielectric properties. On the negative side, however, air has the poorest heat-transfer properties of any of the standard coolants. It also can generate significant amounts of acoustical noise at high flow velocities. Hydrogen is by far the most efficient of the gaseous coolants, but because of safety considerations it is not recommended. Helium, the Freons, and carbon dioxide are all generally superior to air.

If a gas other than air is used as a coolant, care must be taken in sealing the cooling system to prevent leakage. Consideration must also be given to the expansion of the gas because of its temperature rise caused by the electronic equipment. Table 4, adopted from Reference 16, presents properties of gaseous coolants at standard pressure and temperature conditions.

The gaseous cooling techniques are applied to both direct and indirect cooling of electronic equipment. The indirect system, however, is preferred because it eliminates contamination of the equipment. Since air as a coolant has been extensively used for both direct and indirect cooling, its applications are not further discussed. Consideration is given to liquid coolants only.

In the case of indirect liquid cooling, the two major factors that determine whether or not a coolant is suitable for indirect cooling are: (1) its corrosive tendencies and (2) thermal properties. The dielectric properties, which are important in direct cooling, are not important in indirect cooling. This cooling technique, if properly accomplished, minimizes the flow rate and pumping power requirements, besides improving accessibility and component mounting flexibility.

Table 4. Relative Heat Transfer Coefficients of Gases in Forced Convection at Equal Fan Horsepower

COOLING GAS	RELATIVE DENSITY	RELATIVE CONVECTION COEFFICIENT OF HEAT TRANSFER
Air at 1 atm	1	1.00
Air at 2 atm	2	1.38
SF_6 - 1 atm	5	1.51
SF_6 - 2 atm	10	2.17
Hl - 1 atm	0.13	1.79
Hl - 2 atm	0.27	2.57
FC - 75 vapor 1 atm	14	2.48
FC - 75 vapor 2 atm	29	3.66

There are a number of factors which must be considered when choosing a coolant from the large number available. A liquid may be acceptable in some respects, but deficient in others. Reference 17 points out the following properties which must be considered in selecting a proper coolant:

(1) Toxity: Coolants should not be used that are dangerous to the personnel operating the aircraft or ground equipment.

(2) Flammability: Coolants that are flammable within operating and maintenance environmental extremes should not be considered.

(3) Flash Point: A coolant should not be used which has a flash point lower than the highest temperature it will contact during normal use or due to leakage.

(4) Vapor Pressure: The vapor pressure must be sufficiently high at operating temperatures to prevent boiling within the cooling system and pump caviation. Local boiling at the cold plate can generate a blanket of vapor on the surface causing temperature rise.

(5) Pour and Freezing Points: As the temperature is lowered, most coolants become more viscous. The temperature at which the fluid will just begin to pour is defined as the pour point. Fluids such as water do not have a pour point; thus, only the freezing point must be considered. The pour and freezing points define the lower end of the useful coolant operating range. As the pour point is approached, the power required to pump the fluid is increased and heat-transfer effectiveness is decreased.

(6) Thermal Decomposition: Many coolants decompose at high temperatures in the presence of trapped air and as a result of the catalytic action of other compounds within the system. Some fluids may have to be purified and deionized to prevent thermal decomposition.

(7) Dielectric Strength: Dielectric strength will not normally be important in indirect forced convection cooling systems. Only if the coolant should contact the components would the dielectric properties become important.

(8) Effects of Moisture: Moisture can affect coolants in three ways. These are: (1) degradation of dielectric properties, (2) enhanced hydrolysis, and (3) formation of acids and salts which cause corrosion. Many coolants have an affinity for moisture.

(9) Compatibility and Inertness: Coolants should be selected which are chemically compatible with the materials which they will contact within the cooling loop or from leakage. Particular attention should be paid to the selection of seals, gaskets, and adhesives used in the cooling system.

(10) Surface Tension: A coolant with a low value of surface tension will wet the heat-transfer surfaces to a greater degree, thus enhancing the heat transfer effectiveness. However, a low surface tension is more likely to cause leakage problems.

(11) Thermal Expansion: The thermal expansion of the coolant should be considered when designing a closed cooling system. The cooling system should be provided with an adequate expansion tank.

(12) Heat Transfer Properties and Figure of Merit: Properties which directly affect the heat-transfer effectiveness of the coolant are specific heat, viscosity, thermal conductivity, and density. It is desired that the fluid exhibit a high specific heat, because it is proportional to the ability of the coolant to store heat. The thermal conductivity defines the ability of the coolant to transfer heat by conduction and should be high. The fluid viscosity increases pumping power and reduces the heat-transfer effectiveness and, therefore, should be low. Fluid density could have good and bad effects.

A large number of compounds could be considered for use as coolants. Most of these are organic compounds. The compounds which appear to be best suited for electronic-cooling applications are the silicons, fluorinated organics, and the ethylene - glycol-water solution. The silicones are best suited for use when extended temperature ranges and dielectric properties are required.

When a fluid is selected on the basis of heat transfer, a useful figure of merit, η_{Ft}, given by Reference 18 can be used.

$$\eta_{Ft} = \frac{\rho^{0.8}\, k^{0.6}\, C_p^{\,0.4}}{\mu^{0.4}} \tag{28}$$

where ρ = density, gm/cm^3

C_p = specific heat, cal/gm°C

k = thermal conductivity, cal/sec cm^2 °C

μ = coefficient of viscosity, poise

High values of the figure of merit are desirable because such coolants require the least amount of power, while absorbing the largest amount of heat.

Table 5, adapted from Reference 17, presents thermal properties from selected coolants.

Figure 4, adapted from Reference 18, shows the heat-transfer figure of merit for the coolants indicated.

Figures 5 and 6, adapted from Reference 19, compare the pumping power to heat-transfer conductance ratio for gases and liquids, respectively, in laminar and turbulent flow. The X and Y parameters

Table 5. Thermal Properties of Coolants (Ref 17)

FLUID	FREEZE OR POUR POINT °C	FLASH POINT °C	KINEMATIC VISCOSITY (-54°C) CENTI-STOKES	KINEMATIC VISCOSITY (+25°C) CENTI-STOKES	SPECIFIC GRAVITY (25°C) -	THERMAL COND. (25°C) Btu/(hr-ft-°F)	SPECIFIC HEAT (25°C) Btu/(lb$_m$ °F)	THERMAL EXPANSION (25°C) 1/°C
Water	0	[3]	[2]	1.000	1.000	0.35	1.0	0.00006
20% ethylene glycol, 80% water[5]	-9	115[1]	[2]	1.45	1.034	0.31	0.93	
40% ethylene glycol, 60% water[5]	-24	115[1]	[2]	2.44	1.068	0.26	0.84	
60% ethylene glycol, 40% water[5]	-51	115[1]	[2]	4.13	1.114		0.75	0.0007
80% ethylene glycol, 20% water[5]	-47	115[1]	[2]	7.46	1.138	0.19	0.66	
Ethylene glycol	-13	115	[2]	6.1	1.116	0.165	0.56	
FC-75	-93	[3]	7.2	0.65	1.763	0.037	0.248	0.0007
FC-77	-101	[3]	6.9	0.65	1.777	0.037	0.248	0.0009
FC-78	-73	[3]	1.9	0.4	1.707	0.036	0.24	0.0009
Freon E2	-122	[3]	4.5	0.5	1.659	0.045	0.244	0.0014
Freon E1	-115	[3]	21.6	1.2	1.723	0.041	0.243	0.0013
Coolanol 25	-84	163	240	5.0	0.900	0.0754	0.450	0.00083
Coolanol 35	-84	177	930	6.5	0.888	0.077	0.450	0.00085
DC-200(10)	-65	165	140	10.0	0.940	0.0775	0.34	0.00108
DC-200(20)	-60	230	220	20.0	0.955	0.082	0.35	0.00107
DC-200(100)	-55	300	>900	100.0	1.73	0.087	0.35	0.00096
XF-1-3755	-90	215	100	10.5	0.938	0.085	0.430	0.00095
SF-81(50)	-84	316	800	50.0	0.972	0.087	0.36	0.0095
SF-96(20)	-65	>200	100	20.0	0.953	0.082	0.36	0.00107
SF-97(10)	-73	163	110	10.0	0.940	0.075	0.36	0.00138
SF-97(20)	-65	>200	220	20.0	0.953	0.082	0.36	0.00107
SF-1103(10) [L-45(10)]	-65	170	75[4]	10.0	0.940	0.074	0.345	0.00108
SF-1103(20) [L-45(20)]	-60	230	140	20.0	0.955	0.079		0.00107
MIL-H-5606 Hydraulic oil	<-60	>200	<3000	19.0	0.865	0.078	0.45	0.0007

NOTES: [1]For pure ethylene glycol
[2]Frozen
[3]Does not support combustion
[4]Data at -40°C
[5]By weight

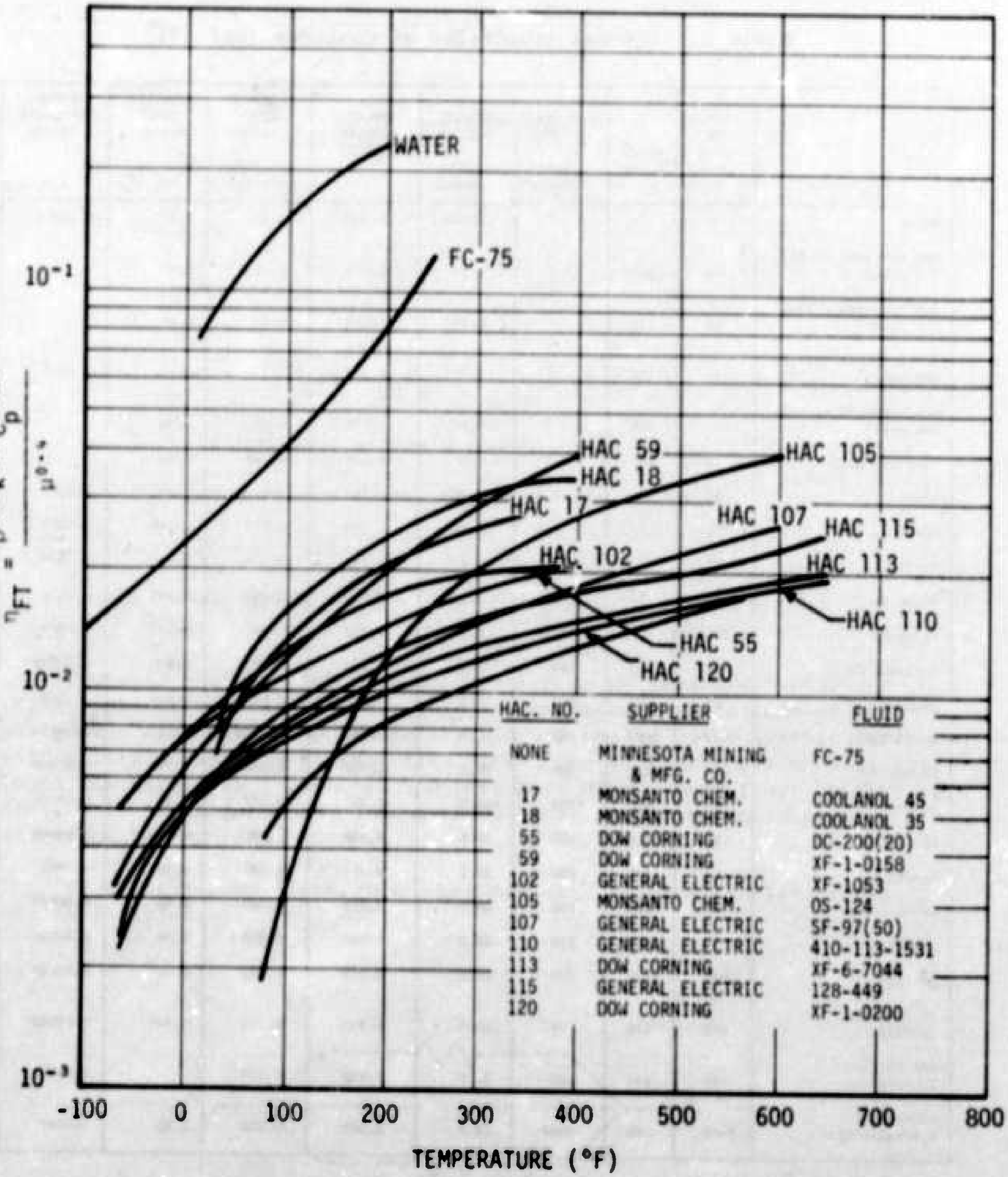

Figure 4. Heat-Transfer Figure of Merit (Ref 18)

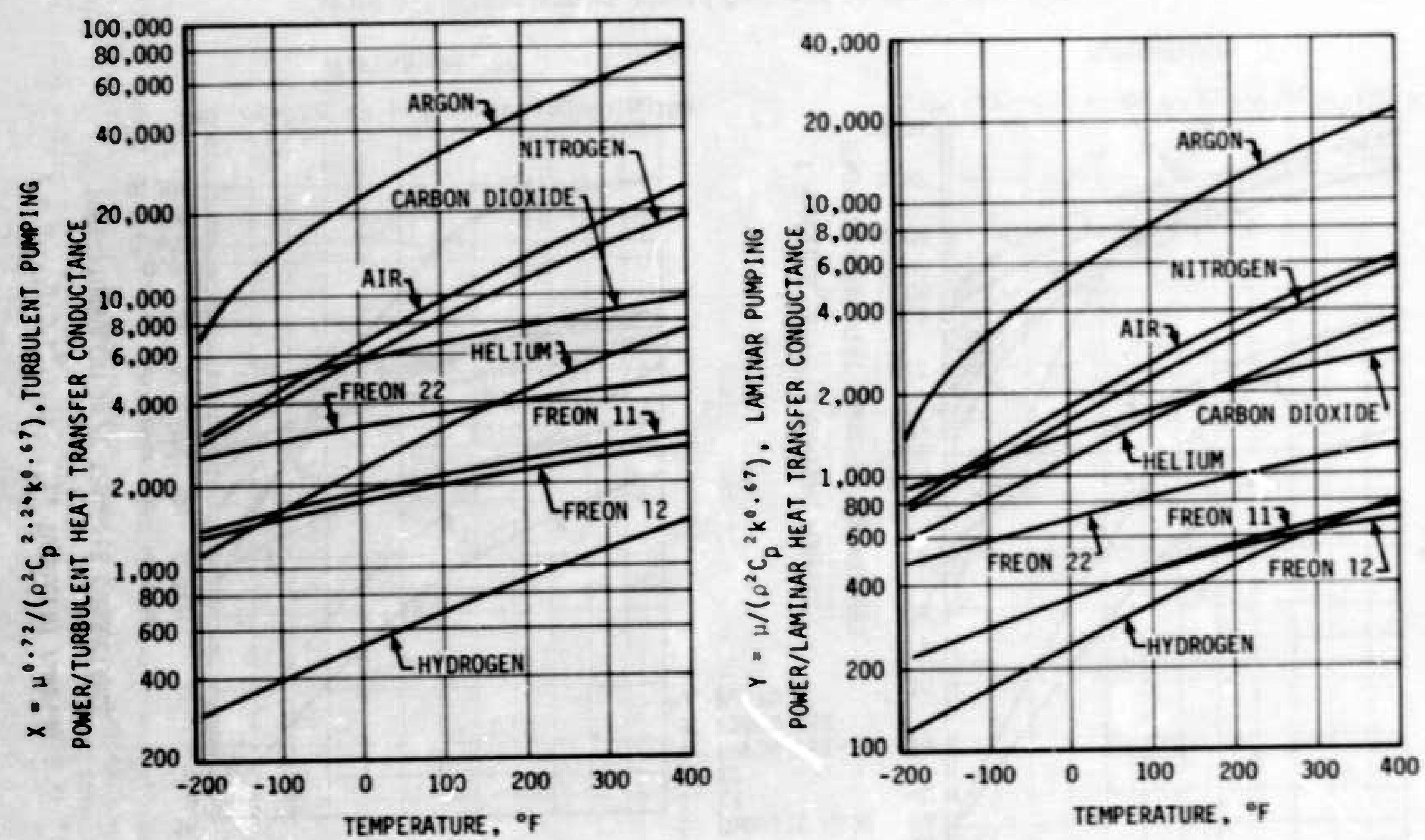

Figure 5. Comparison of Gaseous Coolants on the Basis of Pumping Power and Heat Transfer (Ref 19)

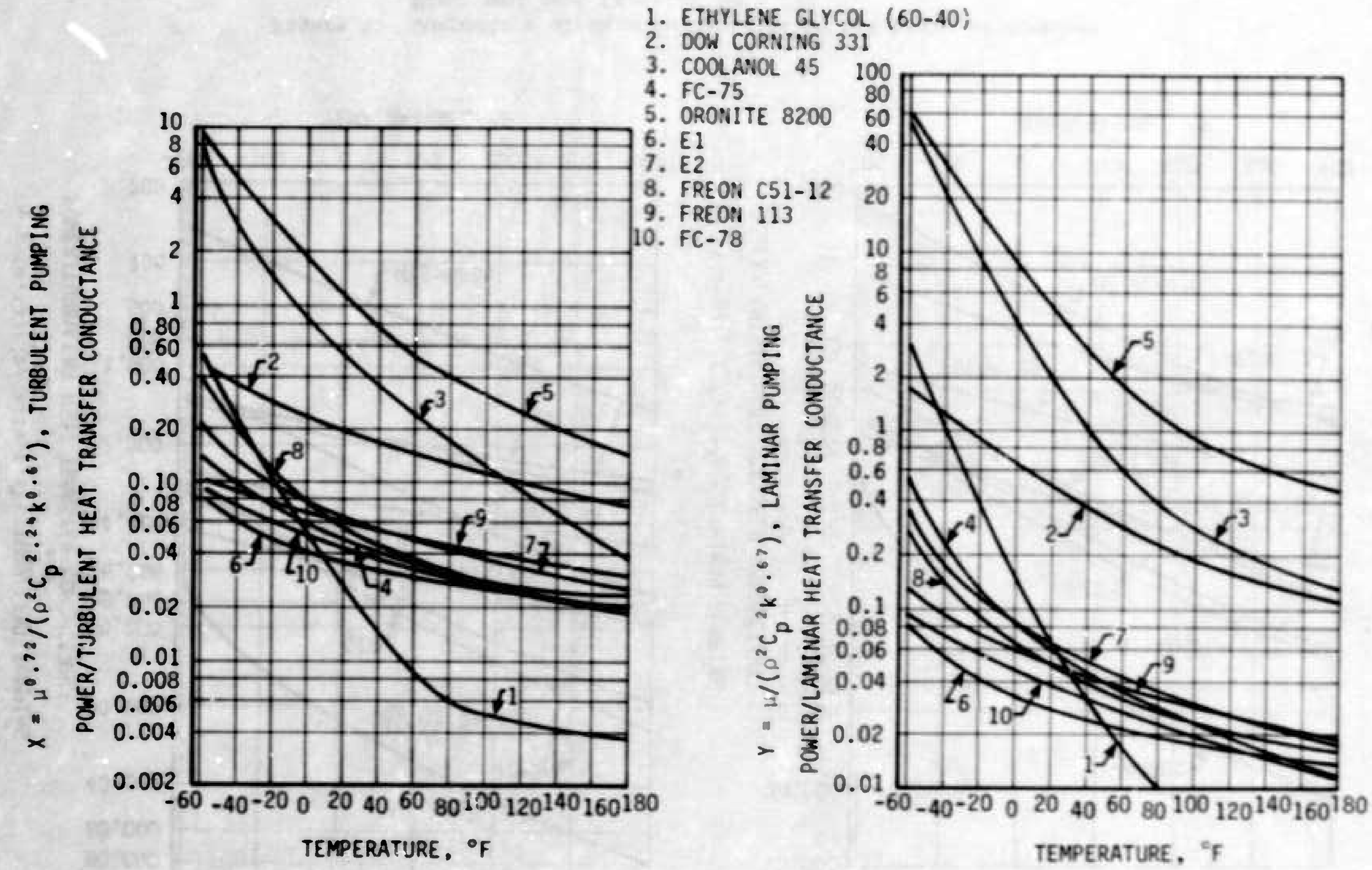

Figure 6. Comparison of Liquid Coolants on the Basis of Pumping Power and Heat Transfer (Ref 19)

represent a ratio of pumping power per unit heat-transfer conductance. Low values of these parameters indicate minimum pumping power penalties for a specified amount of heat removal. It is apparent that liquids are much superior to gases in heat transfer and pumping power. A major advantage of the gases is the wide temperature range over which they operate.

SECTION VI

CONDUCTION HEAT TRANSFER

Heat, generated by electronic or electrical equipment, can be extracted and removed by two general methods: (1) conducting the heat along metallic or other paths to an external heat sink, and (2) transferring the heat to moving gases or liquids. Conduction and radiative cooling have been studied for missiles and spacecraft operating under reduced pressure or complete vacuum conditions. Conductive, or a combination of conductive and convective cooling, is mainly applicable to aircraft electronics equipment. Various types of electronic components (particularly solid state) are excellent for conductive cooling. Not only individual components, but also subassemblies mounted in sealed cases to simplify radio frequency interference protection and avoid airborne moisture and dust, must be cooled by conduction or conduction combined with other modes of heat transfer.

a. Interface Thermal Conductance

Predicting heat transfer and temperature distribution within a solid body does not provide any great difficulties. The difficulties will be experienced when the heat-flow path is interrupted by some kind of mounting joint. Such joints can be formed between the component and/or subassembly and the mounting-base heat sink. Prediction of the temperature drop across a joint causes difficulties which are usually overcome by determining the joint thermal performance experimentally. This method, however, is not very practical. In thermal control system design and analysis, it is of great importance to determine the temperature distribution and heat transfer rates. To do this successfully, some reasonable conductance/resistance data must be obtained for use in the preliminary analysis. Two general approaches can be used to satisfy this requirement: (1) using available experimental data found in published literature, and (2) using developed analytical techniques which can be applied to certain types of joints. Some of the simplified analytical techniques are outlined, and also some experimental data are presented.

The parameters that control the thermal resistance across a joint include surface flatness, roughness, hardness, thermal conductance of the materials making up the joint, and contact pressure. Other items such as temperature, interstitial fluid and its pressure, etc also contribute. The interface thermal conductance is a function of the effective contact area, which is made up of many small contact areas. With increased pressure, the area of each contact point increases, but also the number of points in contact increases. The modes of heat transfer for consideration are: (1) conduction through the direct contact area, (2) gaseous, molecular, or other conduction through the interstitial fluid or filler, and (3) thermal radiation.

The heat-transfer rate across the interface of a joint can be expressed by the following equation:

$$Q = AC\ (\Delta t) \tag{29}$$

and the contact conductance is defined as

$$C = \frac{Q}{A(\Delta t)} \tag{29a}$$

where Q = heat transfer rate, Btu/hr

A = total area of interface, ft^2

C = thermal conductance of joint, Btu/hr $ft^2\,^\circ F$

Δt = temperature differential across the joint, $\Delta t = t_1 - t_2$, $^\circ F$

As an example, consider a plane wall made up of two sheets of similar material as shown in Figure 7a and b

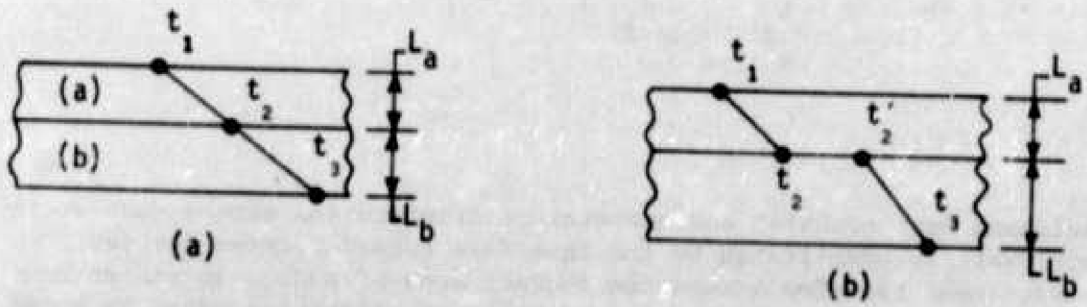

Figure 7. Composite Wall

When the interface thermal resistance (Figure 7a) is neglected, heat flow through the wall can be expressed as follows:

$$Q_a = \frac{kA}{L_a}\left(t_1 - t_2\right) \text{ and } Q_b = \frac{kA}{L_b}\left(t_2 - t_3\right) \tag{30}$$

$$Q_a = Q_b = \frac{A}{\frac{L_a}{k} + \frac{L_b}{k}}\left(t_1 - t_3\right), \text{ Btu/hr} \tag{31}$$

Next, when the resistance of the interface is considered, the following is developed:

$$Q_i = AC\left(t_2 - t_2{}^1\right) \tag{32}$$

Consequently, heat flow across the composite wall can be expressed as follows:

$$Q_a = Q_b = Q_i = \frac{A}{\frac{L_a}{k} + \frac{1}{C} + \frac{L_b}{k}}\left(t_1 - t_3\right) \tag{33}$$

Predicting heat transfer and temperature distribution across such a composite wall is complicated by the interface formed between the two sheets. Heat transfer across the contact area of such a joint can be considered as consisting of two components or conduction paths as shown in Figure 8.

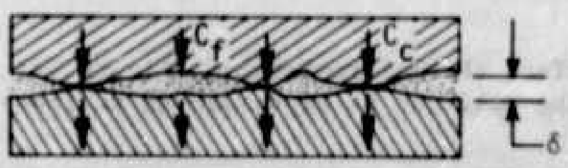

Figure 8. Heat Flow Across the Interface

Thermal conductance of the contact area, therefore, can be expressed as follows:

$$C = C_c + C_f \tag{34}$$

where C_c = direct contact conductance, Btu/hr ft^2 °F

C_f = gap conductance, Btu/hr ft^2 °F

Convection and radiation also take part in the heat transfer process. However, because of the small temperature difference across the interface and small gaps, both radiation and convection modes of heat transfer can be neglected.

Under conditions where only limited information about interface surface conditions is available, the following expression, given in Reference 20, can be used for determining thermal conductance across the area of contact:

$$C = C_c + C_f = \frac{1.56\ k_f}{i_a + i_b} + n\bar{a}k_m \tag{35}$$

$$k_m = \frac{2k_1 k_2}{k_1 + k_2} \tag{36}$$

When joints are made of the same materials, conductivity $k_1 = k_2$ and $k_m = k$. The root mean square (RMS) values of surface irregularity (roughness plus waviness) are i_a and i_b, for surfaces a and b respectively.

k_f = thermal conductivity of the interstitial fluid, Btu/hr ft^2°F/ft

$\bar{a}$ = average radius of contact points

n = number of contact points per unit area

Conduction heat transfer across a gap can be determined from the following expression:

$$C_f = \frac{k_f}{\delta} \tag{37}$$

where δ = average gap thickness, ft.

Figures 9 and 10, adapted from Reference 21, can be used for determining average surface irregularity (based on known RMS surface roughness) and $n\bar{a}$ values when the contact pressure is known. The RMS surface roughness can be measured, or approximate values obtained, when the particular machining process is known. The use of Figure 10 requires knowledge about interface contact pressure. Before this is determined, stress analysis must be performed. Reference 22 recommends an approximate equation for determining the required torque to turn the nut for standard threads with a 60-degree angle and coefficient of friction of 0.15.

$$T = 0.2DF \tag{38}$$

When torque is known, the axial-bolt tensile force can be determined from the following equation:

$$F = \frac{T}{0.2D} \tag{39}$$

where F = induced axial force, lbs

D = bolt diameter, in.

T = torque, in-lbs

An approximate stress distribution of a plate in a bolted joint is shown in Figure 11.

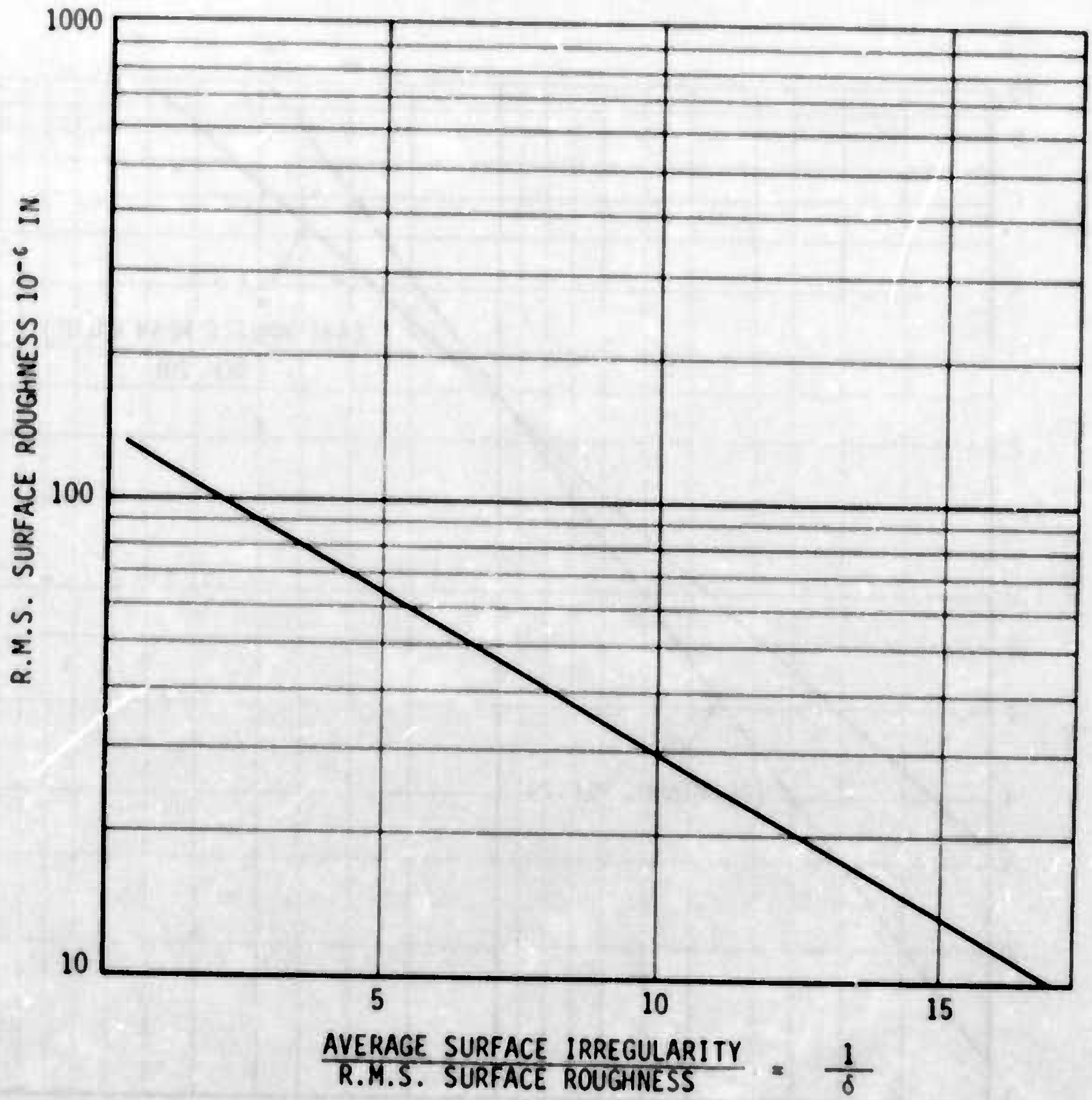

Figure 9. Ratio of Average Surface Irregularity to RMS Surface Roughness vs RMS Surface Roughness

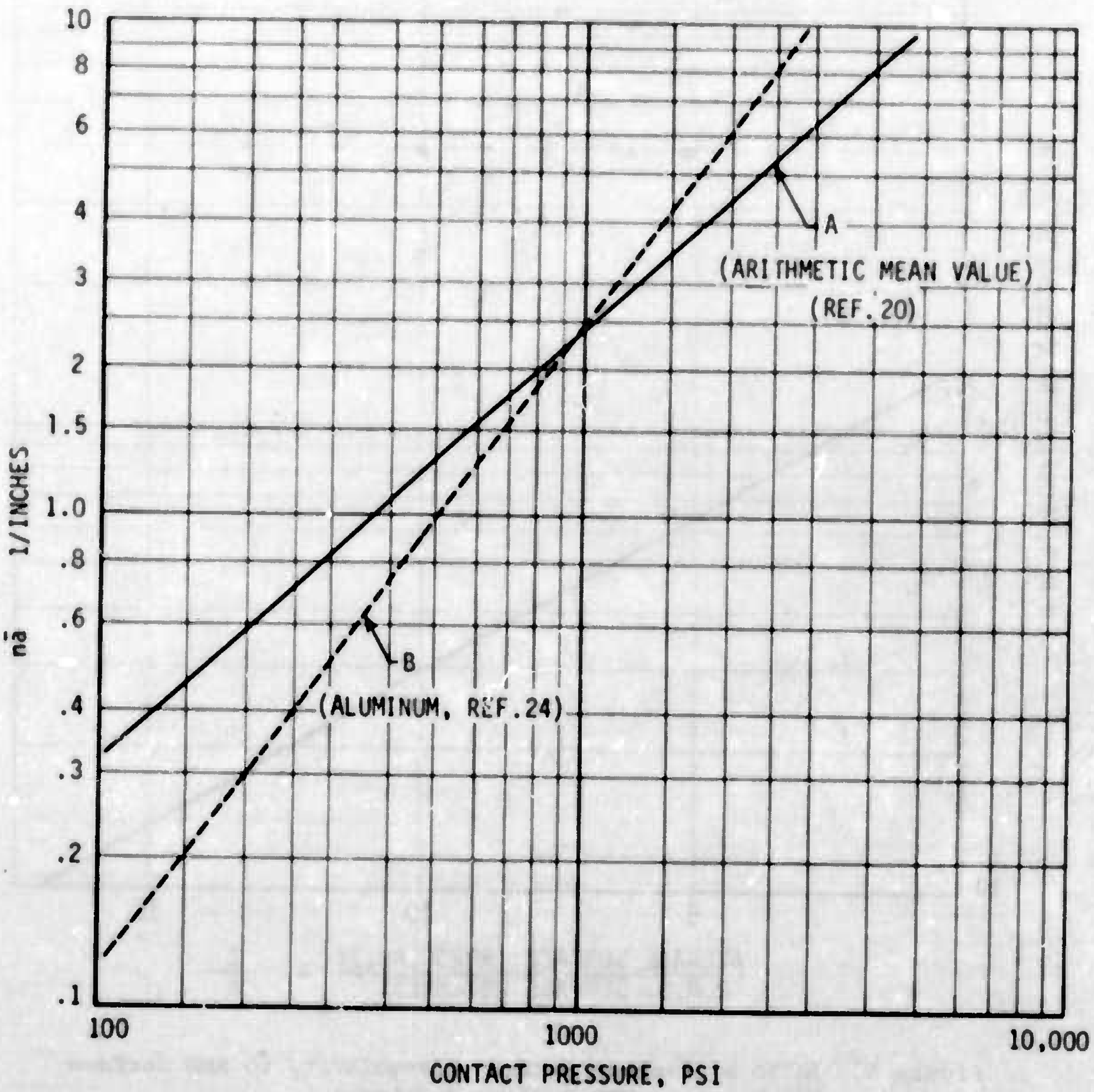

Figure 10. $n\bar{a}$ vs Contact Pressure

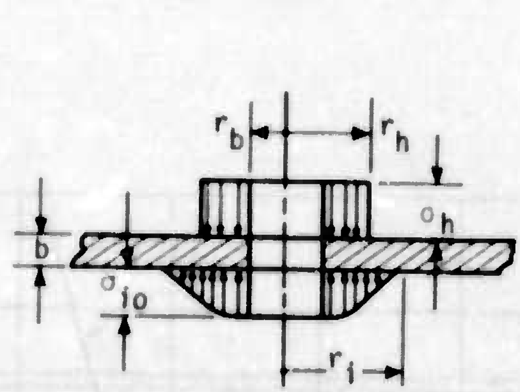

Figure 11. Stress Distribution in a Bolted Joint

Using the stress distribution parameters presented in Reference 23, we can find r_i and also the average interface pressure as follows:

$$\sigma_i = \frac{F}{A_i} \tag{40}$$

$$A_i = \frac{\pi}{4} \left(d_i^{\,2} - d_b^{\,2}\right) \tag{41}$$

If the ratio of r_h/b is known, r_i can be found from Figure 12.

After all the necessary data is substituted into equation 35, the interface conductance across the contact area can be determined. The total interface area of a bolted joint, however, will consist of a direct contact area and a gap area. Figure 13 shows a bolted joint with the area where both plates are in direct contact with each other. This area will depend upon the bolt torque, head size of the bolt, thickness and rigidity of the plates, and will usually be quite small. After a certain distance r from the center of the bolt, the plates, because of deflection caused by the force, separate from each other and a gap results.

Conductance across the contact area can be determined from the procedure outlined above. The next step is to determine conductance across the area where the plates have separated. As previously indicated, thermal conductance across the gap can be determined from equation 37.

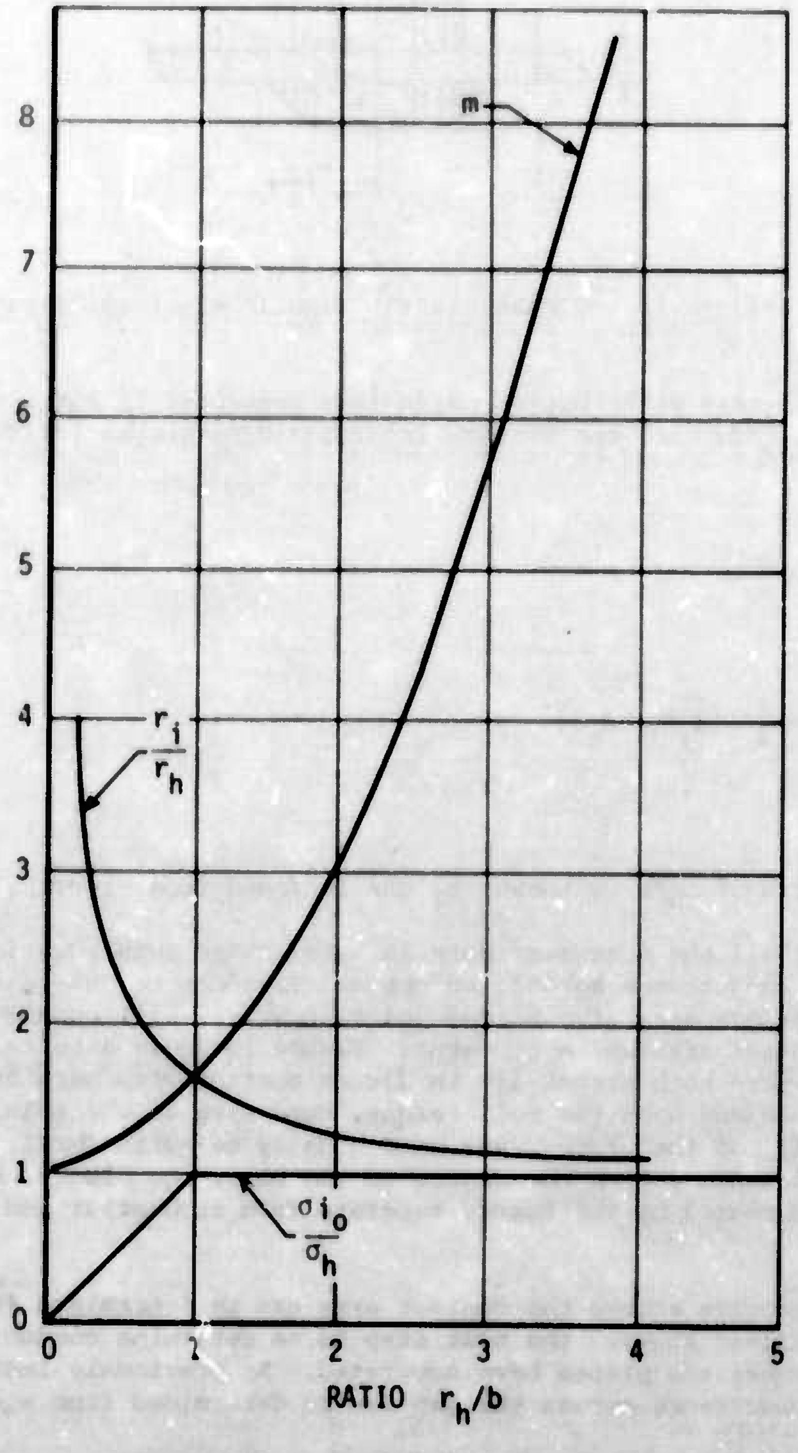

Figure 12. Lieb's Interface Stress Distribution Parameters

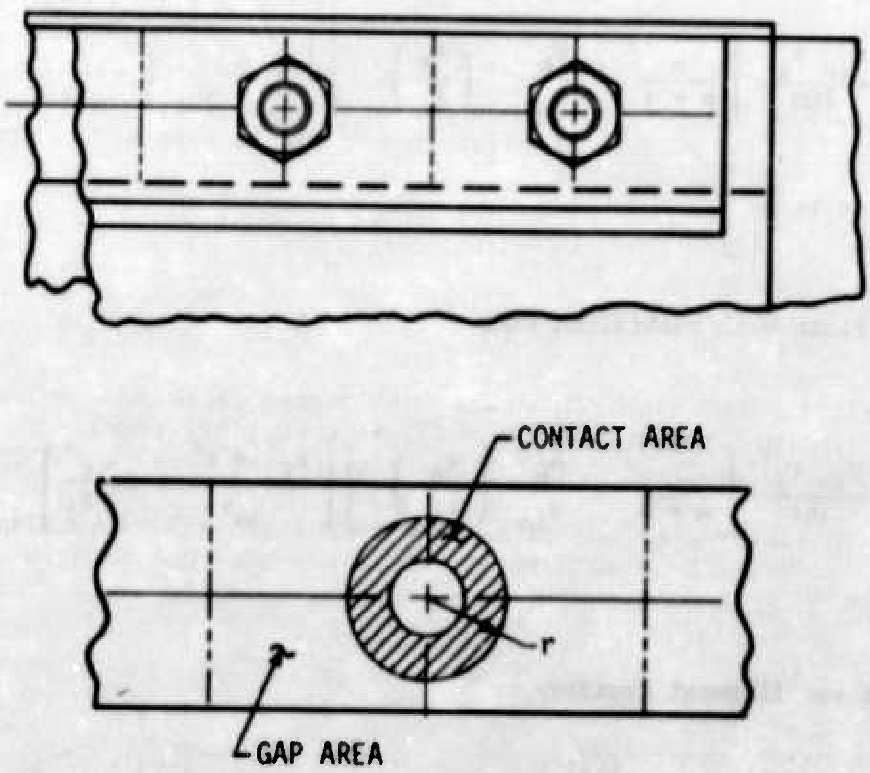

Figure 13. Bolted Joint

To determine this, we must know the thickness of the gap. Reference 23 presents a simplified analytical technique for determining plate deflection, w, as a function of radius for two different plate end conditions. Deflections of each of the end conditions are given as follows:

(1) Plate with free ends:

$$W = \frac{\sigma_{io}\, r_i^{4}}{16D}\left[\frac{m}{m+4} - \frac{\sigma_h}{\sigma_{io}}\left(\frac{r_h}{r_i}\right)^{4}\right]\left[\frac{(1-\mu)}{(1+\mu)}\left(\frac{r^2 - r_i^2}{2R^2}\right) + \ln\frac{r}{r_i}\right] \qquad (42)$$

(2) Plate with restrained ends:

$$W = \frac{\sigma_{io}\, r_i^{4}}{16D}\left[\frac{m}{m+4} - \frac{\sigma_h}{\sigma_{io}}\left(\frac{r_h}{r_i}\right)^{4}\right]\left[\frac{r_i^2 - r^2}{2R^2} + \ln\frac{r}{r_i}\right] \qquad (43)$$

where D is the flexural rigidity

$$D = \frac{Eb^3}{12(1-\mu^2)} \qquad (44)$$

$$m = \frac{r}{\frac{\sigma_{io}}{\sigma_b}\left(\frac{r_i}{r_h}\right)^2 - 1} \qquad (45)$$

Stress distribution on the interface planes can be expressed as:

$$\sigma_i = \sigma_{io} \left[1 - \left(\frac{r}{r_i}\right)^m \right] \tag{46}$$

The variables r_i/r_h, m, and σ_{io}/σ_h are plotted as functions of r_h/b in Figure 12.

where b = plate thickness, in.

μ = Poissons ratio

σ_{io} = interface stress at $r = 0$, psi

σ_i = normal stress at interface plane, psi

σ_h = normal stress under fastener head, psi

r_i = radius at point of zero interface stress, in.

r_h = radius of fastener head, in.

r, R = radial coordinate, in.

It is assumed here that the normal stress, σ_h, exerted by the bolt head is uniform over the entire zone under the head. If both plates are deflected, the gap will be twice the value given by equations.

Any bolted joint, therefore, can be divided into certain areas around each of the bolts, and each of these areas further divided into contact and gap areas. Using the analytical procedures outlined above, the thermal conductance and/or resistance of the joint can be determined as follows:

$$C_j = C_c + C_g \tag{47}$$

$$\frac{1}{R_j} = \frac{1}{R_c} + \frac{1}{R_g} \tag{48}$$

Figure 14 shows schematically the resistance network of a joint.

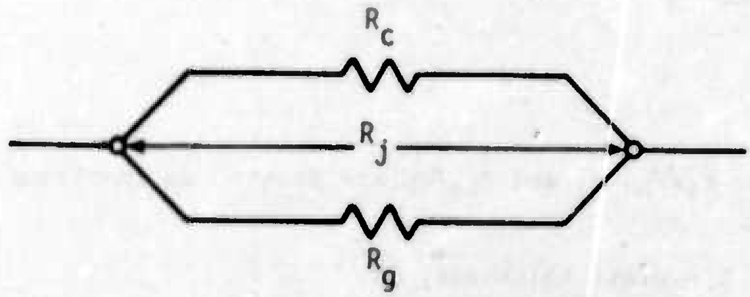

Figure 14. Resistance Network of a Joint

where $R_c = \dfrac{1}{C_c A_c}$ and $R_g = \dfrac{1}{C_g A_g}$

C_c = conductance across contact area, Btu/hr ft^2°F

C_g = conductance across gap area, Btu/hr ft^2°F

A_c = contact area, ft^2

A_g = gap area, ft^2

There is another item of consideration in determining conductance of any type of mounting joint. This is the thermal resistance of the plate or plates making up the joint. In any bolted joint (particularly with thin plates), the contact area around the bolt(s) where most of the heat flow takes place is small and most part of the heat flow; therefore, will be concentrated around these areas, sometimes causing a significant temperature drop.

Figure 15 shows a resistance network of a joint with plate resistances included.

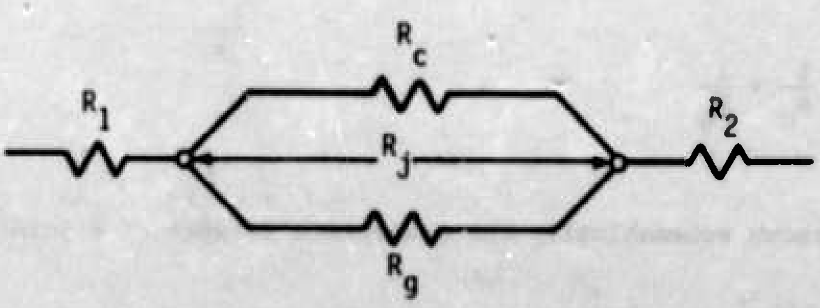

Figure 15. Resistance Network of a Joint and Plates

The total resistance can be expressed as

$$R = R_1 + R_j + R_2 \tag{49}$$

where R_1 and R_2 are resistances of the plates if two plates are present. Consider a simple condition when heat from the contact area is flowing in a radial direction along a disk of thickness, δ, as shown in Figure 16.

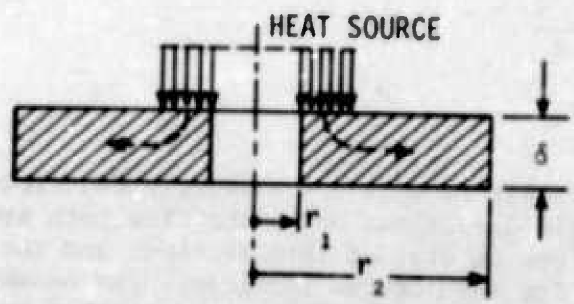

Figure 16. Radial Heat Flow in a Disk

Radial heat conduction in the disk can be expressed as follows:

$$Q = k\delta\ 2\pi r \ \frac{dt}{dr} \tag{50}$$

Integrating within the limits r_1 and r_2 yields

$$Q = k\delta\ 2\pi \ \frac{t_1 - t_2}{\ln r_2 - \ln r_1} \tag{51}$$

Under conditions when computer techniques (R-C networks) are used for thermal analysis, it is convenient to have a simple expression for the heat flow through a cylindrical body or disk of the same form as through a plane wall. This requires determination of a mean area as follows:

$$A_m = \frac{A_2 - A_1}{\ln A_2 - \ln A_1} \qquad (52)$$

where A_1 and A_2 are the inside and outside areas respectively. Heat flow through a cylindrical body can be expressed as:

$$Q = kA_m \frac{t_1 - t_2}{r_2 - r_1} \qquad (53)$$

When the radial heat flow is not uniformly distributed, or the flow takes place in certain directions only, the flow path around the concentrated heat load can be divided into sections and the thermal resistance determined for each of the sections. For example, consider a section of a cold plate (see Figure 17) with attached active devices and cooled by a fluid circulated through passages. Heat generated by the components flows to the cooling-fluid passages. The heat flow and thermal resistance, under such conditions, can be determined by a graphical method known as the flux plot. In this method, each of the heat-flow channels is divided into a member of curvilinear squares consisting of heat-flow lines and isothermal lines. The lines intersect at right angles, and there is no heat flow in the direction of the heat-flow lines.

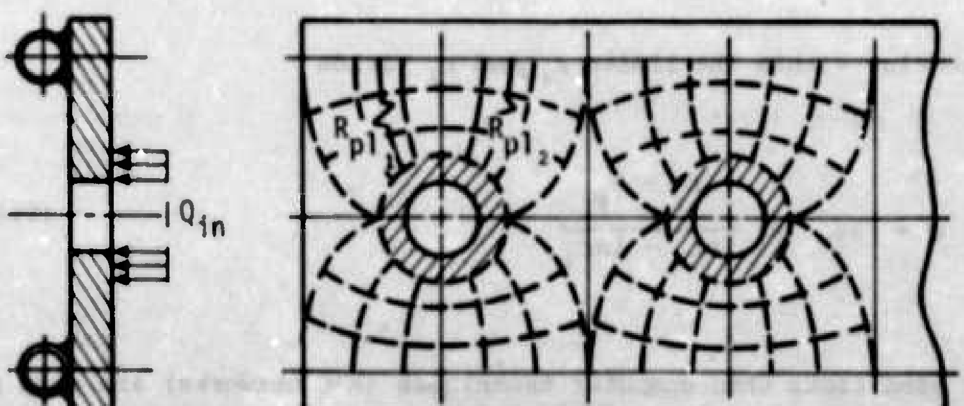

Figure 17. Section of a Cold Plate with Flux Plot

A pair of heat-flow lines present a channel through which heat flows to the sink. If there are M number of curvilinear squares in the channel and N channels of unit thickness, the heat flow can be expressed as

$$Q = \frac{N}{M} k \left(t_1 - t_2\right) \tag{54}$$

and for plate thickness δ

$$Q = \delta \frac{N}{M} k \left(t_1 - t_2\right) \tag{55}$$

Letting $N/M = S$ and $\delta Sk = K$

$$Q = K \left(t_1 - t_2\right) \tag{56}$$

or, introducing thermal resistance

$$Q = \frac{t_1 - t_2}{R}; \quad R = \frac{1}{K} \tag{57}$$

Figure 18 shows the total resistance network from the component mounting flange to the coolant.

Total thermal resistance of each of the two branches can be expressed as

$$R_t = \frac{R_{pl_1} \cdot R_{pl_2}}{R_{pl_1} + R_{pl_2}} + R_{cv} \tag{58}$$

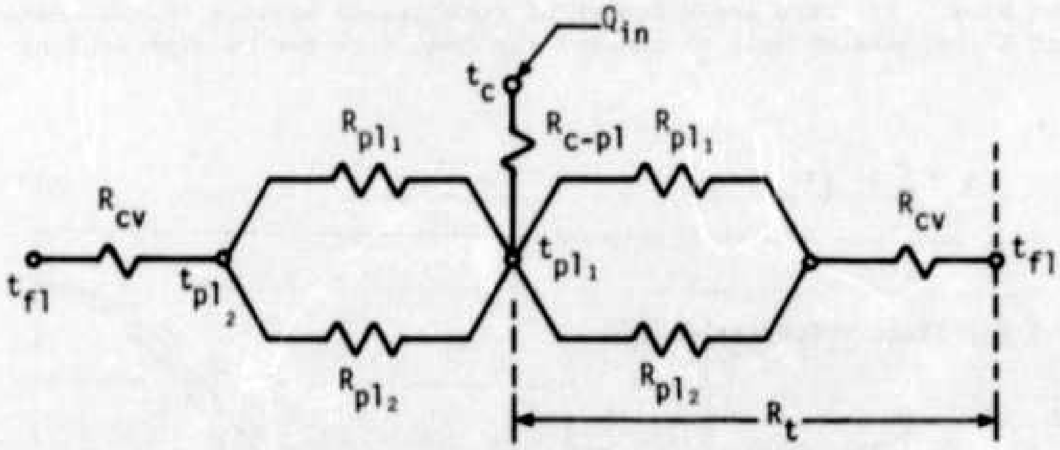

Figure 18. Resistance Network

For a more complex geometry, unsymmetrical loading, or when the cold plate is divided into nodes for computer analysis, sections around the concentrated heat loads can be divided into segments as shown in Figure 19.

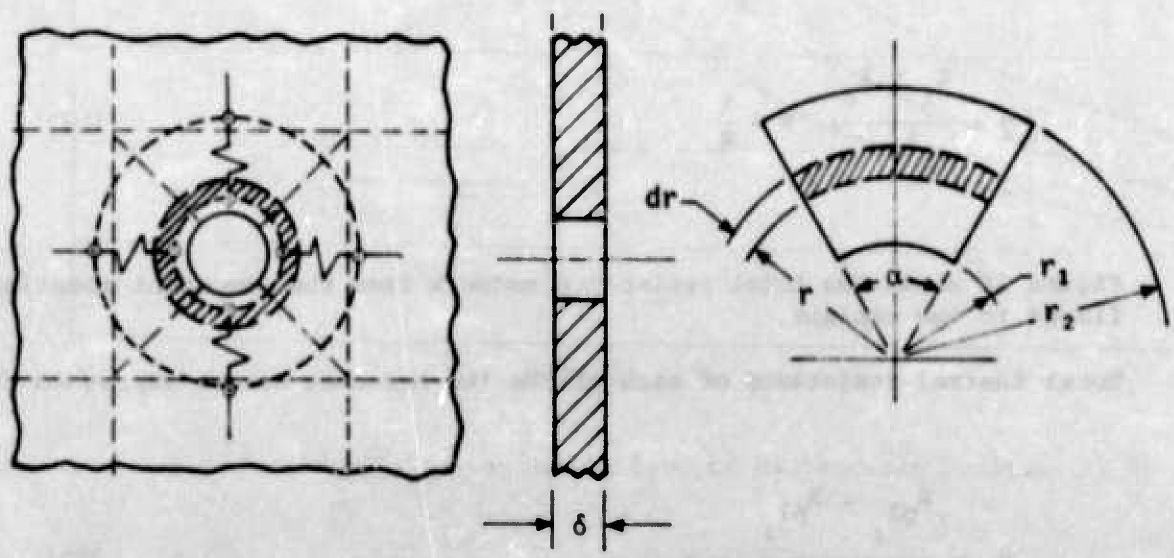

Figure 19. Division of Plate at Concentrated Heat Loads

Heat flow along a conduction path can be expressed as follows:

$$Q = -kA \frac{dt}{dr} \tag{59}$$

Under steady-state conditions, the flow rate is constant and the above equation can be rearranged into the following form:

$$-\frac{dt}{Q} = \frac{dr}{kA} \tag{60}$$

Integrating between the two points yields:

$$\frac{t_1 - t_2}{Q} = \frac{\Delta t}{Q} = \int_{r_1}^{r_2} \frac{dr}{kA(r)} \tag{61}$$

where

$$\frac{\Delta t}{Q} = R \tag{62}$$

and

$$R = \int_{r_1}^{r_2} \frac{dr}{kA(r)} \tag{63}$$

The heat flow area, A(r), varies along the flow path and can be expressed as follows:

$$A(r) = r\,\alpha\delta \tag{64}$$

where α is expressed in radians

$$A(r) = \frac{\pi}{180}\,\alpha\, r\,\delta \tag{65}$$

here α is expressed in degrees

Substituting the value of A(r) yields:

$$R = \int_{r_1}^{r_2} \frac{dr}{kr\alpha\delta} = \frac{1}{k\alpha\delta}\int_{r_1}^{r_2}\frac{dr}{r} = \frac{1}{k\alpha\delta}\left(\ln r_2 - \ln r_1\right) \tag{66}$$

$$R = \frac{1}{k\alpha\delta}\ln\left(\frac{r_2}{r_1}\right) \tag{67}$$

α in radians

SECTION VII

HEAT TRANSFER FROM FINNED SURFACES

The rate of heat transfer from a component and its supporting structure to the ultimate heat sink can be significantly increased by the addition of extended surfaces or fins. Determination of configuration and size of the extended surfaces should be based on the thermal requirements of the electronic equipment and the cooling fluid used.

The literature covers a wide range of fin configurations, including optimization and thermal performance prediction techniques. In this report, however, only the basic equations are presented. Also, extended surface application to cold plate design is discussed.

Consider first a simple analytical method for determining temperature distribution and heat transfer from a rectangular fin. Refer to Figure 20.

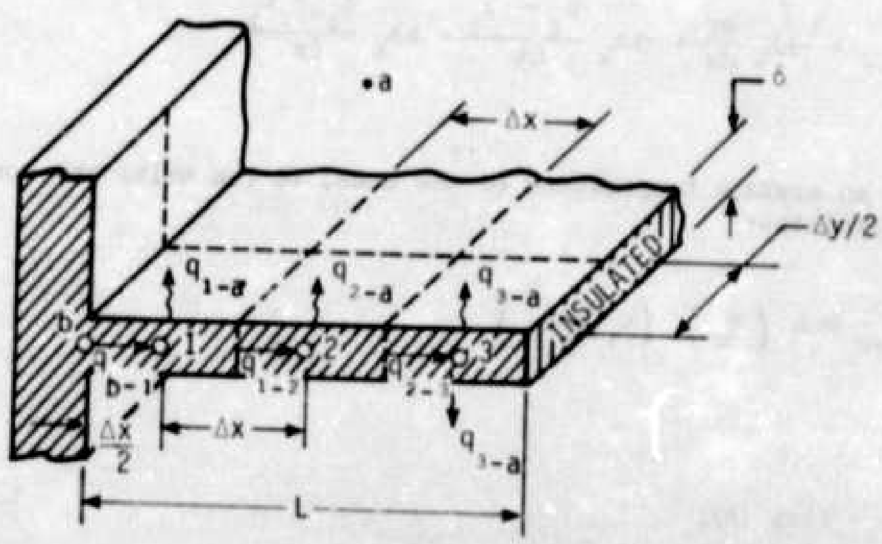

Figure 20. Longitudinal Fin of Rectangular Profile

If the fin is divided into three equal increments or nodes, Δx, the following energy balance at steady-state conditions can be written for each of the nodes:

$$q_{b-1} = q_{1-2} + q_{1-a} \tag{68}$$

$$q_{1-2} = q_{2-3} + q_{2-a} \tag{69}$$

$$q_{2-3} = q_{3-a} \tag{70}$$

where the conduction terms can be written as

$$q_{1-2} = -kA_k \frac{dt}{dx} = -kA_k \frac{t_2 - t_1}{\Delta x} = kA_k \frac{t_1 - t_2}{\Delta x} \tag{71}$$

Assuming an average temperature of the node, we can write the convection terms as follows:

$$q_{1-a} = h \left(A_c \right) \left(t_1 - t_a \right) \tag{72}$$

$$A_c = (\Delta x)\ (\Delta y) \tag{73}$$

When determining the areas for conduction heat transfer, we can distinguish two general conditions.

(1) Convection heat transfer from one side only:

$$A_k = \delta\ (\Delta y) \tag{74}$$

(2) Convection heat transfer from both sides of fin:

$$A_k = \frac{1}{2}\,\delta\,(\Delta y) \tag{75}$$

The rate equations can be written as follows:

$$q_{b-1} = kA_k \frac{t_b - t_1}{\frac{\Delta x}{2}} = 2kA_k \frac{t_b - t_1}{\Delta x} \tag{76}$$

$$q_{1-2} = kA_k \frac{t_1 - t_2}{\Delta x} \tag{77}$$

$$q_{1-a} = hA_c \left(t_1 - t_a\right) \tag{78}$$

$$q_{2-3} = kA_k \frac{t_2 - t_3}{\Delta x} \tag{79}$$

$$q_{2-a} = hA_c \left(t_2 - t_a\right) \tag{80}$$

$$q_{3-a} = hA_c \left(t_3 - t_a\right) \tag{81}$$

Substituting the rate equations into the energy equations yields:

$$\left.\begin{aligned} 2kA_k \frac{t_b - t_1}{\Delta x} &= kA_k \frac{t_1 - t_2}{\Delta x} + hA_c \left(t_1 - t_a\right) \\ kA_k \frac{t_1 - t_2}{\Delta x} &= kA_k \frac{t_2 - t_3}{\Delta x} + hA_c \left(t_2 - t_a\right) \\ kA_k \frac{t_2 - t_3}{\Delta x} &= hA_c \left(t_3 - t_a\right) \end{aligned}\right\} \tag{82}$$

Multiplying by $\Delta x/kA_k$ yields:

$$\left.\begin{aligned} 2\left(t_b - t_1\right) &= \left(t_1 - t_2\right) + \frac{hA_c(\Delta x)}{kA_k}\left(t_1 - t_a\right) \\ t_1 - t_2 &= \left(t_2 - t_3\right) + \frac{hA_c(\Delta x)}{kA_k}\left(t_2 - t_a\right) \\ t_2 - t_3 &= \frac{hA_c(\Delta x)}{kA_k}\left(t_3 - t_a\right) \end{aligned}\right\} \tag{83}$$

$$\text{Let } \frac{hA_c(\Delta x)}{kA_k} = D \tag{84}$$

to obtain the following:

$$
\left.
\begin{aligned}
2\left(t_b - t_1\right) &= \left(t_1 - t_2\right) + D\left(t_1 - t_a\right) \\
\left(t_1 - t_2\right) &= \left(t_2 - t_3\right) + D\left(t_2 - t_a\right) \\
t_2 - t_3 &= D\left(t_3 - t_a\right)
\end{aligned}
\right\}
\tag{85}
$$

When the base temperature of the fin, t_b, and the heat sink temperature, t_a, are known, the node temperatures, t_1, t_2, and t_3, can be computed from the three energy equations.

The heat dissipation rate from the fin can be computed by the following expression:

$$Q = \eta A h \left(t_b - t_a\right) \tag{86}$$

where η is the fin efficiency.

Reference 25 gives the following expression for η:

$$\eta = \frac{t_{avg} - t_a}{t_b - t_a} \tag{87}$$

$$t_{avg} = \frac{1/2\ t_b + t_1 + t_2 + 1/2\ t_e}{3} \tag{88}$$

where t_{avg} is the average temperature of the fin. Figure 21 illustrates the temperature distribution along a fin.

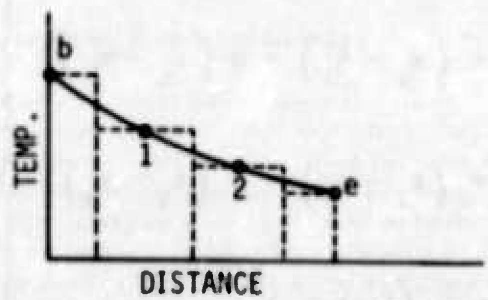

Figure 21. Temperature Distribution Along a Fin

The efficiency of a flat, constant-cross-section fin with negligible heat transfer from the end can be determined from the equation widely used in heat exchanger design:

$$\eta = \frac{\tanh(mL)}{mL} \tag{89}$$

where

$$m = \sqrt{\frac{2h}{k\delta}} \tag{90}$$

The above equations apply for thin sheet fins.

For fin efficiency greater than $\eta = 0.75$, Reference 26 presents the following expression:

$$\eta = \frac{1}{1 + 1/3\ (mL)^2} \tag{91}$$

From solutions of differential equations, we can determine the temperature distribution along a rectangular fin from the following expression:

$$\theta = \theta_0 \frac{\cosh m\,(L-x)}{\cosh\,(mL)} \tag{92}$$

where

$$\theta = t_x - t_a$$

$$\theta_0 = t_b - t_a$$

Neglecting heat dissipation from the end of the fin, we can express heat flow through the base of the fin as follows:

$$Q_0 = k\delta L m\, \theta_0 \tanh\,(mL) \tag{93}$$

Figures 23 and 24 present fin efficiency η and temperature excess ratio θ_e/θ_0 respectively as a function of the fin performance factor mL for longitudinal fins having rectangular cross section.

Similarly as for the longitudinal fin, the temperature distribution and heat dissipation rate can be determined for a radial fin. Refer to Figure 22.

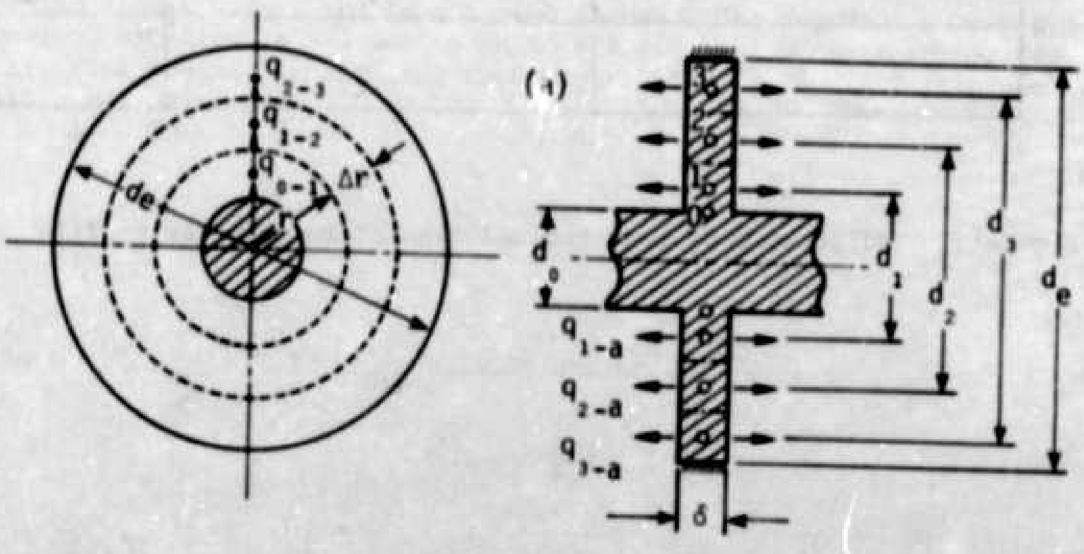

Figure 22. Radial Fin of Rectangular Profile

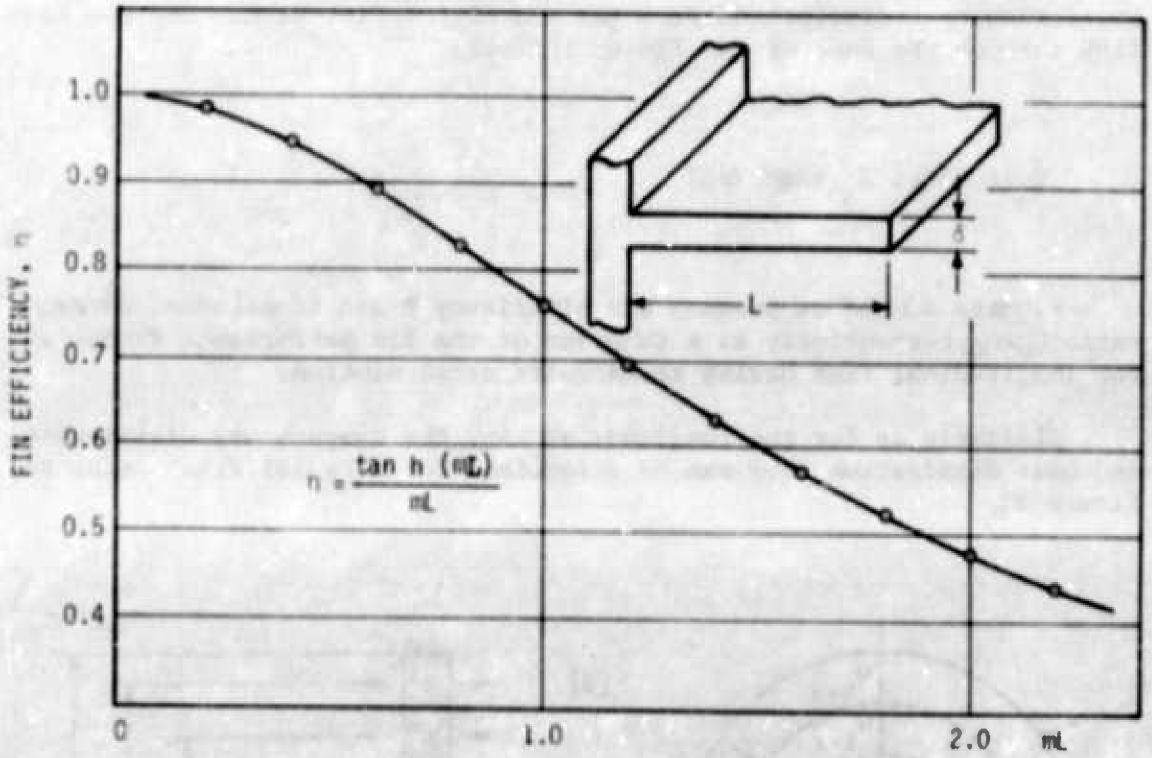

Figure 23. Efficiency of Longitudinal Fins of Rectangular Profile

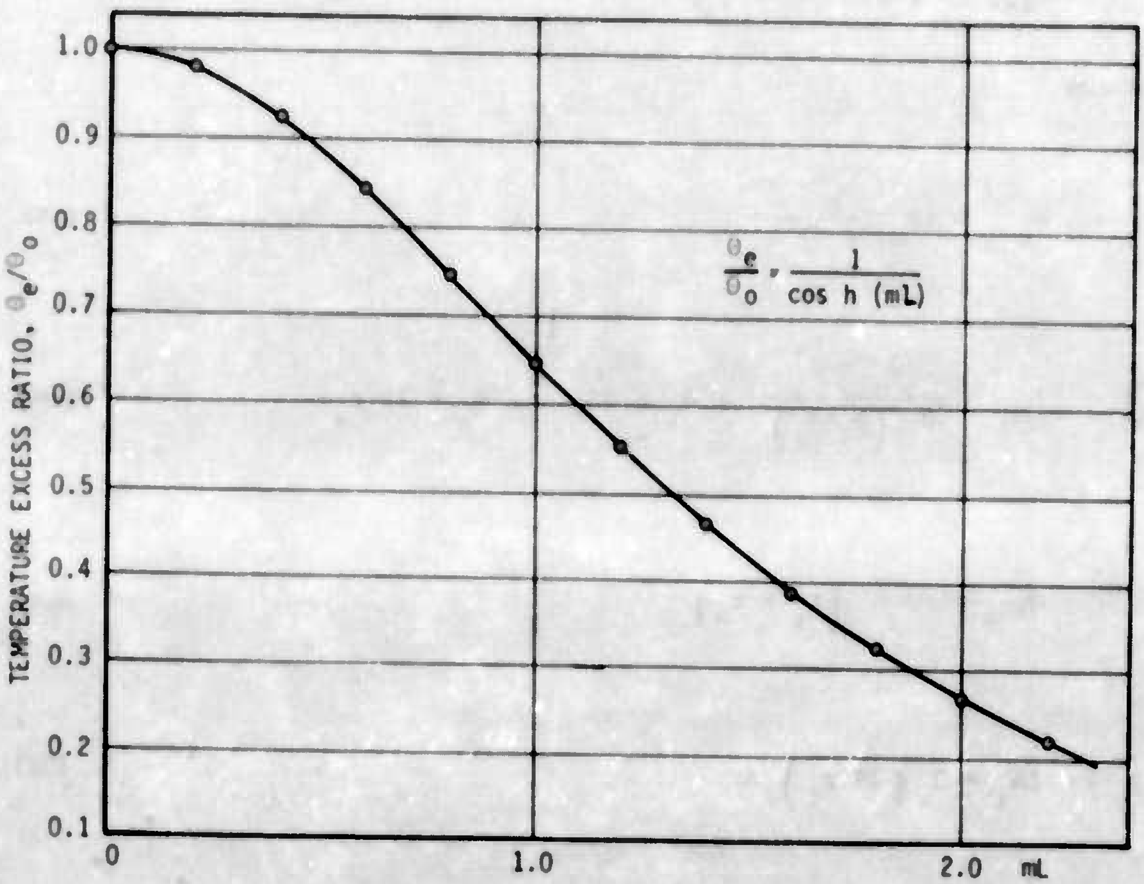

Figure 24. Temperature Excess Ratio of Longitudinal Fins of Rectangular Profile

The energy balance equations can be derived for each of the concentric rings as follows:

$$\left.\begin{aligned} q_{0-1} &= q_{1-2} + q_{1-a} \\ q_{1-2} &= q_{2-3} + q_{2-a} \\ q_{2-3} &= q_{3-a} \end{aligned}\right\} \tag{94}$$

where

$$q_{b-1} = kA_{m1} \frac{t_b - t_1}{r_1 - r_0} \tag{95}$$

$$A_{m1} = \frac{A_1 - A_0}{\ln\left(A_1/A_0\right)} \; ; \; A_1 = 2\pi\, r_1 \delta ; \; A_0 = 2\pi\, r_0 \delta \tag{96}$$

$$q_{1-a} = \Delta A_1 h \left(t_1 - t_a\right) \tag{97}$$

$$\Delta A_1 = 2 \left(2\pi\, r_1\right) \Delta r \tag{98}$$

$$q_{1-2} = kA_{m2} \frac{t_1 - t_2}{r_2 - r_1} \tag{99}$$

$$q_{2-a} = \Delta A_2\, h \left(t_2 - t_a\right) \tag{100}$$

$$q_{2-3} = kA_{m3} \frac{t_2 - t_3}{r_3 - r_2} \tag{101}$$

$$q_{3-a} = \Delta A_3 \, h \left(t_3 - t_a\right) \tag{102}$$

Substituting the rate equations into the energy equations yields:

$$\left.\begin{aligned}
kA_{m1} \frac{t_0 - t_1}{r_1 - r_0} &= kA_{m2} \frac{t_1 - t_2}{r_2 - r_1} + \Delta A_1 h \left(t_1 - t_a\right) \\
kA_{m2} \frac{t_1 - t_2}{r_2 - r_1} &= kA_{m3} \frac{t_2 - t_3}{r_3 - r_2} + \Delta A_2 h \left(t_2 - t_a\right) \\
kA_{m3} \frac{t_2 - t_3}{r_3 - r_2} &= \Delta A_3 h \left(t_3 - t_a\right)
\end{aligned}\right\} \tag{103}$$

Temperature distribution of the fin can be found by solving the three energy equations.

Temperature distribution and heat transfer from a radial fin can also be found from solutions of differential equations. Refer to Figure 25.

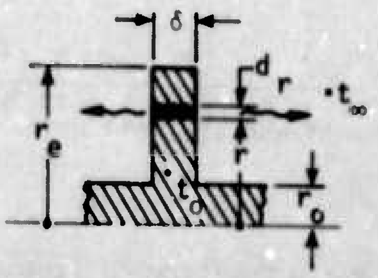

Figure 25. Section of Radial Fin

Heat leaving the element by convection is given by:

$$dq = 2h\,(2\pi\, r dr)\left(t - t_\infty\right) \tag{104}$$

Reference 26 gives the following equation for temperature distribution along a radial fin:

$$\theta = \theta_0 \left[\frac{K_1 \left(mr_e\right) I_0 (mr) + I_1 \left(mr_e\right) K_0 (mr)}{I_0 \left(mr_0\right) K_1 \left(mr_e\right) + I_1 \left(mr_e\right) K_0 \left(mr_0\right)} \right] \tag{105}$$

Heat flow through the base of the fin is given by:

$$q_0 = -2\pi\, kr_0 \delta \left.\frac{d\theta}{dr}\right|_{r = r_0} \tag{106}$$

The general heat-flow relationship is given by:

$$q_0 = 2\pi r_0\, \delta k\, m\theta_0 \left[\frac{I_1 \left(mr_e\right) K_1 \left(mr_0\right) - K_1 \left(mr_e\right) I_1 \left(mr_0\right)}{I_0 \left(mr_0\right) K_1 \left(mr_e\right) + I_1 \left(mr_e\right) K_0 \left(mr_0\right)} \right] \tag{107}$$

The fin efficiency can be determined from the following expression:

$$\eta = \frac{2r_0}{m \left(r_e^2 - r_0^2\right)} \left[\frac{I_1 \left(mr_e\right) K_1 \left(mr_0\right) - K_1 \left(mr_e\right) I_1 \left(mr_0\right)}{I_0 \left(mr_0\right) K_1 \left(mr_e\right) + I_1 \left(mr_e\right) K_0 \left(mr_0\right)} \right] \tag{108}$$

where $m = \sqrt{\frac{2h}{k\delta}}$ is the fin performance factor

where

$$\theta = t - t_\infty$$

$$\theta_0 = t_0 - t_\infty$$

I = modified Bessel function, first kind

K = modified Bessel function, second kind

Reference 26 gives the following simplified equation for a radial fin of rectangular profile:

$$\eta = \frac{1}{1 + 1/3(mb)^2 \sqrt{1/\rho}} \qquad (109)$$

where $b = r_e - r_o$ $\qquad \rho = \dfrac{r_o}{r_e}$

Convection heat transfer from a radial fin can be determined from the following expression:

$$Q_0 = \eta 2\pi \left(r_e^2 - r^2\right) h \left(t_0 - t_\infty\right) \quad \text{(from both sides)} \qquad (110)$$

$$Q_0 = \eta\pi \left(r_e^2 - r_0^2\right) h \left(t_0 - t_\infty\right) \quad \text{(from one side)} \qquad (110a)$$

Figure 26 presents effectiveness of radial fins of rectangular profile at three different radius ratios (r_o/r_e) as a function of the fin performance factor, mb. The computations are based on the simplified equation (Eq. 106). This equation introduces certain errors (somewhat lower η values) which are increasing with decreased ρ values. The charts, however, will provide sufficiently accurate data for ordinary engineering computations.

Figure 27 presents temperature excess ratio of radial fins of rectangular profile at three different radius ratios as a function of the fin performance factor mr . The charts allow determination of temperature differentials within a radial fin or plate when the plate can be divided into some circular areas or sections.

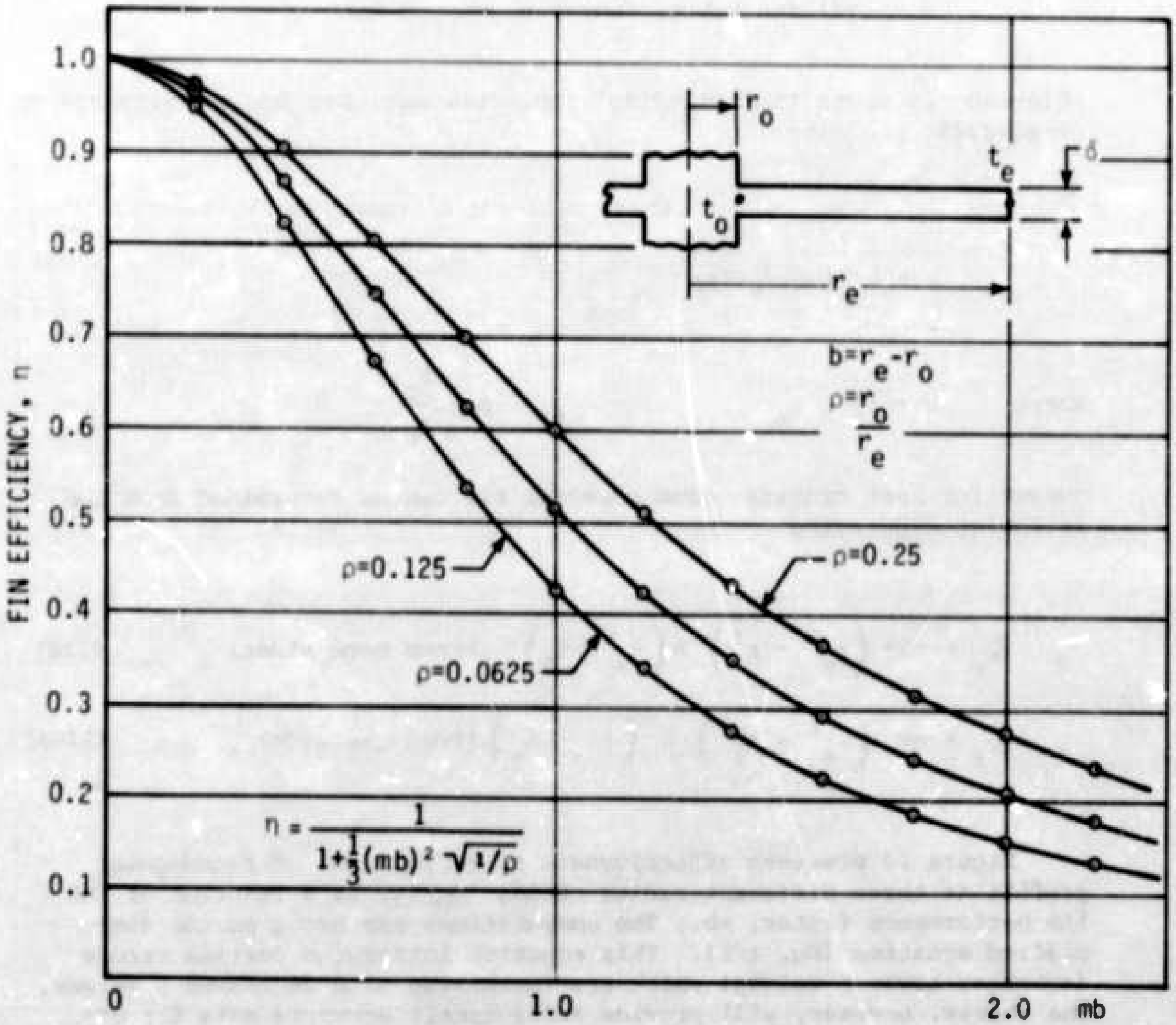

Figure 26. Efficiency of Radial Fins of Rectangular Profile

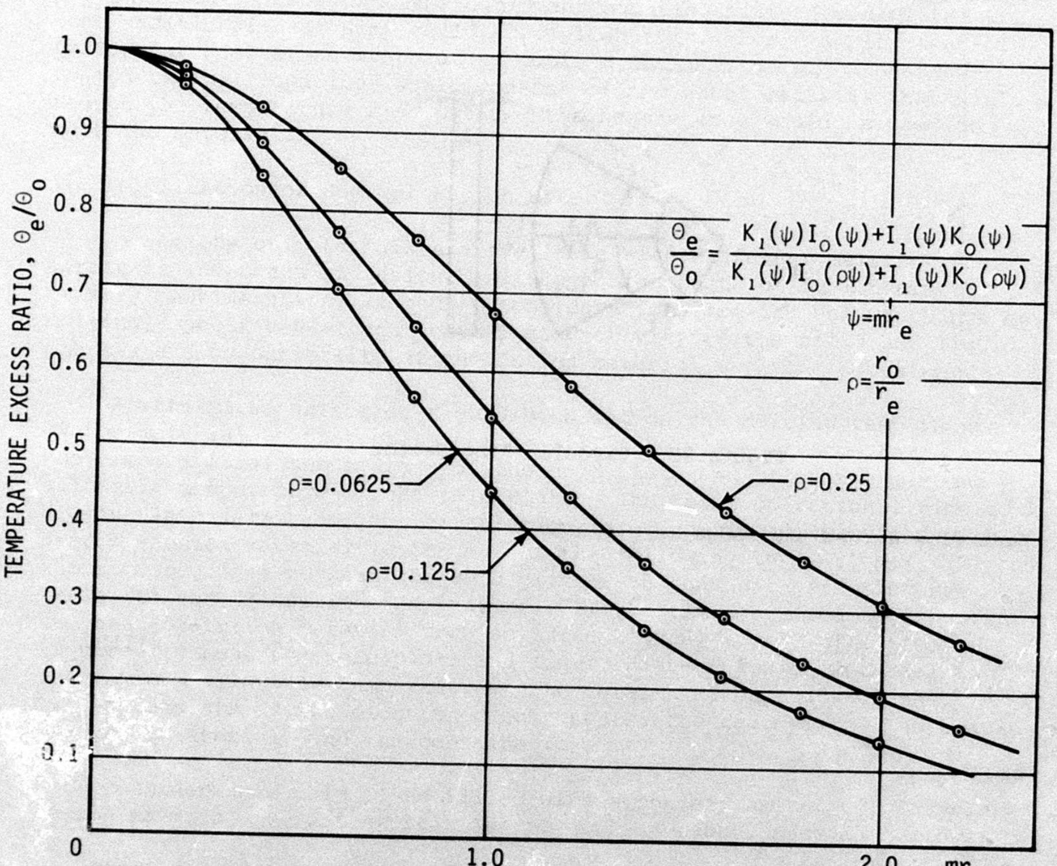

Figure 27. Temperature Excess Ratio of Radial Fins of Rectangular Profile

In cold-plate design, it is often necessary to determine thermal conductances and/or resistances of shapes that differ from the longitudinal and radial fins. Such conditions occur around concentrated heat loads where the surrounding area must be divided into small sections or nodes. Depending on the design of the cold plate, the heat transfer in these sections can take place only by conduction, or conduction and convection (radiation is neglected).

Consider conduction heat transfer across a radial wedge as shown in Figure 28.

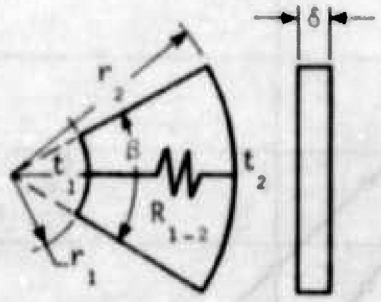

Figure 28. Circular Ring Sector

Heat flow across the wedge is given by:

$$q = -kA \frac{dt}{dr} \tag{111}$$

or

$$\frac{dt}{q} = \frac{dr}{KA} \tag{112}$$

The heat flow area changes with distance from the center and can be expressed as:

$$A(r) = r\beta\delta \text{ (β in radians)} \tag{113}$$

$$\frac{dt}{q} = \frac{dr}{kr\beta\delta} \tag{114}$$

If we integrate, then

$$\frac{t_1 - t_2}{q} = \frac{1}{k\beta\delta} \int_{r_1}^{r_2} \frac{dr}{r} \tag{115}$$

$$\frac{t_1 - t_2}{q} = \frac{\ln r_2 - \ln r_1}{k\beta\delta} \tag{116}$$

$$t_1 - t_2 = q\,\frac{\ln r_2 - \ln r_1}{k\beta\delta} \tag{117}$$

or

$$q = \frac{k\beta\delta}{\ln r_2 - \ln r_1}\left(t_1 - t_2\right) \tag{118}$$

Noting that $\frac{\Delta t}{q}$ = conduction thermal resistance, R, we can determine that

$$R = \frac{\ln r_2 - \ln r_1}{k\beta\delta} \tag{119}$$

This expression can be conveniently used for determining conduction thermal resistances in computer analysis.

The temperature differentials in the above developments are true only for conduction heat transfer. When convection heat transfer also takes place from the ring sector, the temperature distribution can be determined by similar procedures outlined for the radial fin.

Consider next a cold plate with a heat-exchanger core or surface as shown in Figure 29. Figure 29a shows a cold-plate arrangement where both sides of the cold plate can be used for equipment mounting. Figure 29b shows the arrangement when only one side can be used for equipment mounting.

The total heat transfer from a heat exchanger or cold plate of the plate-fin configuration can be divided into two parts: (1) heat transferred from the base or equipment mounting plate and (2) heat transferred from the fins. The total heat transfer is given by:

$$Q = Q_b + Q_f \tag{120}$$

The heat transferred from the fin, applying the definition of fin effectiveness, is:

$$Q_f = \eta_f A_f h_f (\Delta t)_b \tag{121}$$

Assuming effectiveness of the base plate as unity, we can obtain the following:

$$Q_b = A_b h_b (\Delta t)_b \tag{122}$$

The above assumption can be justified if the base plate is divided into the small elements used in computer analysis. Substituting equations 121 and 122 into equation 120, we can obtain:

$$Q = A_b h_b (\Delta t)_b + \eta_f A_f h_f (\Delta t)_b \tag{123}$$

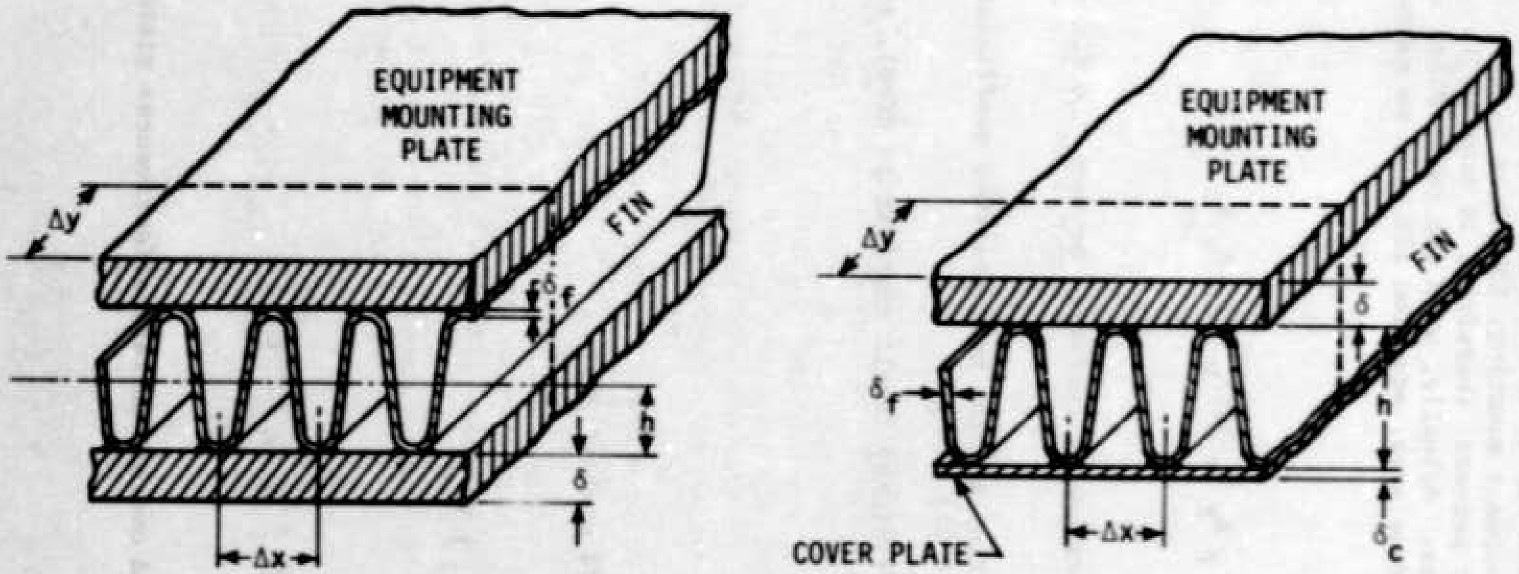

(a) HEAT DISSIPATION FROM BOTH SIDES

(b) HEAT DISSIPATION FROM ONE SIDE

Figure 29. Cold Plates with Finned Surfaces

Equation 123 can be applied for both configurations of the cold plate, except, only half of the fin length must be accounted for when both sides of the plate are used for equipment mounting. If only one side of the plate is used for equipment mounting, the cover plate will also take part in the heat transfer process; therefore, it must be included in the heat transfer surface area. Actually, when the cover plate is included in the heat-transfer surface area, equation 123 must be extended as follows:

$$Q = A_b h_b (\Delta t)_b + \eta_f A_f h_f (\Delta t)_b + \eta_c A_c h_c (\Delta t)_f \tag{124}$$

where $(\Delta t)_f$ is the temperature differential between the fin end and the coolant.

However, for short fins and low heat-transfer coefficients, assumption can be made that $\Delta t_f = \Delta t_b$.

For fins of high efficiency (small temperature drop), assumption can be made that

$$h_b = h_f = h_c = h_o$$

and equations 123 and 124 simplify to

$$Q = h_o \left(A_b + \eta_f A_f \right) \Delta t_b \tag{125}$$

$$Q = h_o \left(A_b + \eta_f A_f + \eta_c A_c \right) \Delta t_b \tag{126}$$

Introducing the weighted overall surface effectiveness yields:

$$\eta_o A = A_b + \eta_f A_f \tag{127}$$

or

$$\eta_o = 1 - \frac{A_f}{A}\left(1 - \eta_f\right) \tag{128}$$

and

$$\eta_o A = A_b + \eta_f A_f + \eta_c A_c \tag{129}$$

or

$$\eta_o = 1 - \frac{A_f}{A}\left(1 - \eta_f\right) - \frac{A_c}{A}\left(1 - \eta_c\right) \tag{130}$$

where

$$A = A_b + A_f + A_c \tag{131}$$

Substituting the weighted effectiveness, we can express the convection heat transfer from a finned surface as follows:

$$Q = \eta_o A h_o (\Delta t)_b \tag{132}$$

where $\Delta t_b = t_b - t_\infty$

t_∞ **= temperature of surroundings,** $^\circ F$

A **= total heat transfer surface area,** ft^2

a. Efficiency of Finned Extended Surfaces

Thermal performance of longitudinal and radial plain rectangular fins has been discussed and some of the important parameters presented in graphical form. However, application of plain heat transfer surfaces for air cooling of electronic equipment will be very limited. In most cases such surfaces, for example the air flow passages of cold plates, will be provided with extended surfaces as shown on Figure 29. Under such conditions both the efficiency and temperature excess of the equipment mounting plate will be significantly affected.

Considering first a longitudinal fin of rectangular cross section provided with a compact heat exchanger core, for example the plain plate-fin surface with 11.1 fins per inch (see Ref. 27). Referring to Figure 29, the heat transfer surface of the mounting plate will be extended by the fins and the cover plate as follows:

$$A_{ext} = A_f + A_c$$

where A_f is surface area of the fins, ft^2

A_c is surface area of the cover plate, ft^2

The overall extended weighted surface effectiveness

$$\eta A_{ext} = \eta_f A_f + \eta_c A_c$$

or

$$\eta_{ext} = \eta_f \frac{A_f}{A_{ext}} + \eta_c \frac{A_c}{A_{ext}}$$

where

$$\eta_f = \frac{\tan h(mb)}{(mb)}$$

$$m = \sqrt{\frac{2 \cdot h}{K\delta_f}}$$

$$\eta_c = F_1 \frac{\tan h(mb)_c}{(mb)_c}$$

Reference 27 gives the following expression for F_1

$$F_1 = \frac{1}{\cosh (mb)_f + \sqrt{\frac{2\delta_c}{\delta_f}} \tan h(mb)_c \sin h(mb)_f}$$

A sample calculation will be performed to determine the overall weighted extended surface efficiency and temperature excess of a fin having a unit width, and length of 3 inches. The Reynolds number of the cooling air flow is assumed to be Re = 2000. The Nusselt number for this flow regime, as obtained from Figure 155, is Nu = 7.7 (fin surface 11.1, Ref. 27)

$$Nu = 7.7 = \frac{D_h h}{k}$$

and $h = 7.7 \frac{k}{D_h} = 7.7 \frac{.0155}{.01012} = 11.79$ Btu/hr ft^2 °F

$$m_f = \sqrt{\frac{2h}{k\delta_f}} = \sqrt{\frac{2(11.79)}{100(.0005)}} = 21.72$$

$$(mb)_f = 21.72(.0208) = 0.4525$$

$$\eta_f = \frac{\tan h(.4525)}{.4525} = 0.938$$

$$\eta_c = F_1 \frac{\tan h(mb)_c}{(mb)_c}$$

$$m_c = \sqrt{\frac{h}{k\delta_c}} = \sqrt{\frac{11.79}{100(.0026)}} = 6.73$$

$$b_c = 1/2(.180)(1/12) = 0.0075 \text{ ft}$$

$$(mb)_c = 6.73(.0075) = 0.0505$$

$$F_1 = \frac{1}{\cosh(.4525) + \sqrt{\frac{2(.0026)}{.0005}} \tanh(.0505) \sinh(.4525)}$$

$$F_1 = 0.847$$

$$\eta_c = .847 \frac{\tanh(.0505)}{.0505} = 0.846$$

For the particular heat exchanger surface, total transfer area/volume between plates, $\beta = 367\ ft^2/ft^3$; fin area/total area = 0.756.

For the given fin volume between plates

$$V = 1 \left(\frac{3}{12}\right)\left(\frac{.25}{12}\right) = 0.00521 \text{ ft}^3$$

Total heat transfer surface area

$$A_t = .00521 \ (367) = 1.91 \text{ ft}^2$$

Fin area $A_f = 1.91 \ (.756) = 1.445 \text{ ft}^2$

Area of cover plate $A_c = 1 \left(\frac{3}{12}\right) = 0.25 \text{ ft}^2$

Area of fin and cover plate

$$A_{ext} = 1.445 + 0.25 = 1.695 \text{ ft}^2$$

$$\eta_{ext} = \frac{1.445}{1.695} \ (.938) + \frac{.25}{1.695} \ (.846) = 0.924$$

For a unit area of fin, there will be extended surface area of

$$A_{ext} = (1) \ (1) \ (.25) \left(\frac{1}{12}\right) \ (367) - 1 = 6.65 \text{ ft}^2/\text{ft}^2$$

As there will be temperature gradients along the extended surfaces, the efficiency of this surface will be reduced by the factor η_{ext}, and the effective extended surface area will be

$$A^1_{ext} = 6.65 \ (.924) = 6.15 \text{ ft}^2/\text{ft}^2$$

This corrected surface area must be included into the fin efficiency and temperature excess equations as follows

$$m = \sqrt{\frac{2\ h\ A^1_{ext}}{k\delta}} \qquad \text{or } m = \sqrt{\frac{h\ A^1_{ext}}{k\delta}}$$

For the surface geometry and flow conditions indicated previously

$$m = \sqrt{\frac{11.79\ (6.15)}{100\ (.0104)}} = 8.34$$

$$mb = 8.34\left(\frac{3}{12}\right) = 2.087$$

$$\eta = \frac{\tanh\ (2.087)}{2.087} = 0.465$$

and

$$\frac{\theta_e}{\theta_o} = \frac{1}{\cosh\ (2.087)} = 0.244$$

Figures 23 and 24 may also be used for determining the fin efficiency and temperature excess ratio. It must be noted, however, that for each core geometry and heat transfer coefficient h the parameter m must be computed separately.

Similarly as for the longitudinal fin, the same procedures may be used to determine fin efficiency and temperature excess ratio of radial fins. Based on the computed mb and mr_e parameters, the fin efficiency η, and the temperature excess ratio θ_e/θ_o may be obtained from Figures 26 and 27, respectively.

SECTION VIII

RADIATION HEAT TRANSFER

As radiant heat transfer takes only a minor part in the overall heat-transfer process considered in this study, only the general equations are presented and briefly discussed.

In accordance to the basic theory, radiant energy is transported either by electromagnetic waves or by photons; it travels at a speed of light. There is a continuous interchange of energy among bodies as a result of the reciprocal process of emittance and absorptance. If one of the bodies in an enclosure is at a higher temperature than the other, it will emit more thermal energy to the colder body than it will receive from it. As a result, the temperature of the colder body will increase. This interchange of energy continues even when both bodies have reached the same temperature, except both of the bodies receive and emit the same amount of energy.

The main factors affecting thermal radiation are temperature, surface properties, and the configuration or geometric factor. The configuration factor between two surfaces is defined as the fraction of radiation leaving one surface and reaching the other surface. Consider first the simplest case: a black surface (perfect absorber) where no reflection occurs. Black surfaces emit in a perfectly diffuse fashion, and the radiation intensity leaving a surface is independent of the direction of emission. This simplifies the radiation heat-transfer computations. For example, the energy radiated from a surface, A_1, that reaches a surface, A_2, is found from the definition of the configuration factor as follows:

$$Q_{1-2} = A_1 F_{1-2} \sigma T_1^4 \tag{133}$$

Similarly, the energy radiated from surface A_2 which reaches surface A_1 is:

$$Q_{2-1} = A_2 F_{2-1} \sigma T_2^4 \tag{134}$$

The net exchange from surface A_1 to surface A_2 is:

$$Q = Q_{1-2} - Q_{2-1} = A_1 F_{1-2} \sigma T_1^4 - A_2 F_{2-1} \sigma T_2^4 \quad (135)$$

From the reciprocity relation, we can determine that

$$A_1 F_{1-2} = A_2 F_{2-1} \quad (136)$$

The net exchange, therefore, can be written in the following form:

$$Q_{1-2} = A_1 F_{1-2} \sigma \left(T_1^4 - T_2^4\right) \quad (137)$$

where σ, the Stefan-Boltzmann constant = 0.1713×10^{-8} Btu/hr ft^{2}°R, T = absolute temperature, °R = 460° + F°.

Actual surfaces, however, cannot be considered as black, and an emittance factor, ϵ, must be introduced into the emissive power equation.

$$E = \epsilon \sigma T^4 \quad (138)$$

where ϵ is defined as the ratio of the emissive power, E, of a given surface to that of a black surface at the same temperature.

$$\epsilon = \frac{E}{E_b} \quad (139)$$

The ratio, ϵ, is also called the total hemispherical emittance.

We can now introduce another item, the total hemispherical absorptance, which is the fraction of the hemispherically incident radiation that is absorbed by the surface over all wave lengths. Therefore, the

radiant energy emitted per unit time and area by a body is $\epsilon\sigma T_1^4$, while the absorbed radiant flux is $\alpha\sigma T_2^4$ (enclosure). Heat exchange between a body and its isothermal enclosure can be expressed as follows:

$$\frac{Q_1}{A} = \epsilon_1 \sigma T_1^4 - \alpha\sigma T_2^4 \tag{140}$$

for gray bodies $\alpha = \epsilon$

and

$$\frac{Q_1}{A} = \epsilon_1 \sigma \left(T_1^4 - T_2^4\right) \tag{141}$$

For general engineering applications, assumption is made that the surfaces involved are gray-body emitters and absorbers ($\alpha = \epsilon$). In such a case, the surface heat-transfer rates can be computed with a minimal knowledge of the radiation properties. Only the hemispherical emittance, ϵ, of each surface is required. To account for emissivities of the participating surfaces a factor, F_ϵ, known as the emissivity factor, is inserted in the heat transfer equation.

$$Q_{1-2} = A_1 F_{1-2} F_\epsilon \sigma \left(T_1^4 - T_2^4\right) \tag{142}$$

$$Q_{2-1} = A_2 F_{2-1} F_\epsilon \sigma \left(T_2^4 - T_1^4\right) \tag{143}$$

For infinite parallel plates, we find that

$$F_{1-2} = 1$$

Substituting, we obtain

$$F_\varepsilon = \frac{1}{1/\varepsilon_1 + 1/\varepsilon_2 - 1} \tag{144}$$

For concentric spheres or infinite cylinders, we also find that

$$F_{1-2} = 1$$

$$F_\varepsilon = \frac{1}{1/\varepsilon_1 + A_1/A_2\ (1/\varepsilon_2 - 1)} \tag{145}$$

Special cases can be found in the literature.

SECTION IX

HEAT STORAGE

In aircraft cooling systems with circulating fluid loops, electronic equipment cooling will be performed mainly by cold plates which are cooled by the circulating fluid. If such a system would develop a leak, over-heating of the electronic equipment would follow within a short time. To avoid a catastrophic failure of the equipment essential to flight, a means must be provided to extend the operational time of the equipment: Providing the equipment mounting plate (cold plate) with some additional heat sink could accomplish this. For example, heat-of-fusion material or an evaporative coolant could be used. A heat-of-fusion thermal capacitor would consist of a mass of material that would reduce the temperature rise because the heat energy would be used to melt the material.

a. Application of Heat of Fusion Materials

A variety of materials are available with different melting temperatures and heats of fusion. Although high heats of fusion are the primary consideration, secondary considerations are the volume change on melting, specific heat and thermal conductivity of the solid and liquid phases, and compatibility of the fusion material with the container.

Furthermore, selection should be based on the melting temperature of the material so that phase change will take place at some temperature above the initial temperature of the cold plate and below the maximum allowable temperature of the cold plate. The total operational time of a cold plate (after coolant circulation is discontinued) provided with heat-of-fusion material is the sum of the following three items: (1) the time required to heat the cold plate with the heat-of-fusion material to the transition temperature, (2) the time required to transfer the heat-of-fusion material from solid to liquid, and (3) the time required to heat the cold plate and liquid heat-of-fusion material to the maximum allowable temperature. The total heat capacity of the system consists of the electronic components, the cold plate, the heat-of-fusion material, and the container.

Considering a cold plate filled with a certain amount of heat-of-fusion material, we can express the total heat capacitance as follows:

$$C_t = C_{fm} + C_{pl} \tag{146}$$

where the heat capacitance $C = Wc$

W = weight in pounds

c = specific heat of the material, Btu/lb°F

When the specific heat is assumed to be constant, the rate of heat flow to a heat storage device can be expressed as follows:

$$Q = Wc \frac{dt}{d\tau} = C \frac{dt}{d\tau} \qquad (147)$$

where $d\tau$ = the time increment

dt = the temperature change during the time increment.

From equation 147, the time during which a certain amount of heat, Q, can be absorbed is:

$$\tau = C \frac{t_1 - t_2}{Q}, \text{ hrs} \qquad (148)$$

where t_1 = the temperature at the beginning of the time interval, °F

t_2 = the temperature at the end of the time interval, °F.

The time required to heat the heat-storage device (cold plate and heat-of-fusion material) to the maximum allowable temperature, therefore, can be determined from the following expression:

$$\tau = \frac{1}{Q}\left[\left(W_{pl}\, c_{pl} + W_f\, c_{fs}\right)\left(t_{tr} - t_i\right) + HW_{fm} + \left(W_{pl}\, c_{pl} + W_f\, c_{fl}\right)\left(t_{max} - t_{tr}\right)\right] \qquad (149)$$

where τ = operational time, hrs

Q = heat input rate, Btu/hr

c_{pl} = specific heat of cold plate, Btu/lb°F

c_{fs} = specific heat of solid heat-of-fusion material, Btu/lb°F

c_{fl} = specific heat of liquid heat-of-fusion material, Btu/lb°F

W_{pl} = weight of cold plate, lbs

W_f = weight of heat-of-fusion material, lbs

t_{tr} = transition temperature of heat-of-fusion material, °F

t_i = initial temperature of cold plate, °F

t_{max} = maximum temperature of cold plate, °F

H = heat of fusion, Btu/lb

As far as thermal performance prediction of heat-storage devices is concerned, very little information is available about heat transfer at the melt interface. Reference 28 provides some information about melting of a solid with a specified heat flux on the boundary. The reference presents a method for determining thickness of melting layer with time and temperature: time history of the surface for melting a solid with an arbitrary heat flux to the surface. The reference presents charts where the expressions $Q(\tau)\ X(\tau)/(\alpha\rho Q_L)$ and $\theta(0,\tau)/(Q_L/C)$ can be found by solving the following equation:

$$\frac{Q(\tau)}{\alpha\,\rho^2 Q_L^{\,2}} \int_0^{\tau} Q(\tau)\,d\tau = \frac{\mu}{6}\left[\mu + 5 + (1 + 4\mu)^{1/2}\right] \qquad (150)$$

where μ is a function of time, τ, for the case $Q(\tau)$ = constant

$$\mu = \tau - \frac{\tau^2}{2!} + \frac{5\tau^3}{3!} + \frac{51\tau^4}{4!} + \frac{827\tau^5}{5!} \qquad (151)$$

The temperature distribution in the liquid melt is given as follows:

$$\frac{\theta(x,\tau)}{Q_L/c} = \frac{1}{2}\left[1 - (1 + 4\mu)^{1/2}\right]\left(\frac{x}{X} - 1\right)$$

$$+ \frac{1}{8}\left[1 - (1 + 4\mu)^{1/2}\right]^2 \left(\frac{x}{X} - 1\right)^2 \qquad (152)$$

and the temperature - time history at the surface x = 0 is given by:

$$\frac{\theta\ (0,\tau)}{Q_L/c} = -\frac{1}{4} + \frac{1}{4}\ (1 + 4\mu)^{1/2} + \frac{1}{2}\mu \qquad (153)$$

Refer to Figure 30.

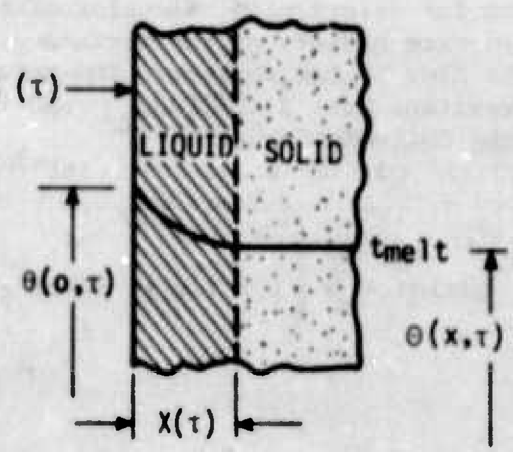

Figure 30. Melting of a Solid with Arbitrary Heat Flux

Q_L = latent heat of fusion

k = thermal conductivity

ρ = mass density

τ = time

α = thermal diffusivity = $k/\rho c_p$, ft^2/hr

θ = temperature difference, $\theta = t - t_m$

c = specific heat

t = temperature of liquid

t_m = melting temperature

$x = X(\tau)$

Because most of the heat-of-fusion materials expand approximately 10 percent when melting, space must be provided for such expansion in the container housing the material. This can be achieved by using a bellows or providing a sufficient void space. Since most of the heat-of-fusion materials have a relatively low thermal conductivity, the heat-transfer matrix should be provided with fins designed for low thermal resistance and low heat flux into the heat-of-fusion material.

The expansion of the heat-of-fusion material could be used to actuate a switch to turn on a warning light or even shut down the system.

Reference 5 presents a simplified computer program that calculates the temperature of the cold plate and at nodes, the heat-of-fusion material temperature as a function of time as the material melts.

Reference 29 gives the following expression for determining the total thermal capacity of the system:

$$C_{syst} = (WC)_F + \left(t_{max} - t_{soak}\right) \sum \left(WC_p\right) \tag{154}$$

where

$$C_F = (C_p)_{solid} \; (t_{melt} - t_{soak}) + H_F + (C_p)_{melt} \; (t_{max} - t_{melt})$$

The last term in equation 154 represents the sum of all the thermal capacitances of the system.

A wide variety of inorganic and organic materials can be used as heat-of-fusion materials. Among the general types available are paraffins, which give a variety of melting points and reasonably high heats of fusion and are not corrosive. They typically have a volume increase of 11 to 15 percent on melting.

Table 6, adapted from Reference 29, lists a number of materials suitable for use in heat-storage systems.

b. Application of Evaporative Coolants

Problems of extreme heat concentration and high ambient temperature are usually solved by the evaporation cooling technique. In this cooling technique, heat is removed from the electronic components and/or systems by a change in state when the coolant evaporates during absorption of heat. For a given weight of coolant, vaporization cooling provides the most effective heat removal compared to any other method. The heat energy absorbed by evaporating a liquid coolant is:

$$Q = M\, h_{fg} \tag{155}$$

Below the boiling point, the heat capacity of the fluid will also add to the overall heat capacity of the system. If the evaporating liquid is stored directly in the cold plate, thermal capacity of the cold plate and its equipment should also be added to obtain the total thermal mass. The total heat capacity, therefore, of a liquid-filled cold plate can be determined from the following expression:

$$C = w_1 c_1 \left(t_{op} - t_b\right) + W_{pl} c_{pl} \left(t_{op} - t_b\right) + W_1\, h_{fg} \tag{156}$$

where W_1 = weight of evaporant, lbs

w_{pl} = weight of equipment mounting plate, lbs

c_1 = specific heat of liquid, Btu/lb °F

C_{pl} = specific heat of the plate material, Btu/lb °F

t_{op} = operating temperature of the cold plate, °F

t_b = boiling temperature of the evaporant, °F

h_{fg} = heat of vaporization, Btu/lb

Table 6. Heat of Fusion Materials and Their Properties

COMPOUND OR SUBSTANCE	FORMULA	MELTING POINT (°F/°C)	HEAT OF FUSION (Btu/lb)	SPECIFIC GRAVITY		HEAT CAPACITY (C_p)	
				Solid	Liquid	Solid	Liquid
Paraffin wax		126/52	63.1	0.90		0.694	
Palmitic acid	$C_{15}H_{31}COOH$	131/55	70.5		0.853	0.430	0.653
o-Xylene Dichloride	$o\text{-}C_8H_8Cl_2$	131/55	52.3	1.393			
Tristearin*	$(C_{17}H_{35}COOH)_3H_5$	133/56 162/72	84.0 98.2		0.862		
Nickel nitrate hydrate	$Ni(NO_3)_2 \cdot 6H_2O$	134/57	65.3	2.05		0.473	
Cadmium nitrate hydrate	$Cd(NO_3)_2 \cdot 4H_2O$	139/59	45.6	2.455			
Heptadecanoic acid* (marjaric acid)	$C_{16}H_{33}COOH$	140/60	81.3 91.6	0.86			
Octacosane	$C_{28}H_{58}$	140/60	96.5	0.775			
Beeswax		143/62	76.2	0.96			
Stearic acid	$C_{17}H_{35}COOH$	152/67	85.7		0.848	0.399	0.550
Azobenzene	$C_6H_5NNC_6H_5$	154/68	52.0	1.203		0.330	
Diphenyl	$C_{12}H_{10}$	156/69	47.0	1.18		0.385	0.313
p-Chloroaniline	$p\text{-}C_6H_4NH_2Cl$	156/69	67.0	1.427	1.170		
Detrio-contant*	$C_{32}H_{66}$	158/70	64.7 94.0		0.775		
Phenyl-acetic acid	$C_6H_5C_2H_3O_2$	170/77	44.1		1.078		
Bromo-camphor	$C_{10}H_{15}OBr$	170/77	75.0	1.444			
m-Xylene dibromide	$m\text{-}C_8H_8Br_2$	170/77	37.6				
Durene	$C_{10}H_{14}$	175/79	67.4		0.838		
Napthalene	$C_{10}H_8$	176/80	64.1	1.004		0.281	0.402

* Compound has two heats of fusion

The time, during which a certain amount of heat can be absorbed, can be expressed as follows:

$$\tau = \frac{C}{Q_{gen}}, \text{ hrs} \tag{157}$$

Q_{gen} = heat transferred by the equipment, Btu/hr

Furthermore, the reservoir must be designed to assure heat transfer to the evaporant when the reservoir is partially full as the liquid evaporates. Wicking material, therefore, often will be required to deliver the liquid to the heat-transfer surface. To prevent loss of the liquid before the emergency condition occurs and control the boiling pressure, thus the temperature, a valve system is required. In designing a vaporization cooling device, the temperature differential (Δt) from the cold plate to the evaporating material must be considered.

Table 7, adapted from Reference 5, lists some of the common liquids for evaporative cooling systems.

Table 7. Evaporative Coolant Properties

LIQUID	TEMPERATURE °F/°C	HEAT OF VAPORIZATION (Btu/lb)	VAPOR PRESSURE (PSIA)	DENSITY (lb/ft^3)
Ammonia	20/-7	553	48.2	40.4
	40/4.5	535	73.3	39.5
	60/15.5	520	107.6	38.5
Water	100/38	1037	1.0	62.0
	150/65.5	1007	3.7	61.5
	200/93	978	11.5	60.4
Methanol	50/10	507	1.05	49.9
	100/38	490	5.0	48.2
	150/65.5	472	15.1	46.7
	200/93	407	40.3	45.0

SECTION X

APPLICATIONS OF HEAT PIPES

Because of the unique heat-transfer characteristics of heat pipes, they are currently used and studied for a wide range of applications, covering almost any temperature range. The heat pipe has found particularly wide applications in spacecraft thermal control, where coolant circulating devices cannot be used because of power limitations and reliability problems. The applications are also more and more extended to avionics equipment cooling. For example, heat-pipe cooling systems have been used for substrate-mounted integrated-circuit chips; electronic-equipment circuit boards; high power-density components such as traveling-wave tubes, Impatt and Trapatt diodes, and modules in airborne phased-array systems; and other specific applications.

It must be noted that extreme care must be exercised in application of heat pipes to avionics equipment cooling. Orientation of the heat pipes with the evaporator end up, and dynamic forces resulting from aircraft maneuvers can significantly reduce thermal performance of heat pipes.

The heat-pipe technology can also be used for thermal control of temperature-sensitive electronic circuitry where not only junction temperatures must be kept low, but also where temperature cycling must be reduced and the mounting-surface temperature uniformly maintained.

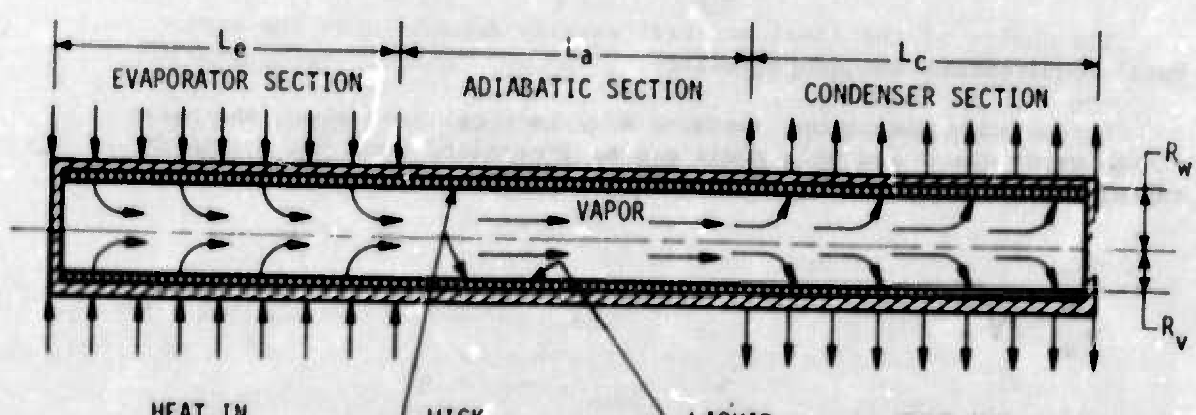

Figure 31. Heat-Pipe Schematic

Figure 31 shows a schematic of a heat pipe consisting of a constant cross-sectional area vapor-flow passage surrounded by an annular wick. The working fluid is evaporated at the evaporator section, transferred through the vapor-flow passage to the condenser section, where it is condensed and returned through the wick by capillary action to the evaporator section. Since both the boiling and condensing process take place at a constant temperature, the internal temperature of the heat pipe is practically constant.

a. Design Principles of Heat Pipes

The heat-pipe design is connected with a number of interrelated problems, and a certain sequence of steps must be undertaken before a successful device can be designed and fabricated. Based on the thermal requirements of the particular equipment or system to be cooled, the working fluid, wick, and shell material of the heat pipe should be selected.

Selection of the working fluid is primarily based upon the expected temperature range. It is important to select fluids with a high latent heat, high thermal conductivity, high surface tension, good wetting ability, and low viscosity. Consideration should also be given to the operating pressure. Extremely high operating pressures may eliminate an otherwise attractive fluid.

In selecting the wick material, the following primary parameters should be considered: (1) thermal conductivity of the wick matrix, (2) the capillary pumping capacity, and (3) the working-fluid pressure drop through the wick.

The choice of the shell material usually depends upon the structural requirements and compatibility.

For optimum operation, assuming a cylindrical heat pipe, the ratio of the vapor space and wall radii can be determined from the following expression given by Cotter in Reference 30.

$$\frac{r_v}{r_w} = \sqrt{\frac{2}{3}} \quad (158)$$

Assuming that the maximum heat flux which the heat pipe can transfer depends upon the capillary pumping pressure, we can develop the following equation:

$$\Delta P_c = \Delta P_l + \Delta P_v + \Delta P_g \quad (159)$$

when the heat pipe orientation is horizontal, $\Delta P_g = 0$, and

$$\Delta P_c = \Delta P_l + \Delta P_v \tag{160}$$

The capillary pumping pressure or driving force results from the adhesive force of interfacial wetting and can be expressed as

$$\Delta P_c = \frac{2\sigma \cos \theta}{r_c} \tag{161}$$

The maximum driving pressure occurs when the wetting angle is zero, $\theta = 0$, and under such conditions:

$$\Delta P_c = \frac{2\sigma}{r_c} \tag{162}$$

The gravity head is given by:

$$\Delta P_g = \rho_l \cdot \frac{g}{g_c} \cdot L \sin \alpha \tag{163}$$

When effects of gravity are neglected, the wick provides the only resistance to liquid flow from the condenser to the evaporator. Because of the low flow rates and velocities encountered in capillary flow, it can be assumed that the flow is laminar and Darcy's law, therefore, will apply:

$$\Delta P_l = \frac{m_l \mu_l L'}{K_p A_w \rho_l} \tag{164}$$

The term L' is the distance from the midpoint of the evaporator section to the midpoint of the condenser section. The wick permeability is expressed as K_p. Another equation, derived from Reference 30, can be used in determining pressure drop of the liquid as follows:

$$\Delta P_l = \rho_l \frac{g}{g_c} L \sin \alpha + \frac{b \mu_l L Q_e}{2\pi \left(r_w^{\,2} - r_v^{\,2}\right) \rho_l \varepsilon r^2_{cmin} h_{fg}} \qquad (165)$$

and for a horizontal pipe, $\alpha = 0$

and

$$\Delta P_l = \frac{b\mu_l L Q_e}{2\pi \left(r_w^{\,2} - r_v^{\,2}\right) \delta_l \varepsilon r^2_{cmin} h_{fg}} \qquad (166)$$

The term b is a dimensionless constant, depending on the detailed geometry of the capillary structure. For nonconnected parallel cylindrical pores, b = 8. For capillary structures with tortuous and interconnected pores, b varies from 10 to 20.

Because of the continuous vapor addition in the evaporator and removal in the condenser, the vapor pressure drop computation is complicated. Solutions for two simplified cases have been obtained; one in which the flow to or from the channel wall is small and the other in which the flow is large.

$$\Delta P_v = P_v (L) - P_v (0) = \frac{4\mu_\ell L Q_e}{\pi \rho_v r_v^{\,4} h_{fg}} \qquad (167)$$

for $Re_r \ll 1$

and for a more practical case when $Re \gg 1$

$$\Delta P_v = P_v(L) - P_v(0) = \frac{\left(1 - 4/\pi^2\right) Q_e^2}{8\rho_v r_v^4 h_{fg}^2} \qquad (168)$$

The axial Reynolds number is defined as follows:

$$Re_z = \frac{2\rho_v r_v \overline{U}_z}{\mu_v} = \frac{2\dot{m}_v}{\pi r_v \mu_v} \qquad (169)$$

where $\overline{U}_z = \dfrac{\dot{m}_v}{\rho_v \pi r_v^2}$

Cotter (Ref 30) states that if $Re_r = 0$ and the axial Reynolds number, Re, is less than 1000; then, laminar flow exists. However, if Re is greater than 1000 and the length exceeds 50 r_v, then fully-developed turbulent flow should exist.

The maximum heat transfer of a heat pipe operating at steady-state conditions can be summarized as follows:

$$\rho_l \frac{g}{g_c} L \sin\alpha + \frac{b\,\mu_l\, Q_e\, L}{2\pi\left(r_w^2 - r_v^2\right)\rho_l \varepsilon\, r_{c_{min}}^2\, h_{fg}}$$

$$+ \begin{cases} \dfrac{4\mu_v\, L\, Q_e}{\pi\rho_v\, r^4\, h_{fg}} & Re_r \ll 1 \\[2ex] \dfrac{\left(1-4/\pi^2\right) Q_e^2}{8\rho_v\, r_v^4\, h_{fg}^2} & Re_r \gg 1 \end{cases} - \frac{2\sigma\cos\theta}{r_{c_{min}}} = 0 \qquad (170)$$

The optimum value of the capillary pore size, $r_{c\ opt}$, can be deduced from the above equation as follows:

$$r_{c\ opt} = \frac{b\ \mu_1\ Q_e\ L}{4\pi\ \left(r_w^2 - r_v^2\right)\ \rho_1 \epsilon\ h_{fg}\ \sigma \cos\theta} \qquad (171)$$

For a horizontal heat pipe, we obtain:

$$\rho_1\ \frac{g}{g_c}\ L \sin\alpha = 0$$

the maximum heat transfer of the steady-state heat pipe can be computed from the following expression:

$$Q_e = \begin{cases} \dfrac{\pi r_w^3\ h_{fg}\ \sigma\cos\theta}{3L} \left(\dfrac{2\epsilon\rho_v\ \rho_1}{3b\ \mu_v\ \mu_1}\right)^{1/2} & Re_r \ll 1 \\[2ex] \dfrac{4\pi r_w^2\ h_{fg}}{3} \left(\dfrac{\rho_v\ \rho_1 \epsilon\sigma^2\ \cos^2\theta}{(\pi^2 - 4)\ bL\ \mu_1}\right)^{1/3} & Re_r \gg 1 \end{cases} \qquad (172)$$

also $Q_e = \dot{m}_1\ h_{fg}$ (173)

In many heat pipe applications, pressure drop in the vapors can be neglected when compared with the pressure drop of the liquid. Consequently, the maximum heat-transfer rate can be expressed as follows:

$$Q_{max} = \frac{\rho_1 \sigma\ h_{fg}}{\mu_1} \left[\frac{2KA_1}{r_c L'} - \frac{KA_1\ \rho_1\ \ L \sin\alpha}{\sigma L'}\right] \qquad (174)$$

where r_c = the single pore radius.

The capillary pumping pressure or driving force, ΔP_C, is impossible to predict accurately because wick surfaces do not exhibit clearly defined uniform circular openings with measurable radii. In addition, wettability is a function of the working fluid and wick material, and values of θ cannot always be obtained or assumed zero. The driving force, ΔP_C, can, however, be determined experimentally by using wick capillary-pressure tests.

b. Radial Heat Flux Limitations

There are two limiting factors which must be considered in the design of heat pipes: (1) when the vaporization rates are too high, the capillary forces may not be sufficient to deliver liquid to the evaporator section of the heat pipe and (2) if vapor does not leave the vaporization interface at the rate it is produced, liquid will be excluded from the interface; and the vapor will expand, forming a blanket of vapor which will cover the heated surface. In either of the two cases, the effects would be a sharp increase in the heat-pipe wall temperature at the evaporator section.

Although there is a very small temperature drop along the longitudinal axis of the heat pipe, the main temperature gradient occurs in the radial direction at both the evaporator and condenser sections. Only limited effort has been devoted to heat-transfer studies of wick-covered surfaces, and only limited data are available about boiling and condensing heat-transfer coefficients from wick-covered surfaces. The heat-transfer rate, based on the overall heat-transfer coefficient, can be expressed as follows:

$$Q = UA(\Delta t) \tag{175}$$

The total thermal resistance of a heat pipe can be expressed as series resistances of the evaporator and condenser

$$R_t = R_e + R_C = \left(\frac{1}{UA}\right)_e + \left(\frac{1}{UA}\right)_C \tag{176}$$

For a tight, low-porosity wick, RCA gives the following radial conduction equation:

$$K_e = \frac{2\pi L_e K_{wlv}}{\ln\left(r_w/r_v\right)} \tag{177}$$

where k_{wlv} is the composite thermal conductivity of the wick, liquid, and possibly trapped vapor bubbles. When nucleate boiling takes place within the wick, the evaporation conductance is expressed by:

$$K_e = 2\pi\, r_w\, L_e\, h \tag{178}$$

where h is the boiling heat-transfer coefficient determined for the specific fluid, heat pipe, and operating heat flux.

Under conditions of low heat flux, the following simple expression can be used:

$$h = \frac{k_{wl}}{\delta_w} \tag{179}$$

where k_{wl} is the thermal conductivity of the liquid-saturated wick and δ_w is the wick thickness.

For heat transfer surfaces covered with thin metallic wicks, equation 179 will give values which are too high, and other analytical expressions must be used for determining evaporative heat-transfer coefficients. Reference 31 has investigated evaporative heat-transfer coefficients for a 1-inch outside-diameter horizontal copper tube embedded in a water-saturated ceramic-fiber wick. The reference points out that at low heat flux, the evaporative heat-transfer coefficient for a wick-covered surface was higher than that for pool boiling from a plain surface. The following reasons are given for the above phenomena: (1) wick fibers increase the effective transfer surface area and provide active sites for bubble formation and (2) the wick fibers greatly increase the ratio of heated surface to liquid volume (this increases the rate of superheat of liquid near the surface, thus aiding the formation of vapor bubbles). Reference 32 presents results of pool boiling of distilled water (at one-atmosphere pressure) from horizontal, stainless-steel tubes spiraled by 1/8- and 1/4-inch diameter organic-fiber wicking in a coil-like manner. The test runs were performed with eight, sixteen, and twenty-six evenly spaced spirals. It was observed that the

wick spirals around the heater section produced much earlier nucleation in the saturated liquid pool. At about 2°F, superheat sites were activated. About 10°F was required without wicking. Also, as the number of spirals increased, the improvement in the film coefficient was increased over no-wicking runs. With twenty-six spirals of wicking around a 6-inch heater length, the film coefficient was four times greater than for a non-wicked surface at Δt_{sat} of 20°F. The wicking spirals, however, did not increase the critical heat flux of the heater surface. The improvement in heat transfer could be observed at the lower heat fluxes only.

Extensive experimental data are presented in Reference 33. Evaporative heat-transfer coefficients were determined from planar wick-covered surfaces, using water and Freon 113 as evaporants. Also, this reference points out that equivalent or superior performance can be obtained with wick-covered surfaces, as compared to surfaces with no wicks. The data, however, indicate that, depending on the structure of the wicking material, the entrapment of vapor bubbles in the wick matrix may cause premature film boiling in the wick at relatively low heat fluxes. The reference indicates that the boiling heat-transfer coefficient of a two-layer thick screen is significantly higher than that of a seven-layer thick wick.

An approximate critical heat flux can be determined by a semi-empirical equation developed by Rohsenow and Griffith (given in Ref 34):

$$q_{cr} = 143\, h_{fg}\, \rho_v \left(\frac{g}{g_c}\right)^{.25} \left(\frac{\rho_l - \rho_v}{\rho_v}\right)^{0.6} \qquad (180)$$

or the following equation developed by Zuber:

$$q_{cr} = 0.18\, h_{fg}\, \rho_v \left[\frac{\sigma\left(\rho_l - \rho_v\right)}{\rho_v^{\,2}}\, g\, g_c\right]^{.25} \left(\frac{\rho_l - \rho_v}{\rho_l}\right)^{0.5} \qquad (181)$$

Correlations with equations 180 and 181 have also been performed for Freons, E2 and C51-12.

Care must be exercised in using the above equations; for thicker wicks and low temperature fluids the equations will give too high values.

If the thermal resistance of the liquid-saturated wick is large compared with the thermal resistance of condensation, the following equation may be used for determining the condensing heat-transfer coefficient:

$$h_c = \frac{k_{wl}}{\delta_w} \tag{182}$$

The following expression is given for determining thermal conductance of a liquid-saturated wick:

$$k_{wl} = \varepsilon k_l + (1 - \varepsilon)\, k_w \tag{183}$$

Both the evaporator and condenser surface areas are important items in heat-pipe thermal performance. When the evaporator is covered with a vapor film, a critical heat flux is reached which will cause a drastic rise in the temperature of the evaporator surface. This condition should be avoided. For a given heat load, the evaporator surface area must be properly sized to ensure operation below the critical heat flux. Similarly, care must be taken for properly designing the condenser section in order to reduce the radial temperature drop. Under gravity conditions, some portion of the condenser can be designed without a wick, significantly reducing the resistance to heat flow.

c. Constant Temperature Heat Pipe

The constant temperature heat pipe, employing an inert gas blanket in the condenser section, was an early development at RCA. Figure 32 shows such an arrangement. The inert or non-condensible gas is employed to control the heat rejection area of the condenser section. Under low heat-transfer rates, the non-condensible gas will occupy most of the condenser length, reducing the heat-transfer area. As the heat load is increased, the non-condensible gas is forced by the working-fluid vapor flow into the reservoir, exposing a larger condensing surface area. As a result, the heat pipe becomes a device of nearly constant temperature regardless of the heat load. Because of the short mean-free path of the vapor molecules at normal internal pressures, the vapor penetration into the non-condensible gas is quite small; and the interface has a sharp temperature gradient.

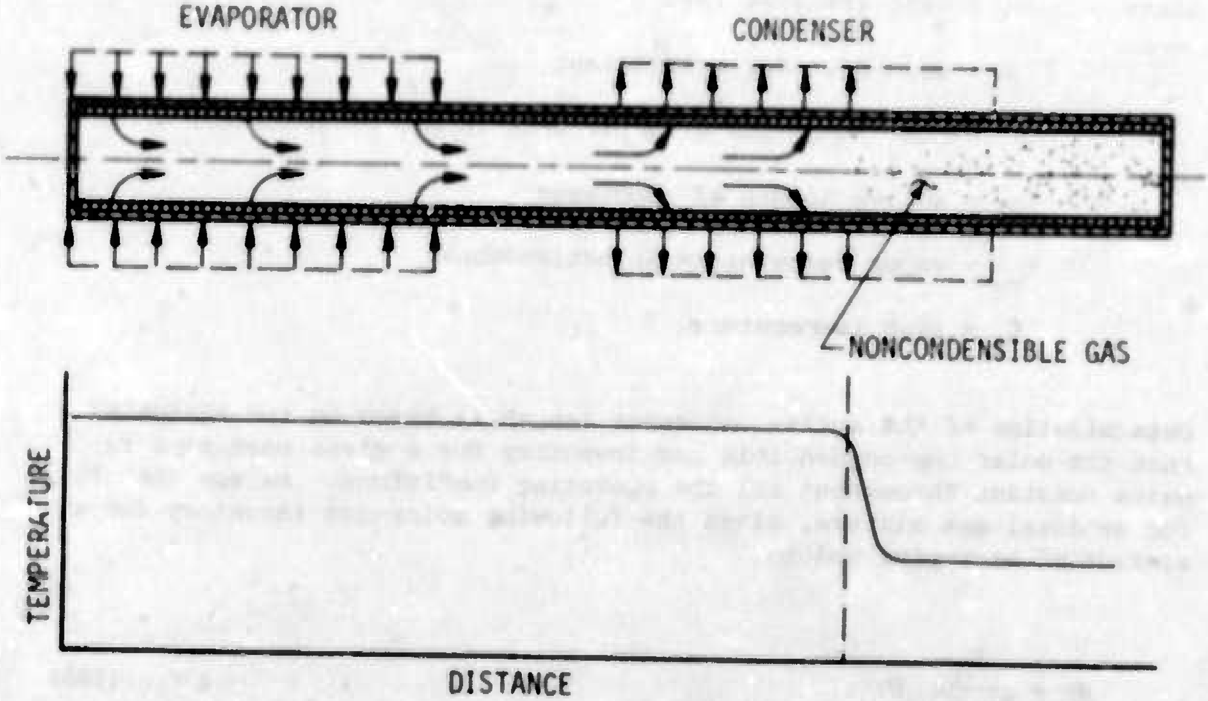

Figure 32. Constant-Temperature Heat Pipe

Although the operating temperature of the constant-temperature heat pipe will be higher at lower heat dissipation rates than the temperature of an equivalent conventional heat pipe, fluctuations caused by heat load changes can be significantly reduced by this simple passive thermal-control technique. This technique of temperature control can be applied to electronic-equipment cooling when the amplitude of thermal cycling must be reduced.

Heat transfer from the condenser can be expressed by the following equation:

$$Q = h\ A'\ L_a\ \left(t_v - t_s\right) \tag{184}$$

where Q = heat transfer rate

h = heat transfer coefficient

A' = heat rejection area per unit length of condenser

L_a = active length of condenser

t_{va} = vapor temperature in active zone

t_s = sink temperature.

Determination of the active condenser length is based on the reasoning that the molar non-condensible gas inventory for a given heat pipe remains constant throughout all the operating conditions. Marcus (Ref 36), for an ideal gas mixture, gives the following molar-gas inventory for an element of heat-pipe volume.

$$dn = \frac{P_g}{R_u T_g} dV \tag{185}$$

where dn = number of moles of gas in the volume element, dv

P_g = partial pressure of gas in dv

T_g = temperature of gas in dv

R_u = universal gas constant.

Assuming a simplified flat-front model for the inactive portion of the condenser, we can integrate the above equation to obtain:

$$n = \frac{P_g \left(L_c - L_a\right)}{R_u T_g} A \tag{186}$$

where A_v = vapor core cross-sectional area

L_c = total condenser length.

Within the gas-blocked region of the condenser, the gas and liquid are at the same temperature (neglecting axial conduction), and the partial pressure of the vapor equals the vapor pressure at the heat-sink temperature, t_s, thus:

$$P_g = P_{va} - P_{vs}, \text{ and } t_g = t_s \tag{187}$$

where P_{va} = total vapor pressure at t_{va}

P_{vs} = vapor pressure at t_s.

Reference 36 gives the following heat-transfer equation for a simple gas-loaded heat pipe:

$$Q = hA' \left(t_{va} - t_s\right) \left[L_c - \frac{n\ Ru\ t_s}{A_v\left(P_{va} - P_{vs}\right)}\right] \tag{188}$$

The term in the brackets represents the active condenser length, which when multiplied by hA' yields the heat-pipe conductance.

For more detailed information about the theory and design of variable-conductance heat pipes, consult Reference 36.

SECTION XI

THERMAL ANALYSIS TECHNIQUES

4. Finite Differences

There are three general techniques available for solution of heat-transfer and temperature-distribution problems: (1) analytical, (2) analog, and (3) finite difference. As the finite difference technique is easily adaptable to digital computations, this technique has found wide applications in solving heat-transfer problems. The heat-transfer device or system is divided into suitable regions or nodes with a reference point located at the center of each region. The number of nodes will depend on the required accuracy, thermal loading, and thermal conductance of the material. For hand calculations, it is advantageous to start with the crudest possible subdivision. All the points from which temperatures are required should be included in the system.

In the numerical or approximate solutions of heat transfer problems, the differential equations are replaced by finite differences, and the problem is solved by a set of algebraic equations. The temperatures, in such a case, are determined at certain discrete points only.

Heat transfer to or from such nodes can take place by conduction, convection, and radiation. Heat can also be generated and stored in these nodes. Consider a section of a rod protruding into a certain environment and losing heat to this environment, as shown in Figure 33.

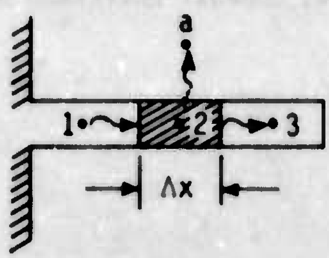

Figure 33. Heat Transfer in a Rod

The energy balance and rate equations can be used directly to arrive at a finite difference formulation. Under steady-state conditions, energy entering an element or node must equal energy leaving the element or

$$q_{in} = q_{out} \tag{189}$$

and

$$q_{12} = q_{23} + q_{2a} \tag{190}$$

The rate of heat transfer by conduction is given by:

$$q_{12} = K_{12} \left(t_1 - t_2\right) \tag{191}$$

or generally

$$\sum q_{ij} = \sum K_{ij} \left(t_i - t_j\right) \tag{192}$$

where

$$K_{12} = kA/\Delta x \text{ and} \tag{193}$$

A = cross-section area of the rod.

The rate of heat transfer by convection is given by:

$$q_{2a} = K_{2a}\left(t_2 - t_a\right) \tag{194}$$

where

$$K_{2a} = hA \text{ and} \tag{195}$$

A = surface area of the rod.

If heat transfer also takes place by radiation, then

$$q_{2-i} = K_{2-i} (t_2 - t_i) \tag{196}$$

where

$$K_{2-i} = A\epsilon\sigma\left(T_2^{\,3} + T_2^{\,2}\,T_i + T_2\,T_i^{\,2} + T_i^{\,3}\right) \tag{197}$$

T = absolute temperature, °R.

Substituting the rate equations into the energy balance equation gives

$$K_{1-2}\left(t_1 - t_2\right) = K_{2-3}\left(t_2 - t_3\right) + K_{2-a}\left(t_2 - t_a\right) \tag{198}$$

Such equations can be set up for each node, and the solution of these equations provides the temperature distribution of the rod. If n points or nodes are selected in a certain system, then n number of equations must be set up. The system of nodal equations can be solved by elimination, matrix inversion, reduction of determinants by Cramer's rule, etc.

Under transient conditions, heat capacity of the node must also be considered. For example, consider the energy balance for a node, i, surrounded by adjacent nodes, j, during a small time interval, $\Delta\tau$. During this time interval, assumption is made that the temperature of the other nodes remains constant. Heat balance of the node, therefore, can be expressed as follows:

$$\sum K_{ij} \left(t_j - t_i\right) = \rho c \, V_i \frac{\Delta t_i}{\Delta \tau} \tag{199}$$

Numerical or approximate techniques are also available for solving transient problems. The numerical methods, however, are restricted to simple geometries and boundary conditions. For more complex systems, particularly under transient conditions, a significant improvement in the analysis technique can be achieved by application of the digital computer.

b. Application of Computer Techniques

The computer technique employs the electrical resistance-capacitance (R-C) network. Similarly, as in an electrical resistance which refers to current flow, thermal resistance refers to heat flow. Computer solutions are obtained by converting the physical system into one consisting of nodes or lumps connected by thermal resistors. The method permits direct solution of complex transient problems involving conduction, convection radiation, and heat storage.

The most time-consuming step is the conversion of the physical system into an equivalent R-C network. All the resistances and capacitances must be calculated and presented in a form acceptable to the particular computer program. Use of the lumping process implies that the lump or node is at a uniform average temperature. By proper selection of the node size and arrangement, any degree of accuracy can be obtained. Consideration, however, should be given to program capacity, anticipated temperature gradients, machine time, etc. There are no general rules which provide guidance in selection of the proper node or lump sizes. Engineering judgement and experience is helpful.

Before going into more complex R-C network applications, some simple heat-transfer problems are presented and discussed. For example, heat flow through a plain wall (see Figure 34) can be expressed as follows:

$$Q = kA \frac{t_1 - t_2}{L} \tag{200}$$

$$Q = \frac{t_1 - t_2}{\frac{L}{kA}} = \frac{t_1 - t_2}{R} \; ; \; R = \frac{L}{kA} \tag{200a}$$

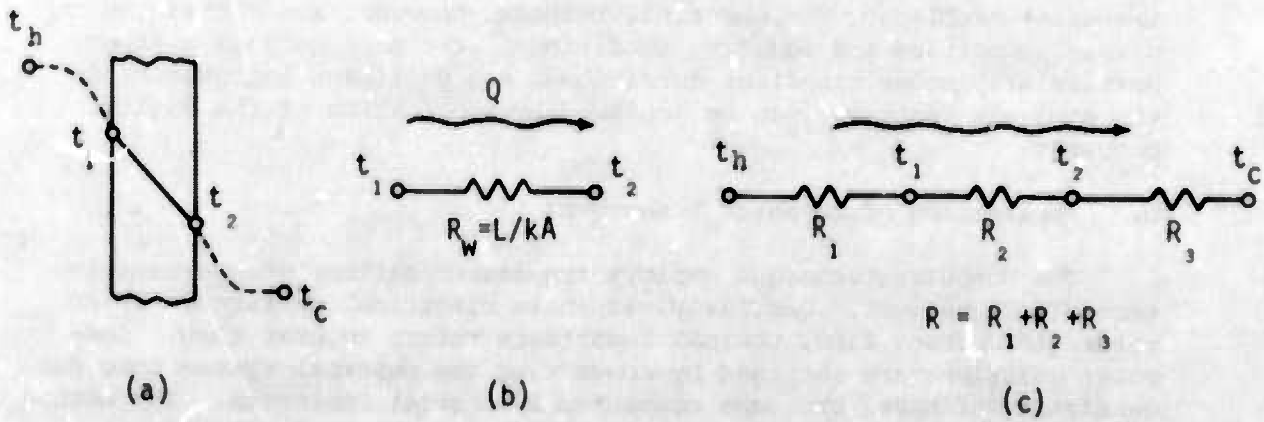

Figure 34. Heat Flow Through a Plain Wall

Figure 34b shows the thermal circuit of the plain wall; Figure 34c shows the thermal circuit of the wall with convection on both sides of the wall.

The convection heat transfer to and from the wall can be expressed by the following equations:

$$Q = A\, h_h \left(t_h - t_1\right) \tag{201}$$

$$Q = A\, h_c \left(t_2 - t_c\right) \tag{202}$$

or

$$Q = \frac{t_h - t_1}{\frac{1}{Ah_h}} = \frac{t_2 - t_c}{\frac{1}{Ah_c}} = \frac{t_h - t_1}{R_h} = \frac{t_2 - t_c}{R_c} \tag{203}$$

Expression L/kA is called the conduction thermal resistance, and expression 1/Ah is called the convection thermal resistance. In any case involving heat transfer between two points at temperatures $t_1 - t_2 = \Delta t$, the heat flow (analogous to Ohm's law) can be expressed as follows:

$$Q = \frac{\Delta t}{R} \tag{204}$$

The relation between the temperatures and the heat flow for the plain wall with convection, can be expressed as follows:

$$Q = \frac{t_h - t_c}{\frac{1}{Ah_h} + \frac{L}{kA} + \frac{1}{Ah_c}} = \frac{t_h - t_c}{R_h + R_w + R_c} \tag{205}$$

Consider next a fin attached to a hot wall or some heat-generating component as shown in Figure 35. Heat from the hot wall is transferred

by conduction to and along the fin, then by convection to the ambient air or other ultimate heat sink. Figure 35 shows the R-C network when only one side of the fin takes part in convection heat transfer. The other side and end could be insulated.

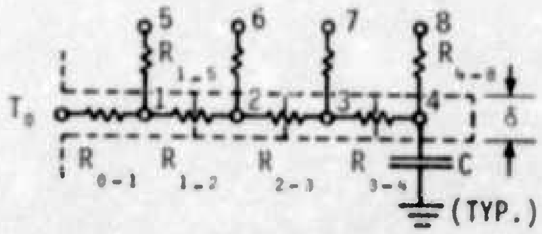

Figure 35. R-C Network of a Longitudinal Fin

Conduction resistances of the fin can be determined as follows:

$$R_{0-1} = \frac{\Delta x}{2kA} \tag{206}$$

$$R_{1-2} = R_{2-3} = R_{3-4} = \frac{\Delta x}{kA} \tag{207}$$

where

$$A = \delta(\Delta y) \tag{208}$$

The convection resistances are:

$$R_{1-5} = R_{2-6} = R_{3-7} = R_{4-8} = 1/hA \tag{209}$$

where $A = (\Delta x)\ (\Delta y)$

When convection heat transfer takes place from both sides of the fin, then

$$A = 2(\Delta x)\ (\Delta y)$$

When heat is dissipated to the ambient air (assumed at uniform temperature), all the ambient nodes (5, 6, 7 and 8) can be combined into one node. Under transient conditions, thermal capacity of the nodes must also be determined. In this particular case, when all the nodes are of the same size, then

$$C_1 = C_2 \quad C_3 = C_4 = \rho c V \tag{210}$$

Because circular fins are finding wide application in heat-transfer equipment, determination of their thermal resistances is presented. Figure 36 shows a circular fin of rectangular cross section and its R-C network. The R-C network shows convection heat transfer from one side of the fin only. The other side can be easily included by multiplying the surface area by two. Heat loss from the end is neglected (thin fin) although it can be easily incorporated into the R-C network.

Heat flow through a cylinder or disk of thickness, δ, can be expressed as follows:

$$Q = 2\pi\ k\delta\ \frac{\Delta t}{\ln(r_2/r_1)} \tag{211}$$

When computer techniques (R-C networks) are used for thermal analysis, it is more convenient to have a simple expression for the heat flow through a cylindrical body of the same form as through a plain wall, or

$$Q = kA_m \frac{\Delta t}{\Delta r} \tag{212}$$

where

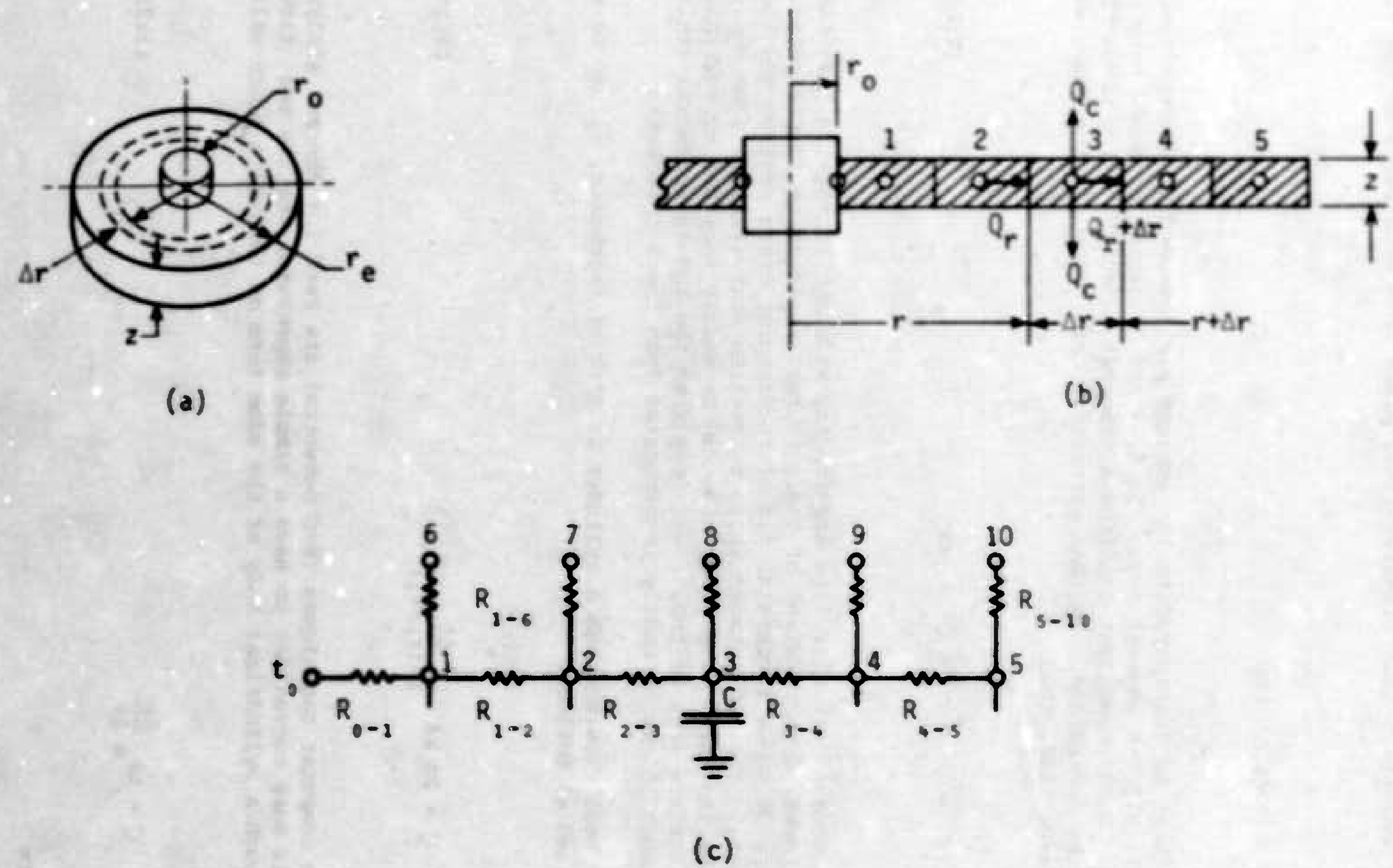

Figure 36. Circular Fin with Rectangular Cross Section

$\Delta t = t_1 - t_2$ and $\Delta r = r_2 - r_1$

A_m is the mean area and can be expressed as follows:

$$A_m = \frac{A_2 - A_1}{\ln (A_2/A_1)} \tag{213}$$

where

$A_1 = 2\pi\ r_1\delta$ and

$A_2 = 2\pi\ r_2\delta$

Thermal resistance of the ring, therefore, is:

$$R = \frac{\Delta r}{kA_m} \tag{214}$$

Convection resistance is given by:

$$R_c = \frac{1}{hA_c} \tag{215}$$

where $A_c = \pi \left(r_2{}^2 - r_1{}^2\right)$ for one side of fin

and $A_c = 2\pi \left(r_2{}^2 - r_1{}^2\right)$ for both sides of fin.

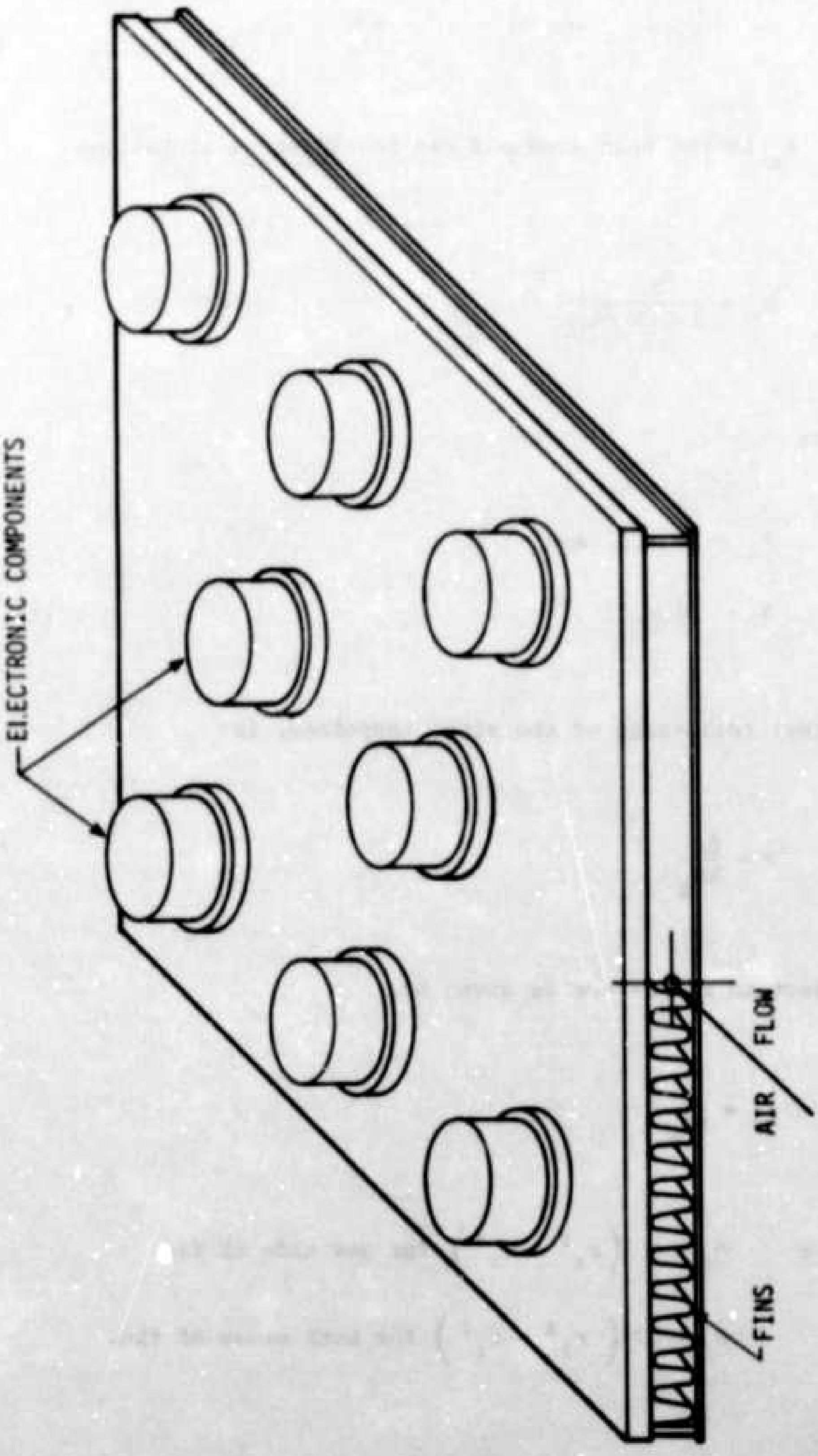

Figure 37. Air-Cooled Cold Plate

A more complex problem is discussed next. For example, it is desired to determine thermal performance of the air-cooled cold plate shown in Figure 37. The cold plate consists of an equipment mounting surface and an air-flow channel through which the cooling air is forced. For more effective cooling and heat transfer, the flow channel is usually provided with extended surfaces, that is, fins. Heat dissipated by the components is transferred across the mounting joint to the plate, then into the cooling air stream. The temperature of the cooling air does not remain constant, but increases along the channel; and a different approach must be used for determining the convection thermal resistances.

Figure 38 shows the R-C network of a section of the cold plate and the air stream. Reference 37 gives the following equations for determining the flow and convection resistances:

$$R_{2-3} = R_{4-5} = R_{6-7} = \cdots \frac{1}{C_p W} \tag{216}$$

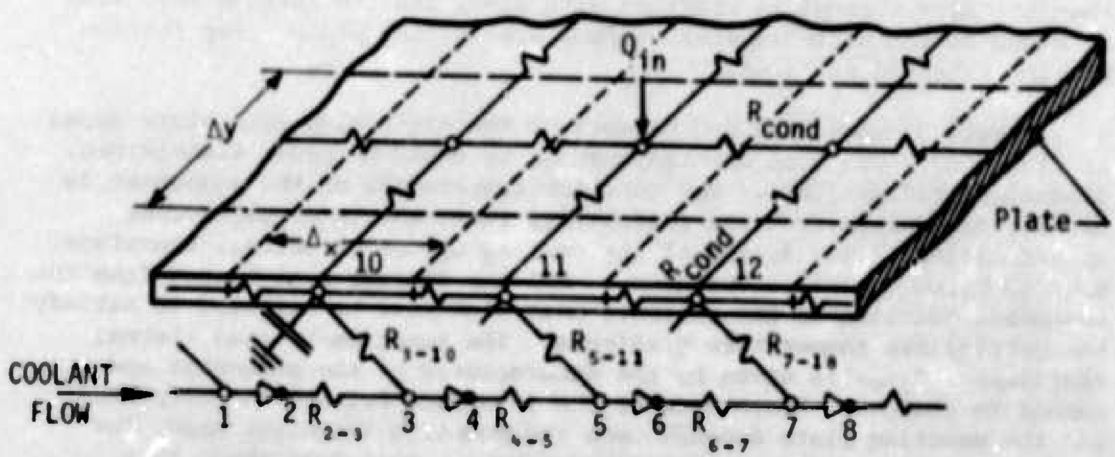

Figure 38. Resistance Network

When the nodes are of equal size, the convection resistances can be expressed as follows:

$$R_{3-10} = R_{5-11} = R_{7-12} = \cdots = \frac{1}{\dot{w}\, c_p \left(e^{\beta} - 1\right)} \tag{217}$$

$$\beta = \frac{hA_c}{\dot{w}c_p} \text{ and} \tag{218}$$

for a flat plate without fins

$$A_c = (\Delta x)\ (\Delta y)$$

When the flow channel is provided with fins, the fin surface must also be added to the heat-transfer surface area of the plate. See Section VII for extended surfaces.

Figure 39 shows the R-C network of the air-cooled cold plate shown in Figure 37. The stud-mounted components could be power transistors, diodes, rectifiers, etc. The junction temperature of the component is usually determined from the reliability requirements or particular specifications. The design of the cooling system or device, therefore, must be based on this temperature. All the thermal resistances from the component junction to the ultimate heat sink must be tailored to satisfy the permissible temperature gradients. The junction-to-case thermal resistance, R_{j-c}, is given by the manufacturer of the component and cannot be changed. Resistance of the interface between the component and the mounting plate depends upon the mounting technique used, for example, with or without insulating washers. Some data about this resistance can be obtained from the open literature. The conduction and convection resistances must be tailored for the particular thermal requirements, especially when both heat source and ultimate heat-sink temperatures are specified. The network shown in Figure 39 may not be the best for the configuration given. Sizing of the plate and fineness of the nodes depend upon the thermal loading. Highly-concentrated heat loads require smaller nodes, particularly around the component mounting areas. It should be noted that all nodes exposed to the cooling air stream must be connected to the air stream by convection resistances.

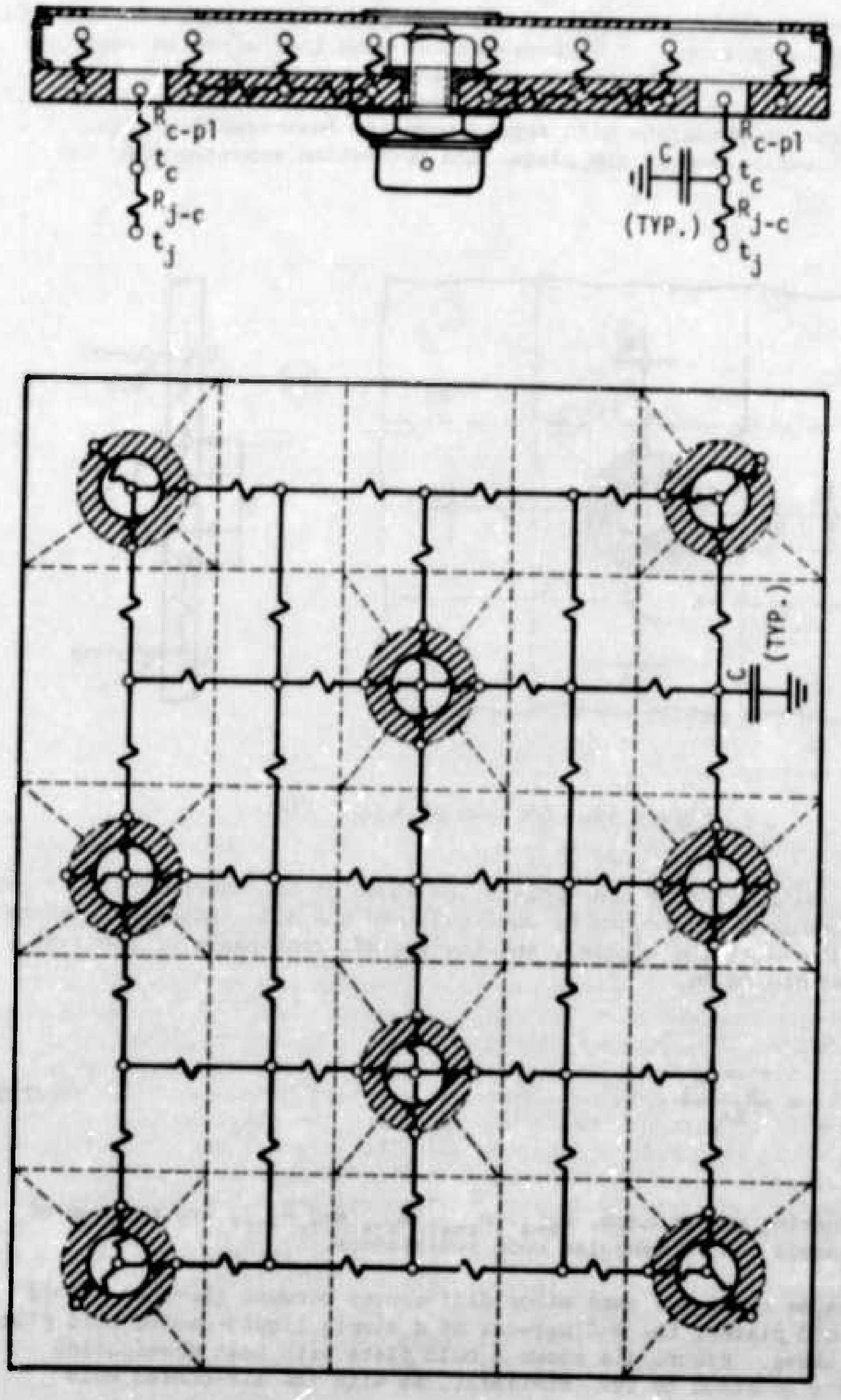

Figure 39. R-C Network of an Air-Cooled Cold Plate

Figure 40 shows a section of the cold plate with the conduction and convection resistances. The cross-hatched area indicates the area over which the dissipated heat of the component is transferred to the plate. From this area, the heat spreads throughout the plate. The magnitude of the temperature gradients will depend upon the heat-transfer rate, conduction resistance of the plate, and convection resistance to the

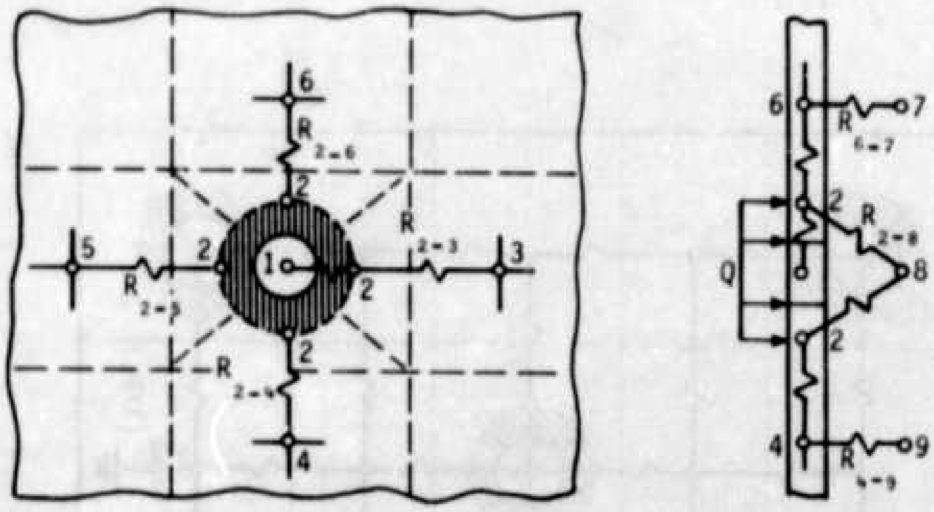

Figure 40. Section of a Cold Plate

coolant. Although four node points are shown on the outer circle of the ring, these node points can be combined into one node (assuming uniform temperature along the circle), and the thermal resistance of the ring can be determined by:

$$R_{1-2} = \frac{r_2 - r_1}{kA_m} \tag{219}$$

The conduction resistances, R_{2-3}, R_{2-4}, R_{2-5} and R_{2-6}, are the sum of the trapezoid and rectangular node resistances.

Because there are some minor differences between air- and liquid-cooled cold plates, the R-C network of a simple liquid-cooled cold plate is also shown. Figure 41a shows a cold plate with heat dissipating components attached to it. Similarly, as with the air-cooled cold

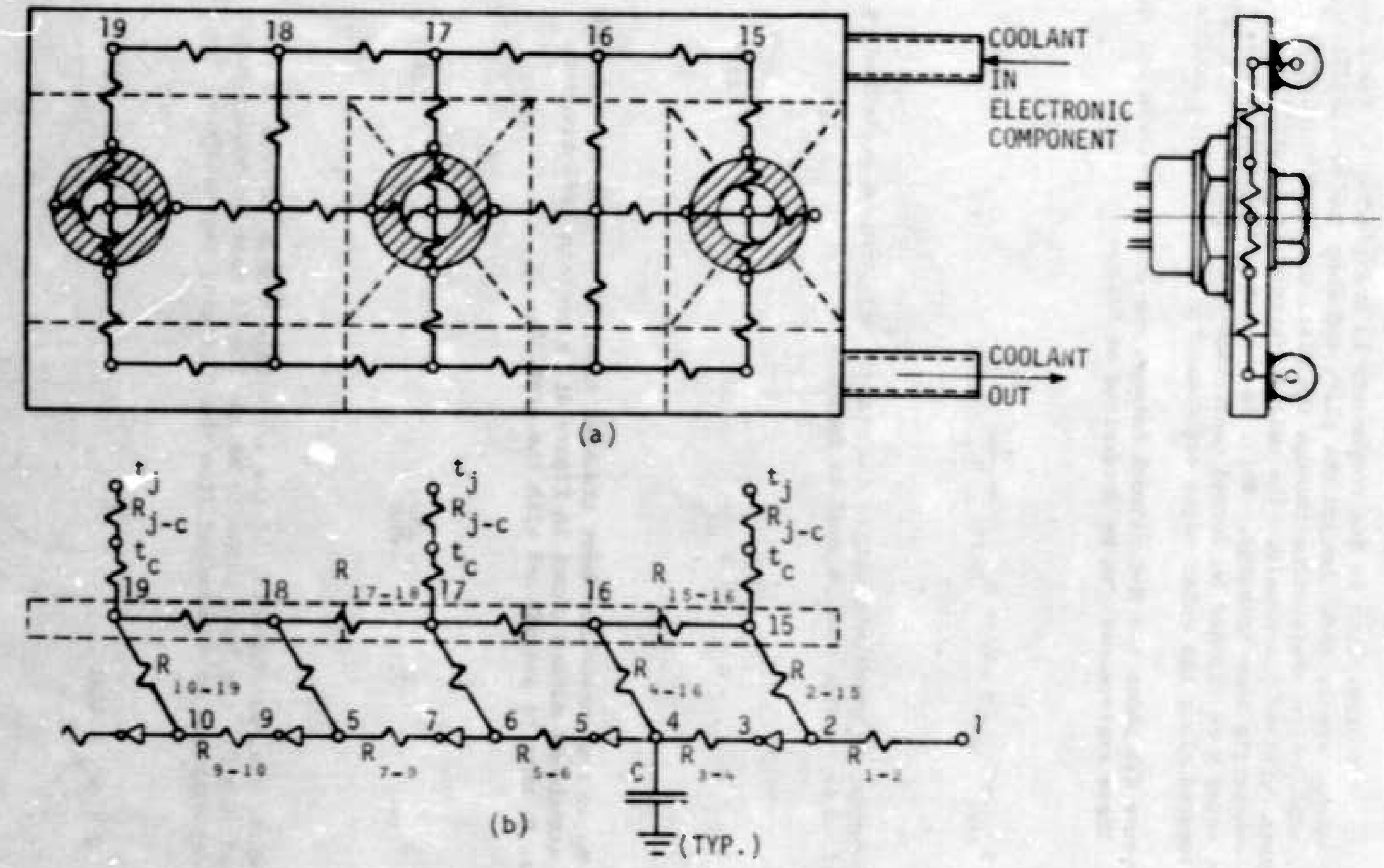

Figure 41. Liquid-Cooled Cold Plate

plate, the heat dissipated by the components is transferred to the plate (cross-hatched area), then through the plate and into the cooling liquid stream. Conduction resistances through the plate can be determined by procedures outlined previously. The only difference is in utilization of the convection heat transfer. While in the air-cooled cold plate, all the nodes were exposed to forced convection heat transfer, here only nodes located along the outer edges are connected to the liquid conduit.

Figure 41b shows the R-C network between the coolant stream and the plate. These resistances can be determined as follows:

$$R_{1-2} = R_{3-4} = \ldots = R_{9-10} = \frac{1}{Wc_p} \tag{220}$$

When temperature gradients within the conduit wall can be neglected, a simplified expression can be used as follows:

$$R_{2-15} = \ldots = R_{10-19} = \frac{1}{hA_c} \tag{221}$$

where A_c is the convection heat transfer area, ft^2. With the tube and plate attachment method shown in Figure 41, a certain effectiveness factor, η, must be introduced with the area, A_c, or

$$R_{2-5} = \ldots = R_{10-19} = \frac{1}{\eta h A_c} \tag{222}$$

While the heat capacity of the air within a node is usually neglected (C = 0), the heat capacity of the liquid must be considered. This capacity can be determined from the following expression:

$$C = \rho c_v A\ (\Delta x) \tag{223}$$

where A is the cross-section area of the tube.

It should be noted that heat is also dissipated from the external surfaces of the plate and components, when not insulated, by natural convection and radiation. However, when the forced convection heat-transfer coefficients are reasonably high, the external heat transfer is usually neglected; although it can be easily incorporated into the R-C network if desired.

Preparation of detailed input data for the computer program is not presented here, because each program would have some differences. Such information can be obtained from user manuals.

SECTION XII

GENERAL THERMAL CONTROL SYSTEMS AND THEIR REQUIREMENTS

The thermal control system should be designed to meet thermal requirements of the electronic equipment within limitations of the aircraft environmental control system and the aircraft weight penalties. There are three main items which must be considered in designing a thermal control system for electronic equipment: (1) the temperature of the component hot-spot or junction must be kept low enough to provide adequate reliability, (2) the component thermal cycling must be limited both as to temperature range and rate of temperature change, and (3) components must be cooled uniformly.

There are many thermal interfaces between the junction of the electronic device and the ultimate heat sink. Because of the maximum allowable junction temperature and the given heat sink temperature, the thermal interfaces must be tailored to the particular requirements. In the case where the thermal interfaces are set, the required temperature of the ultimate heat sink can be determined. Selection of the heat transfer modes or techniques, however, should be made on cost, size, weight, reliability, and serviceability considerations.

The cooling or thermal control systems can be divided into two general categories: (1) direct cooling systems and (2) indirect cooling systems. In the direct cooling systems, the electronic components are directly exposed to the coolant stream. In the indirect cooling systems, the coolant is usually confined to channels in cold plates or chassis to which the electronic components are mounted. In both categories, the coolant can be liquid or gas. The thermal control systems can be further divided into closed and open loops. With few exceptions, liquid is generally used in closed loops; gas coolants (air) are used in open loops. In the direct cooling systems, the component-dissipated heat is rejected directly into the coolant stream by convection (or also evaporation), while in the indirect cooling systems, conduction and convection modes of heat transfer take part in heat removal from the components. Indirect cooling, however, has some advantages such as easier accessibility for maintenance (particularly when liquid coolants are used), less sealing problems, and a wider range of coolant selection.

Because of the high packaging densities and heat dissipation rates of electronic systems presently in use or development stages, natural air cooling is practically obsolete. Forced-convection (including evaporation) liquid and air cooling are considered for present and future electronic systems. For electronic systems having low or medium heat dissipation rates, air cooling, because of its availability, provides simple, cheap, and effective cooling. Both direct and indirect air cooling have been extensively used; however, as air often contains large amounts of moisture and dust, there is a tendency and sometimes

the requirement to employ indirect air cooling by application of cold plates. In this cooling technique, the air is forced through passages and does not come in direct contact with the electronic parts. Forced air cooling is accomplished by using fans or blowers to force the air through the cooling devices.

As far as air cooling is concerned, clean air is one of the most desirable coolants because it is noncorrosive, nontoxic, nonflammable, and possesses good dielectric properties. On the negative side, air has the poorest heat-transfer properties of all the standard coolants, and it can generate significant amounts of acoustical noise at high velocities. In general, noise and vibration become objectionable at velocities above approximately 1500 ft/min (25 ft/sec); although, in some specific applications, the air velocity is limited to approximately 900 ft/min (15 ft/sec).

For high heat-dissipation rates and packaging densities, liquid cooling, because of its high heat-transfer coefficients and low pumping-power requirements, offers outstanding potential for cooling of electronic equipment. The high specific heat of liquids per unit volume enables the use of small sizes for lines, valves, heat exchangers, and pumps. Liquid cooling also minimizes acoustic noise and interference. Liquid-cooling systems are almost always closed loops and usually have a relatively low temperature rise, providing uniform cooling for components of equal power dissipation. Similarly as with air cooling, liquids can be used in direct or indirect cooling. When using cold plates, the liquid is forced through tubes attached directly on one side of the plate, or the liquid-flow passages can be incorporated into the plate.

The liquid-cooling systems will be totally closed, and, because of liquid expansion with temperature increase, some provisions must be made to accommodate these changes. An expansion, or air-cushion tank, should be provided to allow for expansion of the fluid as its temperature increases, to remove air from the coolant, and to cushion the shock in the system if it should become vapor bound. The tank should be large anough to allow for the expansion of all the liquid and still provide an air space.

The cooling systems should be designed for operation under the most severe conditions anticipated. Under less severe conditions, the capacity of the system should be reduced as a function of the cooling demand. Control of a system can be accomplished by using temperature-sensing elements in connection with flow-control valves. The degree of control depends upon the requirements of the most temperature-sensitive part, or parts, in the electronic system. Reference 19 points out that components with a varying duty cycle should be located downstream to protect other equipment and achieve a stabilizing effect. If the duty cycle of a high-power component fluctuates drastically, its improper location could have a significant adverse effect on the reliability of all the downstream components and subassemblies. Problems of this type

can be reduced by proper design of the coolant-flow circuitry. Series, parallel, and a combination of series-parallel circuits can be employed. The choice depends not only on the temperature to be maintained but also upon the weight and power requirements associated with each type of flow circuit. Series circuits have the advantage of mechanical simplicity, tending to minimize the weight of the coolant distribution lines by minimizing the number of connectors and branches. Disadvantages include higher pressure drops for a given flow rate, as compared to other types of circuitry, and a degree of inflexibility with respect to the temperature of the coolant as it passes through the cooling equipment. This latter aspect necessitates greater care in the placement of the components and subassemblies within the electronic equipment when series-flow circuitry is used. With the parallel system, a manifold supplies coolant to the different cooling devices (cold plates and/or heat exchangers) at the same inlet temperature. Component placement in this arrangement is less critical than for series circuits. The parallel concept is particularly advantageous to modular cooling and microminiaturized assemblies, where each unit in the subassembly dissipates approximately the same quantity of heat and is subjected to the same temperature limits. Furthermore, the pressure drop associated with a given flow rate is lower than for other types of circuits. Series-parallel circuitry offers a great degree of design flexibility and allows the advantages of both series and parallel flow configurations. This arrangement is the most likely approach to be used for advanced cooling-system concepts.

The addition of a thermal control system to an aircraft will affect its performance by adding weight, drag, and power consumption. Designers of such a system should have a clear knowledge of the complete electronic cooling load and the pertinent characteristics of the aircraft. It should be pointed out, however, that, except for temperature control of the liquid in the aircraft environmental control system, simple liquid-cooling systems (also air) do not provide any protection against thermal cycling.

SECTION XIII

FLOW DISTRIBUTION IN MANIFOLDS

Not only in a complete cooling system, but also in individual equipment like cold plates and heat exchangers, proper flow distribution of the coolant within the passages is of importance. Configuration and size of the cooling equipment is dictated by the thermal requirements of the electronic equipment, space considerations, and weight and power availability of the vehicle. When the coolant flow passages are arranged in series, no flow distribution problems will occur. Very often, however, the coolant flow passages within a cooling device or equipment must be arranged in parallel. When heat-transfer computations are performed, it is usually assumed that an ideal velocity and flow distribution takes place within the heat transfer matrix. Under actual conditions, however, large deviations from the ideal uniform flow distribution can occur. Such nonuniform flow distribution can even occur within a single passage (in air-cooled equipment) under certain manifold configurations.

Since this report is primarily concerned with cold plates, only some of the manifold configurations applicable in cold plate design are discussed.

The two main factors, inertia and friction, determine the distribution of flow in and out of manifolds. When the inlet manifold has a constant cross section, the velocity reduction in the direction of flow leads to a conversion of velocity pressure into static pressure. The opposite occurs in the discharge manifold. On the other hand, friction causes loss of pressure along the manifold, or any flow passage. The relative magnitude of the pressure regain because of reduced velocity and the pressure loss because of friction determine whether the pressure rises or falls from the inlet end to the closed end of the manifold. If the cross section of the manifold can be changed, it is possible to size the area along the length in a manner that the two opposing factors balance each other, resulting in a uniform discharge along the length. Reference 39 gives the following expression for discharge velocity variation at distances from the dead end of the manifold shown in Figure 42.

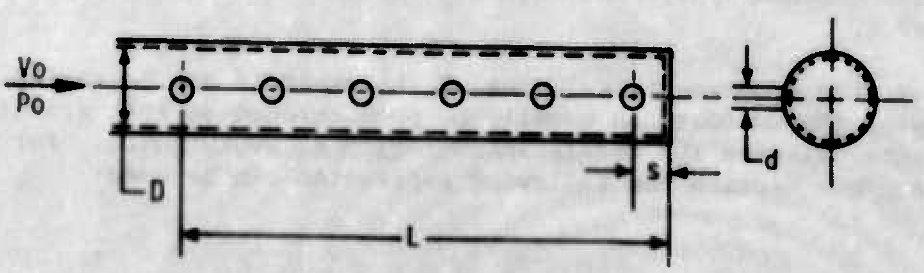

Figure 42. Manifold with Discharge Openings

$$V_i = \frac{V_o}{\sin(kR)} \cos\left(kR\frac{s}{L}\right) \tag{224}$$

where V_o = inlet velocity

L = length of manifold

R = area ratio

k = coefficient of discharge of the holes or slot

$$R = \frac{\text{Sum of areas of all discharge openings}}{\text{Cross-Sectional area of manifold}}$$

In accordance with Reference 39 for a ratio L/D=70, the friction practically cancels the deceleration regain, and the distribution of discharge along the length is practically constant. There is, however, another item of concern, and that is the area ratio. The same reference points out that for an area ratio of R=2, the variation is much greater; and, regardless of the length/diameter ratio, it is not possible to obtain a satisfactory uniformity of discharge. Even for the most favorable length ratio, L/D=70, the variation from uniformity is 7 percent of the average; and for L/D=10, the discharge rate at the inlet end is only 38.7 percent of that at the dead end. Where the area ratio is increased still further, a condition can be reached where the discharge rate at the inlet end reduces to zero, or even reverses. Friction, however, has an equalizing effect; the greater L/D, the greater the area ratio can be without causing the flow to reverse.

Sometimes it is not practical to vary the cross-sectional area of the manifold. In such a case, the distribution of the holes may be varied, or, in the case of a continuous slot, the width of the slot may be varied. Reference 38 points out that for a continuous slot with an area ratio of unity and a short manifold (L/D=10), the slot at the inlet end should be 13 percent wider than the average. At the dead end it should be 5.75 percent narrower than the average. For long manifolds (L/D=80), the required variation of slot length is so small that it can be neglected; and the slot can be made of uniform width. With area ratios larger than unity, the required variation of slot width must be much larger.

Where the cross-sectional area of the manifold can be varied along its length, the contour can usually be proportioned so that friction loss counterbalances the deceleration region at every point. For a circular cross section the following expression can be used:

$$D = (D_o + fgL) \sqrt{\frac{s}{L}} - fgs \tag{225}$$

where D = diameter at a distance, s, from the dead end, ft

D_o = diameter at the inlet end, ft

L = length of the manifold, ft

f = the friction coefficient.

When the manifold arrangements shown in Figure 43 are used, the question arises which is the best configuration to achieve the most uniform flow distribution. The same reference points out that if the entrance end of the inlet manifold is at the same side as the outlet end of the discharge manifold; then, without friction, the pressure rise from entrance or outlet end to dead end would be the same in both manifolds (disregarding volume changes). Even with friction and with different specific volumes, the pressure variation in one manifold tends to counteract that in the other manifold, providing more uniform flow distribution. An exception to this case is manifolds with very large L/D ratios where friction loss far outweighs deceleration regain. In such a case, the inlet and outlet ends should be at opposite sides, as shown with broken lines in Figure 43.

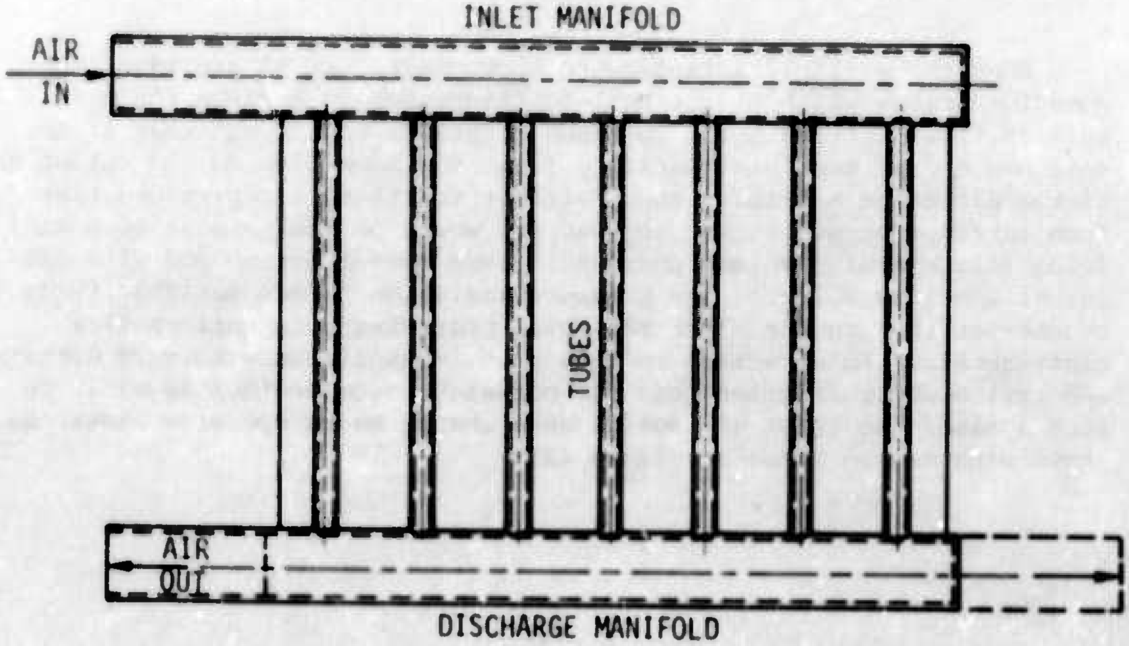

Figure 43. Possible Manifold Arrangements for a Tube Bank

SECTION XIV

THE COLD PLATE

A single fluid heat exchanger designed for removing heat from electronics equipment is called a "cold plate." Depending on the heat load and thermal requirements of the equipment, the coolant can be liquid or gas. Size, heat dissipation rate, and mounting arrangement of the electronic equipment will dictate size and configuration of the cold plate. Because the cold plate is compatible with miniaturization, high power densities and component packaging, its use in military avionics is widely accepted. In this cooling technique, heat from the active component is removed by conduction and convection.

Except for the mounting joint of the component, conduction and convection modes of heat transfer can be quite accurately predicted, which is an important item in thermal control system design. Since heat is removed from the active components by metallic conduction, this packaging technique can be used in unpressurized aircraft equipment bays without noticeable effects upon equipment thermal performance. In the case of air cooling, one of the main advantages of cold plates is to prevent the electronic equipment from having direct contact with the moisture, smoke, and dust contained in the cooling air.

The cold plate or indirect cooling also has other advantages over immersion or direct cooling, particularly when liquid coolants are used. Among these are easier accessibility for maintenance, less possibility of fouling equipment with the coolant, less handling of coolants since the coolants can be contained in a completely closed system, and the ability to use coolants that have good thermal properties.

The cold plates can be divided into two general categories; liquid- and air-cooled cold plates. The most significant difference between these two categories is the way heat is transferred into the coolant stream. While in air-cooled cold plates, a large surface area is exposed to the cooling air stream, in the case of liquid cooling the liquid will be confined in a rather small conduit. This means that practically all the heat generated by the equipment must be transferred through the plate by conduction to the liquid conduit. Particularly high concentrated heat loads might dictate different arrangements of the flow passages.

The air-cooled cold plates, because of the small heat-transfer coefficients, must be provided with large surface areas. These can be achieved with finned surfaces. Both conduction and convection modes of heat transfer, therefore, occur throughout the entire heat-flow path.

In any cold-plate cooling system, the electronic equipment waste heat, dissipated on the mounting surface of the plate, must be transferred by convection to the coolant stream circulated through the passage of the cold plate. The two main equations involved in cold plate design are (1) the rate equation

$$Q = hA\ (\Delta t)_m \tag{226}$$

and (2) the energy equation

$$Q = wc_p\ \left(t_o - t_i\right) \tag{227}$$

where

$$\Delta t_m = \frac{\Delta t_1 - \Delta t_2}{\ln\left(\Delta t_1 / \Delta t_2\right)} \tag{228}$$

h = heat transfer coefficient, Btu/hr ft^2 °F

A = heat transfer surface area, ft^2

Δt_m = log mean temperature difference between the plate and coolant, °F

Δt_1 = temperature difference between fluid and plate at one end, °F

Δt_2 = temperature difference between fluid and plate at the other end, °F.

In most cases, however, the arithmetic average temperature difference can be used for preliminary analysis.

Figure 44 shows a simplified outline of a cold plate with its temperature profile.

It can be seen from equations 226 and 227 that heat dissipated by the plate must equal the heat absorbed by the coolant, or

$$Q = hA\ (\Delta t)_m = \dot{w}c_p\ \left(t_{out} - t_{in}\right) \tag{229}$$

and

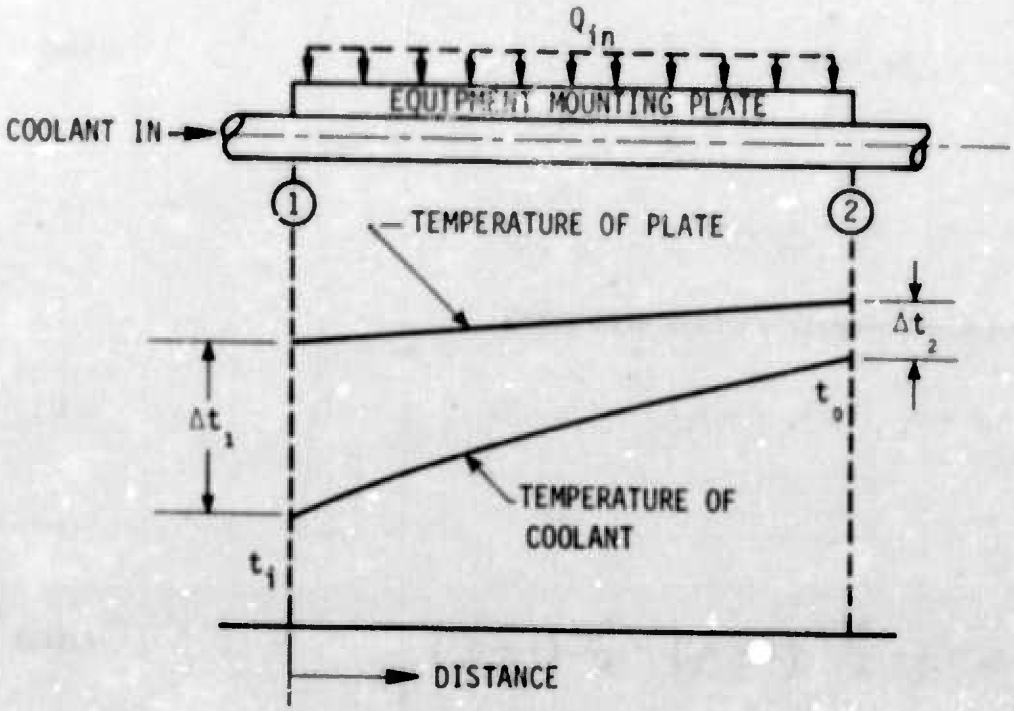

Figure 44. Outline of a Cold Plate and Its Temperature Profile

$$\Delta t_m = \frac{\dot{w} c_p}{hA} \left(t_{out} - t_{in} \right) \quad (229a)$$

If the heat dissipation rate and coolant inlet temperature are known, the mean temperature of the plate can be determined from equation 229.

For an air cooled cold plate with a finned core, the overall surface efficiency, η_o, must be introduced into the rate equation

$$Q = \eta_o \, Ah \, (\Delta t)_m \quad (230)$$

where

$$A = A_b + A_f + A_c \text{ and}$$

η_o = weighted overall surface efficiency

$$\eta_o A = A_b + \eta_f A_f + \eta_c A_c \quad (231)$$

and

$$\eta_o = 1 - \frac{A_f}{A} \left(1 - \eta_f \right) - \frac{A_c}{A} \left(1 - \eta_c \right) \quad (231a)$$

A = total heat transfer surface area

A_b = mounting base surface area

A_f = fin surface area

A_c = surface area of cover plate

η_f = fin efficiency

η_c = efficiency of cover plate

The efficiency of the mounting plate is assumed to be unity.

The forced-convection heat-transfer coefficients depend on flow regimes and types of coolants, and can vary within a very wide range. The coolant flow rate, however, must be based on equipment thermal requirements, pressure drop, and allowable acoustic noise level, and can also vary within a wide range. From the heat-transfer standpoint, there is an advantage in selecting the turbulent flow regime which improves the convection heat-transfer coefficient. Pressure drop requirements and noise level, however, will impose limitations in the selection of too high Reynolds numbers.

In the case of rectangular cross sections, the diameter, D, in both the Reynolds and Nusselt expressions, must be replaced by the hydraulic diameter, D_h,

$$D_h = 4\,\frac{\text{Flow Area}}{\text{Perimeter}} \tag{232}$$

The transition Reynolds number, $VD_h\rho/\mu$, is also found to be approximately 2300, as for circular ducts.

It must be pointed out that all the equations are derived for fully-developed flow which will never occur in an actual cold plate. When heat-transfer coefficients for ducts are determined, two other simplifications are introduced, i.e., constant surface temperature, and constant heat rate per unit of duct length. These simplifications will never occur in an actual cold plate. It should be further emphasized that a high Reynolds number is not a guaranty of a high heat-transfer coefficient. In addition to high velocity, a small diameter is also required; this condition is known as the Holland-Tunnel effect.

More detailed discussions about heat transfer from finned surfaces can be found in Section VII.

SECTION XV

DESCRIPTION OF TEST EQUIPMENT AND APPARATUS

a. Liquid-Cooled Cold Plates

Liquid-cooled cold plates of three different designs were fabricated and tested. Cold Plate Nos. 1 and 2 were made of aluminum (6061-T6), while Cold Plate No. 3 was made of copper. Power transistors and resistors were used as the heat load, and the thermal tests were performed on a hydraulic test bench equipped with a gear pump, a water-cooled heat exchanger, flow meters, and flow control valves. The coolant used in the system was a solution of approximately 60-percent ethylene glycol and 40-percent water. The thermal tests were performed at different electrical power dissipation rates from the electronic components and different coolant flow rates. Temperature measurements were performed using #30-gage copper-constantan thermocouples inserted and secured into small holes drilled in the mounting plate and components. The temperature readings were taken by multichannel recorders. Thermal performance of the cold plates was determined analytically by computer techniques (R-C networks), then compared with actual test results.

1. Liquid-Cooled Cold Plate No. 1

Figure 45 shows the experimental liquid-cooled Cold Plate No. 1. Two of the power transistors were of the type 2N3846, five power transistors of the type 2N1724, and four resistors of the type RER 65. The electronic components were mounted to the cold plate with bolt torques recommended by the manufacturers. Figure 46 shows the mounting arrangement of a power transistor.

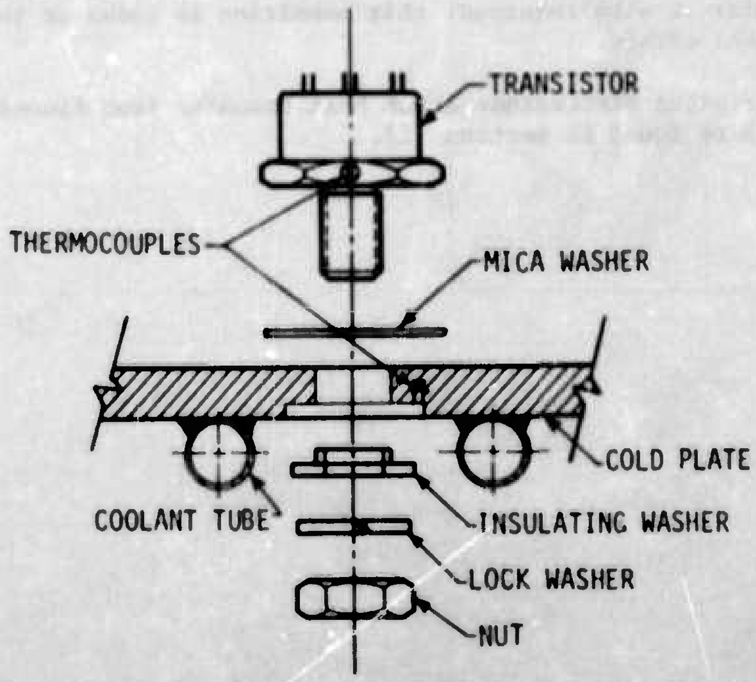

Figure 46. Transistor Mounting on Liquid-Cooled Cold Plate No. 1

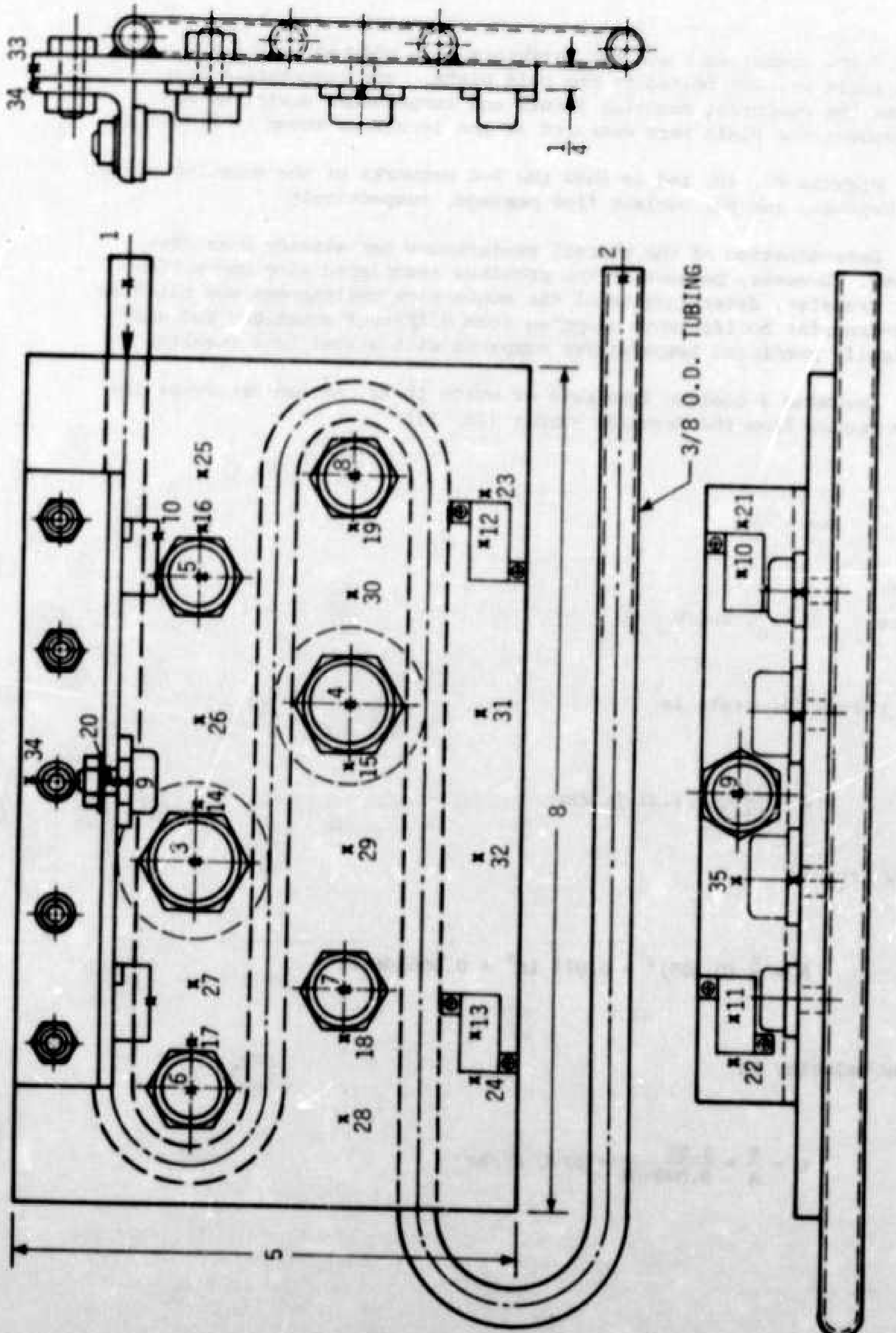

Figure 45. Liquid-Cooled Cold Plate No. 1

One of the transistors and two resistors were mounted on a 1 x 1 x 1/8 inch angle bracket bolted to the cold plate. The temperature drop across the component mounting joints and temperature distribution throughout the plate were measured at the locations shown in Figure 45.

Figures 47, 48, and 49 show the R-C networks of the mounting plate, the bracket, and the coolant flow passage, respectively.

Determination of the thermal resistances has already been discussed. However, because of the problems associated with convection heat transfer, determination of the convection resistances was based on heat-transfer coefficients computed from different equations and analytically predicted temperatures compared with actual test results.

Assuming a coolant flow rate of w=100 lb/hr, we can determine the flow regime from the Reynolds number (Eq. 12)

$$Re = \frac{DU\rho}{\mu}$$

where $U = \frac{V}{A}$, and $V = \frac{w}{\rho}$

The volume flow rate is

$$V = \frac{100}{66.3} = 1.51 \text{ ft}^3/\text{hr}$$

Flow area is

$$A = \frac{\pi}{4} (0.305)^2 = 0.073 \text{ in}^2 = 0.000506 \text{ ft}^2$$

Flow velocity is

$$U = \frac{V}{A} = \frac{1.51}{0.000506} = 2980 \text{ ft/hr}$$

or

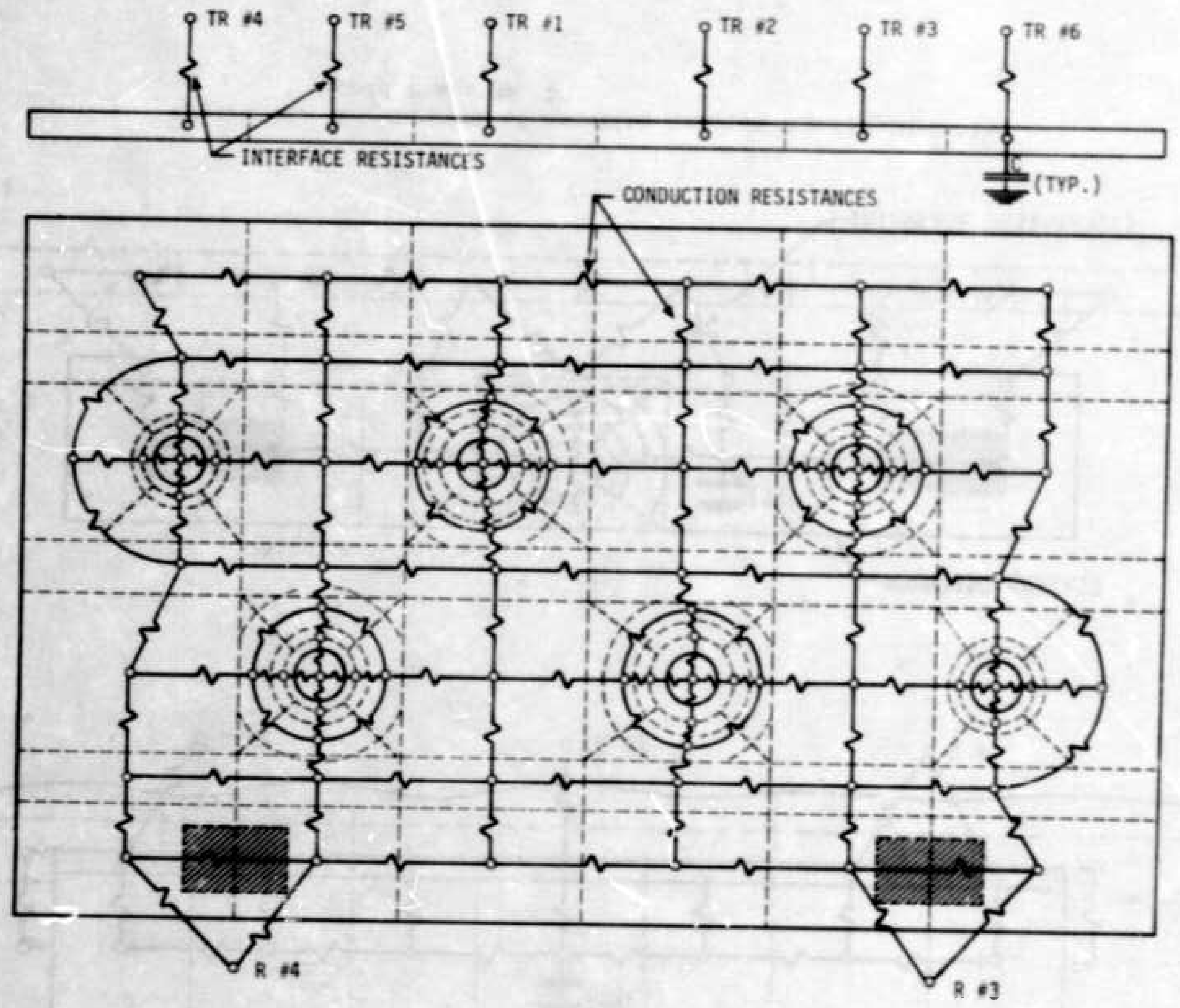

Figure 47. R-C Network of Liquid-Cooled Cold Plate No. 1

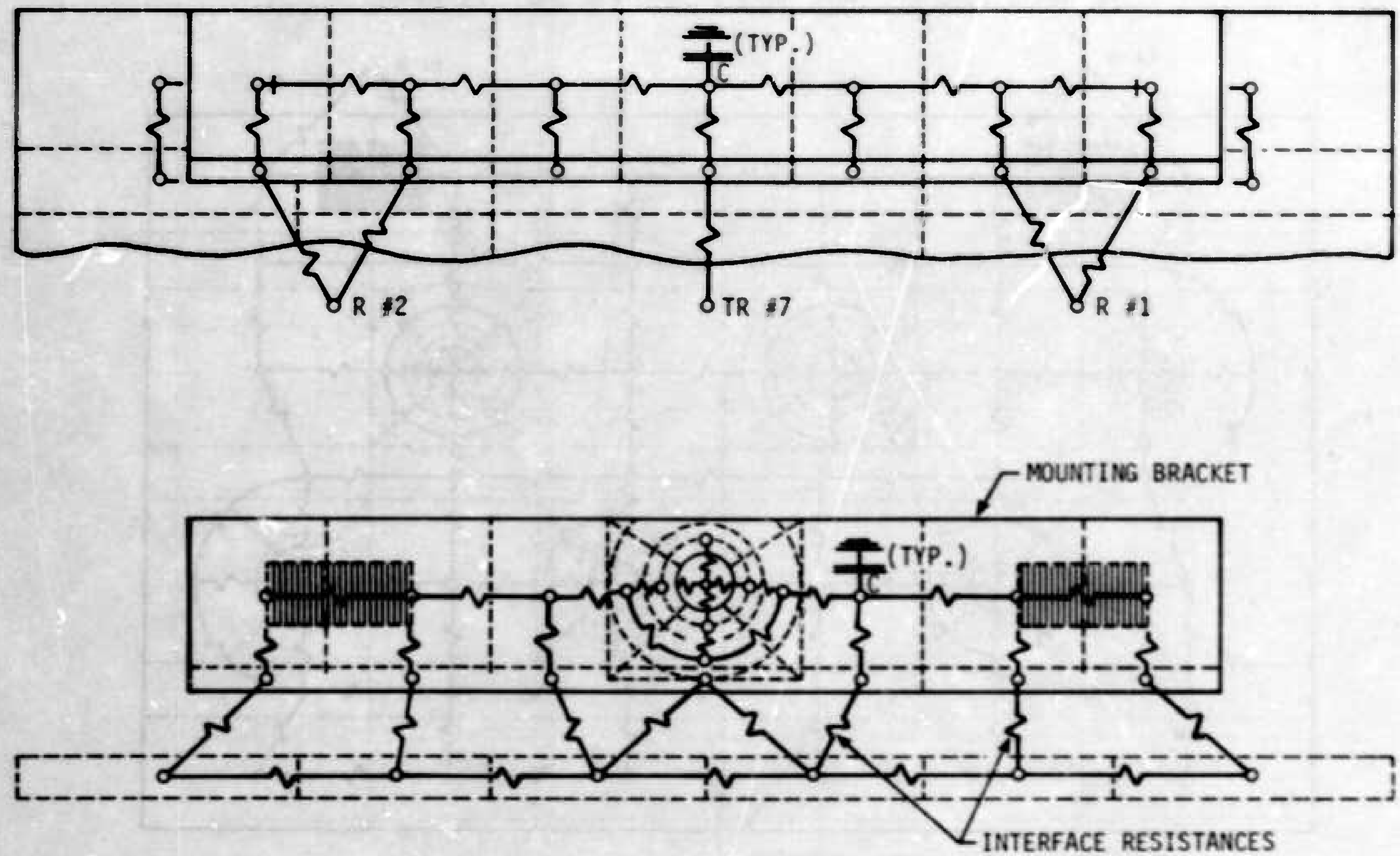

Figure 48. R-C Network of Mounting Bracket for Liquid-Cooled Cold Plate No. 1

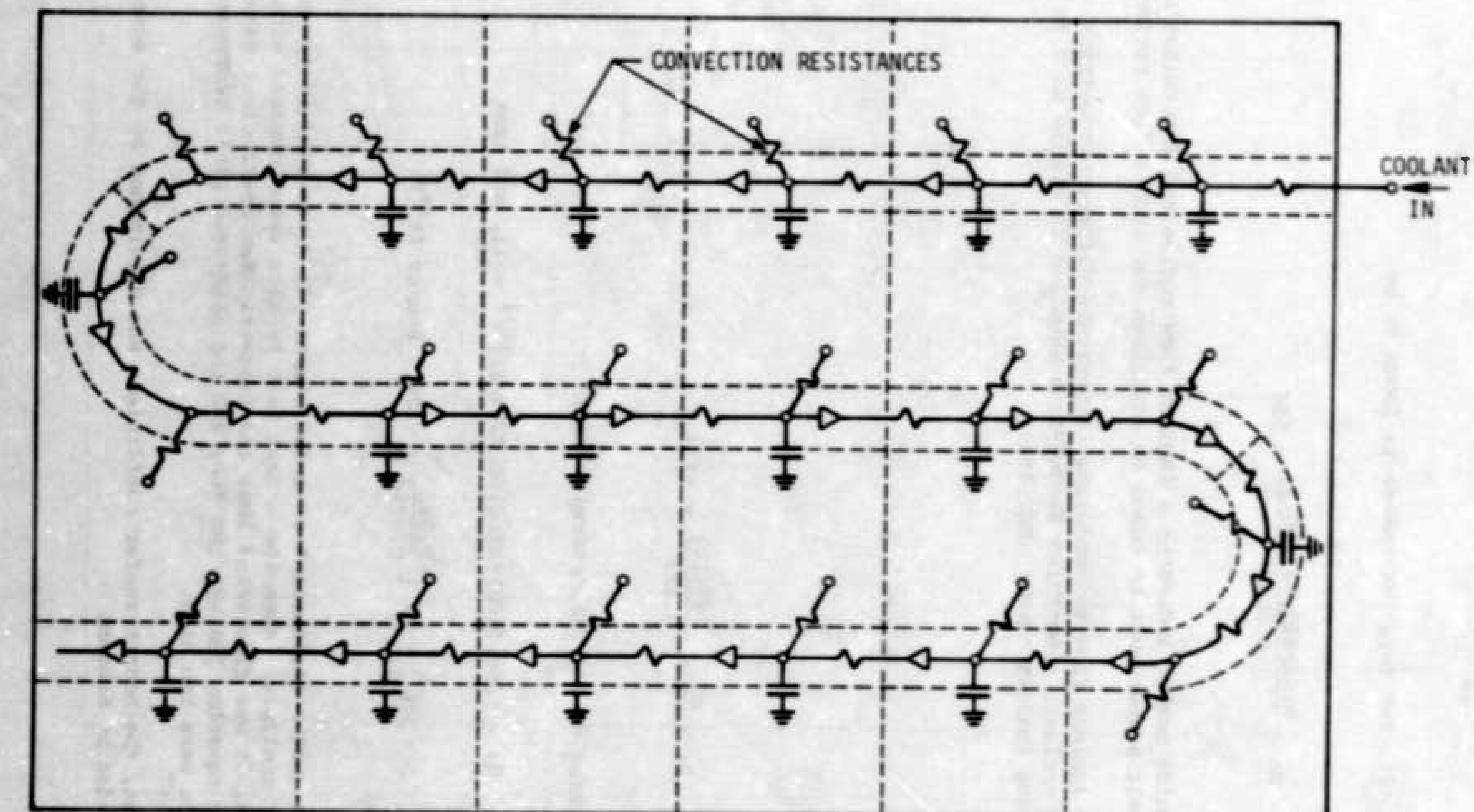

Figure 49. R-C Network of Coolant Flow Passage for Liquid-Cooled Cold Plate No. 1

$U = 0.83$ ft/sec

Consequently, the Reynolds number is found to be

$$Re = \frac{0.0254(0.83)(66.3)}{0.0028} = 500$$

The Reynolds number indicates a laminar flow regime and determination of the Nusselt number must be based on equations for such a flow regime.

For laminar flow and moderate temperature differences between the wall and coolant, a modified Sieder-Tate equation is widely used to determine the Nusselt number (Eq. 18a)

$$Nu = 1.86 \left(Re \cdot Pr \cdot \frac{d}{L}\right)^{1/3}$$

where

$$Pr = \frac{c\mu}{k} = \frac{.745(10)}{0.223} = 33.4$$

Substituting values, we determine that

$$Nu = 1.86[(500)(33.4)(0.0254/2)]^{1/3} = 11, \text{ and that}$$

$$h = Nu\,\frac{k}{d} = 11\left(\frac{0.223}{0.0254}\right) = 96.5 \text{ Btu/hr ft}^{2}\,^{\circ}\text{F}$$

A heat-transfer coefficient of h=100 Btu/hr ft^{2}°F was used in the preliminary analysis. When the actual test results were compared with analysis, it was discovered that the heat-transfer coefficient determined by equation 18a was too low, and the predicted plate temperatures, therefore were too high.

Next, the heat-transfer coefficient was determined by the equation recommended by McAdams

$$Nu = 6.2 \left(\frac{\dot{w}c_p}{kL} \right)^{0.2} \tag{233}$$

Substituting values, we obtain

$$Nu = 6.2 \left[\frac{100(0.745)}{0.223(2)} \right]^{0.2} = 17.3$$

$$h = N \frac{k}{d} = 17.3 \frac{0.223}{0.0254} \cong 150 \text{ Btu/hr ft}^2{}^\circ\text{F}$$

When this value was used in determining the convection resistances, a much closer agreement between analysis and actual test data was achieved. It should be noted that Equation 233 is valid only if $\dot{w}c_p/kL$ exceeds 30, and the Reynolds number is less than 2100.

Figure 50 shows the comparison between test results and analysis of temperature distribution across the plate when heat-transfer coefficients of h=100 and 150 Btu/hr ft^2°F were used in determining the convection resistances. Only transistors #1 and #2 were energized: 75 watts each. The errors introduced in temperature predictions, by selecting heat-transfer coefficients obtained from equations which do not apply to a specific fluid or specific test conditions, can be clearly seen.

A total of fourteen different tests were performed on Cold Plate No. 1. Twelve were steady-state tests, while two were transient tests. To reduce environmental effects upon thermal performance of the cold plate and to simplify analysis, all the tests were performed with the plate insulated (approximately 1-1/2 in. of fiberglass insulation). Mica washers and Dow Corning 340 silicone heat-sink compound was used on all transistor mounting joints. The heat-sink compound was also applied to the resistor and bracket mounting joints. Only case temperatures of the transistors were measured; the junction temperatures were determined from data published by the manufacturer. For example, the 2N3846 transistor maximum junction-to-case thermal resistance is given as:

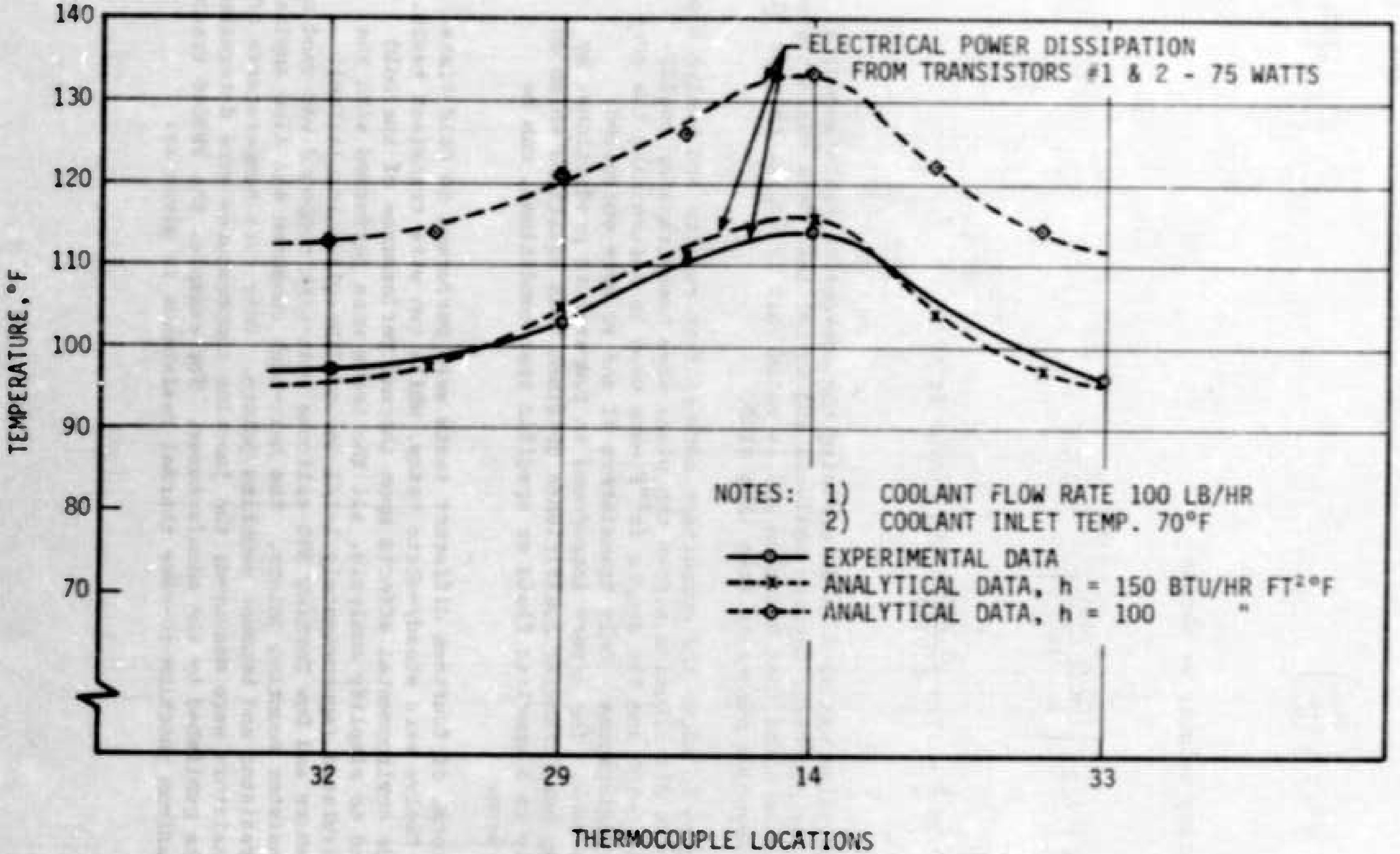

Figure 50. Temperature Distribution of Liquid-Cooled Cold Plate No. 1 (Effects of Convection Heat-Transfer Coefficient)

$$R_{jc} = 0.5°C/watt,$$

and that of the 2N1724 transistor is:

$$R_{jc} = 1.5°C/watt.$$

If the case temperature is known (it can be easily measured), the junction temperature can be determined from Equation 3:

$$t_j = t_c + PR_{j-c}$$

where t_j = the junction temperature of the transistor

t_c = the case temperature of the transistor

P = the electric power dissipation, watts.

Table 8 summarizes all the test conditions. Temperature readings of the thermocouples installed on the plate and electronic components (as shown in Figure 45) are contained in Appendix A.

Figures 51, 52, 53, and 54 show temperature distribution of the plate at the test conditions indicated. Comparison between experimental and analytical results is also shown by plotting the analytically predicted temperatures along the same section of the plate. As can be seen, a good agreement between the predicted and measured results was achieved. The maximum deviation amounts to approximately 5°F which can be considered small. The results indicate that the R-C network computer-analysis technique can provide accurate thermal-performance prediction of cold plates, if sufficiently accurate input data are provided.

Figure 55 shows case temperatures of some of the transistors and resistors as a function of coolant flow rate. Electrical power dissipation from the components was maintained constant throughout the tests. The results show decreased component temperatures with increased coolant flow rates, which is self-explanatory (increased convection heat-transfer coefficients). The large temperature difference between the bracket and plate-mounted components is apparent, and shows the disadvantages of bracket mounting. Even though Transistor #7 dissipated half the electric power that Transistor #5 dissipated, the temperature of Transistor #7 was approximately 40°F higher.

Table 8. Test Conditions of Liquid-Cooled Cold Plate No. 1

TEST NO.	COOLANT FLOW RATE (lb/hr)	ELECTRICAL POWER INPUT TO TRANSISTORS (WATTS)							ELECTRICAL POWER INPUT TO RESISTORS (WATTS)			
		TR#1*	TR#2	TR#3	TR#4	TR#5	TR#6	TR#7	R#1**	R#2	R#3	R#4
1	100	25	25									
2	100	50	50									
3	100	75	75									
4	100			20	20	20	20	20				
5	100			30	30	30	30	20				
6	100			40	40	40	40	20				
7	100	25	25	20	20	20	20	20	13	13	13	13
8	100	50	50	30	30	30	30	20	13	13	13	13
9	100	50	50	40	40	40	40	20	13	13	13	13
10	50	50	50	40	40	40	40	20	13	13	13	13
11	100	50	50	40	40	40	40	20	13	13	13	13
12	200	50	50	40	40	40	40	20	13	13	13	13
13	100	50	50	40	40	40	40	20	13	13	13	13
		TRANSIENT TEST, TR #1 & 2 10 MIN. ON & 10 MIN. OFF										
14	100	50	50	40	40	40	40	20	13	13	13	13
		TRANSIENT TEST, ALL COMPONENTS 10 MIN. ON & 10 MIN. OFF										

* TR - TRANSISTORS

** R - RESISTORS

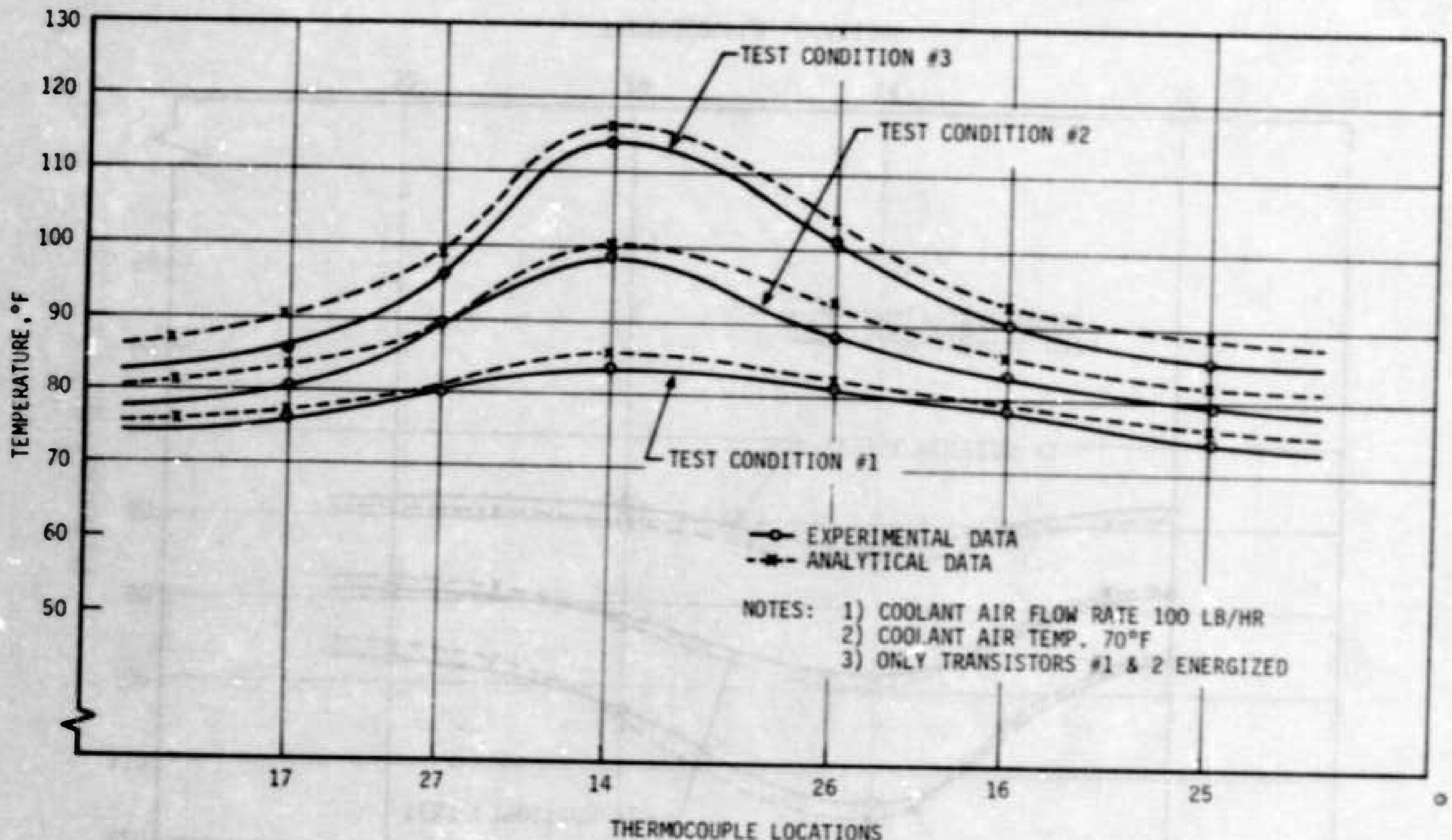

Figure 51. Temperature Distribution of Liquid-Cooled Cold Plate No. 1 at Test Condition Nos. 1, 2, and 3 (TC 17-25)

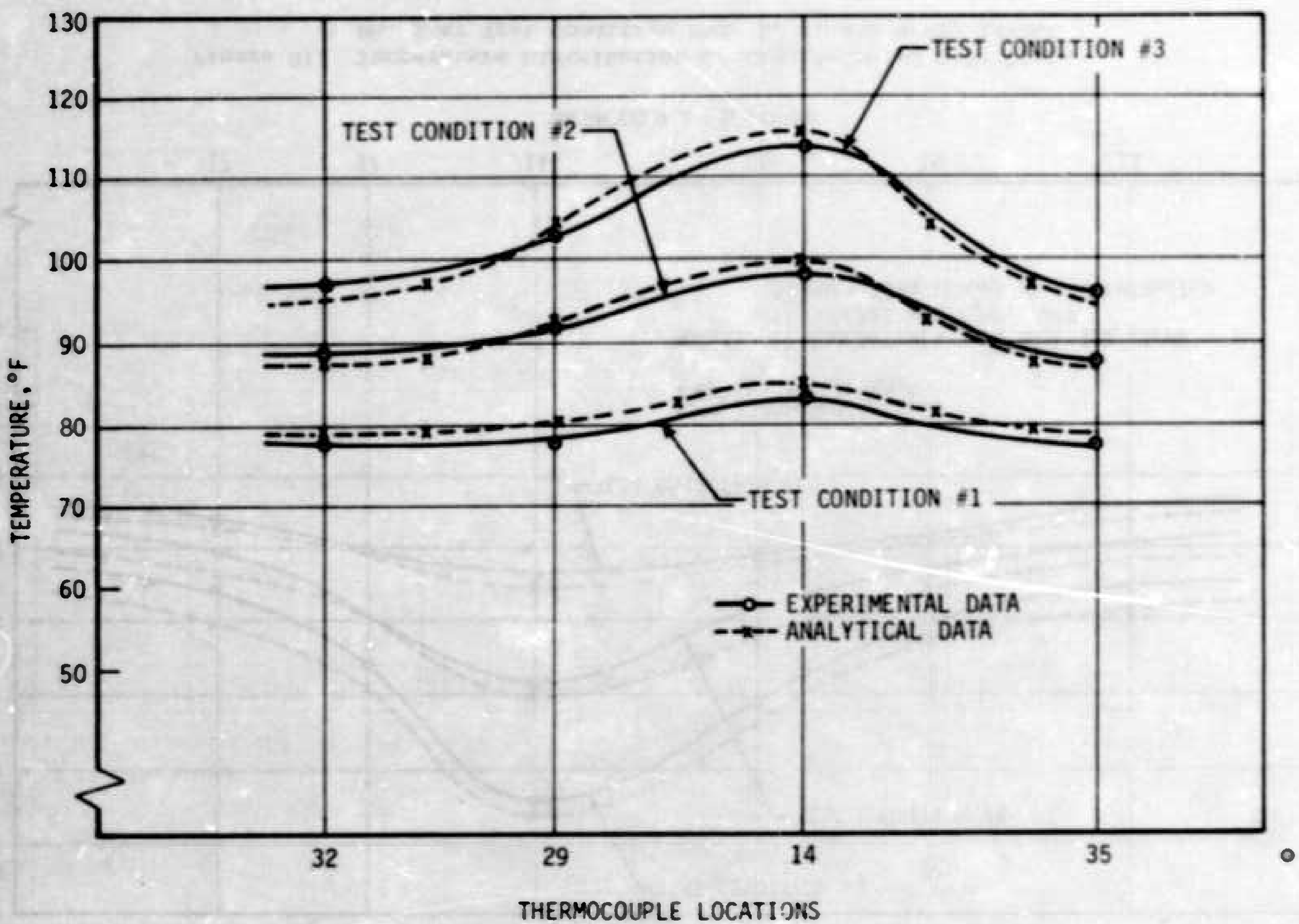

Figure 52. Temperature Distribution of Liquid-Cooled Cold Plate No. 1 at Test Condition Nos. 1, 2, and 3 (TC 32-35)

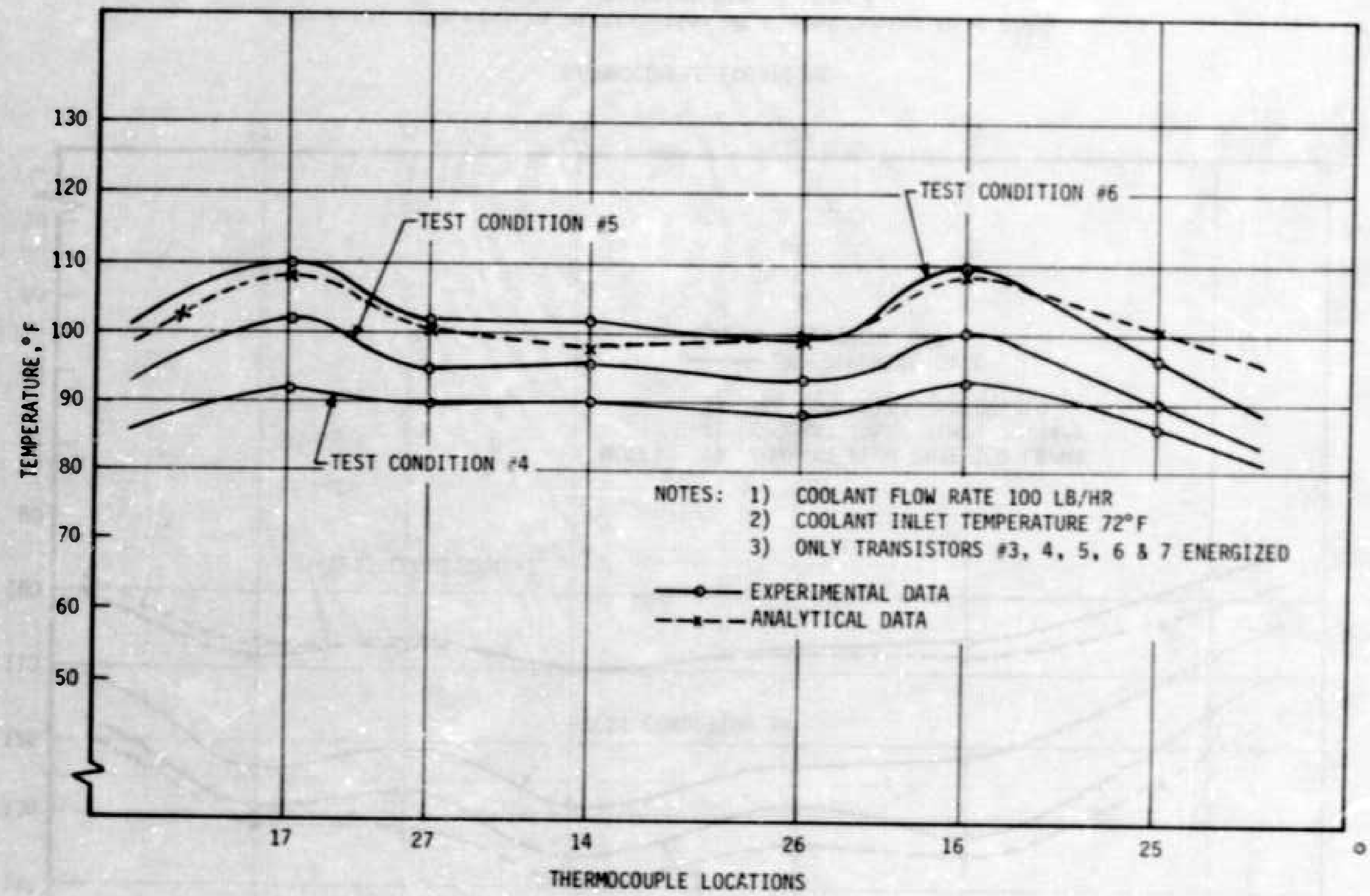

Figure 53. Temperature Distribution of Liquid-Cooled Cold Plate No. 1 at Test Condition Nos. 4 thru 6

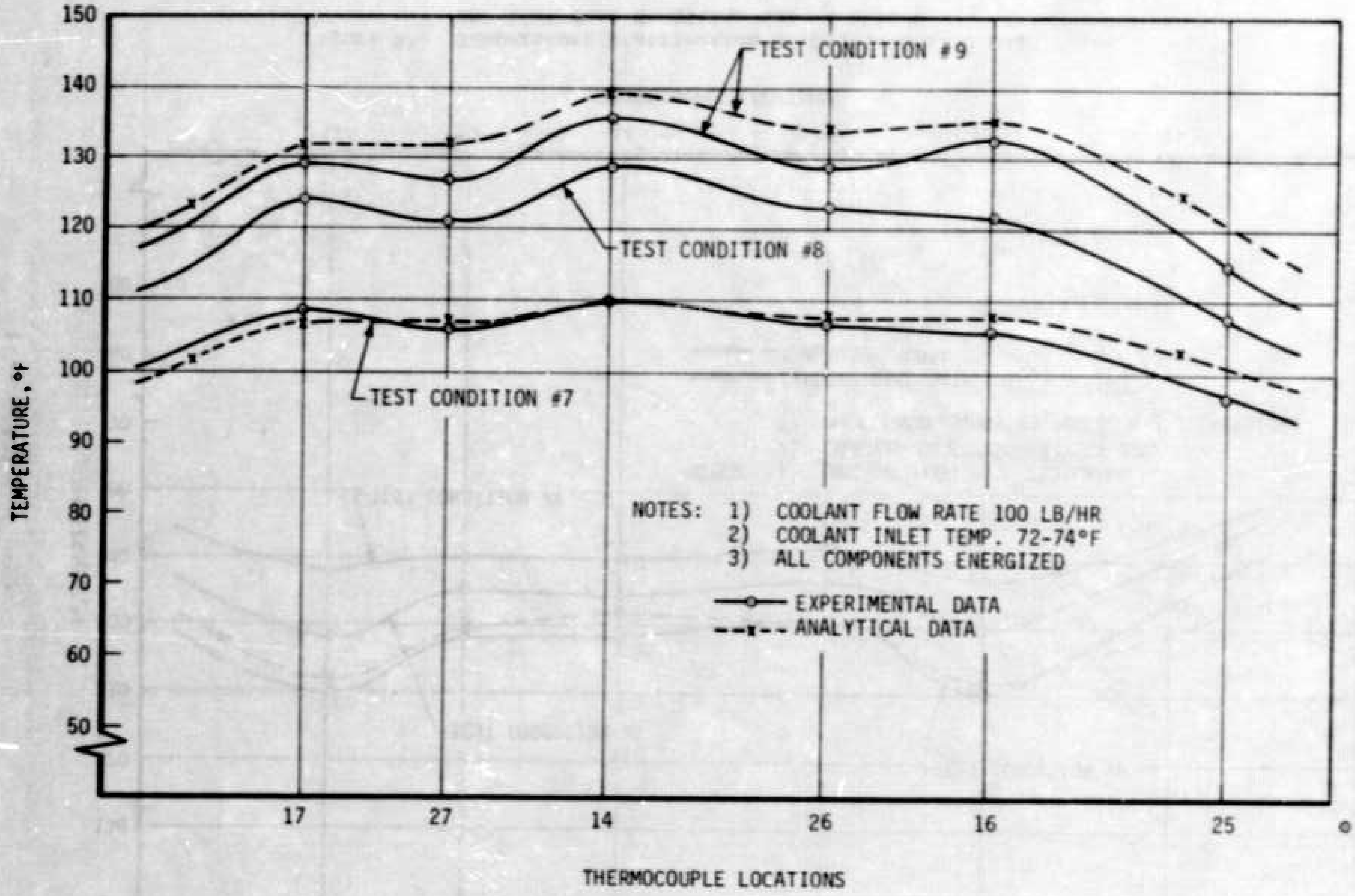

Figure 54. Temperature Distribution of Liquid-Cooled Cold Plate No. 1 at Test Condition Nos. 7 thru 9

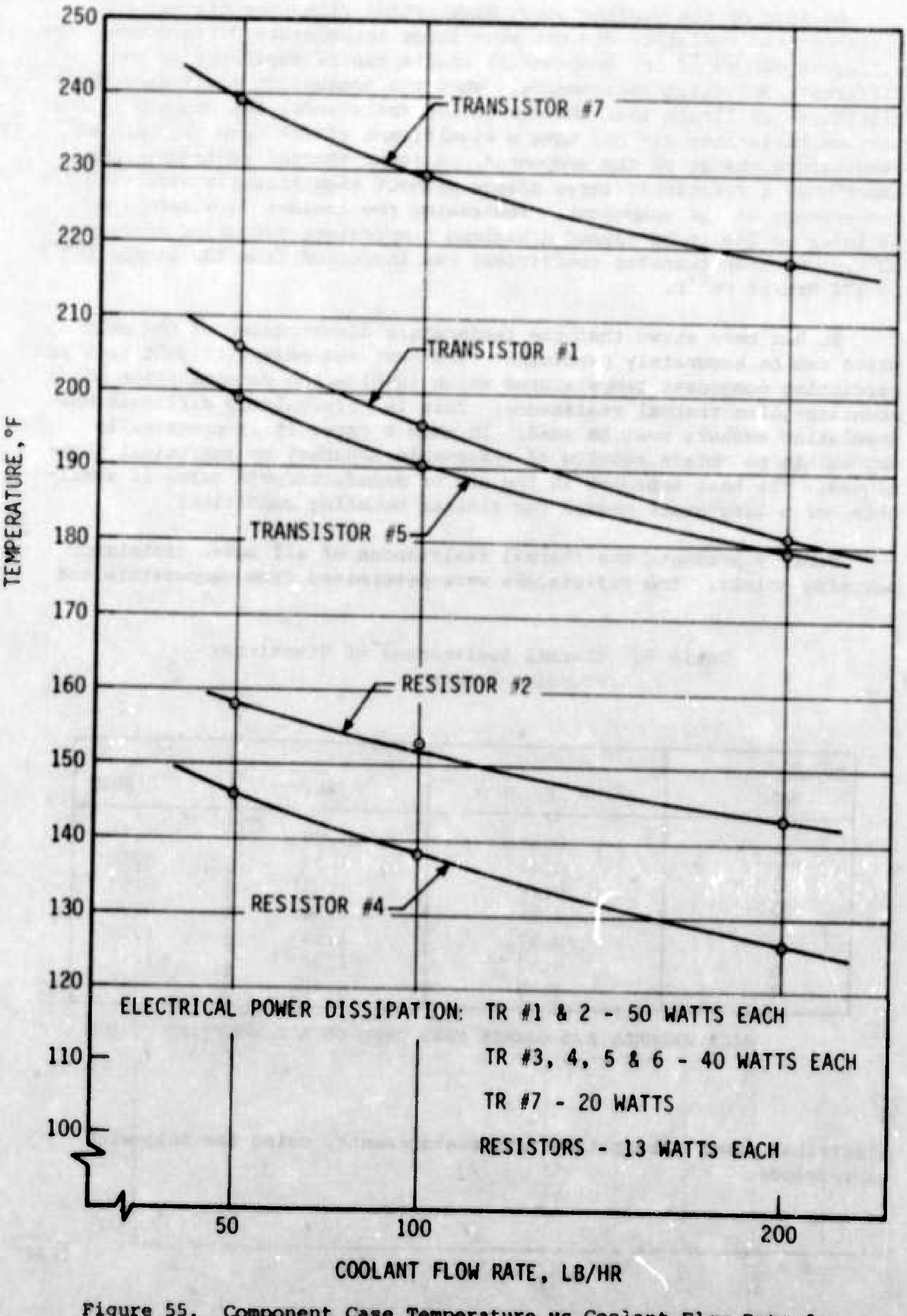

Figure 55. Component Case Temperature vs Coolant Flow Rate for Liquid-Cooled Cold Plate No. 1

Because of the smaller power dissipation rate, the bracket and plate-mounted resistors did not show large temperature differences. The different slopes of the temperature charts can be explained by the different conduction resistances. When the conduction resistance was significantly larger than the convection resistance, the changes in convection resistance did not have a significant effect upon the rate of temperature change of the component. A lower thermal resistance can experience a relatively large change without significantly affecting the temperature of the component. Increasing the coolant flow rate from 50 lb/hr to 200 lb/hr caused a maximum temperature reduction of only 20°F. The heat-transfer coefficient was increased from 132 Btu/hr ft^2°F to 174 Btu/hr ft^2°F.

It has been shown that the temperature distribution of the cold plate can be accurately predicted. The next and most difficult task is predicting component temperatures which involve the determination of mounting-joint thermal resistance. This is particularly difficult when insulating washers must be used. In such a case, it is practically impossible to obtain results of reasonable accuracy by analytical techniques. The best approach is the use of manufacturer's data, if available, or a literature search for similar mounting conditions.

Table 9 presents the thermal resistances of all seven transistor mounting joints. The resistances were determined from temperature and

Table 9. Thermal Resistan es of Transistor Mounting Joints

TRANSISTOR NO.	HR °F/BTU	°F/WATT	°C/WATT
1	0.38	1.29	0.72
2	0.41	1.39	0.78
3	0.48	1.63	0.90
4	0.51	1.74	0.96
5	0.57	1.94	1.10
6	0.57	1.94	1.10
7	1.30	4.40	2.45

MICA WASHERS AND GREASE WERE USED ON ALL MOUNTING JOINTS

electrical power dissipation rate measurements, using the following expression:

$$R = \frac{\Delta t}{Q} \tag{234}$$

where Δt = the temperature differential between the transistor case and mounting surface of the plate, °F or °C

Q = the electrical power dissipation by the transistor, watts.

As already indicated, mica washers and Dow Corning 340 silicone heat-sink compound was used on all mounting joints. Regardless of the condition that the same mounting techniques was used for all similar transistors, there was a difference in thermal resistances. A particularly large resistance was observed at the Transistor #7 mounting joint. This condition was probably caused by the mounting bracket which was made of thinner material with an unfinished surface. The mica washers were not of the same thickness. This condition could have caused variations in the joint thermal resistance. The different electrical power dissipation of each of the transistors could have been another cause. It is the characteristic of a transistor that a temperature increase causes a current increase. It is obvious that transistors provided with larger studs and mounting surfaces will have lower resistances. These are the reasons why the mounting-joint thermal resistances of Transistors #1 and #2 were lower.

Table 10 presents the thermal resistances of the resistor mounting joints, determined by procedures similar to those used for transistors. No electrical isolation was used, and, because of the small fastener size, the mounting torque was not controlled. Heat-sink compound was applied to all mounting surfaces. Variations in mounting-joint thermal resistances (maximum value of approximately 30%) could have been caused by differences in mounting torque, surface conditions, and the application of heat-sink compound.

Table 10. Thermal Resistances of Resistor Mounting Joints

RESISTOR NO.	HR °F/BTU	°F/WATT	°C/WATT
1	0.27	0.92	0.52
2	0.23	0.77	0.42
3	0.25	0.85	0.47
4	0.29	1.00	0.55

DOW CORNING 340 SILICONE HEAT-SINK COMPOUND WAS USED ON ALL MOUNTING JOINTS

Since reliability and performance characteristics of electronic equipment (particularly semiconductor devices) depend on temperature, it is important to determine temperature at the most critical location; this at the junction for transistors. Table 11 presents the junction temperatures of all seven transistors. These temperatures were obtained from test conditions Nos. 10, 11, and 12.

Table 11. Computed Transistor Junction Temperatures

TEST NO.	JUNCTION TEMPERATURE OF TRANSISTORS, °C						
	TR #1	TR #2	TR #3	TR #4	TR #5	TR #6	TR #7
10	121.5	122	153.5	153.5	153.5	154	145
11	118	115	147	148.5	148	146	140
12	107.5	106.5	142	143	141.5	141	134

As can be concluded from the table, the junction temperatures of all of the transistors were within safe operating limits (below 175°C). However, when high equipment reliability is a requirement, power dissipation from Transistors #3, 4, 5, 6, and 7 must be reduced; or the cold plate must be redesigned to provide smaller resistances in the heat-flow path. Another conclusion can be drawn from the data: a significant increase in coolant flow rate (400%) will cause a small reduction in junction temperature. This conclusion can be deduced from the large conduction resistance, as compared to convection resistance. Even though a large change in convection heat transfer takes place, its change will not greatly affect the total resistance.

To obtain some idea of the time lag of such a cold plate, two transient tests were performed by stepwise electrical power input changes. Figure 56 shows a condition when Transistors #1 and #2 were turned on and off within a 20-minute period (10 minutes on and 10 minutes off). Figure 57 shows condition when all the electrical power was turned on and off within a 20-minute period (10 minutes on and 10 minutes off). Because of the high heat-transfer coefficient and low thermal capacity of the cold plate, the rate of temperature change of the components was quite rapid. Such conditions, when repeated more often, will affect equipment reliability. The rate of temperature change can be retarded by increasing the thermal mass of the cold plate.

The correlations between analytical and experimental results indicate an important item. When the cold plate is divided into nodes, care must be exercised in selecting the proper size of the nodes, particularly around the locations of the concentrated heat loads. Figure 58 shows the preliminary R-C network of the cold plate, and Figure 59 shows the comparison between analytical and experimental temperature distribution. The figure shows the trend in temperature increase around the areas of concentrated heat loads. The crude nodes around the concentrated heat loads did not represent the proper heat-flow path causing the errors in temperature distribution.

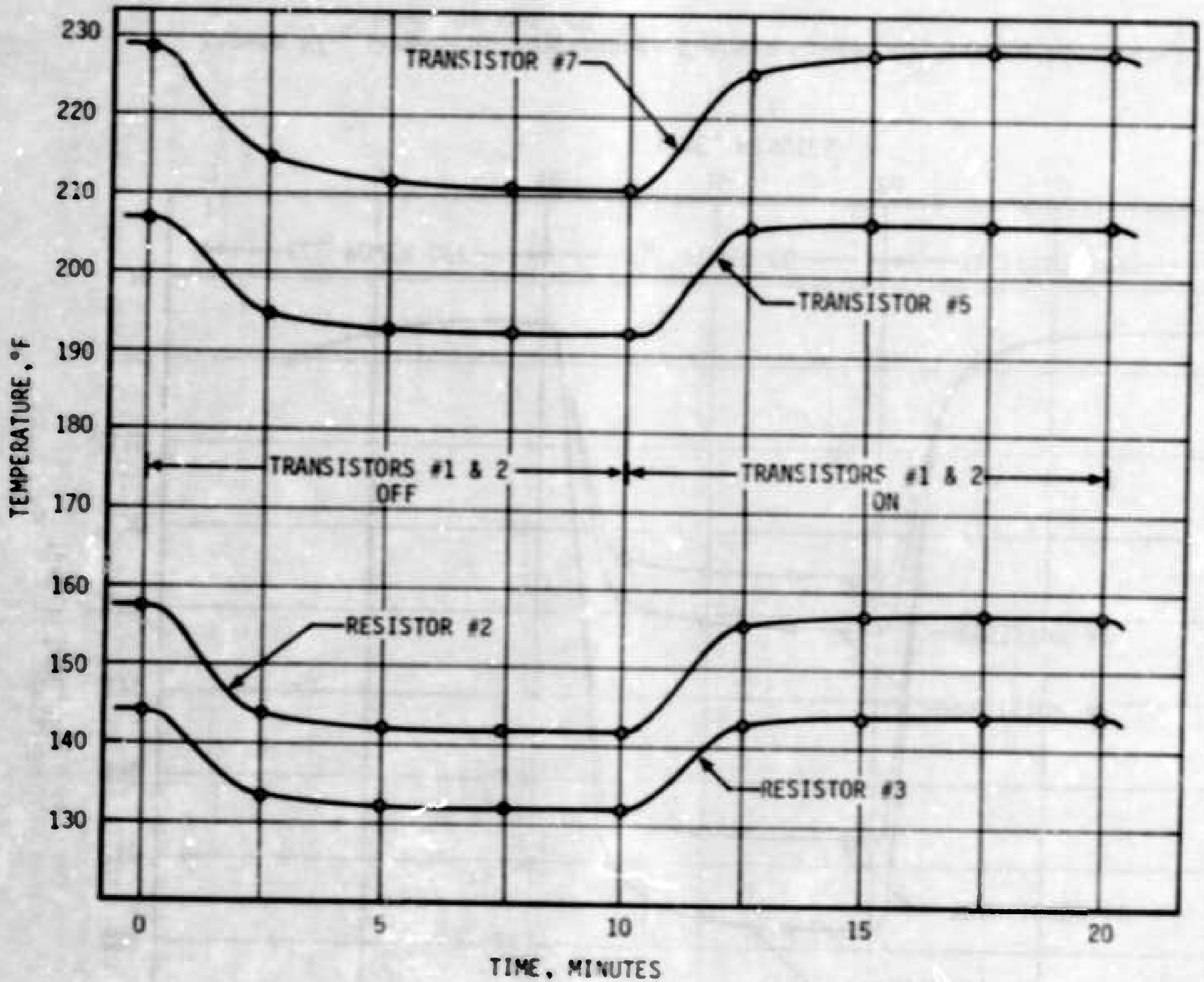

Figure 56. Component Temperature Changes Caused by Heat-Load Changes

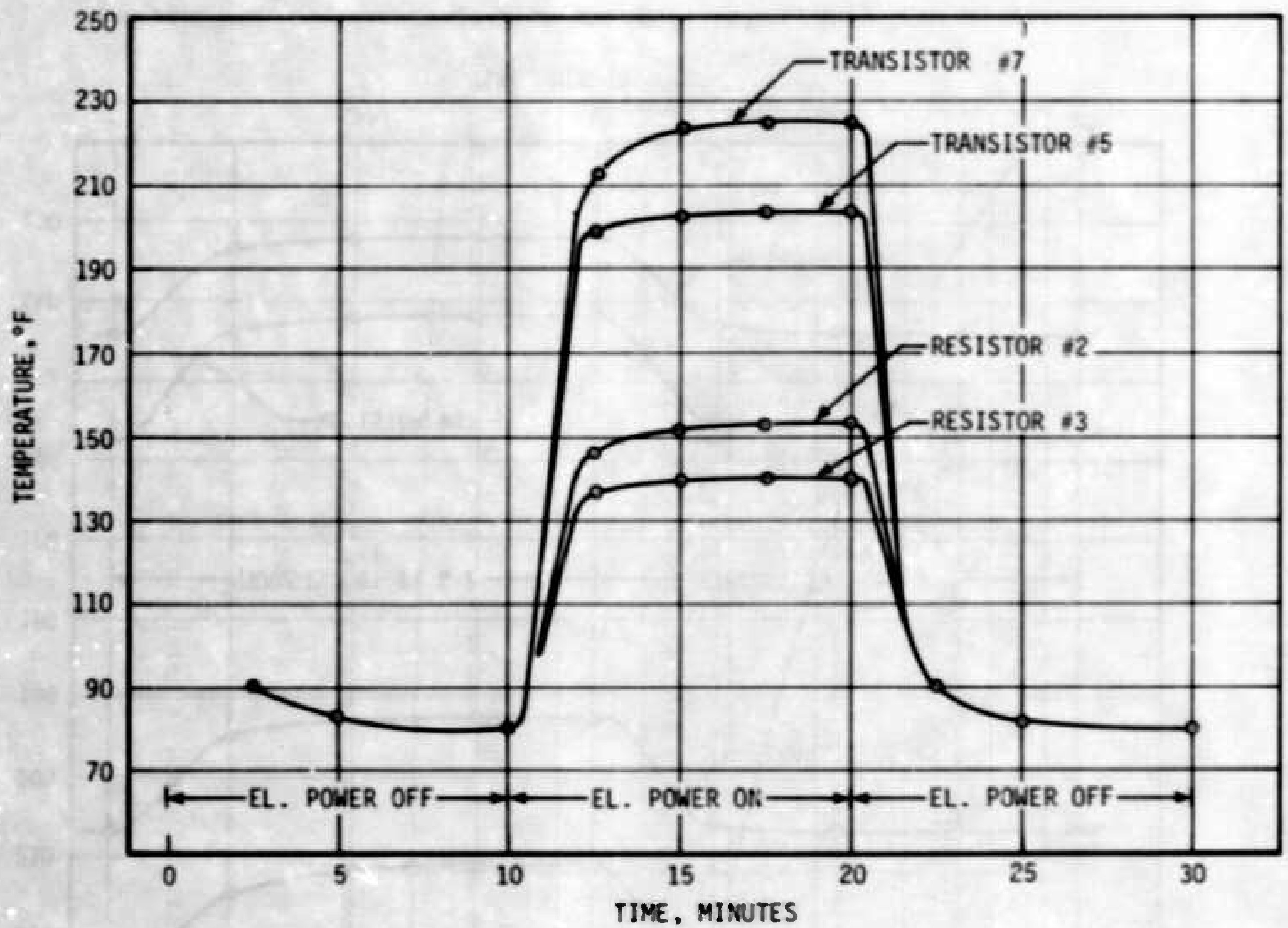

Figure 57. Component Temperature Changes Caused by Turning Electrical Power On and Off

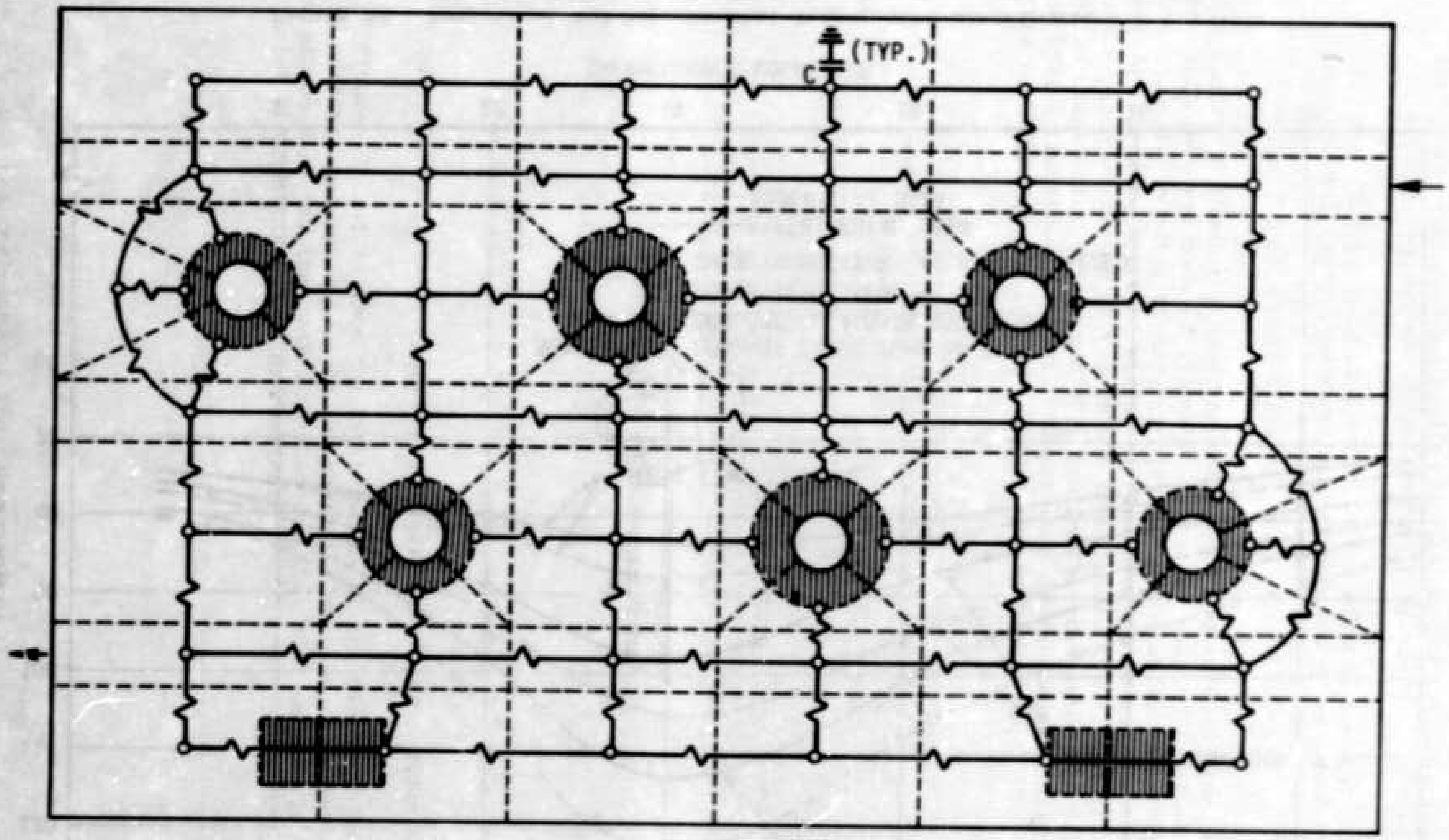

Figure 58. Simplified R-C Network of Liquid-Cooled Cold Plate No. 1 (Preliminary)

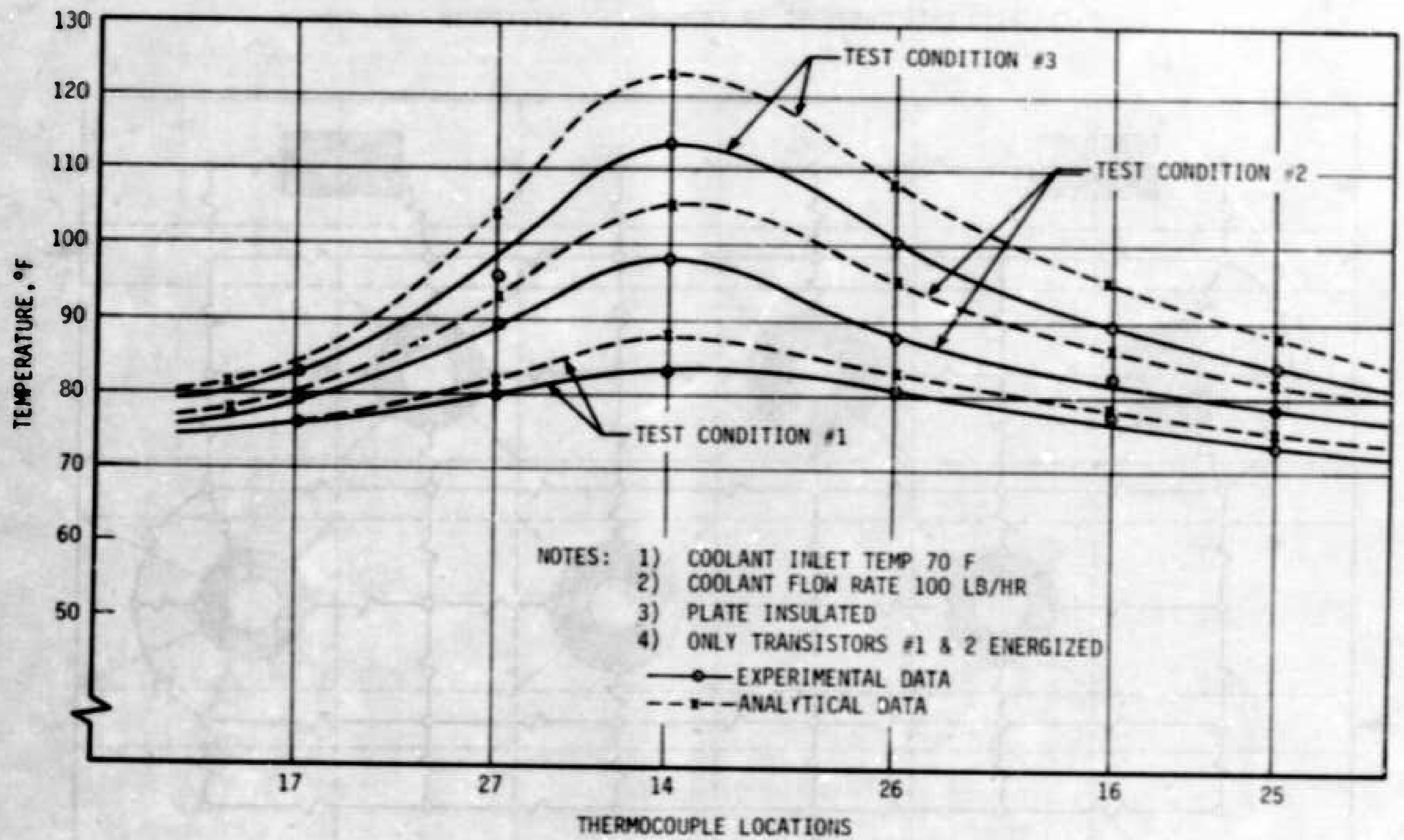

Figure 59. Analytical and Experimental Temperature Distributions For Liquid-Cooled Cold Plate No. 1

2. Liquid-Cooled Cold Plate No. 2

Figure 60 shows the experimental liquid-cooled Cold Plate No. 2. The cold plate was made of aluminum and provided with parallel internal flow passages as shown in the figure. A total of six power transistors and four resistors were mounted on the cold plate as shown. Transistors #1 and #2 were type 2N3846; transistors #3, #4, #5 and #6 were type 2N1724; and the resistors were type NER 65. Temperature measurements throughout the plate were made at the locations indicated.

Figures 61 and 62 show the R-C networks of the plate and the coolant flow passages, respectively. Also, for this plate only, the heat-transfer coefficients of the flow passages were determined. As the plate had two hole sizes, the heat-transfer coefficients were determined for each of the two hole sizes. Since the equation recommended by McAdams previously provided the most accurate results for the coolant used, the same equation was used

$$Nu = 6.2 \left(\frac{\dot{w}c_p}{(kL)} \right)^{0.2}$$

For a coolant flow rate of w = 100 lb/hr, the average heat-transfer coefficient of the 5/16-diameter hole was determined to be:

$$h = 140 \text{ Btu/hr ft}^{2\,\circ}\text{F}$$

and that of the 5/32-diameter hole was determined to be:

$$h = 300 \text{ Btu/hr ft}^{2\,\circ}\text{F}.$$

These values were used for determining the convection resistances in analytical temperature predictions.

A total of twelve steady-state tests at various heat loads and coolant flow rates were performed on Cold Plate No. 2. All of the test data presented were obtained with the plate insulated. Mica washers and Dow Corning heat-sink compound were used on all transistor mounting joints. Only heat-sink compound was used on resistor mounting joints. However, to investigate the effects of mica washers, stud torque, and the application of the heat-sink compound, some of the tests were performed without mica washers, without heat-sink compound, and at different stud torques.

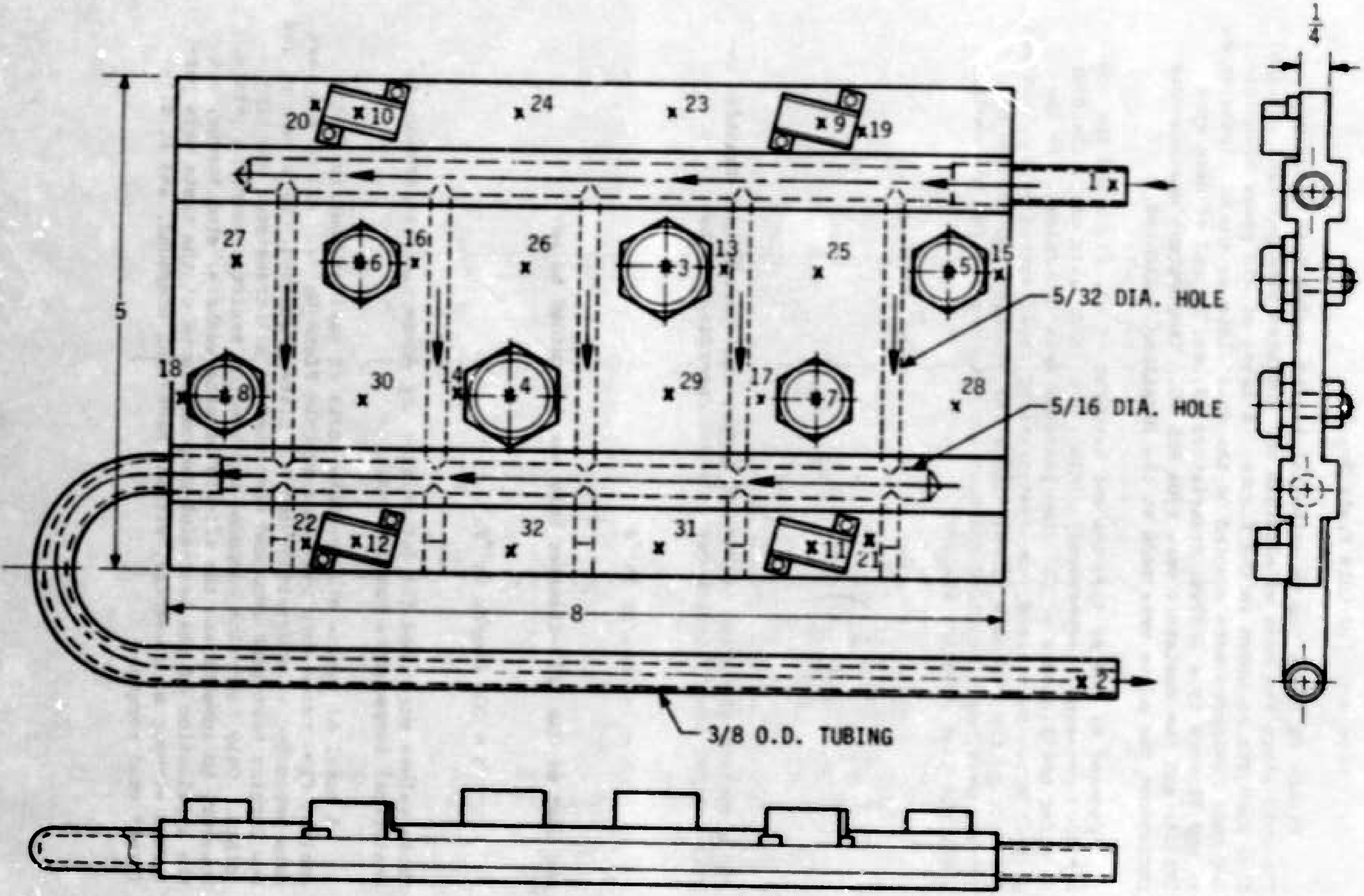

Figure 60. Liquid-Cooled Cold Plate No. 2

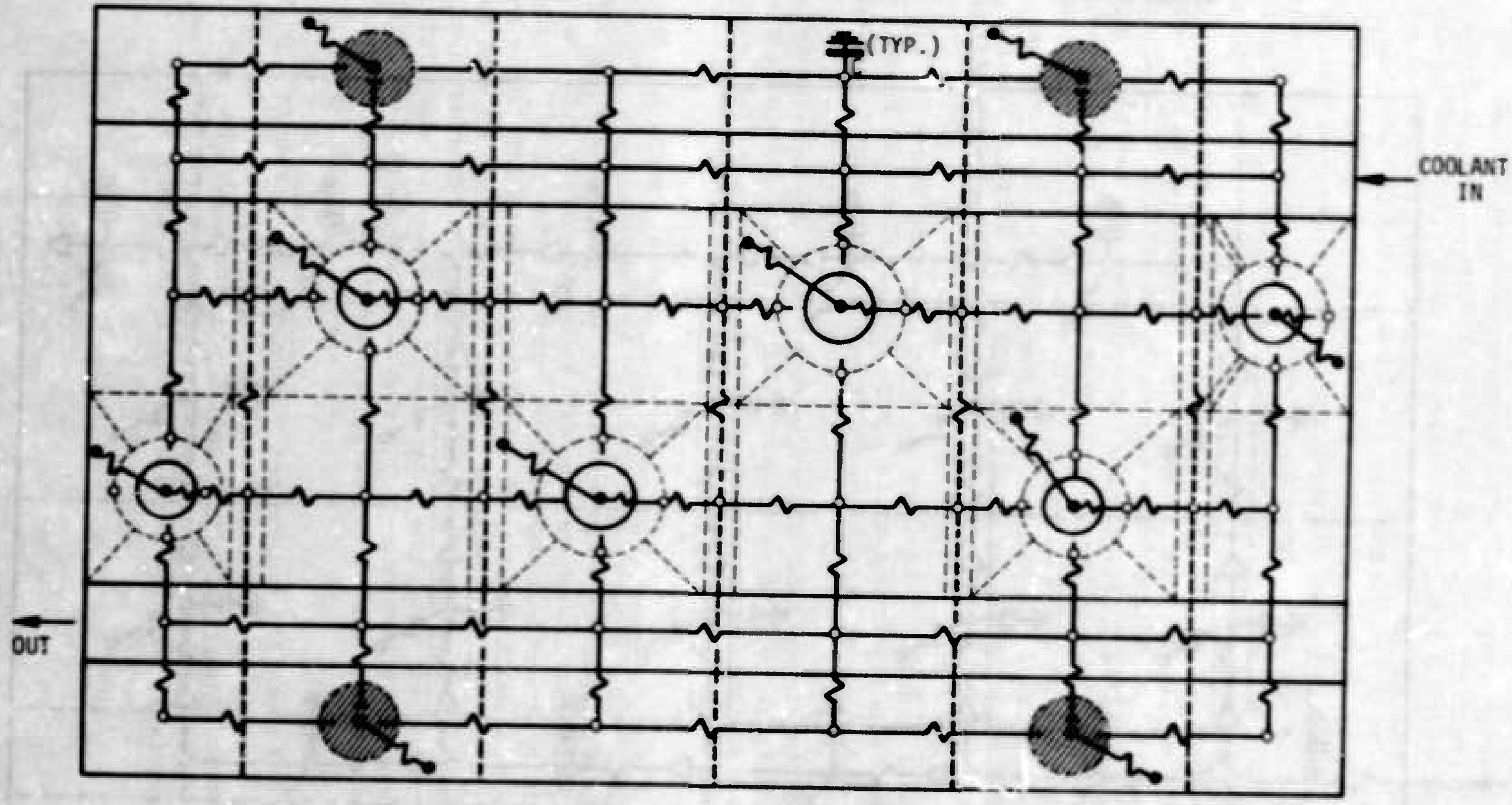

Figure 61. R-C Network of Liquid-Cooled Cold Plate No. 2

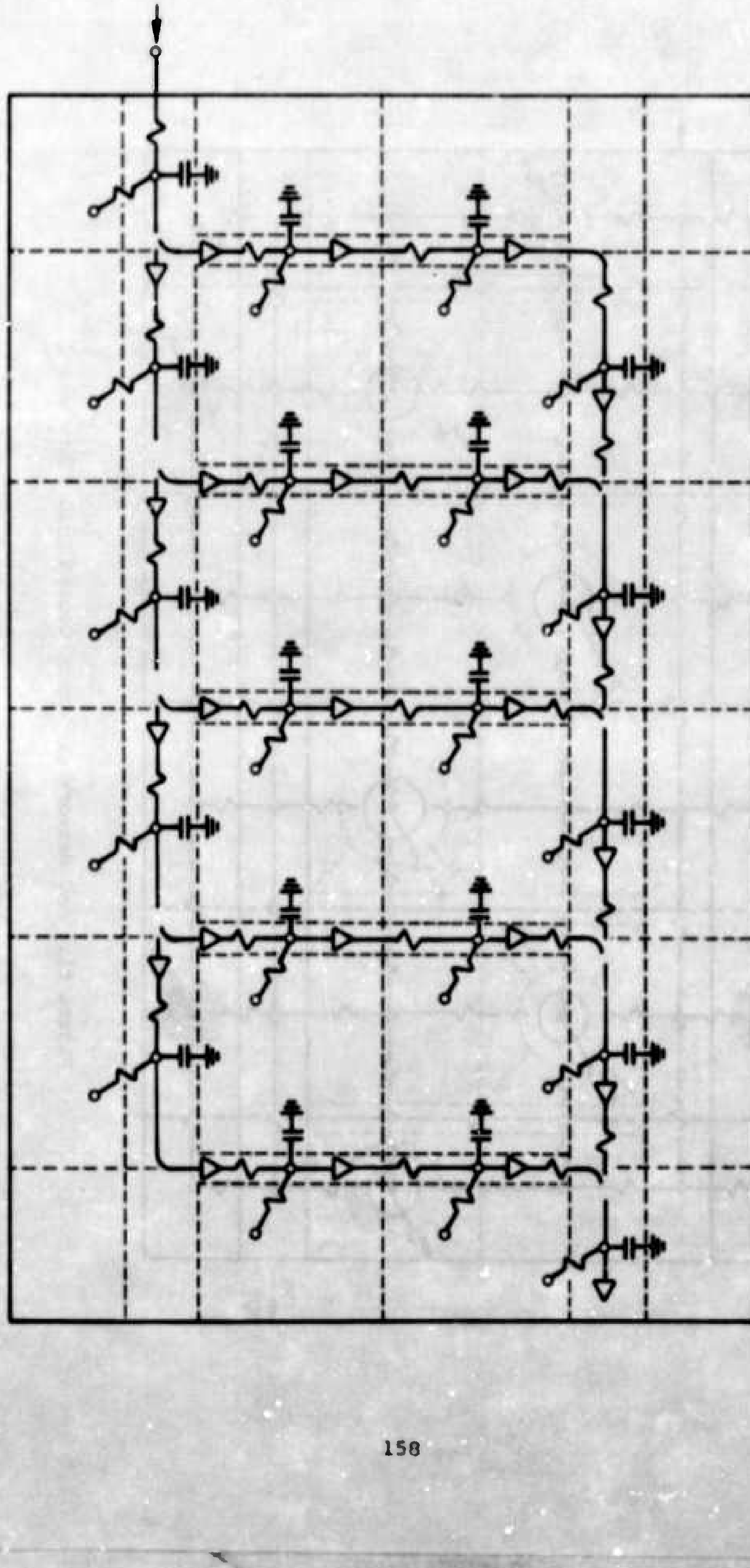

Figure 62. R-C Network of Coolant Flow Passages for Liquid-Cooled Cold Plate No. 2

Table 12 summarizes all the test conditions. Temperature readings of the thermocouples installed on the plate and electronic components (as shown in Figure 60) are contained in Appendix A.

Figures 63, 64, and 65 show the temperature distribution of the plate at the test conditions indicated. Comparison between experimental and analytical data is also made. The maximum deviation of approximately 7°F occurs at test condition 9 (maximum heat load). This value amounts to an error of less than 6 percent, which can be considered small. Some inconsistencies, however, between the experimental and analytical data should be noted. With lower heat loads, the analytically predicted temperatures were lower than those measured. With higher heat loads, they were generally higher than those measured. This condition was probably caused by the convection heat-transfer coefficient changes with temperature. The heat-transfer coefficients of liquids increase with temperature. This is particularly true for liquids of high viscosity. The accuracy of prediction could be improved by selecting small nodes around the areas of the concentrated heat loads, and accounting for coolant property changes with temperature.

Figure 66 shows case temperature changes of some of the electronic components as a function of coolant flow rate changes. The electrical power dissipation from the components was maintained constant throughout the tests. The large temperature differences among the transistors can be explained by differences in the thermal resistances of the mounting joints. Table 13 shows this condition. Different slopes of the temperature changes among the transistors can also be observed. This condition can be explained by the different thermal resistances in the conduction heat-transfer path. The larger conduction resistance reduced the effects of the convection heat-transfer coefficient changes.

Table 13. Thermal Resistances of Transistor Mounting Joints (Cold Plate No. 2)

TRANSISTOR NO.	HR °F/BTU	°F/WATT	°C/WATT
1	0.34	1.14	0.64
2	0.32	1.10	0.60
3	0.59	2.01	1.12
4	0.75	2.56	1.43
5	0.59	2.01	1.12
6	0.49	1.67	0.93

Figure 67 shows transistor case temperature changes as a function of electrical power dissipation rate changes. The temperature charts show a slight deviation from the linear slope. This can be caused by increased heat losses and increased convection heat-transfer coefficients with an increase in the temperature of the plate.

Table 12. Test Conditions of Liquid-Cooled Cold Plate No. 2

TEST NO.	COOLANT FLOW RATE (lb/hr)	ELECTRICAL POWER INPUT TO TRANSISTORS (WATTS)						ELECTRICAL POWER INPUT TO RESISTORS (WATTS)			
		TR #1*	TR #2	TR #3	TR #4	TR #5	TR #6	R #1**	R #2	R #3	R #4
1	100	25	25								
2	100	50	50								
3	100	75	75								
4	100			20	20	20	20				
5	100			30	30	30	30				
6	100			40	40	40	40				
7	100	25	25	20	20	20	20	13	13	13	13
8	100	50	50	30	30	30	30	13	13	13	13
9	100	75	75	40	40	40	40	13	13	13	13
10	50	50	50	40	40	40	40	13	13	13	13
11	100	50	50	40	40	40	40	13	13	13	13
12	200	50	50	40	40	40	40	13	13	13	13

* TR #1 - TRANSISTOR #1

** R #1 - RESISTOR # 1

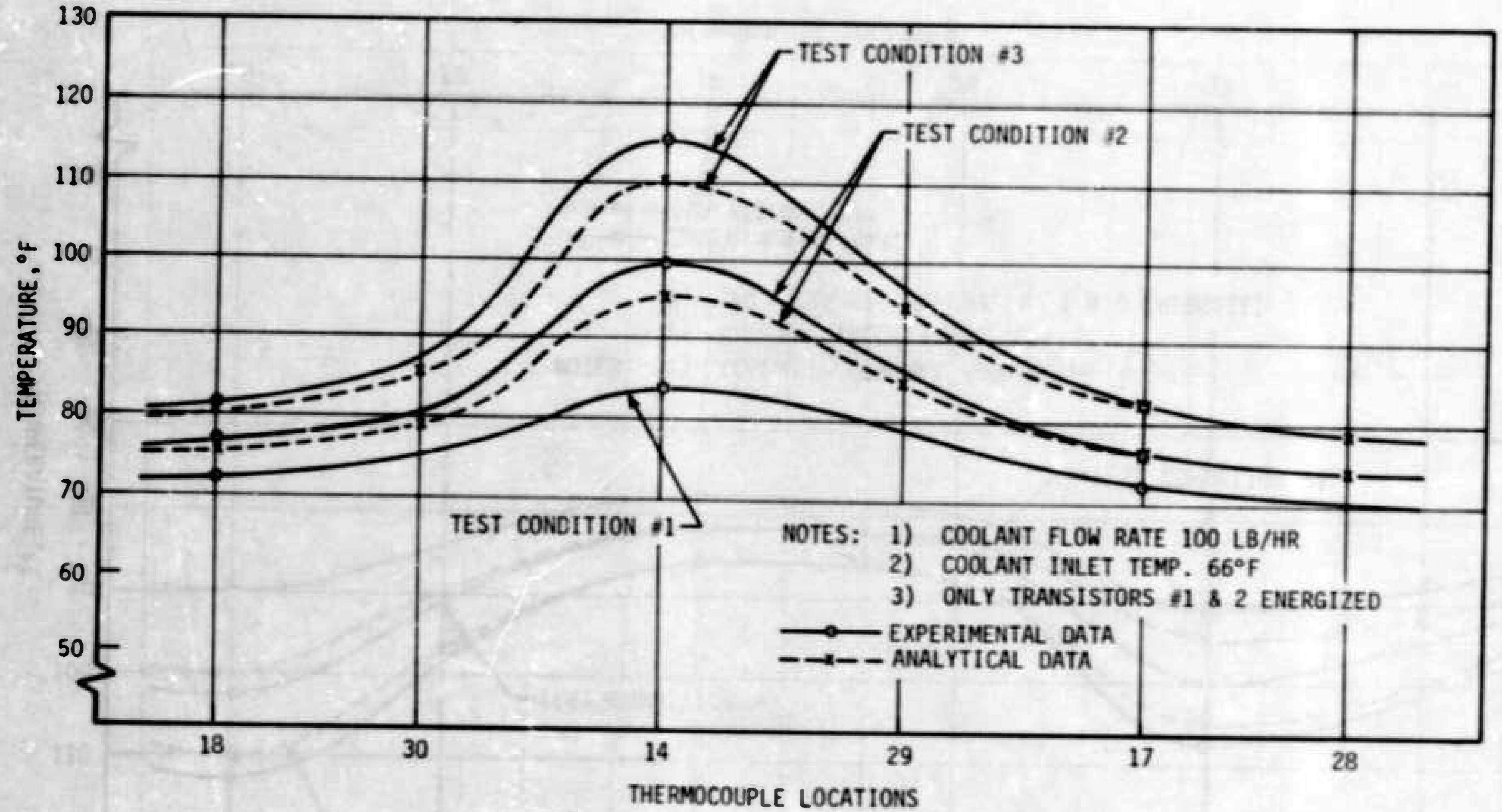

Figure 63. Temperature Distribution of Liquid-Cooled Cold Plate No. 2 at Test Condition Nos. 1 thru 3

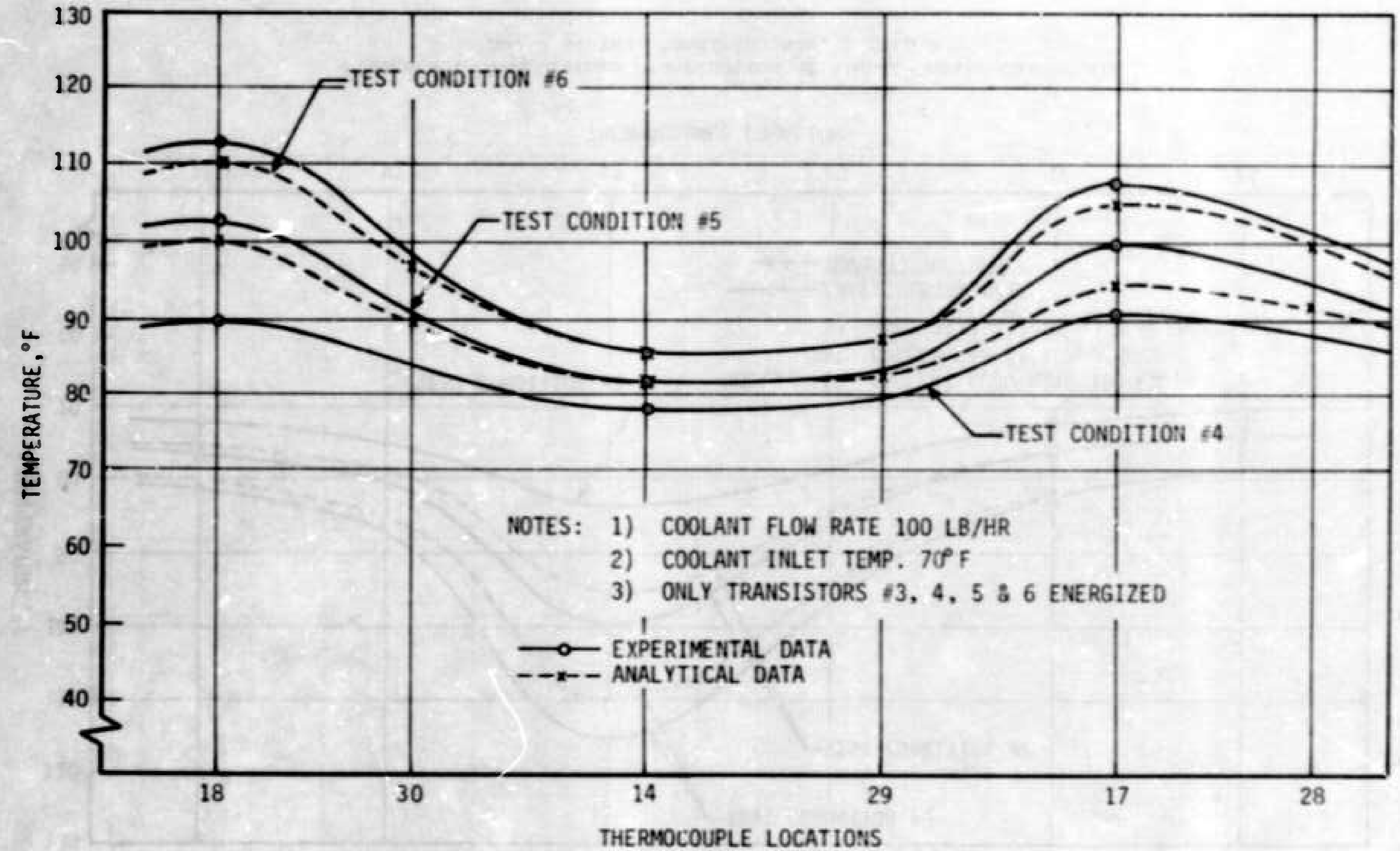

Figure 64. Temperature Distribution of Liquid-Cooled Cold Plate No. 2 at Test Condition Nos. 4 thru 6

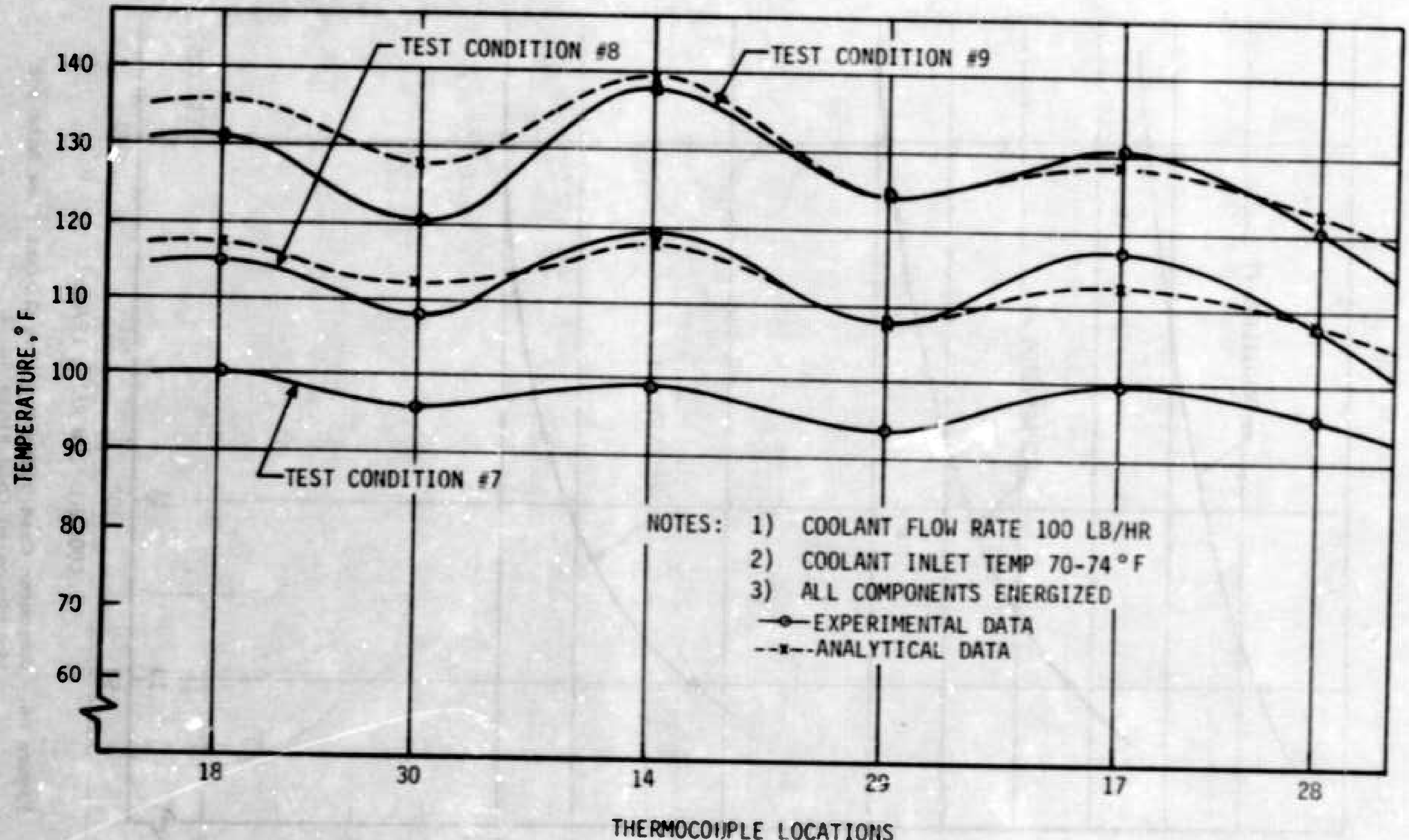

Figure 65. Temperature Distribution of Liquid-Cooled Cold Plate No. 2 at Test Condition Nos. 7 thru 9

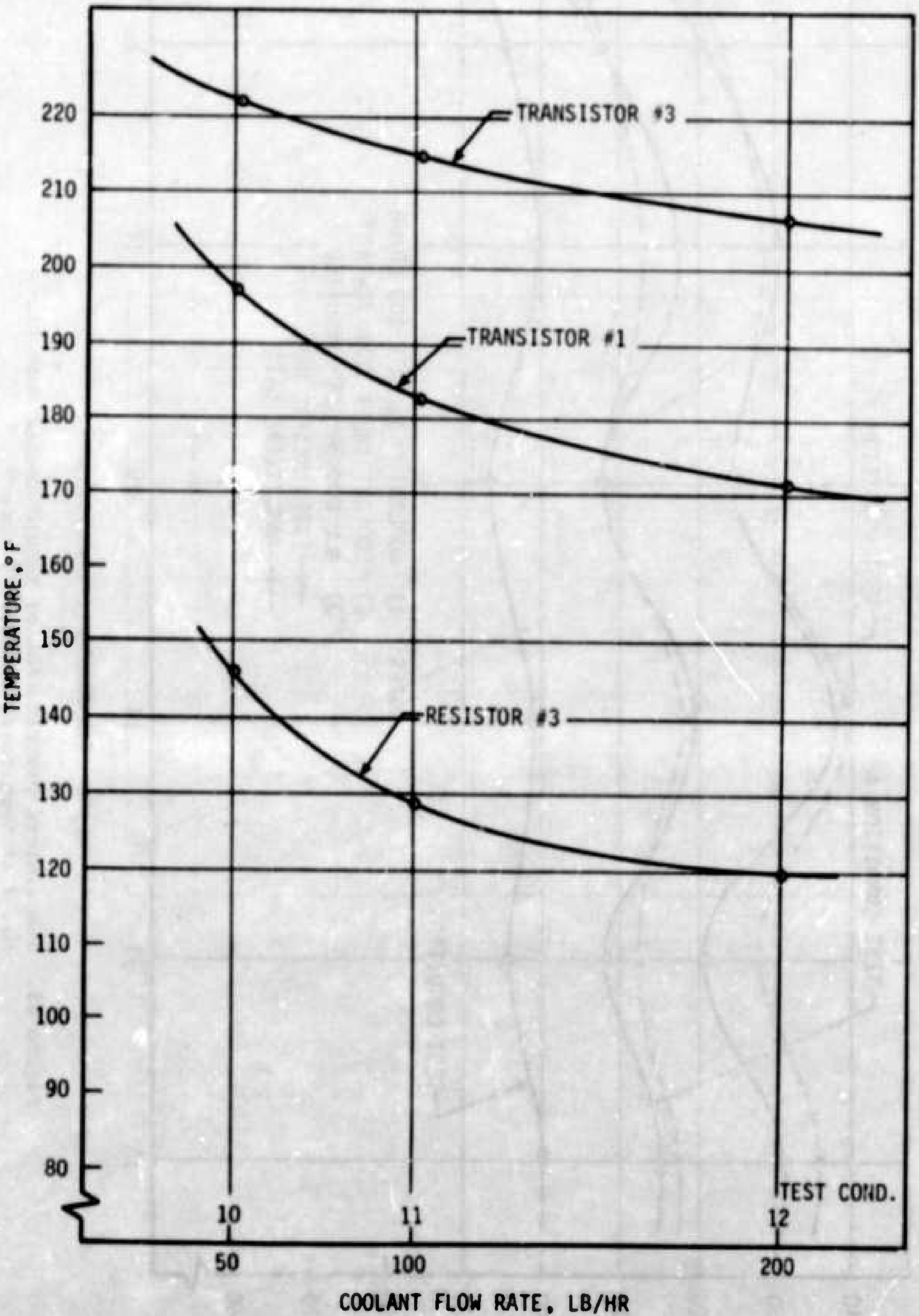

Figure 66. Component Case Temperature vs Coolant Flow Rate for Liquid-Cooled Cold Plate No. 2

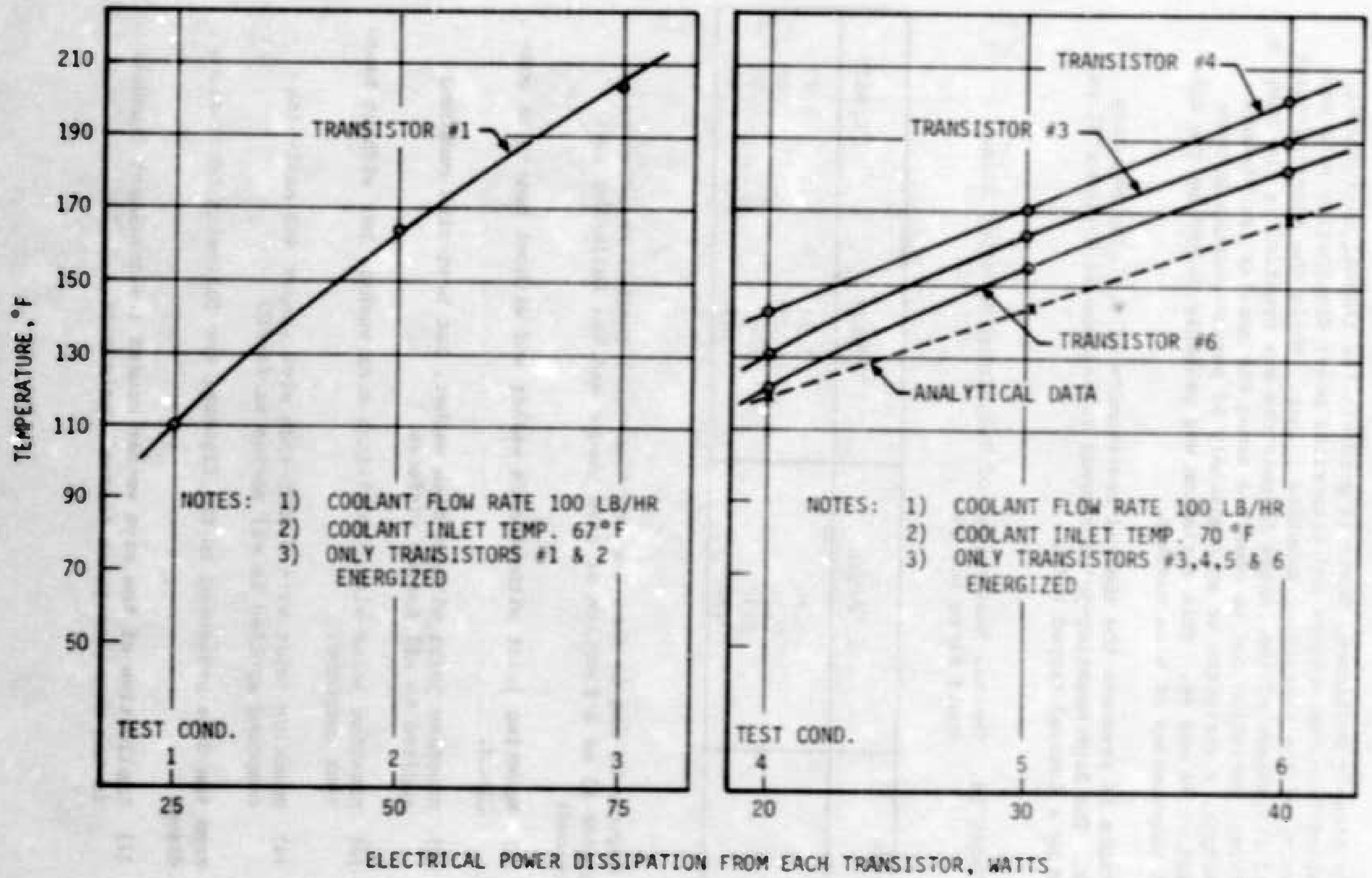

Figure 67. Case Temperature of Transistors vs Electrical Power Dissipation Rate for Liquid-Cooled Cold Plate No. 2

As already mentioned, Table 13 presents the thermal resistances, determined from temperature and electrical power dissipation rate measurements, of the transistor mounting joints. While the mounting-joint thermal resistance of the larger transistors was practically the same, a significant variation can be observed among the smaller transistors. For example, a variation of approximately 50 percent occurs between Transistors #4 and #6. This variation was probably caused by the different thicknesses of mica washers.

Table 14 presents the thermal resistances of resistor mounting joints. The high mounting-joint thermal resistance of Resistor #1 was caused by a damaged tapped hole.

Table 14. Thermal Resistances of Transistor Mounting Joints (Cold Plate No. 2)

RESISTOR NO.	HR °F/BTU	°F/WATT	°C/WATT
1	0.56	1.92	1.07
2	0.36	1.23	0.68
3	0.32	1.07	0.60
4	0.32	1.07	0.60

Figures 68 and 69 show the mounting-joint thermal resistances of Transistor #1 as a function of stud torque and the following test conditions:

(1) Mounting joint without mica washer and without heat-sink compound.

(2) Mounting joint without mica washer, but heat-sink compound applied to all mating surfaces.

(3) Mounting joint with 0.0025-inch mica washer, but without heat-sink compound.

(4) Mounting joint with 0.0025-inch mica washer and heat-sink compound applied to all mating surfaces.

From the data presented in the figures, the following conclusions were drawn:

(1) Application of the mica washer caused a significant increase in the mounting-joint thermal resistance.

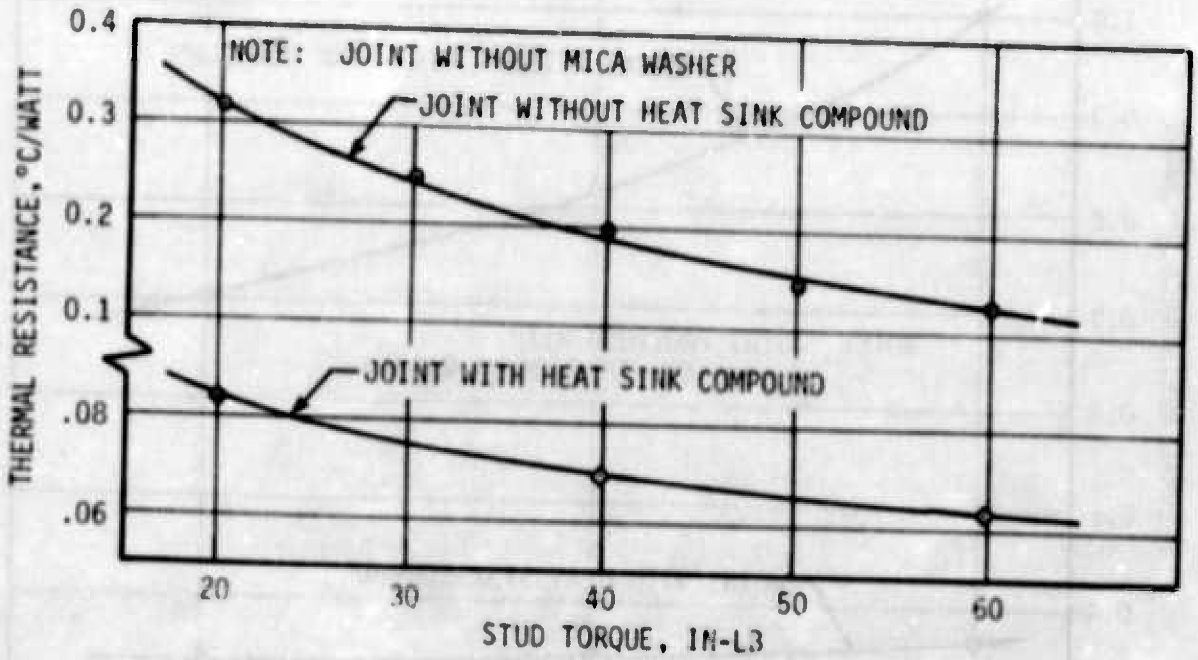

Figure 68. Thermal Resistance of Transistor #1 Mounting Joint vs Stud Torque (without Mounting Washer)

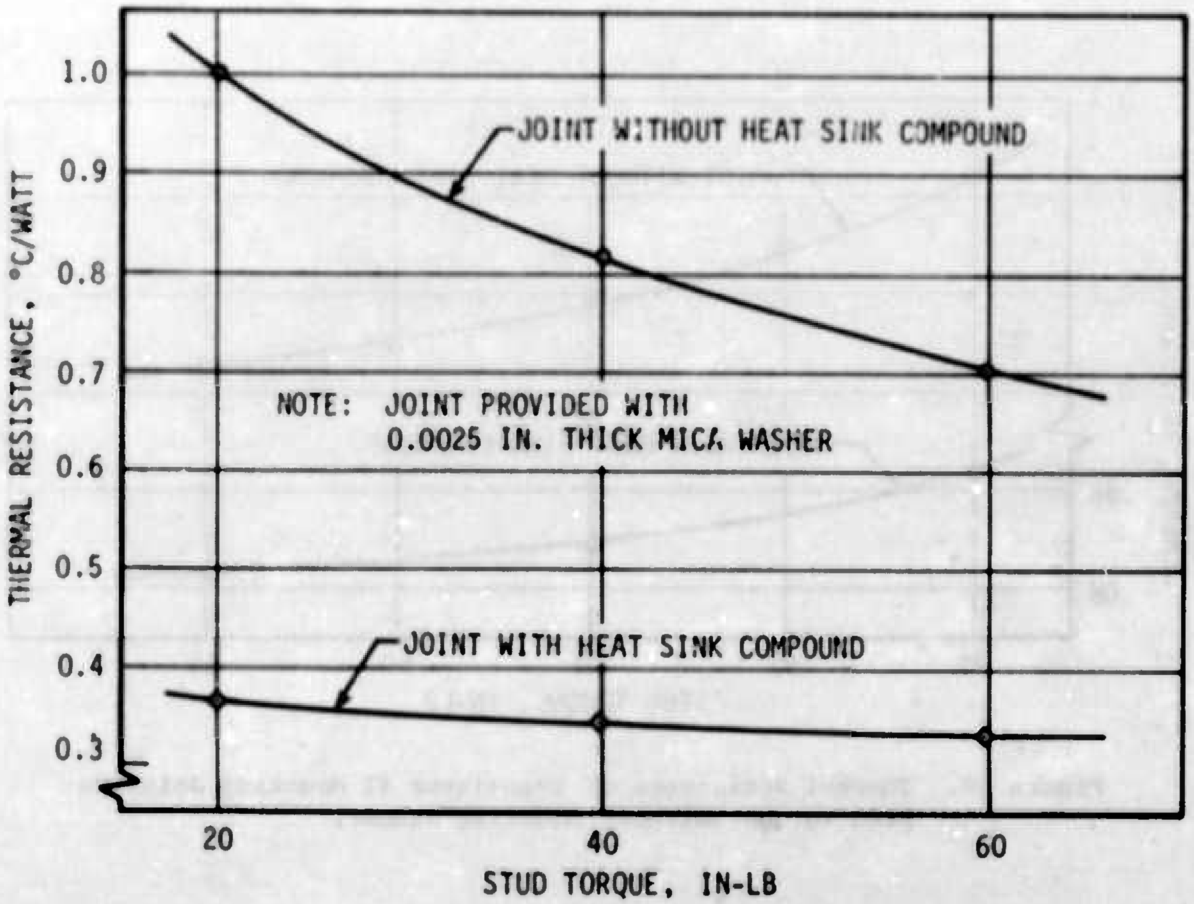

Figure 69. Thermal Resistance of Transistor #1 Mounting Joint vs Stud Torque (with Mounting Washer)

(2) Heat-sink compound applied to the mating surfaces significantly reduced the joint thermal resistance.

(3) The stud torque had a very limited effect upon the joint thermal resistance when heat-sink compound was used.

3. Liquid-Cooled Cold Plate No. 3

Figure 70 shows the experimental liquid-cooled Cold Plate No. 3. The cold plate was made of copper and provided with an internal coolant flow channel. A total of six transistor mounts, as shown in Figure 71, provided finished mounting surfaces. The electronic equipment mounted to the plate consisted of two 2N3896 transistors (TR #1 and #6), two 2N1724 transistors (TR #2 and #5), one 2N2751 transistor (TR #3), and one 2N2109 transistor (TR #4). Temperature measurements through the plate were made at the locations indicated in Figure 70.

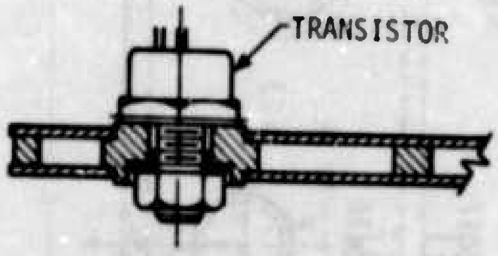

Figure 71. Transistor Mounting on Liquid-Cooled Cold Plate No. 3

Figures 72 and 73 show the R-C networks of the plate and coolant flow channel, respectively. As the coolant flow channel is not circular in this cold plate, the hydraulic diameter, D_h, must be used in the Reynolds and Nusselt number expressions

$$D_h = 4 \frac{A}{P}$$

Where A = the flow area, ft^2

P = the perimeter of the channel, ft.

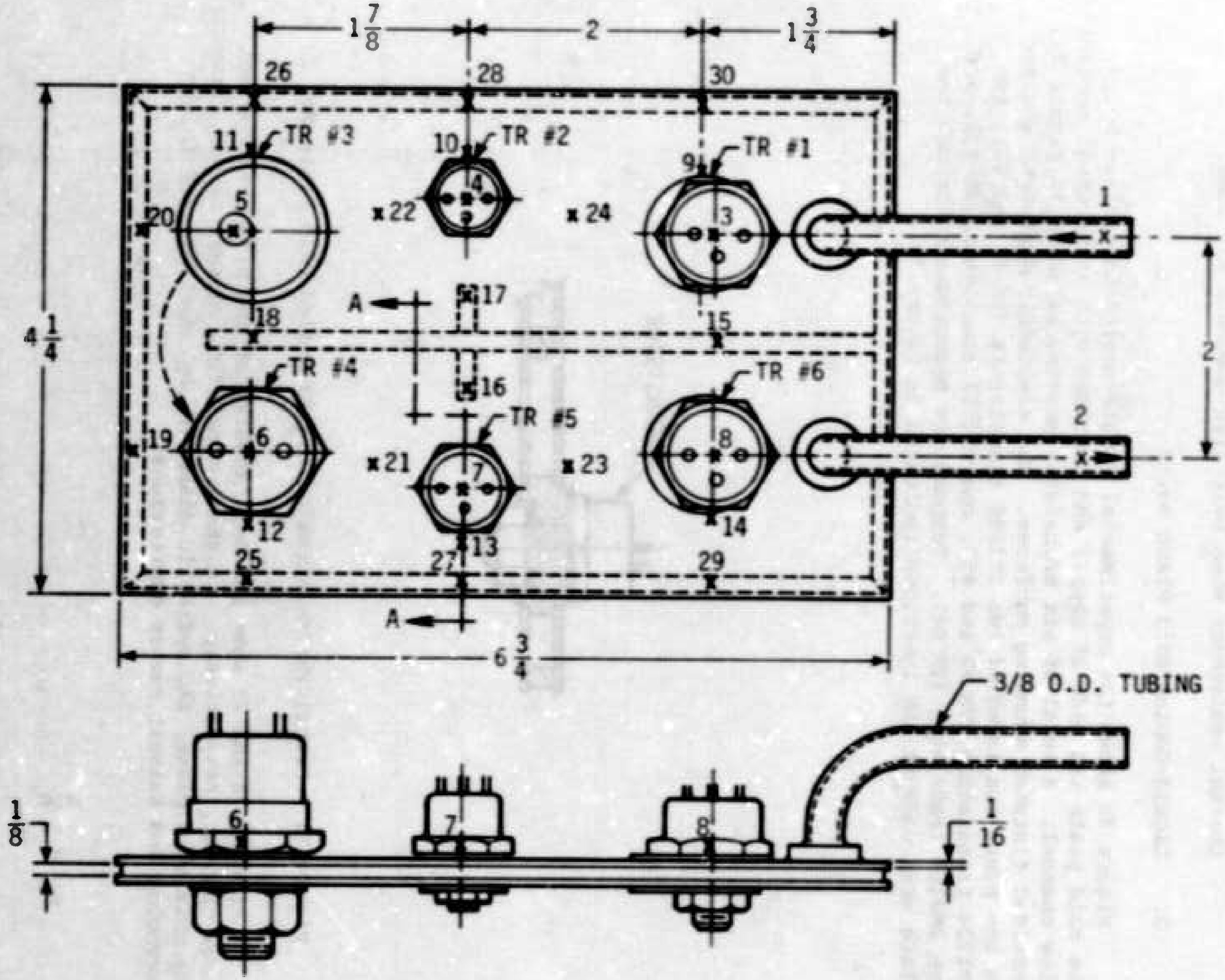

Figure 70. Liquid-Cooled Cold Plate No. 3

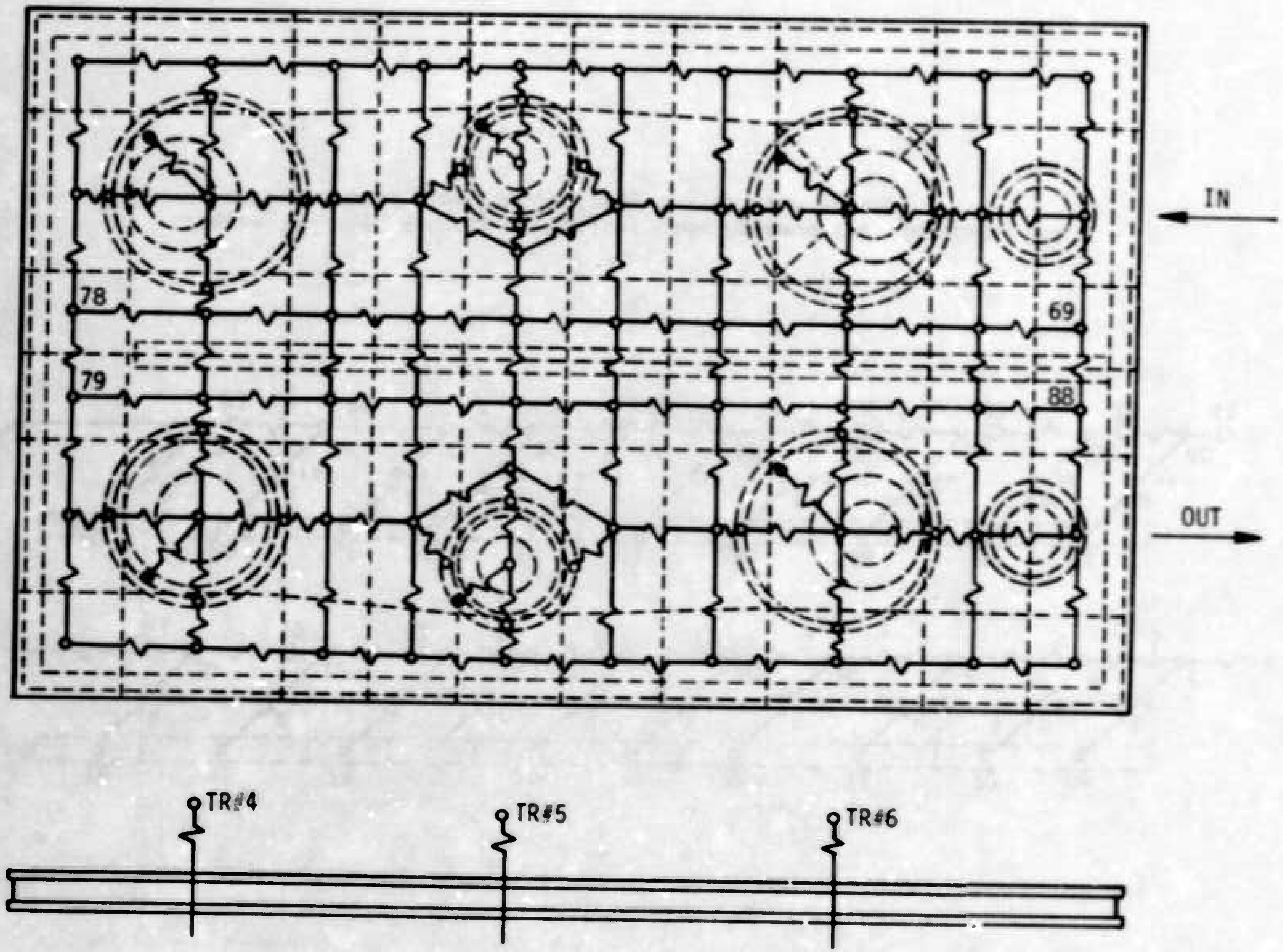

Figure 72. R-C Network of Liquid-Cooled Cold Plate No. 3

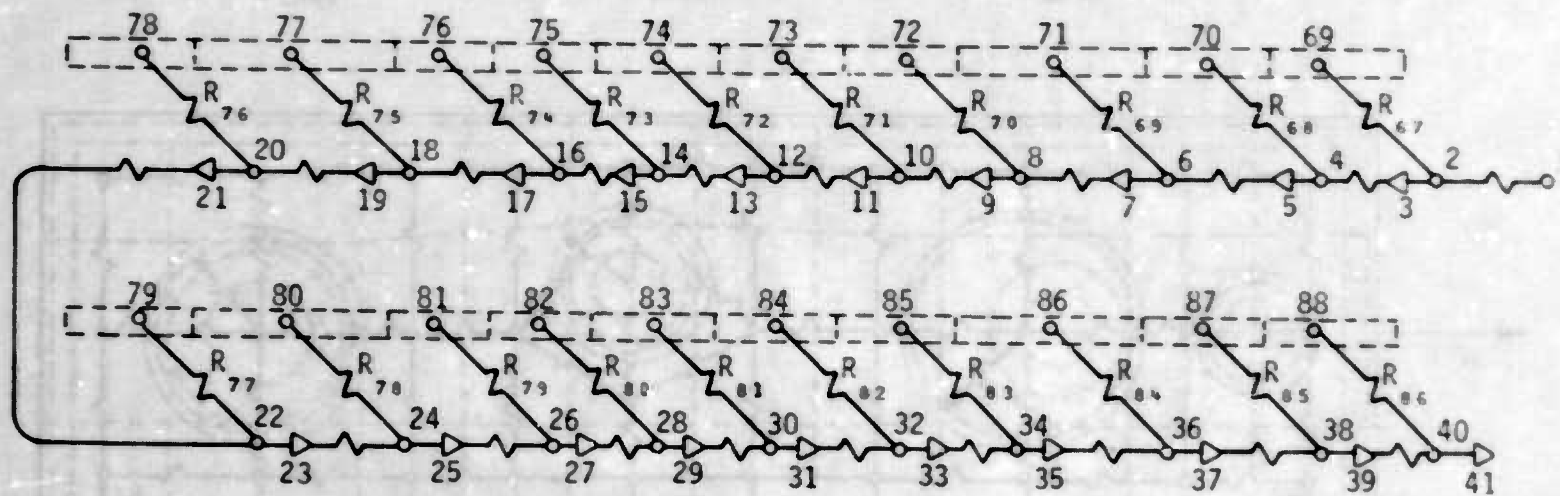

Figure 73. R-C Network of Coolant Flow Passage for Liquid-Cooled Cold Plate No. 3 (Only One Section Shown)

The flow channel here was interrupted by the transistor mounts, therefore, some average width was assumed. The flow area, A, was determined to be approximately 0.00108 ft^2 and the hydraulic diameter, D_h, was found to be 0.019 ft. With a coolant flow rate of w = 100 lb/hr, the Reynolds number, Re, was determined to be 195. As the flow channel of this cold plate was more complex, it was doubtful if any of the standard textbook forced-convection equations would fit this particular configuration. The heat-transfer coefficients, therefore, were determined by using both the Sieder-Tate and McAdams equations and the computed values used in the analytical predictions. As with the previous cold plates, the Sieder-Tate equation gave too low of values for the heat-transfer coefficients (h = 105 Btu/hr $ft^{2\circ}F$), while the McAdams equation gave too high of values (h = 235 Btu/hr $ft^{2\circ}F$). It was determined that a heat-transfer coefficient value of h = 150 Btu/hr $ft^{2\circ}F$ provided a compromise between the experimental and analytical data. All the comparisons, therefore, were based on this heat-transfer coefficient. The reason for this inconsistency can probably be based on fin effects. The heat-transfer coefficients along a fin are not constant, but their value changes along the fin. The same phenomena was also observed with the air-cooled cold plates.

Table 15 summarizes all the test conditions. Temperature readings of the thermocouples installed on the plate and electronic components (as shown on Figure 70) are contained in Appendix A.

Figures 74 and 75 show temperature distribution of the cold plate at the test conditions indicated. Comparison between experimental and analytical data was made by using the heat-transfer coefficient of h = 150 Btu/hr $ft^{2\circ}F$. The results show a good agreement between the experimental and analytical data. A maximum deviation of only 5°F occurred at the concentrated heat load.

Figure 76 shows transistor case temperature changes as a function of coolant flow rate changes. By increasing the coolant flow rate from 50 lb/hr to 200 lb/hr, a maximum case temperature reduction of only 24°F was achieved. The gain was small when the coolant flow rate was increased from 100 lb/hr to 200 lb/hr. No practical gain at all would probably be achieved by increasing the flow rate further. Because of electrical power limitations in aerospace vehicles, the coolant flow rates must be kept as low as possible. If component temperatures must be reduced, it would be more advantageous to reduce resistances in the conduction heat-transfer path.

Figure 77 shows transistor case temperature changes as a function of electrical power dissipation rate. The different rates of temperature changes were caused by the different mounting-joint thermal resistances. The figure is self-explanatory; it indicates the temperature increase of electronic components with increased electrical power dissipation.

Table 15. Test Conditions of Liquid-Cooled Cold Plate No. 3

TEST NO.	COOLANT FLOW RATE (lb/hr)	ELECTRICAL INPUT TO TRANSISTORS (WATTS)					
		TR #1	TR #2	TR #3	TR #4	TR #5	TR #6
1	100	25		25			25
2	100	50		50			50
3	100	75		75			75
4	100				50		
5	100				75		
6	100				100		
7	100		20			20	
8	100		30			30	
9	100		40			40	
10	100	25	20	25	25	20	25
11	100	50	30	50	50	30	50
12	100	75	40	75	75	40	75
13	50	75	40	75	75	40	75
14	100	75	40	75	75	40	75
15	200	75	40	75	75	40	75

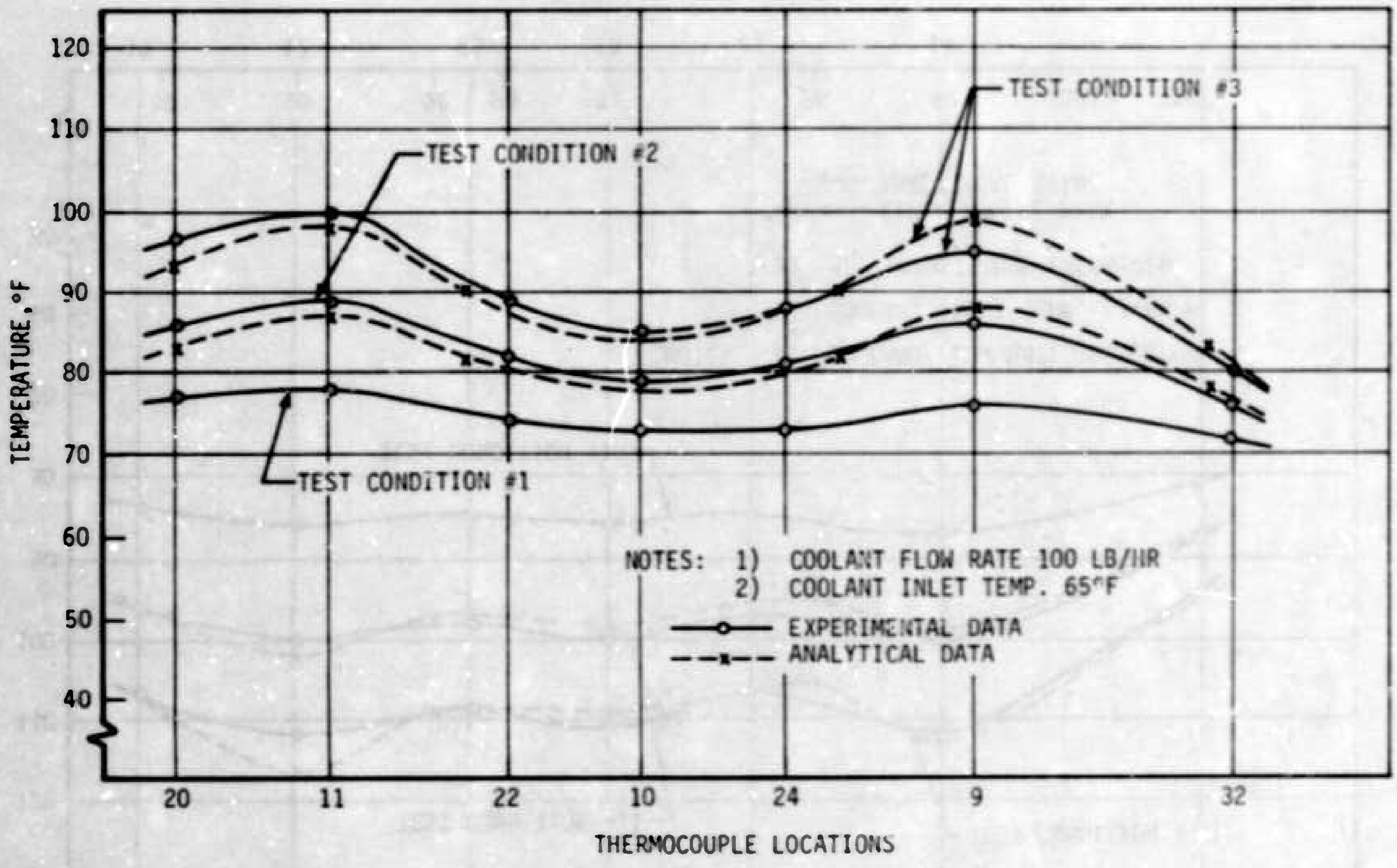

Figure 74. Temperature Distribution of Liquid-Cooled Cold Plate No. 3 at Test Condition Nos. 1 thru 3

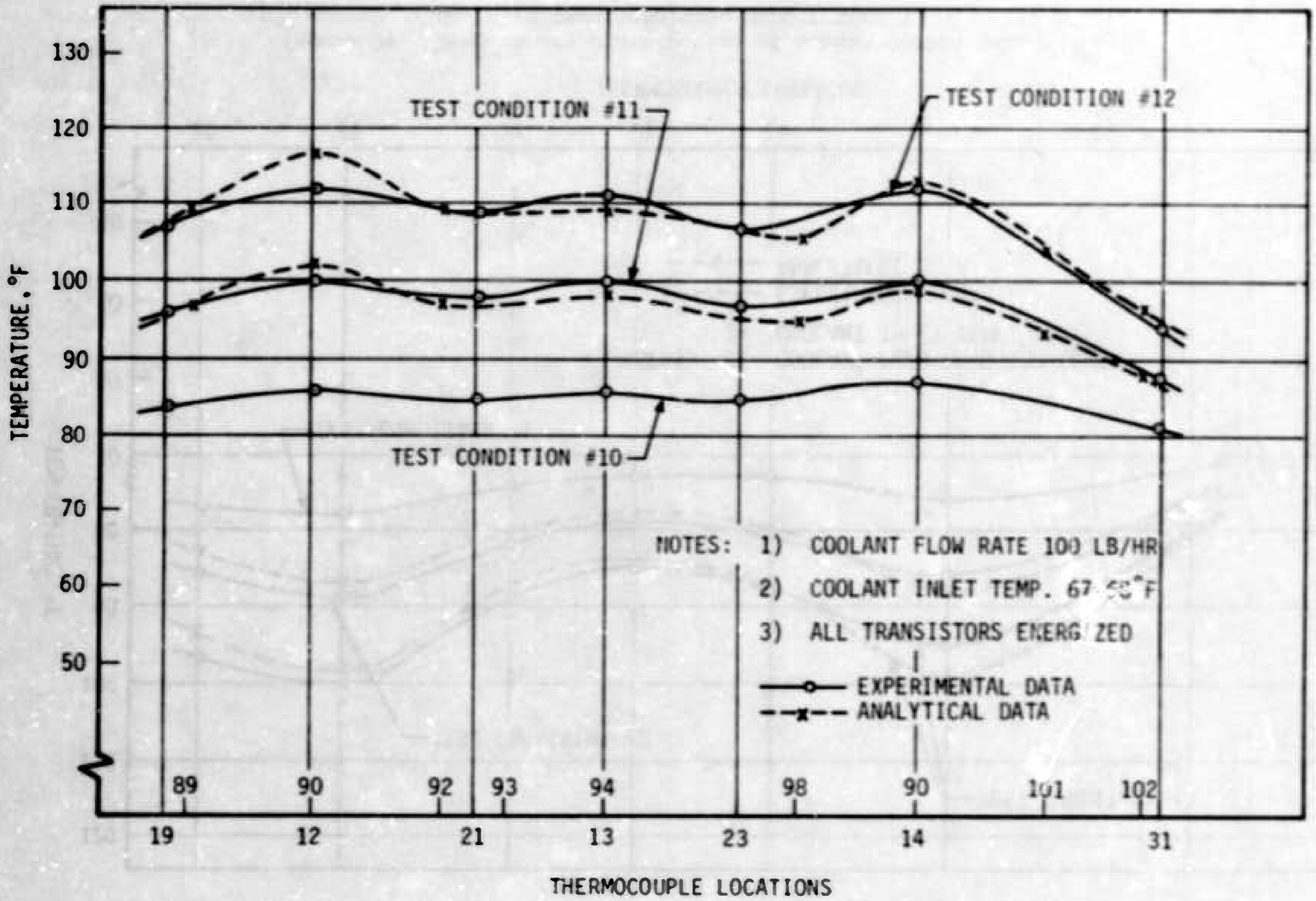

Figure 75. Temperature Distribution of Liquid-Cooled Cold Plate No. 3 at Test Condition Nos. 10 thru 12

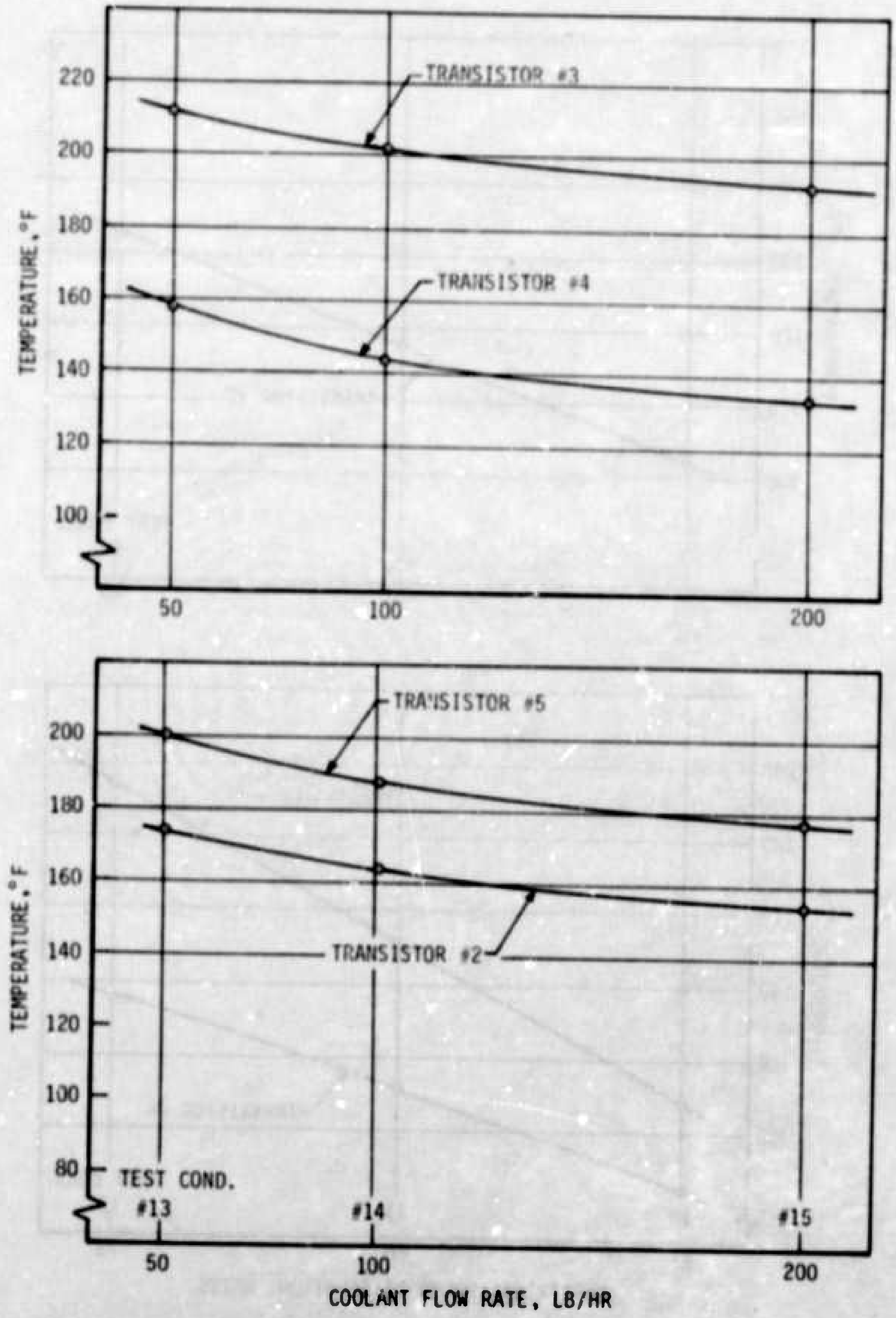

Figure 76. Component Case Temperature vs Coolant Flow Rate for Liquid-Cooled Cold Plate No. 3

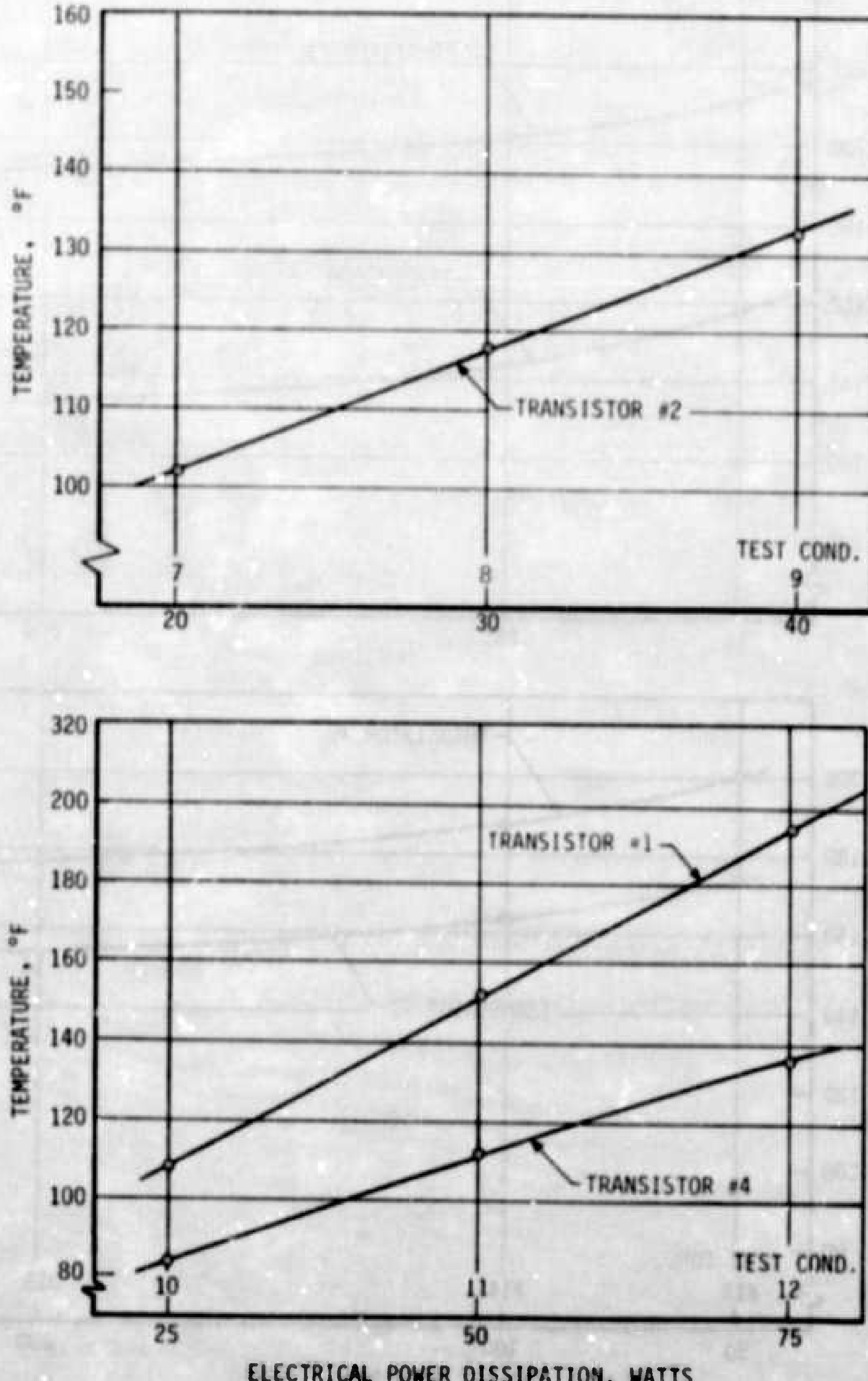

Figure 77. Component Case Temperature vs Electrical Power Dissipation for Liquid-Cooled Cold Plate No. 3

To investigate the effects of mica-washer thickness upon transistor mounting-joint thermal resistance, washers of different thicknesses were selected and used in mounting transistor #2 (2N1724). The mica-washer thicknesses selected were 0.0025 inches, 0.0040 inches, and 0.0080 inches. A stud torque of 20 in-lb was used in all tests, and the heat-sink compound was applied to all mating surfaces. The coolant flow rate was maintained the same throughout all the tests.

Figure 78 shows the temperature changes of Transistor #2 case as a function of electrical power dissipation rate at the three different mica-washer thicknesses. The figure shows the significant effects of washer thickness upon the component temperature. When active electronic components are installed, it is important to select washers which will satisfy the minimum insulation requirements.

Figure 79 shows the case temperature of Transistor #2 as a function of electrical power dissipation. Stud torques of 10 and 20 in-lb were used. The mounting was provided with a 0.0040-inch mica washer and heat-sink compound.

Figure 80 shows the mounting-joint thermal resistance of Transistor #2 as a function of mica-washer thickness. The test points are average values obtained from measurements taken at various heat loads. The heat-sink compound was applied to all mating surfaces and the stud torque was 20 in-lb. The figure is self-explanatory.

4. Thermal Performance Comparison of Liquid-Cooled Cold Plate

Since the cold plates tested were of different design, it is of interest to compare their thermal performance on a common basis. Because of a tendency in electronic-equipment cooling applications to express capability of heat transfer in terms of resistances, such as °F/Btu, °F/watt, or °C/watt, the comparison is based on thermal resistances computed from the following expression:

$$R = \frac{\Delta t}{Q}$$

where

$$\Delta t = \bar{t}_{pl(max)} - \bar{t}_{fl}$$

$\bar{t}_{pl(max)}$ = the mean maximum temperature of the cold plate measured at locations of the concentrated heat loads

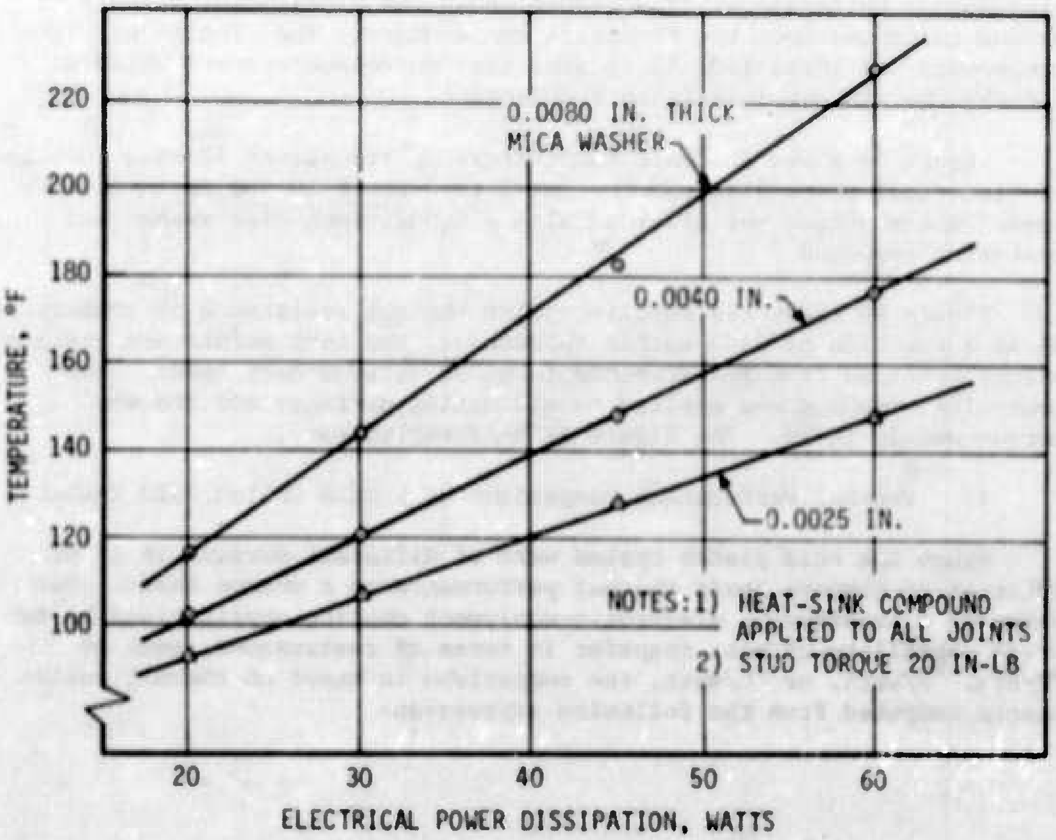

Figure 78. Case Temperature of Transistor #2 vs Electrical Power Dissipation (Effects of Washer Thickness)

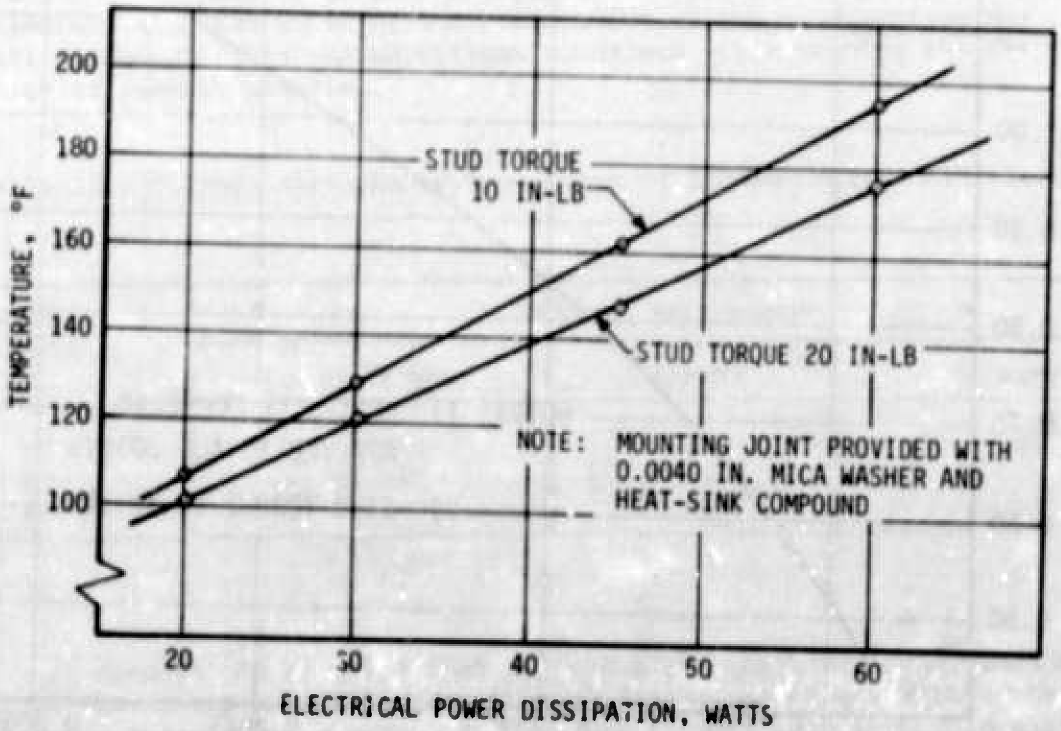

Figure 79. Case Temperature of Transistor #2 vs Electrical Power Dissipation (Effects of Stud Torque)

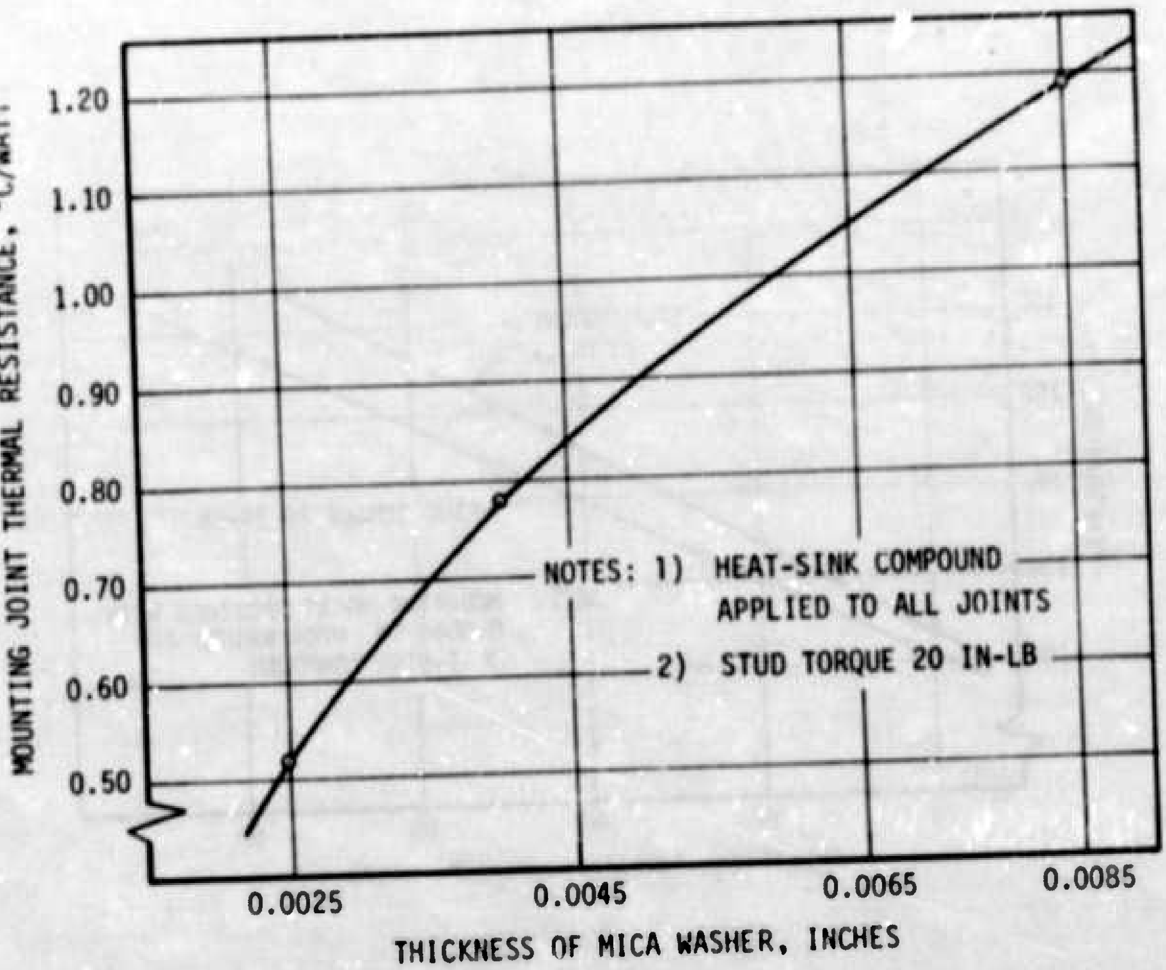

Figure 80. Thermal Resistance of Transistor #2 Mounting Joint vs Thickness of Mica Washer

$\bar{t}_{fl}$ = the mean temperature of the coolant

Q = the total heat or electrical power dissipated by the components.

Table 16 presents thermal resistances obtained as mean values from three different heat loads but with a constant coolant flow rate for each of the cold plates. It can be concluded from the table that Cold Plate No. 3 provided the most effective cooling while Cold Plate No. 1 was most inefficient. It should be noted that Cold Plate No. 3 was made of copper while Cold Plates No. 1 and 2 were made of aluminum. Ease of manufacturing was the reason for selecting copper as the construction material. Because of the higher thermal conductance of copper, Cold Plate No. 3 was made of thinner material. If weight savings must be considered, aluminum would be the best choice as the construction material, although other considerations sometimes might require the selection of another material.

Table 16. Thermal Performance Comparison of Liquid-Cooled Cold Plates

Cold Plate No.	THERMAL RESISTANCES		
	HR °F/BTU	°F/WATT	°C/WATT
1	0.0452	0.153	0.085
2	0.0416	0.142	0.078
3	0.0282	0.095	0.053

It also should be noted that in cold plate configurations, such as that of Nos. 1 and 2, the largest thermal resistance occurs within the convection heat-transfer path. Temperature reduction of such cold plates can be achieved by increasing the convection heat-transfer surface area or by increasing the heat-transfer coefficient, or both. More efficient designs with extended surfaces and mounting arrangements are possible. The design features of a liquid-cooled cold plate are dictated not by the total heat load, but primarily by the magnitude of the concentrated heat load.

5. Sample Calculations

Under preliminary design conditions, it is almost always necessary to perform some simplified thermal analysis of the cooling device. Such analysis can be based on coolant inlet temperature and flow rate, the power dissipation rate from the electronic equipment, and the general outline of the cooling device: a cold plate in this case.

When the general outline of the cold plate and the geometry of the coolant-flow conduits are known, the convection heat-transfer coefficient can be determined from procedures outlined in this report or elsewhere. Starting with the general expression for convection heat transfer, we can state that

$$Q = hA \left(\bar{t}_w - \bar{t}_{fl} \right)$$

where $\bar{t}_{fl}$ = the mean bulk temperature of the coolant and

$$t_{fl} = \frac{t_{in} + t_{out}}{2}$$

On the other hand, heat absorbed by the coolant can be expressed as follows:

$$Q = \dot{w}c_p \left(t_{out} - t_{in} \right) \tag{227}$$

from which we obtain:

$$t_{out} = t_{in} + \frac{Q}{\dot{w}c_p}$$

where Q = total power dissipated by the electronic equipment, Btu/hr

$\dot{w}$ = coolant flow rate, lb/hr

c_p = specific heat of the coolant, Btu/lb°F.

The mean wall temperature of the coolant conduit can be determined from the equation

$$\bar{t}_w = \bar{t}_{fl} + \frac{Q}{hA}$$

When the coolant conduit is attached to one side of the cold plate (Cold Plate No. 1), an efficiency factor, η, must be introduced as follows:

$$\bar{t}_w = \bar{t}_{fl} + \frac{Q}{\eta hA}$$

Based on the mean temperature of the coolant conduit, temperatures of the electronic-component locations can be computed if the power dissipation rates are known.

For example, let's determine the temperature of the cold plate at transistor #1 (TR #1) location (thermocouple #14 reading) under test condition No. 9. At this test condition, the coolant flow rate was $w = 100$ lb/hr, the coolant inlet temperature was $t_{in} = 74°F$, and the total electrical power dissipation rate was $P = 332$ watts or $Q = 1129$ Btu/hr. If a 5-percent heat loss to the environment is assumed, $Q = 1070$ Btu/hr. The outlet temperature of the coolant can be determined as follows:

$$t_{out} = t_{in} + \frac{Q}{wc_p} = 74 + \frac{1070}{100\ (0.75)} = 88.3°F$$

The mean coolant temperature is

$$\bar{t}_{fl} = \frac{74 + 88.3}{2} = 81.15°F$$

$$\bar{t}_{fl} \doteq 81°F$$

Next, the mean temperature of the coolant conduit can be determined from

$$t_w = t_{fl} + \frac{Q}{hA}$$

From the previously given value of h, we know that

$$h = 160 \text{ Btu/hr ft}^{2}{}^\circ\text{F}$$

The surface area of the conduit is found from

$$A = \pi dL$$

$$A = \pi\,(0.305)(24.2) = 23.2 \text{ in}^2 = 0.161 \text{ ft}^2$$

It was determined that $\eta = 0.90$, then

$$\bar{t}_w = 81 + \frac{1070}{0.90\ (160)(0.161)} = 81 + 46 = 127^\circ\text{F}$$

The temperature differential within the mounting plate can be determined by applying two general methods: (1) drawing the flux plot from the contact area of the transistor to the section where the tube is attached or (2) assuming a radial heat flow from the transistor contact area similar to heat flow through a disk.

$$Q = kA_m \frac{t_1 - t_2}{r_2 - r_1}$$

where

$$A_m = \frac{A_2 - A_1}{\ln\left(A_2 / A_1\right)}$$

Refer to Figure 45 (Cold Plate No. 1). Two circles of radii $r_1 = 0.312$ in. and $r_2 = 1.125$ in. can be drawn around TR #1 location, and the heat flow areas can be determined as follows:

$$A_1 = \pi d_1 \delta = \pi(0.625)(0.25) = 0.49 \text{ in}^2$$

$$A_2 = \pi d_2 \delta = \pi(2.25)(0.25) = 1.77 \text{ in}^2$$

Therefore,

$$A_m = \frac{1.77 - 0.49}{\ln(1.77/0.49)} = \frac{1.28}{1.28} = 1 \text{ in}^2 = 0.0069 \text{ ft}^2$$

The temperature of the cold plate at the transistor mounting place can now be computed as follows:

$$t_1 = t_{pl} + \frac{Q}{kA_m}\left(r_2 - r_1\right)$$

where Q, in this case, is the heat dissipated by the transistor.

$$Q = 50\ (3.4) = 170 \text{ Btu/hr}$$

Substituting values, we find that

$$t_1 = 127 + \frac{170}{100(0.0069)}\ (0.094 - 0.026) = 127 + 16 = 143°\text{F}$$

The temperature actually measured was 136°F.

The simplified computation method provided a close agreement with the actual temperature. Based on this temperature and the known interface thermal resistance between the cold plate and the transistor, the junction temperature of the transistor was determined.

It should be noted, however, that this cold plate presented the simplest thermal performance prediction effort. It is possible with this cold-plate configuration to separate convection and conduction modes of heat transfer, and it is not necessary to introduce surface effectiveness factors.

b. Air-Cooled Cold Plates

1. Types of Cold Plates Tested

Limited experimental work performed with air-cooled cold plates in a previous study (Ref 39) revealed that accurate thermal performance prediction, based on standard textbook equations, is impossible. Significant errors can be introduced when thermal performance predictions are based on fully-developed velocity and temperature profiles. To investigate the main parameters affecting the heat transfer and the flow distribution of air-cooled cold plates, a more extensive study was initiated which tested cold plates of different aspect ratios and manifold configurations.

The cold plates tested can be divided into two general categories: (1) cold plates with plain air-flow channels (without finned or extended surfaces) and (2) cold plates with air-flow channels provided with compact heat-exchanger cores. Cold Plate Nos. 1, 2 and 3 were without finned surfaces, while Cold Plate Nos. 4, 5 and 6 were provided with compact heat-exchanger cores. Each of the two categories represented three different aspect ratios and was tested with three or four different manifold configurations. Except for Cold Plate No. 3, all of the cold plates were of approximately the same size as far as the equipment mounting surfaces were concerned, but of different air-flow channel width (flow channels of different aspect ratios). This was done to ease comparison among the different cold plates and manifold configurations by reducing the amount of unknowns which could affect thermal performance.

All of the cold plates were made of aluminum and provided with flanges to allow installation of different manifold configurations. To simulate realistic conditions, actual electronic equipment (power transistors 2N1724) were used as the heat load. Thermal performance of the cold plates was determined at different component power dissipation rates and different cooling-air flow rates. Actual test results were compared with computer analysis, based on the Resistance-Capacitance (R-C) network.

Although it is not likely that a cold plate for cooling of high-density electronic equipment would be made without extended surfaces, it is of interest, from the heat-transfer point of view, to investigate the thermal performance characteristics of such simple cooling devices.

2. Manifold Configurations

Since the cold plates in an actual electronic equipment cooling system would be connected to an air distribution ductwork, a manifold is needed to admit cooling air to the cold plates. The available space and the electronic equipment arrangement would dictate the manifold configuration and arrangement used. Besides effects upon heat transfer and pressure drop, some manifold configurations might cause flow distribution, thus temperature distribution problems.

So that the cooling-air entry effects upon the thermal performance of the cold plates could be investigated, manifolds of four different configurations were fabricated and tested. The manifold configurations and the test results are presented with the particular cold plates that were used.

(1) Air-Cooled Cold Plate No. 1

Figure 81 shows the outline of the experimental air-cooled Cold Plate No. 1, which was a welded construction made of aluminum and provided with flanges for installation of manifolds. The air-flow channel measured 6-1/4 x 1/4 inches, representing an aspect ratio of R = 6.25/0.25 = 25. The hydraulic diameter was D_h = 0.040 ft.

Figure 82 shows the experimental air-cooled Cold Plate No. 1 with the manifold configuration identified as #1. The figure also shows transistor and thermocouple locations. The transistors (type 2N1724) were attached directly to the plate without insulating washers by inserting them into tapped holes. Heat-sink compound was applied to all mounting joints. Transistor case and plate temperatures were measured at different cooling-air flow rates and different electrical power dissipation rates from the transistors.

After the temperature of the plate at the different cooling-air flow rates was measured and the electrical power dissipation from the components was computed, the convection heat-transfer coefficients were determined from the following expression:

$$Q = Ah\ (\Delta t)_m$$

$$h = \frac{Q}{A(\Delta t)_m}$$

where Q = heat transfer rate by convection, Btu/hr

h = heat transfer coefficient, Btu/hr ft^2°F

A = heat transfer area, ft^2

Δt_m = logarithmic mean temperature difference, °F.

$$\Delta t_m = \frac{\Delta t' - \Delta t''}{\ln \frac{\Delta t'}{\Delta t''}}$$

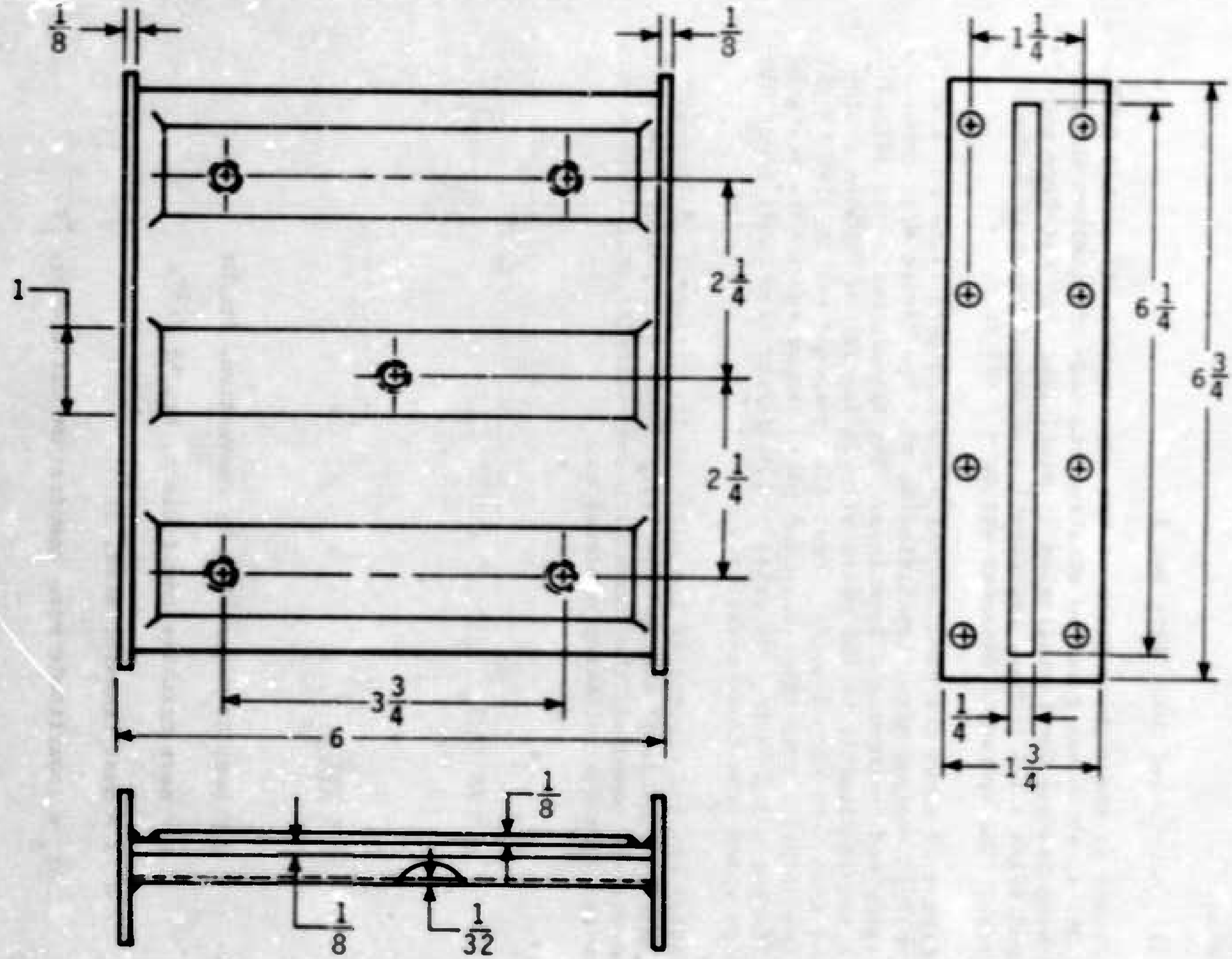

Figure 81. Air-Cooled Cold Plate No. 1

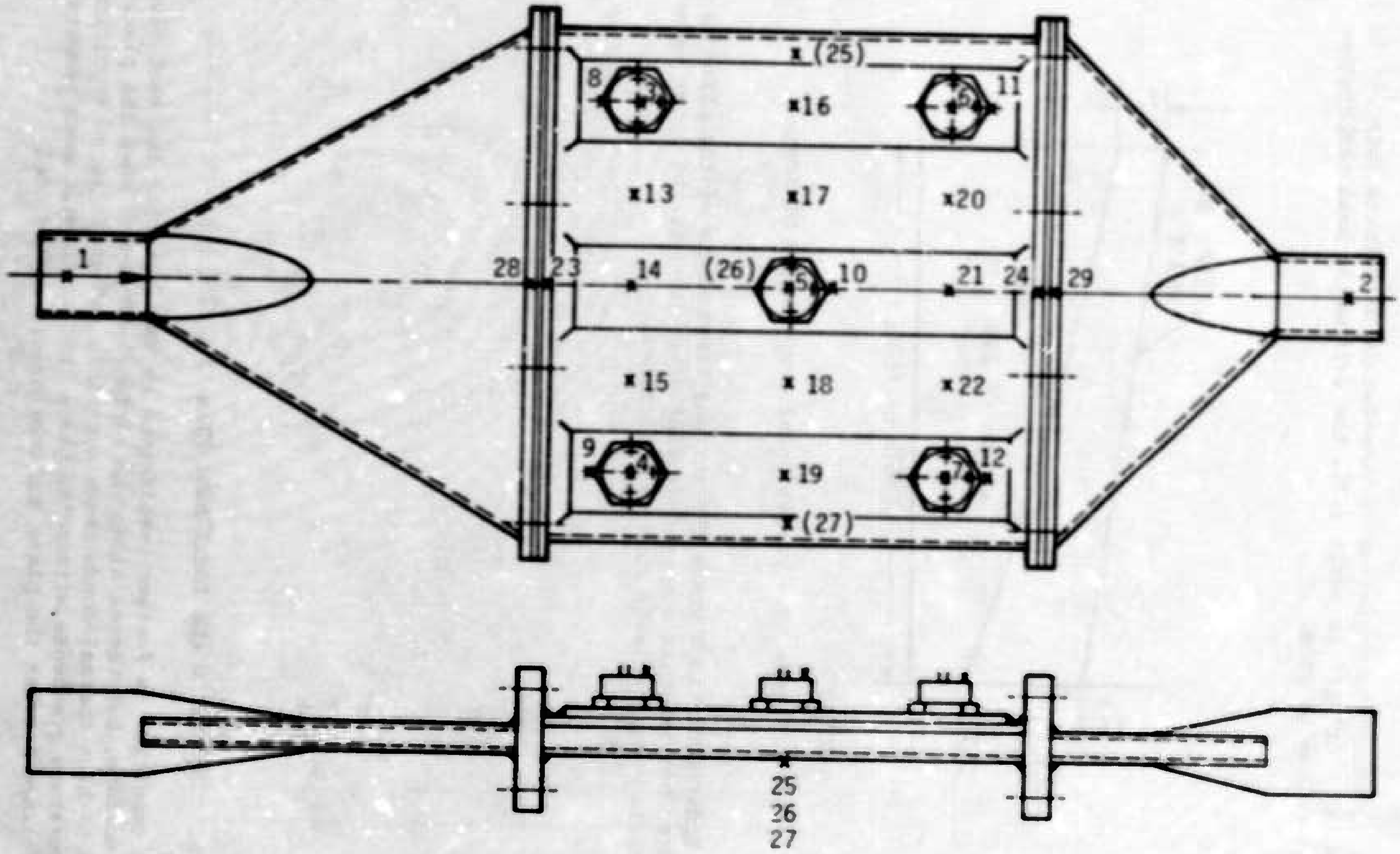

Figure 82. Air-Cooled Cold Plate No. 1 with Manifold Configuration #1

Figure 83 shows the variation of temperature difference from $\Delta t'$ to $\Delta t''$. If the ratio $\Delta t'/\Delta t''$ is small (<2), the arithmetic mean temperature difference can be used.

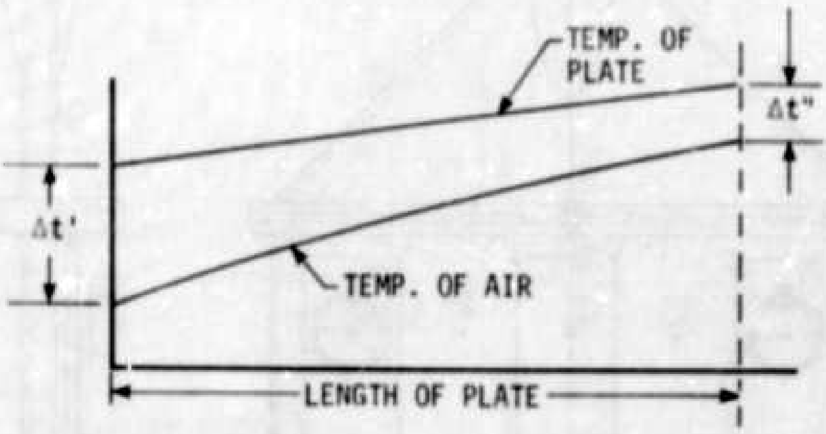

Figure 83. Variation of Temperature Difference

Under conditions where the surface temperature of the plate is not uniform, but exhibits some significant step changes, the local values of the surface coefficients must be determined.

$$h_x = \frac{q''(x)}{\Delta t}$$

and

$$Nu_x = h_x \frac{x}{k}$$

where $q''(x)$ = the local heat flux.

This condition is further complicated by the fact that the heat flux is not uniform, but varies along the surface. However, when the plate is made of high thermal-conductance material, and there is no significant temperature gradients within the plate, the arithmetic mean temperature difference between the plate and cooling air can be used

$$h = \frac{Q}{A(\Delta t)_m}$$

where

$$(\Delta t)_m = \bar{t}_{pl} - \bar{t}_{fl}$$

$\bar{t}_{pl}$ = arithmetic mean temperature of the plate, °F

$\bar{t}_{fl}$ = mean temperature of air, °F.

Table 17 presents all the test conditions of Cold Plate No. 1 with manifold configuration #1. Temperature readings of the thermocouples at the different test conditions are contained in Appendix A.

Figure 84 shows temperature distribution across the plate at the two sections indicated by the thermocouples. The tests were performed at different cooling-air flow rates, but with constant power dissipation rates from the transistors. The figure shows the significant reduction of the temperature of the plate when the cooling-air flow rate is increased. It also shows that the rate of temperature change is reduced at the higher air-flow rates, indicating that there is a limit to which some noticeable temperature reduction can be obtained. As far as temperature gradients within the plate are concerned, no noticeable effects could be observed with the flow-rate changes.

Figure 85 shows temperature distribution across the plate at constant cooling-air flow rates and three different electrical power dissipation rates from the transistors. The figure is self-explanatory.

Figure 86 shows temperature distribution of the cold plate at a cooling-air flow rate of $\dot{w}$ = 68 lbs/hr, and an electrical power dissipation of 100 watts (20 watts from each transistor). The figure shows comparison between experimental and analytical results at two different conditions used in the analysis.

(1) An average heat transfer coefficient based on experimental data was used in determining the convection resistances as follows:

$$Q = \eta_o A_o h_{av} \left(\bar{t}_{(pl)(max)} - \bar{t}_{fl}\right)$$

Table 17. Test Conditions of Air-Cooled Cold Plate No. 1, Manifold Configuration #1

TEST NO.	AIR FLOW RATE (lb/hr)	ELECTRICAL POWER INPUT TO TRANSISTORS (WATTS)				
		TR #1	TR #2	TR #3	TR #4	TR #5
1	22.5	20	20	20	20	20
2	45	20	20	20	20	20
3	68	20	20	20	20	20
4	94	20	20	20	20	20
5	22.5			10		
6	22.5			20		
7	22.5			40		
8	22.5	10	10	10	10	10
9	22.5	15	15	15	15	15
10	22.5	20	20	20	20	20

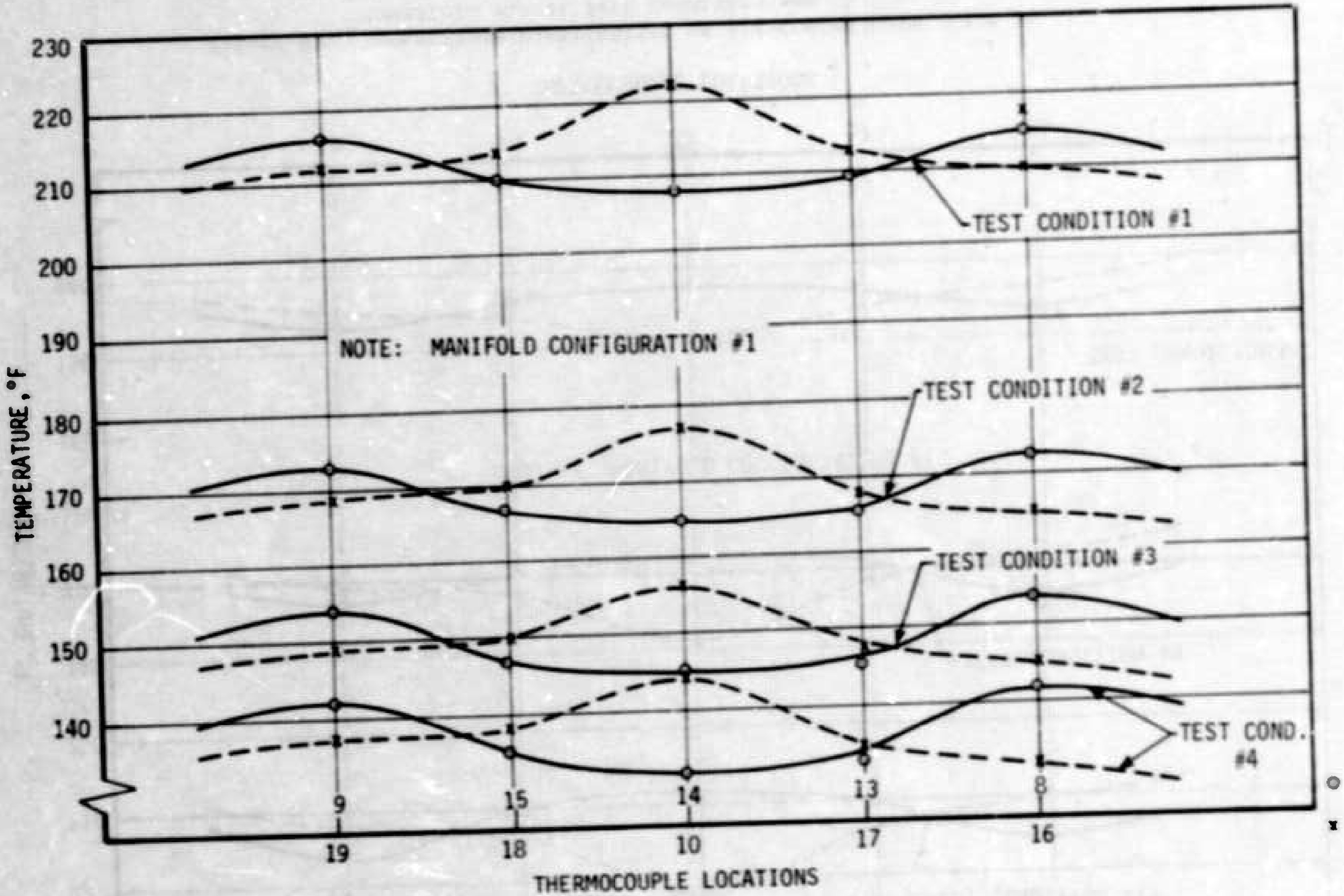

Figure 84. Temperature Distribution of Air-Cooled Cold Plate No. 1 (Manifold #1) at Test Condition Nos, 1 thru 4

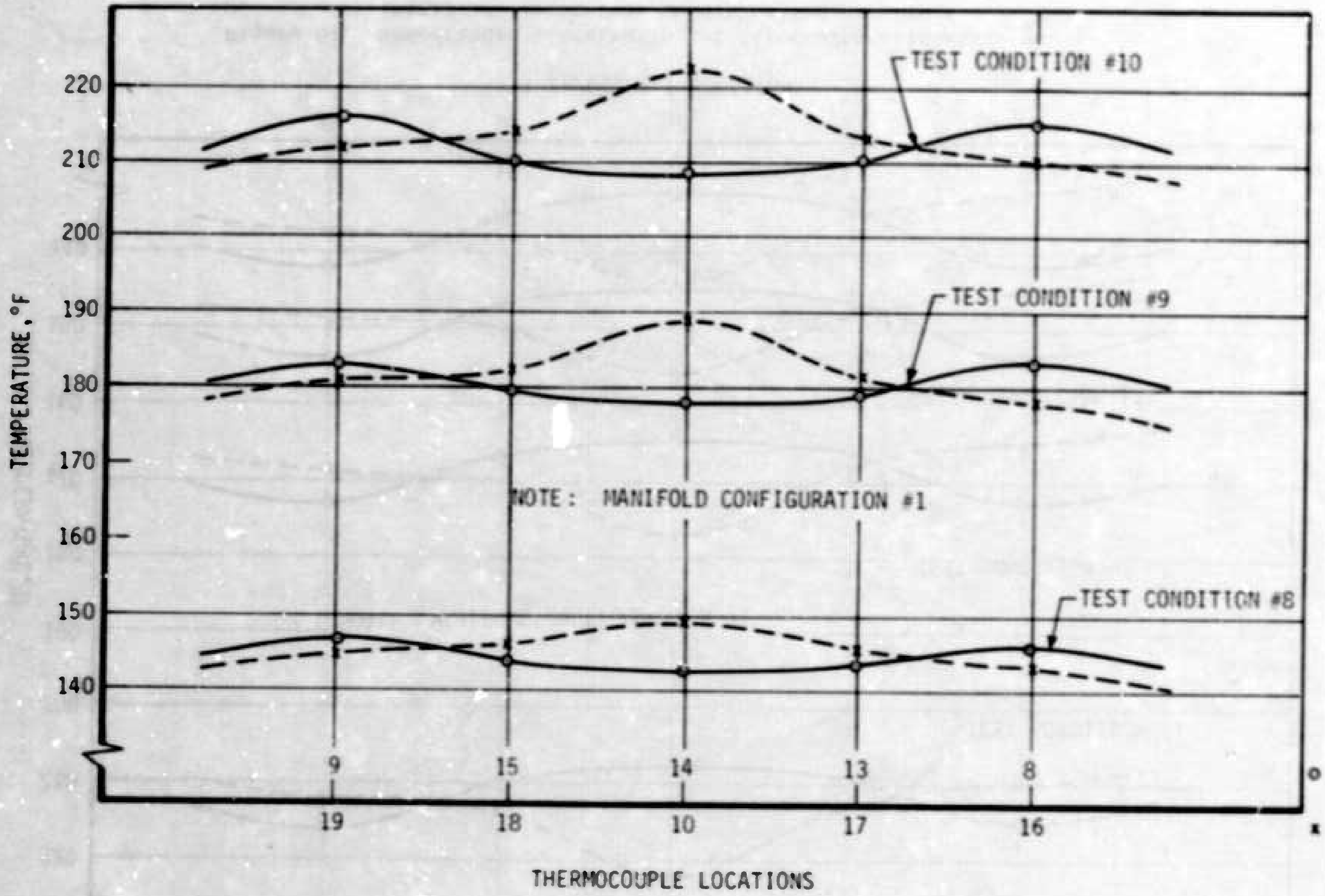

Figure 85. Temperature Distribution of Air-Cooled Cold Plate No. 1 (Manifold #1) at Test Condition Nos. 8 thru 10

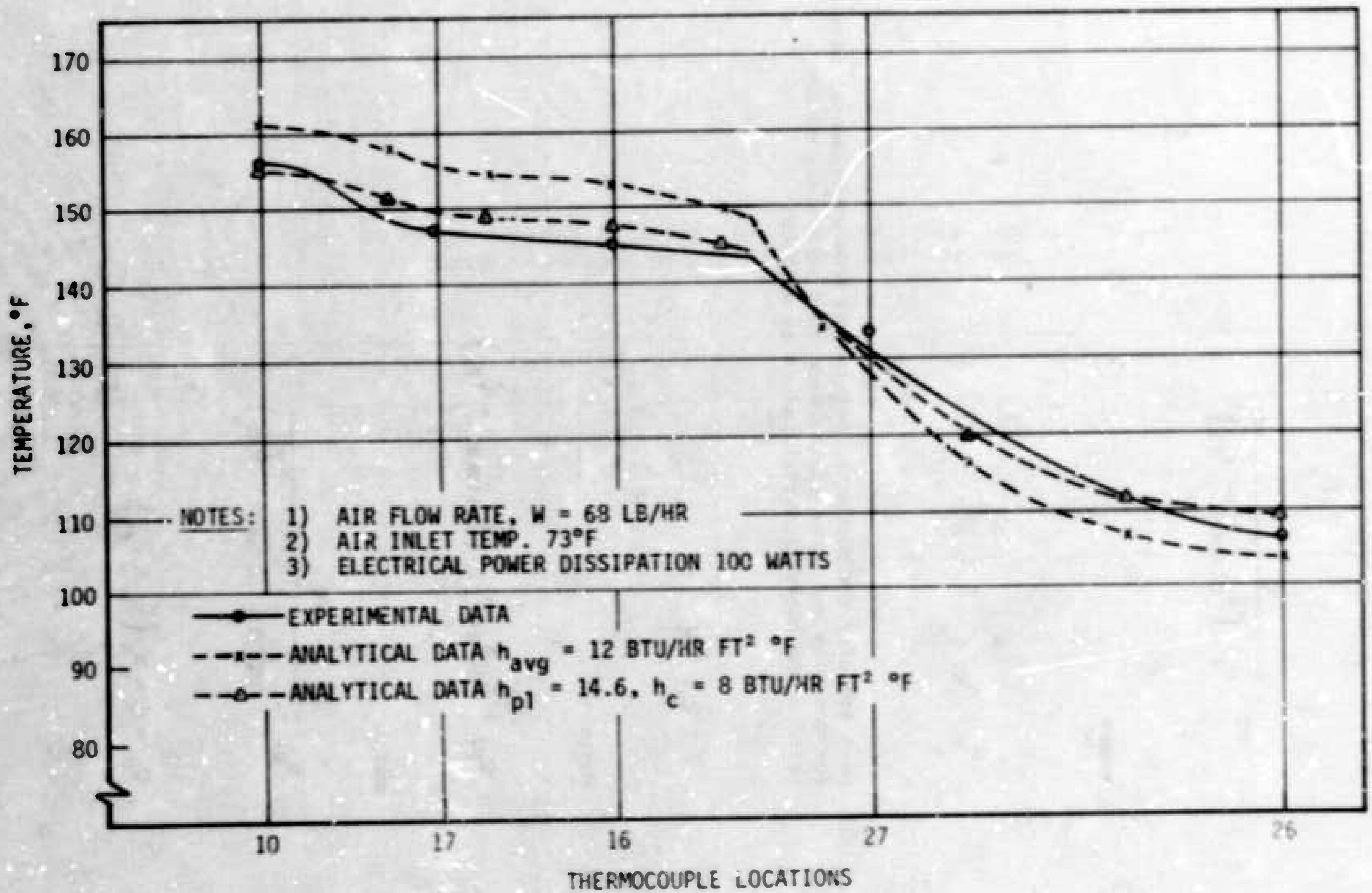

Figure 86. Temperature Distribution of Air-Cooled Cold Plate No. 1 (Manifold #1) Showing Comparison Between Experimental and Analytical Data

and

$$h_{av} = \frac{Q}{\eta_o A_o \left(\bar{t}_{pl(max)} - \bar{t}_{fl} \right)}$$

where

$$\eta_o = \eta_{pl} \frac{A_{pl}}{A_o} + \eta_c \frac{A_c}{A_o}$$

(2) Heat transfer coefficients, determined from experimental data for mounting and cover plates were used separately to determine the convection resistances as follows:

$$Q = Q_{pl} + Q_c$$

where

$$Q_{pl} = \eta_{pl} A_{pl} h_{pl} \left(\bar{t}_{pl(max)} - \bar{t}_{fl} \right)$$

and

$$h_{pl} = \frac{Q_{pl}}{\eta_{pl} A_{pl} \left(\bar{t}_{pl(max)} - \bar{t}_{fl} \right)}$$

$$Q_c = \eta_c A_c h_c \left(\bar{t}_b - \bar{t}_{fl} \right)$$

and

$$h_c = \frac{Q_c}{\eta_c A_c \left(\bar{t}_b - \bar{t}_{f1} \right)}$$

It can be seen that by using the proper heat-transfer coefficients for the mounting and cover plates, a much closer agreement between the experimental and analytical data can be obtained. The average heat transfer coefficient gives higher temperatures for the mounting plate and lower temperatures for the cover plate.

Figure 87 shows temperature distribution of the cold plate at a cooling-air flow rate of w = 94 lbs/hr and a total heat load of 100 watts (20 watts from each transistor). Comparison with experimental data is made at three different cover-plate thicknesses: 1/32 inch, 1/16 inch and 1/8 inch. By increasing the cover plate thickness from 1/32 inch to 1.8 inch, only a minor temperature reduction of the mounting plate could be achieved. It should be noted that the analysis was performed by using the same heat-transfer coefficient for all three fin thicknesses. This probably will not be true under actual conditions; it can be expected that the heat-transfer coefficient of the cover plate will increase with increased temperature uniformity.

Figure 88 shows temperature distribution of the cold plate at a constant cooling-air flow rate of $\dot{w}$ = 22.5 lbs/hr and at three different electrical power dissipation rates from Transistor #3 (only Transistor #3 was energized). Comparison is also made between experimental and analytical data. The largest difference between the two values occurs at the concentrated heat load, and was probably caused by the selection of too large of nodes around the heat input area. Generally, however, the agreement between experimental and analytical data can be considered as good (only 4°F difference). It must be noted that the experimentally determined heat-transfer coefficients were used in the analysis. The figure also shows the significant temperature gradients within the plate at the higher power dissipation rates.

Figure 89 shows case temperature of Transistor #3 versus cooling air flow rate. The electrical power dissipation from the transistors (20 watts from each transistor) was maintained constant throughout the tests. Only Transistor #3 temperature is shown because it was only a few degrees higher than the temperature of the other transistors. The figure shows that equipment temperature can be significantly affected by the cooling-air flow rate. If other parameters are kept constant, selection of the proper air flow rate must be based on the temperature requirements of the electronic equipment. It should be noted, however, that there is a limit beyond which the increased cooling-air flow rate will not noticeably reduce the equipment temperature.

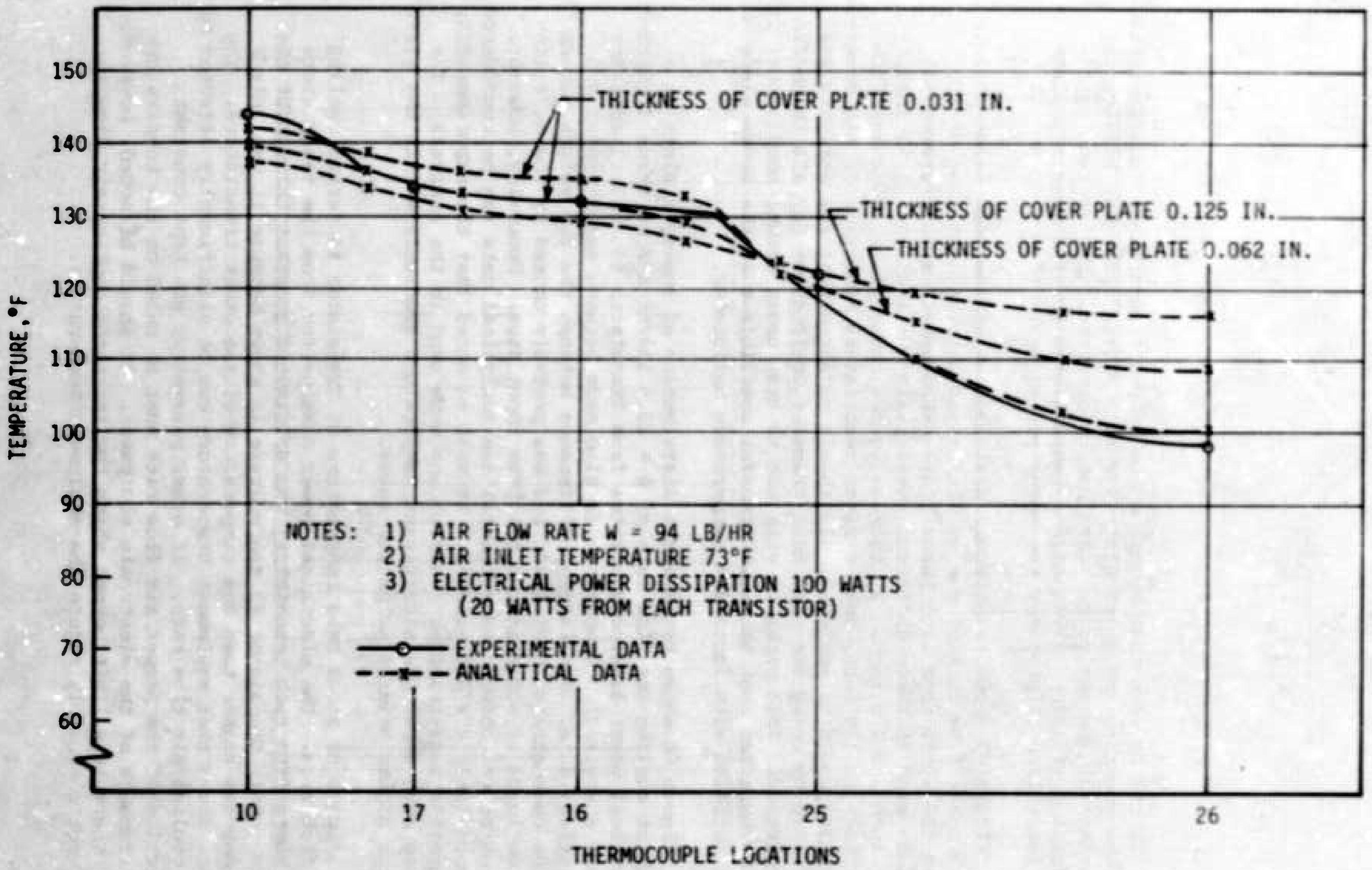

Figure 87. Temperature Distribution of Air-Cooled Cold Plate No. 1 (Manifold #1) Showing Comparison Between Experimental and Analytical Data

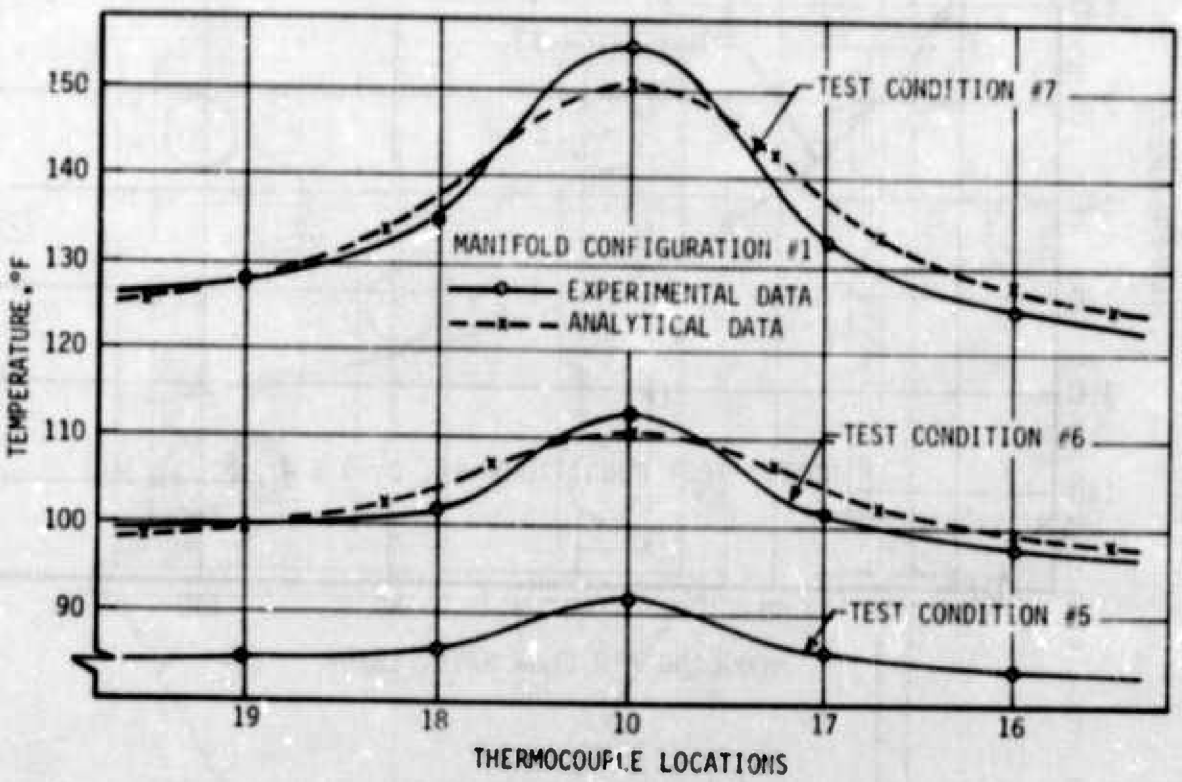

Figure 88. Temperature Distribution of Air-Cooled Cold Plate No. 1 (Manifold #1) at Test Conditions 5 thru 7

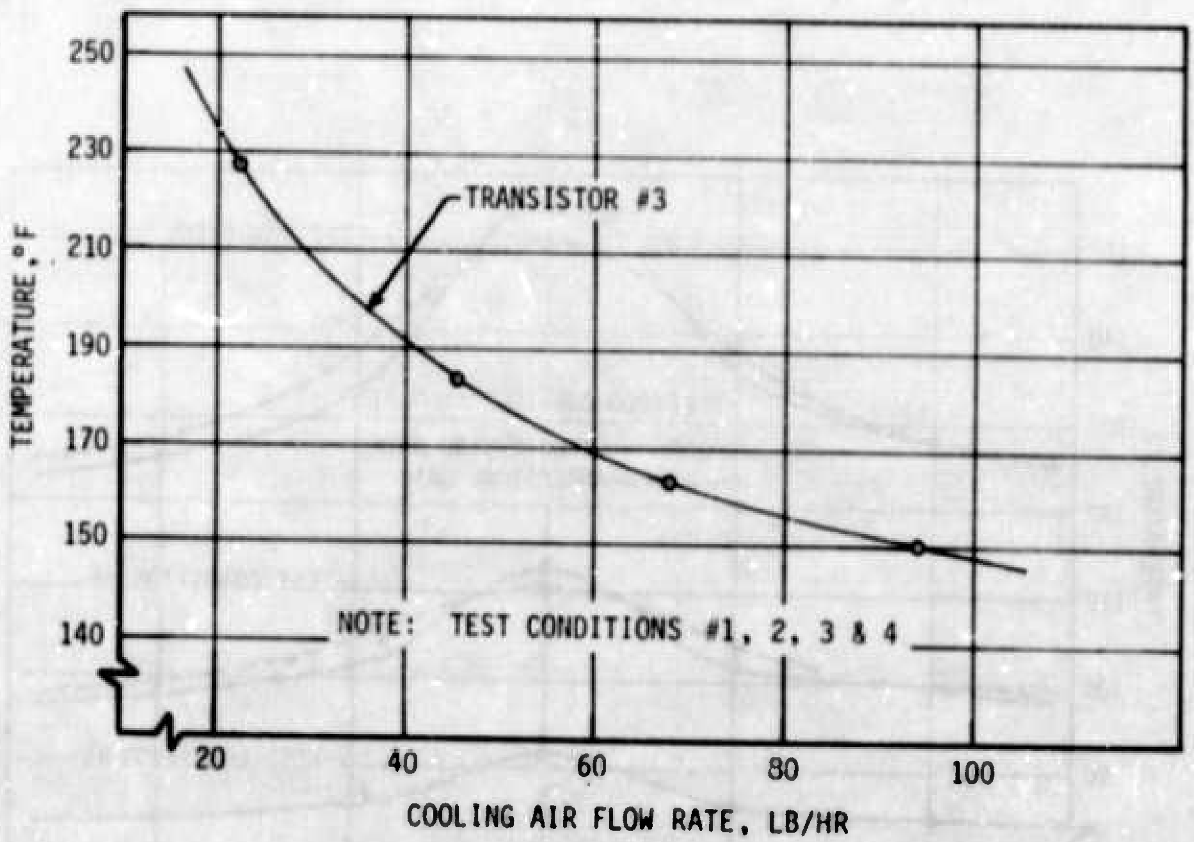

Figure 89. Case Temperature of Transistor No. 3 vs Cooling Air Flow Rate for Air-Cooled Cold Plate No. 1 (Manifold #1)

Figure 90 shows the experimental air-cooled Cold Plate No. 1 with the manifold configuration identified as #2. General configuration of the manifold is the same as #1, except for a 12-inch straight section attached to the cooling-air entrance end of the cold plate. This reduced turbulence effects caused by the manifold. In accordance with Reference 9, the local Nusselt number has closely approached its asymptotic value at a thermal entry length of X/D = 25.

As with the previous configuration, the cold plate was tested at a constant heat load and different cooling-air flow rates to allow determination of the heat-transfer coefficients.

Table 18 presents the test conditions performed with manifold configuration #2.

Table 18. Test Conditions of Air-Cooled Cold Plate No. 1 (Manifold Configuration #2)

TEST NO.	AIR FLOW RATE (lb/hr)	ELECTRICAL POWER INPUT TO TRANSISTORS (WATTS)				
		TR #1	TR #2	TR #3	TR #4	TR #5
1	22.5	20	20	20	20	20
2	45	20	20	20	20	20
3	68	20	20	20	20	20
4	94	20	20	20	20	20

Temperature readings of the thermocouples are contained in Appendix A. The locations of the thermocouples were the same as shown in Figure 82.

Figure 91 shows temperature distribution across the cold plate at the four different air flow rates. When the temperature distribution between the two manifold arrangements is compared, an approximate temperature difference of 10°F can be observed. The higher temperatures of the cold plate with the 24-inch section were caused by reduced turbulence which, in turn, reduced the heat-transfer coefficients. More detailed discussions about determination of the heat-transfer coefficients are provided at the end of this section.

Figure 92 shows the experimental air cooled Cold Plate No. 1 with the manifold configuration identified as #3. Such a manifold configuration would occupy the least space; therefore, it could be used in systems with space limitations. Similarly as with the previous configurations, the thermal tests were performed to determine temperature distribution of the cold plate and provide information for computing the experimental Nusselt numbers and/or heat-transfer coefficients.

Table 19 presents the test conditions of the cold plate.

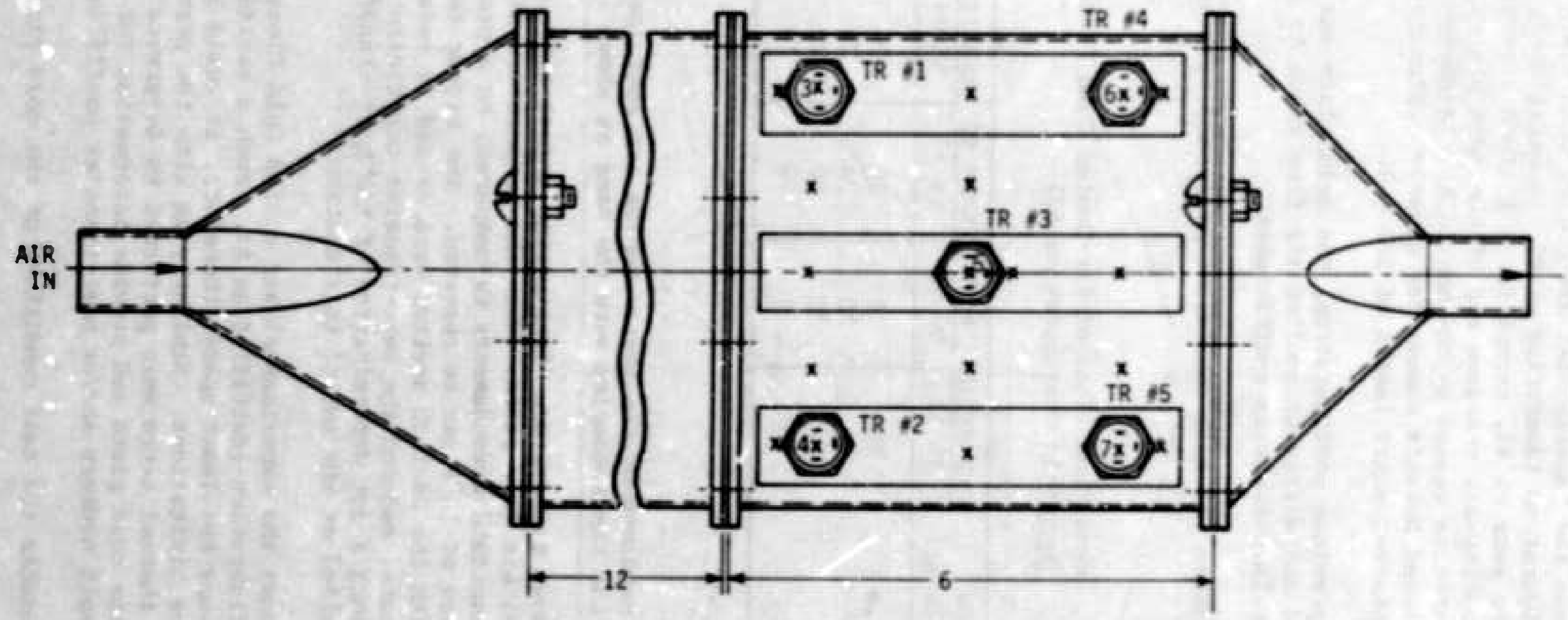

Figure 90. Air-Cooled Cold Plate No. 1 with Manifold Configuration #2

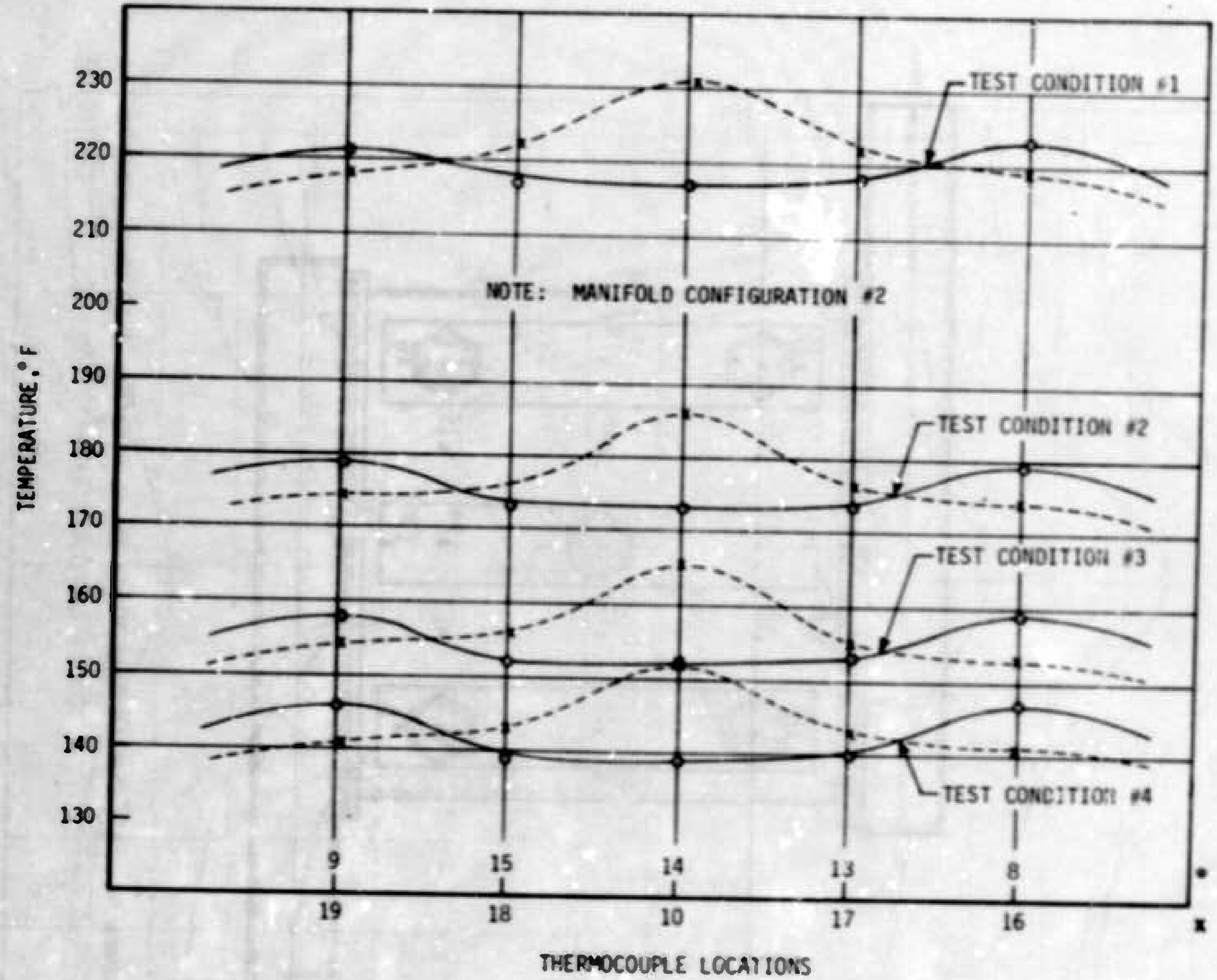

Figure 91. Temperature Distribution of Air-Cooled Cold Plate No. 1 (Manifold #2) at Test Condition Nos. 1 thru 4

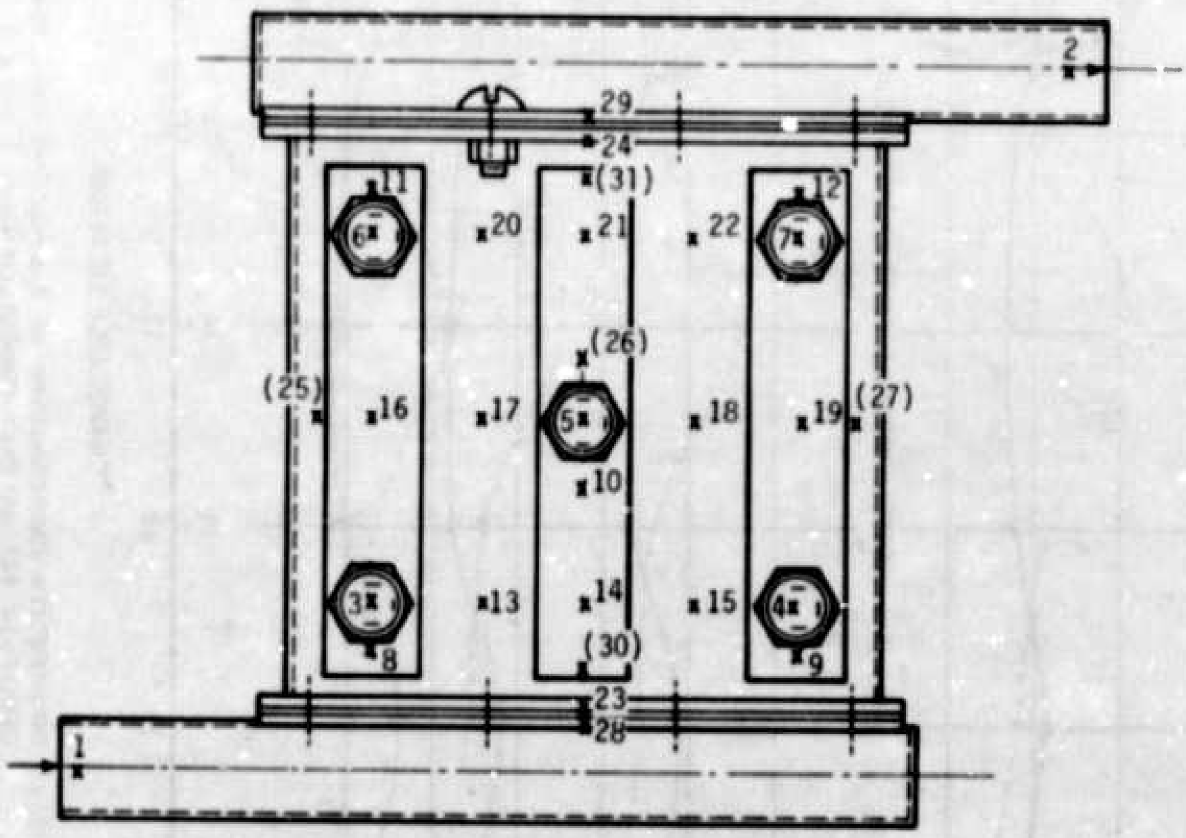

Figure 92. Air-Cooled Cold Plate No. 1 with Manifold Configuration #3

Table 19. Test Conditions of Air-Cooled Cold Plate No. 1 (Manifold Configuration #3)

TEST NO.	AIR FLOW RATE (lb/hr)	ELECTRICAL POWER INPUT TO TRANSISTORS (WATTS)				
		TR #1	TR #2	TR #3	TR #4	TR #5
1	22.5	20	20	20	20	20
2	45	20	20	20	20	20
3	68	20	20	20	20	20
4	94	20	20	20	20	20
5	45			20		
6	45			30		
7	45			40		

Temperature measurements of the cold plate and electronic components at the different test conditions are contained in Appendix A.

Figure 93 shows temperature distribution across the cold plate at four different cooling-air flow rates and at a constant electrical power dissipation rate of 100 watts from the components (20 watts from each transistor). Although a symmetrical heat load was applied to the cold plate, temperature distribution of the plate is distorted. The temperature measurements indicated that the largest cooling-air flow rate occurred at the dead end of the entrance manifold. This condition can be expected with uniform flow-channel width and manifold slot. The flow distribution could be improved by providing the gasket or manifold with a tapered slot. The temperature differentials across the cold plate that can be tolerated depend on the temperature uniformity requirements of the electronic equipment. Manifold slots with reduced cross-sectional areas will increase pressure drop and acoustical noise, and their use, therefore, should be limited to specific applications only. More detailed discussions about flow distribution in manifolds can be found in Section VIII.

Figure 94 shows temperature distribution across the cold plate at different electrical power dissipation rates from Transistor #3 (only Transistor #3 was energized) and a constant cooling-air flow rate of 45 lbs/hr. The temperature distribution is shown at the cooling-air entrance end and central section of the cold plate. As in the previous case, the same trend in temperature distribution can be observed.

The experimentally determined Nusselt numbers were plotted versus Reynolds numbers for the three manifold configurations and are shown in Figure 95. The Nusselt numbers were evaluated from the known expression

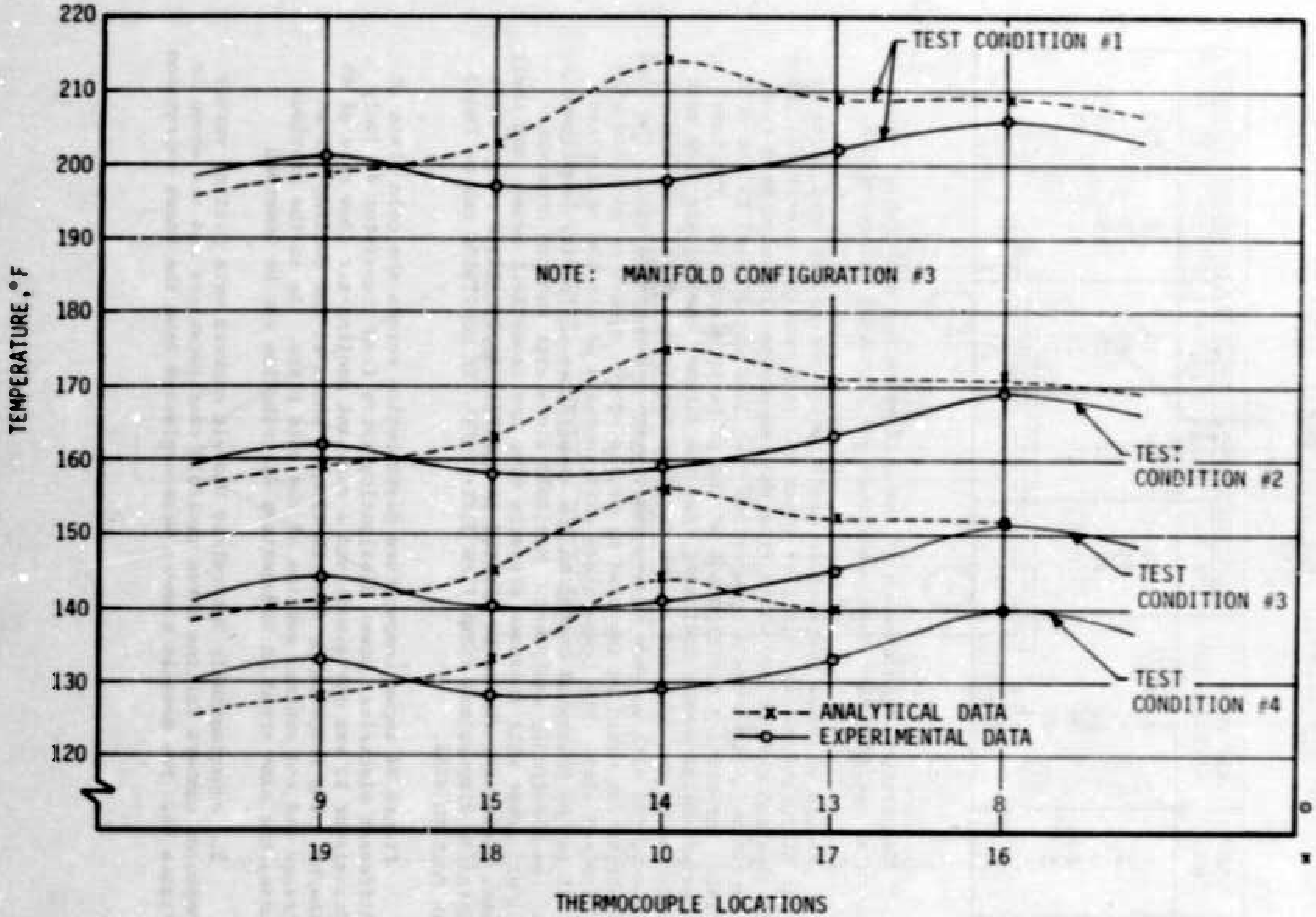

Figure 93. Temperature Distribution of Air-Cooled Cold Plate No. 1 (Manifold #3) at Test Condition Nos. 1 thru 4

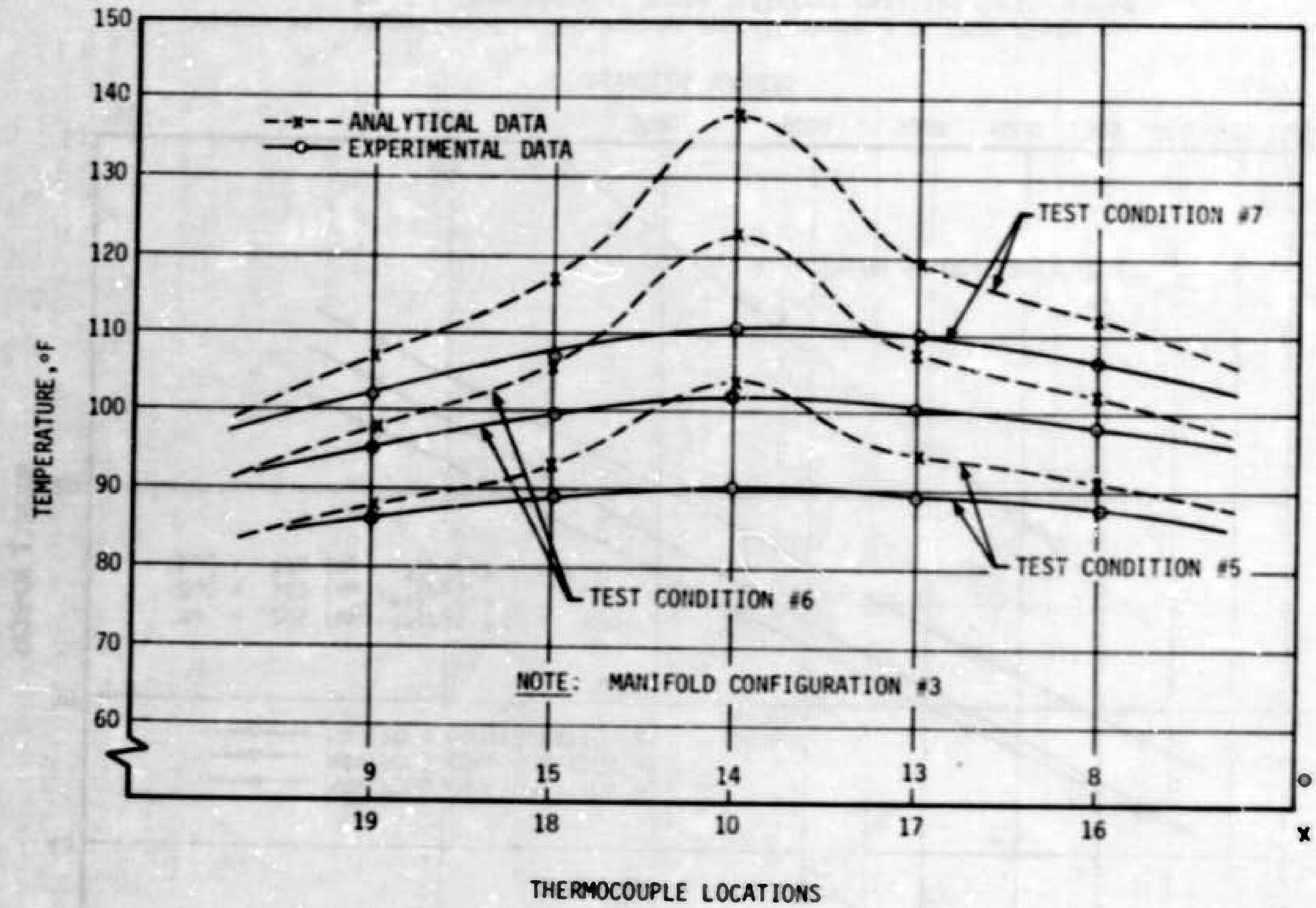

Figure 94. Temperature Distribution of Air-Cooled Cold Plate No. 1 (Manifold #3) at Test Condition Nos. 5 thru 7

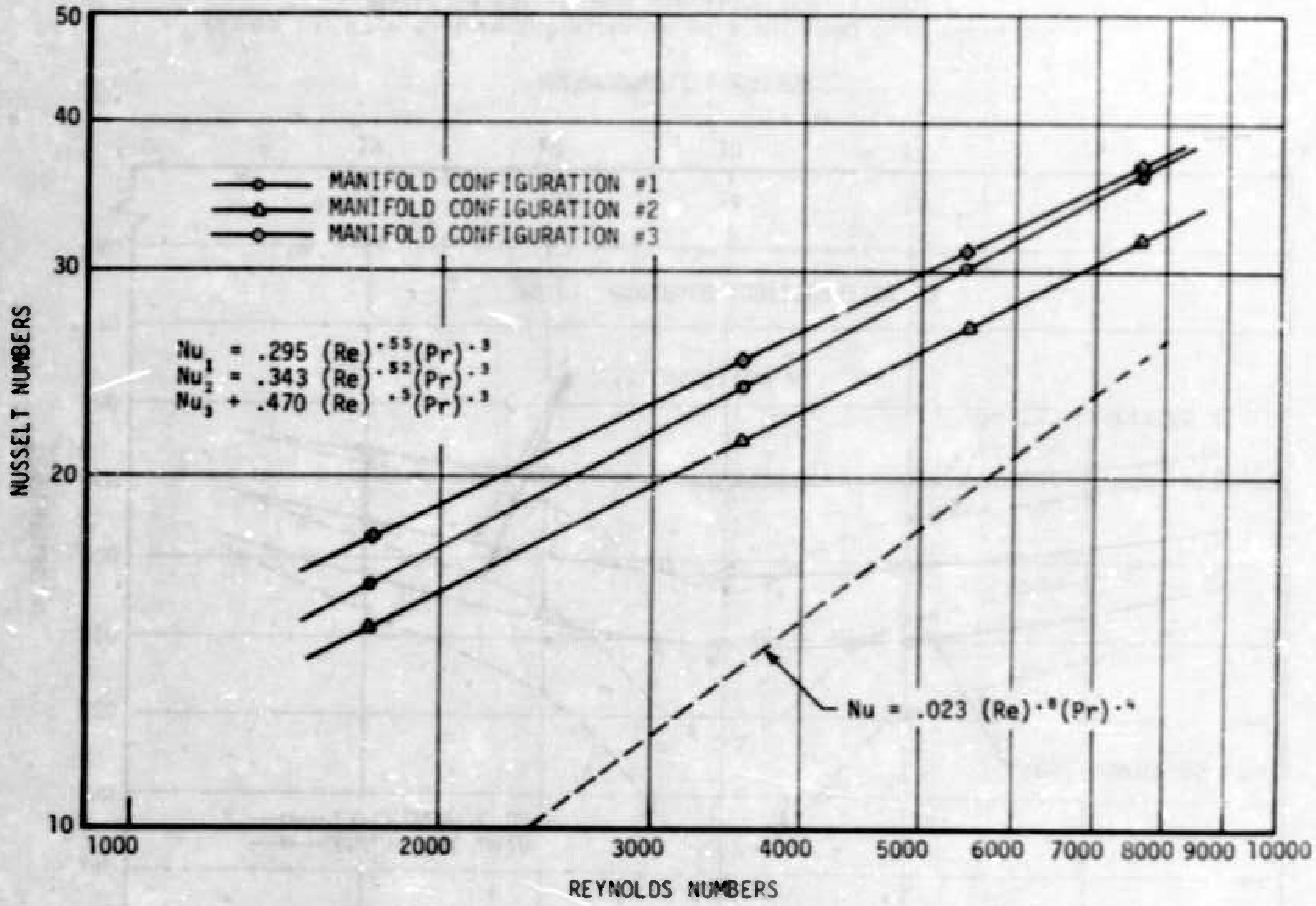

Figure 95. Experimentally Determined Nusselt Numbers of Cold Plate No. 1 - Comparison of Three Different Manifold Configurations

$$Nu = h \frac{D_h}{k}$$

where h = the heat transfer coefficient, Btu/hr ft^2°F

D_h = the hydraulic diameter, ft

k = the thermal conductance of the air, Btu/hr ft°F.

Procedures for determining the forced-convection heat-transfer coefficients have already been discussed. The next step was the determination of constants in the Nusselt expression when written in the general form of:

$$Nu = C(Re)^m(Pr)^n$$

Theoretically, three equations are needed to determine the three constants. However, the Prandtl number was kept constant throughout the experiments, with the Reynolds and Nusselt numbers used as variables. The experimental data was plotted on logarithmic coordinates. After a line was drawn through the plotted points, the exponent, m, was determined from the slope of the line.

Writing the Nusselt equation for two points on the line, we can determine that

$$Nu_1 = C(Re)_1^{\ m}(Pr)_1^{\ n}$$

$$Nu_2 = C(Re)_2^{\ m}(Pr)_2^{\ n}$$

or

$$\log Nu_1 = \log C + m \log(Re)_1 + n \log (Pr)_1$$

$$\log Nu_2 = \log C + m \log(Re)_2 + n \log (Pr)_2$$

Subtracting one equation from the other and rearranging, we can compute the exponent, m, as follows:

$$m = \frac{\log Nu_2 - \log Nu_1}{\log Re_2 - \log Re_1}$$

For a constant Prandtl number and exponent n, the constant C can be computed.

Table 20 summarizes the experimentally determined forced-convection heat-transfer coefficients and Nusselt numbers for the three manifold configurations. It should be noted that both the heat-transfer coefficients and Nusselt numbers are average values determined from the following expression:

$$h = \frac{Q}{\eta_o A_o \left(\bar{t}_{(pl)max} - \bar{t}_{fl}\right)}$$

where η_o = the overall surface effectiveness

A_o = the total heat transfer surface area, ft^2

$\bar{t}_{(pl)max}$ = the average maximum temperature of the cold plate measured at the transistor locations, °F

$\bar{t}_{fl}$ = the arithmetic mean cooling air temperature, °F

Q = the total heat load dissipated by the electronic equipment, Btu/hr.

When thermal performances of the cold plate are compared with the three different manifold configurations, it can be seen that manifold configuration #3 provides the highest Nusselt numbers. This condition can be explained by the larger turbulence induced by the sharp turn of the cooling air stream. Figure 95 shows that the difference in Nusselt numbers between manifold configurations #1 and #3 diminishes with increased Reynolds numbers. It also shows that the manifold configuration, even with the 24-inch straight section, does not have any significant effect upon the Nusselt numbers.

For comparison purposes, the Nusselt numbers determined by the McAdams equation are also plotted on the same figure. It can be seen that there is a significant difference between the predicted and actually measured Nusselt numbers. The difference is particularly large

Table 20. Experimentally Determined Heat-Transfer Coefficients and Nusselt Numbers of Air-Cooled Cold Plate No. 1

MANIFOLD CONFIGURATION	HEAT TRANSFER COEFFICIENTS Btu/hr ft^2°F				NUSSELT NUMBERS			
	TEST #1	TEST #2	TEST #3	TEST #4	TEST #1	TEST #2	TEST #3	TEST #4
1	6.5	9.24	11.6	13.8	16.4	23.8	30.1	36.4
2	5.4	8.37	10.4	10.4	12.25	21.6	27.0	32.0
3	7.0	9.8	12	14.3	18	25.5	31.5	37.7

at the lower Reynolds numbers, indicating that turbulence was induced into the cooling air stream entering the cold plate. Configuration of the flow channel could also have had some effects.

The computed constants were substituted into the Nusselt equation to obtain the following expressions for the three manifold configurations:

(1) Manifold configuration #1

$$Nu = 0.295\ (Re)^{0.55}\ (Pr)^{0.3}$$

(2) Manifold configuration #2

$$Nu = 0.343\ (Re)^{0.52}\ (Pr)^{0.3}$$

(3) Manifold configuration #3

$$Nu = 0.470\ (Re)^{0.5}\ (Pr)^{0.3}$$

Figure 96 shows the resistance-capacitance (R-C) network for air-cooled Cold Plate No. 1. This network was used for predicting temperature distribution of the cold plate at the particular cooling-air flow rates and electrical power dissipation from the components. For uniform flow distribution, all the nodes can be connected to the main coolant stream as shown. When the flow distribution is not uniform, it must be divided into separate channels; and the proper plate nodes must be connected to these channels. Determination of the resistances and capacitances has already been discussed in Section XI and is not, therefore, repeated here. Only the R-C network of this cold plate is shown because the other cold-plate networks are similar.

(2) Air-Cooled Cold Plate No. 2

Figure 97 shows an outline of experimental air-cooled Cold Plate No. 2. The air-flow channel measured 6-1/4 x 1/2 inches, representing an aspect ratio of 6.25/0.5 = 12.5. The hydraulic diameter $\left(D_h = 4A/P\right)$ was 0.0773 ft. The cold plate was provided with flanges to allow installation of different manifold configurations.

Figure 98 shows Cold Plate No. 2 with manifold configuration #1. The figure also shows transistor and thermocouple locations. The transistors (type 2N1724) were attached directly to the plate without insulating washers. Heat-sink compound was applied to all transistor mounting joints. Transistor case and plate temperatures were measured at different cooling-air flow rates and different electrical power dissipation rates from the transistors.

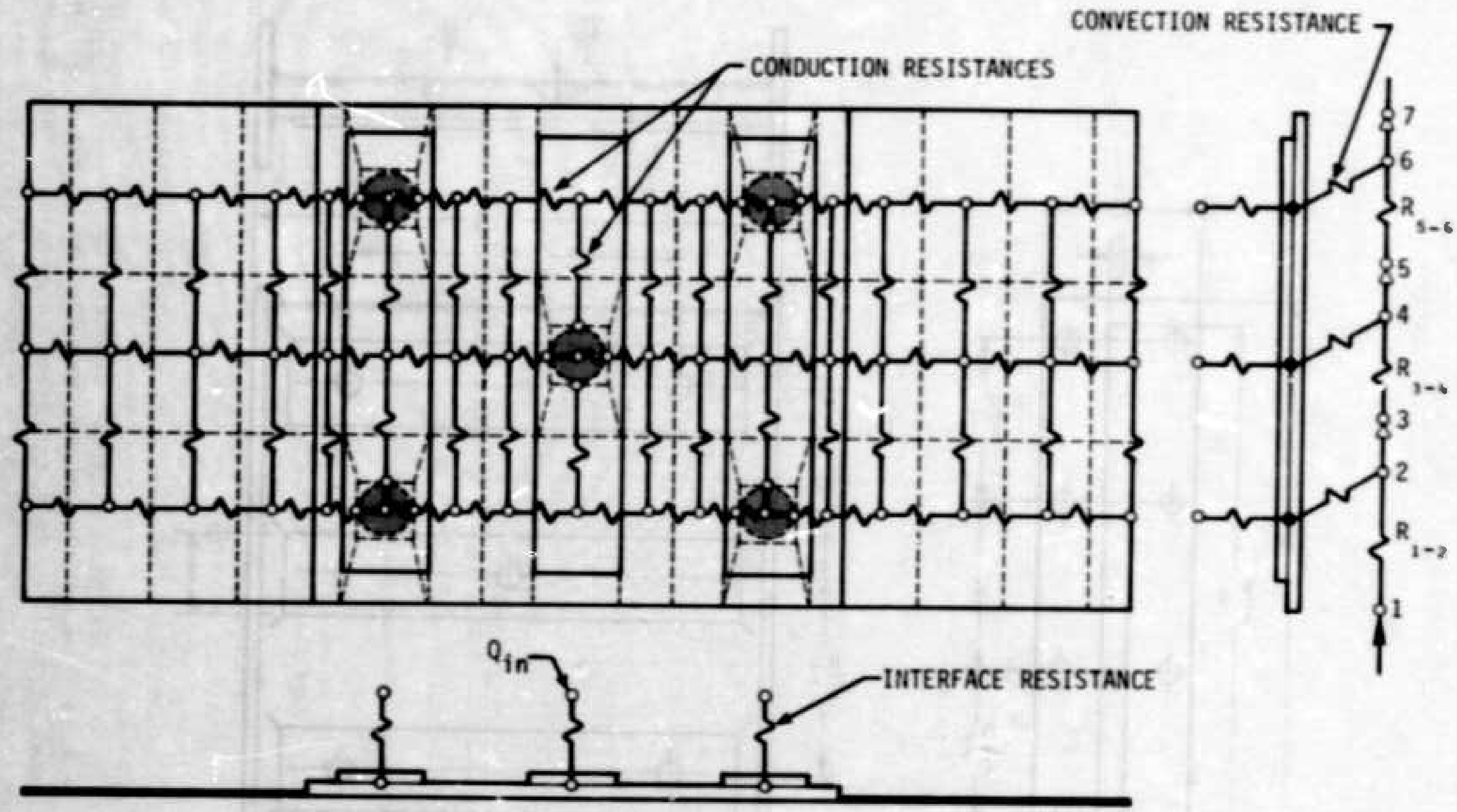

Figure 96. R-C Network of Air-Cooled Cold Plate No. 1

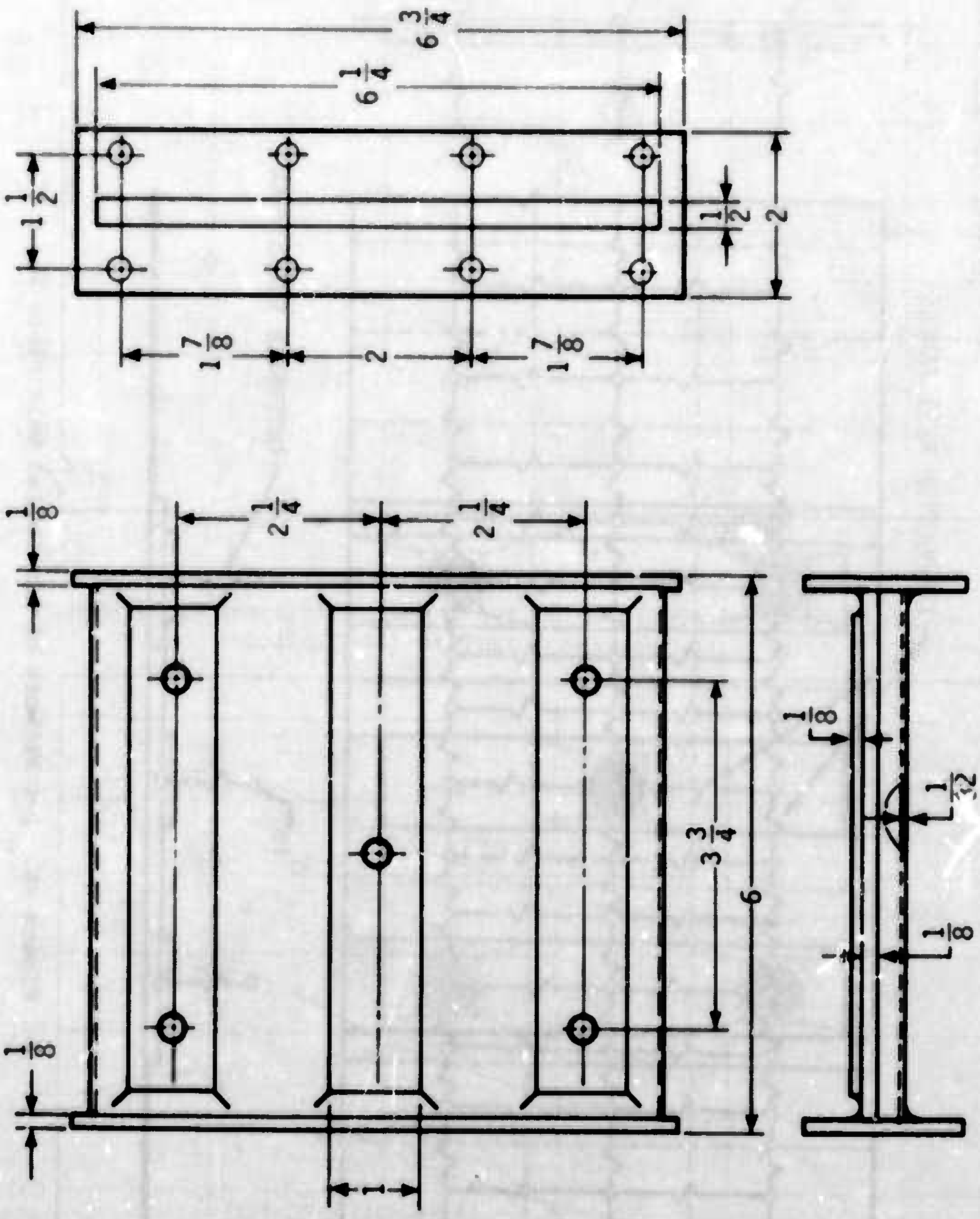

Figure 97. Air-Cooled Cold Plate No. 2

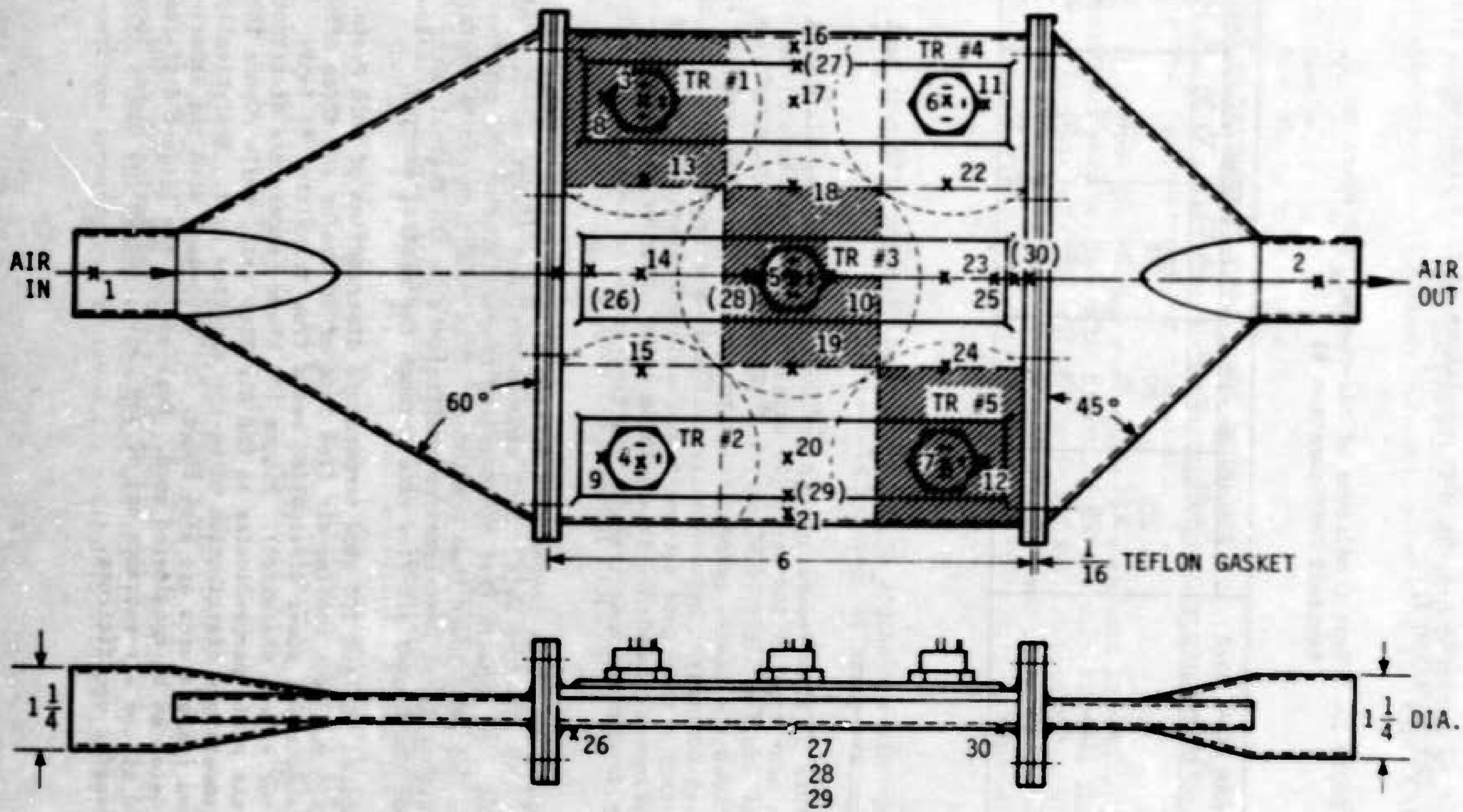

Figure 98. Air-Cooled Cold Plate No. 2 with Manifold Configuration #1

Table 21 presents all the test conditions of Cold Plate No. 2 and manifold configuration #1.

Table 21. Test Conditions of Air-Cooled Cold Plate No. 2, Manifold Configuration #1

TEST NO.	AIR FLOW RATE (lb/hr)	ELECTRICAL POWER INPUT TO TRANSISTORS (watts)				
		TR #1	TR #2	TR #3	TR #4	TR #5
1	45	20	20	20	20	20
2	80	20	20	20	20	20
3	124	20	20	20	20	20
4	80	--	--	20	--	--
5	80	--	--	35	--	--
6	80	--	--	50	--	--

Temperature readings of the thermocouples at the different test conditions are given in Appendix A.

Figure 99 shows temperature distribution of the cold plate at a constant heat load of 100 watts (20 watts from each transistor) and different cooling air flow rates. The temperature measurements were taken across the plate, perpendicular to the air-flow axis. Figure 100 also shows comparison between analytical and experimental data. It can be seen that a very good agreement was achieved between the analysis and the experimental results. It should be noted, however, that experimentally determined heat-transfer coefficients were used in the analysis.

Figure 101 shows temperature distribution of the cold plate parallel to the air-flow axis. Both experimental and analytical data are presented. It appears that the measured temperatures at the cooling-air entrance end were lower than predicted. This condition can be explained by the higher local heat-transfer coefficients in the thermal entry region or the higher air-flow rate through the central section.

Figures 102 and 103 show temperature distribution of Cold Plate No. 2 at a constant cooling-air flow rate of 80 lbs/hr and three different electrical power dissipation rates from Transistor #3 (only Transistor #3 was energized). Figure 102 shows temperature distribution across the plate perpendicular to the air-flow axis, while Figure 103 shows temperature distribution along the air-flow axis. Analytically predicted temperatures are also shown, and agreement with the experimental data can be considered good. Here again, the largest difference occurred at the air-entrance end of the plate, indicating higher local heat-transfer coefficients.

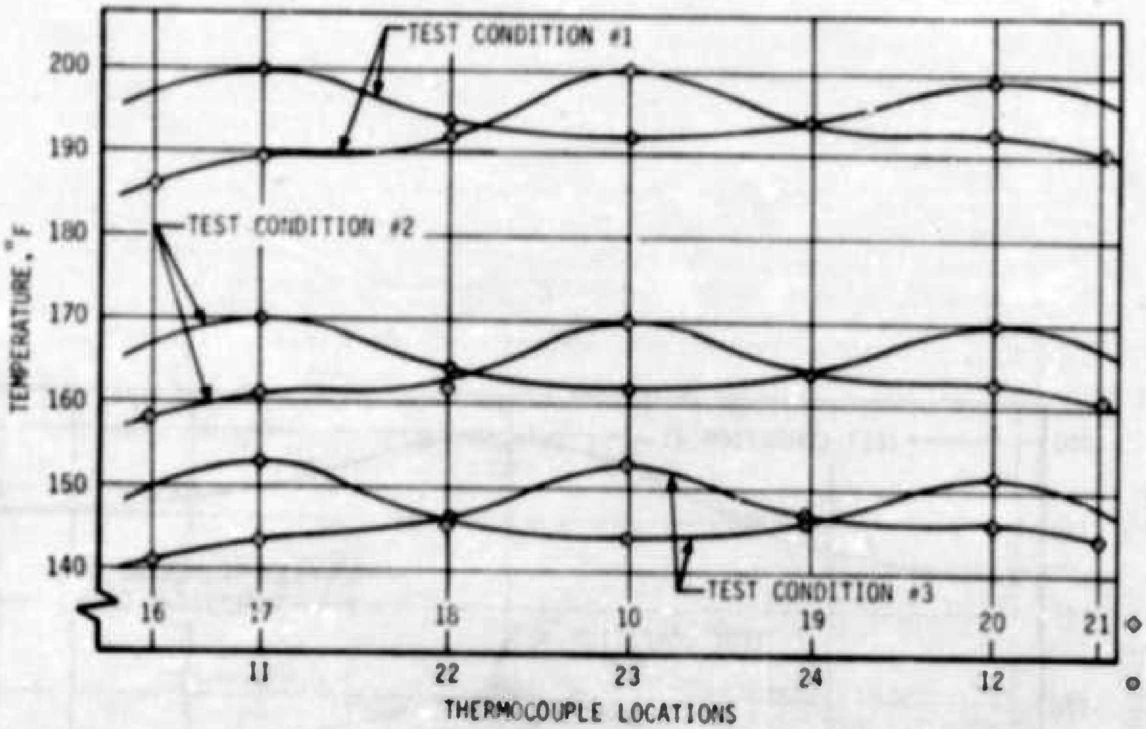

Figure 99. Temperature Distribution of Cold Plate No. 2 (Manifold #1) at Test Condition Nos. 1 thru 3 (TC 16-21)

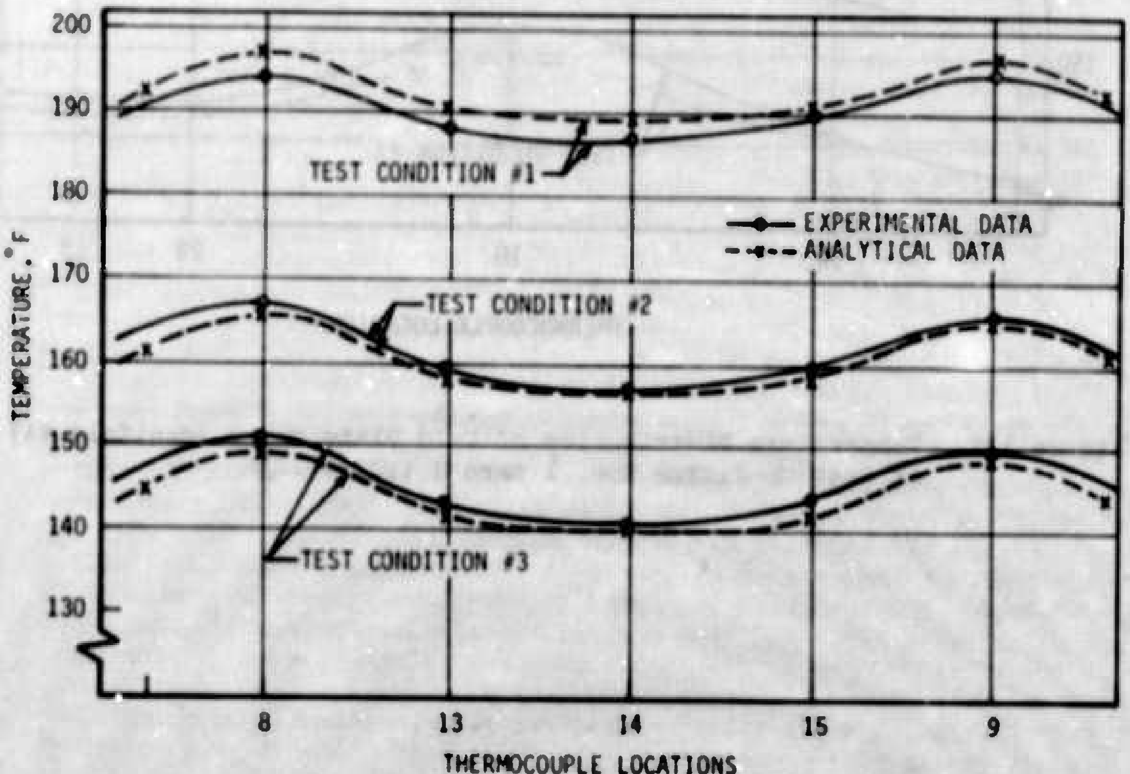

Figure 100. Temperature Distribution of Cold Plate No. 2 (Manifold #1) at Test Condition Nos. 1 thru 3 (TC 8-15)

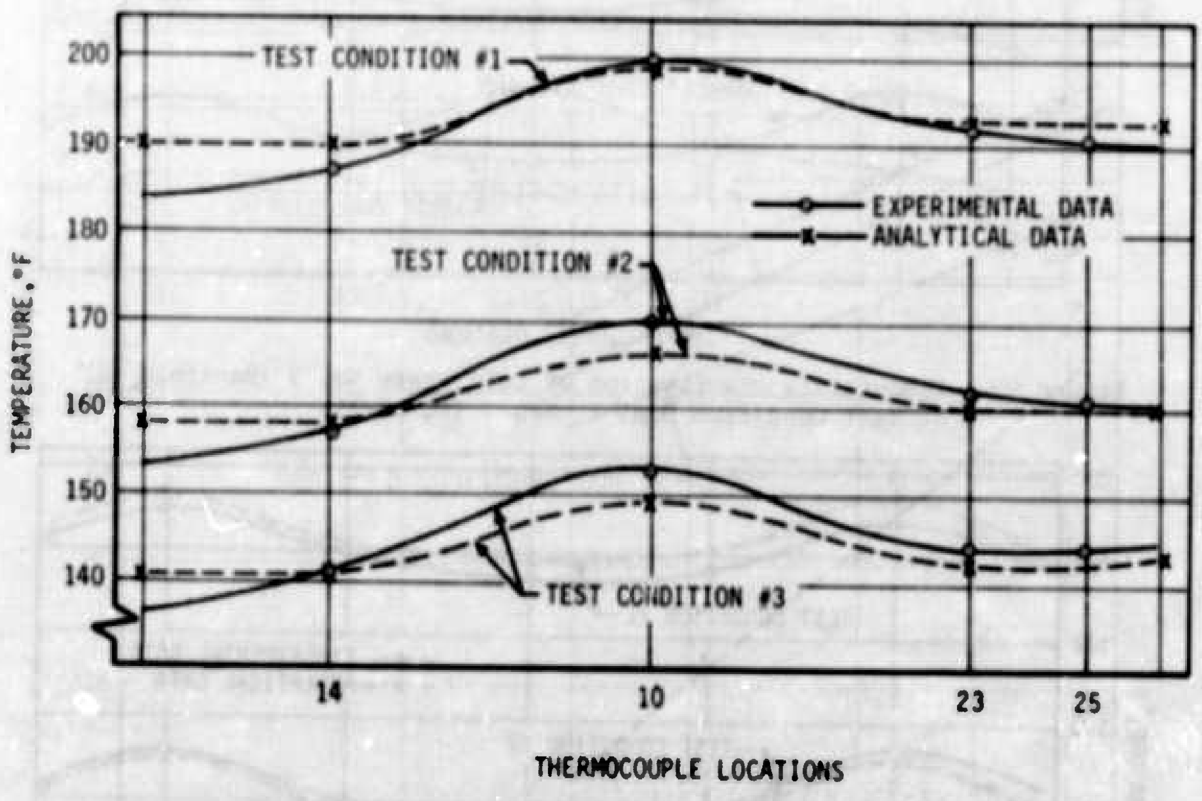

Figure 101. Temperature Distribution of Cold Plate No. 2 (Manifold #1) at Test Condition Nos. 1 thru 3 (TC 10-25)

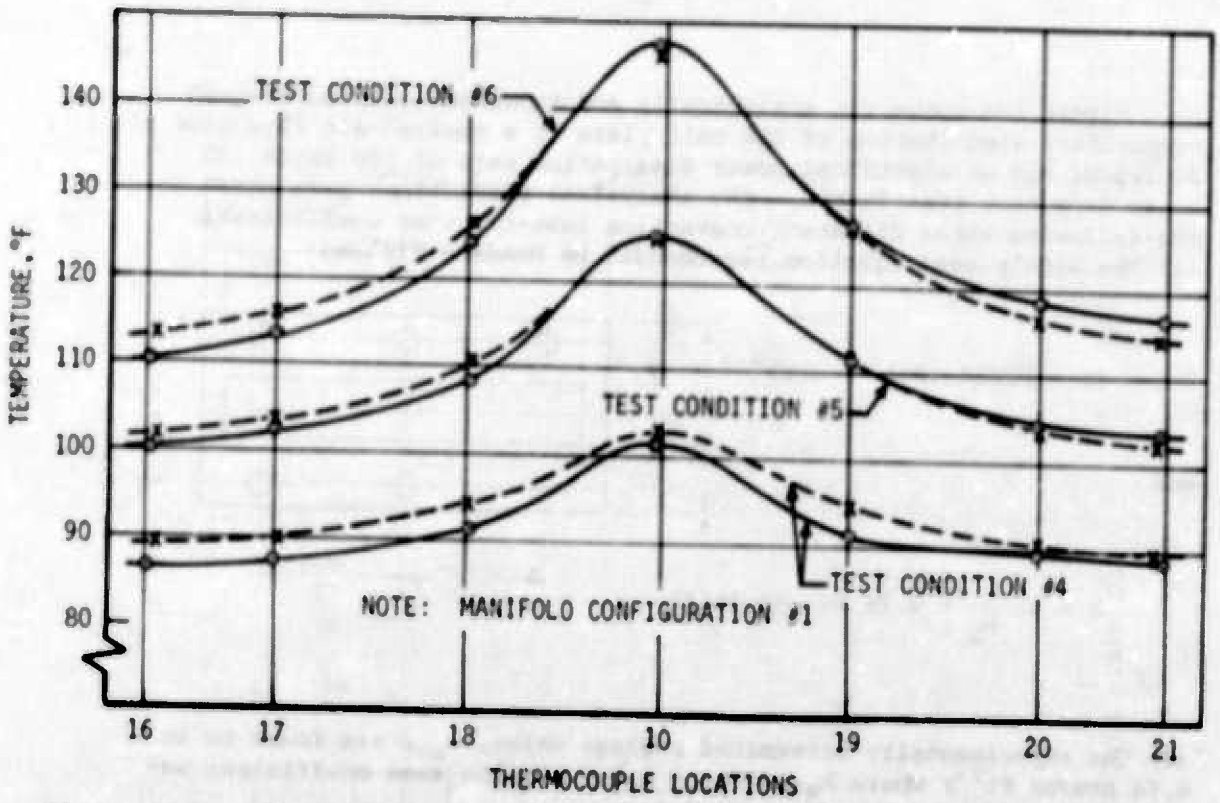

Figure 102. Temperature Distribution of Cold Plate No. 2 (Manifold #1) at Test Condition Nos. 4 thru 6 (TC 16-21)

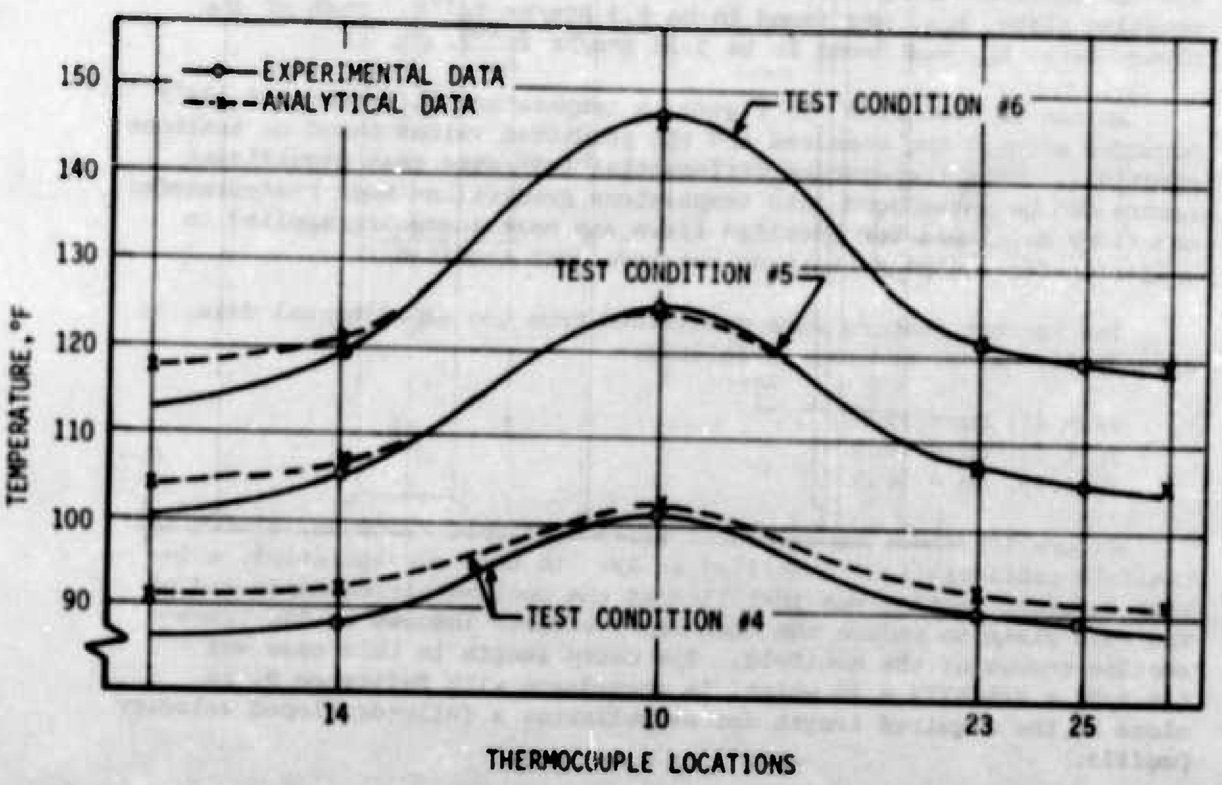

Figure 103. Temperature Distribution of Cold Plate No. 2 (Manifold #1) at Test Condition Nos. 4 thru 6 (TC 14-25)

Figure 104 shows the analytically and experimentally determined temperature distribution of the cold plate at a cooling-air flow rate of 45 lbs/hr and an electrical power dissipation rate of 100 watts (20 watts from each transistor). The analytical predictions were based on the following three different convection heat-transfer coefficients: (1) The widely used equation recommended by McAdams yielded:

$$Nu = 0.023\ (Re)^{0.8}\ (Pr)^{0.4} = 13.8$$

and

$$h = Nu \frac{k}{D_h} = 2.76\ \text{Btu/hr ft}^2\,{}^\circ\text{F}$$

(2) The experimentally determined average value, h_{av}, was found to be 6.74 Btu/hr ft^2°F where $h_{av} = h_{pl} = h_c$, i.e., the same coefficient was used for the mounting and cover plates.

(3) The experimentally determined heat-transfer coefficient of the mounting plate, h_{pl}, was found to be 8.3 Btu/hr ft^2°F. That of the cover plate, h_c, was found to be 5.25 Btu/hr ft^2°F.

As can be seen from the figure, a temperature difference of 134°F occurred between the measured and the predicted values based on textbook equations. This temperature differential indicates that significant errors can be introduced into temperature predictions when heat-transfer equations developed for specific flows and heat loads are applied to heat-transfer equipment that do not have such conditions.

The Nusselt numbers were determined from the experimental data, as already discussed, and are as follows:

Test #1, Nu = 33.5
Test #2, Nu = 45.3
Test #3, Nu = 56.3

Figure 105 shows experimental air-cooled Cold Plate No. 2 with the manifold configuration identified as #2. In this configuration, a 24-inch straight section was installed at the cooling-air entrance end of the cold plate to reduce the turbulence effects induced by the cross-section change of the manifold. The entry length in this case was $L = x/D_h = 2/0.0773 = 26$ which, in accordance with Reference 9, is close to the required length for establishing a fully-developed velocity profile.

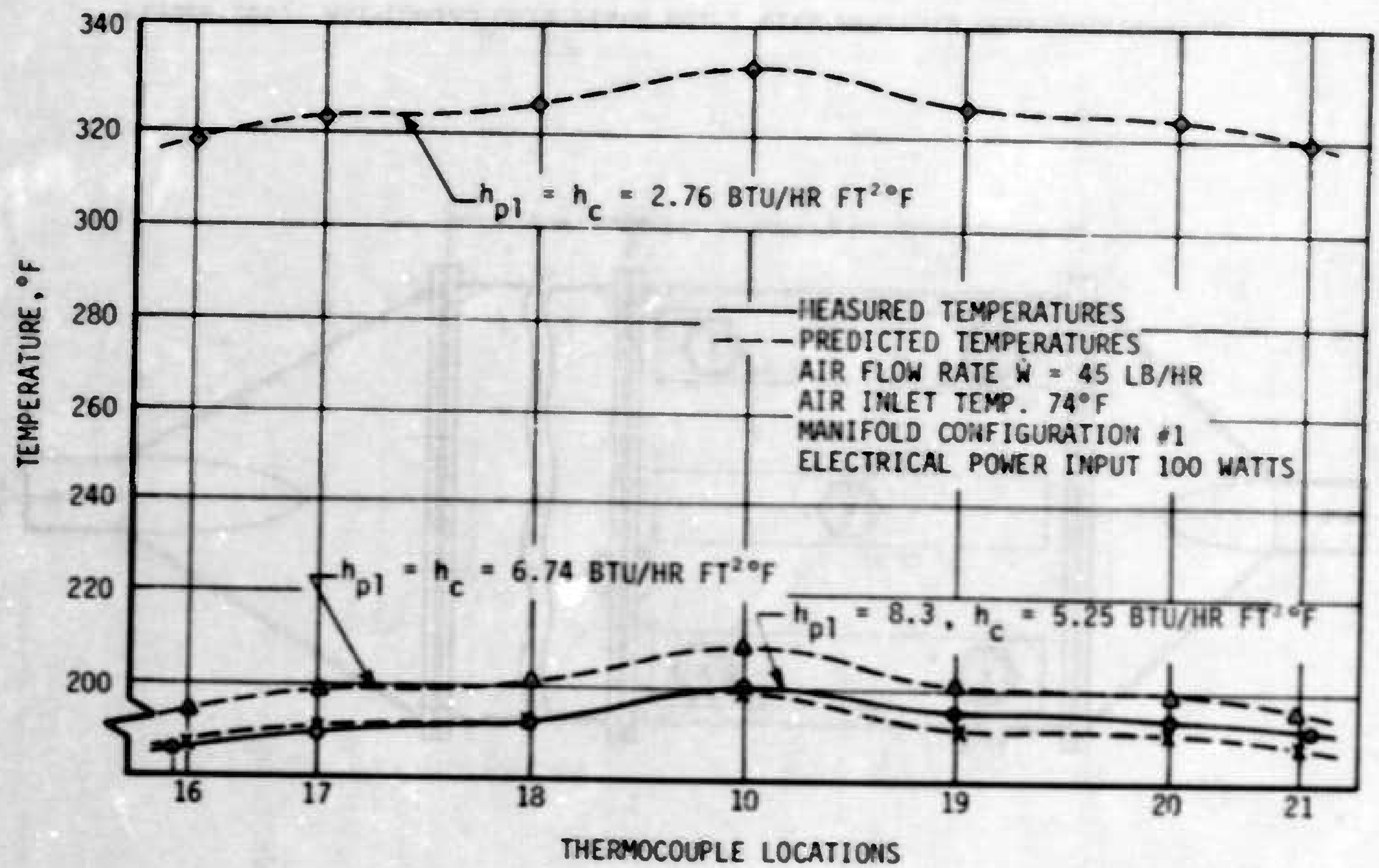

Figure 104. Predicted Temperature Distribution of Cold Plate No. 2 (Manifold #1) at Different Heat-Transfer Coefficients

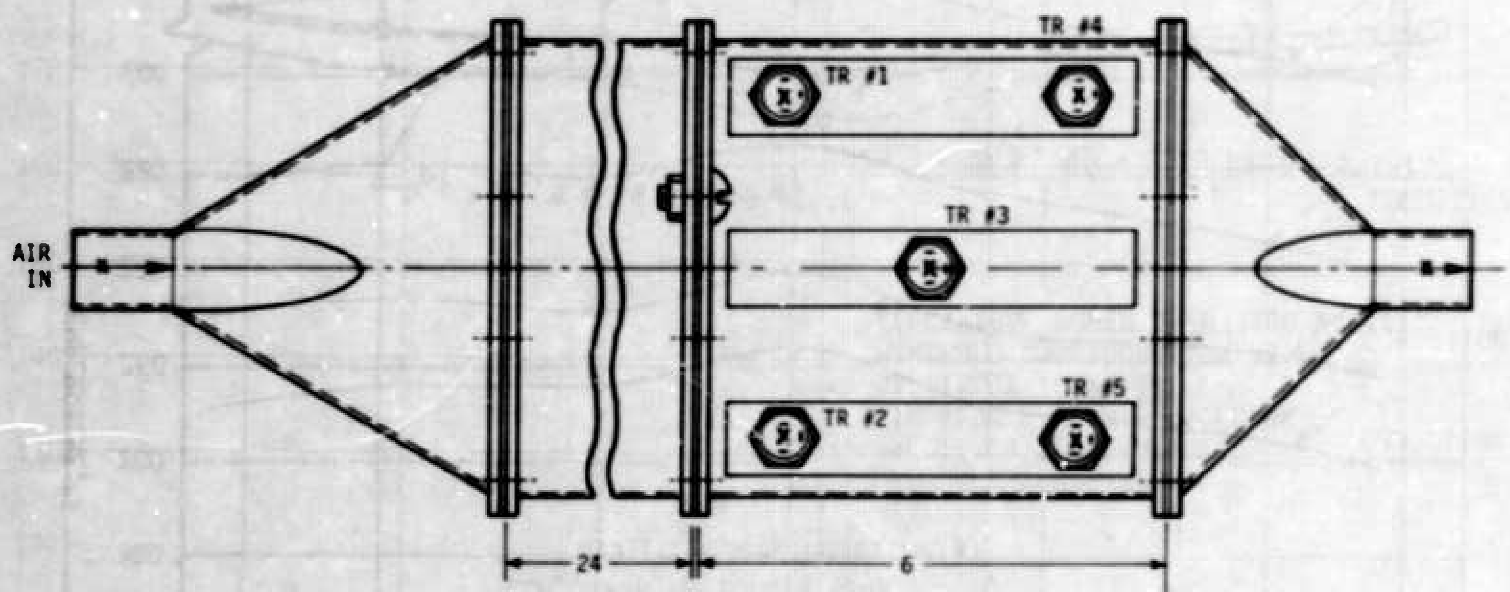

Figure 105. Air-Cooled Cold Plate No. 2 with Manifold Configuration #2

This configuration of the cold plate was tested at a constant heat load of 100 watts and three different cooling-air flow rates. The test conditions are presented in Table 22.

Table 22. Test Conditions of Air-Cooled Cold Plate No. 2, Manifold Configuration #2

TEST NO.	AIR FLOW RATE (lb/hr)	ELECTRICAL POWER INPUT TO TRANSISTORS (watts)				
		TR #1	TR #2	TR #3	TR #4	TR #5
1	45	20	20	20	20	20
2	80	20	20	20	20	20
3	124	20	20	20	20	20
4	80	--	--	20	--	--
5	80	--	--	35	--	--
6	80	--	--	50	--	--

Temperature readings of the thermocouples at the different test conditions are given in Appendix A.

Figures 106 and 107 show temperature distribution of Cold Plate No. 2 at the three different test conditions and the thermocouple locations indicated. The figure is self-explanatory.

The experimentally determined Nusselt numbers are as follows:

Test No. 1, Nu = 28.9
Test No. 2, Nu = 38.1
Test No. 3, Nu = 45.5

Figure 108 shows experimental air-cooled Cold Plate No. 2 with manifold configuration #3. In this manifold configuration, the cooling air entered at one side of the cold plate and left at the other side.

Table 23 presents all the test conditions performed with this manifold configuration.

Temperature readings of the thermocouples at the different test conditions are given in Appendix A.

Figures 109, 110, and 111 show temperature distribution of the cold plate at sections indicated by the thermocouple locations. The figures indicate that a significant temperature distortion occurred across the plate perpendicular to the cooling-air flow stream. This condition was caused by the nonuniform flow distribution. Most of the cooling air was passed through the cold plate opposite the entrance side (dead end of the manifold). Electronic equipment mounted on such a cold plate would also have large temperature differences, causing packaging and electronic system design problems. To reduce this problem, some means must be employed to improve the cooling air distribution.

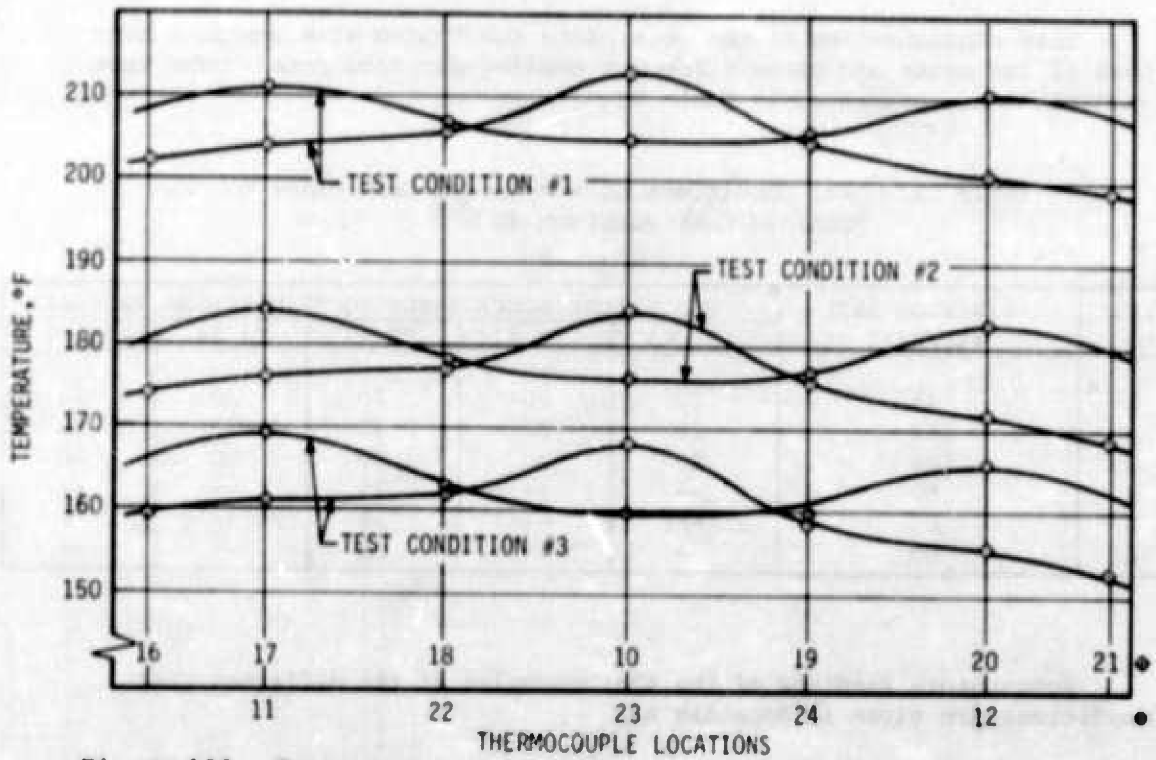

Figure 106. Temperature Distribution of Air-Cooled Cold Plate No. 2 (Manifold #2) at Test Condition Nos. 1 thru 3 (TC 11-24)

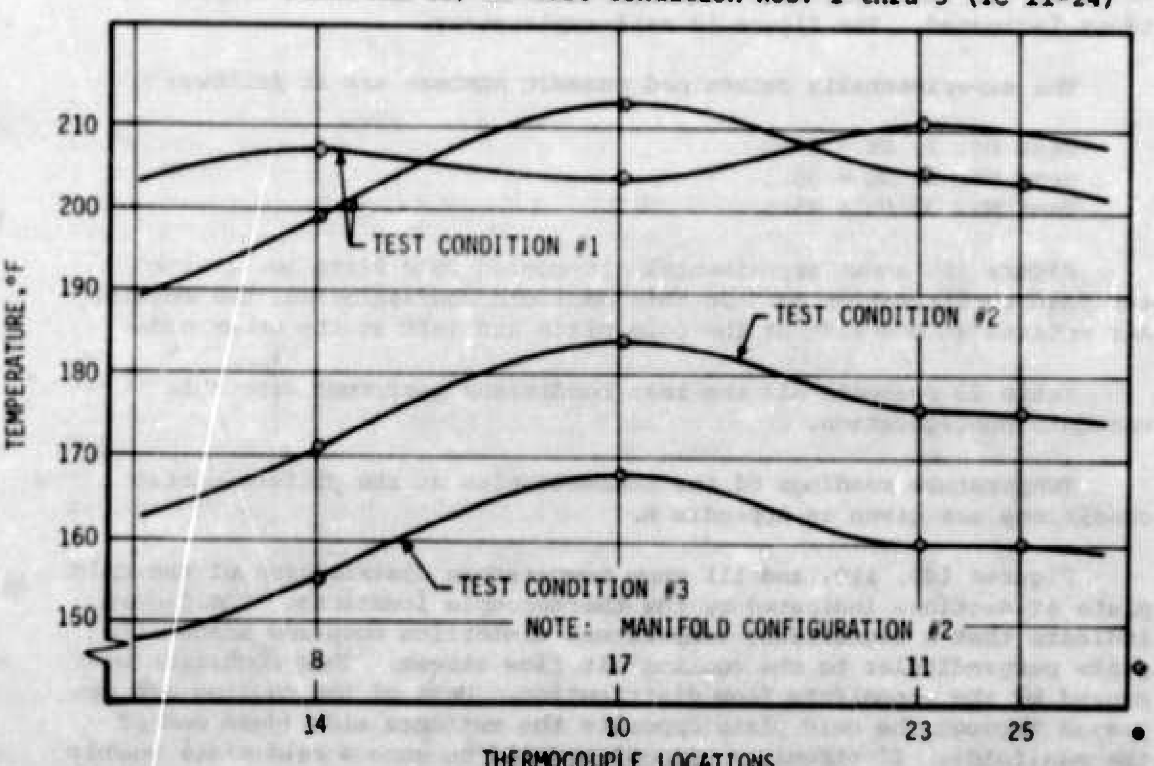

Figure 107. Temperature Distribution of Air-Cooled Cold Plate No. 2 (Manifold #2) at Test Condition Nos. 1 thru 3 (TC 3-25)

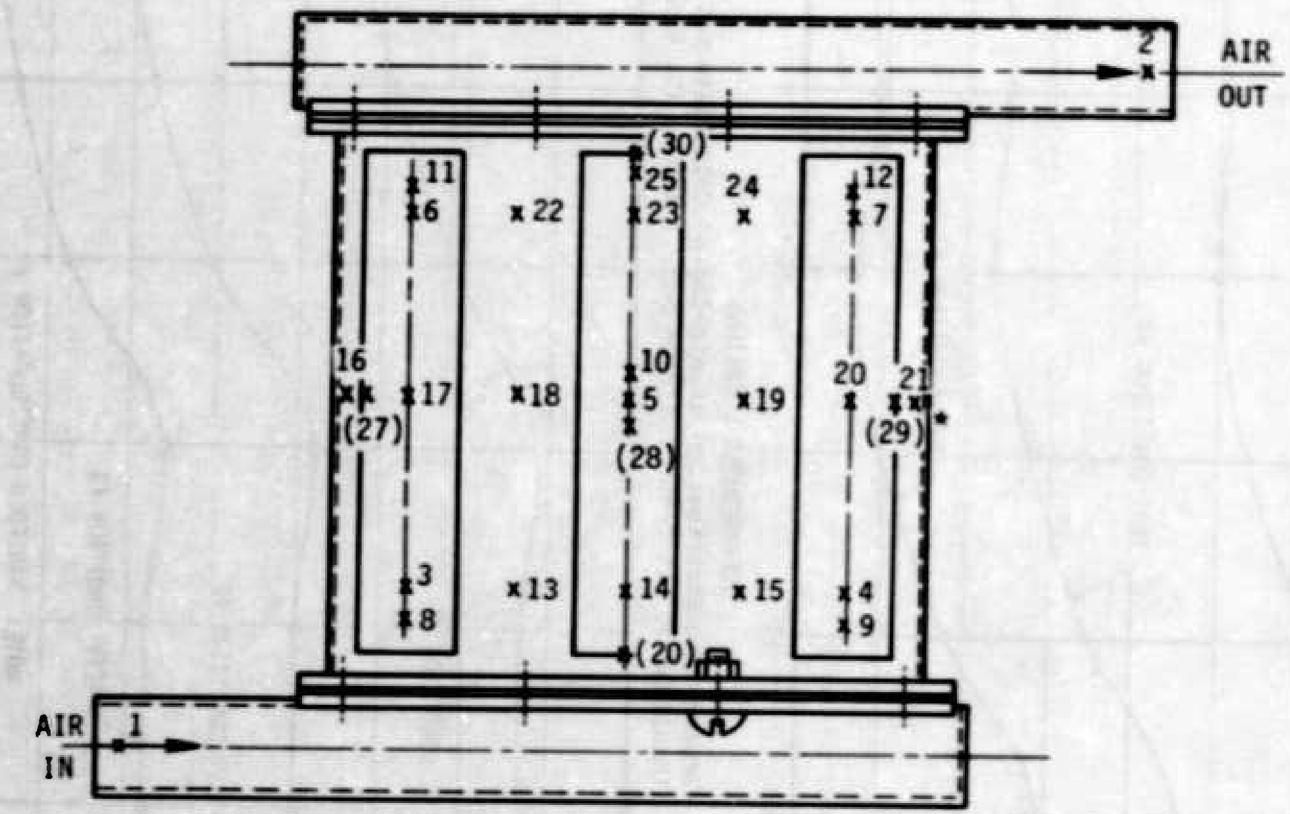

* ( ) THERMOCOUPLES LOCATED AT OTHER SIDE OF PLATE

Figure 108. Air-Cooled Cold Plate No. 2 with Manifold Configuration #3

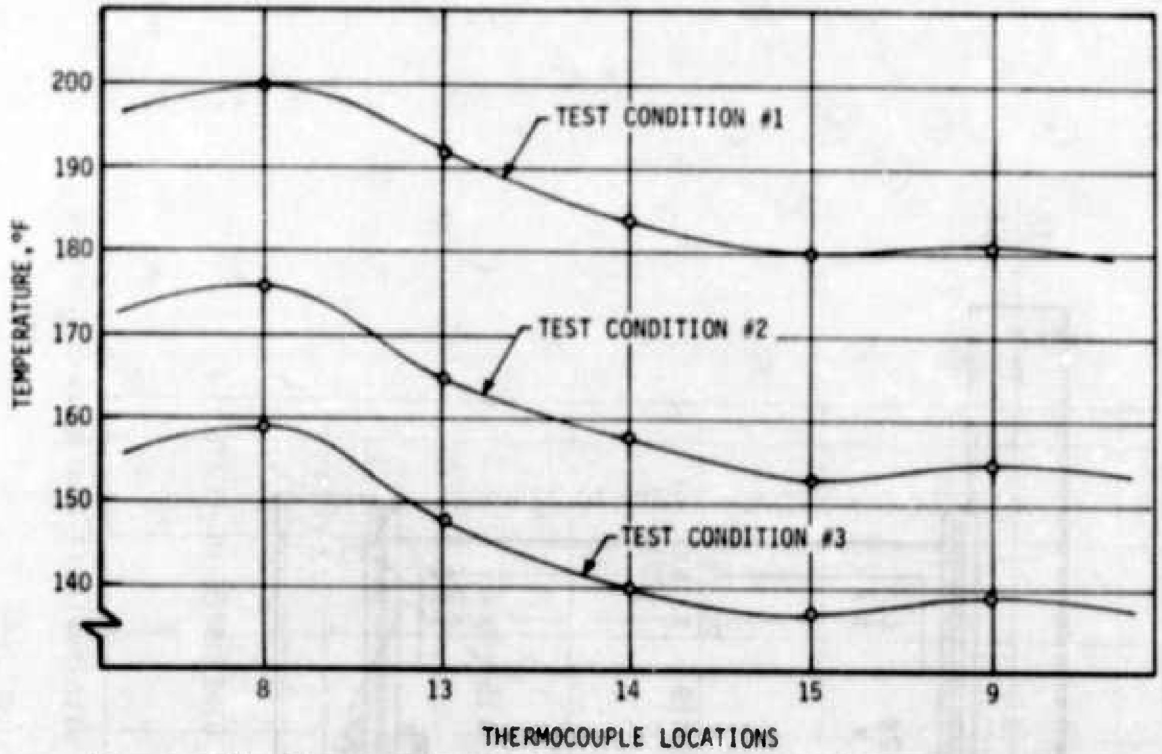

Figure 109. Temperature Distribution of Air-Cooled Cold Plate No. 2 (Manifold #3) at Test Condition Nos. 1 thru 3 (TC 8-15)

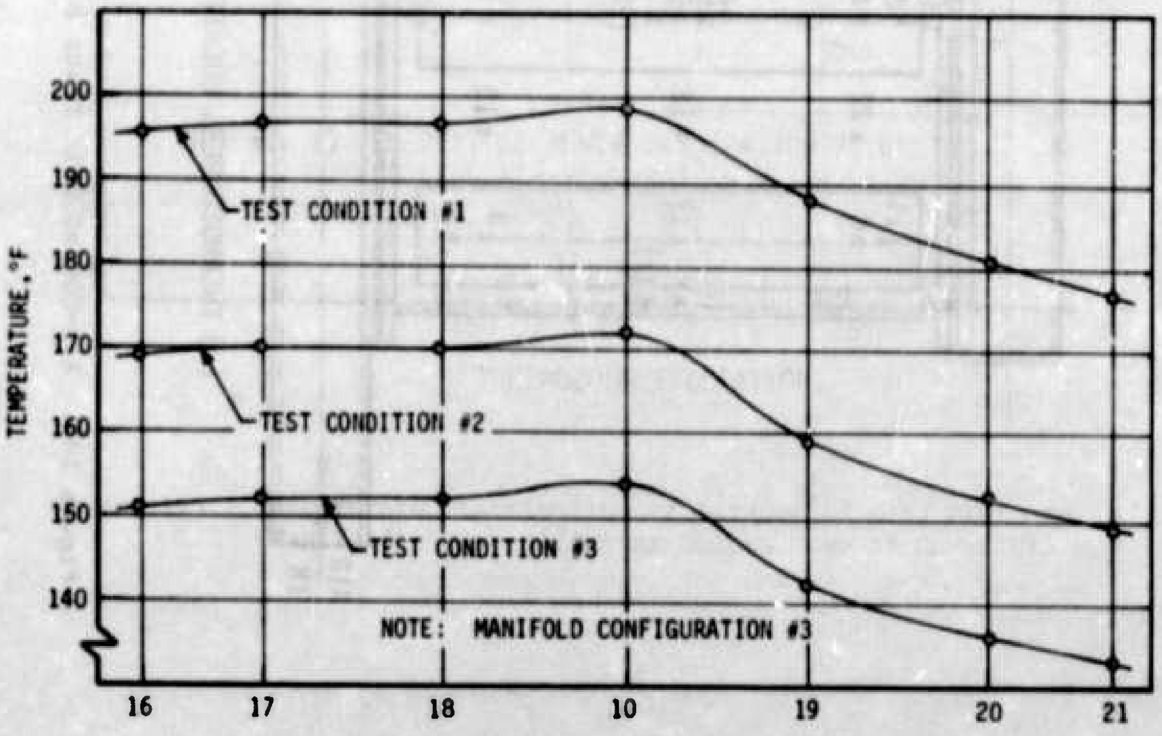

Figure 110. Temperature Distribution of Air-Cooled Cold Plate No. 2 (Manifold #3) at Test Condition Nos. 1 thru 3 (TC 16-21)

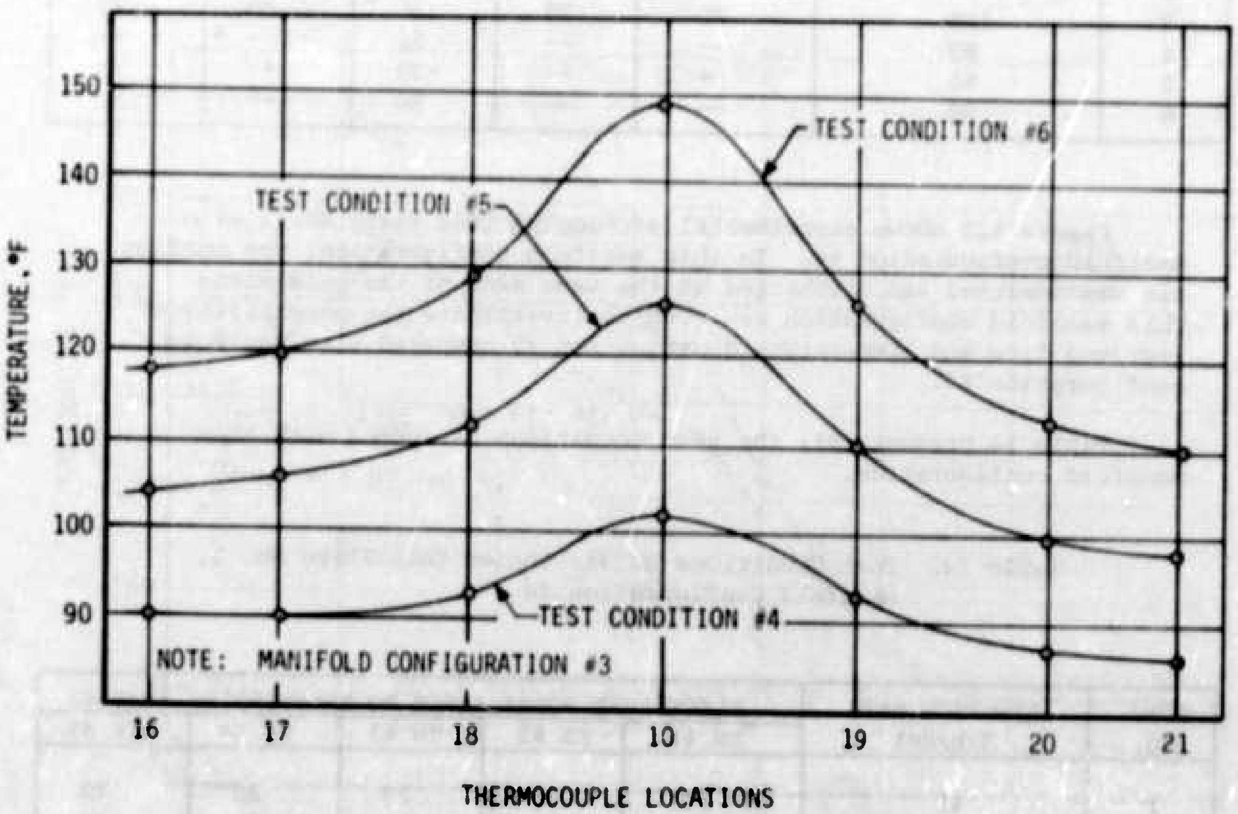

Figure 111. Temperature Distribution of Air-Cooled Cold Plate No. 2 (Manifold #3) at Test Condition Nos. 4 thru 6

Table 23. Test Conditions of Air-Cooled Cold Plate No. 2, Manifold Configuration #3

TEST NO.	AIR FLOW RATE (lb/hr)	ELECTRICAL POWER INPUT TO TRANSISTORS (watts)				
		TR #1	TR #2	TR #3	TR #4	TR #5
1	45	20	20	20	20	20
2	80	20	20	20	20	20
3	124	20	20	20	20	20
4	80	--	--	20	--	--
5	80	--	--	35	--	--
6	80	--	--	50	--	--

Figure 112 shows experimental air-cooled Cold Plate No. 2 with manifold configuration #4. In this manifold configuration, the cooling air was admitted and discharged at the same side of the cold plate. This manifold configuration was used to investigate the possibility of improved flow and temperature distribution as compared with manifold configuration #3.

Table 24 presents all the test conditions performed with this manifold configuration.

Table 24. Test Conditions of Air-Cooled Cold Plate No. 2, Manifold Configuration #4

TEST NO.	AIR FLOW RATE (lb/hr)	ELECTRICAL POWER INPUT TO TRANSISTORS (watts)				
		TR #1	TR #2	TR #3	TR #4	TR #5
1	45	20	20	20	20	20
2	80	20	20	20	20	20
3	124	20	20	20	20	20
4	80	--	--	50	--	--

Temperature readings of all the thermocouples at the different test conditions are given in Appendix A.

Figures 113 and 114 show temperature distribution of the cold plate at sections indicated by the thermocouple locations. Also, this manifold configuration indicated a similar temperature distortion across the cold plate as did the experiment with manifold configuration #3. When the thermal performances of the two manifold configurations are compared, it can be seen that manifold configuration #4 provided smaller temperature differentials across the plate. The plate temperature was also lower.

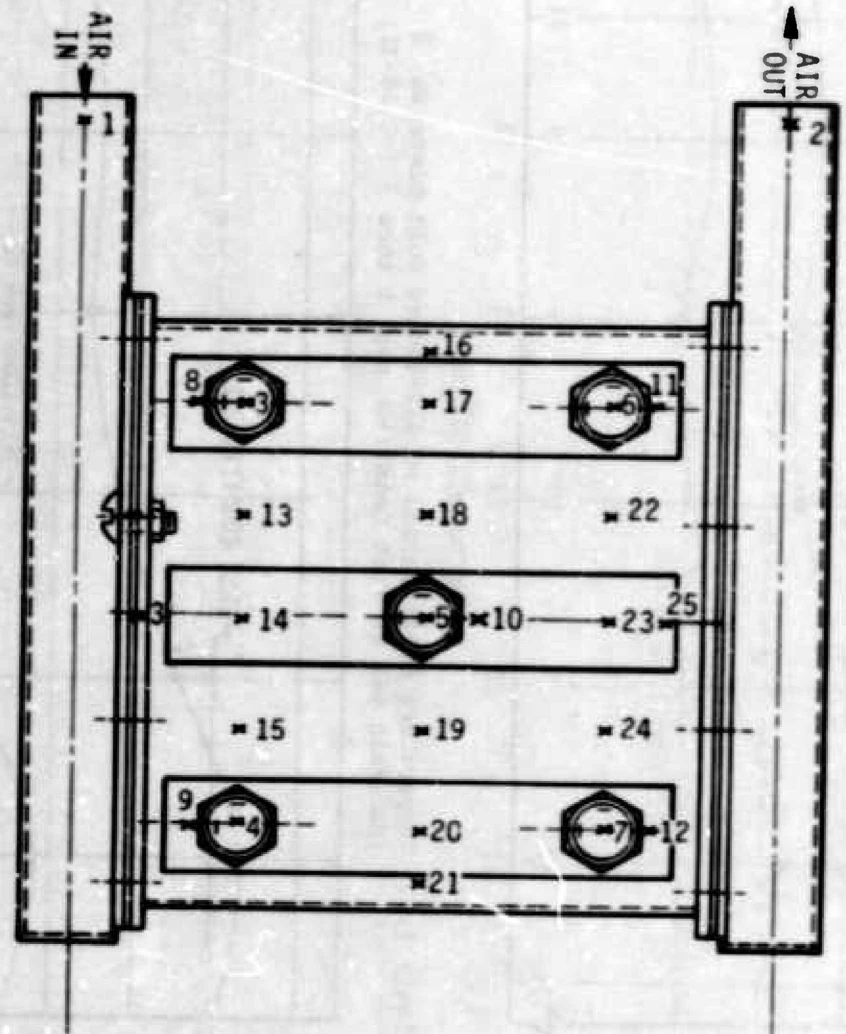

Figure 112. Air-Cooled Cold Plate No. 2 with Manifold Configuration #4

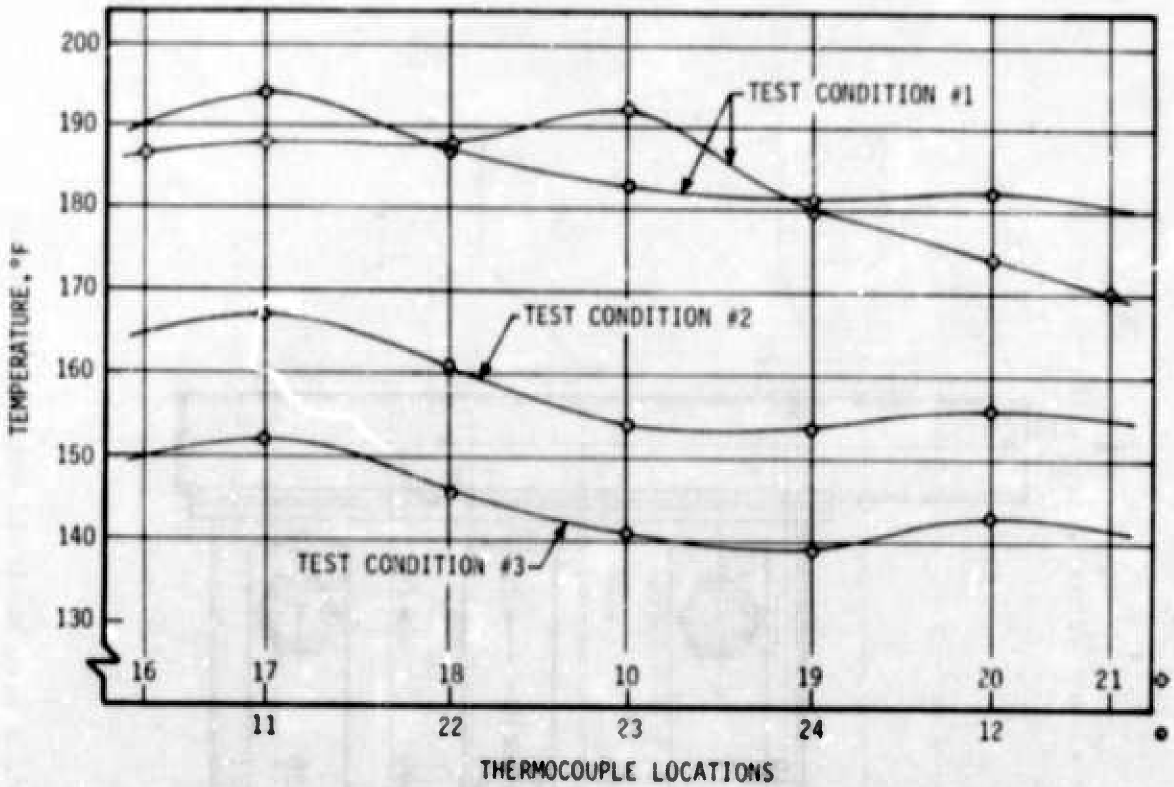

Figure 113. Temperature Distribution of Air-Cooled Cold Plate No. 2 (Manifold #4) at Test Condition Nos. 1 thru 3 (TC 16-21)

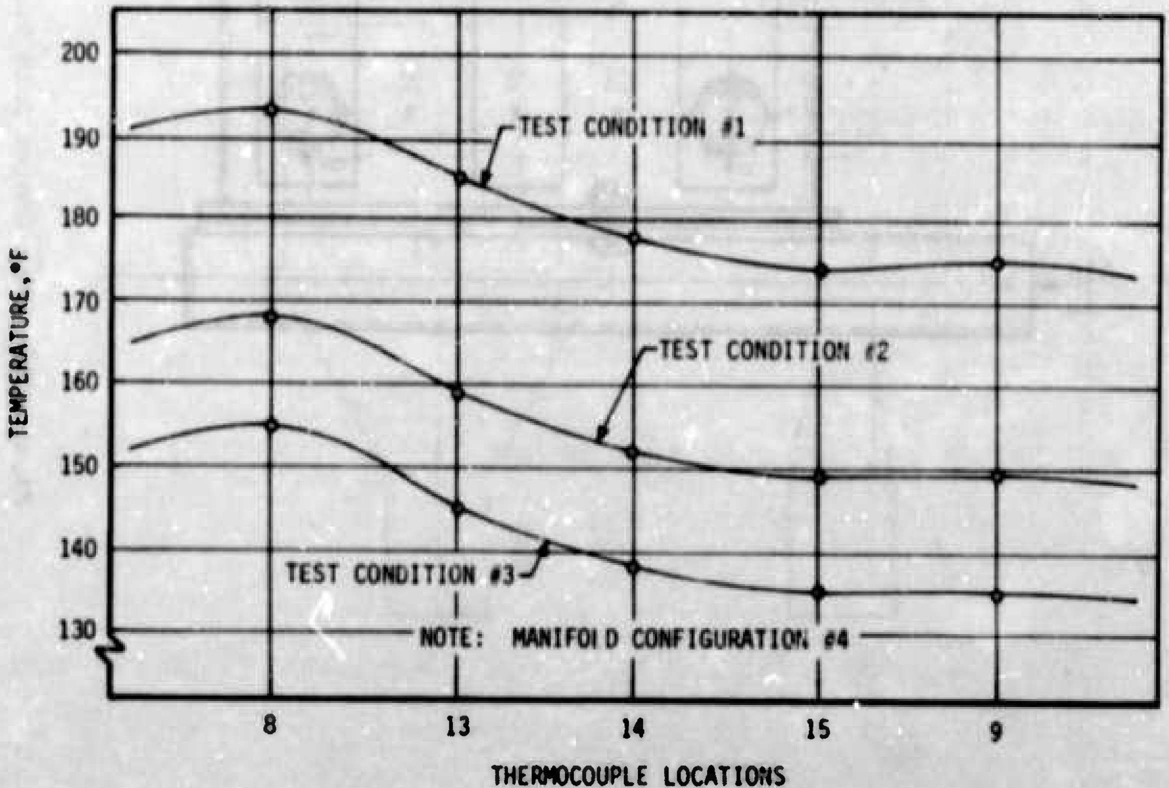

Figure 114. Temperature Distribution of Air-Cooled Cold Plate No. 2 (Manifold #4) at Test Condition Nos. 1 thru 3 (TC 8-15)

Since this manifold configuration demonstrated better thermal performance, the Nusselt numbers were determined only for this configuration.

Test No. 1, Nu = 37.9
Test No. 2, Nu = 50.7
Test No. 3, Nu = 59.8

Because of the smaller space occupied by manifold configurations #3 and #4, it is likely that such manifold configurations would be selected in actual equipment-cooling cold plates.

To improve the thermal performance of such cold plates, additional experiments were performed by inserting gaskets with tapered slots at the cooling-air entrance end of the cold plate. Two gaskets, with slot sizes as shown in Figure 115, were fabricated and inserted between the manifold and cold plate; then, the thermal tests were performed. The

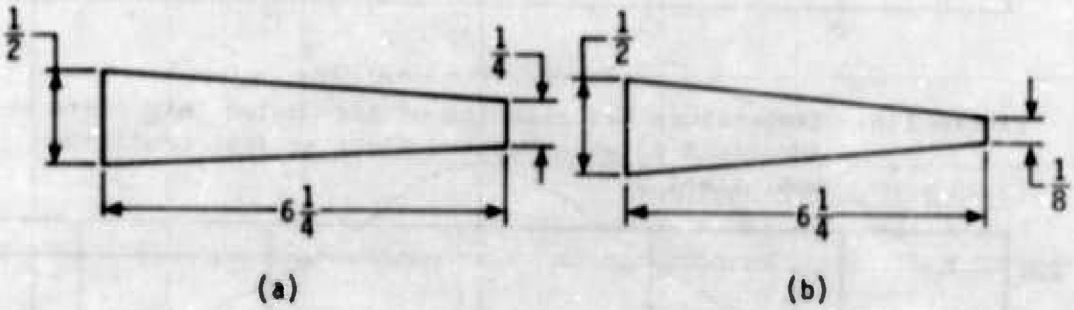

Figure 115. Gasket Slots

narrow end of the slot was placed at the closed end of the manifold. The gasket with the opening shown in Figure 115a did not show any improvement in the temperature distribution. Better results were obtained with the gasket opening shown in Figure 115b. Only the latter results, therefore, are presented. Because transistor #3 burned out, only transistors #1, #2, #4, and #5 were energized. A constant electrical power of 100 watts (25 watts each) was dissipated by the four transistors, and the thermal tests were performed at cooling-air flow rates of 45 lbs/hr and 80 lbs/hr. Similar tests were performed with manifold configurations #3 and #4. Temperature readings of the thermocouples are presented in Appendix A.

Figures 116 and 117 show temperature distribution across the cold plate at the sections indicated by the thermocouples. Although there was improvement in temperature distribution for both manifold configurations when the tapered-slot gasket was installed, almost complete temperature symmetry was achieved for manifold configuration #4. This

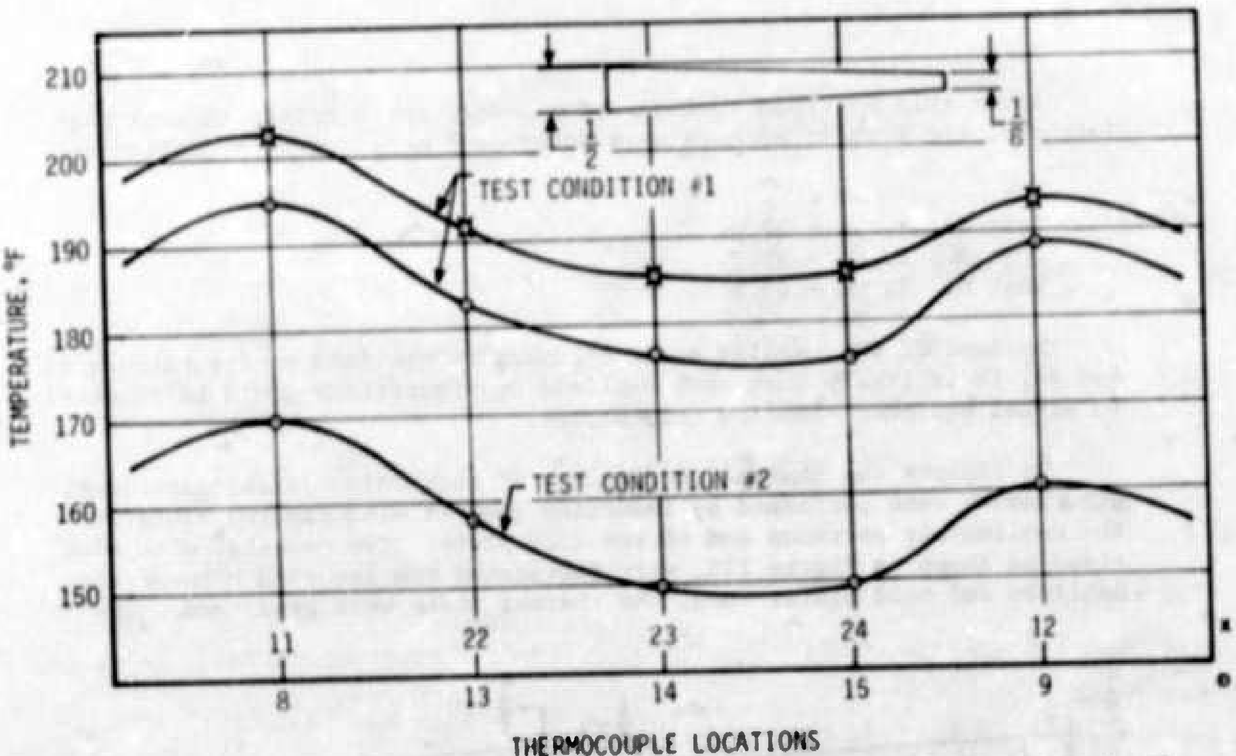

Figure 116. Temperature Distribution of Air-Cooled Cold Plate No. 2 (Manifold #3 with Tapered Slot) at Test Condition Nos. 1 and 2

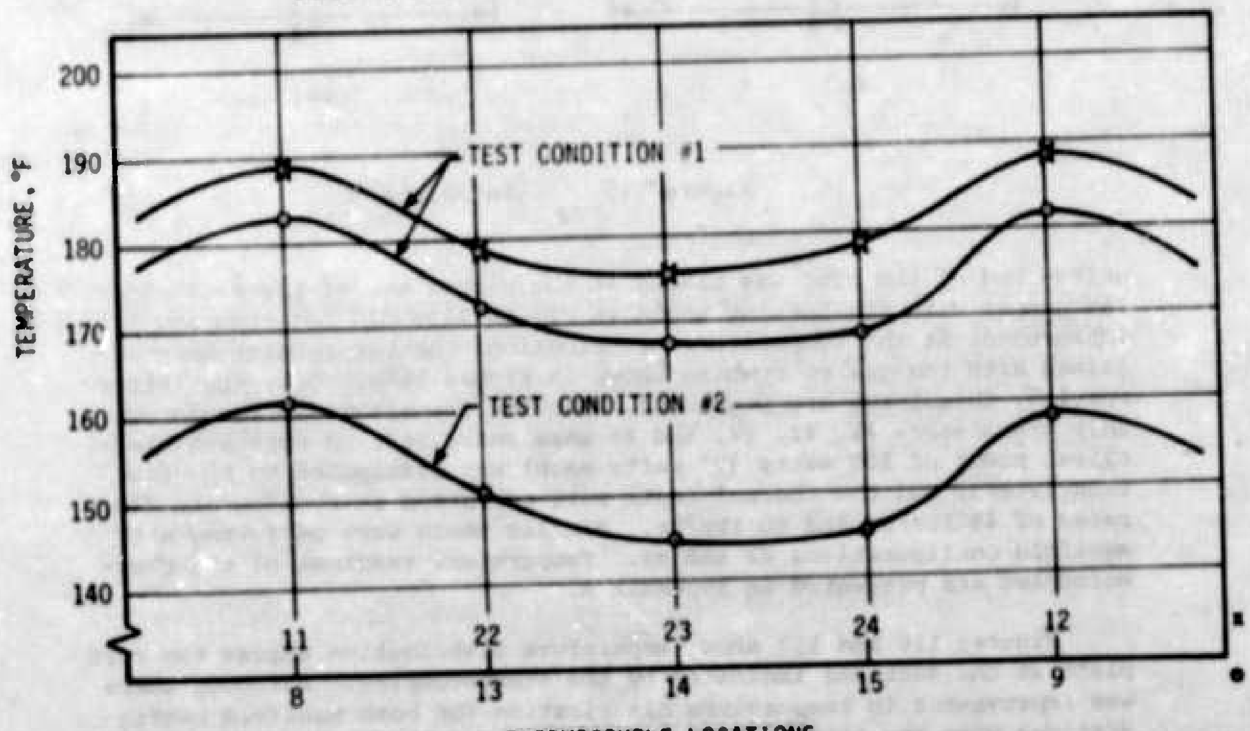

Figure 117. Temperature Distribution of Air-Cooled Cold Plate No. 2 (Manifold #4 with Tapered Slot) at Test Condition Nos. 1 and 2

manifold configuration also provided a lower plate temperature. It should be noted, however, that installation of the tapered-slot gasket caused a larger pressure drop. This condition must be taken into consideration when the pressure drop is limited.

The experimentally determined Nusselt numbers for manifold configurations #1, #2 and #4 are shown in Figure 118. The results of this cold plate experiment show the same trend as that of Cold Plate No. 1: the difference in Nusselt number values between manifold configurations #1 and #4 diminished as the Reynolds numbers were increased. The figure indicates that the different manifold configurations of this cold plate showed larger differences in the Nusselt numbers. The figure also shows a comparison between analytically and experimentally determined Nusselt numbers. The difference is particularly large at the lower Reynolds numbers, indicating the effects of turbulence.

(3) Air-Cooled Cold Plate No. 3

Figure 119 shows the outline of experimental air-cooled Cold Plate No. 3. The air-flow channel of this cold plate measured 3-3/4 x 5/8 inches, the hydraulic diameter, $D_h = 4\ A/P$, was 0.0895 ft; and the aspect ratio, $R = 3.75/0.625$, was 6. The cold plate was provided with flanges to allow installation of different manifold configurations.

Figure 120 shows the cold plate with manifold configuration #1. The figure also shows transistor and thermocouple locations. The transistors (type 2N1724) were attached directly to the cold plate without insulating washers. Heat-sink compound was applied to all transistor mounting joints. Transistor case and cold-plate temperatures were measured at different cooling-air flow rates and different electrical power dissipation rates from the transistors.

Table 25 presents all the test conditions performed on the cold plate with manifold configuration #1.

Temperature readings of the thermocouples at the different test conditions are given in Appendix A.

Figure 121 shows temperature distribution of the cold plate at a constant heat load of 75 watts (25 watts from each transistor) and different cooling-air flow rates. The temperature measurements were taken across the plate perpendicular to the air-flow axis. Figure 122 shows temperature distribution along the cold plate parallel to the cooling-air flow axis. It can be seen from the figures that changes of the cooling-air flow rates practically did not affect temperature gradients within the equipment mounting plate. The plate temperature, however, was significantly reduced when the cooling-air flow rates were increased.

Figure 123 shows temperature distribution of the equipment mounting and cover plates at the test conditions indicated. Only half of the cold plate is shown here. The figure also shows comparison between

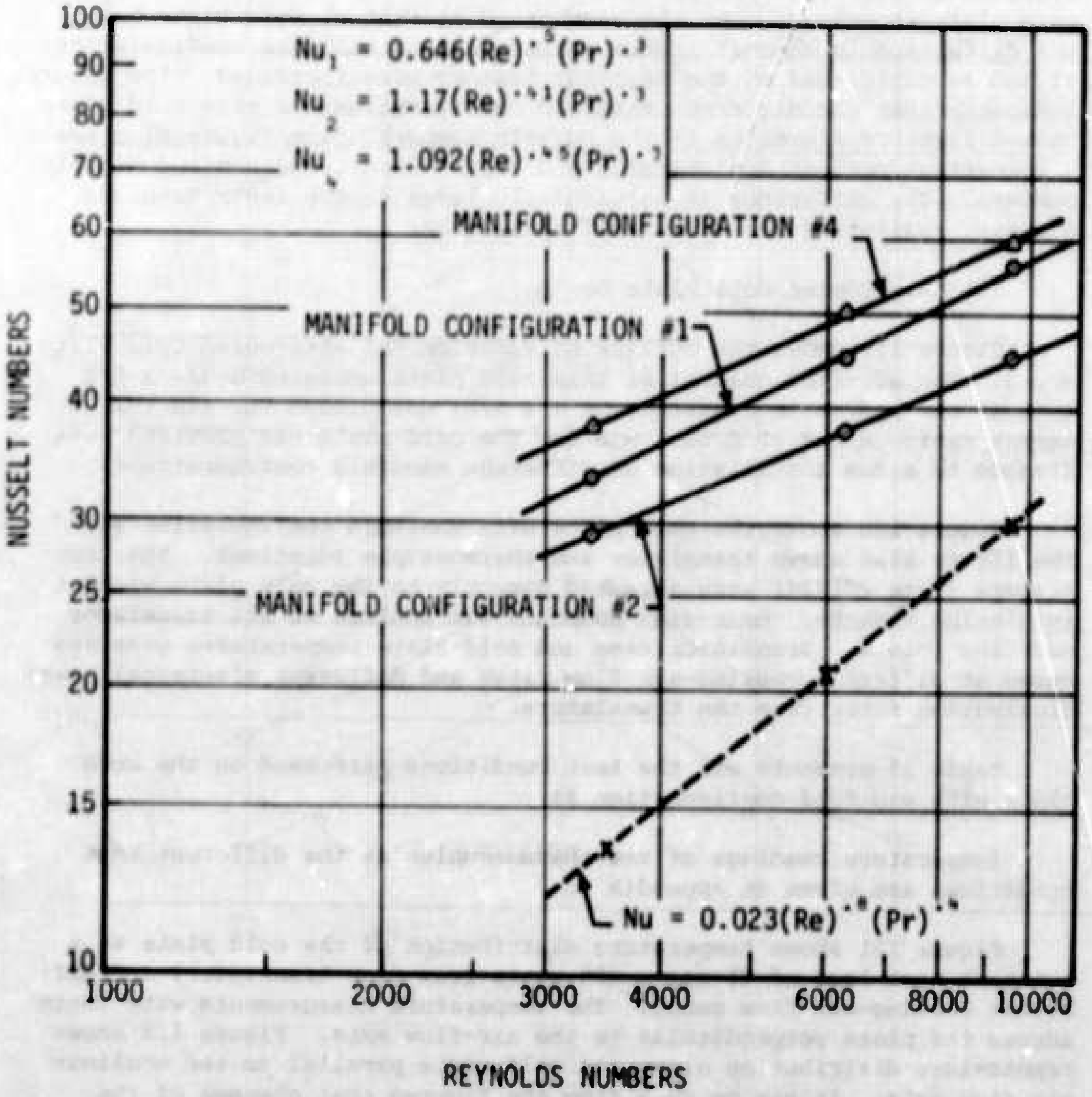

Figure 118. Experimentally Determined Nusselt Numbers vs Reynolds Numbers of Air-Cooled Cold Plate No. 2

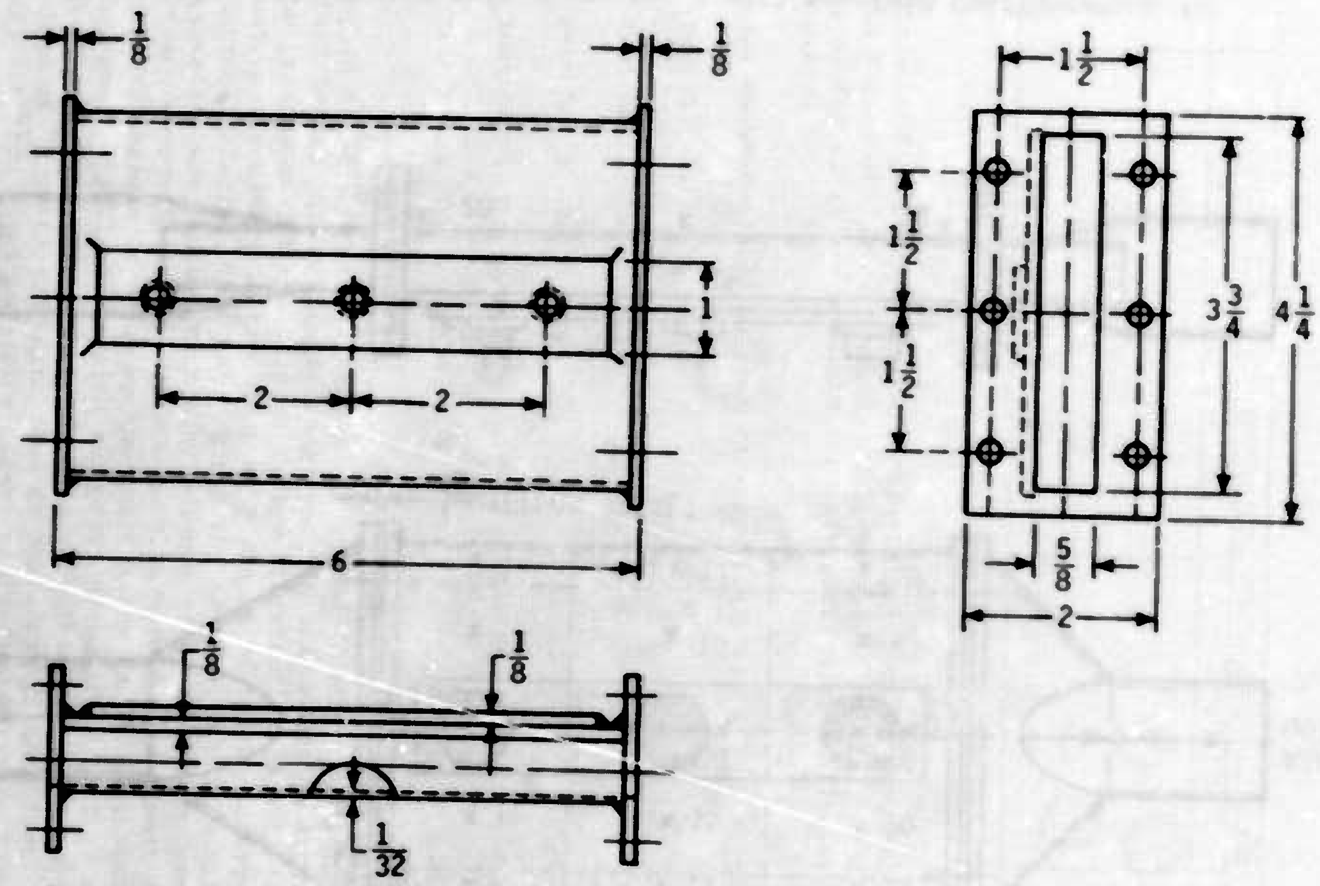

Figure 119. Air-Cooled Cold Plate No. 3

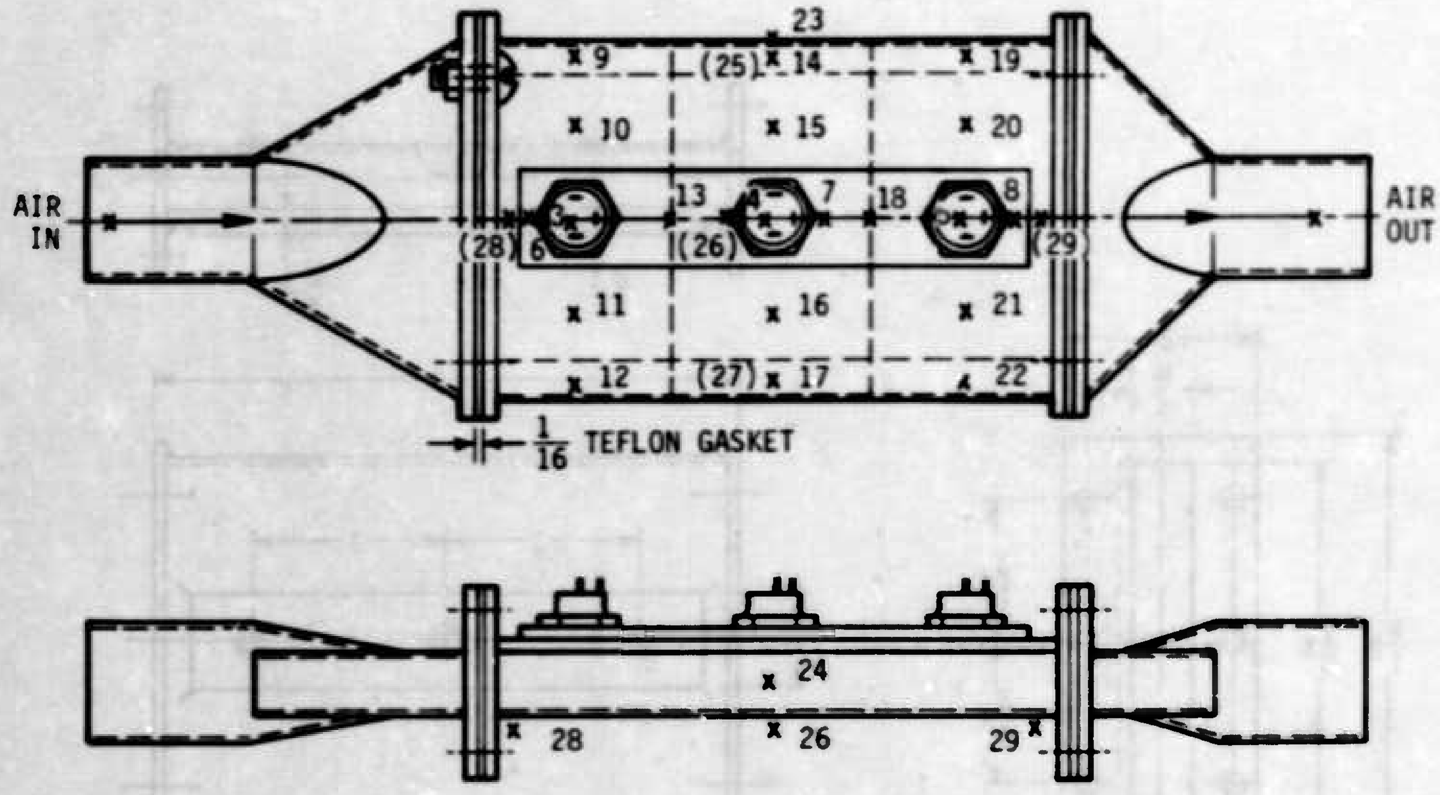

Figure 120. Air-Cooled Cold Plate No. 3 with Manifold Configuration #1

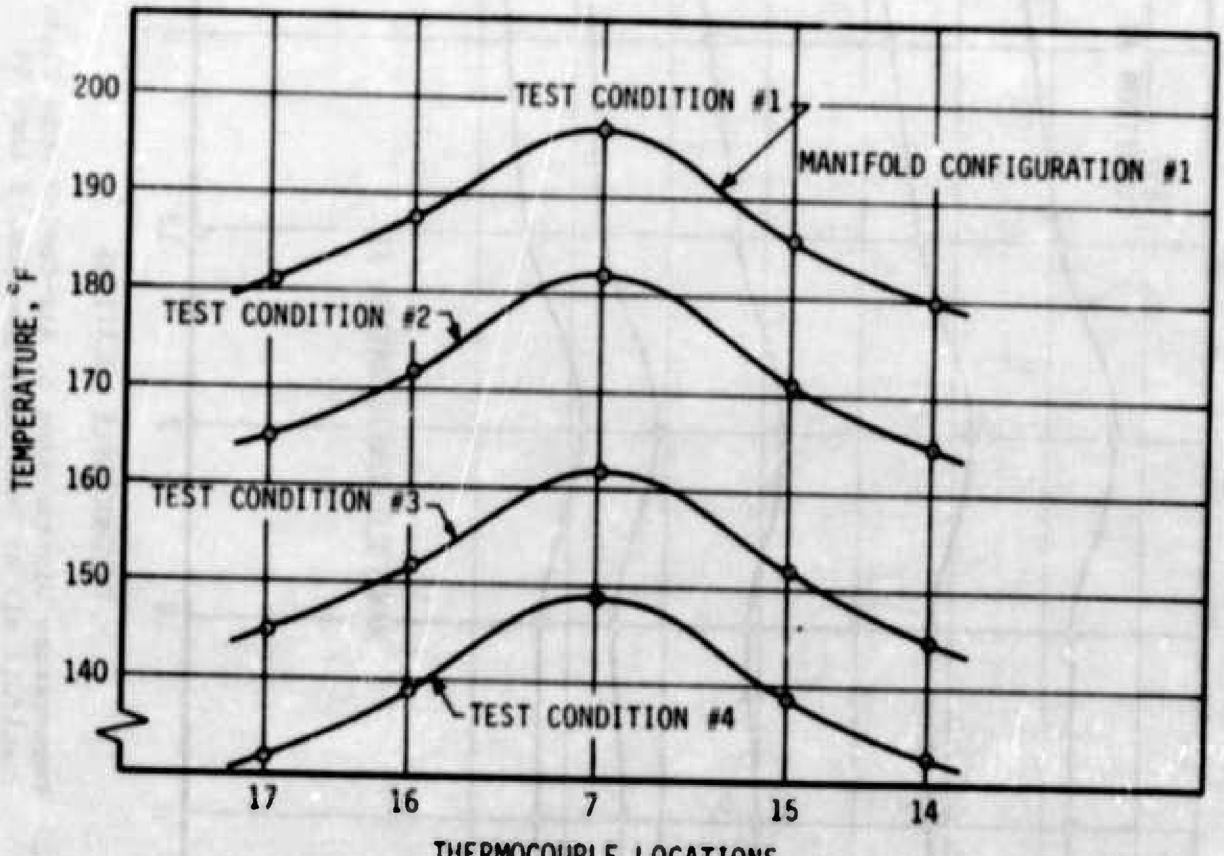

Figure 121. Temperature Distribution of Air-Cooled Cold Plate No. 3 (Manifold #1) at Test Condition Nos. 1 thru 4

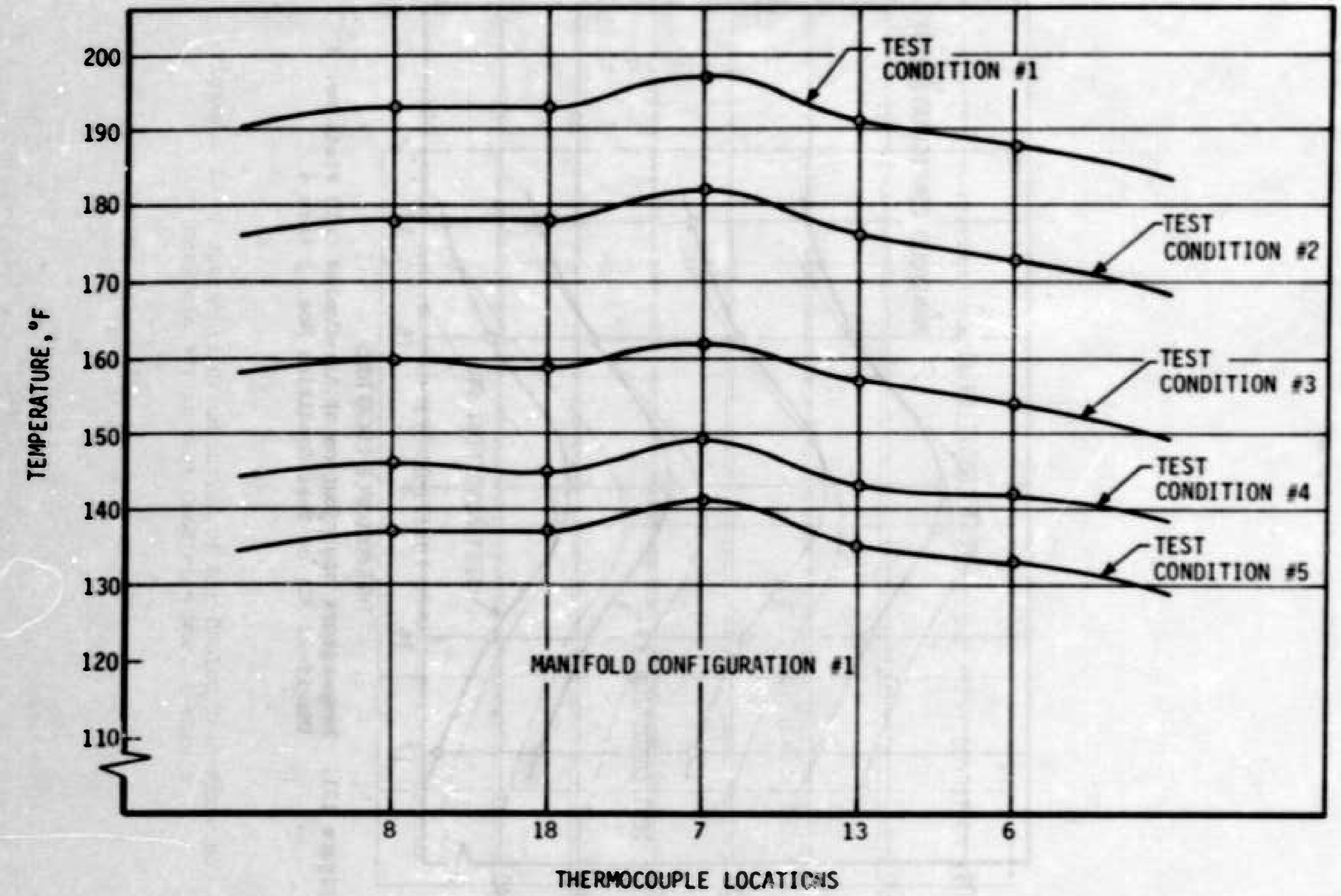

Figure 122. Temperature Distribution of Air-Cooled Cold Plate No. 3 (Manifold #1) at Test Condition Nos. 1 thru 5

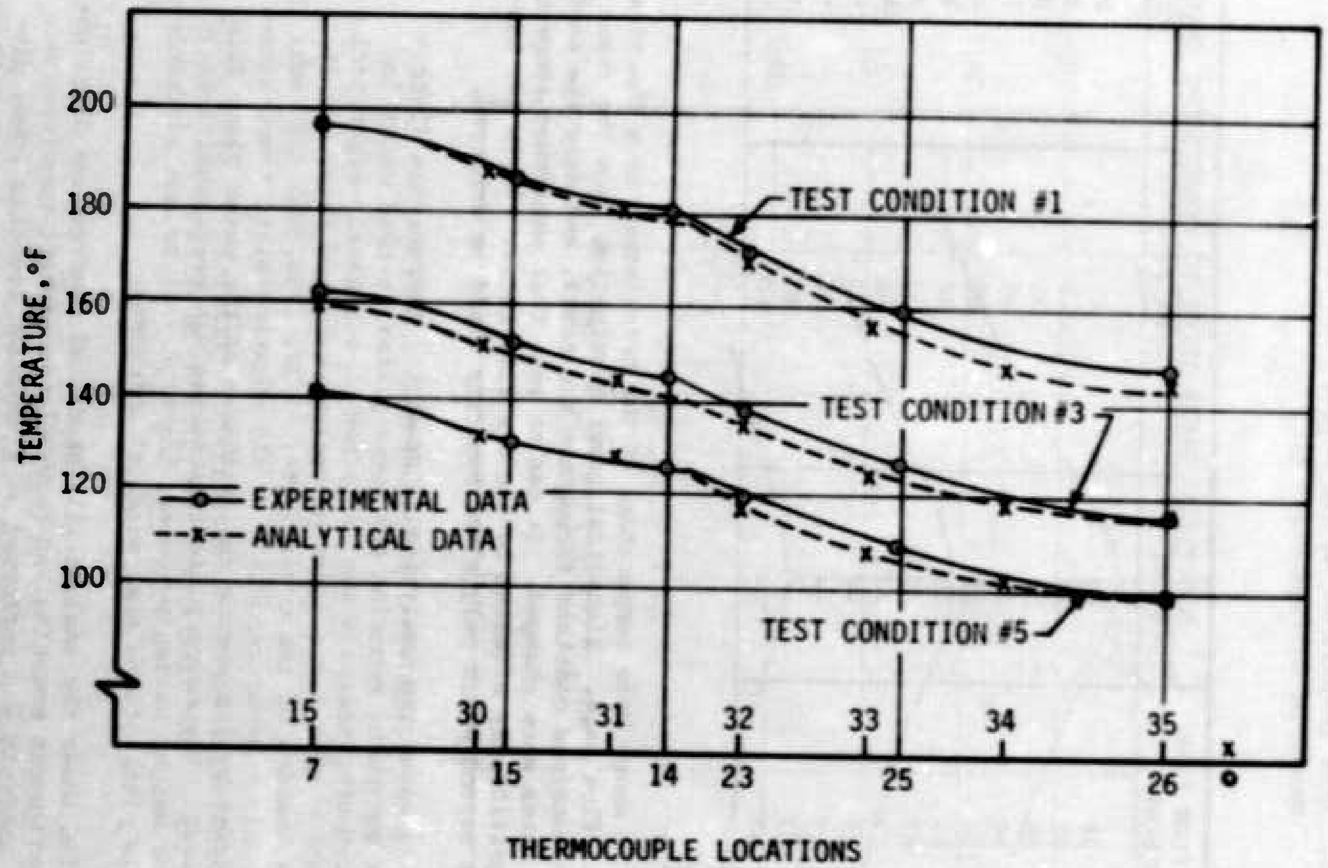

Figure 123. Temperature Distribution of Air-Cooled Cold Plate No. 3 (Manifold #1) at Test Condition Nos. 1 thru 5

experimental and analytical data. It can be seen that an excellent agreement between experimental and analytical data can be achieved when proper computer input data are provided.

Table 25. Test Conditions of Air-Cooled Cold Plate No. 3, Manifold Configuration #1

TEST NO.	AIR FLOW RATE (lb/hr)	ELECTRICAL POWER INPUT TO TRANSISTORS (watts)		
		TR #1	TR #2	TR #3
1	34	25	25	25
2	45	25	25	25
3	68	25	25	25
4	94	25	25	25
5	124	25	25	25
6	67	20	20	20
7	67	30	30	30
8	67	40	40	40
9	67	--	20	--
10	67	--	30	--
11	67	--	40	--
12	67	--	50	--

Figure 124 shows case temperature of the transistors as a function of cooling-air flow rate. Electrical power dissipation from the transistors was maintained constant throughout the tests, and only the cooling-air flow rates were changed. It can be seen that equipment temperatures are significantly affected by the air flow rates. There is, however, a limit beyond which only minor benefits could be achieved.

Figure 125 shows the analytically predicted temperature distribution of the equipment mounting and cover plates at test condition No. 5. The computer analysis was performed at a constant electrical power dissipation rate and a constant cooling-air flow rate, but at different thicknesses of the cover plate: 1/32, 1/16, and 1/8 inch. As can be seen, only a minor reduction of the mounting-plate temperature could be achieved by increasing the thickness of the cover plate from 1/32 to 1/8 inch. The cover plate temperature was more significantly affected. For weight saving purposes, therefore, it is not advisable to make the whole plate of the same material thickness.

Figure 126 shows the analytically predicted temperature distribution of the equipment mounting and cover plates at test condition No. 1. The computer analysis was performed at a constant electric power dissipation rate and a constant cooling-air flow rate, but at two different applications of the heat-transfer coefficients as shown in the figure. The heat-transfer coefficients used in the analysis were determined from experimental data discussed previously. It has been already noted that the convection heat-transfer coefficients for the equipment mounting and

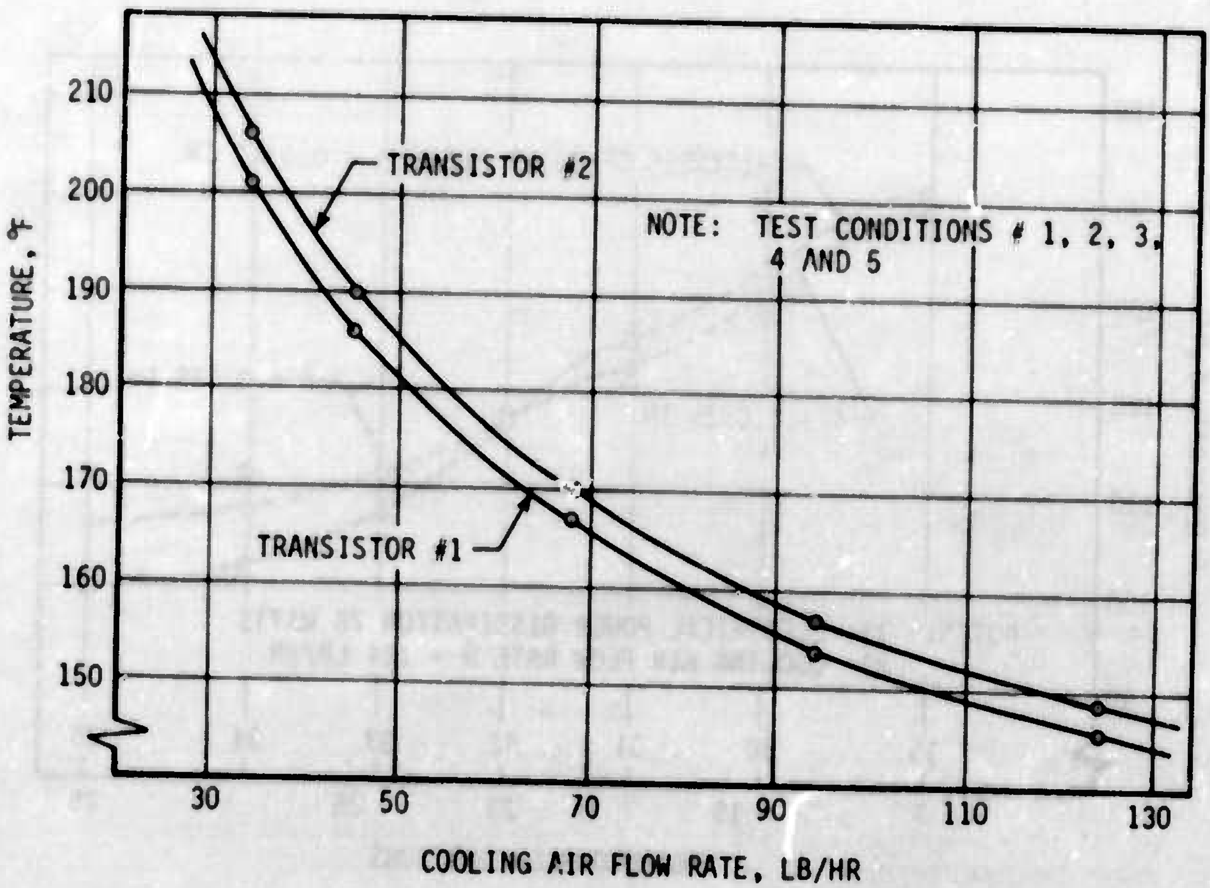

Figure 124. Case Temperature of Transistors vs Cooling Air Flow Rate for Air-Cooled Cold Plate No. 3 (Manifold #1)

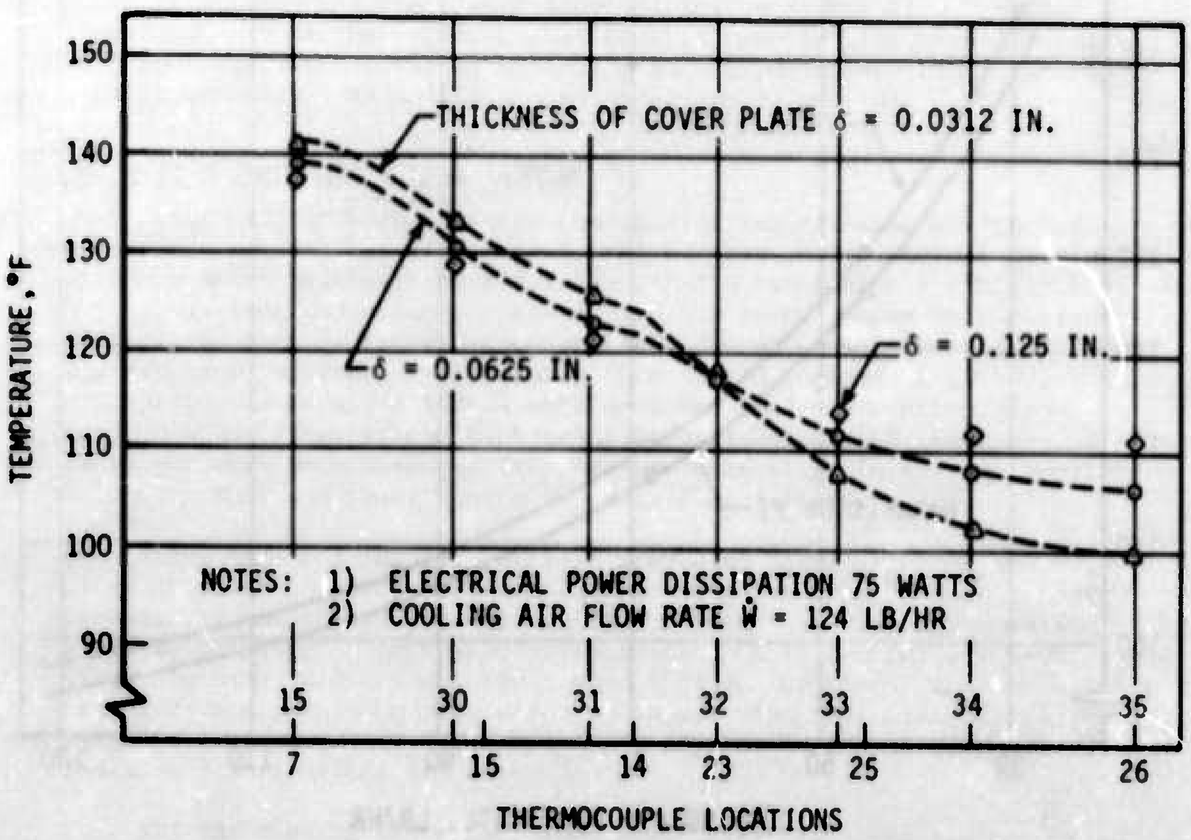

Figure 125. Temperature Distribution of Air-Cooled Cold Plate No. 3 (Manifold #1) at Different Thicknesses of Cover Plate

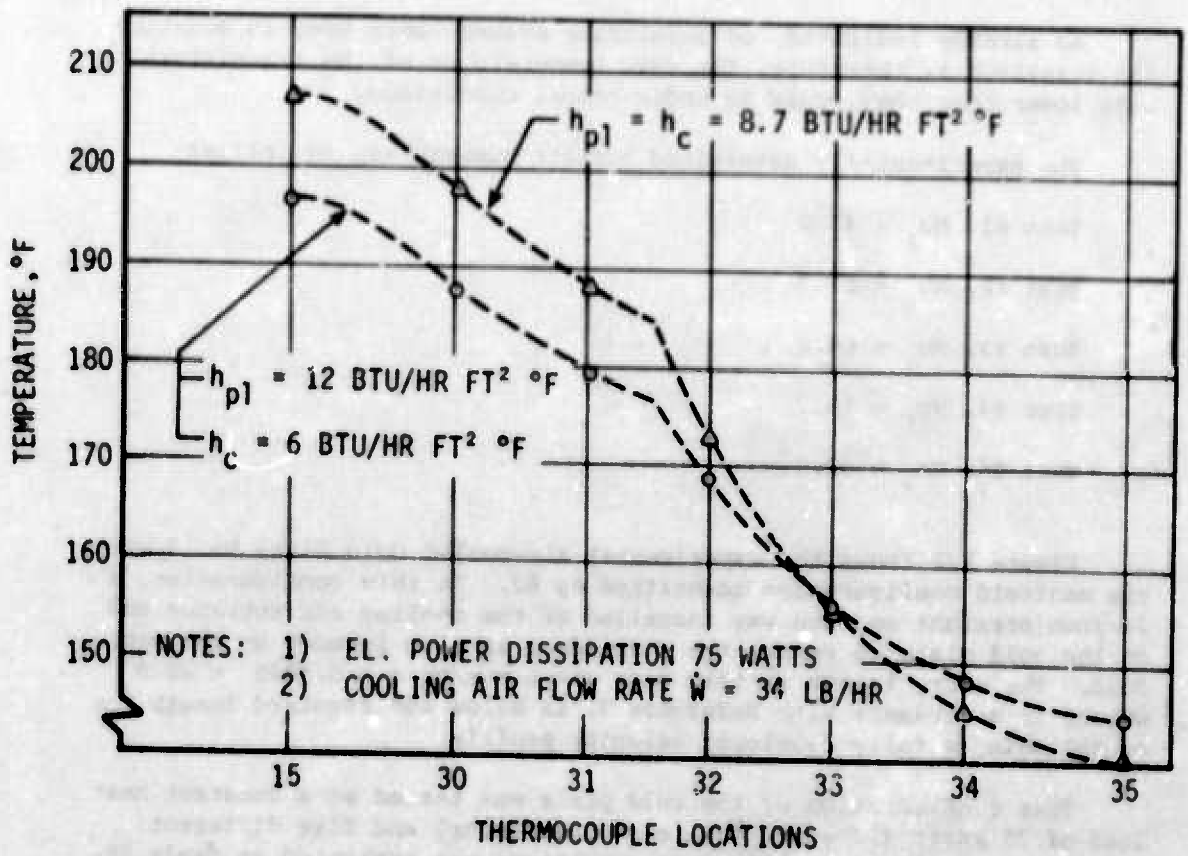

Figure 126. Temperature Distribution of Air-Cooled Cold Plate No. 3 (Manifold #1) at Different Heat-Transfer Coefficients

cover plates are not the same; and, if accurate thermal performance prediction is required, different heat-transfer coefficients for the mounting and cover plates must be used. It can be seen that when the average heat-transfer coefficient is used, the predicted mounting plate temperature will be higher, while the cover plate temperature will be lower. These are obvious results.

Figure 127 shows the case temperature of transistor #2 as a function of the electrical power dissipation rate from the transistor. The figure is self-explanatory.

As already indicated, no insulating washers were used in mounting the transistors; therefore, the case temperatures of the transistors were lower than they would be under actual conditions.

The experimentally determined Nusselt numbers are as follows:

Test #1, $Nu_1 = 43.2$

Test #2, $Nu_2 = 51.7$

Test #3, $Nu_3 = 64.8$

Test #4, $Nu_4 = 78.7$

Test #5, $Nu_5 = 92.3$

Figure 128 shows the experimental air-cooled Cold Plate No. 3 with the manifold configuration identified as #2. In this configuration, a 24-inch straight section was installed at the cooling-air entrance end of the cold plate to reduce the turbulence effects induced by the manifold. The entry length in this case was $L = x/D_h = 2/0.0895 = 22.3$ which, in accordance with Reference 9, is below the required length for establishing a fully-developed velocity profile.

This configuration of the cold plate was tested at a constant heat load of 75 watts (25 watts from each transistor) and five different cooling-air flow rates. The test conditions are presented in Table 26.

Temperature measurements of the thermocouples at the different cooling-air flow rates are given in Appendix A.

Figure 129 shows temperature distribution of Cold Plate No. 3, manifold configuration #2, at the five different cooling-air flow rates.

When the thermal performances of manifold configurations #1 and #2 are compared, it can be seen that the plate temperature was noticeably higher when the 24-inch straight section was installed. For example, at test condition No. 1, the temperature difference between the two configurations at the central section (TC #1) of the plate reached a value

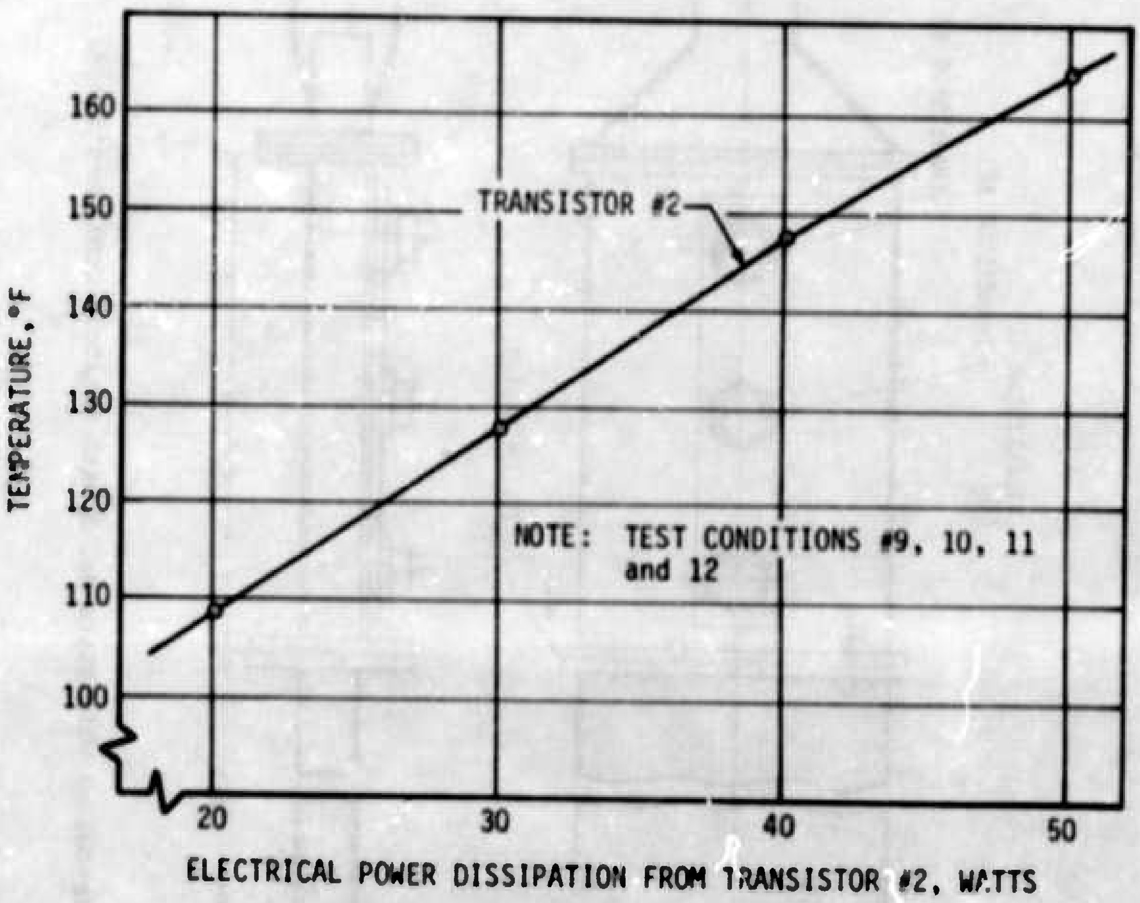

Figure 127. Case Temperature of Transistor #2 vs Electrical Power Dissipation Rate (Cold Plate No. 3, Manifold #1)

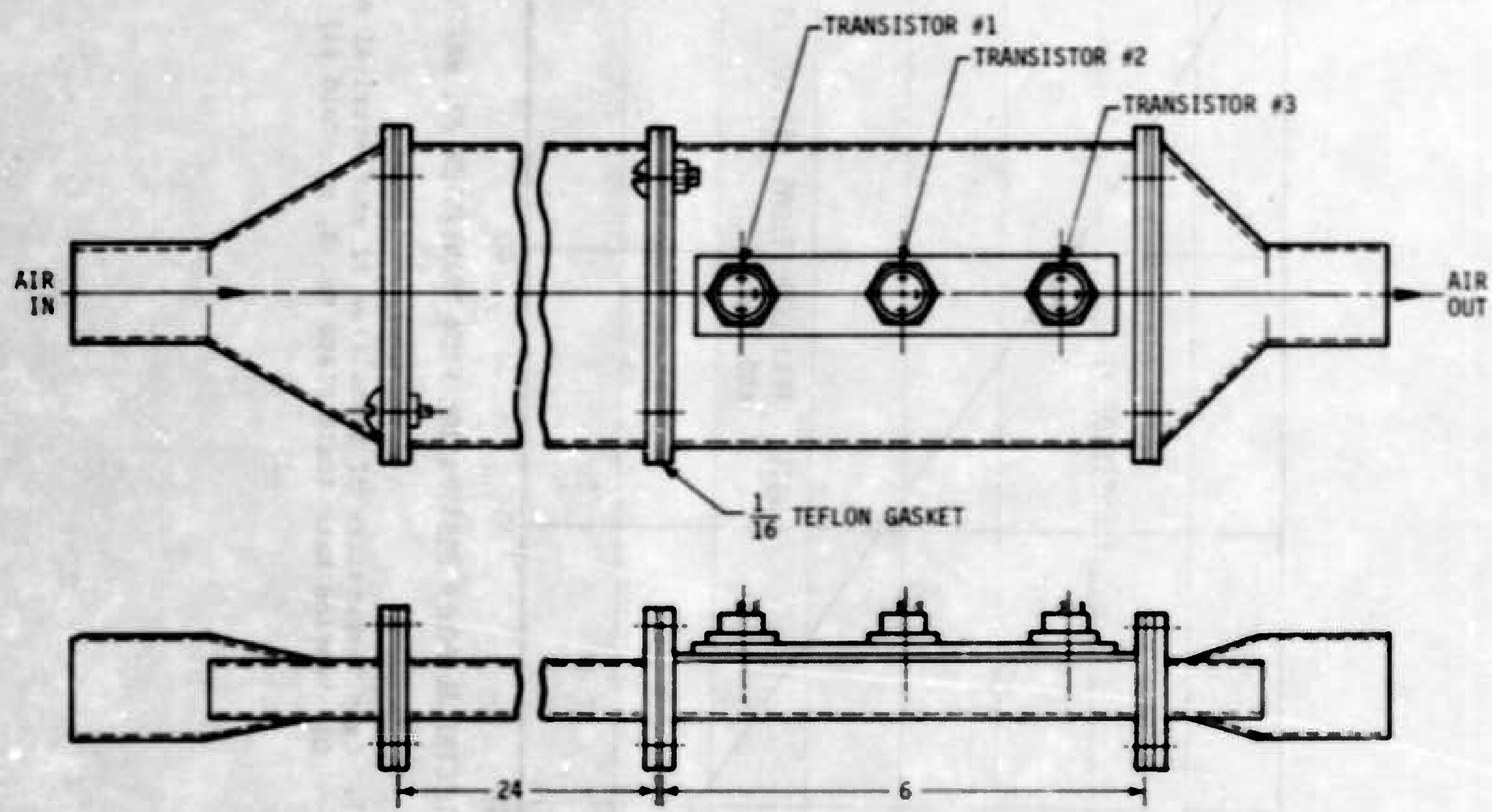

Figure 128. Air-Cooled Cold Plate No. 3 with Manifold Configuration #2

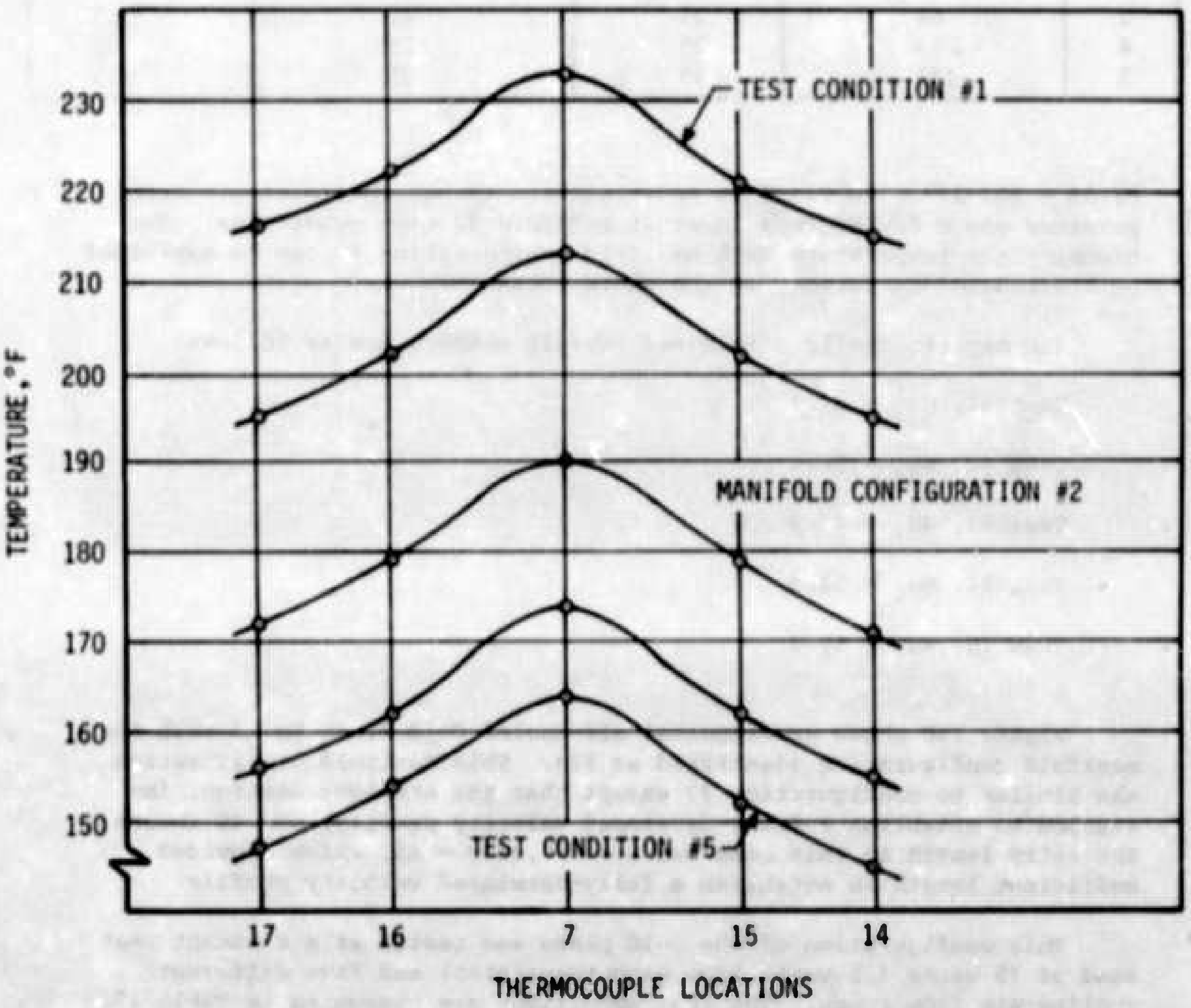

Figure 129. Temperature Distribution of Air-Cooled Cold Plate No. 3 (Manifold #2) at Test Condition Nos. 1 thru 5

Table 26. Test Conditions of Air-Cooled Cold Plate No. 3, Manifold Configuration #2

TEST NO.	AIR FLOW RATE (lb/hr)	ELECTRICAL POWER INPUT TO TRANSISTORS (watts)		
		TR #1	TR #2	TR #3
1	34	25	25	25
2	45	25	25	25
3	68	25	25	25
4	94	25	25	25
5	124	25	25	25

of $\Delta t = 233-197 = 36°F$. This occurred even though the inlet air temperature was a few degrees lower at manifold #2 test conditions. The higher plate temperature with manifold configuration #2 can be explained by the reduced turbulence at the plate entrance.

The experimentally determined Nusselt numbers are as follows:

Test #1, $Nu_1 = 31.7$

Test #2, $Nu_2 = 36.2$

Test #3, $Nu_3 = 43.2$

Test #4, $Nu_4 = 52.3$

Test #5, $Nu_5 = 59.7$

Figure 130 shows experimental air-cooled Cold Plate No. 3 with the manifold configuration identified as #2a. This manifold configuration was similar to configuration #2 except that the straight section, installed to establish a fully-developed velocity profile, was 48 inches. The entry length in this case was $L = 4/0.0895 = 45$, which provided sufficient length to establish a fully-developed velocity profile.

This configuration of the cold plate was tested at a constant heat load of 75 watts (25 watts from each transistor) and five different cooling-air flow rates. The test conditions are presented in Table 27.

Temperature measurements of the thermocouples at the different cooling-air flow rates are contained in Appendix A.

Figure 131 shows temperature distribution across Cold Plate No. 3, manifold configuration #2a, at the five different cooling-air flow rates. Although length of the straight section in this configuration was twice the length of configuration #2, only a slight increase in temperature was observed between the two manifold configurations. This

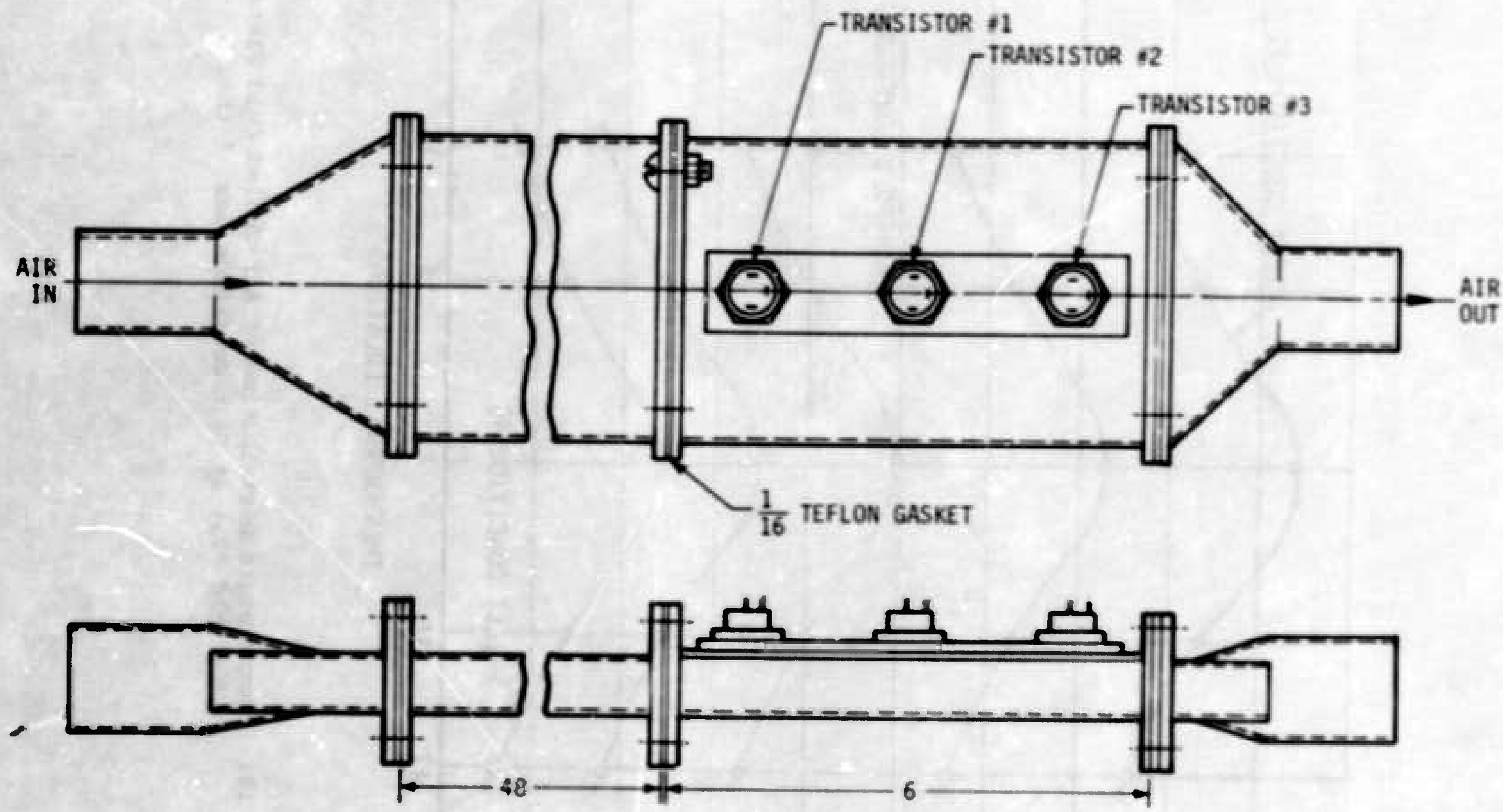

Figure 130. Air-Cooled Cold Plate No. 3 with Manifold Configuration #2a

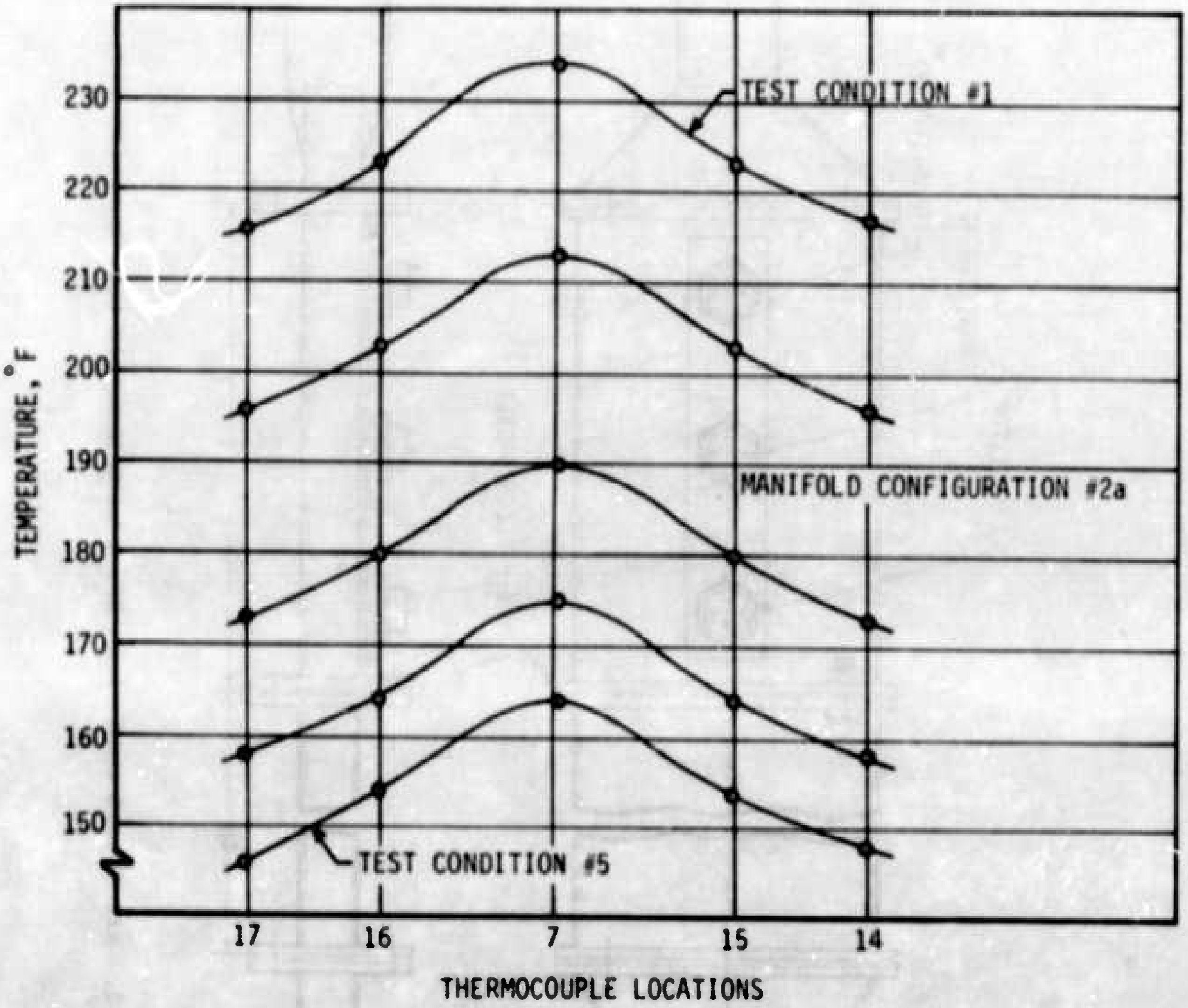

Figure 131. Temperature Distribution of Air-Cooled Cold Plate No. 3 (Manifold #2a) at Test Condition Nos. 1 thru 5

Table 27. Test Conditions of Air-Cooled Cold Plate No. 3, Manifold Configuration #2a

TEST NO.	AIR FLOW RATE (lb/hr)	ELECTRICAL POWER INPUT TO TRANSISTORS (watts)		
		TR #1	TR #2	TR #3
1	34	25	25	25
2	45	25	25	25
3	68	25	25	25
4	94	25	25	25
5	124	25	25	25

condition indicates that the 24-inch straight section provided the entry length for establishing a nearly fully-developed velocity profile, at least as far as it was possible for this particular configuration of the cold plate.

The experimentally determined Nusselt numbers are as follows:

Test No. 1, $Nu_1 = 29.5$

Test No. 2, $Nu_2 = 34.7$

Test No. 3, $Nu_3 = 42.9$

Test No. 4, $Nu_4 = 50.3$

Test No. 5, $Nu_5 = 58.5$

Figure 132 shows experimental air-cooled Cold Plate No. 3 with the manifold configuration identified as #3. In this mounting arrangement of the transistors, the cooling-air flow distribution is not very important, particularly if the mounting plate is of thick and high thermal conductance material. The main reason for tests with this manifold configuration was to investigate turbulence effects upon the convection heat-transfer coefficients. This type of manifold arrangement is also of interest because it occupies the least space as far as installation is concerned. Similarly as with the previous manifold configuration, the cold plate was tested at two general conditions: (1) a constant heat load of 75 watts (25 watts from each transistor) and five different cooling-air flow rates and (2) a constant air-flow rate of 67 lb/hr and three different heat loads.

The test conditions are presented in Table 28.

Temperature measurements of the thermocouples at all the test conditions are given in Appendix A.

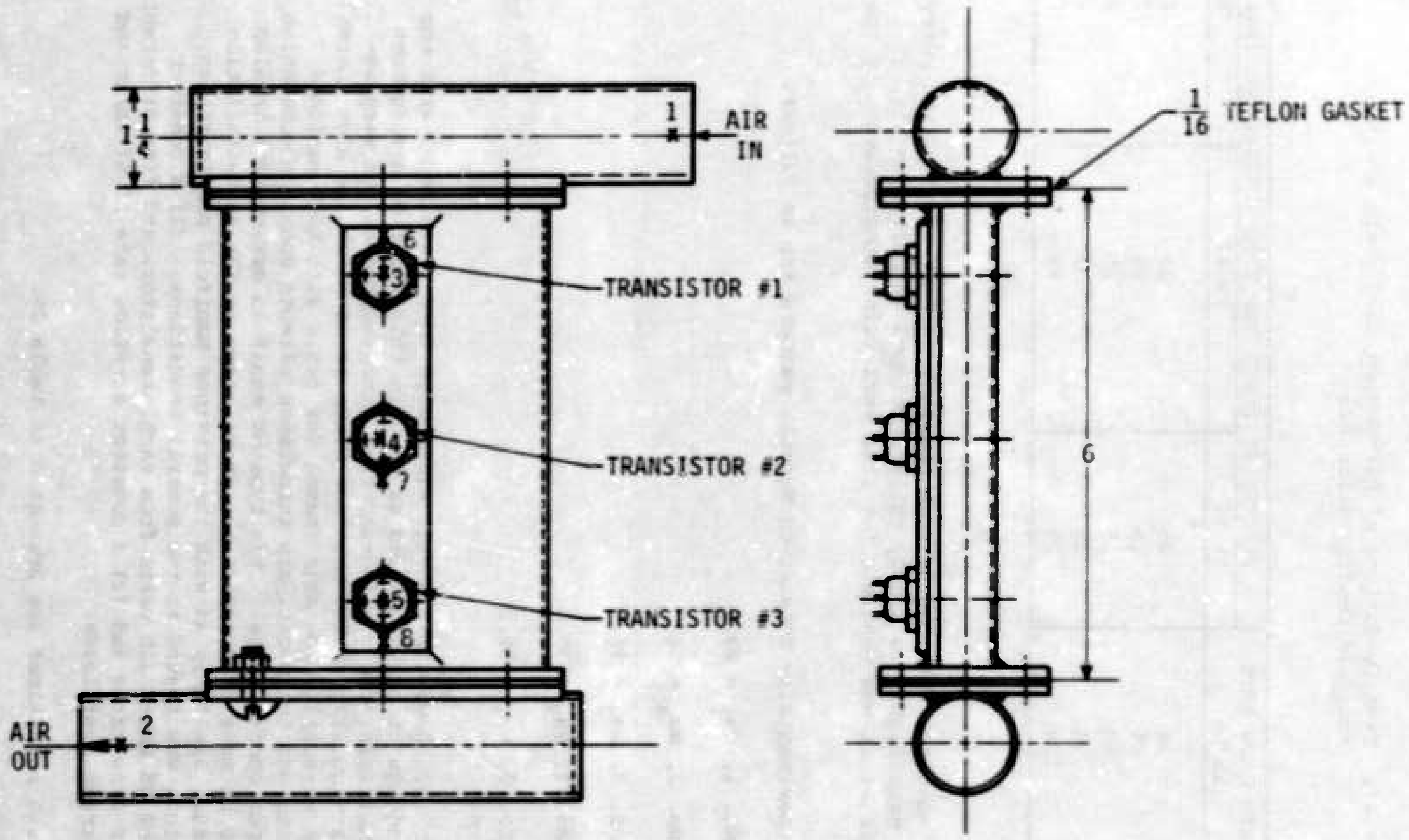

Figure 132. Air-Cooled Cold Plate No. 3 with Manifold Configuration #3

Table 28. Test Conditions of Air-Cooled Cold Plate No. 3, Manifold Configuration #3

TEST NO.	AIR FLOW RATE (lb/hr)	ELECTRICAL POWER INPUT TO TRANSISTORS (watts)		
		TR #1	TR #2	TR #3
1	34	25	25	25
2	45	25	25	25
3	68	25	25	25
4	94	25	25	25
5	124	25	25	25
6	67	20	20	20
7	67	30	30	30
8	67	40	40	40

Figure 133 shows temperature distribution across the cold plate at a constant electrical power dissipation rate of 75 watts (25 watts from each transistor) and five different cooling-air flow rates. Figure 134 shows temperature distribution of the cold plate at a constant cooling-air flow rate, but three different heat loads. Both figures show unsymmetrical temperature distribution across the plate, indicating non-uniform flow distribution. With the transistor mounting arrangement of this cold plate, the flow and temperature distributions are not important; consequently, no other manifold arrangement was tested.

Figure 135 the case temperature of transistor #2 as a function of the cooling-air flow rate at the different manifold configurations. Because of the small difference in transistor temperature between the manifold #2 and #2a configurations, only one condition is shown on the figure. The figure shows that the 24-inch section had a significant effect upon the component temperature. This indicates that the straight section reduced the entry turbulence effects, thus reducing the heat-transfer coefficients. No noticeable temperature difference was observed between manifold #1 and #3 configurations.

The experimentally determined Nusselt numbers are as follows:

Test #1, $Nu_1 = 48.6$

Test #2, $Nu_2 = 60.8$

Test #3, $Nu_3 = 70.9$

Test #4, $Nu_4 = 83.6$

Test #5, $Nu_5 = 90.4$

Figure 136 shows a comparison of Nusselt numbers among the four manifold configurations of Cold Plate No. 3. The figure clearly shows the turbulence effects upon the Nusselt numbers. Manifold configurations #2 and #2a with the extended straight sections showed the lowest

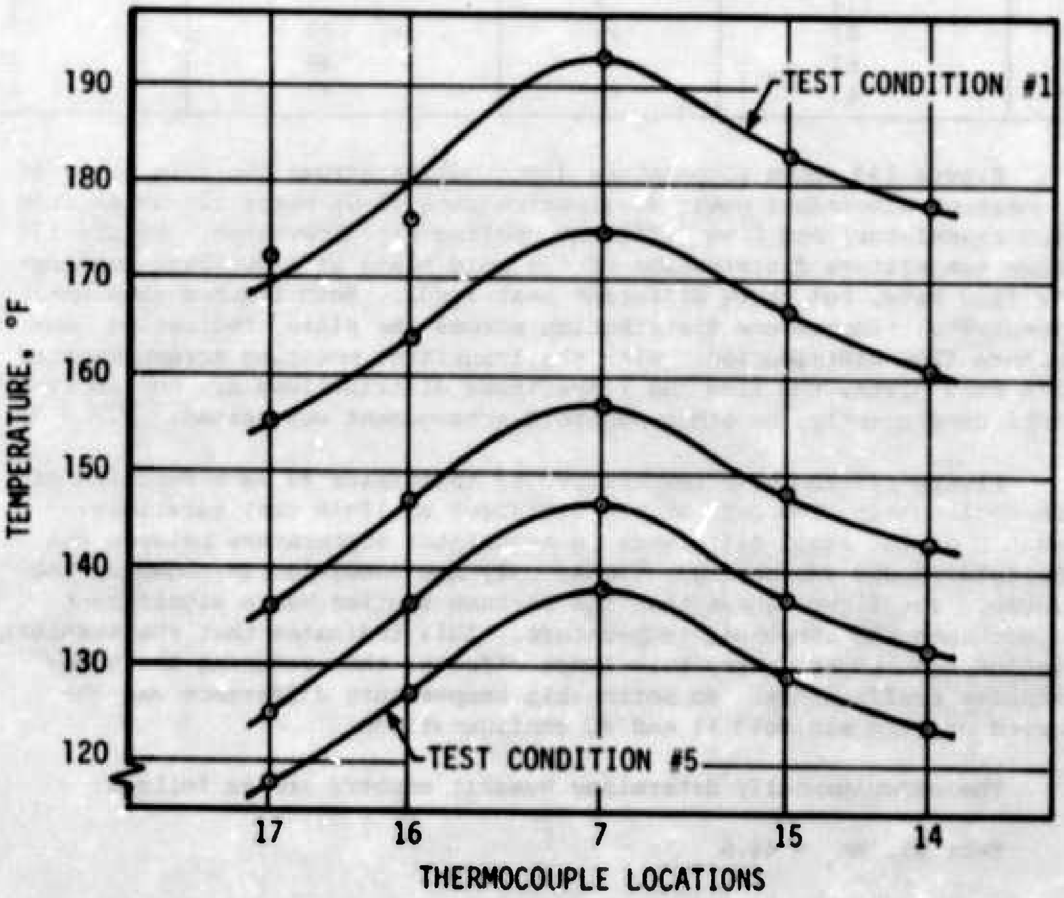

Figure 133. Temperature Distribution of Air-Cooled Cold Plate No. 3 (Manifold #3) at Test Condition Nos. 1 thru 5

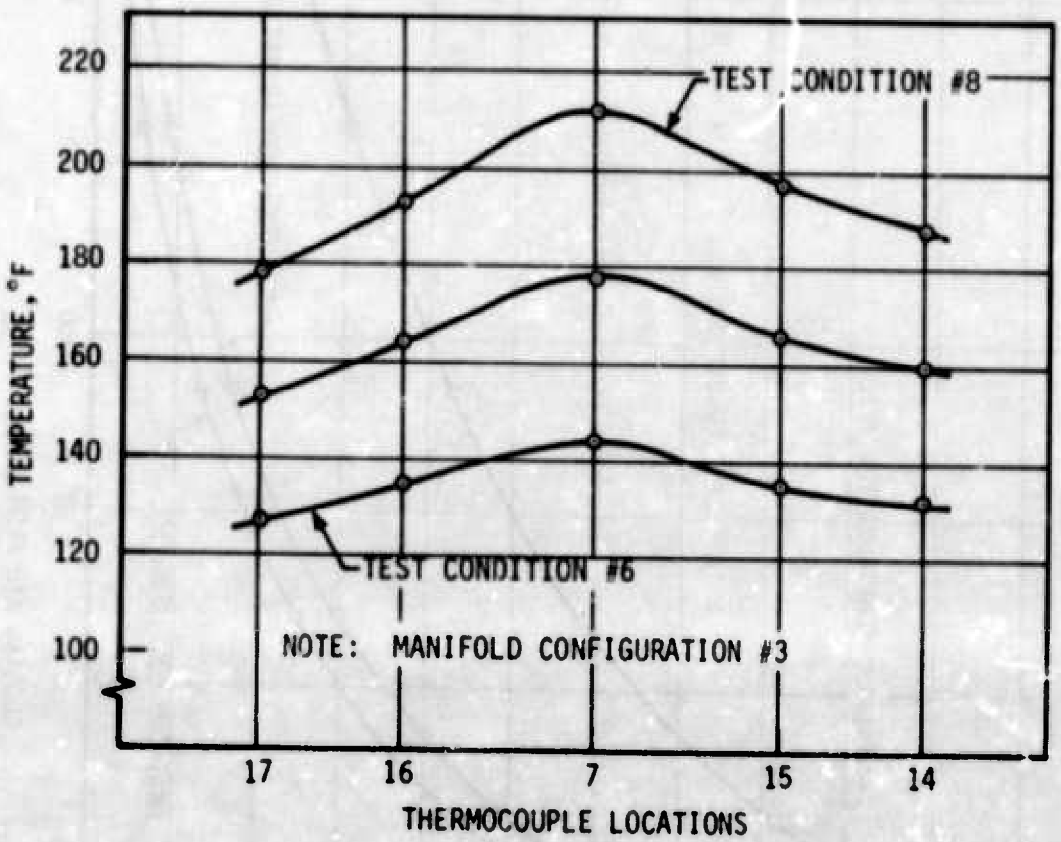

Figure 134. Temperature Distribution of Air-Cooled Cold Plate No. 3 (Manifold #3) at Test Condition Nos. 6 thru 8

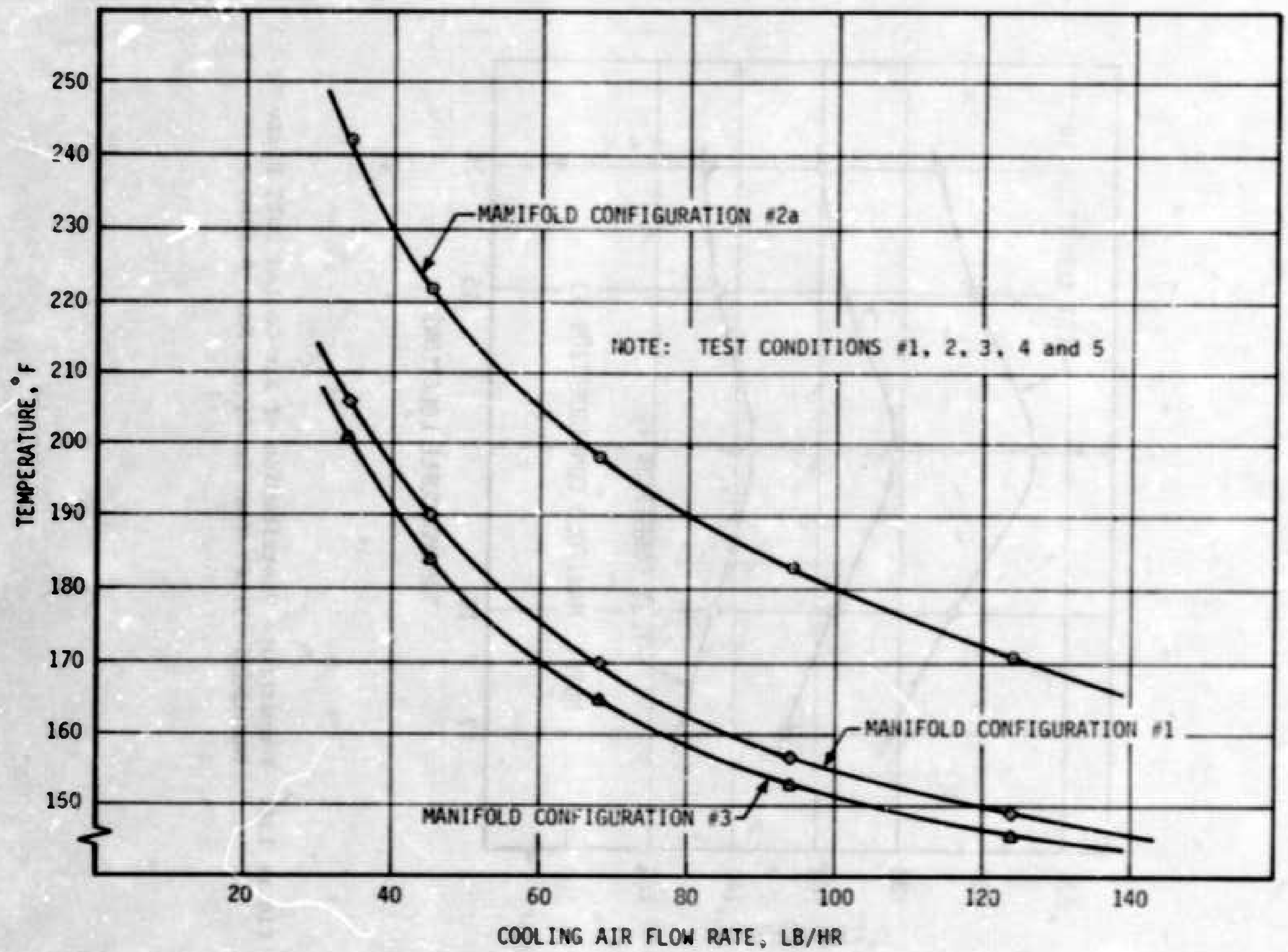

Figure 135. Temperature of Transistor #2 vs Cooling Air Flow Rate Comparison among Manifold Configurations Cold Plate No. 3

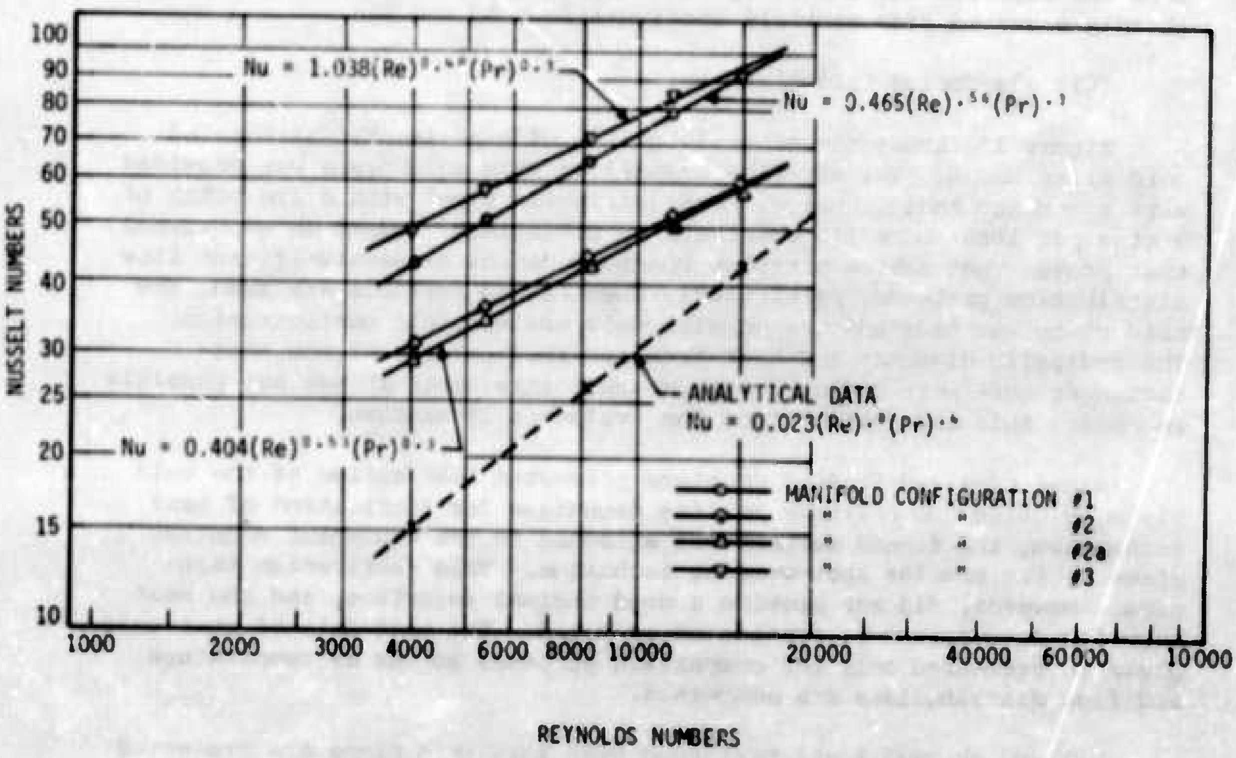

Figure 136. Experimentally Determined Nusselt Numbers vs Reynolds Numbers of Air-Cooled Cold Plate No. 3

Nusselt numbers; however, they did not provide the fully-developed velocity profile expected from the length to diameter ratio (x/D_h). The small difference in Nusselt numbers between manifold configurations #1 and #3 and #2 and #2a diminishes almost completely at a Reynolds number of approximately 15,000. As with the other cold plates, a significant difference can be observed between the analytical and experimental results. The difference is particularly large at the lower Reynolds numbers. Both the higher Nusselt numbers and the different slopes of the curves can be explained by the turbulence induced by the cooling-air entry conditions and also by the geometry of the flow passage. It is obvious that the turbulence effects were greater at the lower flow rates and diminished in significance as the flow rate is increased. It can be expected that at sufficiently high Reynolds numbers the experimental and analytical data will coincide. This can be clearly observed from manifold configurations #2 and #2a.

(4) Air-Cooled Cold Plate No. 4

Figure 137 shows the general outline of experimental air-cooled Cold Plate No. 4. The air-flow channel of this cold plate was provided with a compact heat exchanger core (strip-fin type) with a fin pitch of 9 fins per inch and a fin thickness of 0.010 inch. Based on experience that proves that narrow air-flow channels do not cause significant flow distribution problems, particularly when finned surfaces are used, the cold plate was made and tested with only one manifold configuration. The hydraulic diameter and heat-transfer surface area of the heat-exchanger core were computed from measurements since it was not possible to obtain this information from the available literature.

Since time and funding problems prevented fabrication of the cold plate by using the ordinary brazing technique for fabrication of heat exchangers, the finned surface was attached to the equipment mounting plate by the simpler spot-welding technique. This fabrication technique, however, did not provide a good thermal interface, and the heat transfer data cannot be considered as valid. The test data of this cold plate is presented only for comparison purposes as far as temperature and flow distributions are concerned.

All the thermal tests performed with this cold plate are presented in Table 29.

The temperature readings obtained from the different test conditions are given in Appendix A.

Figures 138 and 139 show temperature distribution of Cold Plate No. 4 at a constant power dissipation rate of 100 watts (20 watts from each transistor) and different cooling-air flow rates. The temperature distribution is shown at two sections across the cold plate indicated by the thermocouple locations. When the temperature distribution of this

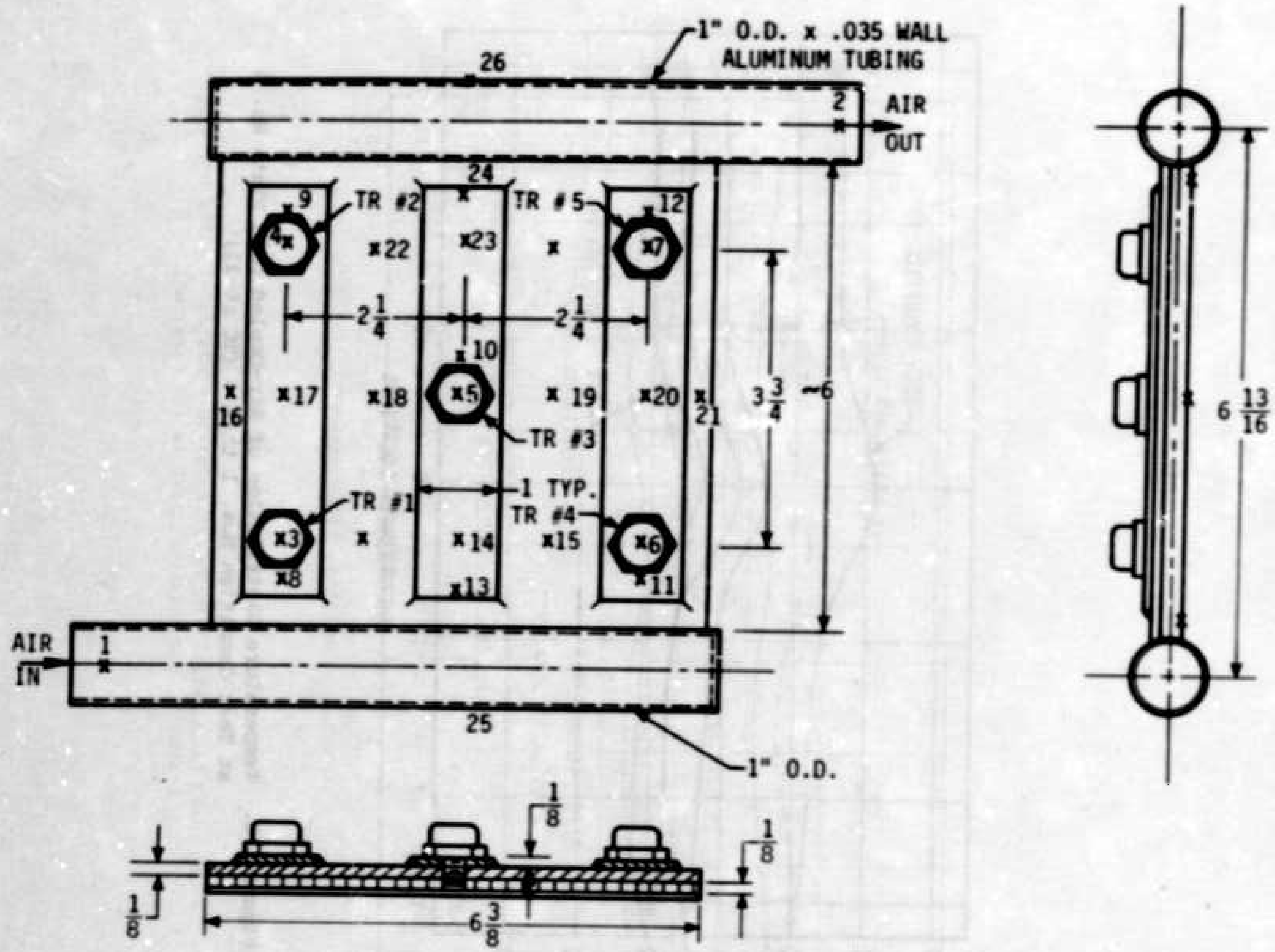

Figure 137. Air-Cooled Cold Plate No. 4

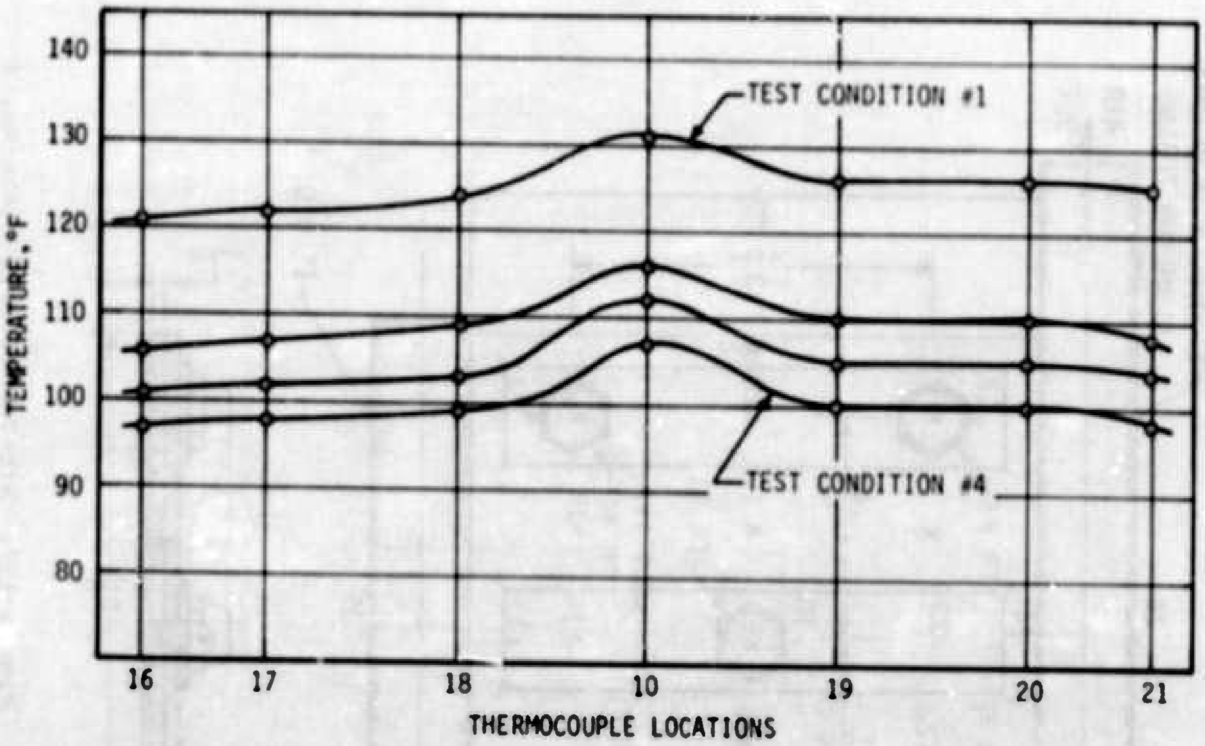

Figure 138. Temperature Distribution of Air-Cooled Cold Plate No. 4 at Test Condition Nos. 1 thru 4 (TC 16-21)

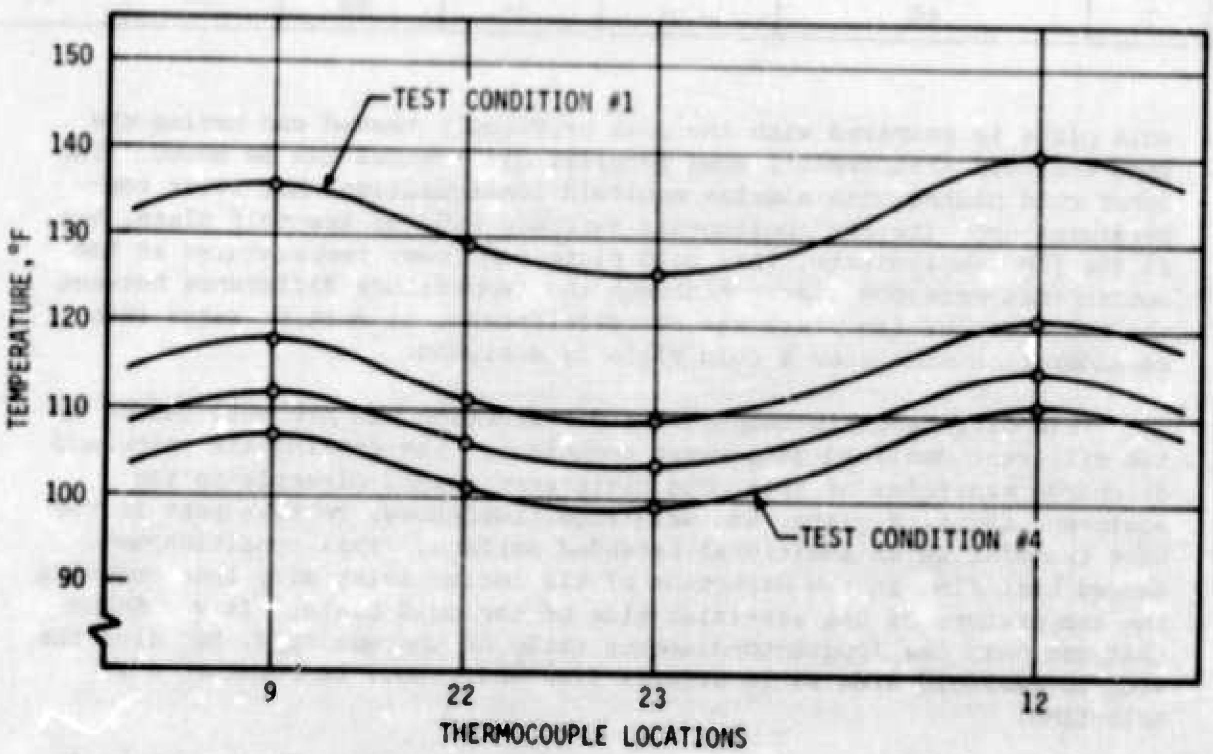

Figure 139. Temperature Distribution of Air-Cooled Cold Plate No. 4 at Test Condition Nos. 1 thru 4 (TC 9-23)

Table 29. Test Conditions of Air-Cooled Cold Plate No. 4

TEST NO.	AIR FLOW RATE (lb/hr)	ELECTRICAL POWER INPUT TO TRANSISTORS (watts)				
		TR #1	TR #2	TR #3	TR #4	TR #5
1	34	20	20	20	20	20
2	56	20	20	20	20	20
3	94	20	20	20	20	20
4	124	20	20	20	20	20
5	68	--	--	20	--	--
6	68	--	--	35	--	--
7	68	--	--	50	--	--

cold plate is compared with the ones previously tested and having the same manifold arrangement, some peculiar differences can be noted. The other cold plates with similar manifold configurations had lower temperatures opposite the cooling-air entrance side of the cold plate, but, as the figures indicate, this cold plate had lower temperatures at the cooling-air entrance side. Although the temperature difference between the two sides of the plate was not significant, it must be taken into consideration when such a cold plate is designed.

This difference in temperature distribution was probably caused by the different manifold attachment technique. The cooling-air inlet and discharge manifolds of this cold plate were welded directly to the equipment mounting plate, and were able, therefore, to take part in the heat transfer as an additional extended surface. This condition enhanced heat flow in the direction of the cooler inlet air, thus reducing the temperature of the air-inlet side of the cold plate. It was found that not only the length-to-diameter ratio of the manifold, but also the slot-to-manifold area ratio affects flow and, thus, temperature distribution.

Figure 140 shows temperature distribution across the cold plate at a constant air flow rate of 68 lbs/hr, but at different power dissipation rates from transistor #3 (only transistor #3 was energized). This thermal loading provided an almost completely symmetrical temperature distribution across the cold plate.

Figure 141 shows the case temperature of transistors #1 and #2 versus the cooling-air flow rate. Power dissipation from the transistors was maintained constant (100 watts total, 20 watts from each transistor) while the cooling-air flow rate was varied from 34 lbs/hr to 124 lbs/hr. It can be seen from the figure that only a minor reduction of transistor temperature can be achieved by increasing the cooling-air flow rate above approximately 70 lbs/hr.

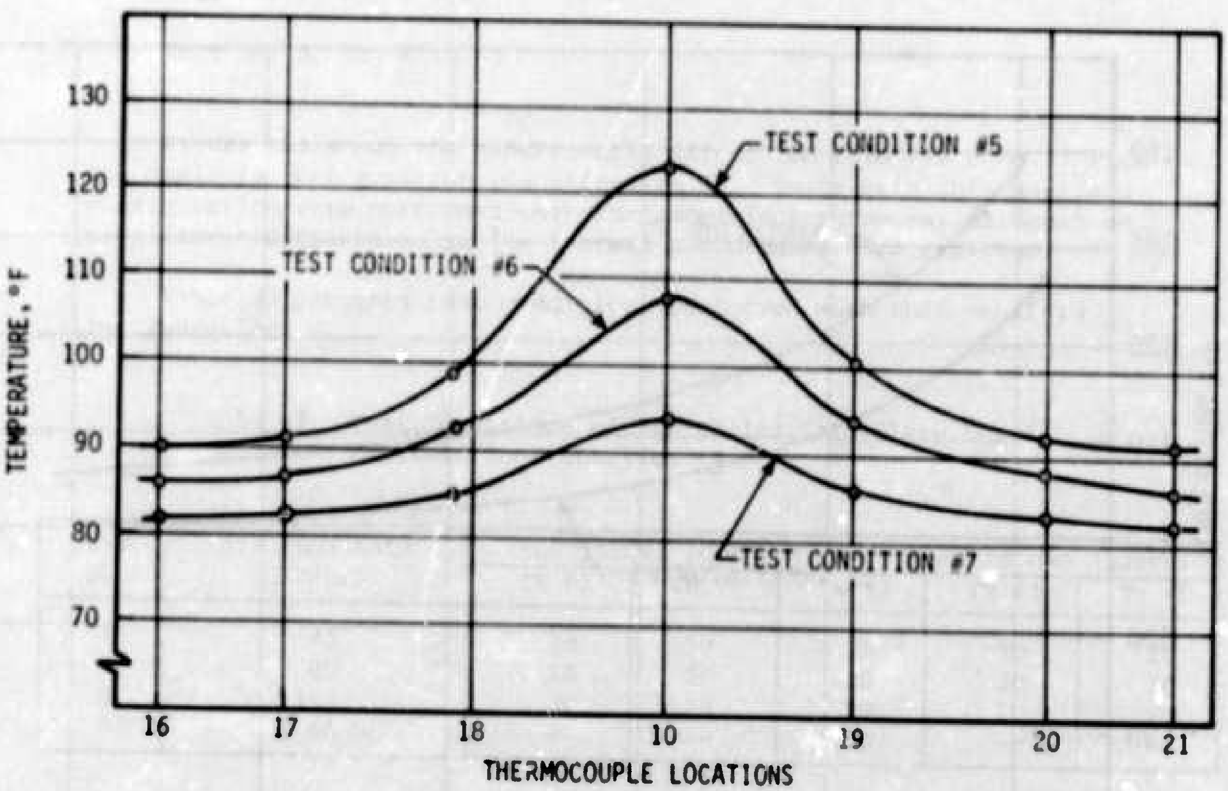

Figure 140. Temperature Distribution of Air-Cooled Cold Plate No. 4 at Test Condition Nos. 4 thru 6

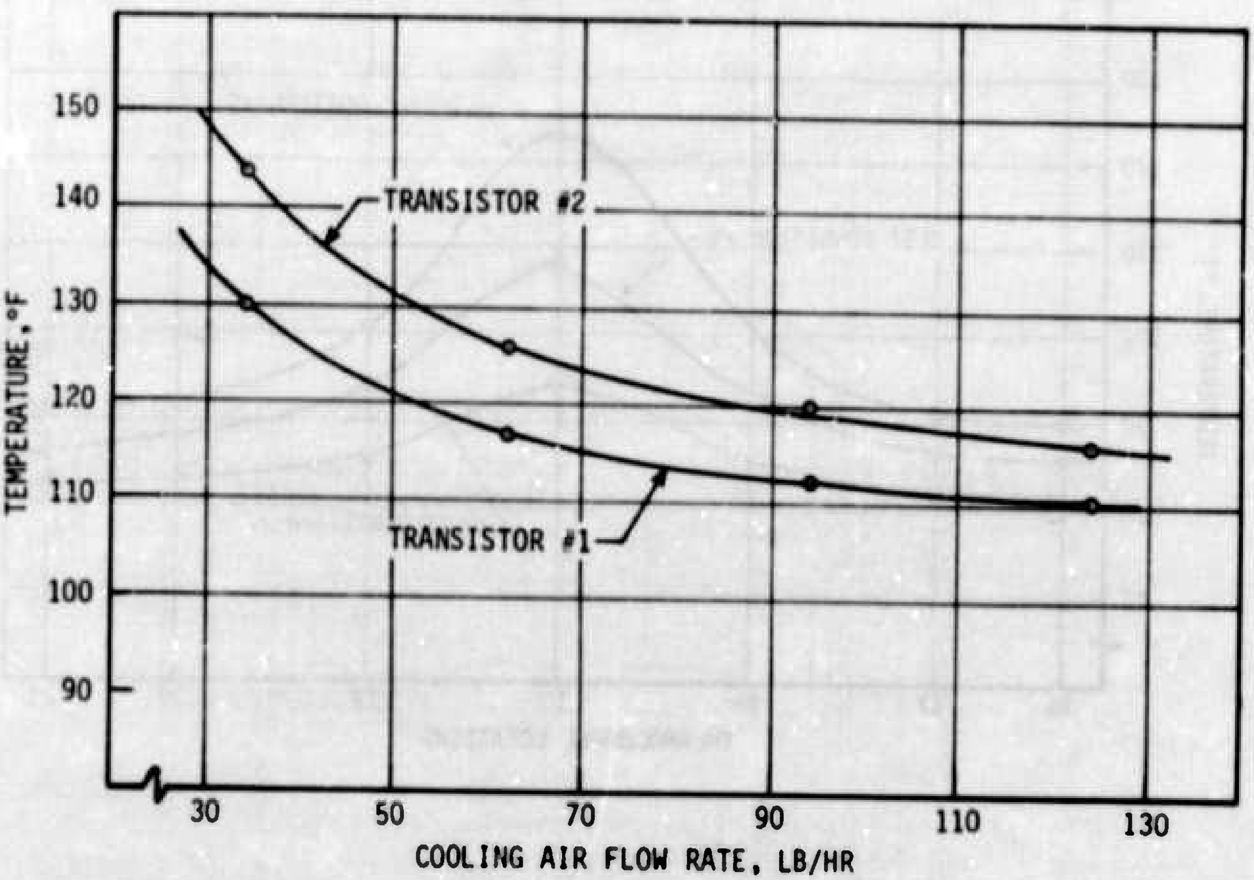

Figure 141. Case Temperature of Transistors vs Cooling Air FLow Rate for Air-Cooled Cold Plate No. 4

(5) Air-Cooled Cold Plate No. 5

Figure 142 shows the outline of experimental air-cooled Cold Plate No. 5. The air-flow channel of this cold plate measured 1/4 x 6 inches and was provided with a finned core having a surface geometry identified in Reference 27 as plate-fin surface 11.1 (11.1 fins per inch). The hydraulic diameter, D_h, of this surface geometry was 0.01012 ft; the total heat transfer area/volume between plates, $\beta = 367\ ft^2/ft^3$; and the fin area/total area was 0.756. The cold plate was provided with flanges to allow installation of different manifold configurations.

The fabrication of this cold plate was performed in accordance with the practice used in the fabrication of heat exchangers (heat exchanger core brazed to the plates), and the experimentally determined heat-transfer coefficients and Nusselt numbers, therefore, are presented and compared with available test data and/or analysis.

Figure 143 shows the cold plate with manifold configuration #1. The figure also shows transistor and thermocouple locations. Two mounting arrangements were used for mounting the power transistors to the cold plate. One of the transistors was mounted on a flat reinforcement strip, while the others were mounted on angle brackets brazed on the cold plate.

Figure 144 shows the transistor mounting arrangement on the bracket with insulating washers, although such washers were not used in these tests. The primary purpose of these tests was to determine the thermal performance of the cold plates. If the heat-sink (cold plate) temperatures can be accurately predicted; then, the component temperatures can be computed, based on known mounting-joint thermal resistances.

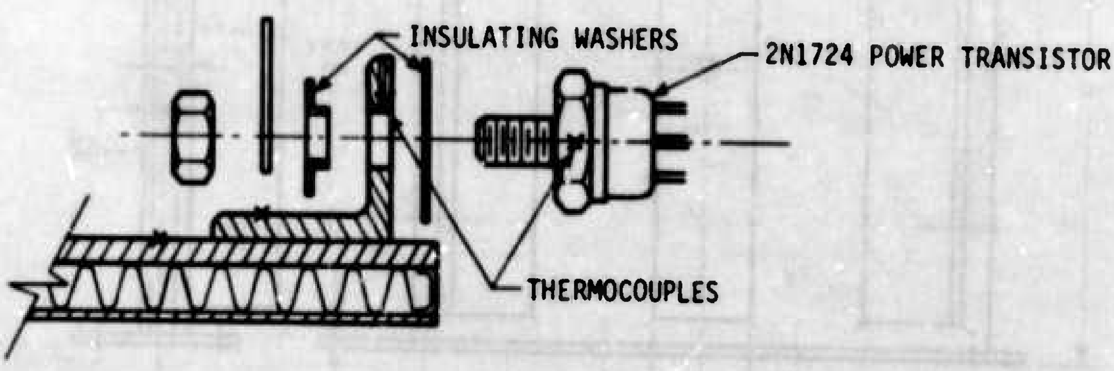

Figure 144. Mounting of Transistor on Bracket

Transistor case and cold plate temperatures were measured at different cooling-air flow rates and different electrical power dissipation rates from the transistor.

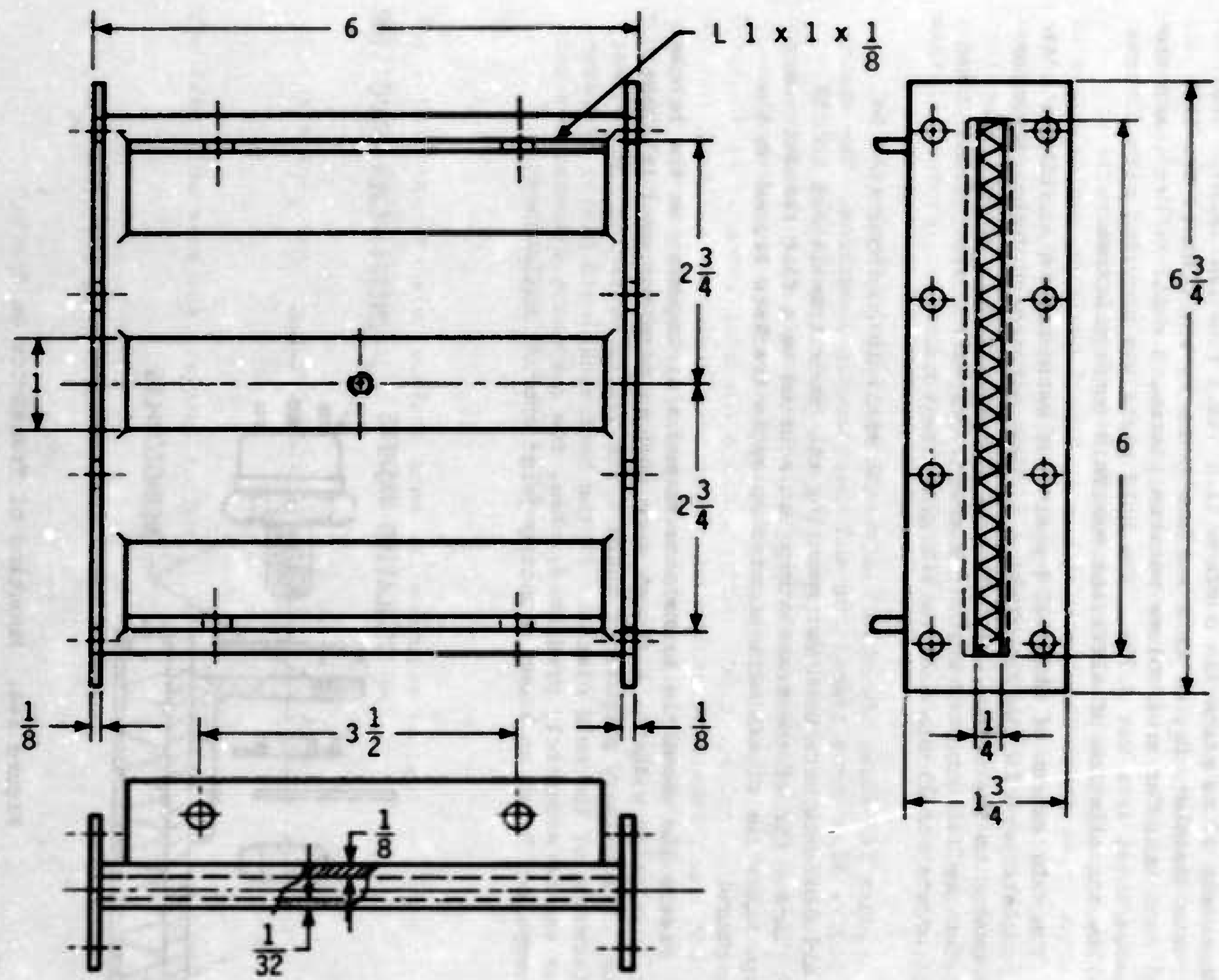

Figure 142. Air-Cooled Cold Plate No. 5

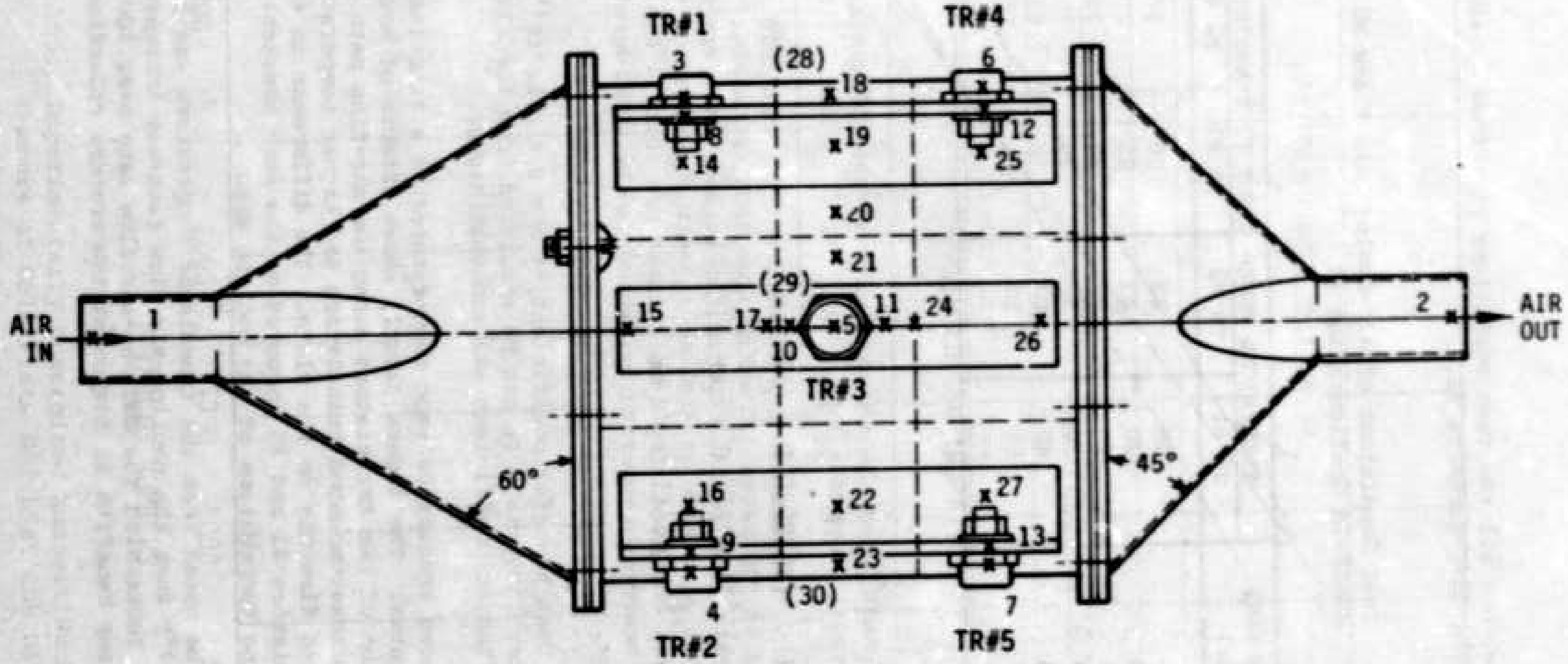

Figure 143. Air-Cooled Cold Plate No. 5 with Manifold Configuration #1

Table 30 presents all the test conditions performed on the cold plate with manifold configuration #1.

Table 30. Test Conditions of Air-Cooled Cold Plate No. 5, Manifold Configuration #1

TEST NO.	AIR FLOW RATE (lb/hr)	ELECTRICAL POWER INPUT TO TRANSISTORS (watts)				
		TR #1	TR #2	TR #3	TR #4	TR #5
1	45	20	20	20	20	20
2	80	20	20	20	20	20
3	124	20	20	20	20	20
4	68	30	30	30	30	30
5	68	40	40	40	40	40
6	68	50	50	50	50	50
7	68	--	--	50	--	--

Temperature readings of the thermocouples at the different test conditions are given in Appendix A.

Figure 145 shows temperature distribution of the cold plate at a constant heat load of 100 watts (20 watts from each transistor) and different cooling-air flow rates. Comparison between analysis and experimental data is also made at the cooling-air flow rate of 45 lbs/hr. As can be seen, the predicted temperatures are about 4°F higher than the actually measured temperatures, which can be considered an excellent agreement.

A convection heat-transfer coefficient of h = 8 Btu/hr ft^2°F was used in the computer analysis. It can be concluded from the figure that the actual heat-transfer coefficient was somewhat higher.

Figure 146 shows transistor case temperatures as a function of cooling-air flow rates. The figure clearly shows effects of mounting methods and location of the transistors along the air-flow path. As can be expected, the bracket-mounted transistors had higher temperatures than the one mounted directly on the plate. The difference in temperature between transistors #1 and #5 (mounted on the same bracket) was caused by the rising temperature of the cooling air.

It must also be noted that the transistor temperature was reduced by approximately 17°F when the cooling-air flow rate was increased from 45 to 124 lbs/hr. Increasing the cooling-air flow rate over 100 lbs/hr would not provide any benefits in component temperature reduction.

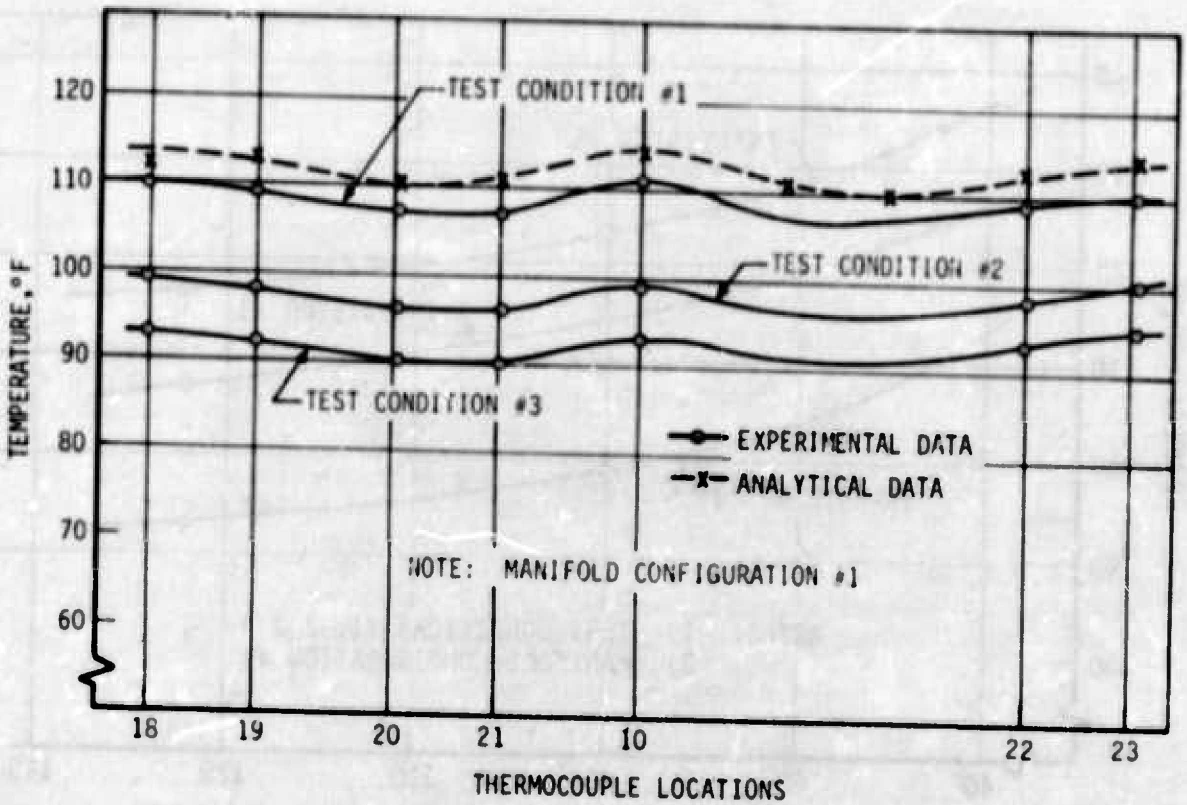

Figure 145. Temperature Distribution of Air-Cooled Cold Plate No. 5 (Manifold #1) at Test Condition Nos. 1 thru 3

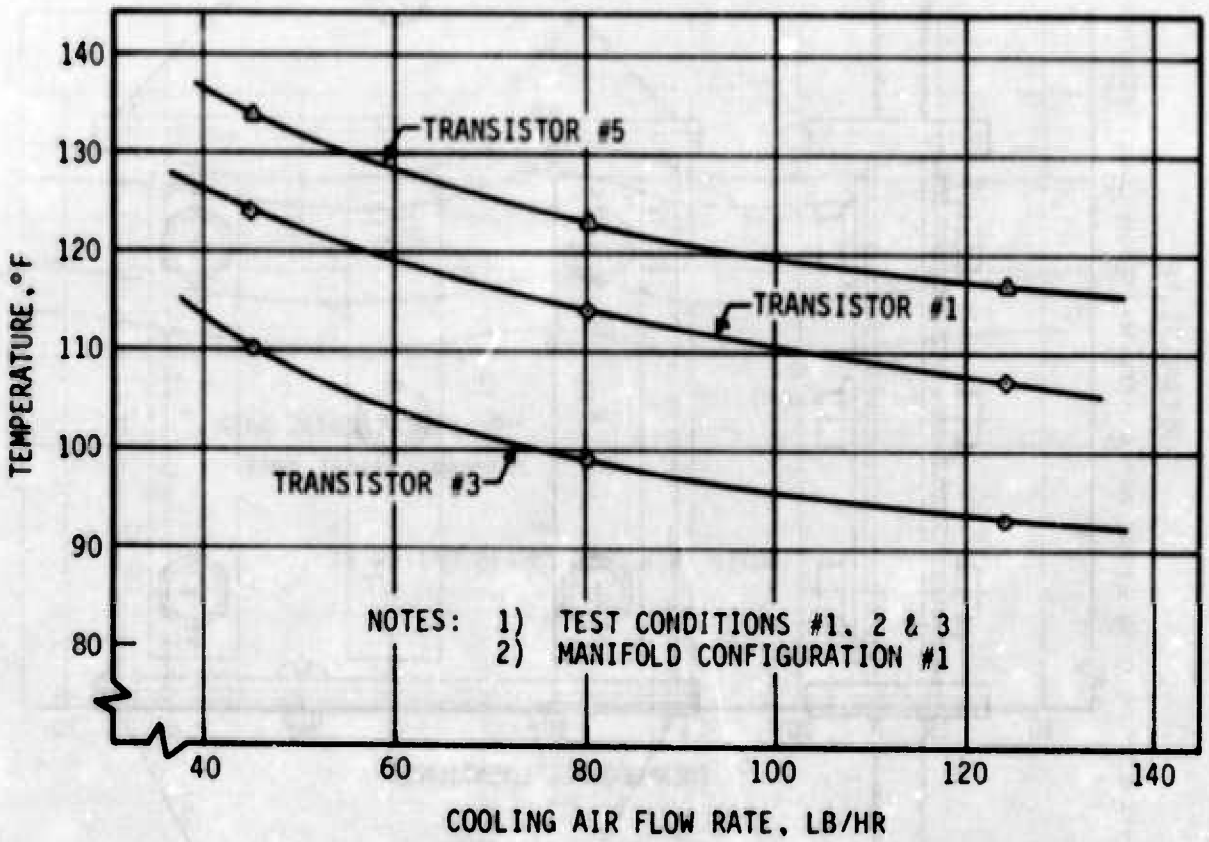

Figure 146. Case Temperature of Transistors vs Cooling Air Flow Rate for Air-Cooled Cold Plate No. 5 (Manifold #1)

Regardless of the smaller Nusselt numbers (as compared with the other cold plates) the plate and component temperatures were much lower, indicating the effectiveness of finned air-flow channels.

Figure 147 shows the case temperature of the transistors as a function of the electrical power dissipation rates from the transistors. A constant cooling-air flow rate of 68 lbs/hr was maintained throughout the three test conditions. All the transistors were energized with approximately the same electrical power (exact power adjustments were difficult because two transistors were energized by one power supply).

It can be seen that with increased power dissipation, the temperature difference among the transistors was increased. The rate of temperature increase was the largest for transistor #5 which was located at the cooling-air discharge end of the cold plate. The figure clearly shows the importance of mounting methods and the location of components of high power dissipation rates. If bracket mounting must be used for high power dissipating components, brackets of thicker material should be selected.

The experimentally determined Nusselt numbers are as follows:

Test No. 1, $Nu_1 = 5.74$

Test No. 2, $Nu_2 = 8.73$

Test No. 3, $Nu_3 = 11.71$

Figure 148 shows experimental air-cooled Cold Plate No. 5 with the manifold configuration identified as #2. In this configuration, a 12-inch straight section was installed at the cooling-air inlet end of the cold plate to reduce the turbulence effects induced by the manifold.

This configuration of the cold plate was tested at a constant heat load of 100 watts (20 watts from each transistor) and three different cooling air flow rates. The test conditions are presented in Table 31.

Table 31. Test Conditions of Cold Plate No. 5, Manifold Configuration #2

TEST NO.	AIR FLOW RATE (lb/hr)	ELECTRICAL POWER INPUT TO TRANSISTORS (watts)				
		TR #1	TR #2	TR #3	TR #4	TR #5
1	45	20	20	20	20	20
2	80	20	20	20	20	20
3	124	20	20	20	20	20

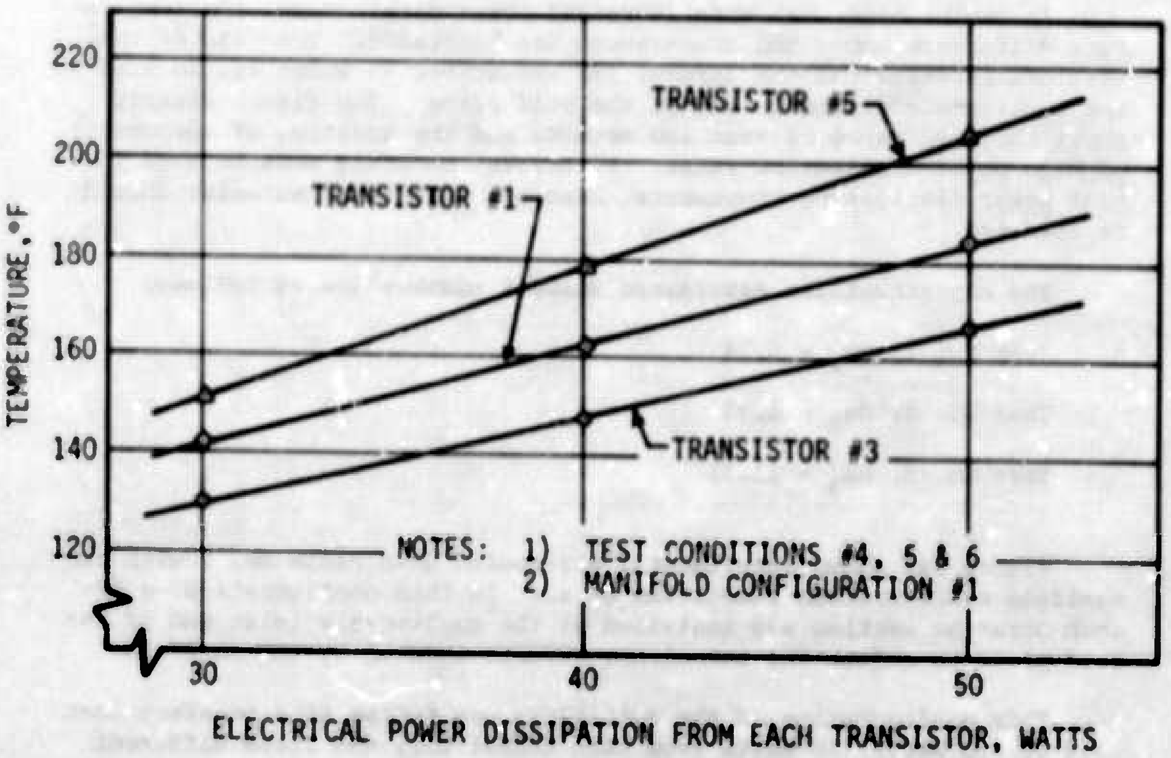

Figure 147. Case Temperature of Transistors vs Electrical Power Dissipation Rates for Air-Cooled Cold Plate No. 5 (Manifold #1)

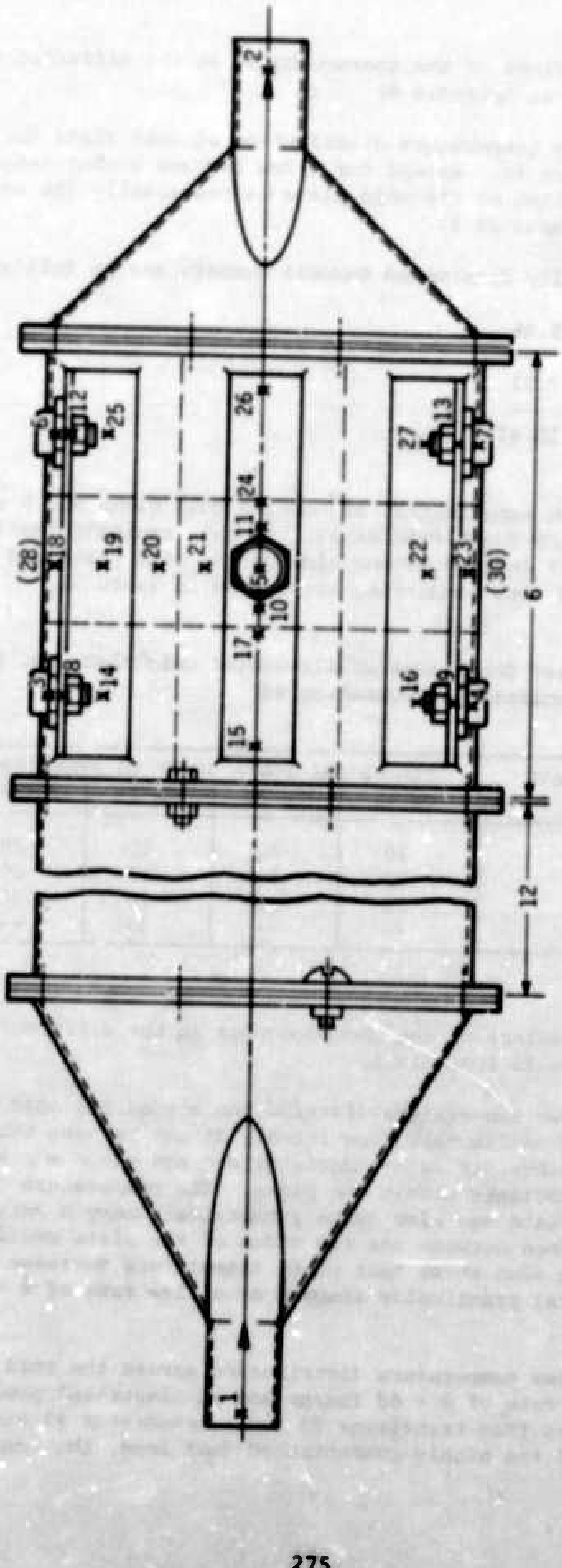

Figure 148. Air-Cooled Cold Plate No. 5 with Manifold Configuration #2

Temperature readings of the thermocouples at the different test conditions are given in Appendix A.

Figure 149 shows temperature distribution of Cold Plate No. 5 with manifold configuration #2. Except for a few degrees higher temperature, temperature distribution of the cold plate is practically the same as with manifold configuration #1.

The experimentally determined Nusselt numbers are as follows:

Test #1, $Nu_1 = 5.86$

Test #2, $Nu_2 = 7.93$

Test #3, $Nu_3 = 10.41$

Figure 150 shows experimental air-cooled Cold Plate No. 5 with the manifold configuration identified as #3. In this manifold configuration, the cooling air entered at one side of the cold plate and left at the other side. The test conditions are listed in Table 32.

Table 32. Test Conditions of Air-Cooled Cold Plate No. 5, Manifold Configuration #3

TEST NO.	AIR FLOW RATE (lb/hr)	ELECTRICAL POWER INPUT TO TRANSISTORS (watts)				
		TR #1	TR #2	TR #3	TR #4	TR #5
1	45	20	20	20	20	20
2	80	20	20	20	20	20
3	124	20	20	20	20	20
4	68	--	--	50	--	--

Temperature readings of the thermocouples at the different test conditions are given in Appendix A.

Figure 151 shows temperature distribution across the cold plate at the three different cooling-air flow rates. It can be seen that a power dissipation of 20 watts per each transistor did not cause any significant temperature gradients within the plate. The temperature distribution across the plate was also quite symmetrical; only a very small temperature difference between the two sides of the plate could be observed. The figure also shows that plate temperature decrease (with increased flow rates) practically stopped at a flow rate of $\dot{w} = 124$ lbs/hr.

Figure 152 shows temperature distribution across the cold plate at a cooling-air flow rate of $\dot{w} = 68$ lbs/hr and an electrical power dissipation of 50 watts from transistor #3 (only transistor #3 was energized). Because of the highly concentrated heat load, the temperature

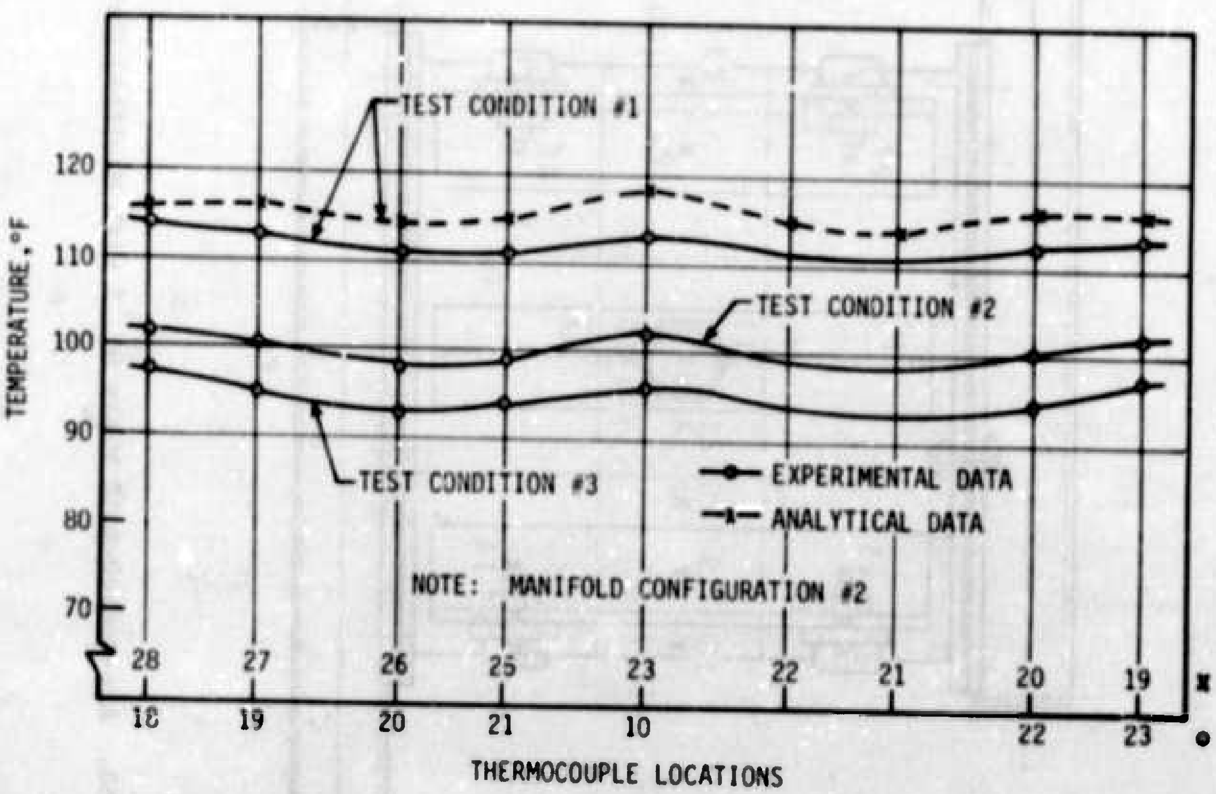

Figure 149. Temperature Distribution of Air-Cooled Cold Plate No. 5 (Manifold #2) at Test Condition Nos. 1 thru 3

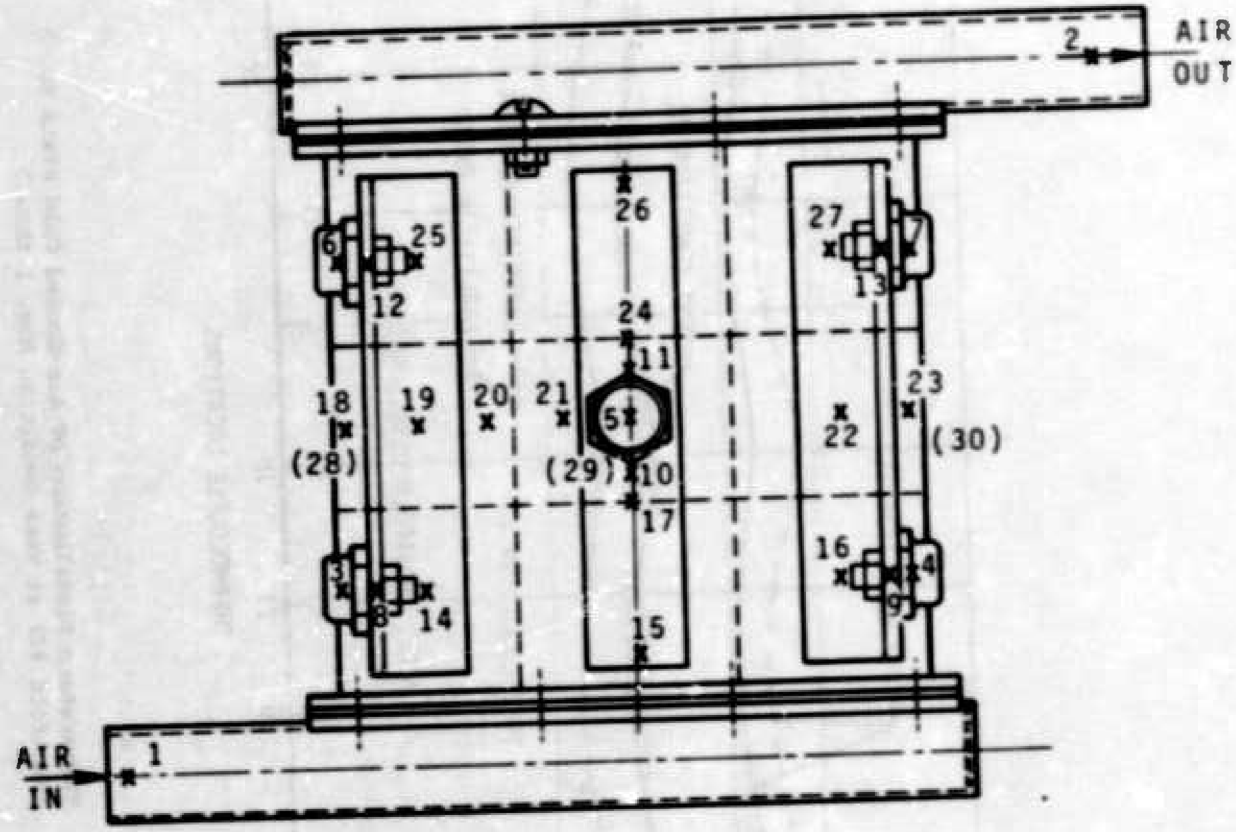

Figure 150. Air-Cooled Cold Plate No. 5 with Manifold Configuration #3

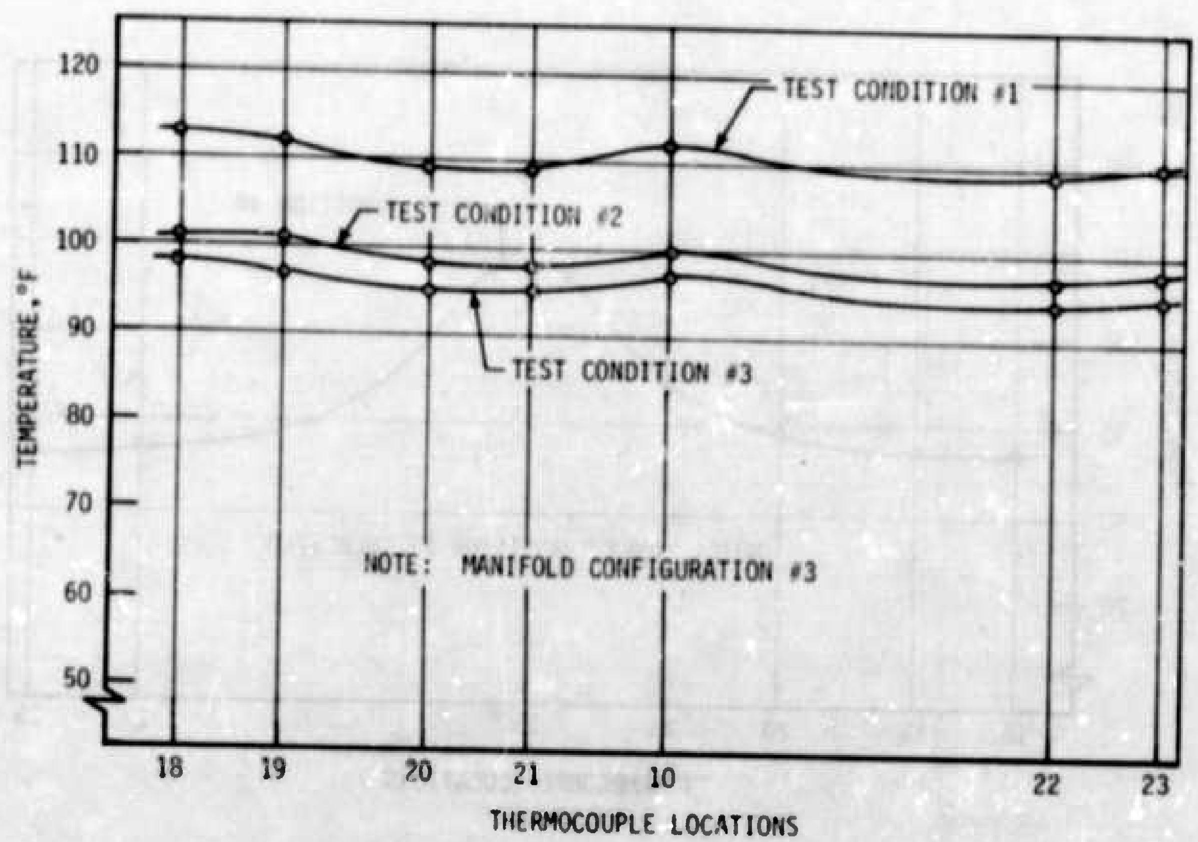

Figure 151. Temperature Distribution of Air-Cooled Cold Plate No. 5 (Manifold #3) at Test Condition Nos. 1 thru 3

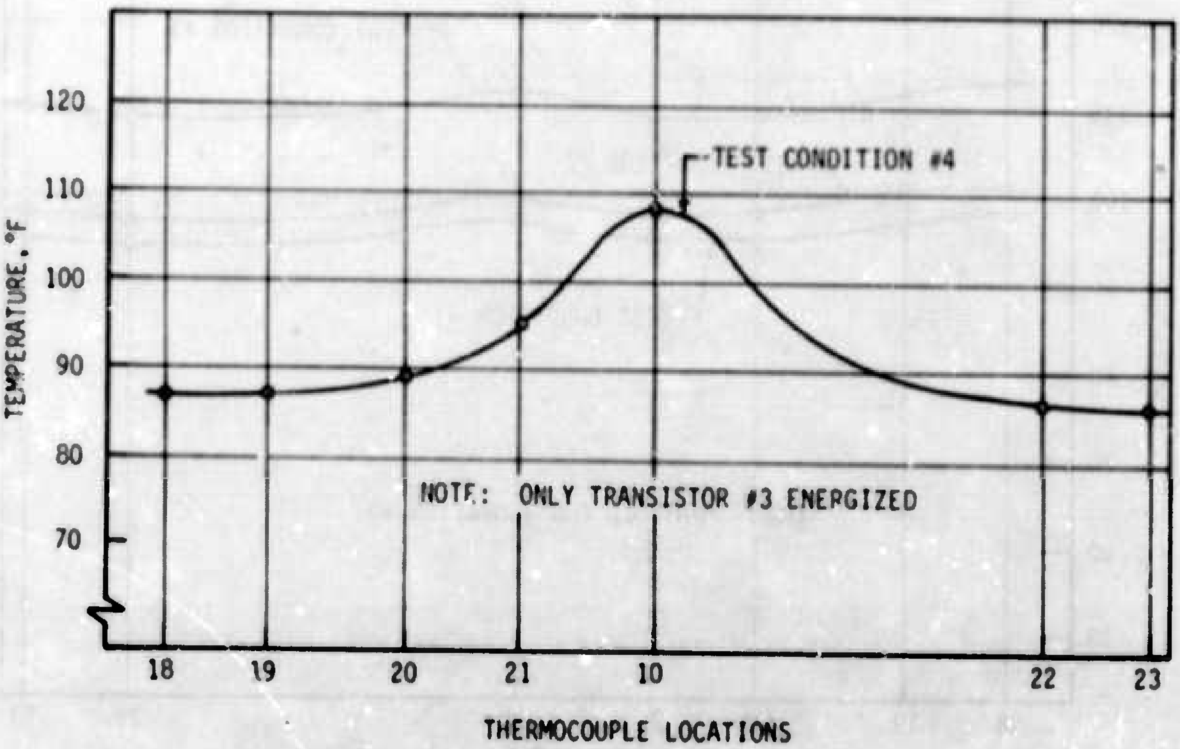

Figure 152. Temperature Distribution of Air-Cooled Cold Plate No. 5 (Manifold #3) at Test Condition No. 4

gradient within the mounting plate was increased; it was, however, significantly lower than that of the cold plates without the finned surfaces.

The experimentally determined Nusselt numbers are as follows:

Test No. 1, $Nu_1 = 6.8$

Test No. 2, $Nu_2 = 9.43$

Test No. 3, $Nu_3 = 10.03$

Figure 153 shows the experimental air-cooled Cold Plate No. 5 with the manifold configuration identified as #4. Tests with this manifold configuration were performed only for comparison purposes, although no significant differences in the thermal performance were expected.

Table 33 presents test conditions performed with this manifold configuration.

Table 33. Test Conditions of Air-Cooled Cold Plate No. 5, Manifold Configuration #4

TEST NO.	AIR FLOW RATE (lb/hr)	ELECTRICAL POWER INPUT TO TRANSISTORS (watts)				
		TR #1	TR #2	TR #3	TR #4	TR #5
1	45	20	20	20	20	20
2	80	20	20	20	20	20
3	124	20	20	20	20	20
4	68	--	--	50	--	--

Temperature readings of the thermocouples at the different test conditions are given in Appendix A.

Figure 154 shows temperature distribution across the cold plate at a constant heat load of 100 watts (20 watts from each transistor) and different cooling-air flow rates. As can be seen from the figure, temperature distribution across the cold plate was almost completely symmetrical indicating a uniform flow distribution.

The experimentally determined Nusselt numbers are as follows:

Test No. 1, $Nu_1 = 6.79$

Test No. 2, $Nu_2 = 9.31$

Test No. 3, $Nu_3 = 12.21$

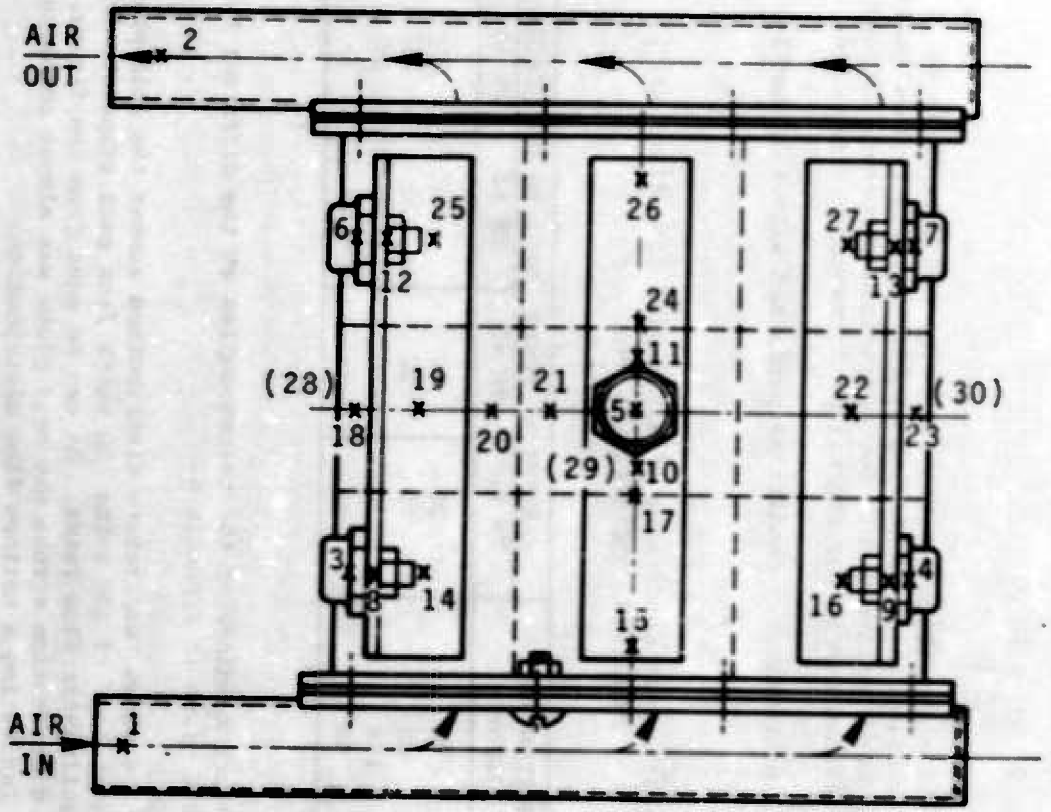

Figure 153. Air-Cooled Cold Plate No. 5 with Manifold Configuration #4

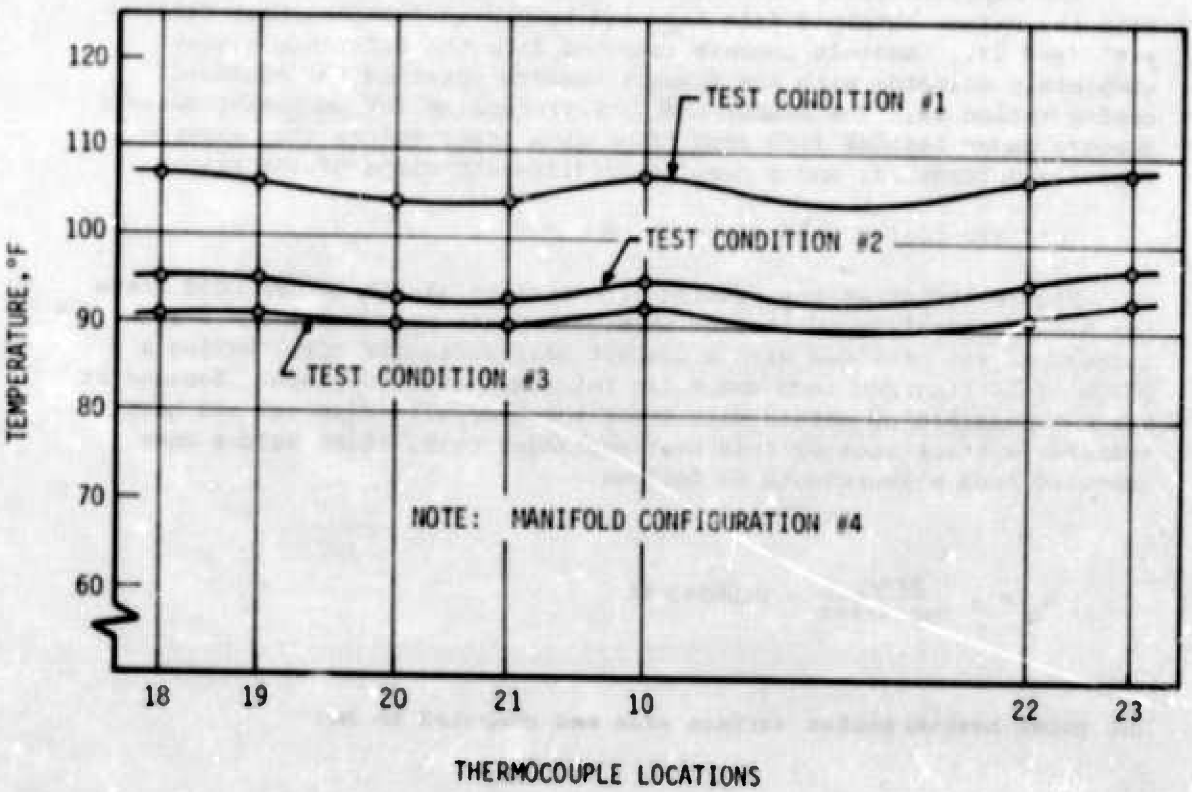

Figure 154. Temperature Distribution of Air-Cooled Cold Plate No. 5 (Manifold #4) at Test Condition Nos. 1 thru 3

Figure 155 shows experimentally determined Nusselt numbers as a function of Reynolds numbers for air-cooled Cold Plate No. 5. The figure shows comparison of the Nusselt numbers among the different manifold configurations. Results obtained from manifold configuration #3 are not presented because the values obtained fall between those for manifold configurations #2 and #4. As can be concluded from the figure, the different manifold configurations and arrangements did not have significant effects upon thermal performance of this cold plate.

The experimentally determined Nusselt numbers were also compared with the values obtained from Kays and London in "Compact Heat Exchangers" (Ref 27). Nusselt numbers computed from the reference almost completely coincide with the Nusselt numbers obtained for manifold configuration #1. The Sieder and Tate expression for computing Nusselt numbers under laminar flow conditions gave lower values than experimentally determined, and a completely different slope of the graph.

(6) Air-Cooled Cold Plate No. 6

Figure 156 shows the outline of experimental air-cooled Cold Plate No. 6. The air-flow channel of this cold plate measured 1/2 x 6-1/4 inches and was provided with a compact heat-exchanger core, having a pitch of 14 fins per inch and a fin thickness of 0.006 inch. Because it was not possible to obtain data about the hydraulic diameter and heat transfer surface area of this heat exchanger core, these values were computed from measurements as follows:

$$D_h = 4 \frac{\text{Area}}{\text{Perimeter}} = 0.00943 \text{ ft}$$

The total heat-transfer surface area was computed to be:

$$A = A_{fin} + A_{pl} = 3.990 \text{ ft}^2$$

The free flow area was computed to be:

$$A_{pl} = 0.0179 \text{ ft}^2$$

Time and funding problems prevented application of the more expensive ordinary heat exchanger fabrication techniques. A spot-welding technique was used for attaching the heat-exchanger core to one side of

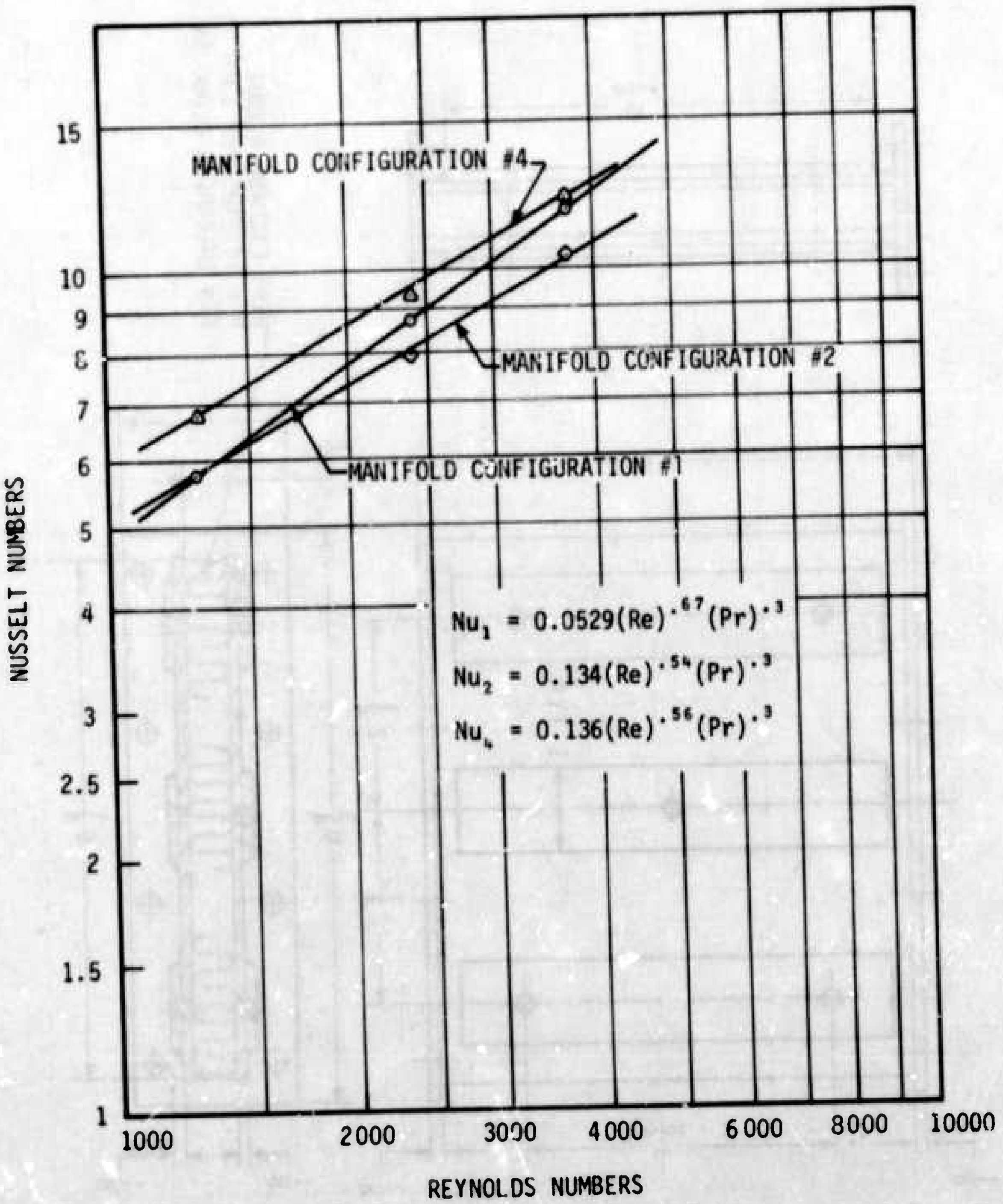

Figure 155. Experimentally Determined Nusselt Numbers vs Reynolds Numbers of Cold Plate No. 5 at the Different Manifold Configurations

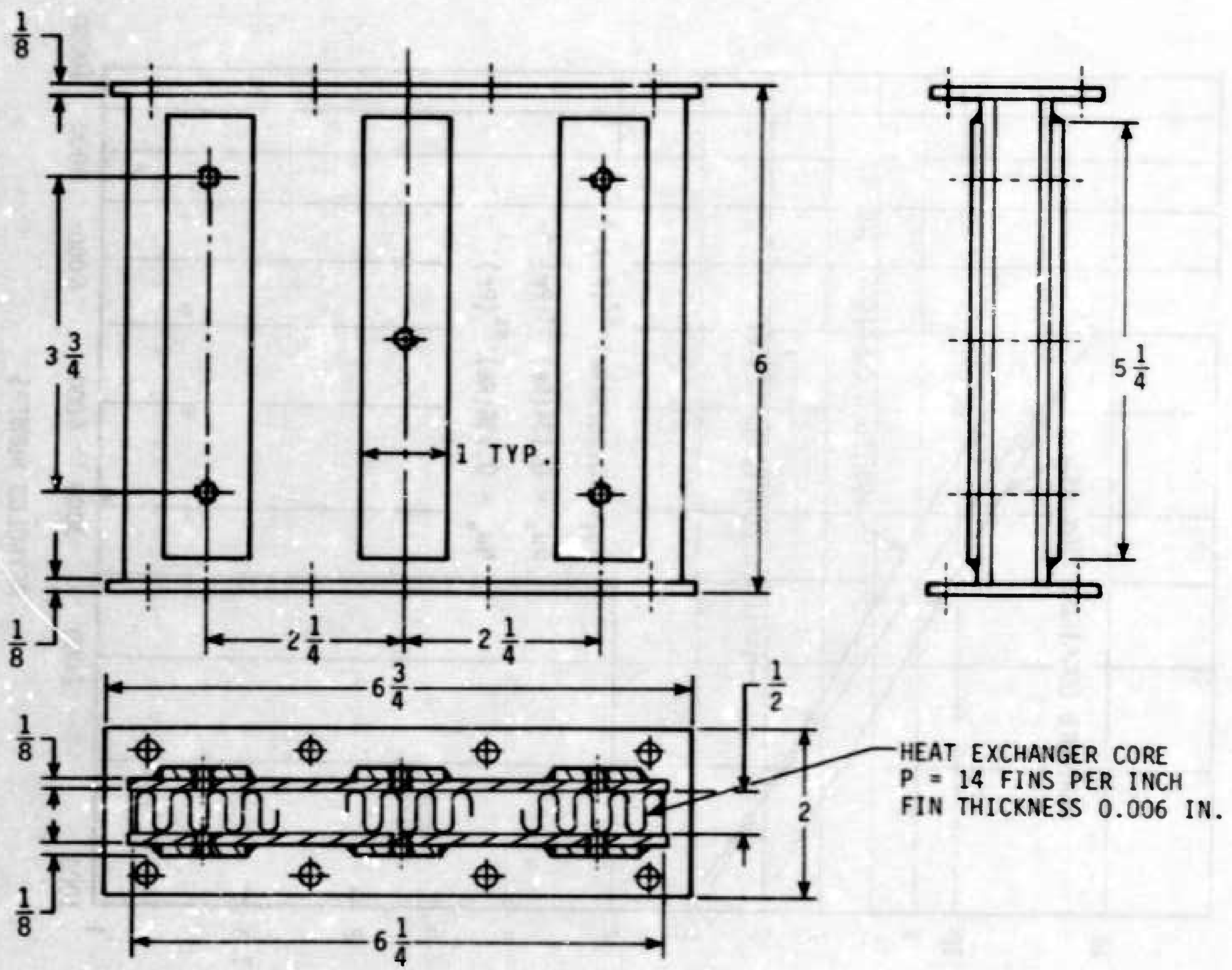

Figure 156. Air-Cooled Cold Plate No. 6

the equipment mounting surface; conductive epoxy was used on the other side. Both sides of the cold plate were provided with equipment mounting surfaces; and to investigate the effects of different manifold configurations upon flow distribution and heat transfer. The cold plate was provided with flanges.

When a symmetrical heat load was applied to both sides of the cold plate, temperature measurements indicated that a lower interface thermal resistance between the heat-exchanger core and equipment mounting surface occurred at the side where the conductive epoxy was used (just the opposite was expected). The heat transfer coefficients, therefore, cannot be considered as valid and will not be presented. The temperature measurements and temperature distribution graphs will be mainly presented for comparison purposes, and to demonstrate the effects of manifold configuration upon the particular flow passage geometry.

Figure 157 shows experimental air-cooled Cold Plate No. 6 with the manifold configuration identified as #1. The figure also shows transistor and thermocouple locations. Only the side of the cold plate is shown where epoxy was used for attaching the heat-exchanger core to the equipment mounting surface. The transistors (type 2N1724) were attached directly to the cold plate without insulating washers. Heat-sink compound was used on all transistor mounting joints. Because of limited temperature measuring instruments, the case temperature of all the transistors was not measured.

The thermal tests performed with this manifold configuration are presented in Table 34.

Table 34. Test Conditions of Air-Cooled Cold Plate No. 6, Manifold Configuration #1

TEST NO.	AIR FLOW RATE (lb/hr)	ELECTRICAL POWER INPUT TO TRANSISTORS (watts)				
		TR #1	TR #2	TR #3	TR #4	TR #5
1	45	18	22	20	20	20
2	80	18	22	20	20	20
3	124	18	22	20	20	20
4	80	--	--	50	--	--

Temperature readings of the thermocouples at the different test conditions are given in Appendix A.

Figure 158 shows temperature distribution across the cold plate perpendicular to the flow stream. Figures 159 and 160 show temperature distribution along the cooling-air flow stream. The tests were performed at different cooling-air flow rates, but constant electrical power dissipation rates from the transistors. Only the transistors

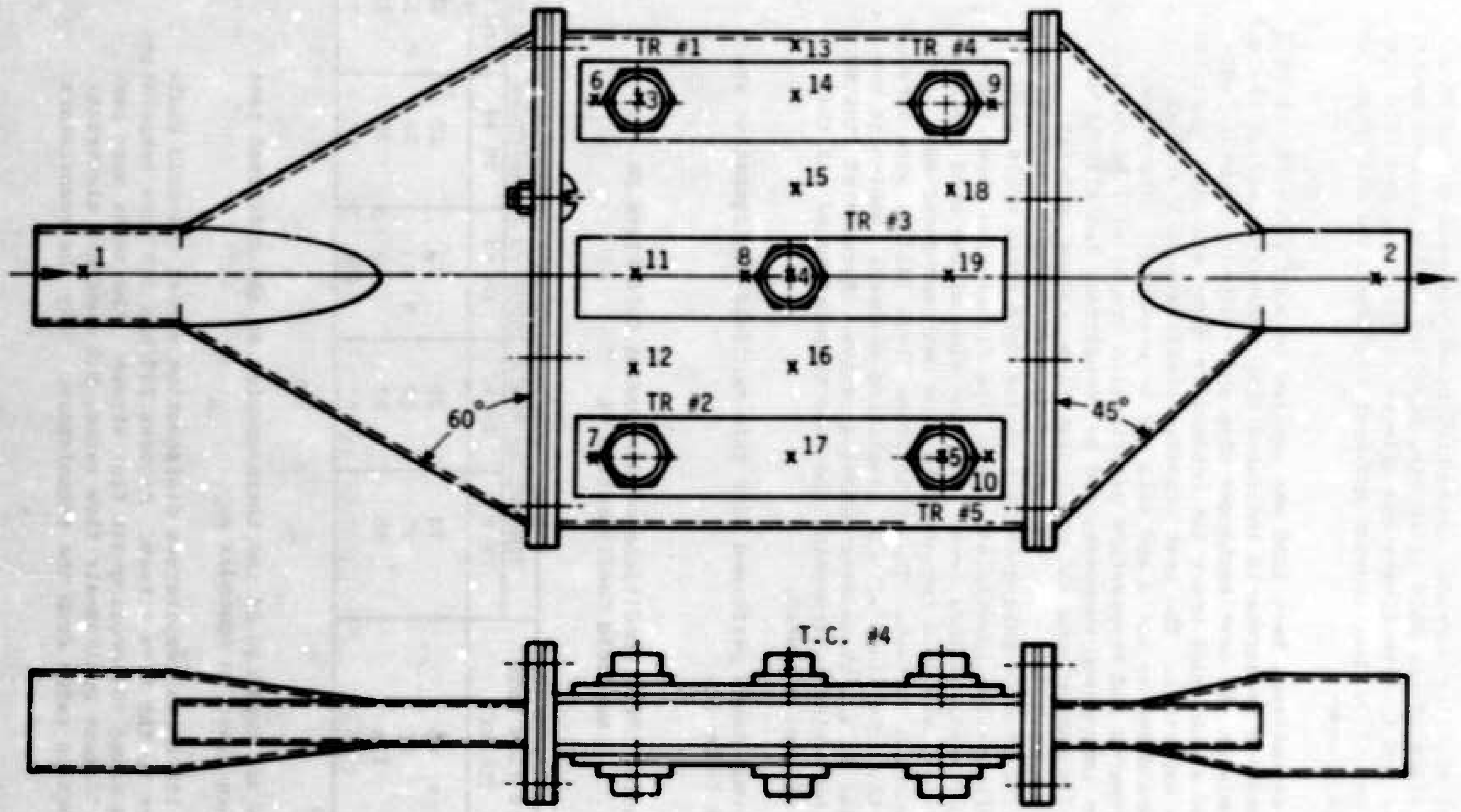

Figure 157. Air-Cooled Cold Plate No. 6 with Manifold Configuration #1

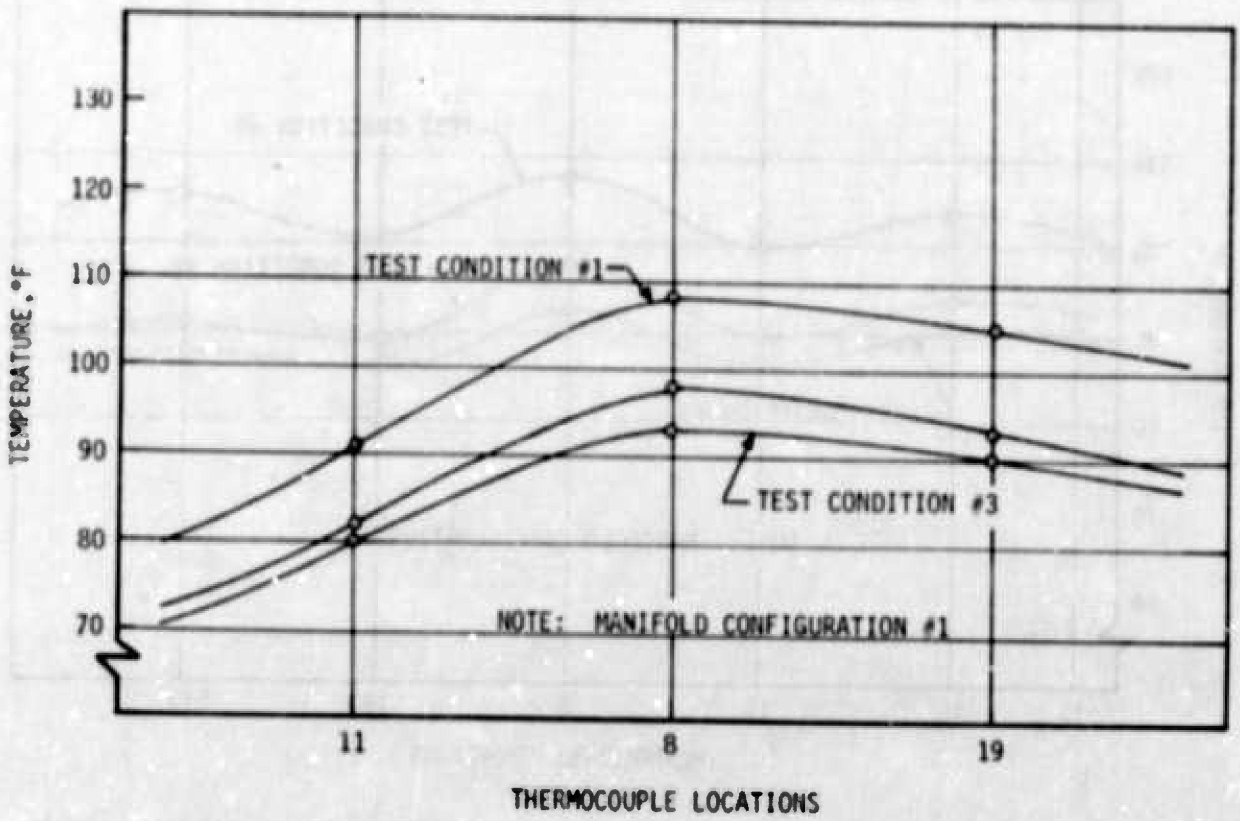

Figure 158. Temperature Distribution of Air-Cooled Cold Plate No. 6 (Manifold #1) at Test Condition Nos. 1 thru 3 (TC 13-17)

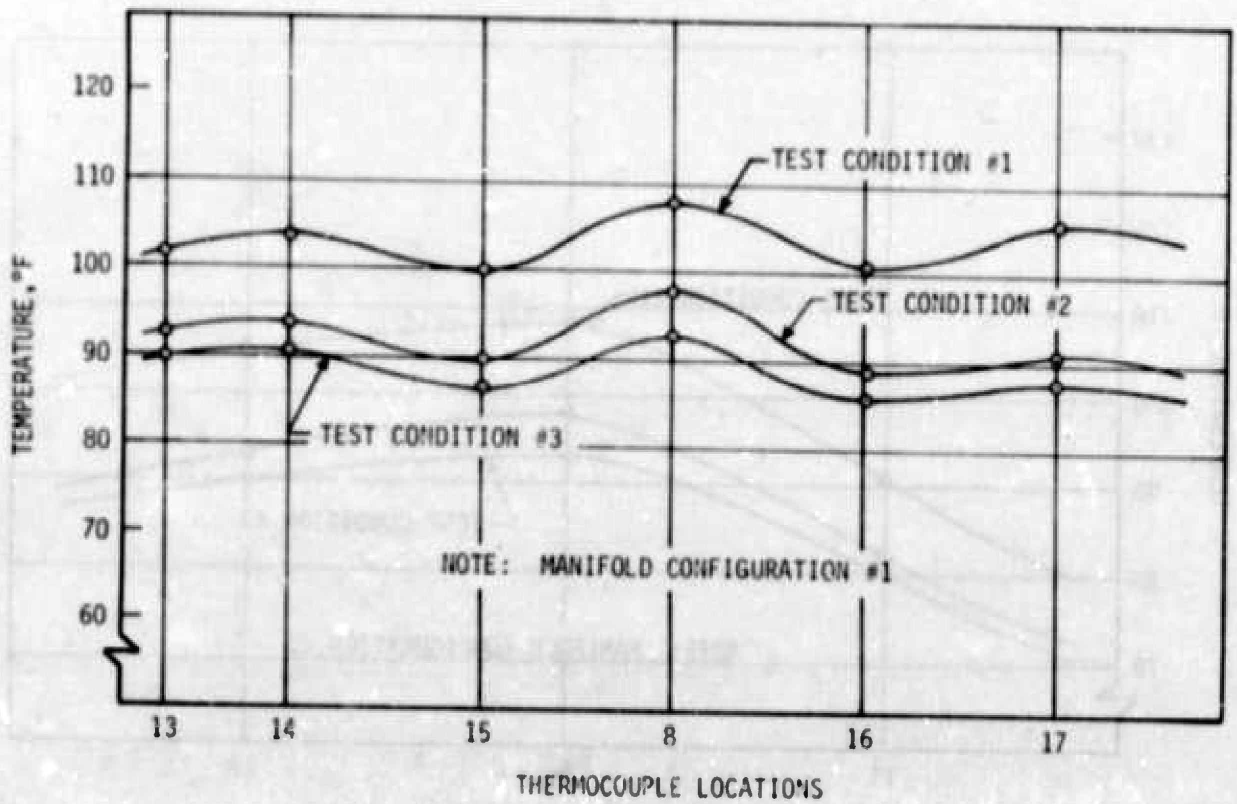

Figure 159. Temperature Distribution of Air-Cooled Cold Plate No. 6 (Manifold #1) at Test Condition Nos. 1 thru 3 (TC 11-19)

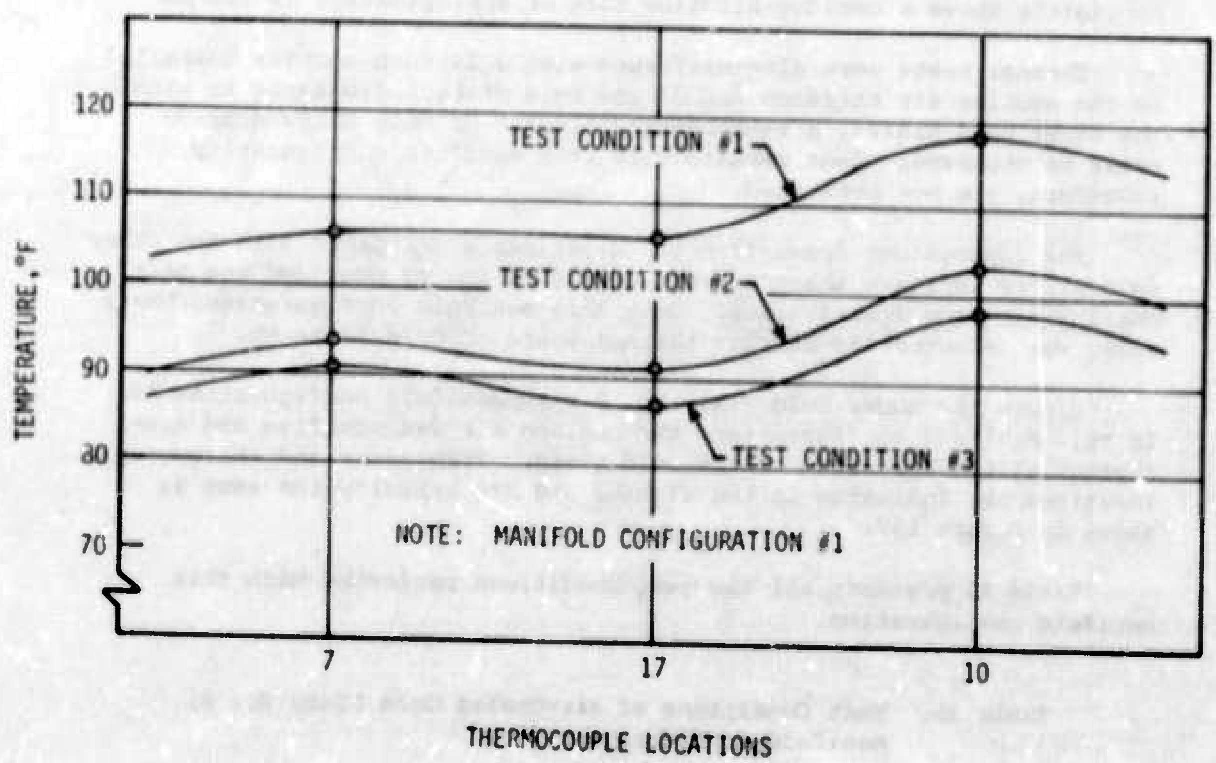

Figure 160. Temperature Distribution of Cold Plate No. 6 (Manifold #1) at Test Condition Nos. 1 thru 3 (TC 7-17)

mounted on the side shown were energized. As can be expected, the largest temperature differences of the cold plate occurred along the cooling-air flow stream. The figures are self-explanatory and clearly show the trend in temperature distribution when air is used as a cooling medium.

Figure 161 shows the case temperature of transistor Nos. 1 and 3 versus the cooling-air flow rate. Similarly as with the other cold plates provided with compact heat-exchanger cores, there was no significant reduction in component temperature within the flow-rate range in which the tests were performed. The gain in temperature reduction was negligible above a cooling-air flow rate of approximately 80 lbs/hr.

Thermal tests were also performed with a 24-inch section installed at the cooling-air entrance end of the cold plate. Similarly as with the other cold plates, a temperature increase of only a few degrees could be observed. Test results with this manifold configuration, therefore, are not presented.

The conclusions drawn from the experiments performed with the other cold plates indicate that manifold configuration #4 provided the best cooling-air flow distribution. Only this manifold configuration, therefore, was selected for further thermal tests of Cold Plate No. 6.

Figure 162 shows Cold Plate No. 6 with manifold configuration #4. In this manifold configuration, the cooling air was admitted and discharged at the same side of the cold plate. Transistor and thermocouple locations are indicated in the figure, and are actually the same as shown in Figure 157.

Table 35 presents all the test conditions performed with this manifold configuration.

Table 35. Test Conditions of Air-Cooled Cold Plate No. 6, Manifold Configuration #4

TEST NO.	AIR FLOW RATE (lb/hr)	ELECTRICAL POWER INPUT TO TRANSISTORS (watts)				
		TR #1	TR #2	TR #3	TR #4	TR #5
1	45	22	20	20	20	20
2	80	22	20	20	20	20
3	124	22	20	20	20	20
4	80	--	--	50	--	--

Temperature readings of the thermocouples at the different test conditions are given in Appendix A.

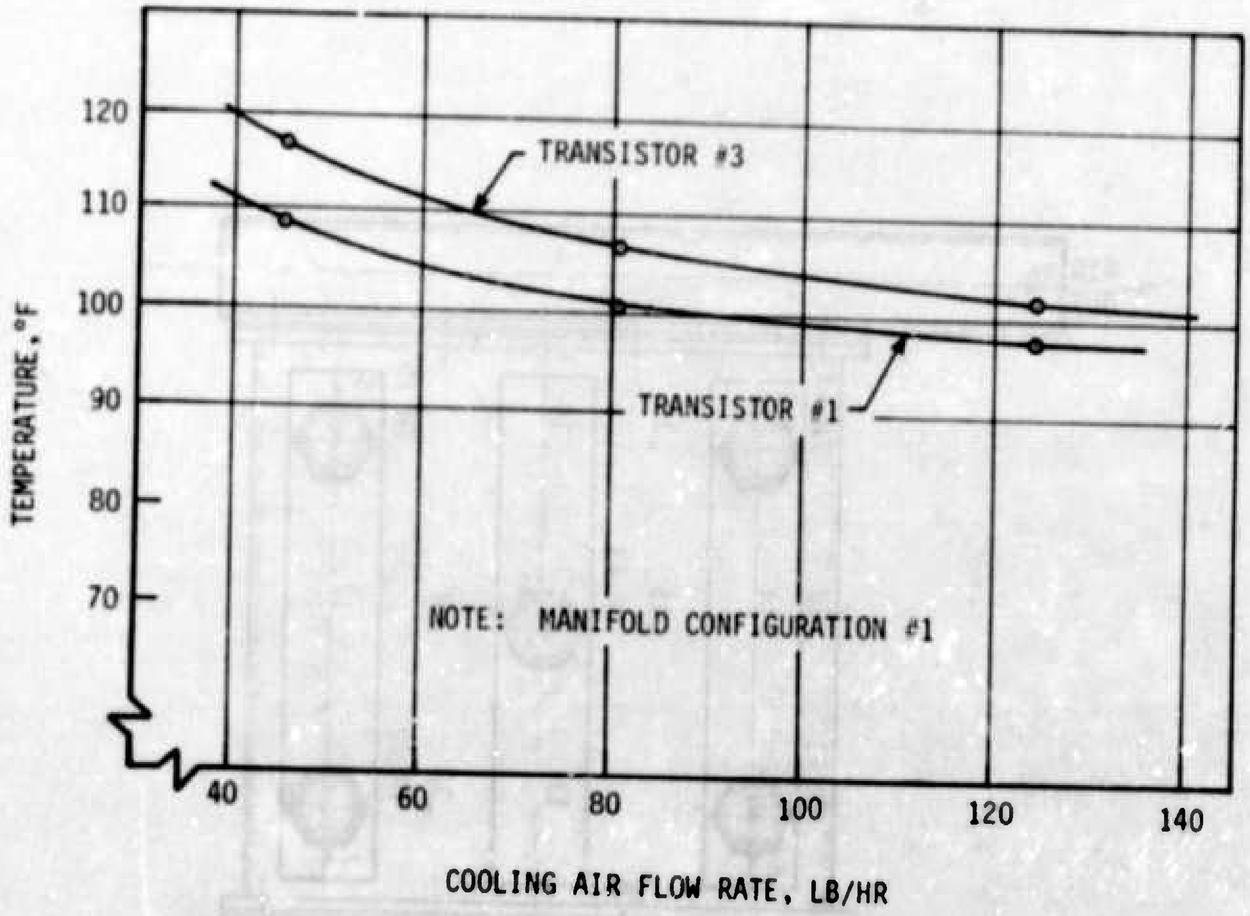

Figure 161. Case Temperature of Transistors vs Cooling Air Flow Rate for Cold Plate No. 6 (Manifold #1)

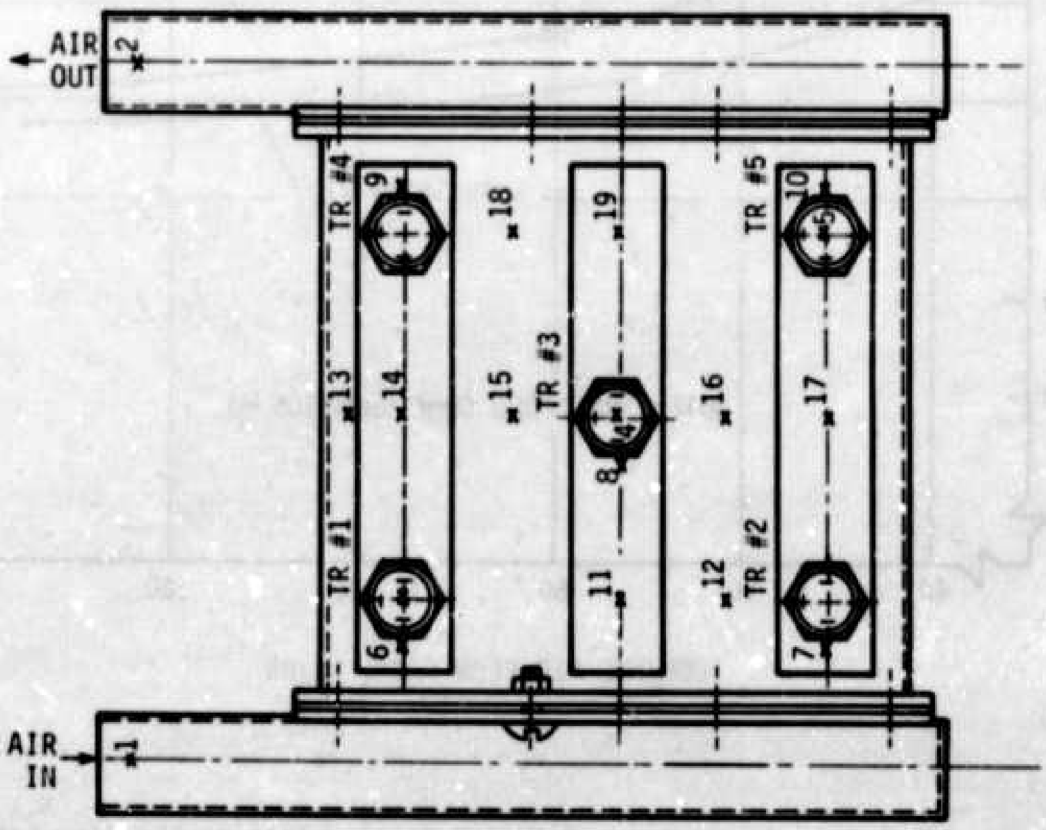

Figure 162. Air-Cooled Cold Plate No. 6 with Manifold Configuration #4

Figure 163 shows temperature distribution across the central section of the cold plate perpendicular to the cooling air flow stream. As can be seen from the figure, quite a symmetrical temperature distribution across the cold plate was achieved with this manifold configuration even though no special means for improving flow distribution were employed.

Figure 164 shows temperature distribution across the cold plate at the cooling-air entrance end, while Figure 165 shows temperature distribution along the cooling-air flow stream at the thermocouple locations indicated. From Figure 164, it can be concluded that the cooling-air flow distribution was quite uniform.

Because of the improper extended surface attachment techniques used, the experimentally determined Nusselt numbers cannot be considered as valid and, therefore, are not presented.

3. Thermal Performance Comparison of Air-Cooled Cold Plates

Because of the many possible configurations and manifold arrangements of the air-cooled cold plates, it is of interest and importance to the thermal designer to acquire knowledge about the different parameters affecting heat transfer and flow distribution of electronic-equipment cold plates. Thermal performance characteristics of all the cold plates with the different manifold configurations, therefore, are compared and the parameters affecting heat transfer and flow distribution are discussed. Since two general types of cold plates were tested (with and without finned surfaces), each of the two types is discussed. Comparisons are based on both heat transfer and the cooling-air flow distribution.

First, comparison is made among the cold plates without extended surfaces.

Figure 166 shows experimentally determined convection heat-transfer coefficients, Btu/hr ft^{2}°F, as a function of Reynolds numbers of Cold Plate Nos. 1, 2 and 3. It can be seen that Cold Plate No. 1 had the highest heat-transfer coefficient, and Cold Plate No. 2 had the lowest. Both of the cold plates had equipment mounting surfaces of exactly the same size and similar transistor arrangements. The only difference was in the width of the cooling-air flow channel. Results of the comparison confirm the phenomena discussed in Section V: high Reynolds numbers do not necessarily provide high heat-transfer coefficients; the hydraulic diameters must be small. The figure also reveals that a difference in the heat-transfer coefficients increased with increased Reynolds numbers.

Comparison with Cold Plate No. 3 is difficult because of the different transistor mounting arrangement.

The test results that are presented were obtained with manifold configuration #1.

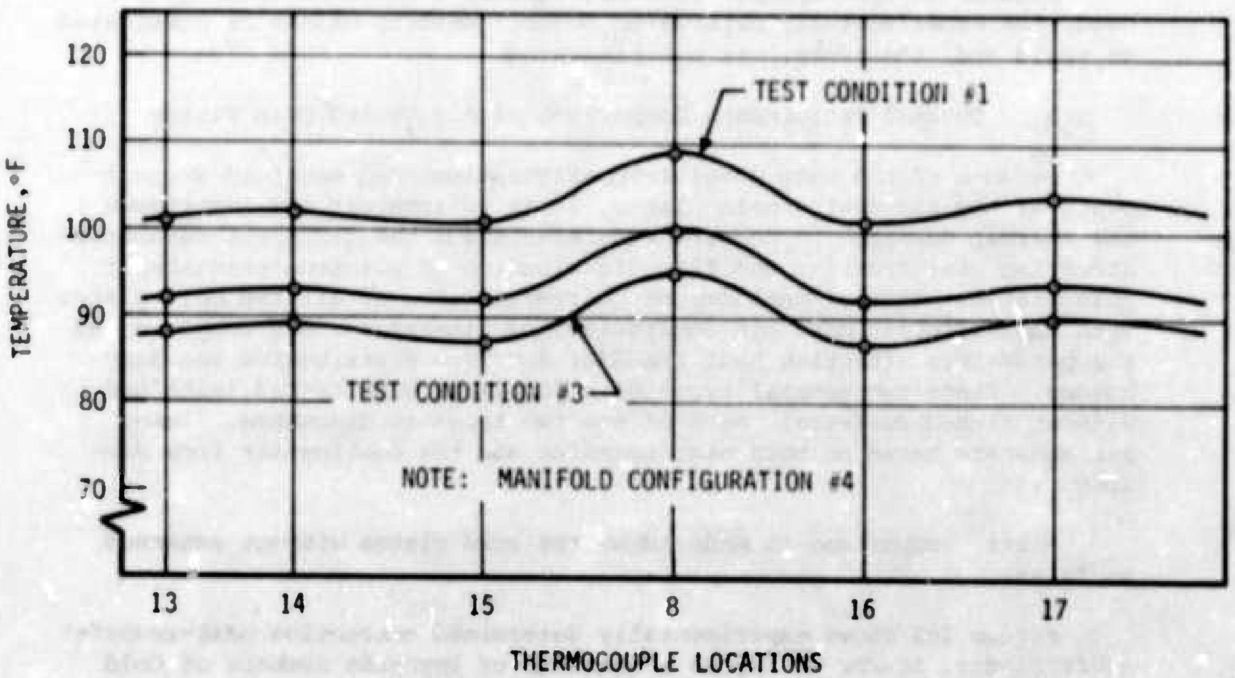

Figure 163. Temperature Distribution of Air-Cooled Cold Plate No. 6 (Manifold #4) at Test Condition Nos. 1 thru 3 (TC 13-17)

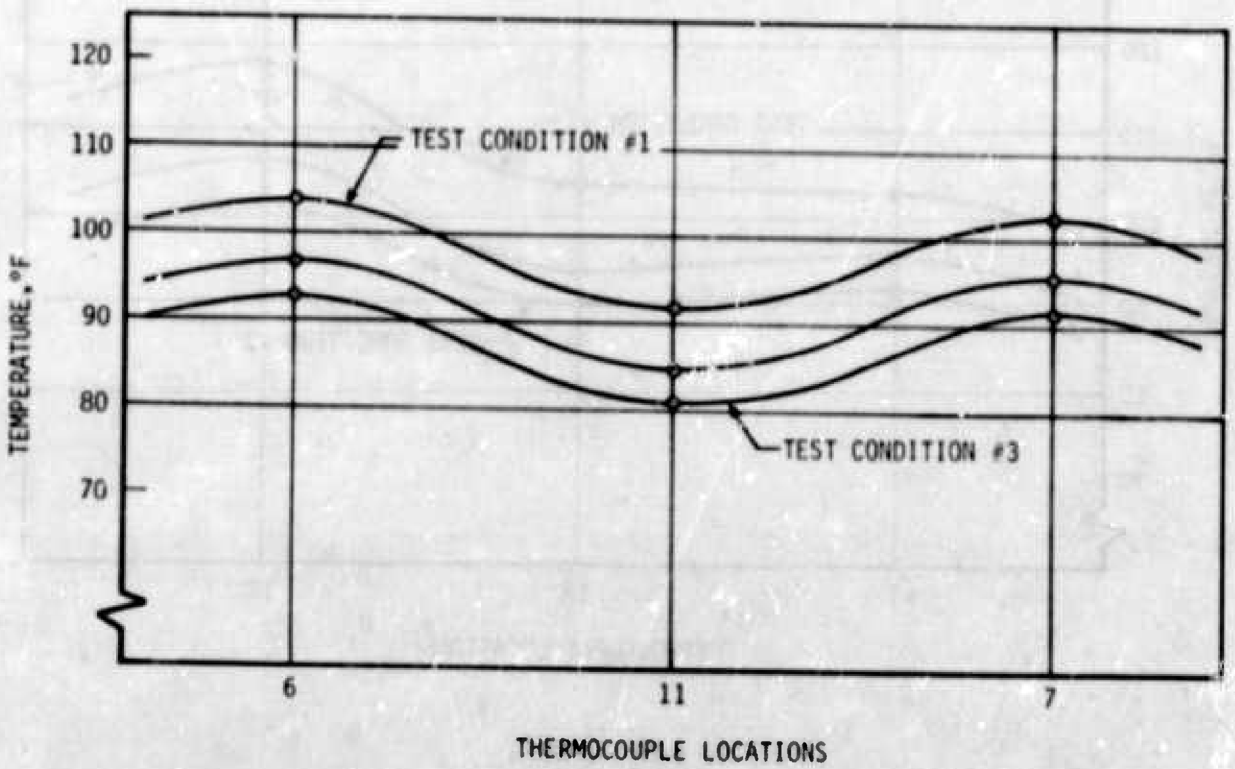

Figure 164. Temperature Distribution of Air-Cooled Cold Plate No.6 (Manifold #4) at Test Condition Nos. 1 thru 3 (TC 6-11)

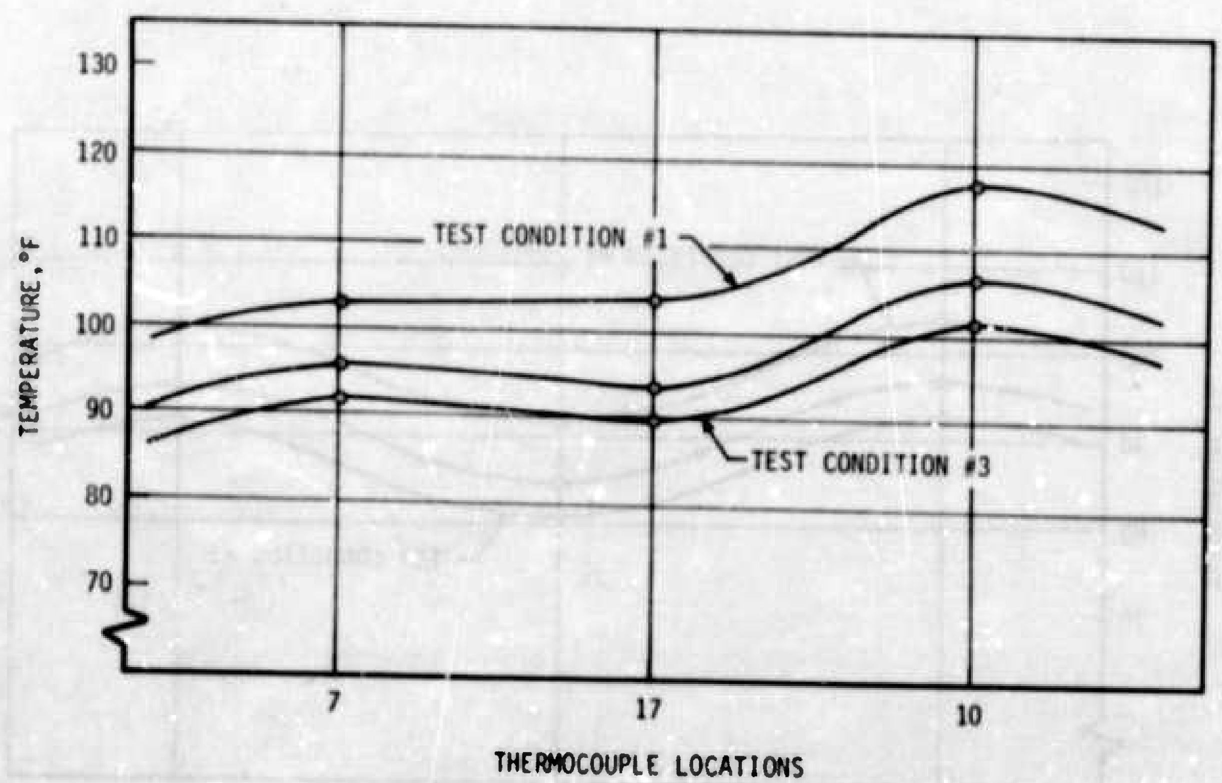

Figure 165. Temperature Distribution of Cold Plate No. 6 (Manifold #4) at Test Condition Nos. 1 thru 3 (TC 7-17)

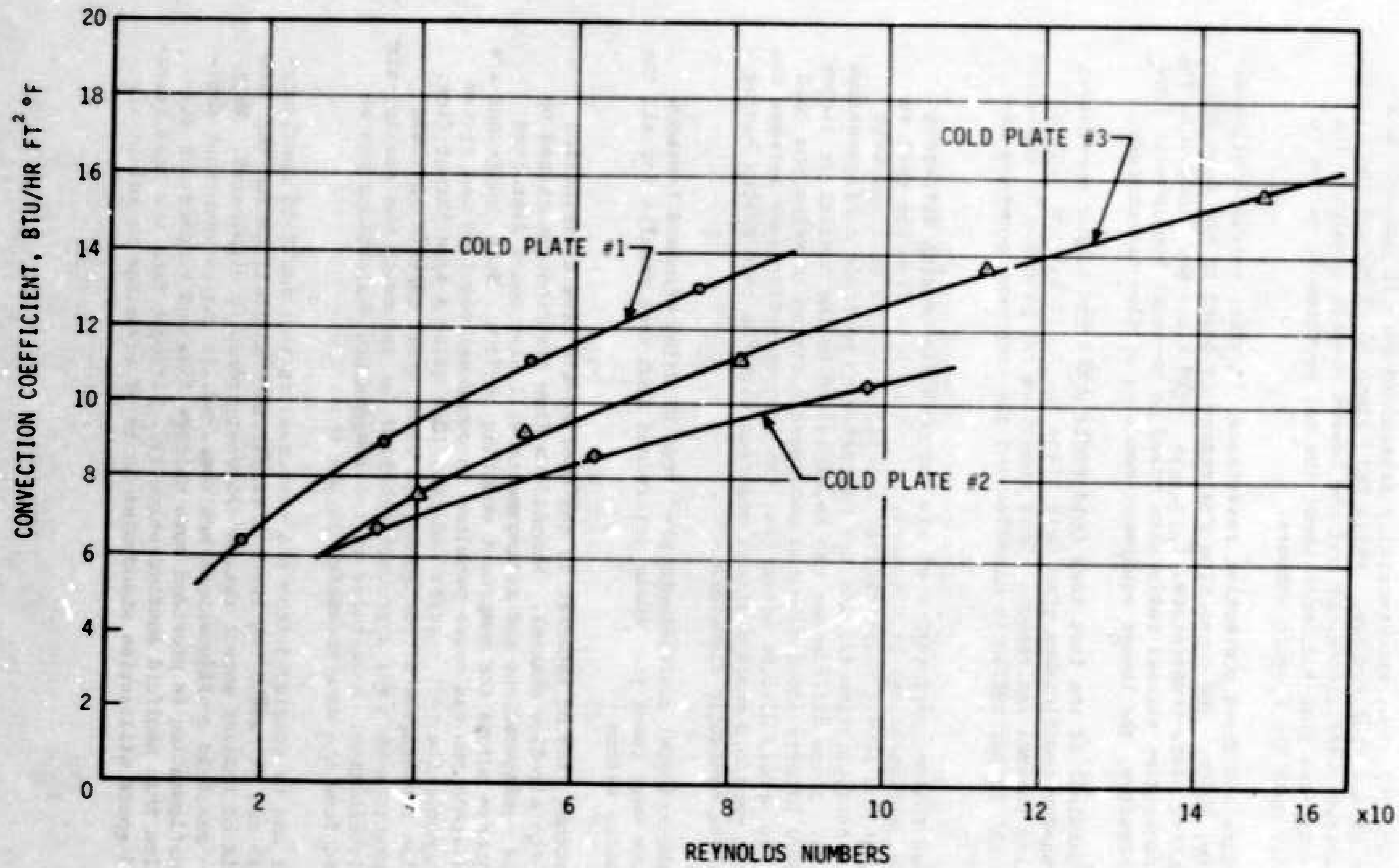

Figure 166. Experimentally Determined Convection Heat-Transfer Coefficients vs Reynolds Numbers (Comparison Among Cold Plates Nos. 1 thru 3)

Figure 167 shows experimentally determined Nusselt numbers as a function of Reynolds numbers. While Cold Plate No. 1 showed the highest heat-transfer coefficients, it had the lowest Nusselt numbers. The figure indicates that judgement about thermal performance cannot be based only upon the Nusselt numbers.

Figure 168 shows convection resistance, °C/watt, versus cooling-air flow rate, lb/hr. The convection resistance is based on the mean maximum mounting plate temperature, $\bar{t}_{pl(max)}$. Cold Plate No. 1 provided the lowest convection thermal resistance based on an equal cooling-air flow rate, therefore, the lowest equipment-mounting surface temperature.

Regardless of the fact that Cold Plate No. 3 had higher convection heat-transfer coefficients than Cold Plate No. 2, it had the highest convection thermal resistance. This condition can probably be explained by both the larger hydraulic diameter and the component mounting arrangement.

When thermal performance of similar cold plates with different manifold configurations is compared, it can be seen from the test results that the lowest heat-transfer coefficients were obtained with manifold configuration #2, and the highest with manifold configurations #3 and #4. These differences can be explained by the smaller or larger turbulence effects induced to the cooling-air stream entering the cold plate. It should also be noted that the largest differences between the different manifold configurations occurred with the cold plates having the largest hydraulic diameters.

Heat-transfer coefficients predicted by using standard textbook equations were lower than those determined from test results for all the cold plates tested.

Another item of interest is the cooling-air flow distribution within the air-flow channel. Nonuniform flow distribution caused by manifold configurations and arrangements will also cause distorted temperatures across the component mounting surface. Such conditions are not desirable and can cause problems in component mounting and system performance. The test results indicate that quite a significant flow, thus also temperature distortions, can occur under certain manifold configurations when means are not provided for improving the cooling-air flow distribution. Magnitudes of the temperature distortions can be obtained from the data presented in the text.

It can be concluded from the test results that manifold configurations #3 and #4 caused the largest temperature distortions for the flow channels of smaller aspect ratios (largest hydraulic diameters). When the two manifold configurations are compared, it can be seen that manifold configuration #4 provided more uniform flow and temperature distribution than manifold configuration #3. Although from the heat transfer and space utilization standpoint it is of advantage to select the

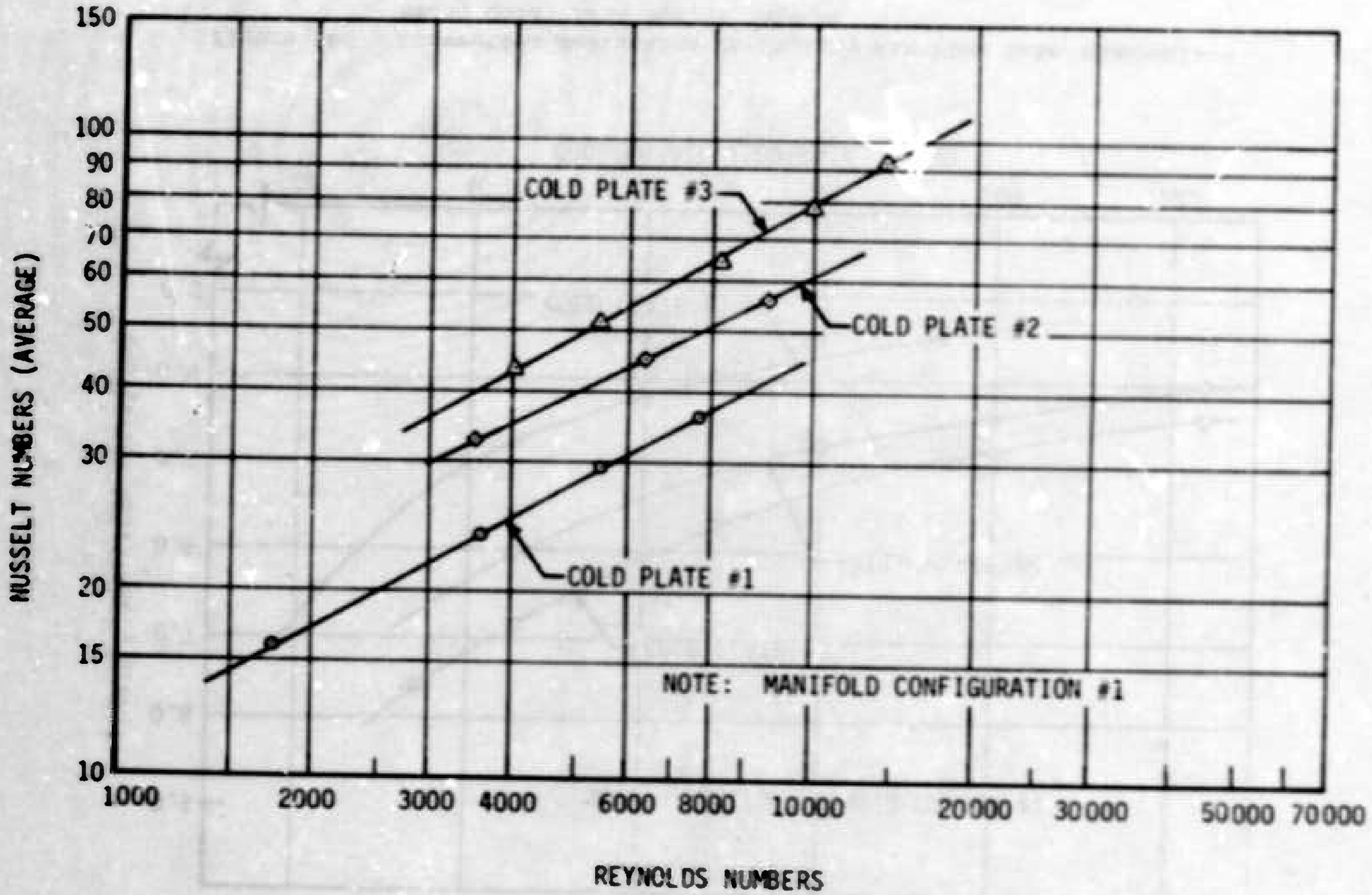

Figure 167. Experimentally Determined Nusselt Numbers vs Reynolds Numbers (Comparison Among Cold Plate Nos. 1 thru 3)

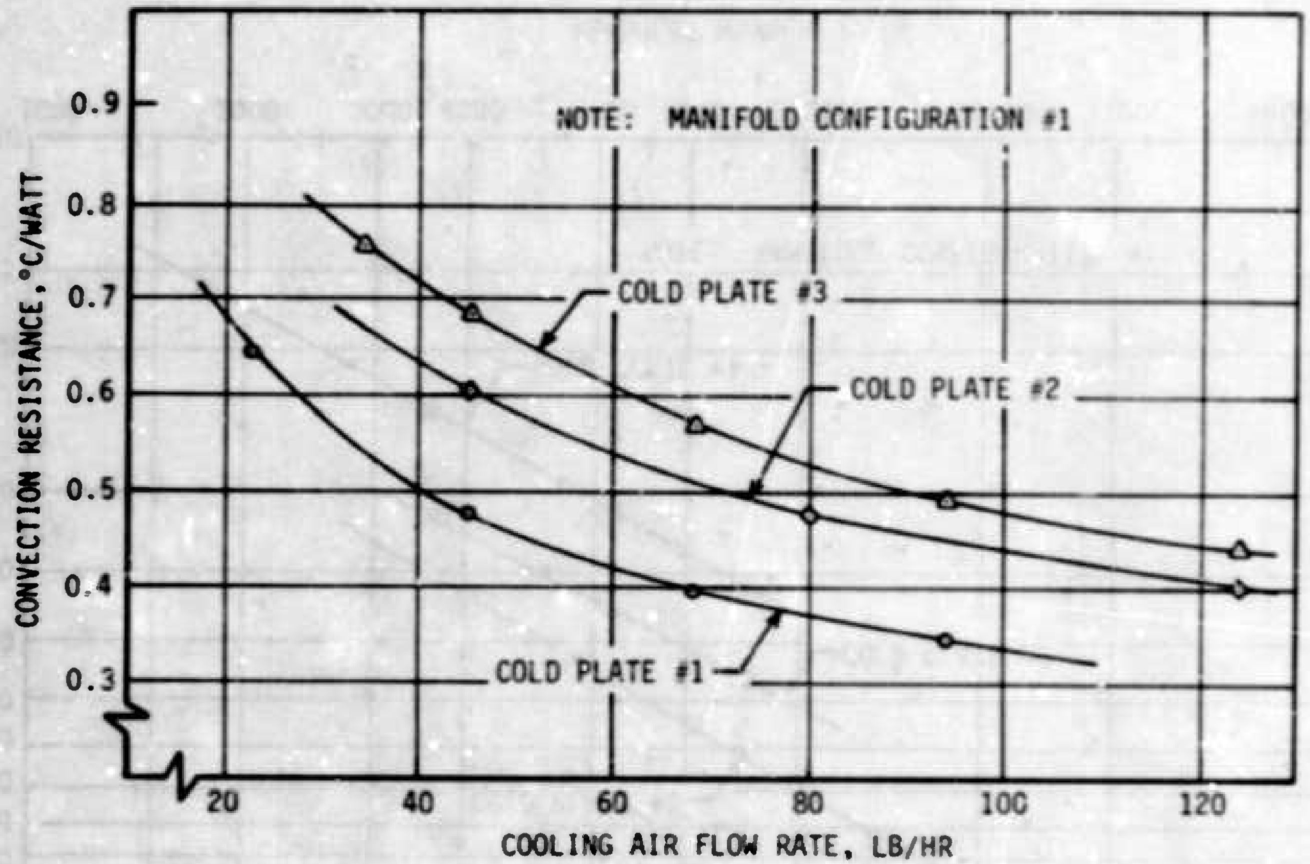

Figure 168. Convection Resistance vs Cooling Air Flow Rate (Comparison Among Cold Plate Nos. 1 thru 3)

above manifold configurations, pressure drop and flow distribution problems must be taken into consideration when cold plates are designed. Pressure drop is significantly increased when tapered slots are used for improving cooling-air flow distribution.

Thermal performance comparison among the cold plates provided with finned surfaces cannot be made because of the different manufacturing techniques used for attaching the heat-exchanger cores to the equipment mounting surfaces. Important conclusions, however, can be drawn from the different cold plates and manifold configurations as far as flow and temperature distributions are concerned. While flow distribution of cold plates without finned surfaces was significantly affected by manifold configurations #3 and #4, the flow distribution of cold plates provided with finned surfaces was not, although the cooling-air flow channels of some of the cold plates were similar. It can be concluded that cross flow within the channel contributes to the nonuniform flow distribution. This conclusion is supported by comparing the temperature distribution of the finned cold plates. Cold Plate No. 4, having the largest aspect ratio, showed the largest temperature distortion. This condition can be explained by the strip-fin heat-exchanger core which allowed some cross flow. Because of the uninterrupted fins of Cold Plate Nos. 5 and 6, no cross flow was possible within the flow channels of these cold plates.

Although it is obvious that cold plates provided with finned surfaces have much higher cooling effectiveness, the thermal performance of Cold Plate Nos. 1 and 5 (having similar air-flow channels) is compared for the convenience of the reader.

Figure 169 shows the comparison (between Cold Plate Nos. 1 and 5) of experimentally-determined, forced-convection heat-transfer coefficients and Reynolds numbers. The figure clearly shows the significant difference in the heat-transfer coefficients.

Figure 170 shows the comparison of convection resistances and cooling-air flow rate among the four cold plates. A significant reduction in convection heat-transfer resistance can be achieved by extending the heat transfer surface area by the application of fins.

Figure 171 shows the comparison among the three cold plates of Transistor #3 case temperature and the cooling-air flow rate. The location on the cold plate and the mounting of Transistor #3 was the same for all the cold plates. The figure clearly shows the advantage in temperature reduction of components when extended surfaces are used. It should be noted that Cold Plate Nos. 1 and 2 experienced more significant temperature changes with cooling-air flow rate changes than Cold Plate No. 5. Cold plates without finned surfaces experienced larger temperature variations than cold plates with finned surfaces in all the tests performed.

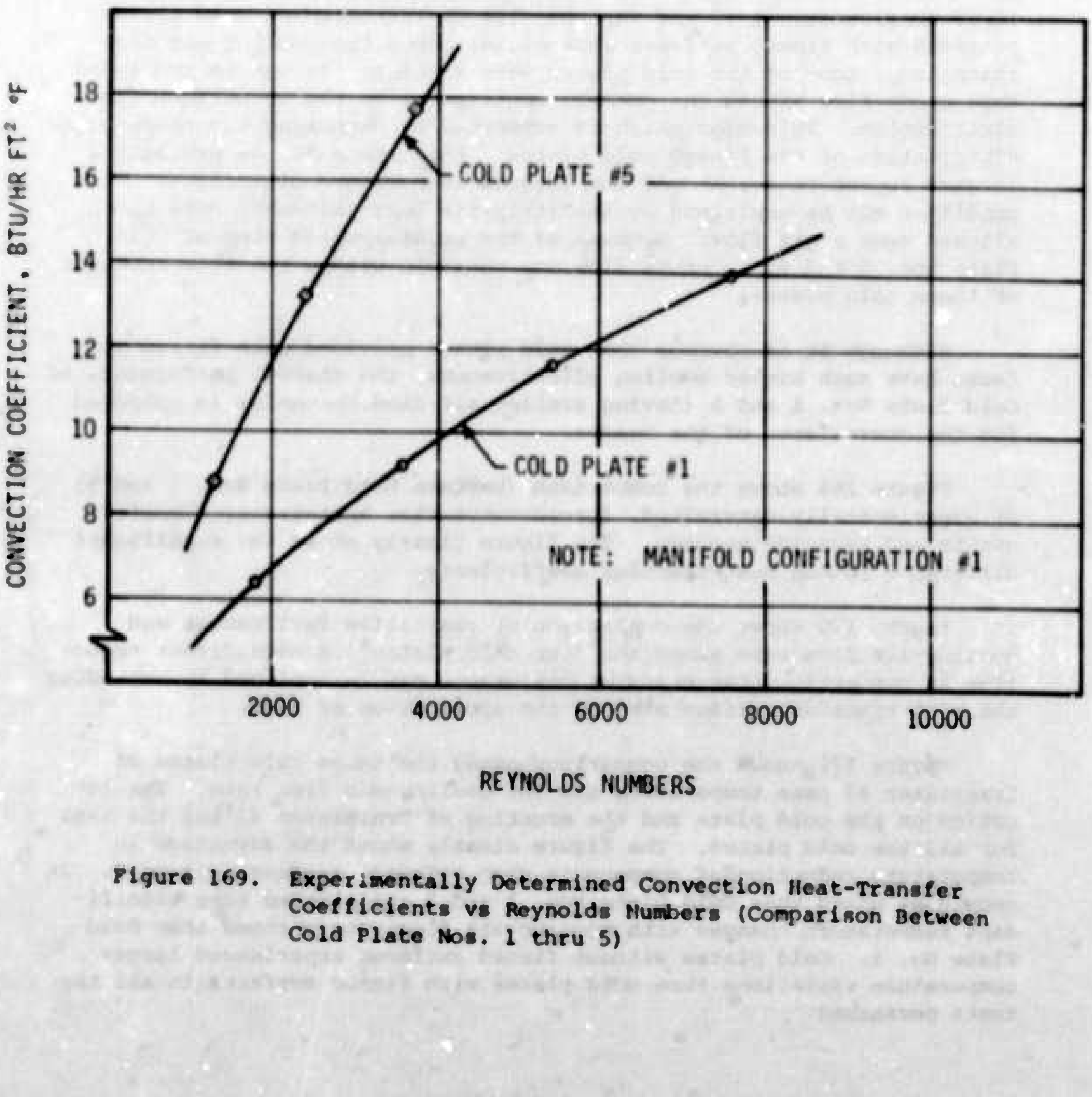

Figure 169. Experimentally Determined Convection Heat-Transfer Coefficients vs Reynolds Numbers (Comparison Between Cold Plate Nos. 1 thru 5)

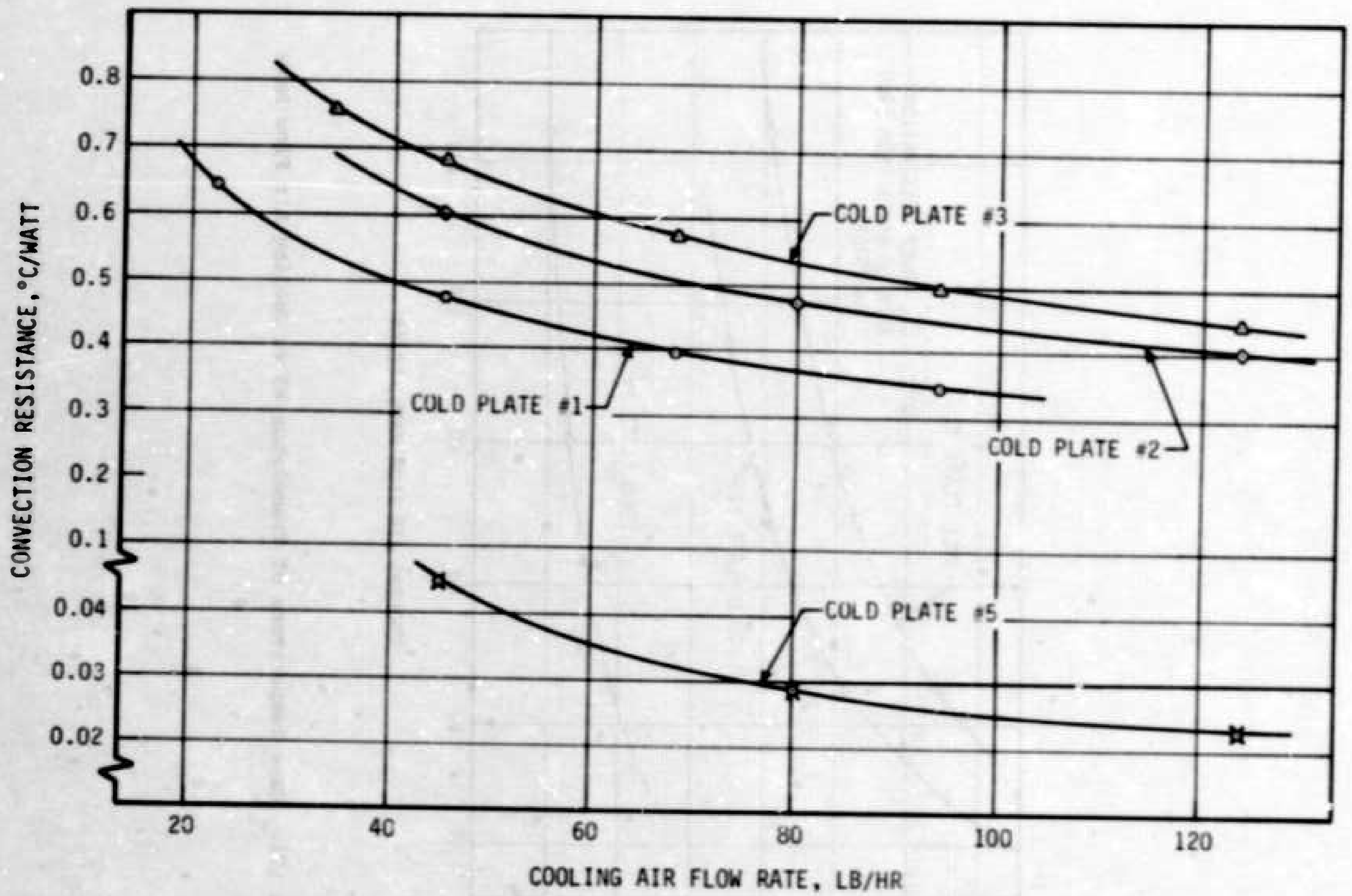

Figure 170. Convection Resistance vs Cooling Air Flow Rate (Comparison Among Cold Plate Nos. 1, 2, 3, and 5)

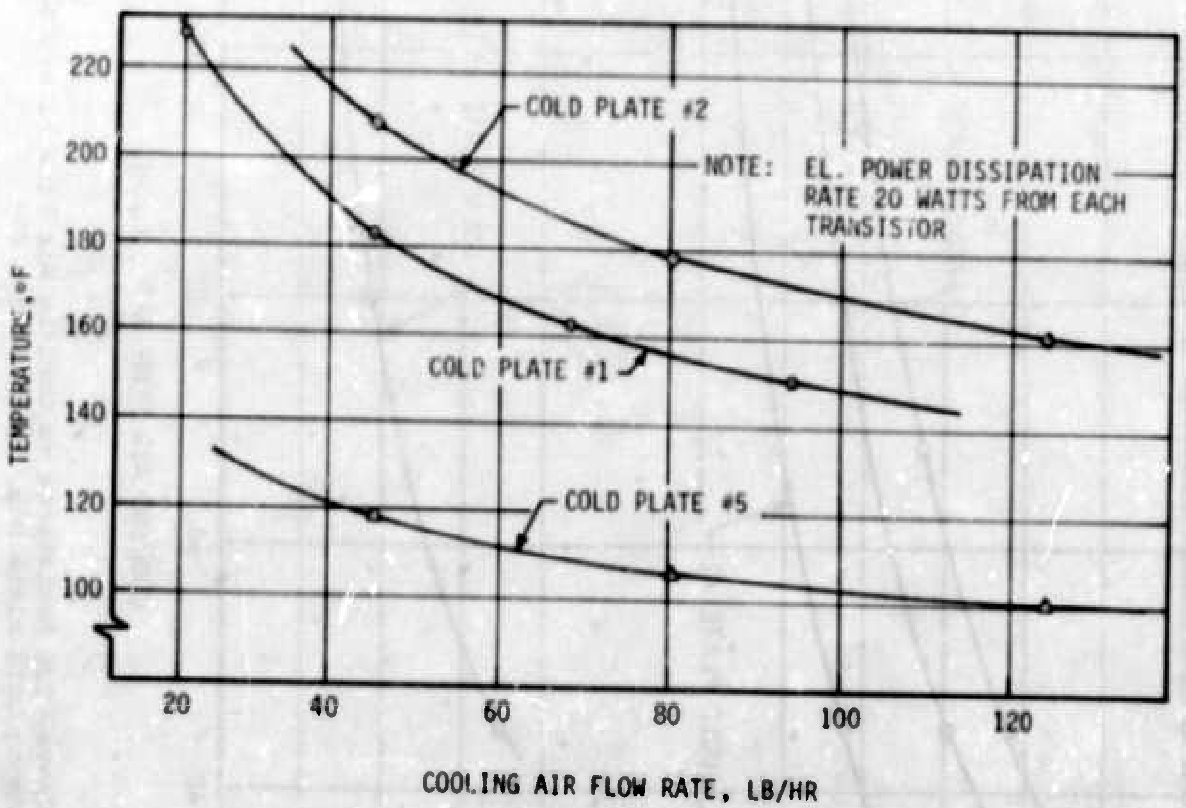

Figure 171. Case Temperature of Transistor #3 vs Cooling Air Flow Rate

4. Sample Calculations of Air-Cooled Cold Plates

Simplified manual calculations for predicting temperature of the equipment mounting surface will be performed on cold plates with and without finned surfaces. Such calculations will be always required during preliminary design of the cooling equipment. Only one cold plate of each of the two types will be selected.

(1) Cold Plates Without Finned Surfaces

As Cold Plate No. 1 showed the best thermal performance characteristics among the simple cold plates tested, a simplified manual thermal performance prediction procedure will be outlined for this cold plate. The thermal performance predictions will be based on some specific test conditions when electrical power dissipation rate from the components, coolant flow rate and inlet temperature are known.

It is assumed in this sample calculation that a waste heat load of 100 watts (340 Btu/hr) must be dissipated by the cold plate. The cooling-air flow rate may be specified in lb/hr, or a certain maximum flow velocity may also be given. High cooling-air flow velocities enhance heat transfer, but cause acoustical noise and pressure drop problems. An air flow velocity of $U = 15$ ft/sec and inlet temperature of 75°F was selected in this example.

Cooling air volume and mass flow rates, and mean temperature may be determined as follows:

$$V = AU = 0.01085\ (54000) = 586\ \text{ft}^3/\text{hr}$$

Mass flow rate of the cooling-air based on a mean temperature of 80°F

$$w = V\rho = 586\ (0.0734) = 43\ \text{lb/hr}$$

A mass flow rate of $\dot{w} = 45$ lb/hr was selected because such a flow rate was used in some of the tests.

The cooling-air outlet temperature can be determined from the following expression:

$$Q = wc_p \left(t_{out} - t_{in}\right)$$

and

$$t_{out} = t_{in} + \frac{Q}{wc_p} = 75 + \frac{340}{45(0.24)}$$

$$t_{out} = 106.5°F$$

The mean air temperature is

$$\bar{t}_{fl} = \frac{75 + 106.5}{2} = 90.75°F$$

and

$$\bar{t}_{fl} = 91°F$$

The recalculated volume flow rate of the air is

$$V = \frac{\dot{w}}{\rho} = \frac{45}{0.072} = 625 \text{ ft}^3/\text{hr}$$

The flow velocity is

$$U = \frac{V}{A} = \frac{625}{0.01085} = 57{,}600 \text{ ft/hr}$$

or

$$U = 57600/3600 = 16 \text{ ft/sec}$$

This flow velocity will not cause any acoustical noise problems.

The Reynolds number is

$$Re = \frac{D_h U \rho}{\mu}$$

and

$$Re = \frac{0.04\ (57600)\ (0.072)}{0.0455} = 3645$$

The cooling-air flow regime can be considered as turbulent.

To determine the temperature of the equipment mounting surface, the convection heat-transfer coefficient must be known. Based on conclusions obtained from the experimental work, this is not an easy task. First, the heat-transfer coefficient is not constant along the periphery of the cold plate, and second, the standard textbook equations do not provide realistic values. To show effects of convection heat-transfer coefficients upon predicted cold-plate temperature, the sample calculations are performed by using first a predicted, then, an actual heat-transfer coefficient. Since the Reynolds number indicates turbulent flow, the heat-transfer coefficient is determined from the equation recommended by McAdams.

$$Nu = 0.023\ (Re)^{0.8}\ (Pr)^{0.4} = 0.023\ (3645)^{0.8}\ (0.7)^{0.4}$$

and

$$Nu = 14$$

$$Nu = h \frac{D_h}{k} \qquad h = Nu \frac{k}{D_h} = 14 \frac{0.0155}{0.04} = 5.4 \text{ Btu/hr ft}^2\ {}^\circ F$$

This value will be used for both the equipment mounting and cover surfaces of the cold plate. As the cold plate consists of surfaces having different material thicknesses, these surfaces will also have different effectiveness factors. The total heat transfer from the cold plate, therefore, must be divided into two parts: (1) heat transferred from the base or equipment mounting surface and (2) heat transferred from the cover plate.

$$Q = Q_b + Q_c$$

Two general approaches can be used in predicting heat transfer from the base or equipment mounting plate: (1) it can be assumed that $\eta_b = 1$ and the mean temperature of the mounting plate can be used in the heat-transfer calculations.

$$Q_b = A_b h_b \left(\bar{t}_b - \bar{t}_{fl}\right)$$

where $\bar{t}_b$ = the mean temperature of the mounting plate, °F

$\bar{t}_{fl}$ = the mean temperature of the cooling air, °F.

(2) When $\eta_b \neq 1$, then

$$Q_b = \eta_b A_b h_b \left(\bar{t}_{b(max)} - \bar{t}_{fl}\right)$$

where $t_{b(max)}$ = the mean maximum temperature of the mounting plate, °F.

The heat transferred from the cover plate, applying the definition of fin effectiveness, is

$$Q_c = \eta_c A_c h_c \left(\bar{t}_b - \bar{t}_{fl}\right)$$

Assumption is made here that the edge of the cover plate has a temperature equal to $\bar{t}_b$. A small error will be introduced by this assumption which can be neglected. It should be further pointed out that the predicted temperature of the equipment mounting plate will be higher and

that of the cover plate lower when an average heat-transfer coefficient is used. This condition has been discussed under test conditions. The sample calculations, therefore, are based on the assumption that $\eta_b = 1$.

Assuming that $h_b = h_c = h_o$, we can express the heat dissipated from the cold plate as follows:

$$Q = A_b h_o \left(\bar{t}_b - \bar{t}_{fl}\right) + \eta_c A_c h_o \left(\bar{t}_b - \bar{t}_{fl}\right)$$

or

$$Q = h_o \left(A_b + \eta_c A_c\right) \left(\bar{t}_b - \bar{t}_{fl}\right)$$

Introducing the weighted overall surface effectiveness yields

$$\eta_o A = A_b + \eta_c A_c$$

and

$$\eta_o = \frac{A_b}{A} + \eta_c \frac{A_c}{A}$$

where

$$A = A_b + A_c, \ A_b = A - A_c$$

Substituting and rearranging yields

$$\eta_o = 1 - \frac{A_c}{A} \left(1 - \eta_c\right)$$

From previous developments

$$\eta_c = \frac{\tanh\ (mL)}{mL}$$

where

$$m = \sqrt{\frac{h}{k\delta}} = \sqrt{\frac{5.4}{90(0.0026)}} = 4.8$$

$$L = 0.25 + 3.125 = 3.375 \text{ in.} = 0.281 \text{ ft}$$

$$mL = 4.8\ (0.281) = 1.35$$

$$\eta_c = \frac{\tanh\ (1.35)}{1.35} = \frac{0.874}{1.35} = 0.647$$

$$\eta_c = 0.647$$

$$\eta_o = 1 - \frac{0.281}{0.542}\ (1 - 0.647) = 0.82$$

Substituting values, we can determine that

$$\bar{t}_b = 91 + \frac{340}{(0.82)(0.542)(5.4)} = 91 + 142 = 233°F$$

When this value is compared with the actual test results where $\bar{t}_b$ was approximately 170°F, it is obvious that the computed heat-transfer coefficient is too low.

Next, temperature prediction of the cold plate is based on a heat-transfer coefficient obtained from experimental data shown in Figure 95. For a Reynolds number of Re = 3645 and manifold configuration #1, the Nusselt number of Nu = 24.5 was obtained from the figure.

$$h = Nu \frac{k}{D_h} = 24.5 \frac{0.0155}{0.04}$$

$$h = 9.5 \text{ Btu/hr ft}^2 \text{ °F}$$

$$m = \sqrt{\frac{9.5}{90(0.0026)}} = 6.37$$

$$mL = 6.37 \quad (0.281) = 1.79$$

$$\eta_c = \frac{\tanh (1.79)}{1.79} = \frac{0.946}{1.79} = 0.528$$

$$\eta_o = 1 - \frac{A_c}{A} \left(1 - \eta_c\right)$$

$$\eta_o = 1 - \frac{0.281}{0.542} \quad (1 - 0.528) = 0.755$$

$$\bar{t}_h = \bar{t}_{fl} + \frac{Q}{\eta_o A h_o} = 91 + \frac{340}{(0.755)(0.542)(9.5)} = 178°F$$

This temperature is much closer to the actual test data of 170°F. By using a mean heat-transfer coefficient, the predicted mounting plate temperature is always higher, and in this case it is the maximum temperature of the cold plate as measured at the location of transistor #3. If the concentrated heat loads are not significantly high, the outlined thermal performance prediction technique can be considered as sufficient. For heat loads causing large temperature gradients within the mounting plate, effectiveness of the base plate must also be included into the weighted overall surface effectiveness as follows:

$$\eta_o A = \eta_b A_L + \eta_c A_c$$

and

$$\eta_o = \eta_b \frac{A_b}{A} + \eta_c \frac{A_c}{A} A_b$$

Using the overall effectiveness of the cold plate, we can obtain the mean maximum temperature of the mounting plate from the following expression:

$$Q = \eta_o A h_o \left(\bar{t}_{b(max)} - \bar{t}_{fl} \right)$$

and

$$\bar{t}_{b(max)} = \bar{t}_{fl} + \frac{Q}{\eta_o A h_o}$$

Determination of the mounting plates effectiveness depends upon the distribution and magnitude of the heat loading, among other factors. Under conditions of symmetrical component mounting with an equal heat dissipation rate from the components, the mounting surface can be divided into approximately equal sections and the fin effectiveness of these sections determined.

(2) Cold Plates with Finned Surfaces

Since the fabrication of Cold Plate No. 5 was performed in accordance with the general practice used in the fabrication of heat exchangers, this cold plate was selected for the sample calculations. For comparison purposes, the same test conditions were selected as in the previous sample calculation: a waste heat load of 100 watts (340 Btu/hr) with a cooling-air flow rate of w = 45 lb/hr. A cooling-air inlet temperature of 70°F was selected because this temperature is close to the actual air temperature at Test Condition #1.

The cooling-air outlet temperature is

$$t_{out} = t_{in} + \frac{Q}{w\ C_p} = 70 + \frac{340}{45\ (0.24)} = 101.5°F$$

and the mean air temperature is

$$t_{fl} = \frac{70 + 101.5}{2} = 86°F$$

Based on this temperature, the air volume flow rate, velocity, and Reynolds number can be computed as follows:

$$V = \frac{w}{\rho} = \frac{45}{0.073} = 616.4\ ft^3/hr$$

$$U = \frac{V}{A} = \frac{616.4}{0.0075} = 82185\ ft/hr$$

or

$$U = 82185/3600 = 22.8\ ft/sec$$

$$Re = \frac{D_h\ U\ \rho}{\mu}$$

$$D_h = 0.0101\ ft$$

$$Re = \frac{0.0101\ (82185)\ (0.073)}{0.045} = 1346$$

The Reynolds number indicates a laminar flow regime, and prediction of the Nusselt number must be based on this flow regime. Sieder and Tate have proposed the following correlation:

$$Nu = h \frac{D_h}{k} = 1.86 \left(Re \cdot Pr \cdot \frac{D_h}{L} \right)^{1/3}$$

Substituting values, we obtain

$$Nu = 1.86 \left[(1346)(0.7) \quad \frac{0.0101}{0.5} \right]^{1/3} = 4.96 = 5$$

and

$$h = Nu \frac{k}{D_h} = 5 \frac{0.0154}{0.0101} = 7.6 \text{ Btu/hr ft}^2 \text{ °F}$$

The actual Nusselt number, as determined from the experimental data with manifold configuration #1, was

$$Nu = 5.8$$

and

$$h = 5.8 \frac{0.0154}{0.0101} = 8.8 \text{ Btu/hr ft}^2 \text{ °F}$$

Prediction of the cold plate temperature, therefore, is based on the convection heat transfer coefficient of 8.8 Btu/hr ft^2°F.

From the test results obtained, it can be seen that no significant temperature gradients occurred within the equipment mounting surface at the particular heat load. The mean temperature of the mounting surface, therefore, will provide sufficiently accurate data for predicting component temperatures.

For a given heat load, mean temperature of the cooling-air stream, heat-transfer surface area, and known convection heat-transfer coefficient, the average temperature of the equipment mounting surface can be determined from the following simple expression:

$$Q = Ah \left(\bar{t}_{pl} - \bar{t}_{fl} \right)$$

and

$$\bar{t}_{pl} = \bar{t}_{fl} + \frac{Q}{Ah}$$

The total heat transfer surface area was determined to be $A = 1.55\ ft^2$. Substituting values yields

$$\bar{t}_{pl} = 86 + \frac{340}{1.55\ (8.8)} = 86 + 25 = 111°F$$

The average temperature of the cold plate, as determined from Test Condition #1 temperature measurements, was 108°F. The results are in excellent agreement, showing that for symmetrical and moderate heat loads, the simplified thermal performance prediction technique can provide sufficiently accurate data. However, with highly concentrated heat loads and unsymmetrical heat loads, an overall fin-effectiveness factor must be introduced as outlined in the previous example and also in Section VII.

$$Q = \eta_o\ A\ h_o \left(\bar{t}_{pl(max)} - \bar{t}_{fl} \right)$$

and

$$\bar{t}_{pl(max)} = \bar{t}_{fl} + \frac{Q}{\eta_o\ A\ h_o}$$

For more complex geometrics of the cold plates and highly-concentrated, unsymmetrical heat loads, computer analysis must be employed when more accurate results are required.

The presented sample calculations can be used when the cold plate configuration and the equipment arrangement are known. Under conditions when only the heat load, cooling-air flow rate, and/or velocity, and inlet temperature are given, the cold plate must be designed to satisfy the electronic-equipment thermal requirements. These requirements may include maximum allowable junction or case temperatures and temperature uniformity. Design of the cold plate(s) in such a case will be more or less a "cut and try" procedure.

Space limitations and packaging density, usually encountered in avionics equipment thermal design, will probably always require finned heat-transfer surfaces. Compact heat-exchanger surfaces (fins or cores) of different configurations and materials are available from many sources. Selection of these surfaces should be based on both heat-transfer and pressure-drop requirements. Information pertaining to heat-transfer and flow-friction design data for these surfaces may be obtained from heat-exchanger handbooks or the published literature of manufacturers.

The preliminary thermal analysis must be started from the maximum allowable temperature of the most temperature-sensitive electronic equipment and its electrical power dissipation rate. When the maximum allowable junction temperature of the component(s) and its power dissipation rate are known, the case temperature of the component can be computed from procedures previously outlined. The interface resistance between the component mounting surface and the cold plate depends on the mounting arrangement (with or without insulating washers) and can be found in published literature, or must be determined from experiments. No accurate analytical techniques for predicting interface thermal resistance are available, particularly when insulating washers are used.

The thermal performance prediction procedure outlined so far provides the maximum temperature of the cold plate at the locations of the concentrated heat loads. If the concentrated heat loads are moderate and symmetrically arranged, the surface area of the cold plate can be computed if the convection heat-transfer coefficient is known. This will be the total heat transfer area, consisting of fin and mounting surface, or surfaces, if both sides of the cold plate are used for equipment mounting. The heat transfer surface area may be computed from the known simple expression

$$Q = \eta_o A h_o \left(\bar{t}_{pl(max)} - \bar{t}_{fl} \right)$$

from which

$$A = \frac{Q}{\eta_o h_o \left(\bar{t}_{pl(max)} - \bar{t}_{fl} \right)}$$

Several possible variables might come into consideration in selecting the proper geometry of the heat-transfer surface. For example, if limitations are imposed on the equipment-mounting surface area, longer fins will be required. Such fins, however, will have a lower efficiency factor, η, thus requiring a larger heat-transfer surface area. On the other hand, if limitations are imposed on the volume of the cold plate, a very compact heat exchanger surface (many fins per inch) must be selected. Such fin geometry will cause a larger pressure drop of the cooling air. Furthermore, heat dissipation rates from components will dictate component spacing and the selection of a certain material thickness of the mounting surface to reduce temperature gradients.

It is impossible at this time to establish standard design and thermal performance prediction techniques and procedures, unless the electronic equipment and/or systems are also standardized. Different equipment mounting arrangements, heat loads, and general thermal requirements require different cold plate configurations and design approaches. When no particular restrictions are imposed as to weight and volume requirements, it is a simple matter to design a cold plate by following the presented data and analytical procedures.

Figure 172 shows cold-plate effectiveness versus cooling-air flow rate as determined from coolant and mounting plate temperature measurements. The following equations define Q and effectiveness, ε.

$$Q = wCp \left(t_{out} - t_{in}\right) = wCp\ \varepsilon \left(t_w - t_{in}\right)$$

and

$$\varepsilon = \frac{t_{out} - t_{in}}{t_w - t_{in}}$$

where t_{out} = coolant outlet temperature, °F

t_{in} = coolant inlet temperature, °F

t_w = average temperature of mounting plate, °F.

The general trend of reduced surface effectiveness can be explained by the increased heat-transfer coefficients caused by increased coolant flow rates. When the rate of effectiveness change is compared, a significant difference can be observed between Cold Plates No. 5 and No. 6.

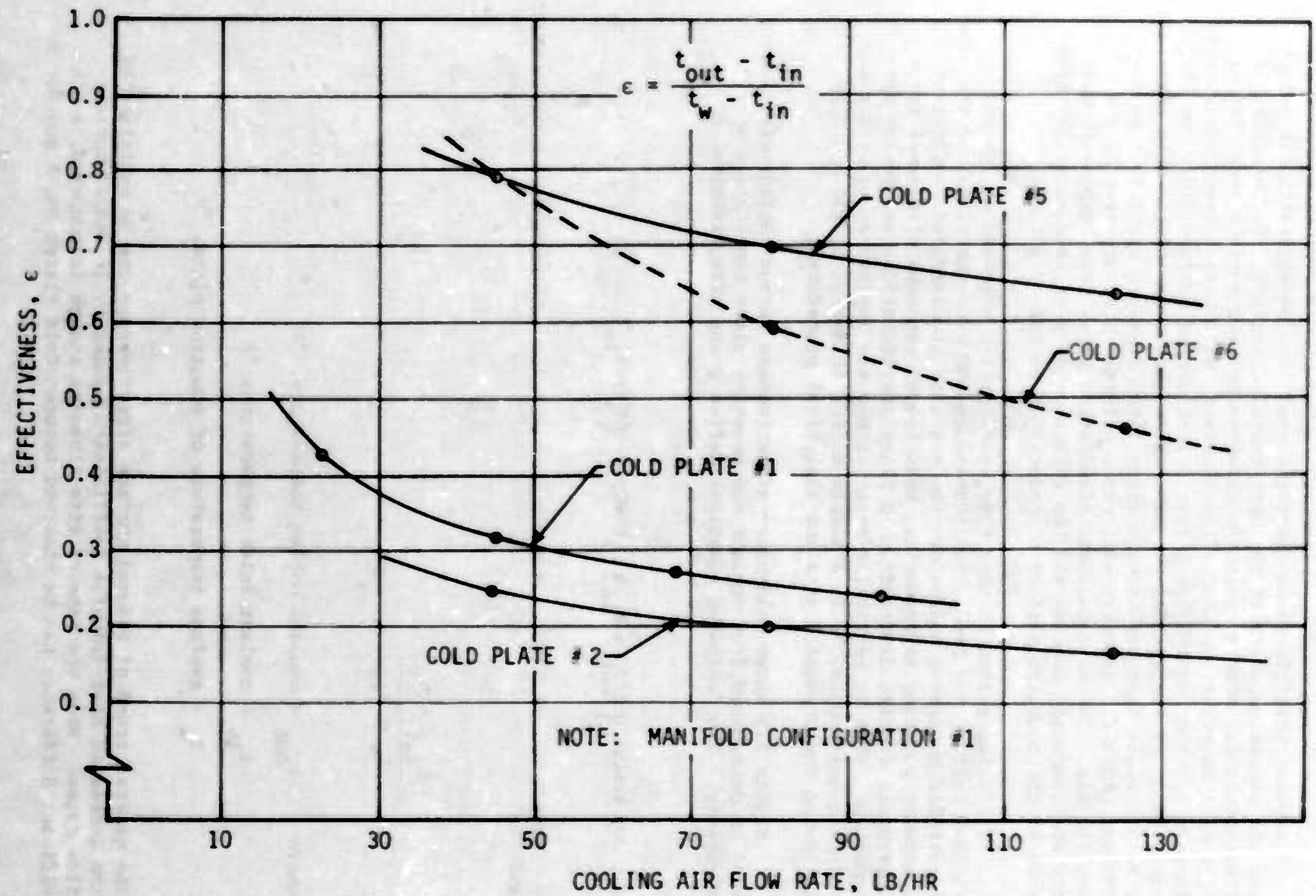

Figure 172. Cold-Plate Effectiveness vs Cooling Air Flow Rate

Since fin effectiveness is affected not only by heat-transfer coefficients, but also by fin length, Cold Plate No. 6 (with the longer fins) experienced a more significant reduction in effectiveness than Cold Plate No. 5.

(3) Sample Calculations for Determining Heat Transfer Coefficients from Experimental Data

Two sample calculations, one for a cold plate without finned surfaces (Cold Plate No. 1) and the other for a cold plate with finned surfaces (Cold Plate No. 5) are performed.

(Cold Plate No. 1)

In accordance with the Newton's law of cooling, the average heat-transfer coefficient, h, can be computed by dividing the convective heat flux by the difference between the average surface and coolant temperature.

$$Q = Ah\ (\Delta t)$$

and

$$h = \frac{Q/A}{\Delta t}$$

The calculation procedure is complicated here by the condition that the cold plate must be divided into two sections: the mounting and cover plates. The total convective heat transfer, therefore, must also be divided into two parts: heat transferred from the equipment mounting plate and heat transferred from the cover plate, or

$$Q = Q_{pl} + Q_c$$

where

$$Q_{pl} = \eta_{pl}\ A_{pl}\ h_{pl}\ \left(\bar{t}_{pl\,(max)} - \bar{t}_{fl}\right)$$

or

$$Q_{pl} = A_{pl}\, h_{pl} \left(\bar{t}_{pl} - \bar{t}_{fl}\right)$$

$$Q_c = \eta_c\, A_c\, h_c \left(\bar{t}_b - \bar{t}_{fl}\right)$$

Because of the many unknowns in the above equations, a direct solution of these equations is impossible. It is convenient in this case to determine first the heat-transfer coefficient of the cover plate (based on the temperature drop) from the following expression (Ref 26).

$$\theta_x = \theta_b \frac{\cosh\ m\ (L - x)}{\cosh\ (mL)}$$

At x = L, the central section of the plate, we find that

$$\theta_e = \frac{\theta_b}{\cosh\ (mL)}$$

where

$$m = \sqrt{\frac{h}{k\delta}}$$

$$\theta_b = \bar{t}_b - \bar{t}_{fl}$$

$$\theta_e = \bar{t}_e - \bar{t}_{fl}$$

$$\bar{t}_{fl} = \frac{t_{in} + t_{out}}{2}$$

and L = 3.125 + 0.25 = 3.375 in. = 0.281 ft.

Under Test Condition #1, obtained from Table A-4 and Figure 173,

$$\bar{t}_{f1} = \frac{72 + 133}{2} = 102.5°F$$

$$t_b = 208°F, \; t_e = 159°F$$

$$\theta_b = 208 - 102.5 = 105.5°F$$

$$\theta_e = 159 - 102.5 = 56.5°F$$

From the known temperatures, the heat-transfer coefficient of the cover plate can be computed as follows:

$$\cosh (mL) = \frac{\theta_b}{\theta_e} = \frac{105.5}{56.5} = 1.867$$

$$mL = 1.234$$

$$m = \frac{1.234}{0.281} = 4.39; \quad \sqrt{\frac{h}{90(0.0026)}} = 4.39$$

$$h = 19.28(0.234) = 4.5 \text{ Btu/hr ft}^2 °F$$

Next, the fin effectiveness of the cover plate can be computed

$$\eta_c = \frac{\tanh (mL)}{mL} = \frac{\tanh (1.235)}{1.235} = \frac{0.844}{1.235} = 0.685$$

Heat transfer rate from the cover plate is found with

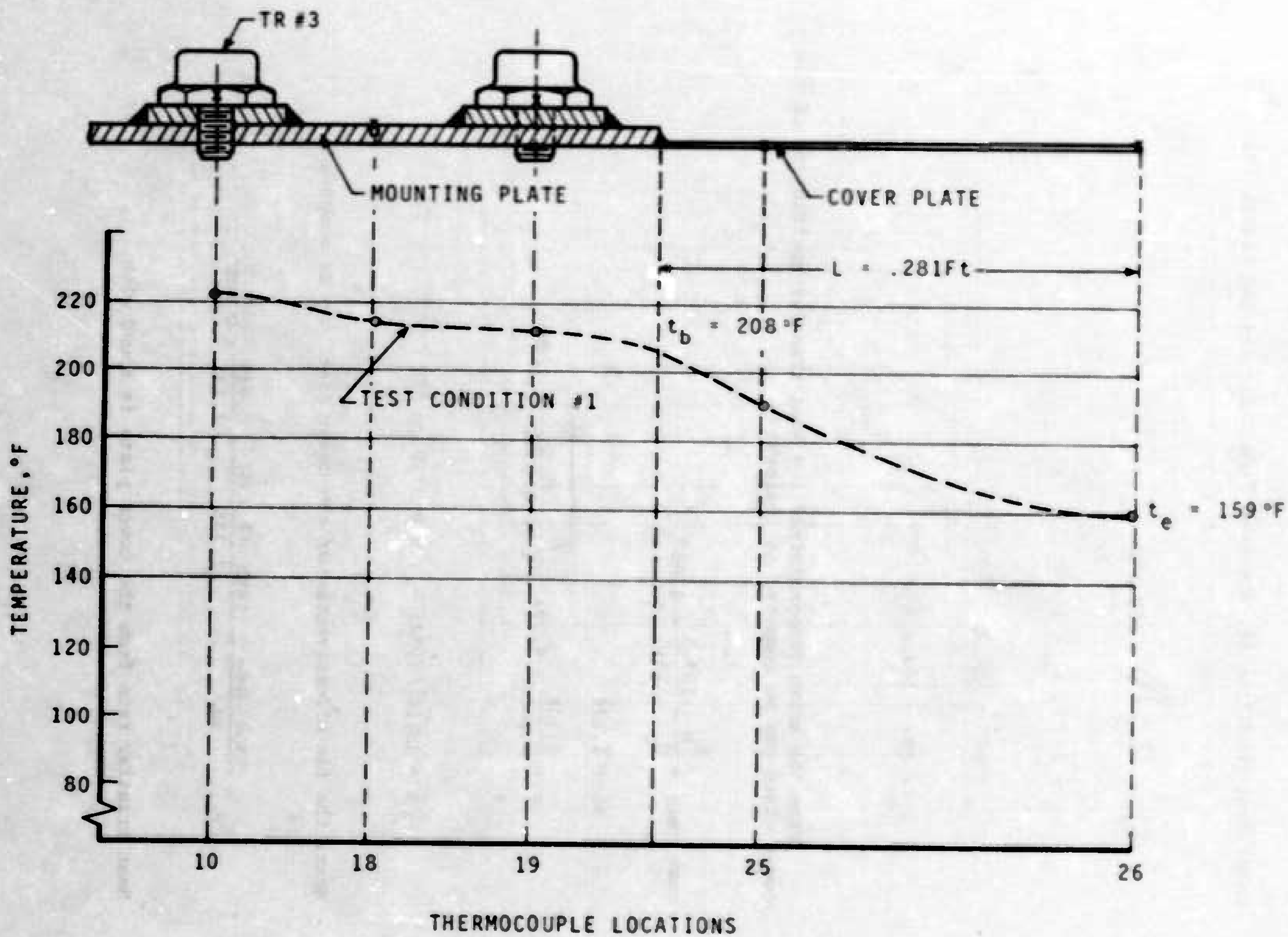

Figure 173. Temperature Distribution of Cold Plate No. 1 with Manifold Configuration #1

$$Q_c = \eta_c A_c h_c \left(t_b - \bar{t}_{f1}\right) = (0.685)(0.281)(4.5)(2.08 - 102.5)$$

$$= 91 \text{ Btu/hr}$$

Assuming a 5% heat loss to the environment, we can compute the total heat dissipated by the cold plate as follows:

$$Q = 340 - 17 = 323 \text{ Btu/hr}$$

The heat dissipated by the cover plate is

$$Q_{p1} = 323 - 91 = 232 \text{ Btu/hr}$$

From the expression $Q_{p1} = A_{p1} h_{p1} \left(\bar{t}_{p1} - \bar{t}_{f1}\right)$, we find that

$$h_{p1} = \frac{Q_{p1}}{A_{p1}\left(\bar{t}_{p1} - \bar{t}_{f1}\right)}$$

Determination of the cold plate average temperature is based on two sets of temperature readings as indicated below (see Figure 82):

$$\bar{t}_{p1} = \frac{t(8) + t(9) + t(10) + t(11) + t(12) + t(14) + t(16) + t(19) + t(21)}{9}$$

$$= \frac{215 + 216 + 222 + 220 + 220 + 209 + 210 + 212 + 211}{9}$$

$$= \frac{1935}{9} = 215°F$$

$$\bar{t}_{pl} = \frac{t(8) + t(9) + t(10) + t(11) + t(12) + t(13) + t(14) + t(15)}{15}$$

$$+ \frac{t(16) + t(17) + t(18) + t(19) + t(20) + t(21) + t(22)}{15}$$

$$= \frac{215 + 216 + 222 + 220 + 220 + 209 + 209 + 210 + 210 + 213}{15}$$

$$\frac{+ 214 + 212 + 212 + 211 + 213}{15} = \frac{3206}{15} = 213.7°F$$

Because of the small difference between the two average temperatures, only the first value, based on the nine temperature readings, is used for computing h_{pl}. If more significant temperature gradients occur within the plate, then some average temperature for each of the nine areas should be determined.

Substituting values yields

$$h_{pl} = \frac{Q_{pl}}{A_{pl}\left(\bar{t}_{pl} - \bar{t}_{fl}\right)} = \frac{232}{(0.26)(215 - 102.5)} = 7.93$$

$$h_{pl} = 8 \text{ Btu/hr ft}^{2}°F$$

From the computed heat-transfer coefficient and the maximum average temperature, $\bar{t}_{pl(max)}$, the effectiveness of the mounting plate, η_{pl}, can be determined.

$$\eta_{pl} = \frac{Q_{pl}}{A_{pl}\, h_{pl}\left(\bar{t}_{pl(max)} - \bar{t}_{fl}\right)}$$

where

where $\bar{t}_{pl(max)} = \frac{t(8) + t(9) + t(10) + t(11) + t(12)}{5}$

$$= \frac{215 + 216 + 222 + 220 + 220}{5} = \frac{1093}{5} = 218.5°F$$

and

$$\eta_{pl} = \frac{232}{(0.26)(8)(218.5 - 102.5)} = 0.962$$

For simplified computations and data presentation, it is convenient to introduce an overall heat transfer coefficient, h.

$$Q = \eta_o A_o h_o \left(\bar{t}_{pl} - \bar{t}_{fl}\right)$$

and

$$h_o = \frac{Q}{\eta_o A_o \left(\bar{t}_{pl} - \bar{t}_{fl}\right)}$$

The overall surface effectiveness, η_o, can be determined from the following expression:

$$\eta_o A_o = \eta_{pl} A_{pl} + \eta_c A_c$$

and

$$\eta_o = \eta_{pl} \frac{A_{pl}}{A_o} + \eta_c \frac{A_c}{A_o}$$

where

$$A_{pl} = 0.26 \text{ ft.}^2, \; A_c = 0.281 \text{ ft.}^2, \; A_o = 0.541 \text{ ft}^2$$

Substituting values yields

$$\eta_o = 0.962 \frac{0.26}{0.541} + 0.685 \frac{0.281}{0.541} = 0.462 + 0.356 = 0.818$$

and

$$\eta_o = 0.818$$

Therefore,

$$h_o = \frac{323}{(0.818)(0.541)(215 - 102.5)} = 6.5 \text{ Btu/hr ft}^2 \text{ °F}$$

The Nusselt number is found by

$$Nu = h \frac{D_h}{k} = 6.5 \frac{0.040}{0.0158} = 16.4$$

Similar procedures may be applied for determining the average heat-transfer coefficients and Nusselt numbers for the other test conditions.

(Cold Plate No. 5)

Since the cooling-air flow channel of this cold plate is provided with a compact heat-exchanger core, the total heat-transfer surface area must be used in the convection heat-transfer equation. With the short fins extending from the equipment mounting plate, an average heat-

transfer coefficient value can be assumed for the whole surface area. The heat-transfer coefficient, therefore, is computed from the average equipment mounting plate and cooling-air temperatures.

$$h = \frac{Q}{A\left(\bar{t}_{pl} - \bar{t}_{fl}\right)}$$

where A is the total heat transfer surface area which was determined to be 1.55 ft^2.

Under Test Condition #1 and manifold configuration #1,

$$\bar{t}_{fl} = \frac{69 + 100}{2} = 84.5°F \quad \text{and} \quad Q = 323 \text{ Btu/hr}$$

$$\bar{t}_{pl} = \frac{t(11) + t(14) + t(15) + t(16) + t(19) + t(22) + t(25) + t(26) + t(27)}{9}$$

$$= \frac{104 + 109 + 116 + 94 + 111 + 110 + 103 + 109 + 115}{9}$$

$$= \frac{971}{9} = 107.88 = 108°F$$

Substituting values yields

$$h = \frac{323}{1.55\ (108 - 84.5)} = 8.86 \text{ Btu/hr ft}^2 °F$$

The Nusselt number is found from

$$Nu = h\frac{D_h}{k} = 8.86\ \frac{0.0101}{0.0155} = 5.77$$

Introducing the overall surface effectiveness, we obtain

$$Q = \eta_o Ah \left(\bar{t}_{pl(max)} - \bar{t}_{fl} \right)$$

$$\eta_o = \frac{Q}{Ah \left(\bar{t}_{pl(max)} - \bar{t}_{fl} \right)}$$

where

$$t_{pl(max)} = \frac{t(14) + t(16) + t(11) + t(25) + t(27)}{5}$$

$$= \frac{104 + 116 + 111 + 103 + 115}{5} = \frac{549}{5} = 109.8 = 110°F$$

Substituting values yields

$$\eta_o = \frac{323}{1.55\ (8.86)(110 - 84.5)} = 0.922$$

Sample Problem - Air-Cooled Cold Plate

It is required to design an air-cooled cold plate for cooling electronic assembly consisting of 12 power transistors with power dissipation of 20 watts from each transistor. The maximum allowable junction temperature of the transistors is given as $t_j = 125°C$. Cooling air inlet temperature is 80°F, temperature rise across the cold plate is limited to $\Delta t = 20°F$, and the maximum air velocity is limited to 25 ft/sec.

All of the transistors will be mounted on one side of the cold plate using indium washers for electrical isolation. Assuming package outline as TO-66 with junction-to-case thermal resistance $R_{j-c} = 3°C/watt$. Contact resistance between the transistor flange and mounting surface of the cold plate is given in Table 3 as $R_{c-pl} = 0.16°C/watt$.

As heat dissipation rates from the individual transistors are not high, a mounting plate with thickness of $\delta = 1/8$ inch is selected. It is further assumed that width of the cold plate is not limited, and a plate-fin surface 10-27T heat exchanger core is selected. Reference 27 presents the following data for the above surface geometry:

Fin pitch - 10.27 per inch

Plate spacing, b - 0.544 inch

Hydraulic diameter, D_h = 0.01259 ft

Fin metal thickness, δ_f = 0.010 in. aluminum

Total heat transfer area/volume between plates, β = 289.93 ft^2/ft^3

Fin area/total area = 0.863

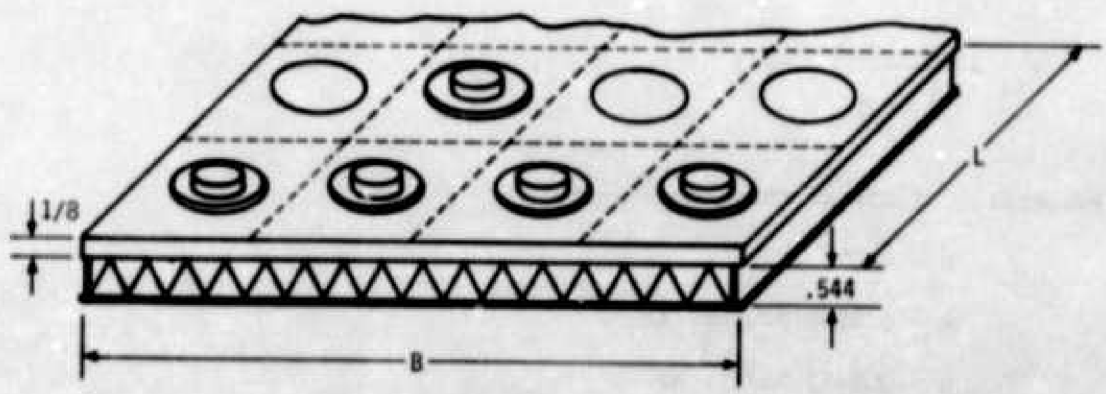

Figure 174. Section of Sample Cold Plate

The equipment mounting surface area of the cold plate must be computed to satisfy thermal requirements of the transistors.

Based on heat rejection rate and temperature rise of the cooling air, the weight flow rate of the air may be determined from the following equation

$$Q = \dot{w}C_p\ (\Delta t)$$

$$Q = 20(12)\ (3.41) = 818\ \text{Btu/hr}$$

Neglecting natural convection and radiation to the surrounding environment, all of this heat must be absorbed by the cooling air, and

$$\dot{w} = \frac{Q}{C_p(\Delta t)} = \frac{818}{.24(20)} = 170 \text{ lb/hr}$$

Outlet temperature of the air

$$t_{out} = t_{in} + 20 = 80 + 20 = 100°F$$

Mean temperature of the air

$$t_{fl} = \frac{80 + 100}{2} = 90°F$$

Properties of air at this temperature

$$\rho = 0.072 \text{ lb/ft}^2$$

$$k = 0.0155 \text{ Btu/hr. ft °F}$$

$$\mu = 0.0455 \text{ lb/ft. hr.}$$

$$Pr = 0.70$$

Volume flow rate of cooling air

$$V = \frac{w}{\rho} = \frac{170}{.072} = 2361 \text{ ft}^3\text{/hr}$$

For the given air flow velocity, the required free flow area will be

$$A = \frac{V}{U} = \frac{2361}{25(3600)} = 0.02623 \text{ ft}^2 = 3.78 \text{ in}^2$$

Width of the cold plate can be determined from the following expression:

$$A = B(.544) - B(10.27)(.544)(.010) = B(.488)$$

$$B = \frac{A}{.488} = \frac{3.78}{.488} = 7.75 \text{ in}$$

The Reynolds number

$$Re = \frac{D_h U \rho}{\mu} = \frac{.01259(25)(3600)(.072)}{.0455} = 1793$$

From Reference 27

$$(h/GC_p)(Pr)^{2/3} = 0.00495$$

$$G = \frac{\dot{w}}{A} = \frac{170}{.02623} = 6481 \text{ lb/hr. ft}^2$$

$$h/GC_p = \frac{.00445}{.788} = 0.00565$$

$$h = .00565(6481)(.24) = 8.8 \text{ Btu/hr. ft}^2 \text{ °F}$$

As geometry of the heat exchanger surface and the heat transfer coefficient are known, the overall weighted extended surface efficiency can be computed from the following expression

$$\eta_{ext} = \frac{A_f}{A_{ext}} \eta_f + \frac{A_c}{A_{ext}} \eta_c$$

$$\eta_f = \frac{\tan h\ (mb)_f}{(mb)_f}, \quad m = \sqrt{\frac{2\ (8.8)}{100(.000833)}} = 14.53$$

$$(mb)_f = 14.53 \left(\frac{.544}{12}\right) = 0.6588$$

$$\eta_f = \frac{\tan h\ (.6588)}{.6588} = 0.877$$

$$\eta_c = F_1 \ \frac{\tan h\ (mb)_c}{(mb)_c}$$

$$F_1 = \frac{1}{\cos h\ (mb)_f + \sqrt{\frac{2(.0026)}{.000833}}\ \tan h\ (.0471)\ \sin h\ (.6588)} = 0.764$$

$$\eta_c = 0.764 \ \frac{\tan h\ (.0471)}{.0471} = 0.763$$

The area ratios can be determined from the following reasoning:

Assuming a section of the cold plate having heat transfer surface area of unity. In accordance with the given data, fin area/total area = 0.863, thus $A_f = (1)(0.863) = 0.863$. As the cover and mounting plates' surface areas are equal

$$A_c = A_{pl} = \frac{1.0 - 0.863}{2} = 0.0685 \text{ ft}^2 \text{ of total area}$$

$$A_{ext} = 0.863 + 0.0685 = 0.9315 \text{ ft}^2 \text{ of total area}$$

Substituting the computed values

$$\eta_{ext} = \frac{.863}{.9315}\ (.877) + \frac{.0685}{.9315}\ (.763)$$

$$\eta_{ext} = 0.868$$

Depending upon spacing of the electronic components, the cold plate will have larger or smaller efficiency. Accurate determination of the efficiency, therefore, is not possible before size of the cold plate and equipment mounting arrangement is not known. On the other hand, size of the cold plate will also depend upon the allowable Δt between the cooling air stream and the equipment mounting plate.

For a given cooling air temperature and maximum allowable junction temperature of the transistors, Δt's within the equipment mounting surface and between coolant and cold plate must be tailored to satisfy the equipment thermal requirements.

Presenting the total thermal resistances and Δt's in graphical form

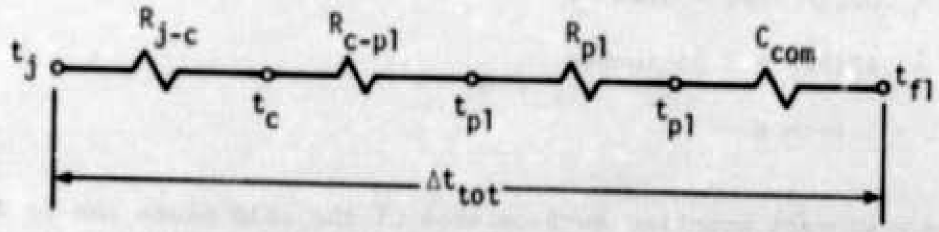

The following Δt's can already be determined

$$t_j = 125°C = \frac{9}{5}(125) + 32 = 257°F$$

$$\overline{t}_{fl} = 90°F$$

$$\Delta t_{tot} = 257 - 90 = 167°F$$

$$\Delta t_{j-c} = 20\ (3) = 60°C = \frac{9}{5}(60) = 108°F$$

$$\Delta t_{c-pl} = 20(.18) = 3.6C = \frac{9}{5}(3.6) \doteq 5.5°F$$

From the above $\Delta t_{pl} + \Delta t_{conv} = 167 - (108 + 5.5) = 52.5°F$

Because of the rather low concentrated heat loads spacing among the components and temperature gradients within the mounting surface will be small, and the largest portion of the 52.5°F temperature differential can be utilized for the convection heat transfer. Assuming first a $\Delta t_{conv} = 30°F$, and introducing efficiency of the extended surface $\eta_{ext} = 0.868$

$$A = \frac{Q}{\eta h(\Delta t)_{conv}} = \frac{818}{.868(8.8)(30)} = 3.57 \text{ ft}^2$$

Volume of the cold plate $V = A/\beta$

$$V = 3.57/289.93 = 0.0123 \text{ ft}^3$$

Length of the cold plate $L = V/A$

where $A = .544(7.75) = 4.216 \text{ in}^2 = .0293 \text{ ft}^2$

$$L = .0123/.0293 = 0.42 \text{ ft}$$

or $L = .42(12) = 5.04$ inches

Assume $L = 5$ inches.

The equipment mounting surface area of the cold plate can be divided into 12 equal sections and the transistors located on these sections. Heat, dissipated by the transistors, will spread within the sections which may be considered as radial fins. In accordance with size of the cold plate and equipment arrangement, the approximate values of the two radii were determined to be $r_o = 0.25$ in. and $r_e = 1.0$ in.

From procedures outlined in Section VIIa, the extended surface area per unit area of the mounting plate are determined to be:

$$A_{ext} = (1)(1)(.544)\left(\frac{1}{12}\right)(289.93) - 1 = 12.14 \text{ ft}^2/\text{ft}^2$$

and the effective area

$$A^{1}_{ext} = A_{ext}\, \eta_{ext} = 12.14(.924) = 11.2 \text{ ft}^2/\text{ft}^2$$

$$m = \sqrt{\frac{h A^{1}_{ext}}{k\,\delta}} = \sqrt{\frac{8.8(11.2)}{100(.0104)}} = 9.735$$

$$mr_e = 9.735 \left(\frac{1}{12}\right) = 0.8112$$

$$\rho = r_o/r_e = 0.25$$

From Figure 27 the temperature excess ratio

$$\frac{\theta_e}{\theta_o} = 0.75 = \frac{t_e - t_\infty}{t_o - t_\infty}$$

where t_∞ is the coolant temperature, °F

t_o is the temperature at radius r_o = .25 in.

t_e is the temperature at radius r_e = 1.0 in.

From the known parameter mb efficiency of the equipment mounting plate can be obtained from Figure 26.

$b = 1.0 - .25 = .75$ in $= .0625$ ft

and $mb = 9.735(.0625) = .608$

$\eta = 0.80$

Based upon this efficiency the maximum Δt between the equipment mounting plate and the cooling air can be computed

$$\Delta t = t_o - t_\infty = \frac{Q}{\eta A h} = \frac{818}{.8(3.57)(8.8)} = 32.5°F$$

$$t_o = 32.5 + 90 = 122.5°F$$

$$\frac{t_e - t_\infty}{t_o - t_\infty} = 0.75 \quad \therefore \quad t_e - t_\infty = 0.75(t_o - t_\infty)$$

$$t_e = 0.75\ (122.5 - 90) + 90 = 114^\circ F$$

$$t_o - t_e = \Delta t_p = 122.5 - 114 = 8.5^\circ F$$

Based on the computed values of $\Delta t_{conv} = 30^\circ F$ and $\Delta t_{pl} = 8.5^\circ F$, the actual junction temperature of the transistors will be

$$t_j = t_{fl} + \Delta t_{conv} + \Delta t_{pl} + \Delta t_{c-pl} + \Delta t_{j-c}$$

Substituting values

$$t_j = 90 + 30 + 8.5 + 5.5 + 108 = 242^\circ F$$

This temperature is below the allowable maximum junction temperature of 125°C (257°F).

c. Cold Plates Provided with Heat Pipes

The electronic-equipment thermal requirements of uniform-temperature equipment mounting surfaces can be most easily satisfied by incorporating heat pipes into the equipment mounting chassis or cold plates. Cold plates provided with heat pipes were fabricated and tested to demonstrate the feasibility and performance characteristics of this technique.

The cold plates presented in this section can be divided into three general categories: (1) cold plates provided with conventional heat pipes, (2) cold plates provided with conventional heat pipes and phase change materials, and (3) cold plates provided with variable conductance heat pipes. The data presented in this report were obtained from References 5 and 40.

1. Cold Plates Provided with Conventional Heat Pipes

(1) Heat-Pipe Cold Plate No. 1

Figure 175 shows Cold Plate No. 1 which was made of aluminum and contained a continuous 0.5-inch heat pipe bent in a U-shape, thus forming two evaporator sections and one condenser section. Copper tubing (1/4-inch outside diameter), through which coolant was circulated, was attached to the condenser section of the heat pipe. A tape-type electric heater, attached to the plate as shown, was used to simulate the equipment dissipated heat load. The heat pipe was designed for a heat load of approximately 100 watts (340 Btu/hr), and ammonia was used as the working fluid. Temperature distribution of the plate was almost completely uniform. This condition can be explained by the uniform heat input from the tape heater. Concentrated heat loads would cause certain temperature gradients within the plate.

Figure 176 shows temperature changes of the cold plate (thermocouple #2 readings) resulting from electrical power input changes. The temperature change is linear to an electrical power input rate of 75 watts; there is some deviation thereafter. This phenomena could have been caused by some noncondensible gas left in the heat pipe or more heat dissipation to the ambient air at the higher plate temperatures.

Figure 177 shows the same plate with two silicon power transistors (2N1016) and a "dummy" component attached to it. The transistors were fastened to the plate with the manufacturer's recommended torque of 50 in-lb. Temperature measurements were made with copper-constantan thermocouples inserted into small holes drilled into the plate and the component mounting flanges and/or studs.

Figure 178 shows comparison of temperature distribution of the cold plate under conditions when the plate was cooled by a circulating liquid coolant and natural convection to the ambient air. Electrical power input rates to both transistors were the same under both conditions. As expected, there was a significant temperature difference of the transistor mounting base between the two test conditions, thus showing the effectiveness of liquid cooling.

It should be noted that the temperature of the heat pipe increased by 69°F without the coolant flow and was uniform throughout the plate, except around the transistor mounting base. The temperature increase of the components would be much larger for an ordinary liquid-cooled cold plate without the coolant flow. The heat-pipe cold plate can provide a significant advantage as a heat sink under emergency conditions by increasing the fin effectiveness, thus the heat dissipation rate.

(2) Heat-Pipe Cold Plate No. 2

Figure 179 shows Cold Plate No. 2 provided with rectangular heat pipe passages. The cold plate was made of 1/8-inch thick aluminum sheets welded in a configuration to adapt electronic equipment heat flux

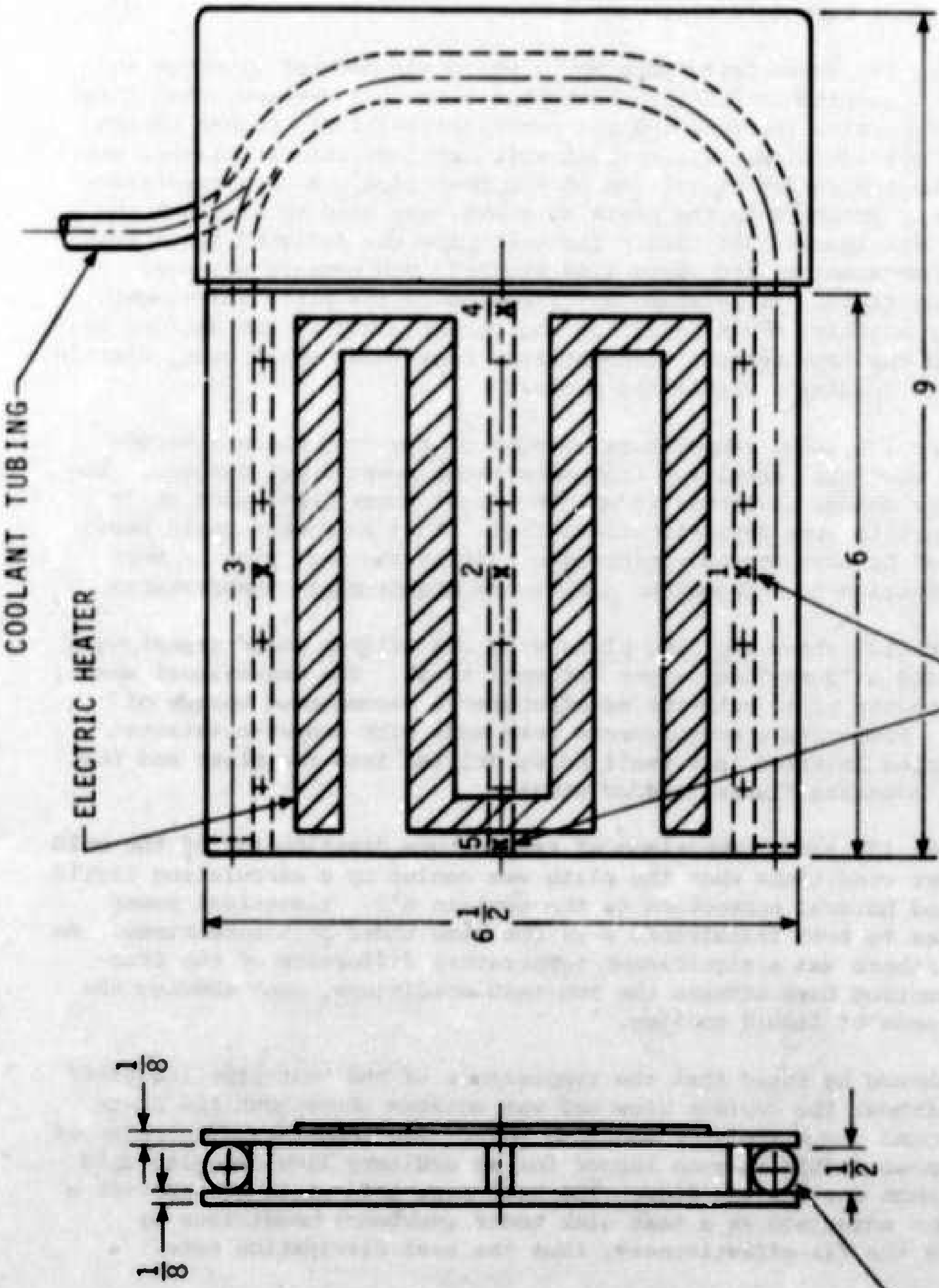

Figure 175. Heat-Pipe Cold Plate No. 1

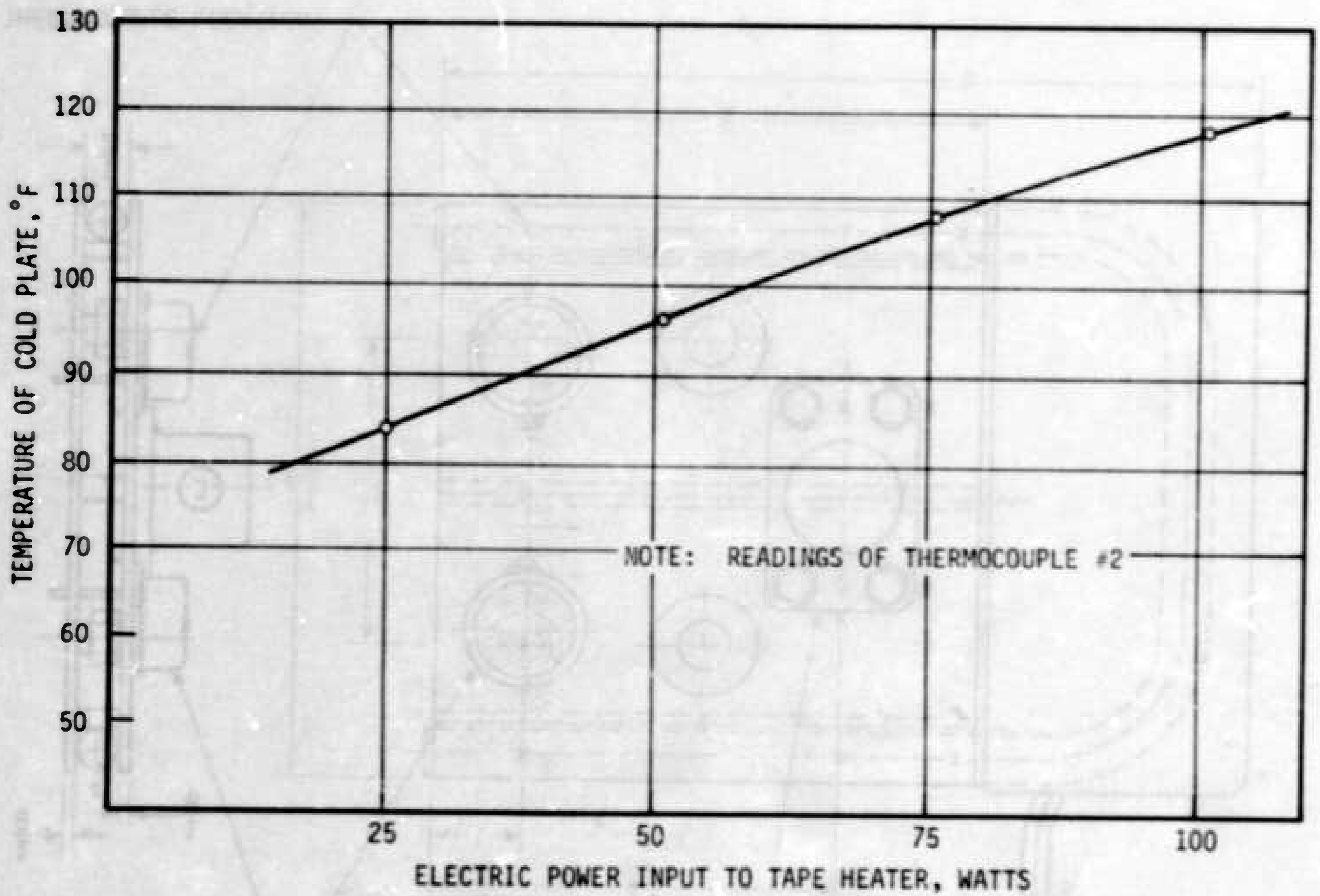

Figure 176. Temperature Changes of Heat-Pipe Cold Plate No. 1 vs Electrical Power Input Rates

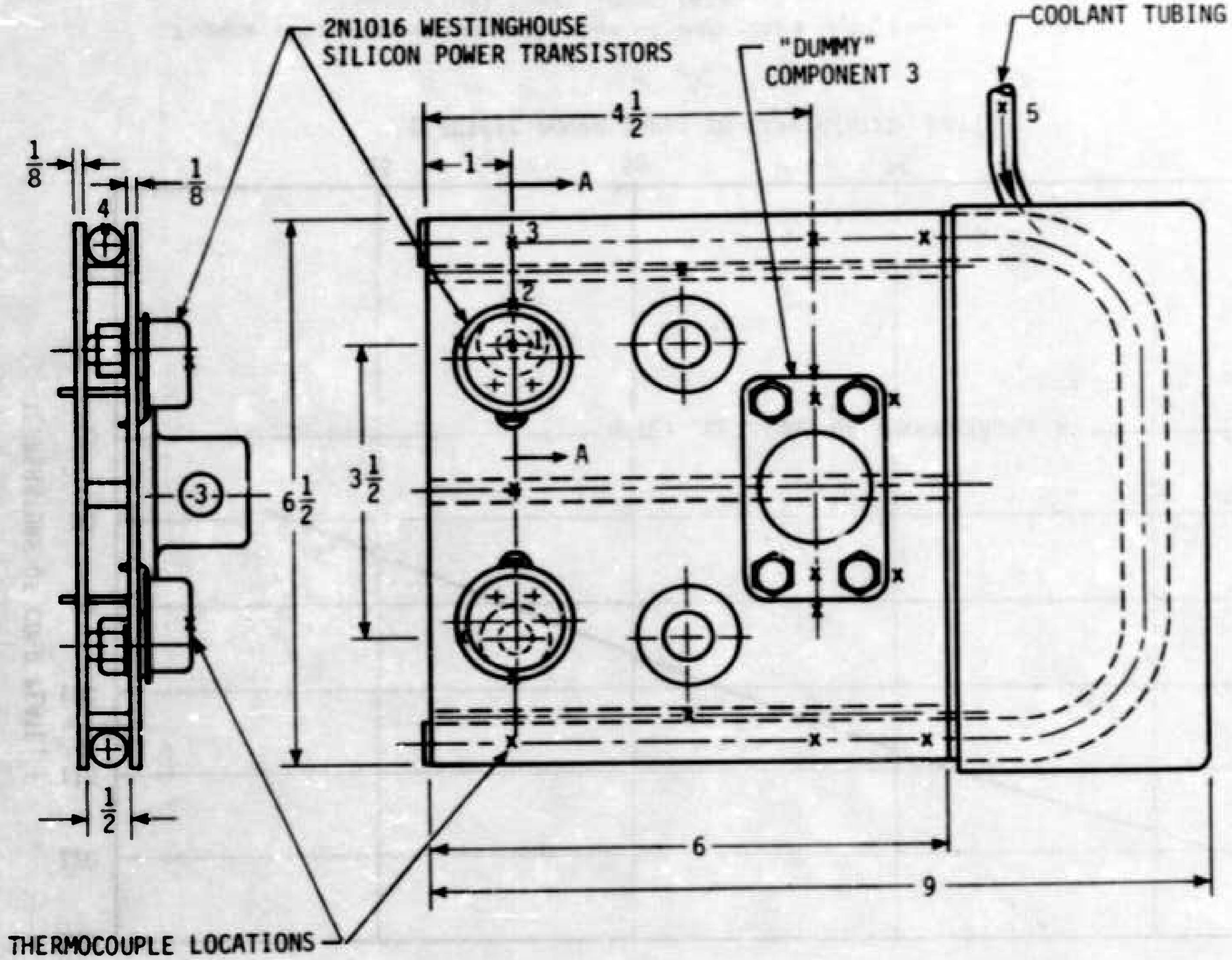

Figure 177. Cold Plate No. 1 with Attached Components

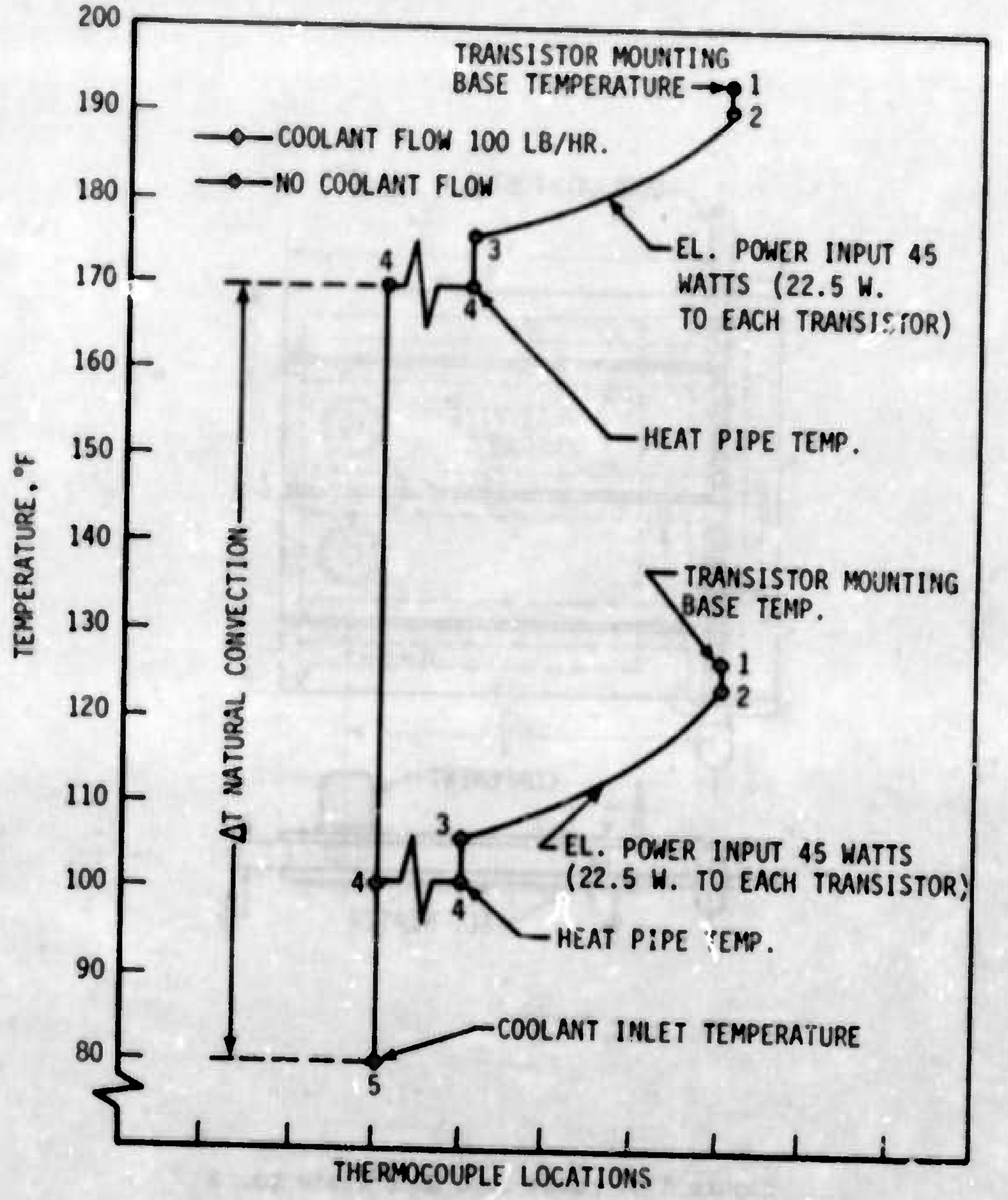

Figure 178. Temperature Distribution of Heat-Pipe Cold Plate No. 1 under Coolant Flow and No-Flow Conditions

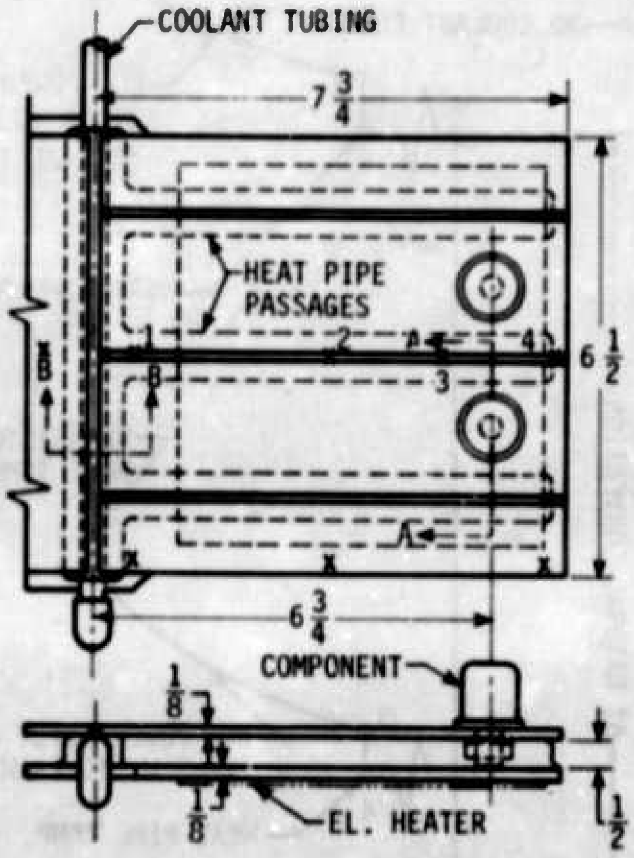

Figure 179. Heat-Pipe Cold Plate No. 2

simulators. Only one end of the plate is shown; the other end is similar. The heat-pipe passages were lined with two layers of 100-mesh copper screen and charged with Freon 11. The electronic-equipment heat load was simulated by two "dummy" components and a blanket-type electric heater. A total heat load of 230 watts (40 watts from each component and 150 watts from the electric heater) could be generated by the heat flux simulators.

Figure 180 shows Section A-A (evaporator section) and Figure 181 shows Section B-B (condenser section) of the cold plate.

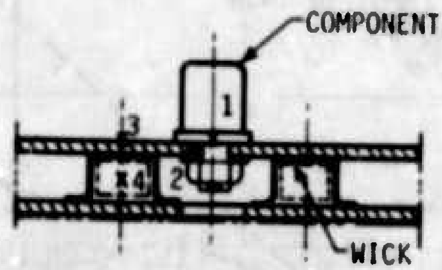

Figure 180. Section A-A of Cold Plate

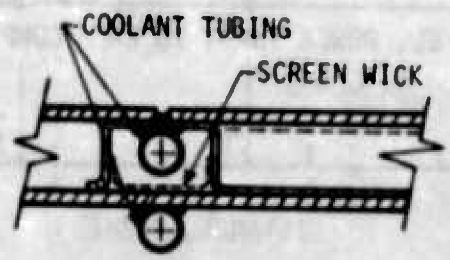

Figure 181. Section B-B of Cold Plate

Figure 182 shows temperature distribution of the cold plate as measured along the external surface of the central heat pipe at thermocouple locations 1, 2, 3, and 4. The tests were performed at three different levels of electrical power input to the electronic component heat-flux simulators. A condition was also investigated when the heat-pipe passages were not charged with the working fluid. It can be seen that temperature gradients within the cold plate can be significantly reduced by the application of heat pipes.

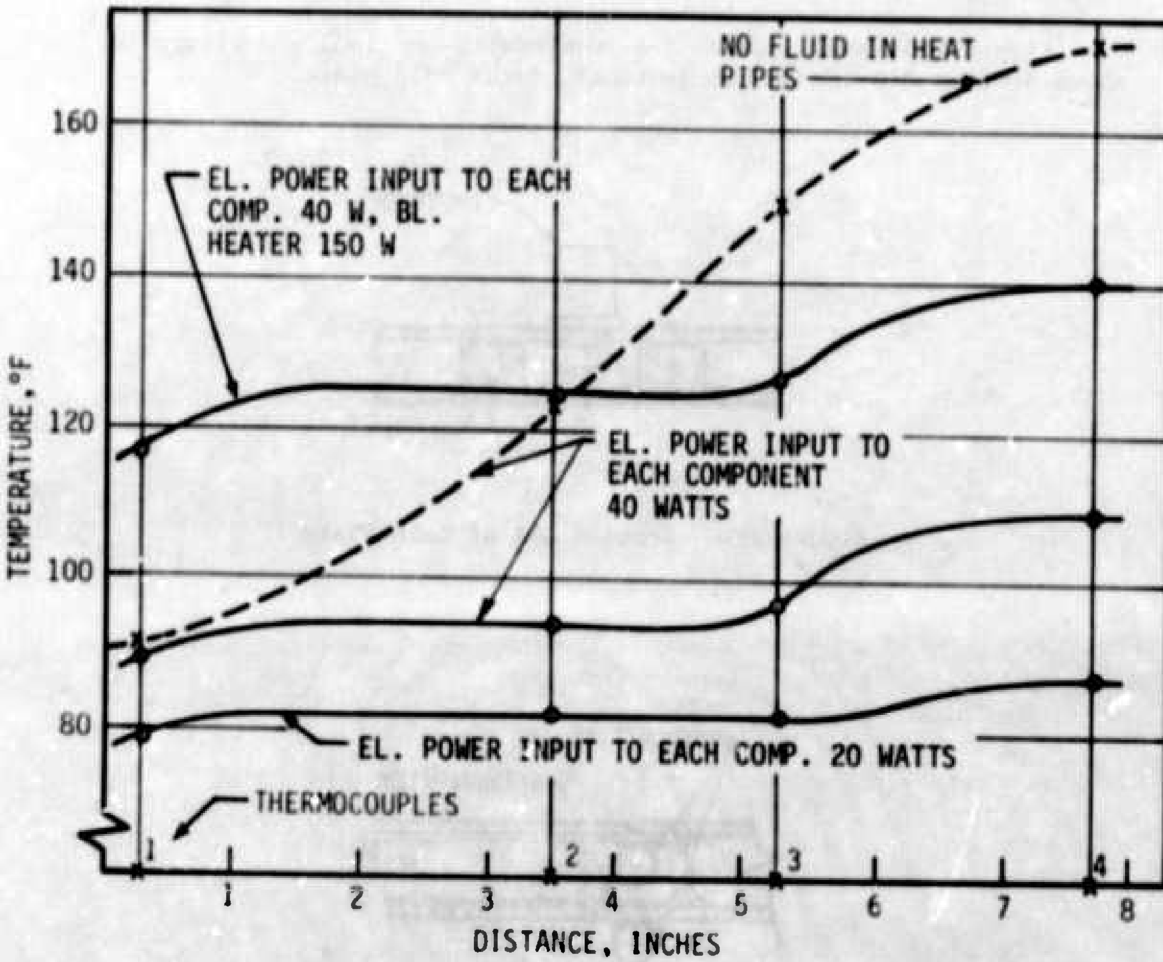

Figure 182. Temperature Distribution of Heat-Pipe Cold Plate No. 2

Figure 183 shows temperature distribution from the component mounting base to the circulating coolant at three different electrical power input rates. The figure clearly shows that the largest temperature differentials occurred within the component mounting surfaces (conduction heat transfer) and at the condenser section (convection heat transfer). If thermal requirements dictate lower component temperatures, critical sections of the cold plate must be properly increased or spacings reduced.

(3) Heat-Pipe Cold Plate No. 3

Thermal tests performed on the conventionally-designed (fin-tube arrangement) cold plates indicated that a significant temperature drop can occur within the mounting surfaces. This condition can introduce restrictions for cooling components with high power dissipation rates unless thick mounting plates are used. To reduce temperature gradients within the component mounting plates, a new design was devised. Figure 184 shows Cold Plate No. 3 which was made of two thin sheets forming a 3/16-inch-wide internal cavity. A 100-mesh copper screen was used as a wick and was charged with a working fluid. Because of ease of fabrication, the cold plate was made of copper instead of aluminum, which would be a more realistic material for airborne applications. The electronic components, generally silicon power transistors, were mounted to inserts as shown in Figures 185 and 186 of the cold plate. Heat generated by the electronic components was transferred through the inserts to the working fluid, and from there to the coolant, which was circulated through 1/4-inch-diameter tubing attached to the condenser section. The arrangement of the heat-pipe cavity and component mounting surface shortened the conduction path significantly, thus reducing the temperature differential from the insert to the working fluid. Evaporative heat transfer took place from the insert and internal surface of the plates.

Heat transfer from extended surfaces has been discussed in Section VII and will not, therefore, be discussed here. Only the resistance network from the component mounting base to the working fluid of the heat pipe is shown. See Figure 187.

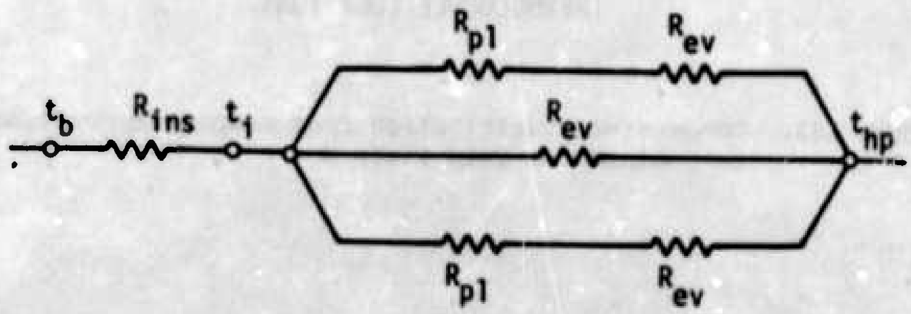

Figure 187. Resistance Network of Evaporator Section

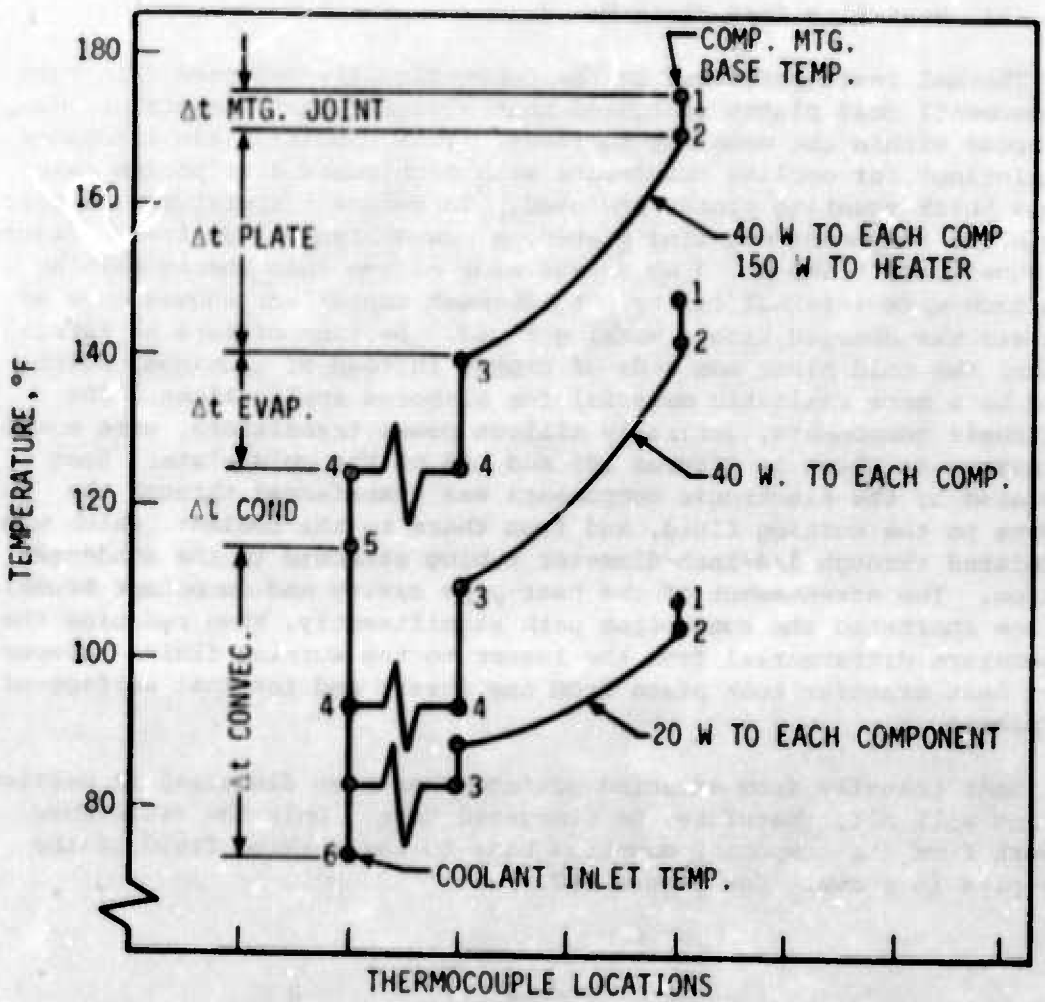

Figure 183. Temperature Distribution from Component Mounting Base to Coolant for Cold Plate No. 2

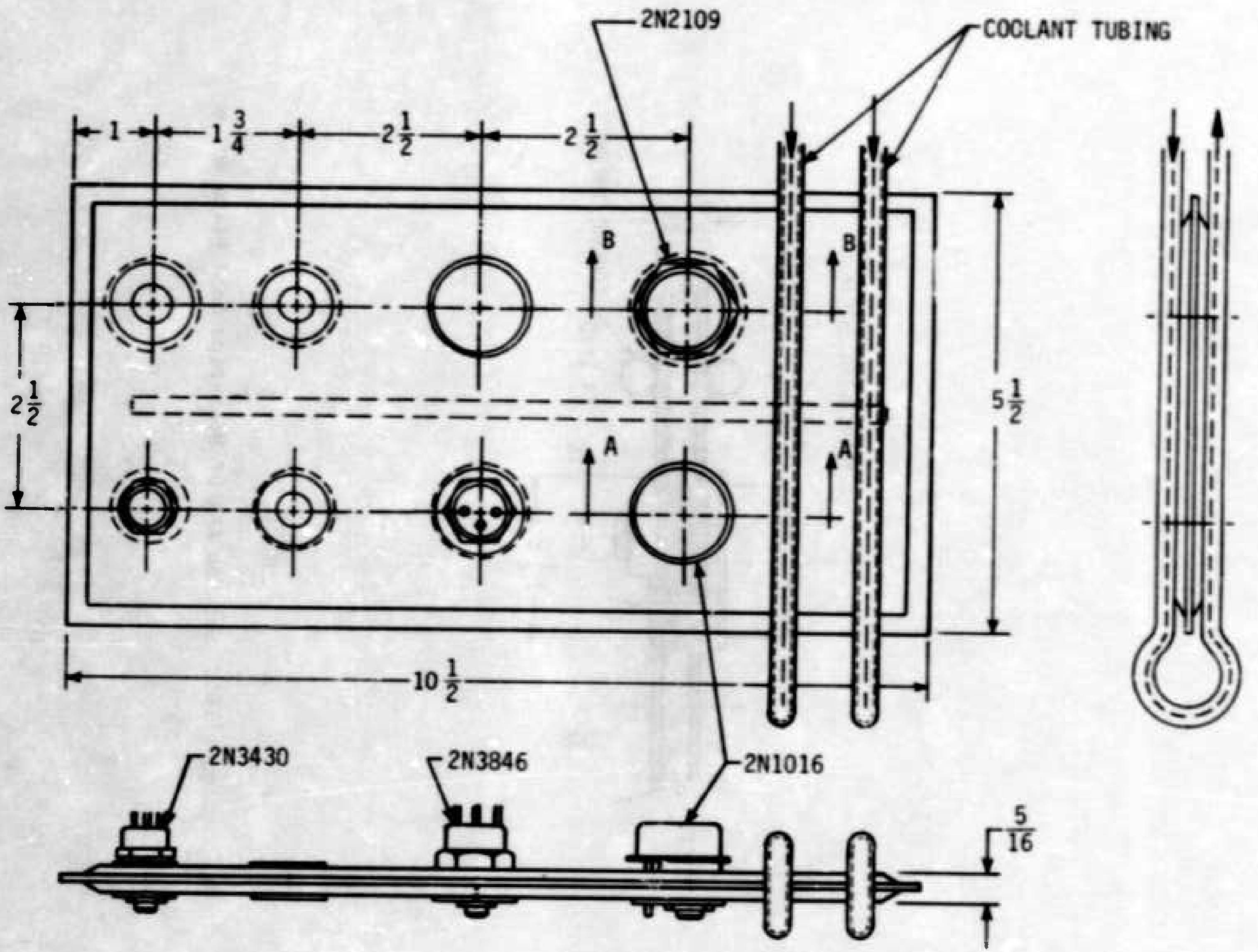

Figure 184. Heat-Pipe Cold Plate No. 3

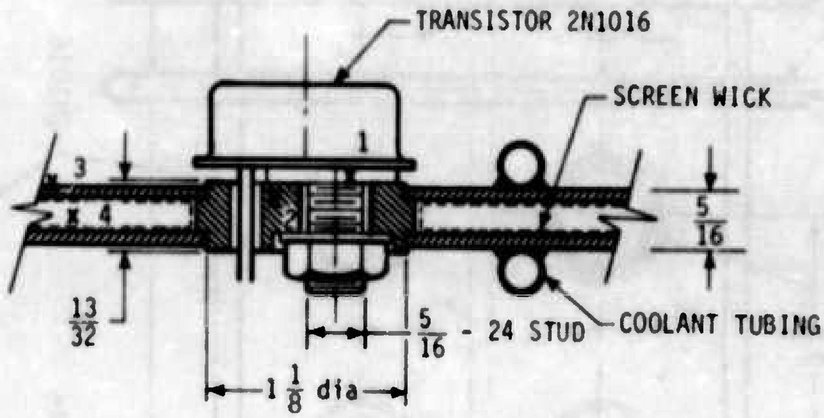

Figure 185. Section A-A of Heat-Pipe Cold Plate No. 6

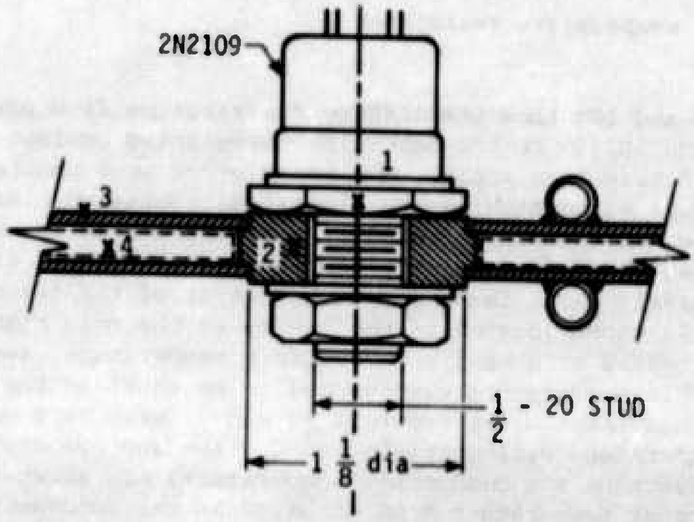

Figure 186. Section B-B of Heat-Pipe Cold Plate No. 6

This resistance can be expressed as follows:

$$R = R_j + R_{ins} + \cfrac{1}{\cfrac{1}{R_{pl} + R_{ev}} + \cfrac{1}{R_{ev}} + \cfrac{1}{R_{pl} + R_{ev}}}$$

where R_j = thermal resistance of mounting joint

R_{ins} = thermal resistance of insert

R_{pl} = thermal resistance of plate

R_{ev} = evaporative resistance

Figures 188 and 189 show temperature distribution from power transistors 2N1016 and 2N2109 to the heat-sink circulating coolant at three different power dissipation rates. The transistors were mounted directly to the plate without using any electrical isolation. As can be seen, temperature differentials caused by conduction heat transfer through the plates were significantly reduced. Thermocouple #3 was located approximately 1-3/8 inches from the center of the insert. Thermocouple #4 is shown located in the cavity of the cold plate. Actually, it was located at a section of uniform temperature, away from heat sources. This temperature was assumed to be equal to the vapor temperature. Since temperature readings #3 and #5 were hard to specify, the combined temperature differentials (conduction and evaporation temperature and convection and conduction temperature) are shown in the figure. The largest temperature drop occurred at the condenser section of the cold plate and was primarily caused by the convection heat transfer to the circulating coolant. This temperature differential, however, can be reduced by providing a larger convection heat-transfer area.

An attempt was also made to determine the maximum concentrated heat-load removal rate. An electrical power input of 165 watts was applied to the 2N2109 power transistor without any indication of dry-out of the wick. Because of the cold-plate internal pressure and transistor temperature considerations, no further increase was made in the electrical power input. At an electrical power input of 165 watts, the transistor case temperature reached a value of 180°F. Based on a junction-to-case thermal resistance of R_{jc} = 0.35°C/watt = 0.63°F/watt, the transistor junction temperature was determined to be

$$t_j = t_c + R_{jc}P = 180 + 0.63\ (165) = 284°F = 140°C$$

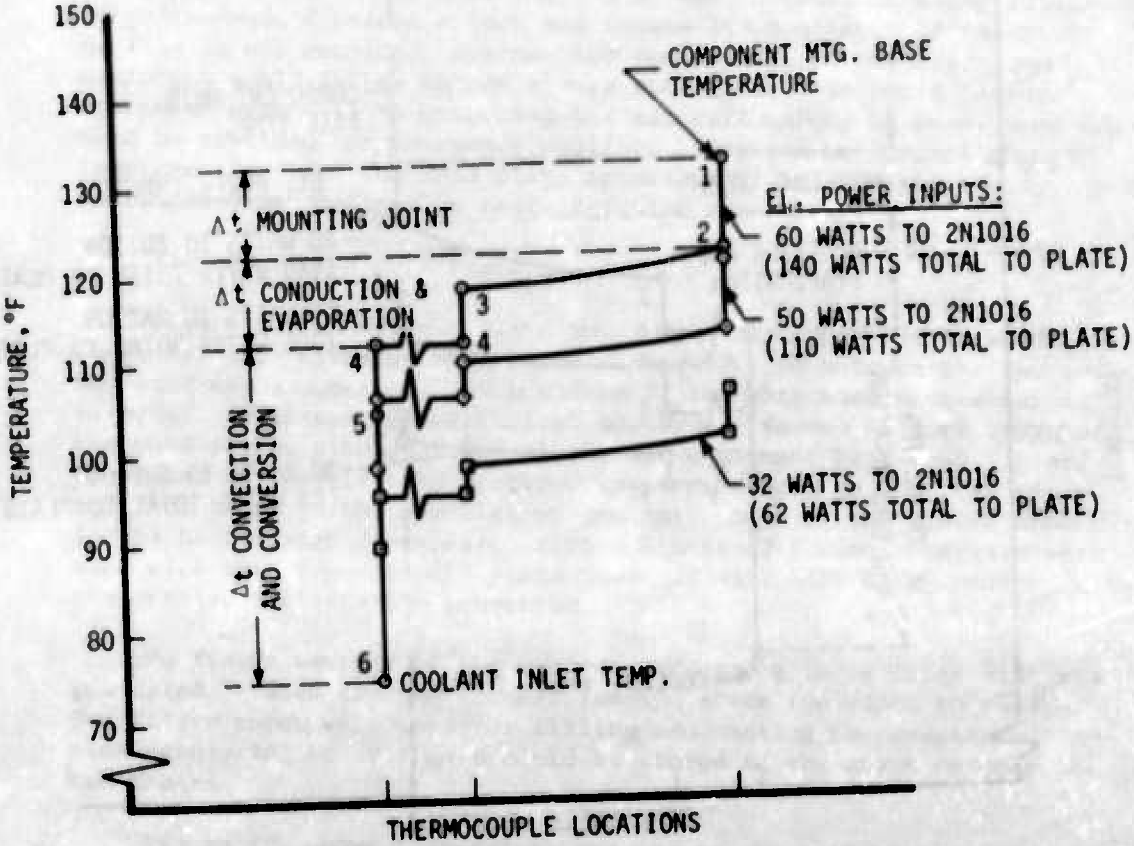

Figure 188. Temperature Distribution from Transistor to Coolant for Heat-Pipe Cold Plate No. 3

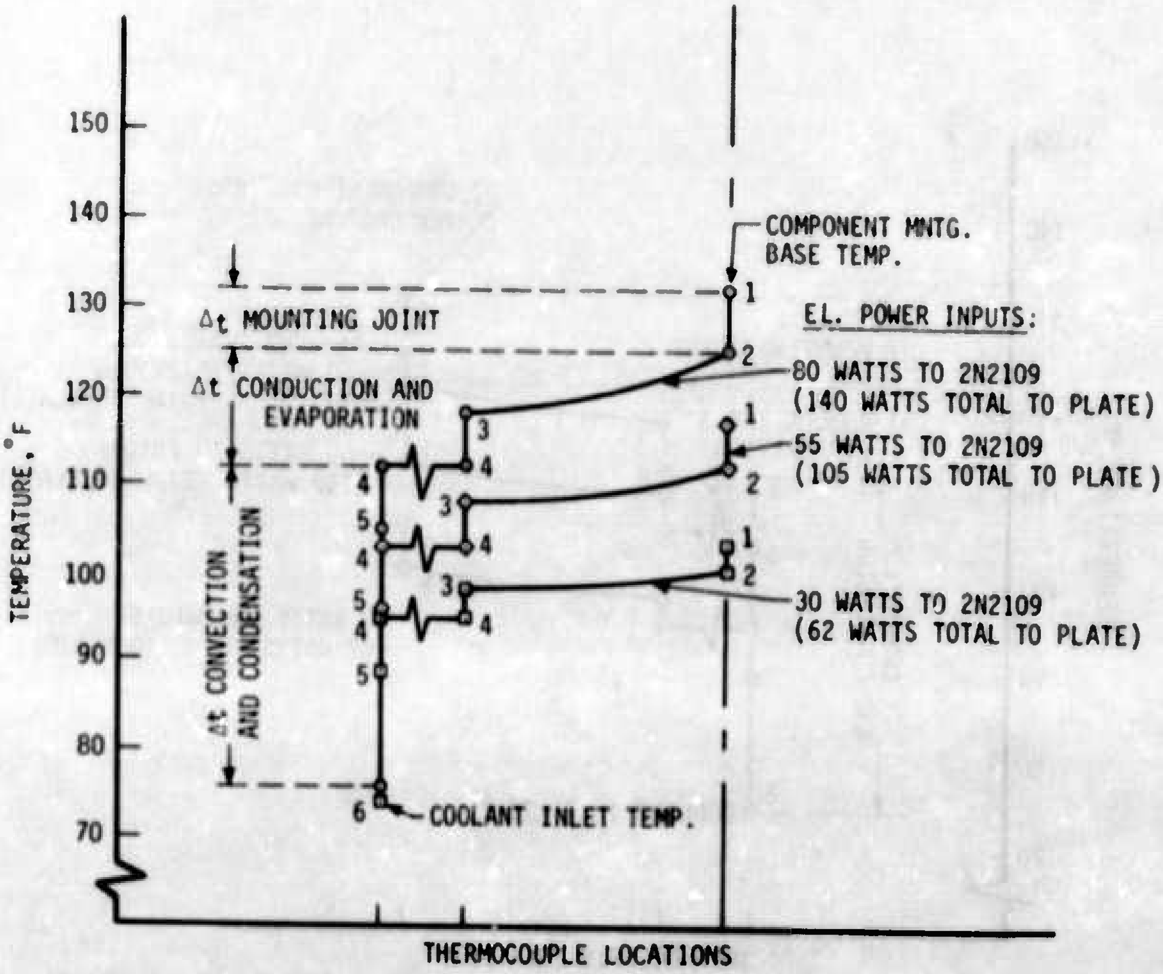

Figure 189. Temperature Distribution from Transistor to Coolant for Heat-Pipe Cold Plate No. 3

This temperature was below the maximum allowable junction temperature of 175°C. It must be noted, however, that no insulating washer was used between the transistor and cold plate.

2. Cold Plates Provided with Heat Pipes and Phase Change Materials

In a liquid-cooled system where cold plates are used for cooling of electronic equipment, some means must be provided to avoid a catastrophic failure of equipment essential to "safe return." Such condition can occur when a closed-loop cooling system, because of enemy action or other reasons, develops a leak and looses its coolant. If emergency cooling is not provided, overheating and failure of the electronic equipment would follow within a very short time. To avoid failure of equipment essential to returning the aircraft safely to base, some means must be provided for emergency cooling. This can be accomplished by incorporating into the cold plate materials of high heat capacity, such as evaporative coolants or heat-of-fusion materials.

(1) Heat-Pipe Cold Plate No. 1

Figure 190 shows Cold Plate No. 1 made of copper and provided with three 1/2-inch-diameter heat pipes. Space formed betwnen the two mounting surfaces was sealed. It could be filled with some heat-absorbing material. Blanket-type electrical heaters, attached to both sides of the cold plate, simulated the electronic-equipment heat load. Heat, generated by the electric heaters, was transferred to the heat pipes, and from there to the circulating coolant. Both of the plates took part in the heat transfer process. Although heat-of-fusion materials were used with this type of cold plate (see Ref 41), only data obtained with evaporative coolants are presented.

To insure wetting of the heated surfaces, a loose fiber wick was installed between the two plates, leaving space for vapor to escape. Two filler tubes were used for filling and venting the evaporant. Approximately 262 cc of liquid could be stored in the space between the two plates.

Figure 191 shows temperature changes of the cold plate versus time after the circulating coolant was turned off. The results are presented for two fluids, water and Freon 113, and two different heat loads for each fluid. As can be seen from the figure, water provided the best heat sink as far as operating time is concerned. The 262 cc of water provided an operational time of over 4 hours at a heat load of 50 watts after the coolant flow was turned off. The temperature of the plate, however, was quite high because operation occurred at sea level. When Freon 113 was used as the heat sink, the plate temperature was maintained at quite a low level, but the operational time, because of the low latent heat of evaporation, was short. The operation time can be increased by providing additional space for the evaporant.

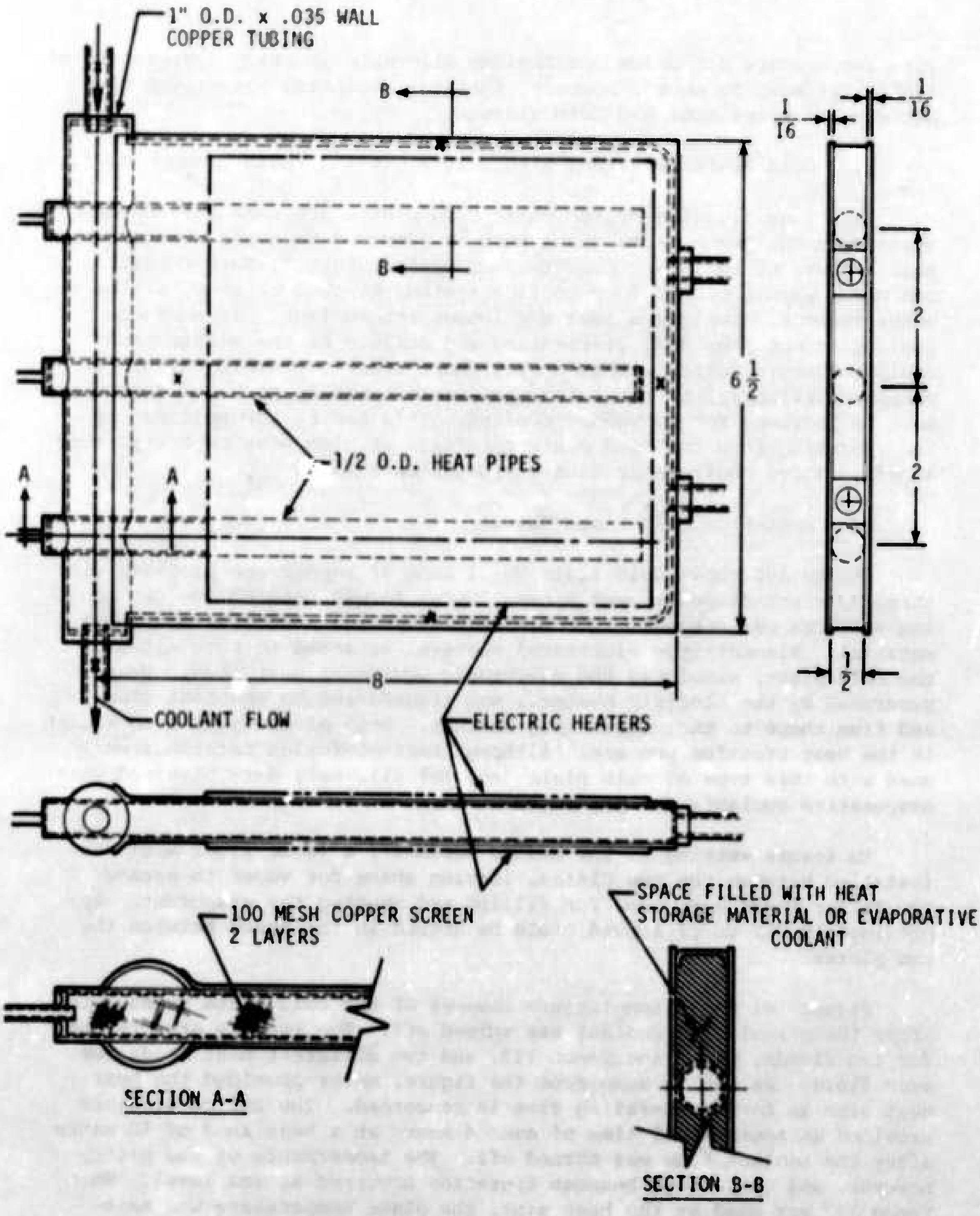

Figure 190. Heat-Pipe Cold Plate No. 1 with High Thermal Capacity

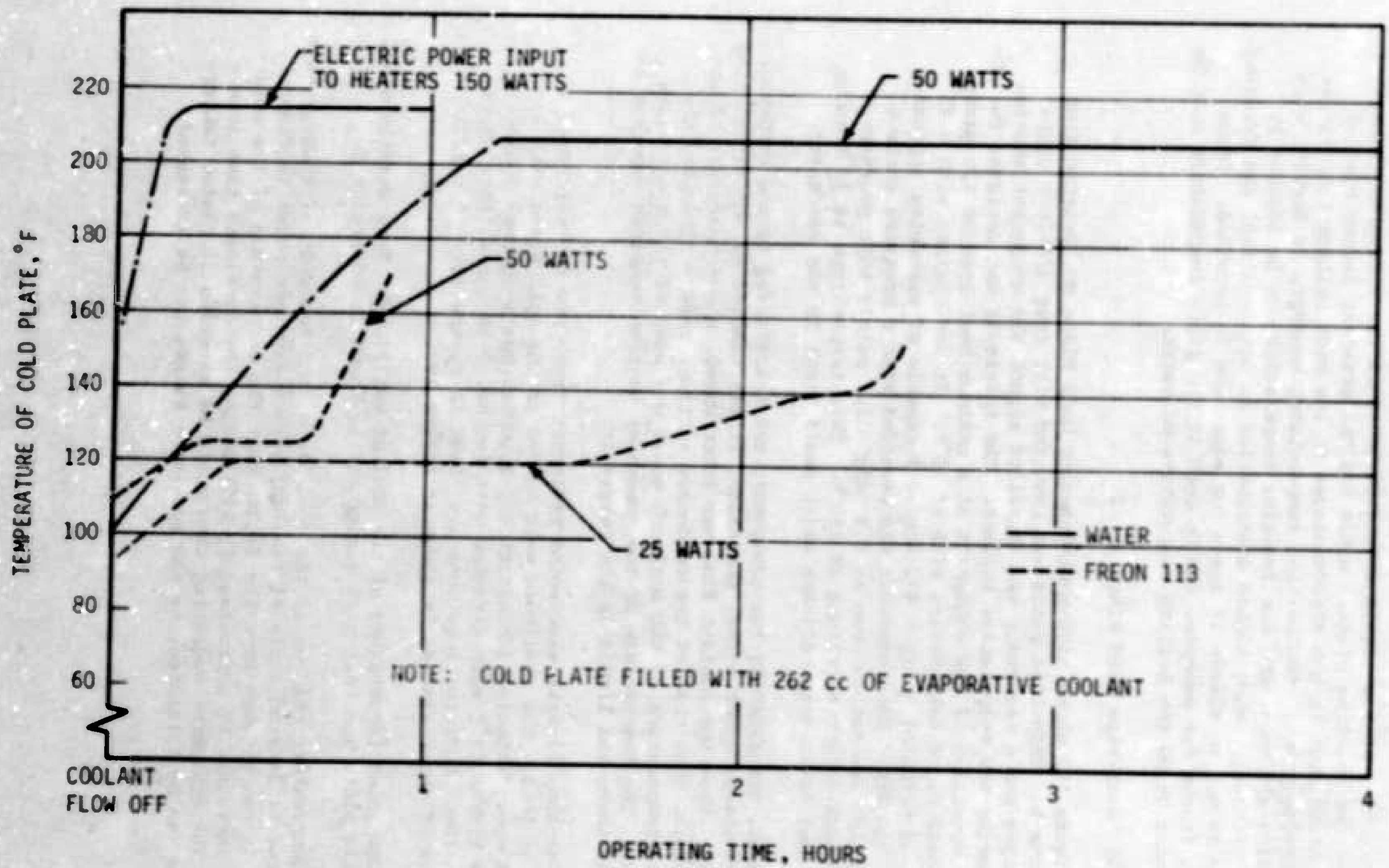

Figure 191. Temperature Changes vs Time of Heat-Pipe Cold Plate No. 1 at Different Test Conditions

Selection of the liquid should be based on the allowable temperature of the mounting plate. Water has the greatest latent heat of vaporization, but it has disadvantages in its high boiling temperature and freezing point. The boiling temperature, however, is lowered with increasing altitude, and the freezing temperature can be lowered by adding methanol. When liquid distribution is not required, the freezing problem is not so severe if space for expansion is provided. Other fluids, Freons for example, can be used if the plate temperature must be maintained below the boiling temperature of water.

(2) Heat-Pipe Cold Plate No. 2

Figure 192 shows high-heat-capacity Cold Plate No. 2 taken from Reference 5. This cold plate was provided with four 3/8-inch copper heat pipes and a reservoir was installed around the condenser section for storing the evaporative coolant. The reservoir was designed for 30-minute operation of the equipment at a maximum heat load of 120 watts and a cold plate temperature rise of 30°F. It was charged with 0.45 pounds of methanol (h_{fg} = 472 Btu/lb) capable of absorbing approximately 210 Btu. The reservoir was provided with a pressure control valve which was set to open at 0.4 psig (15.1 psia); this pressure corresponds to a temperature of 150°F. This temperature is 13°F above the normal maximum temperature which could occur in the condenser.

Heat, generated by the equipment, was transferred to the condenser section where, under normal operation, it was removed by the circulating coolant. When the coolant flow was interrupted, the temperature of the heat pipes, thus that of the condenser section, rose and reached the boiling temperature of the methanol which was used as the evaporative coolant. The temperature of the condenser section remained constant as long as there was liquid in the reservoir.

One-ohm, 10-watt wire-wound resistors (type RER 65) were used as the heat load. The resistors were bonded to the cold plate with a filled epoxy adhesive (Ablestick 465-9) which has a thermal conductivity of 0.4 Btu/hr ft°F were attached with two No. 2-56 screws torqued to 1.5 in-lbs. Resistor locations are shown in Figure 192. A circuit diagram of the resistors is shown in Figure 193.

The inlet temperature of the coolant was 110°F. More details about the cold plate and heat-pipe design can be found in Reference 5.

Temperature changes of the cold plate (thermocouple #2 reading) and resistor #4 (thermocouple #1 reading) versus time are shown in Figure 194. It can be seen from the figure that the temperature of the cold plate increased by approximately 25°F during the 30-minute time interval. The equipment operating time could be extended if higher temperatures can be tolerated, or the reservoir volume can be increased.

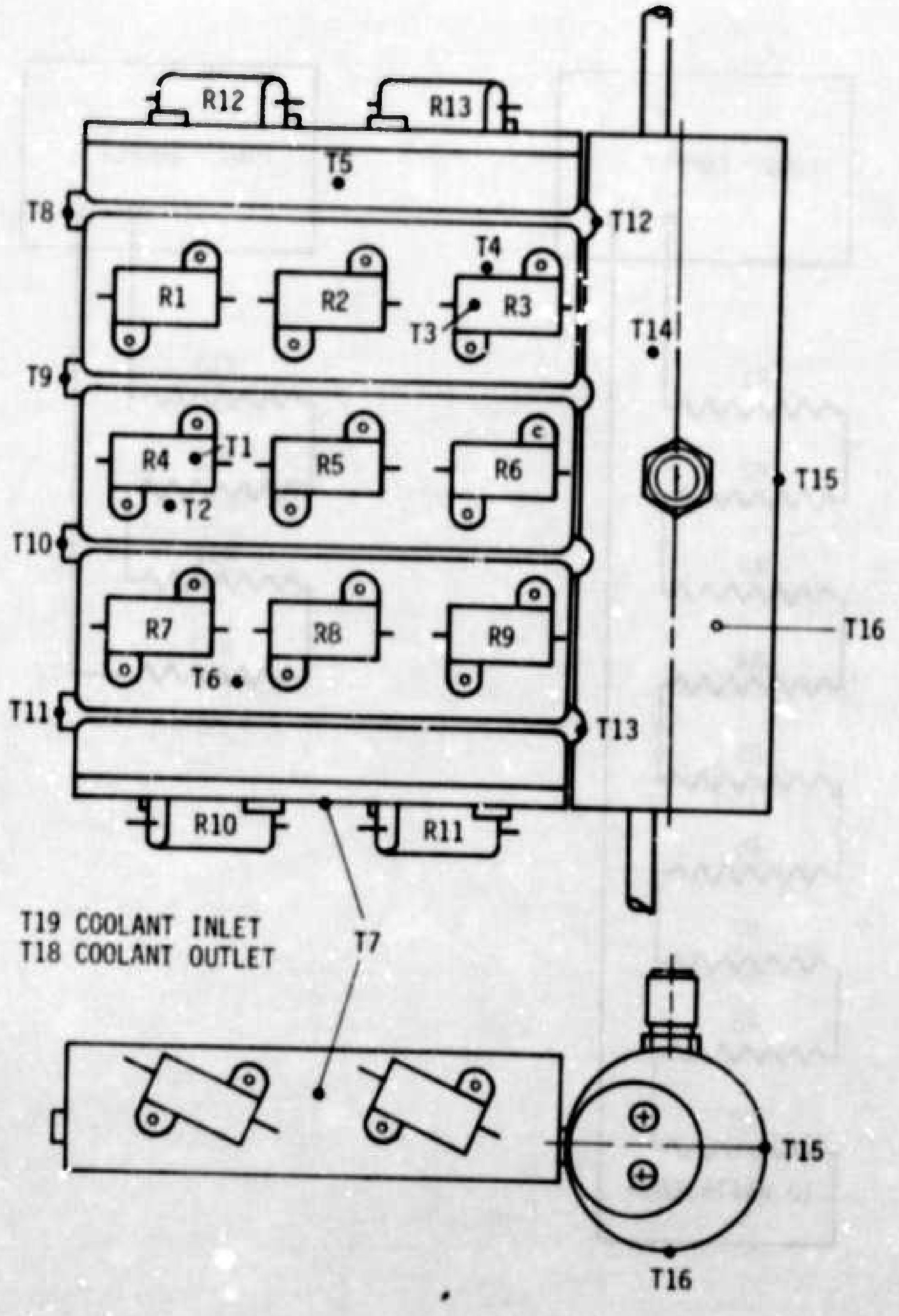

Figure 192. Heat-Pipe Cold Plate No. 2 with High Thermal Capacity

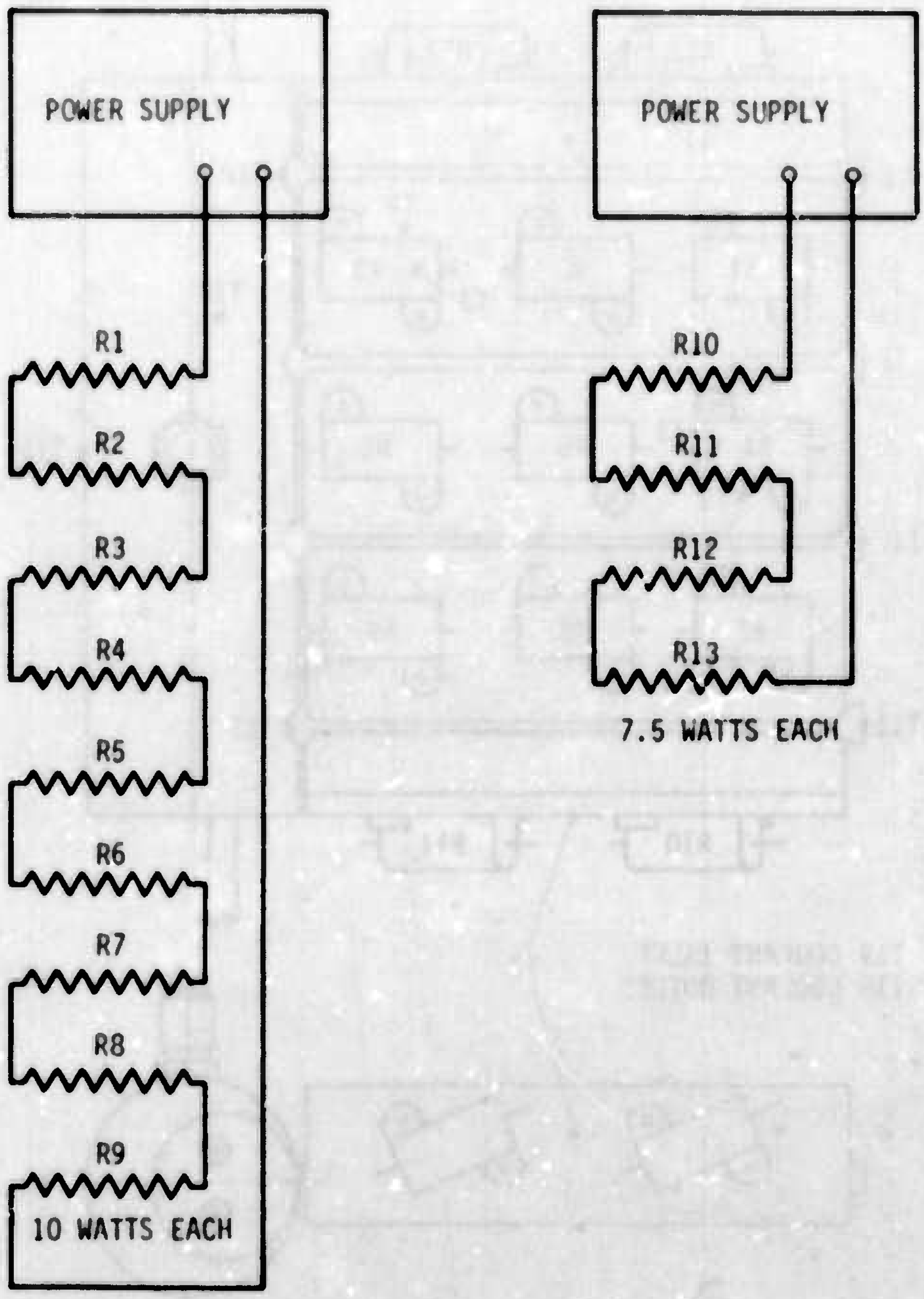

Figure 193. Resistor Circuit Diagram

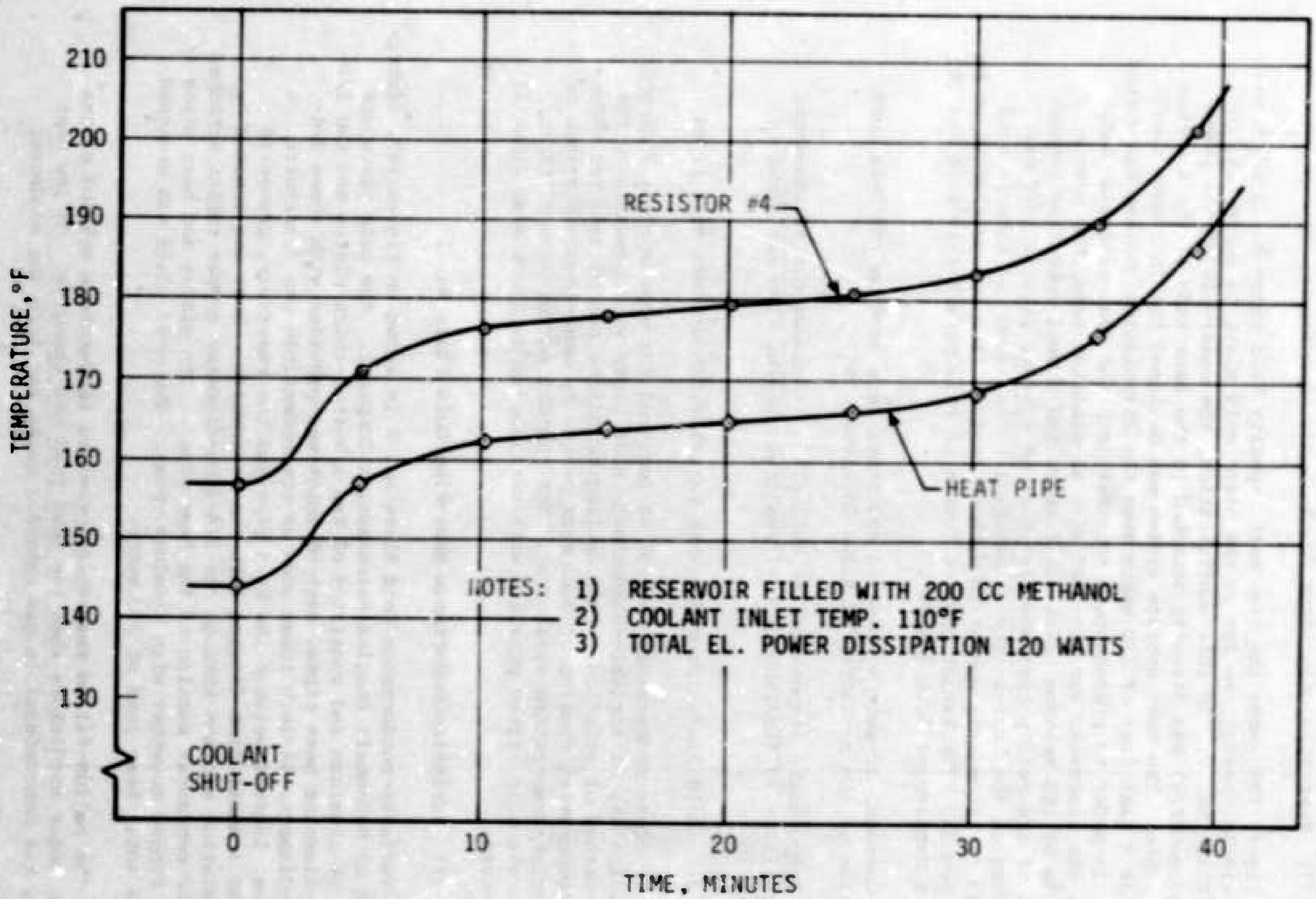

Figure 194. Temperature Changes of Resistor and Heat-Pipe Cold Plate No. 2 vs Time After Coolant Shut-Off

(3) Heat-Pipe Cold Plate No. 3

Figure 195 shows the high heat capacity Cold Plate No. 3 which was of a similar design, as far as the basic cold plate is concerned, to Cold Plate No. 2. In this configuration, the reservoir of the phase-change material was directly attached to the back side of the aluminum cold plate. The heat storage system was designed for 15-minute operation at a heat load of 120 watts when the circulating coolant was turned off. In order to promote heat transfer into the heat-of-fusion material, the reservoir was provided with an aluminum honeycomb matrix. Because of its melting point (15°F above the normal operating temperature of the cold plate) and high heat of fusion, stearic acid was selected as the heat-of-fusion material. The amount of stearic acid needed for 15-minute operation without coolant flow was determined to be 1.23 pounds. The latent heat of fusion of this material is 85.6 Btu/lb, with a density of 52.8 lbs/ft^3.

One-ohm, 10-watt wire-wound resistors were used as the heat load. Location of the resistors is shown in Figure 195.

Temperature changes of the cold plate (thermocouple #2 readings) and resistor #4 (thermocouple #1 readings) versus time are shown in Figure 196.

3. Cold Plates Provided with Variable Conductance Heat Pipes

If close temperature control is required for some special equipment only, the use of variable-conductance heat pipes will probably be the best method of solution. This cooling technique can be used for reducing temperature cycling of equipment caused by heat-load variations or heat-sink temperature variations. The thermal performance of three different cold plates provided with variable-conductance heat pipes is presented.

(1) Variable-Conductance Heat-Pipe Cold Plate No. 1

Variable-conductance Cold Plate No. 1 is shown on Figure 197, (fabricated by McDonnell Douglas Astronautics Company). The cold plate was made of aluminum and consisted of two 1/8-inch-thick plates and two 1/2-inch-diameter heat pipes, each of which was provided with three 3/4-inch-diameter 14-inch tubes used as noncondensible gas reservoirs. A device, located between the heat pipe and the reservoir, prevented liquid ammonia from flowing into the reservoirs. Heat was removed by circulating coolant through the 1/4-inch-diameter copper tubing attached to the condenser section of the heat pipes. The plates and heat pipes were bonded together with aluminum epoxy. The cold plate was designed for a total heat load of 250 watts.

The helium-filled reservoirs provided temperature control of the plate under conditions when the heat load was changing. At low heat load, the noncondensible gas extended quite far into the condenser

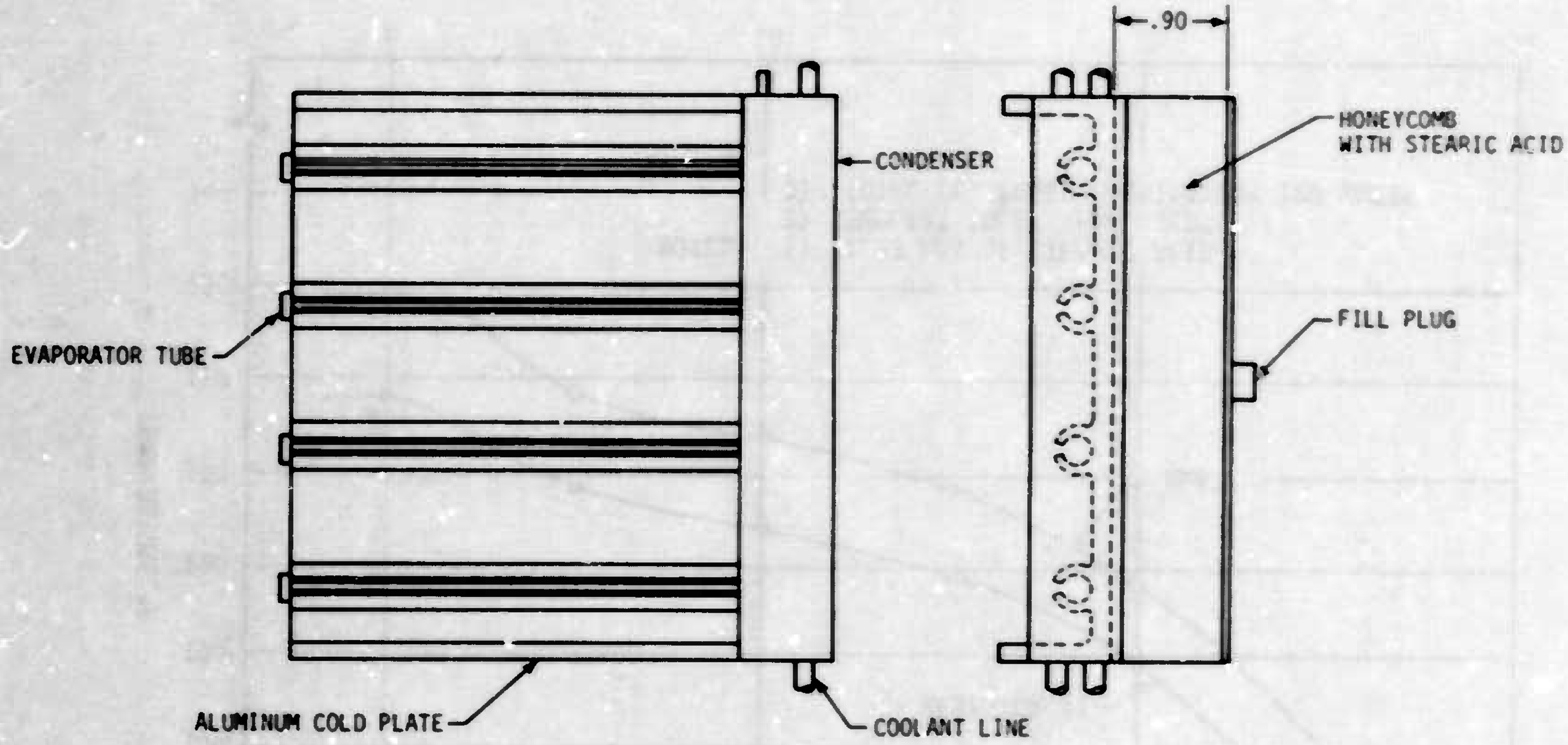

Figure 195. Heat-Pipe Cold Plate No. 3 with High Thermal Capacity

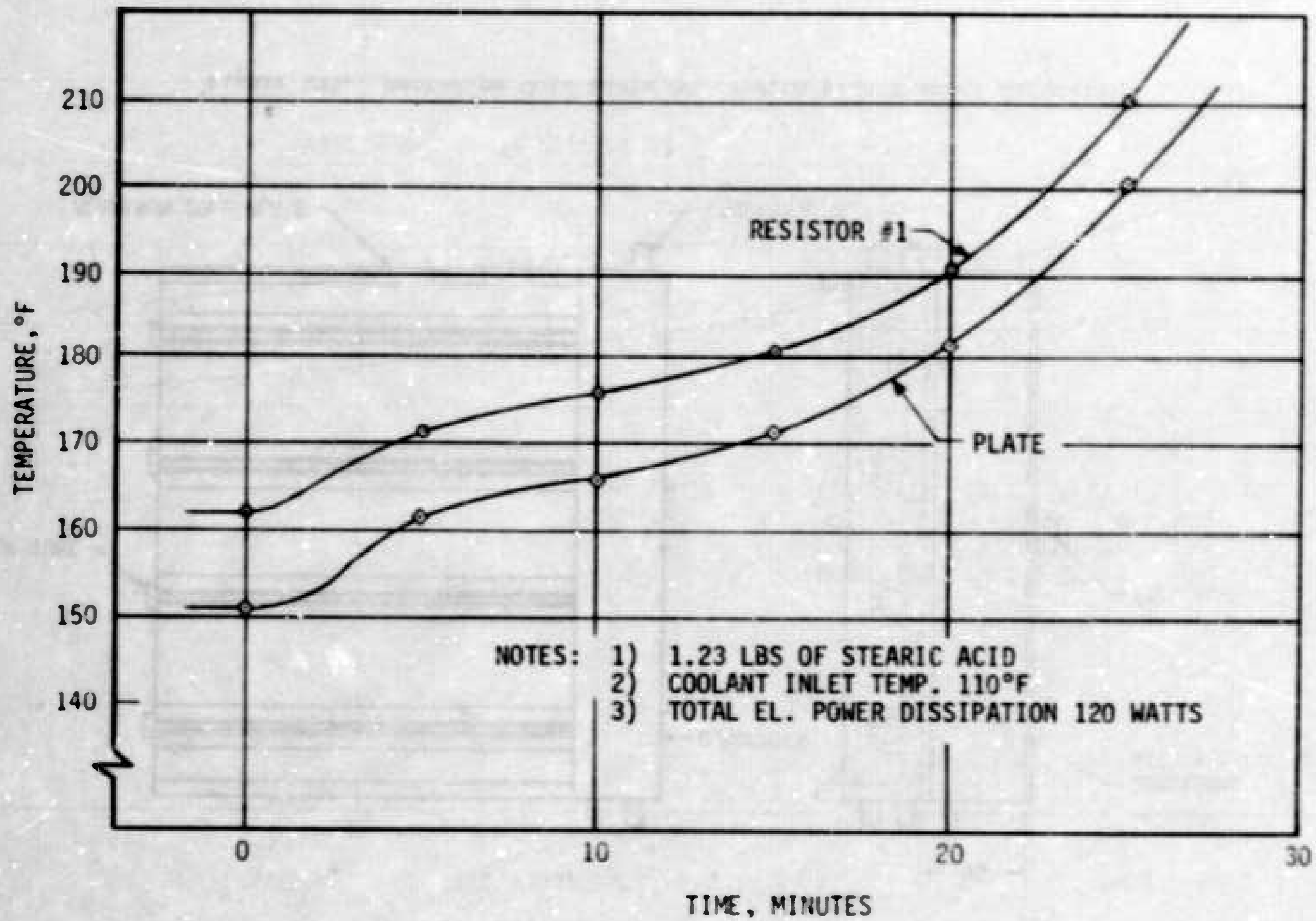

Figure 196. Temperature Changes of Resistor and Heat-Pipe Cold Plate No. 3 vs Time After Coolant Shut-Off

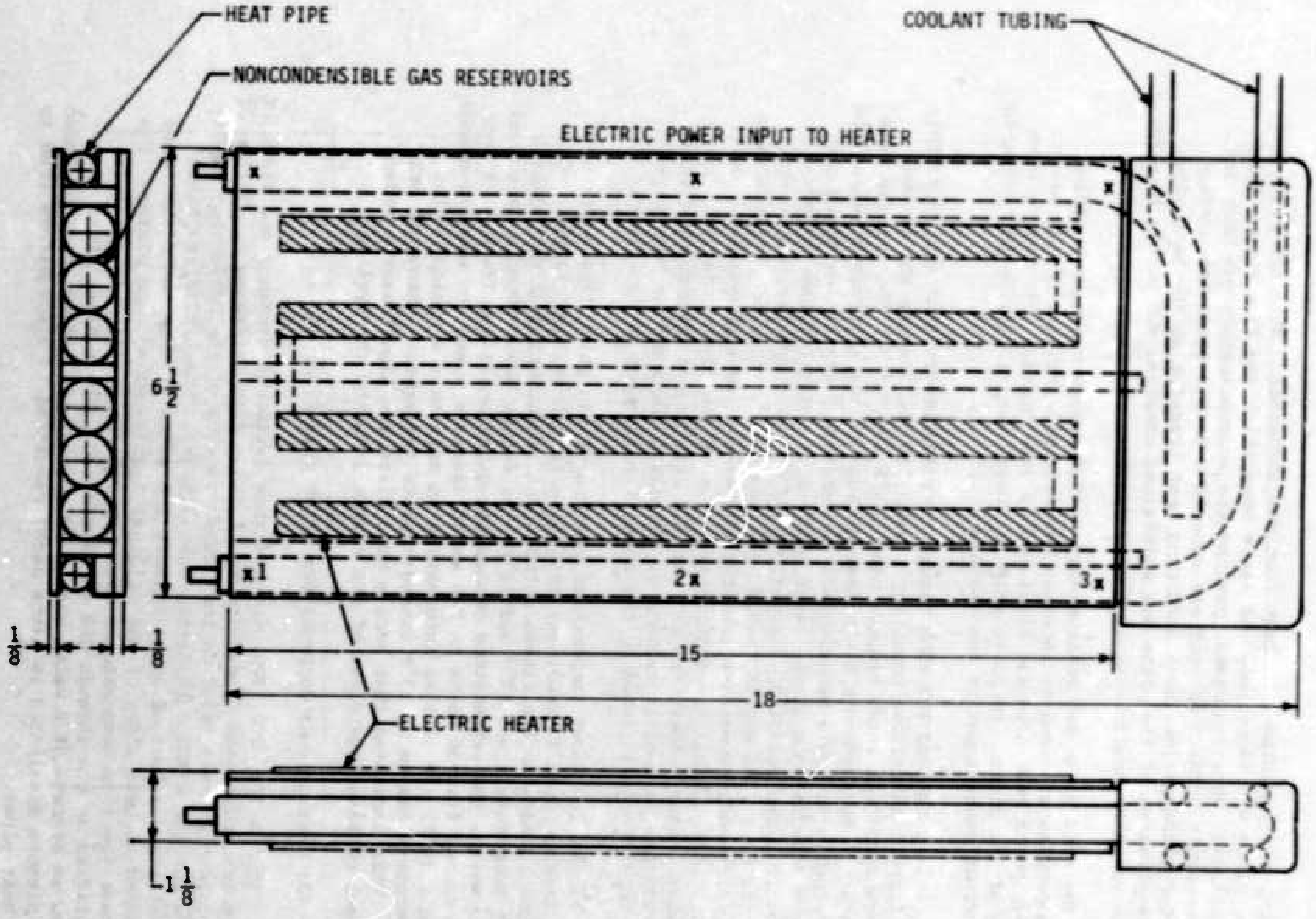

Figure 197. Variable-Conductance Heat-Pipe Cold Plate No. 1

section, and resistance to heat flow was increased. When the heat load of the plate was increased, the vapor generation and flow rates, thus the pressure, were increased, pushing the noncondensible gas back into the reservoir. The displaced gas exposed a larger condenser surface area for condensation, thus promoting heat transfer of the heat pipe. The temperature of the plate was maintained constant and stable because of the variable conductance of the condenser.

The cold plate was instrumented with #30-gage copper-constantan thermocouples attached to internal and external surfaces of the plate. The equipment heat load was simulated by tape heaters attached to both sides of the plate. DC power supplies were used to provide controllable electrical power input to the heaters.

Figures 198 and 199 show temperature distribution of the cold plate at different electrical power input rates to the heaters and at two different coolant inlet temperatures (55°F and 72°F). The figures show temperature measurements taken near an edge of the cold plate (along the heat pipe). As could be expected, temperature distribution along the plate was nonuniform at the lower heat input rates because the noncondensible gas occupied a large portion of the condenser. However, when the heat load was increased, the vapor flow rate and pressure were also increased, exposing a larger surface area for condensation. As a result, only a small temperature increase of the plate occurred. Somewhat larger temperature changes and also higher temperatures were observed at the central section of the plate (between the heat pipes). This condition was caused by the thermal resistance of the plate.

Figure 200 shows temperature changes of the cold plate (obtained from thermocouple #2 readings) resulting from heat load changes. Comparison is made in the figure between the conditions when the coolant inlet temperature was 55°F and 72°F. As can be seen, above a heat load of 80 watts, the temperature change was quite small and linear. A heat load change from 80 watts to 240 watts caused a plate temperature change of only 10°F. It is also interesting to note that a coolant inlet temperature change of 17°F caused a plate temperature change of only 2°F. This indicates that such a cold plate can significantly reduce thermal cycling regardless of the source inducing the cycling.

(2) Variable-Conductance Heat-Pipe Cold Plate No. 2

Figures 201, 202, 203, and 204 show different sections and views of variable-conductance Cold Plate No. 2 taken from Reference 5. Design of the cold plate was based on the Hughes version of the deflection amplifiers for the AWACS cathode-ray-tube display. The amplifiers had a normal thermal load of approximately 120 watts in components that were attached to both sides of the original liquid-cooled cold plates. The highest junction temperatures were experienced by eight transistors identified as Q11 through Q18 in Figure 204. These transistors dissipated an average of 8 watts each. In some display modes, four of these transistors dissipated 16 watts each, resulting in a nonuniform load to the heat pipes.

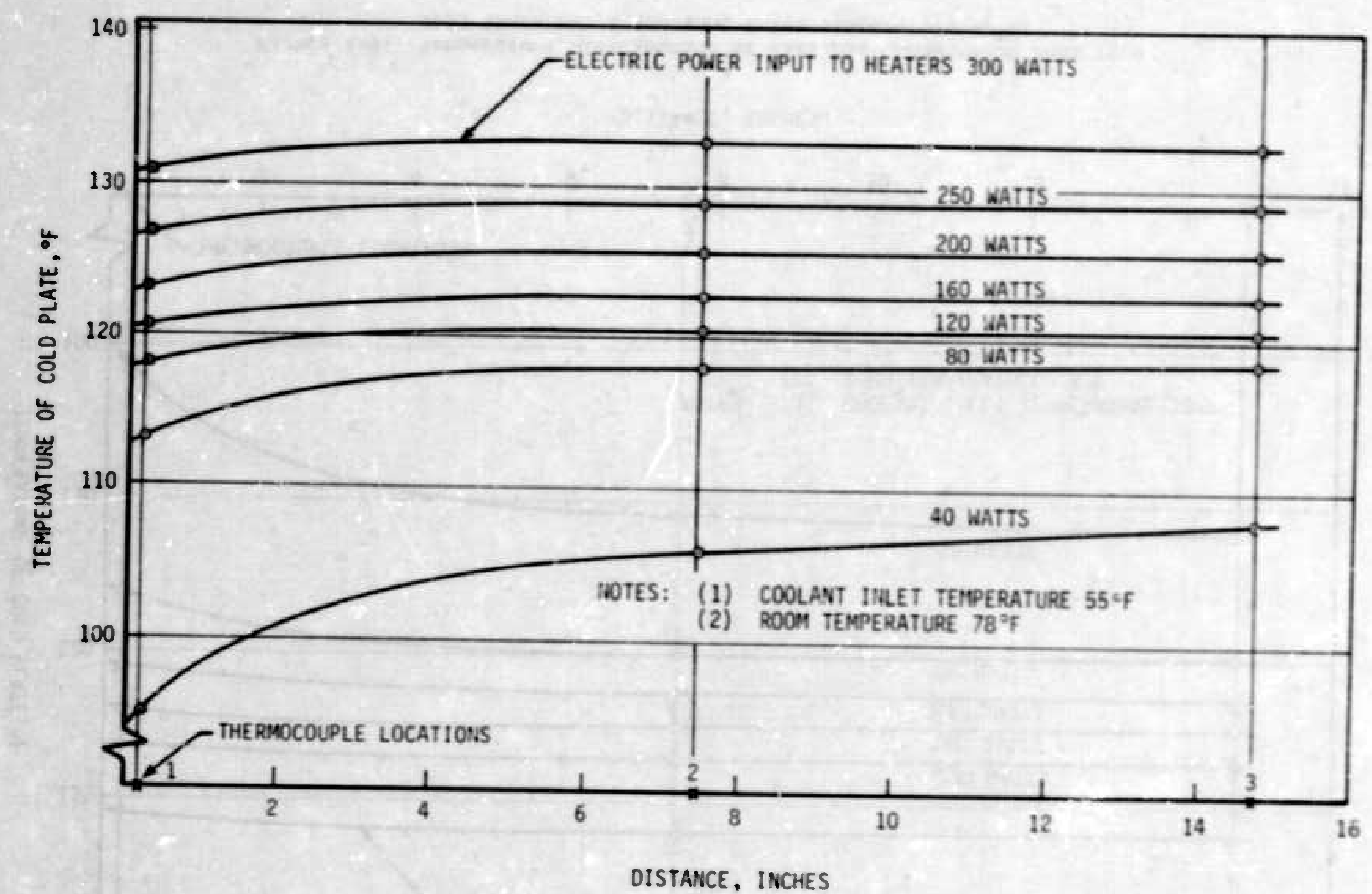

Figure 198. Temperature Distribution of Variable-Conductance Heat-Pipe Cold Plate No. 1 (Coolant Inlet Temperature 55°F)

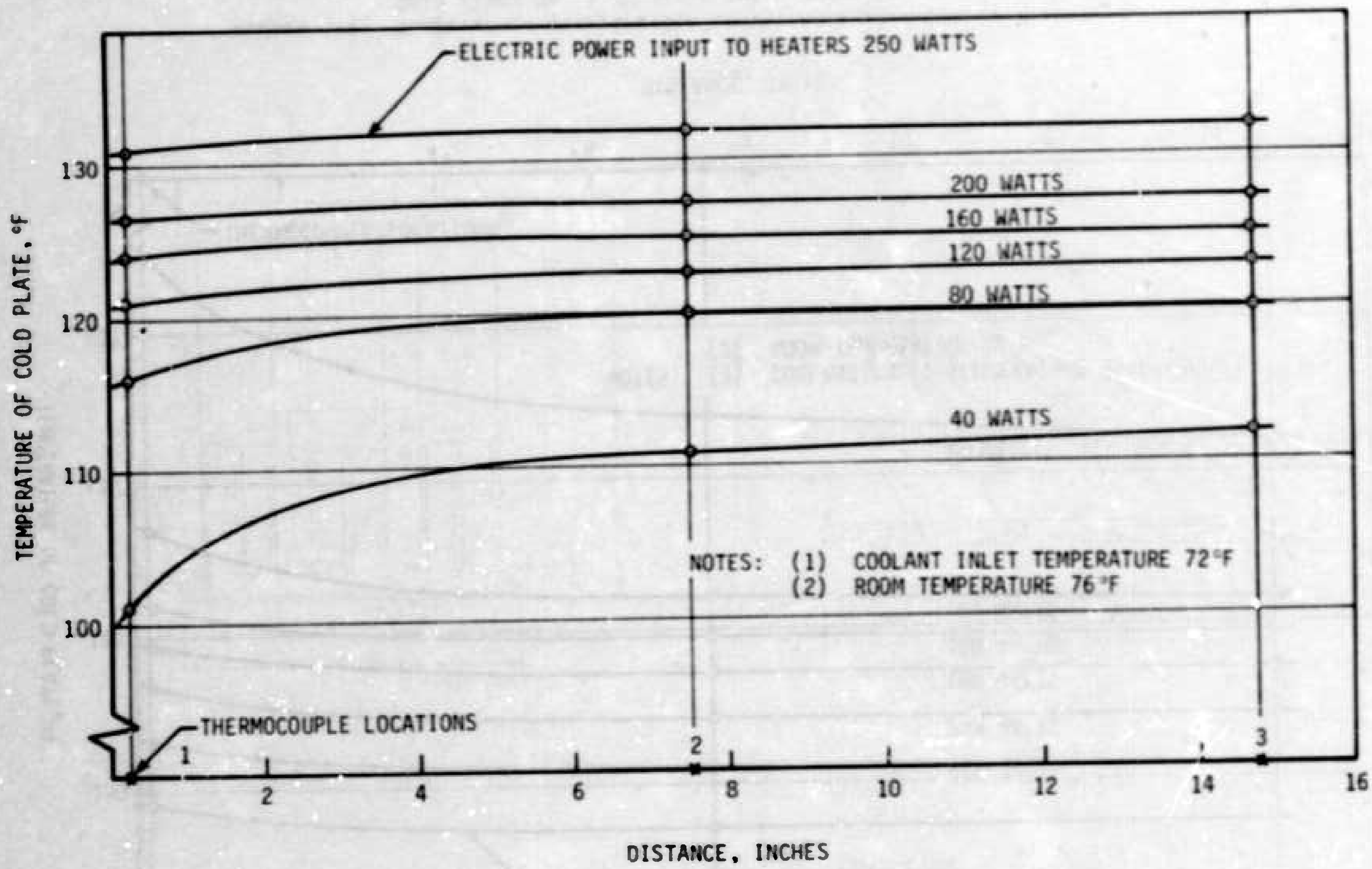

Figure 199. Temperature Distribution of Variable-Conductance Heat-Pipe Cold Plate No. 1 (Coolant Inlet Temperature 72°F)

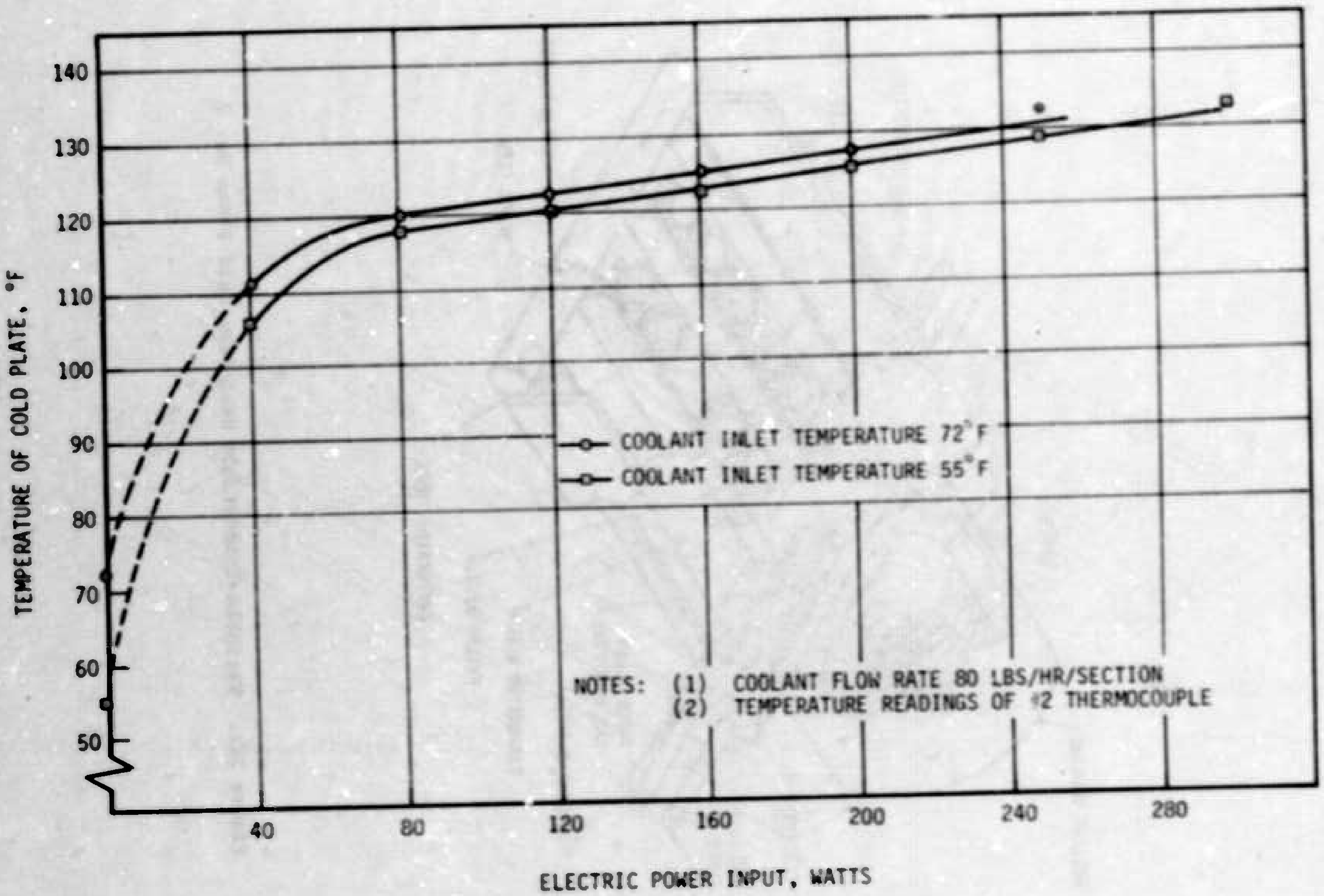

Figure 200. Temperature Changes of Variable-Conductance Heat-Pipe Cold Plate No. 1 vs Electrical Power Input Rates

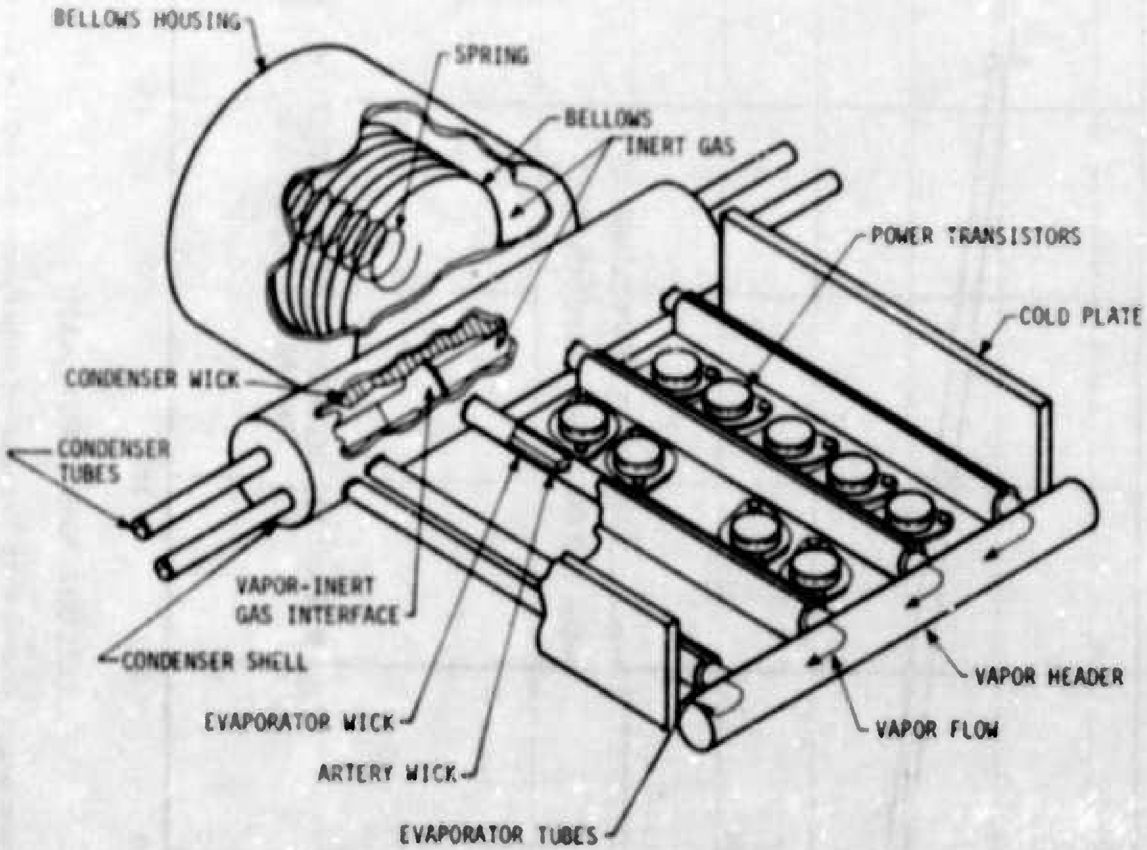

Figure 201. Variable-Conductance Heat-Pipe Cold Plate No. 2

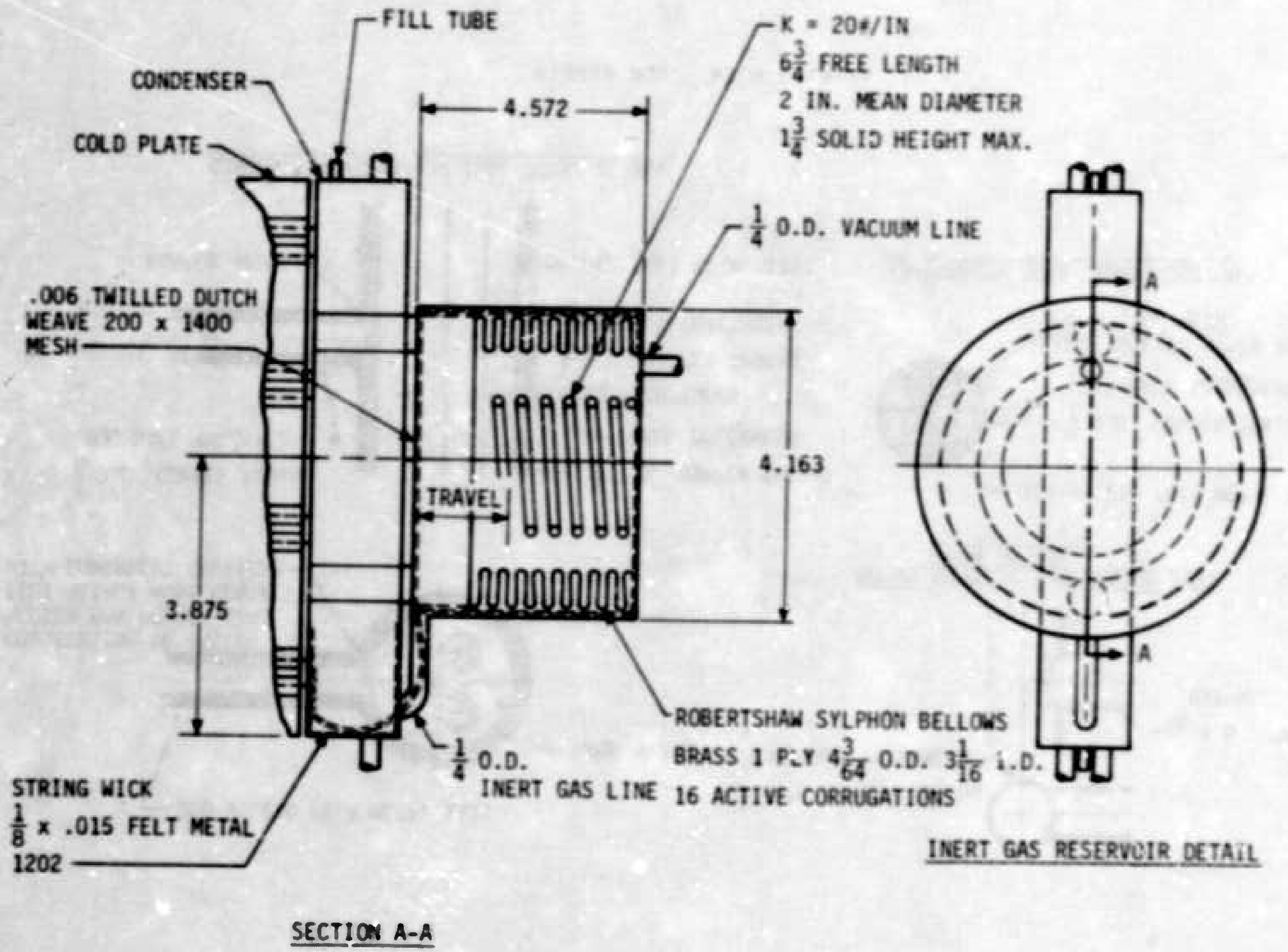

Figure 202. Inert Gas Bellows

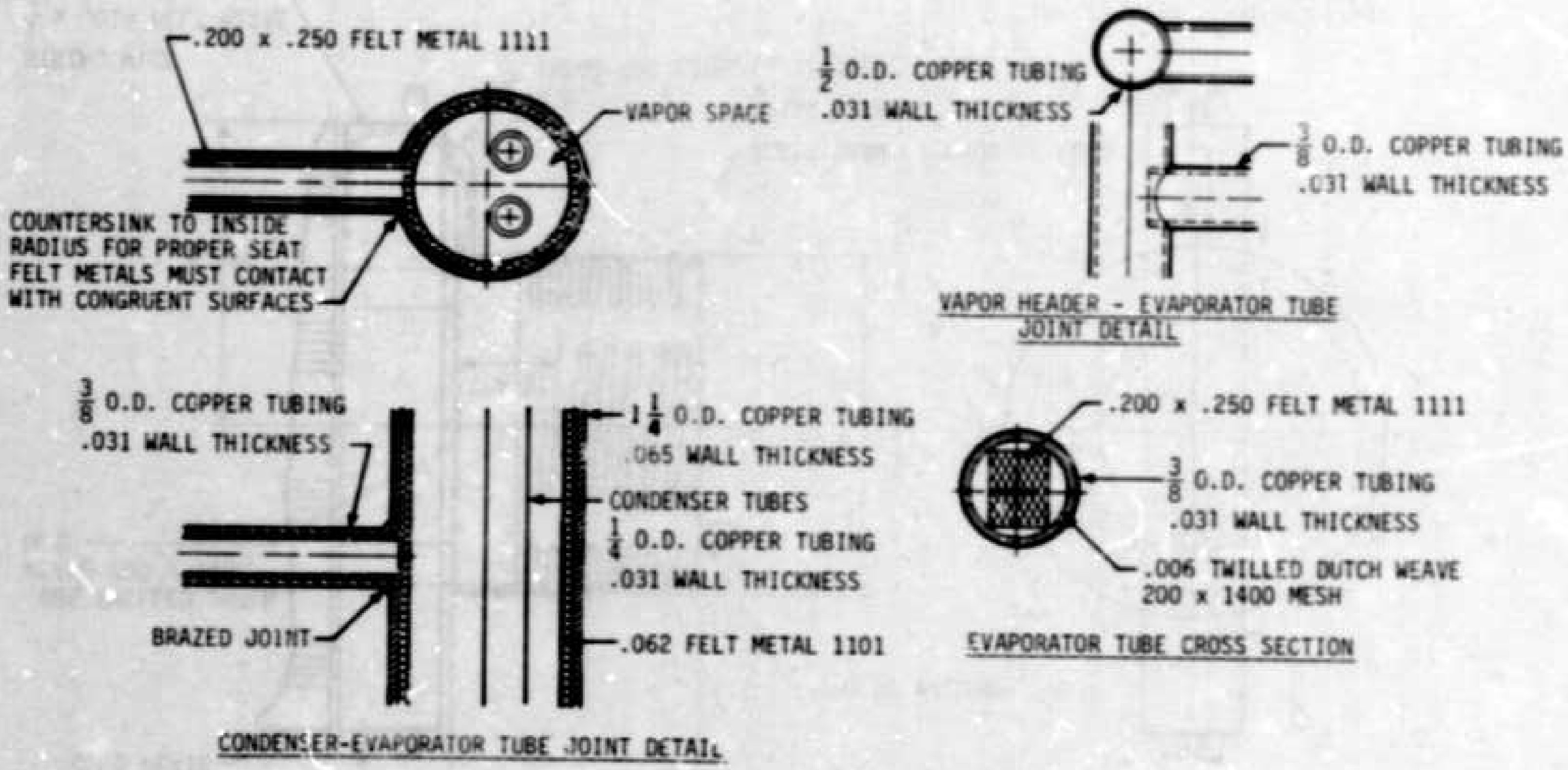

Figure 203. Wick Details

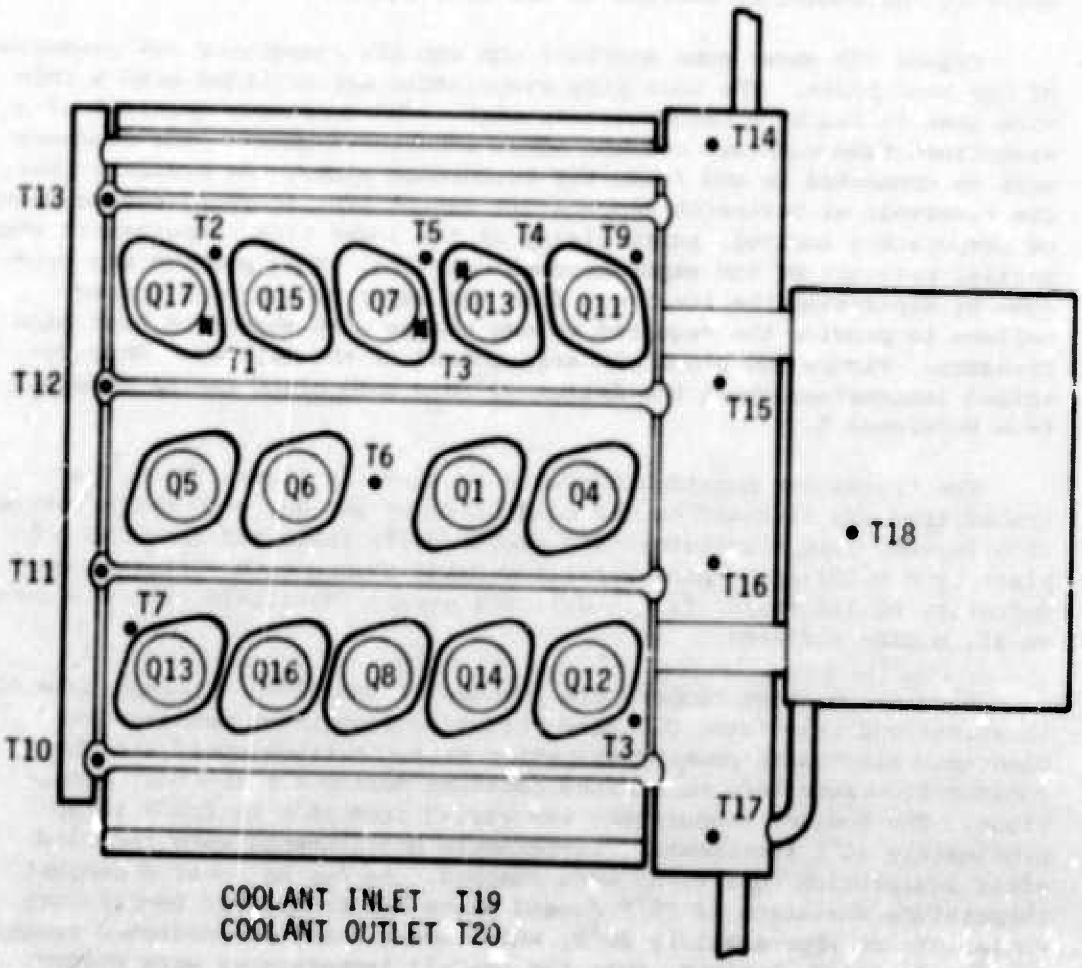

Figure 204. Transistor and Thermocouple Locations

The cold plate was designed to limit temperature change to 20°F with a change in coolant temperature from 35°F to 120°F or with a change in dissipated power from 30 watts to 120 watts. A coolant flow rate of 0.4 gal/minute of 62/38 ethylene-glycol and water solution was used for evolving the condenser section of the cold plate.

Figure 203 shows some sections through the evaporator and condenser of the heat pipes. The heat pipe evaporators are provided with a thin wick that is fed by a larger artery wick. The condenser consists of a wick-lined tube with two coolant tubes located as shown. The condenser wick is connected to and feeds the evaporator wicks. An ordinary inert gas reservoir at heat-sink temperature cannot provide an effective means of temperature control, particularly at the lower sink temperatures when partial pressure of the vapor becomes very low. This problem was overcome by separating the inert gas from the vapor by use of a spring bellows to provide the required volume change with change in heat pipe pressure. Figure 202 shows the arrangement of the bellows. More detailed information about the design of this cold plate can be obtained from Reference 5.

The transistor mounting hardware is shown in Figure 205. The transistors are fastened to the cold plate by two No. 4-40 bolts torqued to 5 in-ibs. The transistors are electrically insulated from the cold plate by a 0.064-inch-thick beryllium-oxide washer with a thermal conductivity of 140 Btu/hr ft°F. Silicone grease (Wakefield 120) was used on all mating surfaces.

Figure 206 shows temperature changes of the plate (thermocouple #2 location) and transistor Q17 case versus coolant inlet temperature changes. Electrical power dissipation from the transistors and the coolant flow rate were maintained constant during all the test conditions. The coolant temperature was varied from 35°F to 120°F in approximately 20°F increments. Temperature measurements were recorded after equilibrium conditions were reached. As can be seen, a coolant temperature variation of 85°F caused plate and transistor temperature variations of approximately 20°F, which are within the predicted range. It must be noted, however, that the overall temperatures were higher than predicted.

Figure 207 shows case temperature of transistor Q17 versus different electrical power dissipation rates from the transistors. A constant coolant flow rate of 0.4 gal/minute was maintained throughout all the test conditions with a coolant inlet temperature of 120°F. The test results show that a power dissipation rate increase from 20 watts to 120 watts (ΔQ = 100 watts) caused a temperature increase from 144°F to 163°F (Δt = 19°F).

(3) Variable-Conductance Heat-Pipe Cold Plate No. 3

Figure 208 shows variable-conductance Cold Plate No. 3 which was of similar design to Cold Plate No. 2, except for the stud-mounted high power components. These components, two high power transistors (2N3846)

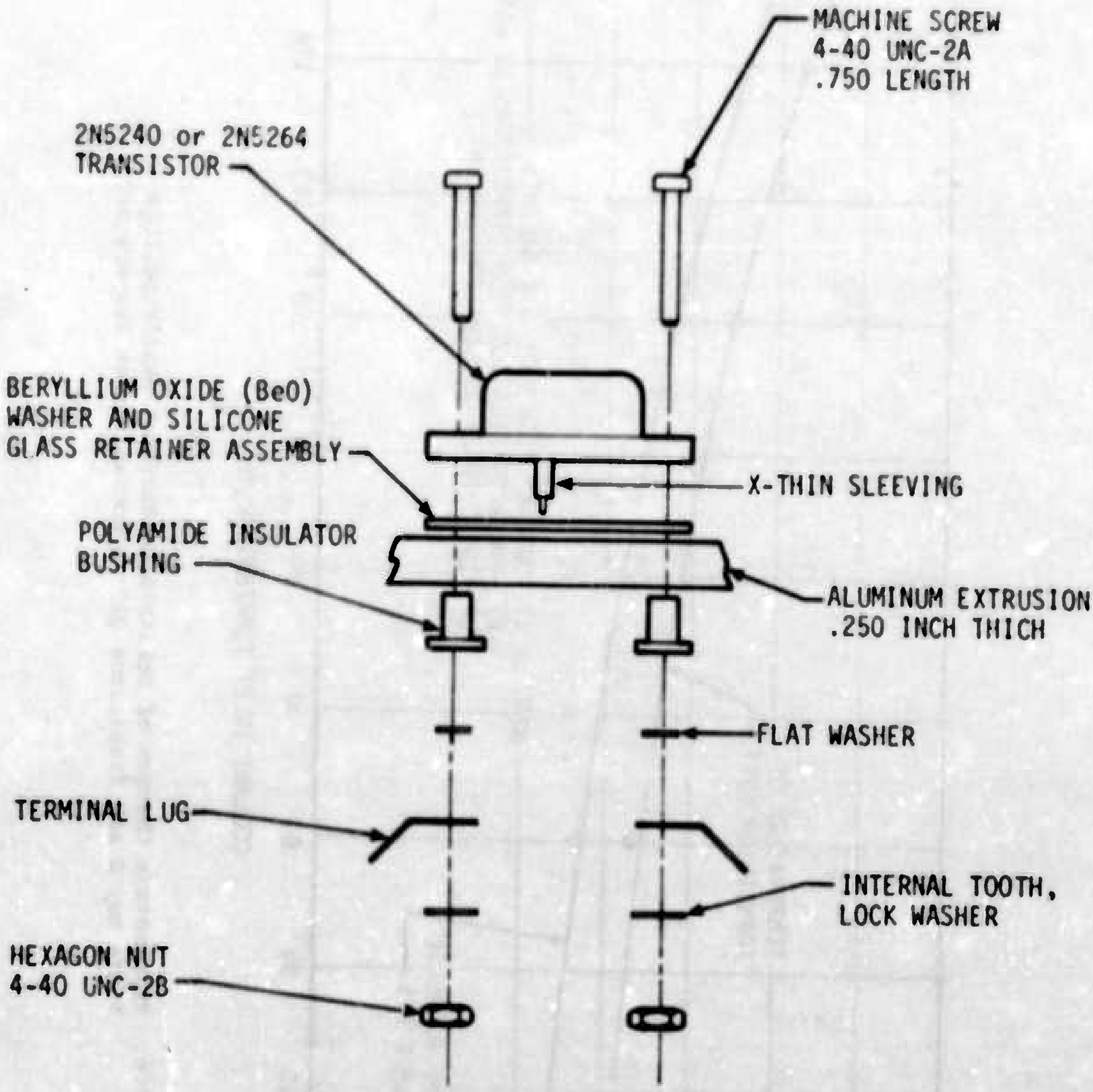

Figure 205. Transistor Mounting Detail

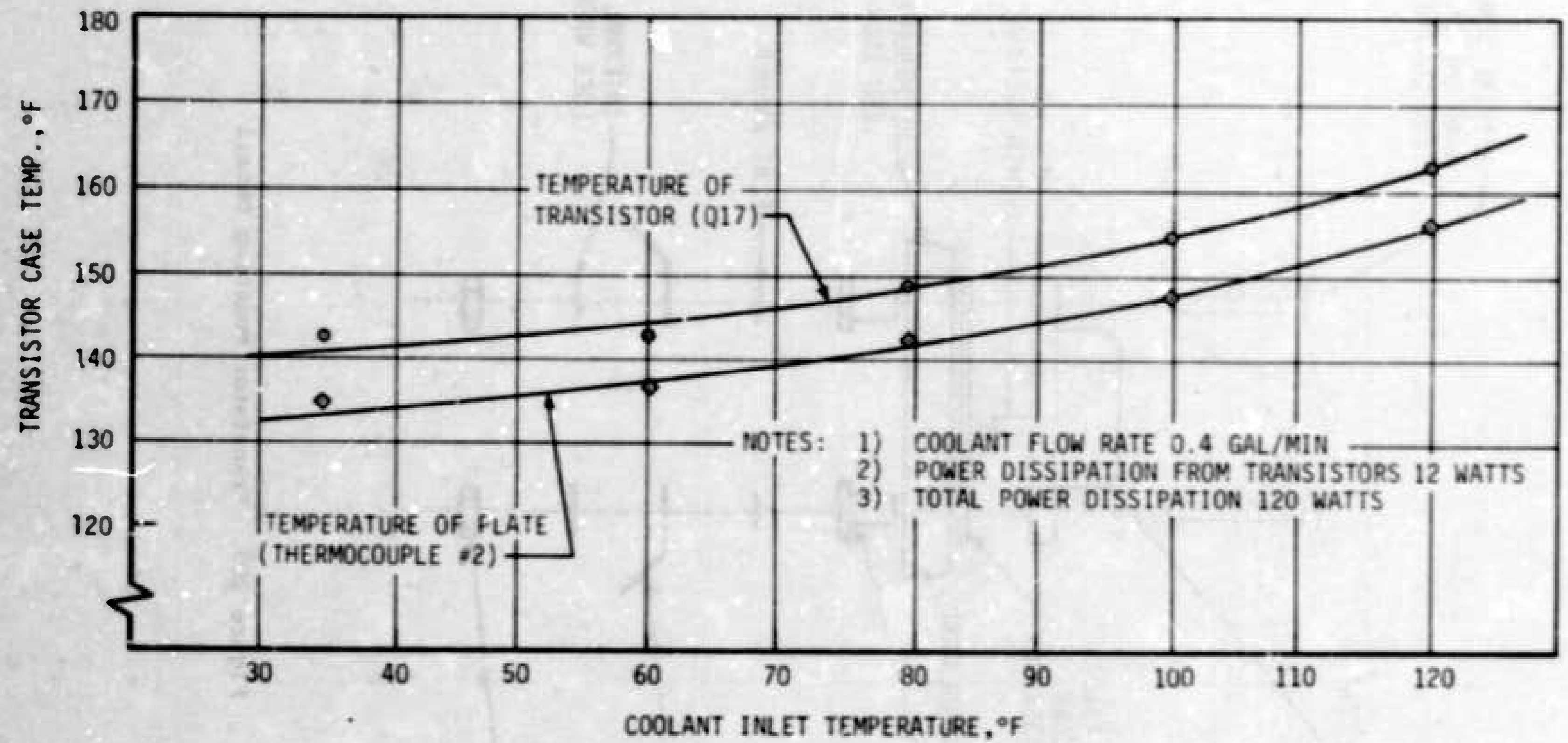

Figure 206. Temperature Changes of Variable-Conductance Heat-Pipe Cold Plate No. 2 and Transistor Q17 vs Coolant Inlet Temperature

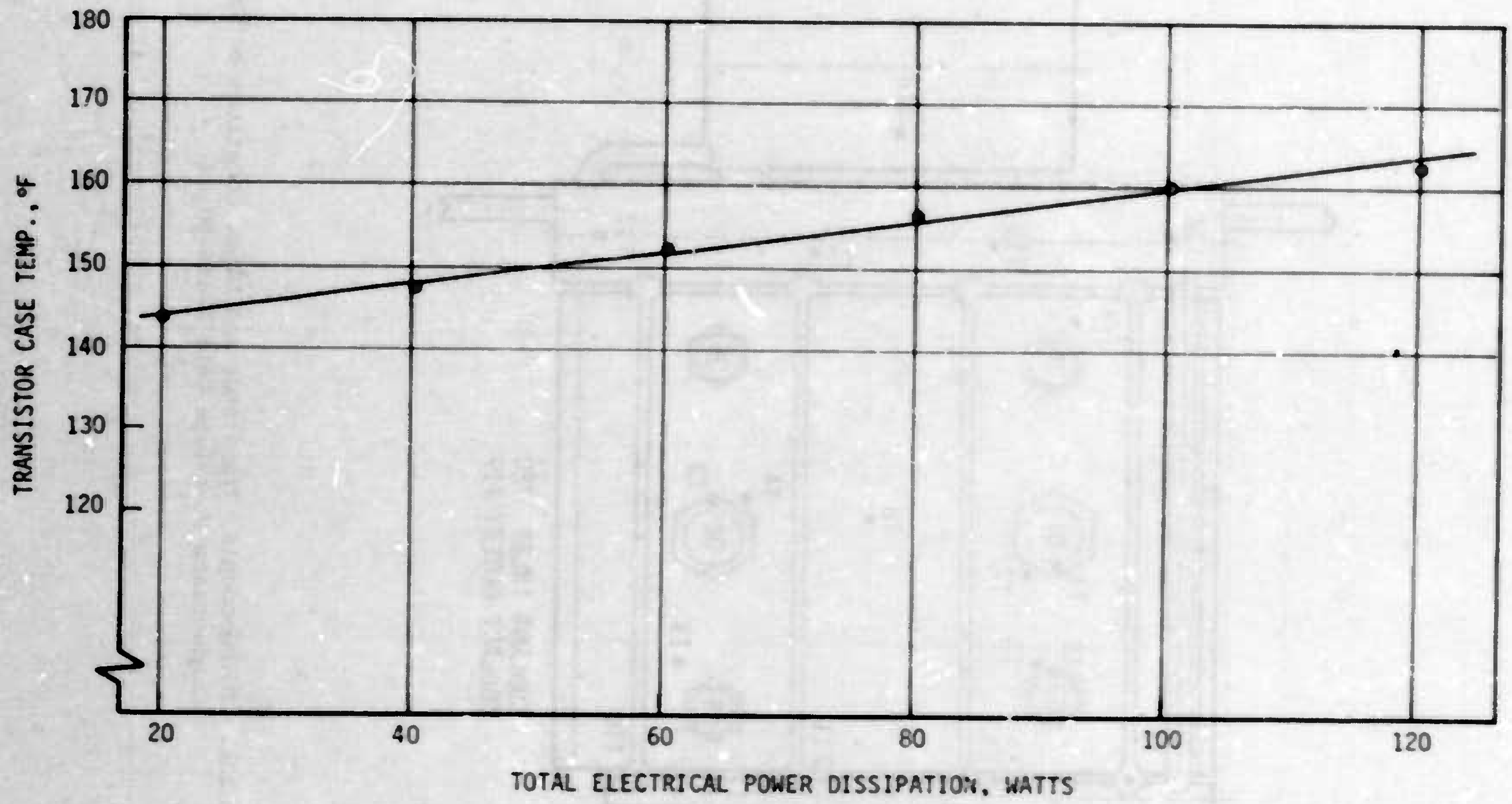

Figure 207. Case Temperature Changes of Transistor Q17 vs Electrical Power Dissipation Rate

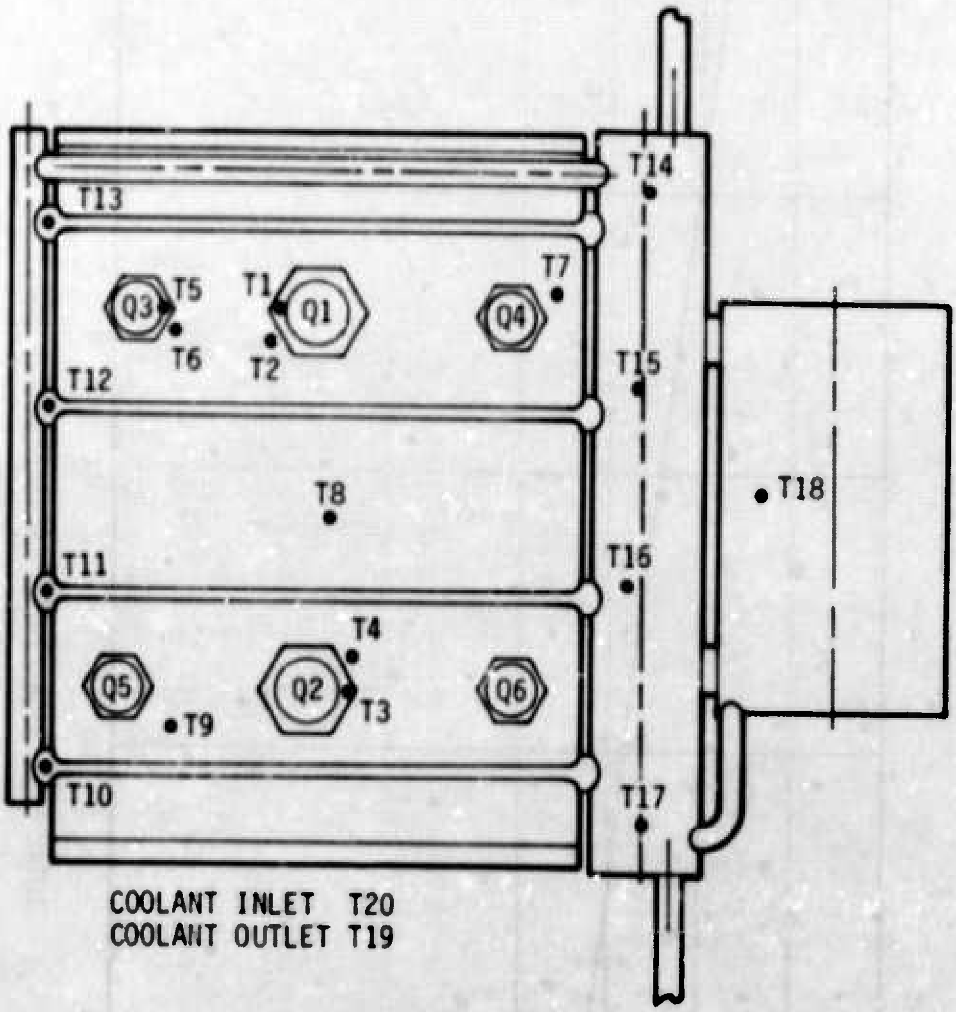

Figure 208. Thermocouple, Transistor and Diode Locations on Variable-Conductance Heat-Pipe Cold Plate No. 3

and four diodes (1N3885), were selected to investigate effects of concentrated heat loads. One of the transistors was bolted directly to the cold plate, while the other was provided with a 0.031-inch-thick beryllia washer for electrical isolation. Thermal compound (Wakefield 120) was used on all interfaces. The power transistor 5/16-24 studs were torqued to 160 in-lbs; the diode 10-32 studs were torqued to 30 in-lbs. The diodes were mounted directly to the cold plate with the thermal compound used on all mounting joints.

Thermal performance of the cold plate was investigated under conditions of variable coolant temperatures and variable electrical power dissipation rates from the components.

Figure 209 shows temperature changes of the cold plate (thermocouple #2 location) and transistor Q1 case versus coolant inlet temperature changes from 35°F to 120°F. A constant coolant flow rate of 0.4 gal/minute was maintained throughout the tests. Also, the electrical power dissipation rate of 120 watts was maintained constant; the power dissipation rate from the transistor was 40 watts. A coolant temperature increase from 35°F to 120°F (Δt = 85°F) caused the plate and transistor case temperature to increase 26°F, which is 6°F higher than results obtained from Cold Plate No. 2 tested at similar conditions.

Figure 210 shows temperature changes of the cold plate and transistor Q1 case as a function of electrical power dissipation rates from the components. There was no power input to transistor Q1 at Test Condition 1; 20 watts were applied at Test Condition 2 and 40 watts at Test Conditions 3 and 4. A constant coolant flow rate of 0.4 gal/minute and an inlet temperature of 120°F were maintained throughout the tests.

Figure 211 shows the cold-plate temperature and case temperature of transistors Q1 and Q2 as a function of different electrical power dissipation rates from the transistors. It must be noted that only one of the transistors was energized at any one time. While the temperature of the cold plate increased from 142°F to 169°F (Δt = 27°F), the case temperature of transistor Q1 increased from 146°F to 196°F (Δt = 50°F) when the transistor electric power dissipation rate was increased from 20 watts to 100 watts.

Similar tests were also performed with transistor Q2 which was mounted to the cold plate with a 0.031-inch beryllia washer. Because of the high mounting joint thermal resistance, the rate of temperature increase was much higher. The test results show that maintaining the heat-sink temperature at a constant level does not provide a satisfactory control for equipment having high mounting-joint thermal resistance and for significant changes in power dissipation rates.

4. Circuit Card Heat Pipe

A thin, flat circuit-card heat pipe was developed under a study described in Reference 5. The circuit-card heat pipe was designed for a total heat load of 24 watts, consisting of twelve 1.2-inch x 1.0-inch

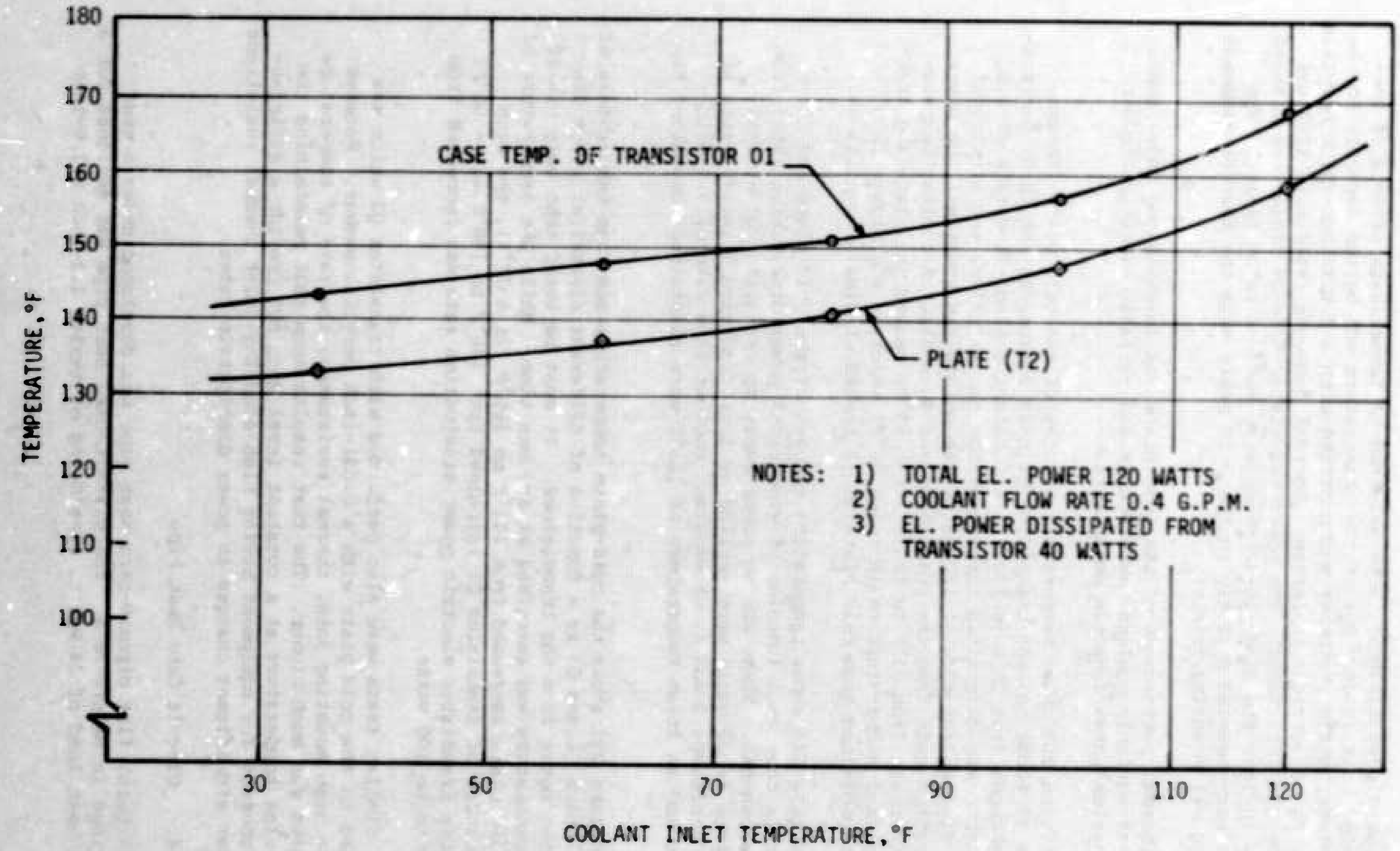

Figure 209. Temperature Changes of Variable-Conductance Heat-Pipe Cold Plate No. 3 and Transistor vs Coolant Inlet Temperature

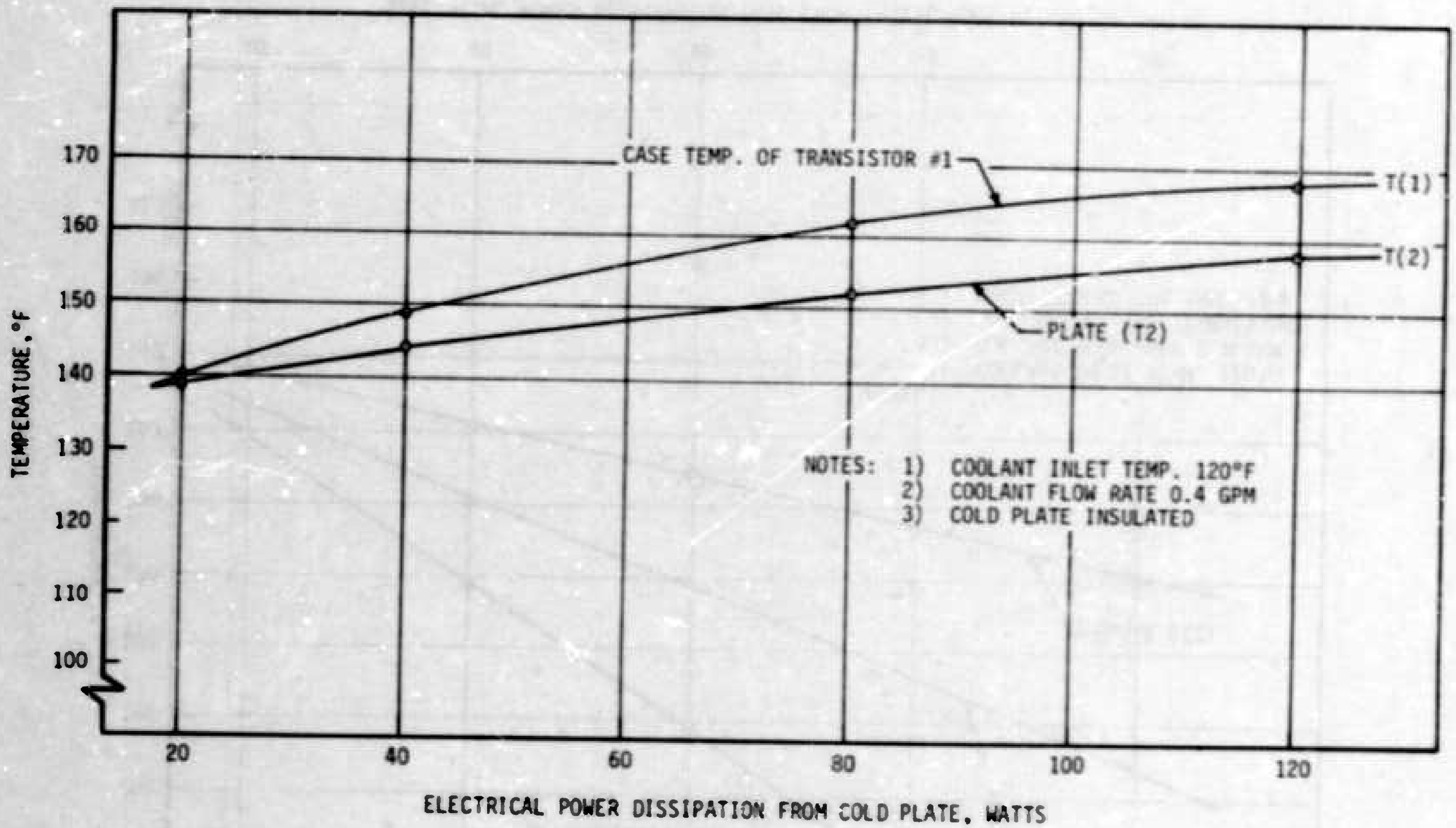

Figure 210. Temperature Changes of Variable-Conductance Heat-Pipe Cold Plate No. 3 and Transistor Q21 vs Electrical Power Dissipation Rate

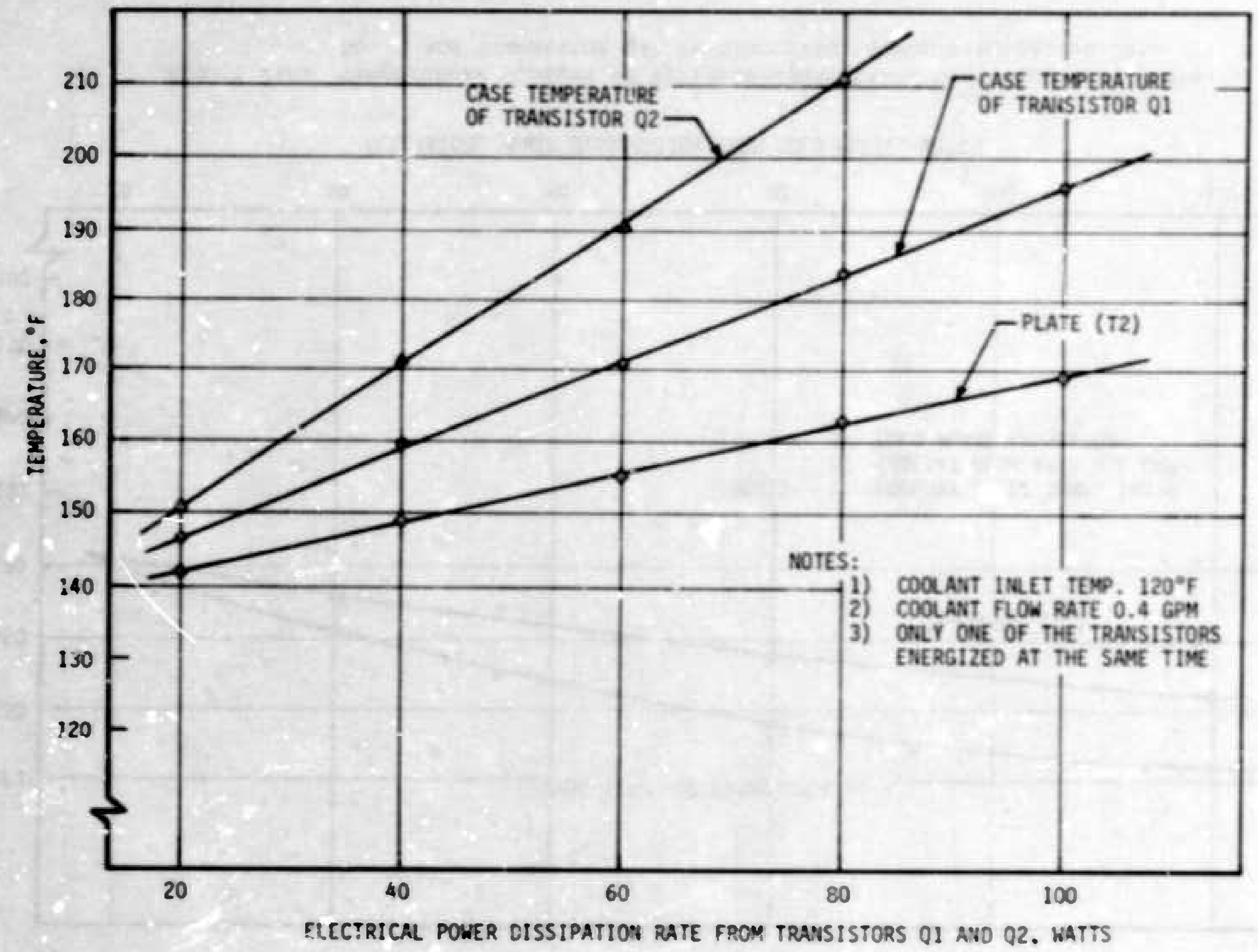

Figure 211. Case Temperature of Transistors Q1 and Q2 vs Electrical Power Dissipation Rate

hybrid circuit packages which were bonded to the card. Each of the packages dissipated 2 watts. Figure 212 shows the outline of the circuit-card heat pipe made of beryllium copper. The wick is composed of a single layer of 200 x 1400-mesh twilled-dutch-weave nickel screen in combination with a stainless-steel felt-metal artery wick. Methanol was used as the working fluid.

Figure 213 shows the circuit card with the hybrid circuit packages, Figure 214 shows wedge clamps of the circuit card. The circuit card was installed vertically with heat sinks at both ends of the card. Coolant tubes were attached to the card slot fixture.

Thermal tests of the circuit card were performed at card slot temperatures of 50°F and 140°F. At the card slot temperature of 50°F, the heat pipe appeared to be practically non-operative, showing a large temperature differential along the length of the card. However, when the card slot temperature was increased to 140°F, temperature of the card was almost uniform. The poor performance at the low condensor temperature can be explained by some non-condensible gas left in the cavity or by sonic flow problems at the low vapor pressure. At low heat-sink temperatures, a working fluid with lower boiling temperature could be selected.

Figure 215 shows temperature distribution of the circuit card at a card-slot temperature of 140°F. A temperature difference of approximately 4°F occurs between the central section and edges of the card. Even a solid copper card of similar thickness could not achieve such a temperature uniformity.

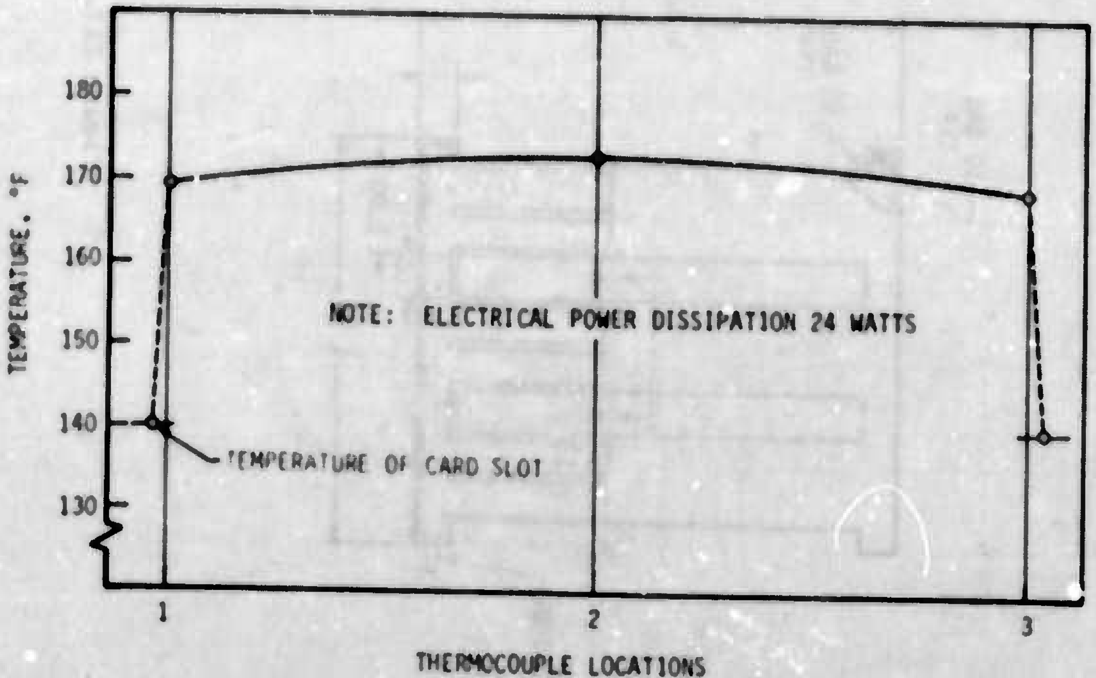

Figure 215. Temperature Distribution of Circuit Card

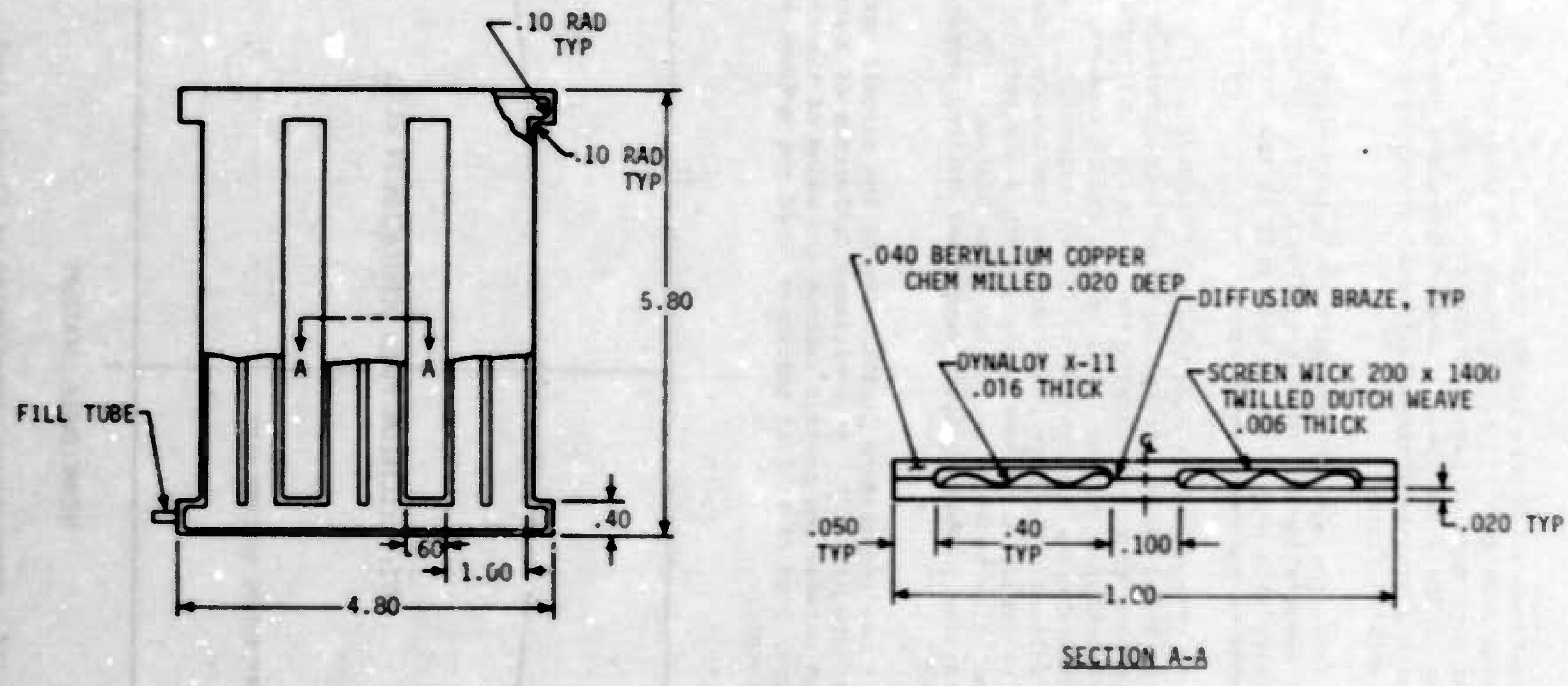

Figure 212. Circuit-Card Heat-Pipe

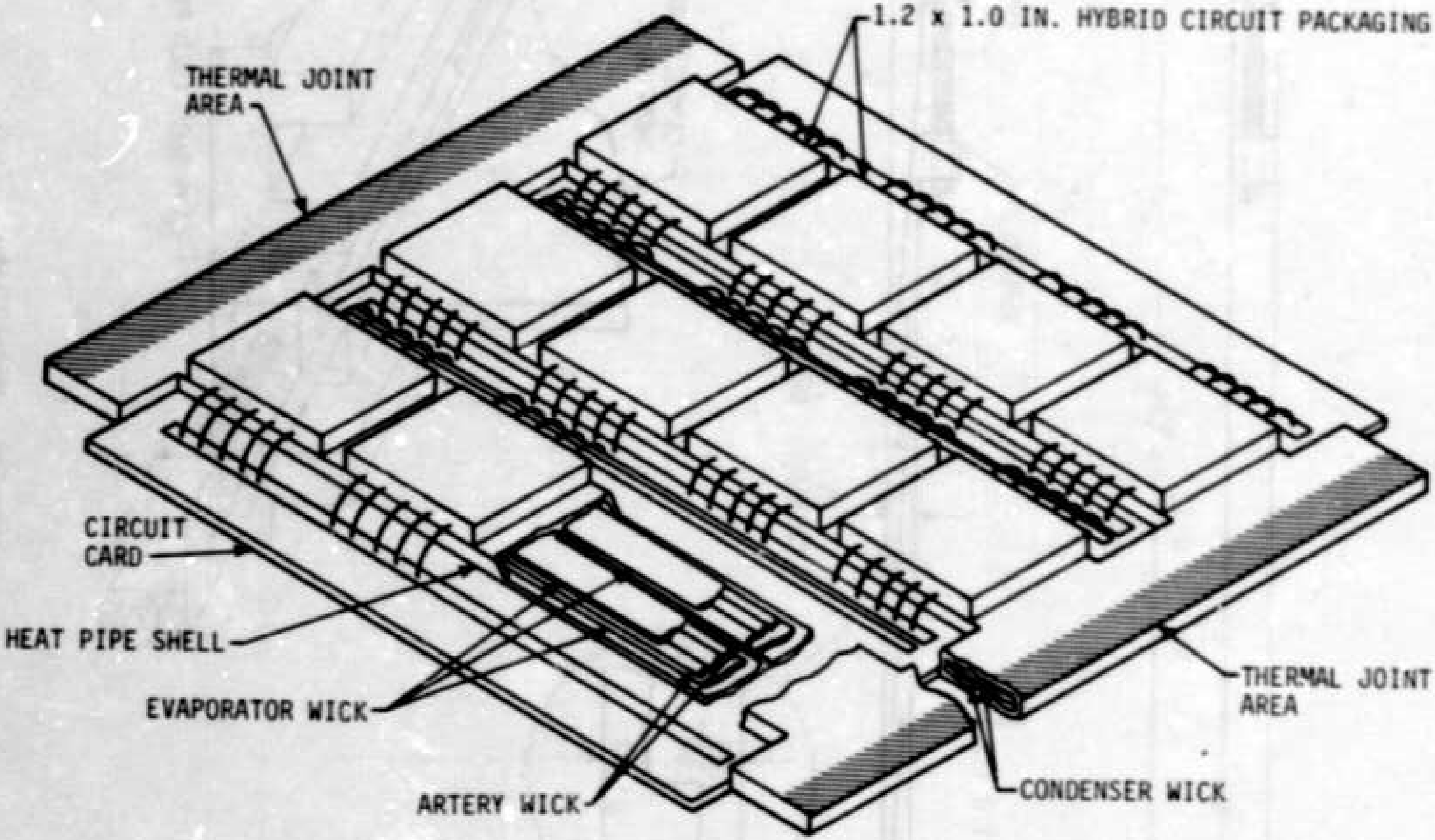

Figure 213. Circuit-Card Heat-Pipe with Hybrid Circuit Packages

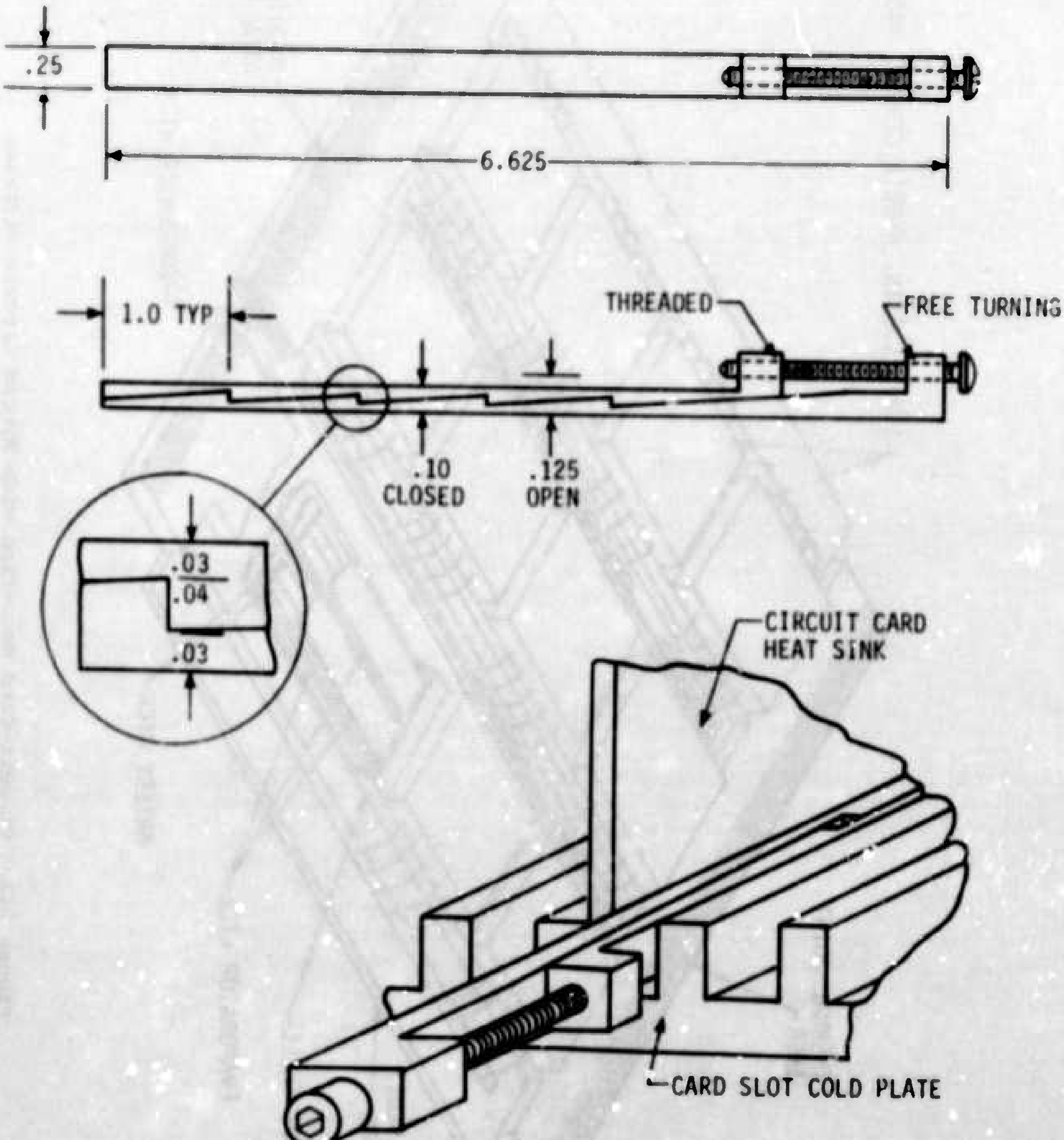

Figure 214. Wedge Clamp

The temperature drop across the clamping device appeared to be too high, and some improvements are required for the high-power circuit cards.

5. Thermal Performance Characteristics of Cold Plates Provided with Heat Pipes

Because of the different configurations and equipment mounting arrangements, no direct comparison of the thermal performance among the cold plates is possible; only some of the thermal performance characteristics, therefore, are discussed.

Cold Plates Nos. 1 and 2, which were generally of similar design, showed quite significant temperature gradients within the equipment mounting surfaces and at the condenser section. Besides the uniform temperature along the heat pipe axis, there is no advantage in using heat pipes instead of simple liquid flow passages.

Cold Plate No. 3 showed significant improvement in reducing temperature gradients within the equipment mounting surface. The main advantage of such a cold plate is temperature uniformity across the whole equipment-mounting surface area. Electronic equipment mounted on such a cold plate will have almost uniform temperatures regardless of the power dissipation rates. This condition is becoming a requirement in microelectronic systems. There was a noticeable temperature drop at the condenser section because of the small convection heat-transfer surface area. This is a general problem in applications of heat pipes.

Great advantages can be gained by using heat pipes in cold plates provided with heat-of-fusion materials or evaporative coolants. Even though the heat-absorbing materials are located outside the cold plate, heat, generated by the distant components, is transferred to the heat sink with a very small temperature gradient.

The use of variable-conductance heat pipes for temperature control of special electronic equipment is presently finding wide application in space flight. The use of heat pipes in avionics equipment cooling is generally hampered by the effects of dynamic and gravity forces. It is anticipated, however, that with special precautions and design procedures these problems can be solved and the unique characteristics of the heat pipes will find wider applications in avionics equipment cooling.

REFERENCES

1. J. T. Pogson and J. L. Franklin, "Analysis and Temperature Control of Hybrid Microcircuits," ASME Paper No. 73-ENAS-6, August 1973.

2. W. F. Hilbert and F. H. Kube, "Effects on Electronic Equipment Reliability of Temperature Cycling in Equipment," Grumman Aircraft Engineering Corporation, Report EC-69-400, February 1969.

3. D. M. Cawthon and J. I. Gonzalez, "Effects of Aircraft Environmental Thermal Transients on Component Part Thermal and Electrical Parameters," Martin Marietta Corporation, Report OR 10, 164, December 1969.

4. J. H. Seely and R. C. Chu, "Heat Transfer in Microelectronic Equipment," Marcel Dekker, Inc., New York, 1970.

5. R. J. Gimetti, M. A. Merrigan and L. A. Nelson, "Thermal Control of Airborne Electronic Equipment," AFFDL-TR-73-12, June 1973.

6. R. Haumesser, J. B. Coleman, R. Child and J. Welsh, "Reliability and Design Handbook, Thermal Applications," NAVELEX Publication No. 0967-437-7010, July 1973.

7. RADC-TR-60-22, "Methods of Cooling Semiconductor Devices."

8. Charles A. Harper, Editor, "Handbook of Electronic Packaging," McGraw-Hill Book Co., New York.

9. W. M. Kays, "Convection Heat Transfer," McGraw-Hill Book Company, New York.

10. Edited by Warren M. Rohsenow and James P. Hartnett, "Handbook of Heat Transfer," McGraw-Hill Book Company, New York.

11. W. M. Rohsenow and H. Y. Choi, "Heat Mass and Momentum Transfer," Prentice-Hall, Inc., Englewood Cliffs, N. J.

12. E. N. Sieder and G. E. Tate, Ind. Eng. Chem., 28: 1429 (1936).

13. Warren H. Giedt, "Principles of Engineering Heat Transfer," D. Van Nostrand Company, Inc., New York, 1959.

14. R. Haumesser, J. B. Coleman, R. Child and J. Welsh, "Reliability/Design Handbook, Thermal Applications," NAVELEX Publication No. 0967-437-7010, July 1973.

15. D. Q. Kern and A. D. Kraus, "Extended Surface Heat Transfer," McGraw-Hill Book Company, New York.

16. L. F. Kilham, R. R. Ursch & J. F. Ahern, Electrical Manufacturing, August, 1959.

REFERENCES (CONT'D)

17. J. L. Haws, F. A. Richards and D. E. Yakel, "Thermal Control of Airborne Phased Array Systems," AFFDL-TR-73-44, November 1973.

18. S. W. Coffman, et al, "Advanced Heat Transfer Fluids," WADD-TR-61-186, April 1962, Hughes Aircraft Company.

19. B. G. Helenbrook and F. M. Anthony, "Development of Liquid Cooling Techniques for Advanced Airborne Electronic Equipment," AFFDL-TR-71-129, March 1972.

20. J. E. Fontenot, "Thermal Conductance of Contacts and Joints," Boeing Document No. D5-12206.

21. C. A. Whitehurst, "The Thermal Conductance of Bolted Joints" NASA CR 94738, May 1968.

22. M. F. Spotts, "Design of Machine Elements," Prentice-Hall, Inc., New York.

23. K. G. Lindh, et al, "Studies on Heat Transfer in Aircraft Structure Joints," University of California Report No. 57-50, May 1957.

24. T. N. Centinkale and M. Fishenden, "Thermal Conductance of Metal Surfaces in Contact," General Discussion on Heat Transfer, IME and ASME, 1951, pp. 271-294.

25. G. M. Dusinberre, "Heat Transfer Calculations by Finite Differences," International Textbook Company, Scranton, Pennsylvania 1961.

26. A. D. Kraus, "Extended Surfaces," Spartan Books, Inc., Baltimore, Maryland 1964.

27. W. M. Kays and A. L. London, "Compact Heat Exchangers," McGraw-Hill Book Company, New York.

28. E. R. G. Eckert and Robert M. Drake, "Analysis of Heat and Mass Transfer," McGraw-Hill Book Company, New York.

29. Ronald S. Woodard, Paul J. Kendall and Karl W. Fagin, "Cooling Systems Studies for Neodymium Doped Glass and Yag Lasers," AFFDL-TR-70-8, March 1970.

30. T. P. Cotter, "Theory of Heat Pipes," Los Alamos Scientific Laboratory Report LA-3246-MS, Los Alamos, New Mexico, February 1965.

31. W. D. Allingham and J. A. McEntire, "Determination of Boiling Film Coefficient for a Heater Horizontal Tube in Water-Saturated Wick Material," ASME Paper No. 60-HT-11, September 1960.

32. R. S. Gill, "Pool Boiling in the Presence of Capillary Wicking Materials," M.S. Thesis, Massachusetts Institute of Technology, August 1967.

REFERENCES (CONCLUDED)

33. H. R. Kunz et al, "Vapor-Chamber Fin Studies," NASA CR-812, June 1967.

34. A. E. Bergles et al, "Cooling of High Power Density Computer Components," MIT, Report DSR-70712-60, November 1968.

35. V. Ash, "A Survey of Liquid Boiling Phenomena, Their Prediction and Analysis," IEEE Transactions, March 1963.

36. B. C. Marcus, "Theory and Design of Variable Conductance Heat Pipes."

37. NASA-CR-65581, "Thermal Analyzer Computer Program for the Solution of General Heat Transfer Problems," NASA Manned Spacecraft Center, Houston, Texas.

38. J. D. Keller, "Flow Distribution in Manifolds," Journal of Applied Mechanics, March 1949.

39. C. J. Feldmanis, "Application of Integral Air-Cooled Cold Plates," AFFDL-TR-73-156, Air Force Flight Dynamics Laboratory.

40. Carl J. Feldmanis, "Application of Cold Plates to Electronic Equipment Cooling," AFFDL-TR-72-128, Air Force Flight Dynamics Laboratory, November 1972.

APPENDIX A

TEST DATA

Table A-1. Test Data of Liquid-Cooled Cold Plate No. 1

THERMO-COUPLE NO.	TEMPERATURE, °F		
	TEST COND #1	TEST COND #2	TEST COND #3
1	70	70	71
2	72	74	78
3	115	165	210
4	122	172	220
5	79	90	93.5
6	75.5	80	88
7	77	86	92
8	76	81.5	87
9	78	87	97
10	75.5	81.5	88
11	77	87.5	95
12	77	85	90
13	77	84	90
14	83.5	98.5	114
15	87	102	117
16	78	83	90
17	76	80	85
18	76	82	88.5
19	80	33	85
20	77	88	96
21	78	83	86
22	76	88	94
23	75	82	86
24	77	83	89
25	74	79	85
26	81	88	101
27	80	90	96
28	76	80	85
29	78	92	103
30	80	90	96
31	80	90	98
32	78	89	97
33	78	88	96
34	78	88	96
35	78	91	98

Table A-1. Test Data of Liquid-Cooled Cold Plate No. 1 (Cont)

THERMO COUPLE NO.	TEMPERATURE, °F		
	TEST COND #4	TEST COND #5	TEST COND #6
1	72	72	72
2	76	78	80
3	90	94	100
4	87	91	98
5	123	150	180
6	125	155	181
7	130	159	187
8	132	161	190
9	208	216	225
10	87	94	100
11	87	94	99.5
12	83	88.5	94
13	84	90.5	96.5
14	90.5	96	102
15	86.5	90	96
16	93.5	101	110
17	92	102	110
18	93	99	107
19	94	101	110.5
20	120	126	130
21	90	94	98
22	91	95	101
23	83	90	95
24	82	92	97
25	87	91	97
26	89	94	100
27	90	95	102
28	86	92	100
29	88	91.5	97
30	84	91	96
31	82	90	94
32	85	90	95
33	88	92	99
34	93	97	103
35	101	106	112

Table A-1. Test Data of Liquid-Cooled Cold Plate No. 1 (Cont)

THERMO-COUPLE NO.	TEMPERATURE, °F		
	TEST COND #7	TEST COND #8	TEST COND #9
1	72	73	74
2	81	86	88
3	138	190	200
4	143	191	199
5	141	177	200
6	145	186	218
7	140	185	210
8	148	186	215
9	230	245	248
10	132	145	150
11	132.5	147	152.5
12	114	126	131
13	116	131	138
14	110	129	136
15	110	129	134
16	106	122	133
17	108.5	124	129
18	106.5	120	127.5
19	106	126	133
20	143	156	160
21	120	133	139
22	124.5	137	143
23	102	115	120
24	105	118	123
25	97	108	115
26	107	123	129
27	106	121	127
28	97	110	117
29	105	120	126
30	106	118	125
31	101	114	119
32	103	117	121
33	108	120	127
34	109		129
35	122	136	140

Table A-1. Test Data of Liquid-Cooled Cold Plate No. 1 (Cont)

THERMO-COUPLE NO.	TEMPERATURE, °F		
	TEST COND #10	TEST COND #11	TEST COND #12
1	66	74	78
2	93	88	84
3	206	200	181
4	207	194	179
5	200	189	180
6	200	191	181
7	200	190	179
8	201	187	178
9	239	229	218
10	156	151	141
11	158	152	143
12	144	131	121
13	146	138	126
14	144	135	123
15	143	131	119
16	136	126	116
17	126	117	107
18	138	127	115
19	136	117	107
20	174	164	154
21	146	139	127
22	150	141	132
23	136	116	106
24	132	121	110
25	121	113	103
26	139	128	117
27	136	127	115
28	125	117	106
29	137	126	113
30	136	125	113
31	135	119	107
32	132	119	107
33	135	127	116
34	134	125	115
35	147	140	127

Table A-2. Test Data of Liquid-Cooled Cold Plate No. 2

THERMO-COUPLE NO.	TEMPERATURE, °F		
	TEST COND #1	TEST COND #2	TEST COND #3
1	66	66	66
2	68	70	73
3	110	157	197
4	111	156	196
5	69	73	78
6	73	78.5	84.5
7	73	78	84
8	73	77	81.5
9	72	75.5	81
10	72	76	82.5
11	72	77	81
12	73	79	86
13	82	97	112
14	84	100	115.5
15	71	74	78
16	74	79	85.5
17	72	76	82.5
18	72	77	81.5
19	72	76	80
20	72	76	81
21	73	76.5	81
22	72	78	85
23	70	72	75
24	71	75	80
25	74	80	87
26	72	79	85
27	73	76	80
28	72	76	79
29	75	84	94
30	73	78	84
31	70	74	78
32	77	86	96
33	74	80	88
34	76	84	91
35	74	88	88
36	74		88

NOTE: ONLY TRANSISTORS #1 & 2 ENERGIZED

Table A-2. Test Data of Liquid-Cooled Cold Plate No. 2 (Cont)

THERMO-COUPLE NO.	TEMPERATURE, °F		
	TEST COND #4	TEST COND #5	TEST COND #6
1	69	70	70
2	73	73	77
3	78	82	85
4	80	82	87.5
5	131	164	189
6	142	171	202
7	133	161	185
8	121	155	182
9	78	82	85
10	81	86	91
11	88	93	99
12	90	95	98
13	79	83	87
14	72	82	86
15	92	101.5	109
16	88	95.5	103
17	91	100	108
18	90	103	113
19	78	82	84
20	81	85	90
21	83	88	93
22	80	85	89
23	81	85	89
24	83	88	94
25	76	80	82
26	76	80	83
27	82	90	94
28	86	94	101
29	78	82	86
30	80	87	91
31	84	94	100
32	80	82	88
33	82	90	96
34	78	80	86
35	78	82	87
36	78	82	87

NOTE: ONLY TRANSISTORS #3, 4, 5 & 6 ENERGIZED

Table A-2. Test Data of Liquid-Cooled Cold Plate No. 2 (Cont)

THERMO-COUPLE NO.	TEMPERATURE, °F		
	TEST COND #7	TEST COND #8	TEST COND #9
1	70	70	74
2	78	82	89
3	128	176	223
4	124	173	220
5	141	183	218
6	151	184	222
7	142	174	209
8	133	162	197
9	120	129	137
10	115	124	135
11	114	125	135
12	112	123	134
13	99.5	118	137
14	99	119.5	138
15	99	116	130
16	99	113	127
17	100	118	131
18	100	115	131
19	95	104	115
20	99	108	122
21	99	111	124
22	99	109	120
23	90	100	117
24	90	99	114
25	92	104	116
26	92	104	118
27	96	104	119
28	96	108	121
29	94	108	125
30	96	108	121
31	93	104	116
32	94	106	118
33	88.5	97	106
34	91	101	113

NOTE: ALL COMPONENTS ENERGIZED

Table A-2. Test Data of Liquid-Cooled Cold Plate No. 2 (Cont)

THERMO-COUPLE NO.	TEMPERATURE, °F		
	TEST COND #10	TEST COND #11	TEST COND #12
1	69	74	76
2	95	87	83
3	197	183	172
4	192	179	170
5	222	215	207
6	244	237	227
7	226	209	200
8	214	200	189
9	136	127	114
10	136	123	114
11	136	123	114
12	147	130	120
13	139	126	115
14	137	125	115
15	142	135	127
16	143	132	122
17	146	129	120
18	146	131	120
19	118	109	102
20	128	116	106
21	134	116	106
22	133	118	108
23	111	104	97
24	130	111	100
25	112	104	97
26	114	105	97
27	125	112	102
28	132	118	107
29	122	110	102
30	121	110	102
31	129	117	109
32	127	114	105
34	126	110	101
35	124	109	100
36	124	110	100

Table A-3. Test Data of Liquid-Cooled Cold Plate No. 3

THERMO-COUPLE NO.	TEMPERATURE, °F				
	TEST COND #1	TEST COND #2	TEST COND #3	TEST COND #4	TEST COND #5
1	66	65	65	72	72
2	69	72	75	74	75
3	107	147	188	74	74
4	73	79	86	75	75
5	106	142	178	77	78
6	71	77	83	106	122
7	72	77	83	79	82
8	117	172	229	75	76
9	76	86	95	74	74
10	73	79	85	74	75
11	78	89	100	77	79
12	72	76	81	90	98
13	72	76	81	80	83
14	77	89	100	76	78
15	74	82	89	75	75
16	73	78	85	77	79
17	73	78	84	76	77
18	74	82	89	80	84
19	72	77	83	84	90
20	77	86	97	77	78
21	72	76	82	83	88
22	74	82	89	75	76
23	74	81	89	76	78
24	73	81	88	74	74
25	72	74	80	84	90
26	78	88	98	75	76
27	72	77	82	79	82
28	75	80	87	74	74
29	76	85	94	76	76
30	74	82	89	72	72

Table A-3. Test Data of Liquid-Cooled Cold Plate No. 3 (Cont)

THERMO-COUPLE NO.	TEMPERATURE, °F				
	TEST COND #6	TEST COND #7	TEST COND #8	TEST COND #9	TEST COND #10
1	71.5	67	66	66	68
2	75	69	69	69	75
3	74	70	70	70	108
4	76	102	118	133	112
5	80	72	74	74	116
6	137	71	72	73	94
7	85	112	136	159	123
8	77	71	72	74	128
9	74	70	71	71	81
10	76	78	82	85	86
11	82	72	73	74	87
12	106	71	71	72	86
13	86	77	81	85	86
14	79	72	74	74	87
15	75	70	71	72	80
16	81	74	78	80	84
17	79	74	76	79	83
18	88	71	73	74	84
19	97	70	71	72	84
20	80	70	71	73	85
21	93	73	75	78	85
22	77	74	76	78	85
23	80	74	76	79	85
24	74	72	74	75	81
25	95	72	73	74	84
26	77	73	74	75	86
27	86	76	77	82	86
28	75	77	79	83	86
29	78	73	75	76	85
30	73	71	71	71	80

Table A-3. Test Data of Liquid-Cooled Cold Plate No. 3 (Cont)

THERMO-COUPLE NO.	TEMPERATURE, °F				
	TEST COND #11	TEST COND #12	TEST COND #13	TEST COND #14	TEST COND #15
1	68	67	68	74	79
2	80	84	98	90	87
3	153	195	212	205	201
4	132	160	174	164	155
5	154	192	212	202	192
6	112	137	158	144	134
7	150	181	200	188	178
8	188	241	250	238	228
9	93	102	116	109	105
10	98	108	124	114	106
11	101	114	134	121	110
12	100	112	133	118	108
13	100	111	131	118	108
14	100	112	130	118	108
15	89	97	113	103	97
16	95	104	122	110	100
17	93	102	119	108	99
18	97	108	128	114	103
19	96	107	127.5	114	103
20	99	111	131	118	105
21	98	109	130	116	105
22	97	106	124	113.5	104
23	97	107	126	113	104
24	91	100	114	107	100
25	94	102	123	104	100
26	98	110	126	112	103
27	97	106	124	107	102
28	97	104	116	105	99
29	97	107	124	108	102
30	90	96	108	98	96

Table A-4. Test Data of Air-Cooled Cold Plate No. 1, Manifold Configuration #1

THERMO-COUPLE NO.	TEMPERATURE, °F			
	TEST COND #1	TEST COND #2	TEST COND #3	TEST COND #4
1	72	73	73	73
2	133	104	94	88
3	227	186	167	154
4	222	178	157	145
5	228	183	163	150
6	226	179	161	148
7	224	179	160	148
8	215	173	154	141
9	216	173	154	142
10	222	177	156	144
11	220	175	155	142
12	220	175	155	143
13	209	165	145	132
14	209	165	145	132
15	210	167	147	135
16	210	165	145	132
17	213	167	147	134
18	214	170	150	138
19	212	169	149	137
20	212	167	147	133
21	211	166	146	133
22	213	168	148	135
23	203	160	141	128
24	208	162	142	130
25	190	150	133	122
26	159	121	106	98
27	194	152	134	123
28	123	102	94	89
29	190	146	127	116

Table A-4. Test Data of Air-Cooled Cold Plate No. 1, Manifold Configuration #1 (Cont)

THERMO-COUPLE NO.	TEMPERATURE, °F		
	TEST COND #5	TEST COND #6	TEST COND #7
1	71	72	72
2	77	83	96
3	83	96	121
4	84	98	126
5	94	119	168
6	83	96	122
7	84	97	125
8	83	95	120
9	83	97	124
10	92	113	155
11	83	96	123
12	83	97	125
13	84	98	125
14	84	99	129
15	84	99	128
16	84	98	125
17	86	102	133
18	86	102	135
19	85	100	128
20	85	99	127
21	85	100	130
22	85	99	129
23	84	98	124
24	84	98	126
25	82	94	116
26	80	90	105
27	83	96	118
28	77	82	92
29	83	96	117

Table A-4. Test Data of Air-Cooled Cold Plate No. 1, Manifold Configuration #1 (Cont)

THERMO-COUPLE NO.	TEMPERATURE, °F		
	TEST COND #8	TEST COND #9	TEST COND #10
1	72	72	72
2	102	119	132
3	152	193	227
4	150	188	221
5	152	193	228
6	150	189	226
7	151	190	224
8	145	183	215
9	146	183	216
10	149	188	222
11	147	185	220
12	149	186	220
13	142	178	209
14	142	178	208
15	143	179	210
16	143	178	210
17	145	181	213
18	146	182	214
19	145	181	212
20	144	180	212
21	144	179	211
22	145	181	213
23	140	174	203
24	141	177	208
25	131	166	190
26	116	140	159
27	135	167	194
28	99	112	123
29	132	162	190

Table A-5. Test Data of Air-Cooled Cold Plate No. 1, Manifold Configuration #2

THERMO-COUPLE NO.	TEMPERATURE, °F			
	TEST COND #1	TEST COND #2	TEST COND #3	TEST COND #4
1	73	73	73	73
2	134	104	93	88
3	236	193.5	171	159
4	226	183	163	151.5
5	237	192	171	158
6	231	188	165	156
7	233	189	170	155
8	223	179	159	147
9	221	179	158	146
10	231	186	165	152
11	226	182	160	150
12	227	183	165	150
13	218	173	153	140
14	217	173	152	139
15	217	173	152	139
16	219	174	153	141
17	222	176	155	143
18	222	177	156	143
19	218	174	154	141
20	220	175	154	142
21	220	175	154	141
22	221	176	156	142
23	210	167	147	135
24	215	170	150	137
25	200	154	134	123
26	170	127	110	100
27	198	154	135	124
28	115	97	90	86
29	196	153	133	123

Table A-6. Test Data of Air-Cooled Cold Plate No. 1, Manifold Configuration #3

THERMO-COUPLE NO.	TEMPERATURE, °F			
	TEST COND #1	TEST COND #2	TEST COND #3	TEST COND #4
1	72	73	73	73
2	133	104	94	88
3	218	181	163	151
4	207	168	151	139
5	221	182	164	151
6	222	185	167	154
7	213	173	154	142
8	206	169	151	140
9	201	162	144	133
10	214	175	156	144
11	217	180	162	149
12	208	168	150	137
13	202	163	145	133
14	198	159	141	129
15	197	158	140	128
16	209	171	152	140
17	209	171	152	140
18	203	163	145	133
19	199	159	141	128
20	210	172	153	140
21	206	167	148	135
22	204	165	146	133
23	191	152	134	123
24	204	165	145	133
25	194	157	140	128
26	159	125	110	101
27	176	139	122	112
28	146	114	100	93
29	176	140	122	111
30	148	115	102	94
31	170	134	113	107

Table A-6. Test Data of Air-Cooled Cold Plate No. 1, Manifold Configuration #3 (Cont)

THERMO-COUPLE NO.	TEMPERATURE, °F		
	TEST COND #5	TEST COND #6	TEST COND #7
1	71.5	72	72
2	77	81	84
3	88.5	98.5	106
4	86	95	103
5	110	133	152
6	90	101	110
7	88	97.5	105
8	88	98	106
9	86	95	102
10	104	123	138
11	90	101	110
12	89	97.5	105
13	89	100	110
14	90	102	110
15	89	99	107
16	91	102	112
17	94	107.5	119
18	93	106	117
19	88	98	106
20	91	103	113
21	91	103	113
22	90	101	110
23	88	97	105
24	89	101	110
25	88	98	106
26	81	89	94
27	82	92	98
28	80	83	89
29	85	93	99
30	80	85	89
31	80	90	98

Table A-7. Test Data of Air-Cooled Cold Plate No. 2, Manifold Configuration #1

THERMO-COUPLE NO.	TEMPERATURE, °F		
	TEST COND #1	TEST COND #2	TEST COND #3
1	74	74	74
2	104	92	86
3	201	174	158
4	202	173	156
5	208	178	161
6	206	177	159
7	206	176	159
8	194	167	151
9	195	166	150
10	200	170	153
11	200	170	153
12	199	170	152
13	188	159	143
14	187	157	141
15	190	160	144
16	186	158	141
17	189	161	143
18	192	162	145
19	195	164	147
20	193	163	146
21	191	161	144
22	194	164	146
23	192	162	144
24	194	164	146
25	191	161	144
26	134	114	102
27	158	132	117
28	136	114	102
29	169	140	124
30	142	116	105

Table A-7. Test Data of Air-Cooled Cold Plate No. 2, Manifold Configuration #1 (Cont)

THERMO-COUPLE NO.	TEMPERATURE, °F		
	TEST COND #4	TEST COND #5	TEST COND #6
1	72	72	73
2	75	79	82
3	86	99	109
4	87	101	114
5	109	138	166
6	86	100	111
7	87	102	114
8	85	98	108
9	87	101	114
10	101	125	147
11	86	99	111
12	87	101	114
13	86	101	113
14	88	105	119
15	90	104	118
16	86	100	110
17	87	102	113
18	91	108	124
19	91	111	127
20	89	104	118
21	88	103	116
22	89	104	116
23	90	107	121
24	89	105	119
25	89	105	119
26	79	86	91
27	80	91	98
28	78	86	91
29	82	95	104
30	79	86	93

Table A-8. Test Data of Air-Cooled Cold Plate No. 2, Manifold Configuration #2

THERMO-COUPLE NO.	TEMPERATURE, °F		
	TEST COND #1	TEST COND #2	TEST COND #3
1	72	73	73
2	102	91	84
3	212	185	168
4	214	185	170
5	221	191	175
6	216	188	174
7	219	191	174
8	207	180	164
9	204	176	161
10	213	184	168
11	211	184	169
12	211	183	166
13	202	174	158
14	199	171	155
15	200	170	154
16	202	174	159
17	204	176	161
18	206	177	162
19	205	176	159
20	201	172	156
21	199	169	153
22	206	178	163
23	205	176	160
24	206	177	160
25	204	176	159
26	140	116	106
27	174	150	136
28	147	122	110
29	169	141	126
30	154	128	114

Table A-8. Test Data of Air-Cooled Cold Plate No. 2, Manifold Configuration #2 (Cont)

THERMO-COUPLE NO.	TEMPERATURE, °F		
	TEST COND #4	TEST COND #5	TEST COND #6
1	72	72	72
2	76	78	81
3	90	105	121
4	89	102	117
5	112	142	175
6	91	107	123
7	90	104	120
8	91	105	121
9	89	102	116
10	105	129	157
11	91	107	123
12	90	105	119
13	92	108	125
14	93	110	128
15	92	106	124
16	92	107	124
17	92	108	126
18	95	115	136
19	95	114	134
20	91	106	122
21	90	104	119
22	93	109	127
23	94	112	131
24	93	109	126
25	93	110	128
26	80	87	94
27	86	98	110
28	81	87	96
29	84	93	104
30	82	90	98

Table A-9. Test Data of Air-Cooled Cold Plate No. 2, Manifold Configuration #3

THERMO-COUPLE NO.	TEMPERATURE, °F		
	TEST COND #1	TEST COND #2	TEST COND #3
1	74	74	74
2	105	92	86
3	207	181	164
4	189	162	146
5	206	179	161
6	212	185	164
7	197	170	154
8	200	176	159
9	181	155	139
10	199	172	154
11	206	180	159
12	190	163	147
13	192	165	148
14	184	158	140
15	180	153	137
16	196	169	151
17	197	170	152
18	197	170	152
19	188	159	142
20	181	153	136
21	177	149	133
22	198	170	152
23	192	164	147
24	190	161	145
25	190	163	145
26	123	108	99
27	173	148	132
28	140	116	106
29	149	124	109
30	146	122	109

Table A-9. Test Data of Air-Cooled Cold Plate No. 2, Manifold Configuration #3 (Cont)

THERMO-COUPLE NO.	TEMPERATURE, °F		
	TEST COND #4	TEST COND #5	TEST COND #6
1	72	73	73
2	75	79	82
3	89	102	115
4	85	96	107
5	109	139	167
6	89	103	117
7	86	99	110
8	88	102	115
9	85	96	106
10	102	126	149
11	88	102	117
12	85	99	111
13	89	104	119
14	90	105	119
15	88	102	114
16	90	104	118
17	90	106	120
18	93	112	129
19	93	110	126
20	87	100	113
21	86	98	110
22	91	106	121
23	91	108	123
24	90	104	118
25	90	105	120
26	78	84	90
27	86	96	106
28	80	87	93
29	81	90	97
30	82	88	96

Table A-10. Test Data of Air-Cooled Cold Plate No. 2, Manifold Configuration #4

THERMO-COUPLE NO.	TEMPERATURE, °F			
	TEST COND #1	TEST COND #2	TEST COND #3	TEST COND #4
1	74	74	74	73
2	103	91	85	81
3	199	174	161	114
4	183	157	143	106
5	199	172	158	165
6	200	173	158	114
7	189	163	150	109
8	193	168	155	113
9	175	149	135	106
10	192	165	151	147
11	194	167	152	113
12	182	156	143	108
13	185	159	145	117
14	178	152	138	119
15	174	149	135	114
16	187	160	146	115
17	188	162	147	118
18	188	162	148	127
19	180	154	139	124
20	174	147	133	111
21	170	144	130	108
22	187	161	146	118
23	183	156	141	121
24	181	154	139	115
25	181	154	139	117
26	124	106	97	88
27	162	138	124	104
28	131	110	101	90
29	144	119	107	95
30	134	111	102	90

Table A-11. Test Data of Air-Cooled Cold Plate No. 2

THERMO-COUPLE NO.	Manifold Configuration #3 TEMPERATURE, °F TEST COND #1	Manifold Configuration #3 TEMPERATURE, °F TEST COND #2	Manifold Configuration #4 TEMPERATURE, °F TEST COND #1	Manifold Configuration #4 TEMPERATURE, °F TEST COND #2
1	83	82	81	81
2	111	100	113	100
3	202	178	190	168
4	202	174	195	170
5	181	155	172	149
6	208	183	195	173
7	202	177	197	175
8	195	170	183	162
9	189	161	182	159
10	182	156	172	149
11	203	177	189	166
12	194	169	189	166
13	183	158	172	151
14	177	150	168	145
15	176	150	169	146
16	189	164	176	154
17	190	165	178	155
18	186	160	175	152
19	181	155	174	151
20	182	156	176	153
21	181	154	174	151
22	192	166	179	156
23	186	160	176	153
24	187	161	179	157
25	187	160	177	154
26	122	105	115	100
27	166	143	152	132
28	134	114	124	108
29	153	129	148	128
30	144	122	133	115

Table A-12. Test Data of Air-Cooled Cold Plate No. 3, Manifold Configuration #1

THERMO-COUPLE NO.	TEMPERATURE, °F				
	TEST COND #1	TEST COND #2	TEST COND #3	TEST COND #4	TEST COND #5
1	73	73	73	73	73
2	105	97	89	84	82
3	201	186	167	154	146
4	206	190	170	157	149
5	206	191	171	159	149
6	188	173	154	142	133
7	197	182	162	149	141
8	193	178	160	146	137
9	173	159	140	128	121
10	181	166	147	135	127
11	181	166	147	135	125
12	175	161	140	128	119
13	191	176	157	143	135
14	180	165	145	133	126
15	186	171	152	139	131
16	188	172	152	139	131
17	181	165	145	132	122
18	193	178	159	145	137
19	178	164	145	132	125
20	186	170	150	139	130
21	186	170	150	138	130
22	179	164	144	131	122
23	172	157	138	127	120
24	173	157	138	125	116
25	160	146	127	116	110
26	148	134	116	105	99
27	160	146	126	114	105
28	143	130	113	104	97
29	153	140	121	110	103

Table A-12. Test Data of Air-Cooled Cold Plate No. 3, Manifold Configuration #1 (Cont)

THERMO-COUPLE NO.	TEMPERATURE, °F			
	TEST COND #6	TEST COND #7	TEST COND #8	TEST COND #9
1	72	73	74	72
2	86.5	95	102	76
3	148	187	224	92
4	150	191	229	109
5	152	194	231	92
6	137	172	203	90
7	144	182	216	102
8	142	178	210	90
9	126	156	181	89
10	131	164	192	90
11	132	164	193	90
12	128	157	184	89
13	139	175	207	95
14	130	162	190	93
15	135	169	200	95
16	136	170	201	96
17	131	162	190	93
18	141	177	209	95
19	130	161	188	91
20	135	169	199	91
21	135	169	198	91
22	130	160	188	90
23	125	153	178	91
24	125	153	178	91
25	116	139	160	88
26	107	125	141	84
27	115	138	158	88
28	105	122	138	83
29	111	132	150	86

Table A-12. Test Data of Air-Cooled Cold Plate No. 3
Manifold Configuration #1 (Cont)

THERMO-COUPLE NO.	TEMPERATURE, °F		
	TEST COND #10	TEST COND #11	TEST COND #12
1	72	72	72
2	79	81	83
3	102	112	122
4	128	148	165
5	103	113	123
6	100	109	119
7	118	134	147
8	101	111	121
9	99	107	115
10	100	110	118
11	100	110	119
12	99	108	116
13	109	122	132
14	104	115	124
15	108	120	132
16	109	121	133
17	104	115	124
18	109	121	132
19	100	109	118
20	101	111	120
21	101	111	121
22	100	110	118
23	100	110	118
24	100	110	118
25	96	104	110
26	91	97	102
27	96	104	110
28	90	95	100
29	92	98	104

Table A-13. Test Data of Air-Cooled Cold Plate No. 3, Manifold Configuration #2

THERMO-COUPLE NO.	TEMPERATURE, °F				
	TEST COND #1	TEST COND #2	TEST COND #3	TEST COND #4	TEST COND #5
1	71	71	71	71	71
2	102	93	86	82	79
3	234	215	192	176	167
4	241	221	198	181	172
5	243	222	199	182	173
6	220	201	179	163	153
7	233	213	190	174	164
8	229	209	186	169	160
9	205	186	164	148	139
10	213	194	172	156	147
11	213	194	172	156	147
12	205	187	165	149	140
13	226	205	183	167	157
14	215	195	171	155	145
15	221	202	179	162	152
16	222	202	179	162	154
17	216	195	172	156	147
18	229	209	185	170	159
19	213	194	170	154	145
20	221	201	178	161	152
21	221	201	178	161	152
22	214	194	171	155	146
23		187	164	149	138
24		187	165	149	139
25	196	176	153	138	128
26	184	165	143	127	118
27	195	176	153	138	128
28	173	155	135	121	112
29	187	170	147	132	122

Table A-14. Test Data of Air-Cooled Cold Plate No. 3, Manifold Configuration #2a

THERMO-COUPLE NO.	TEMPERATURE, °F				
	TEST COND #1	TEST COND #2	TEST COND #3	TEST COND #4	TEST COND #5
1	70	70	70	70	70
2	100	92	85	81	79
3	236	215	192	178	168
4	242	222	198	183	171
5	243	222	200	185	174
6	221	202	179	165	155
7	234	213	190	175	164
8	230	209	187	172	161
9	208	188	165	150	141
10	216	196	173	158	148
11	215	195	173	158	148
12	207	187	165	149	140
13	227	211	183	169	160
14	217	196	173	158	148
15	223	203	180	164	154
16	223	203	180	164	154
17	216	196	173	158	146
18	230	209	186	171	160
19	215	194	172	157	147
20	222	201	179	164	153
21	222	201	179	164	153
22	215	194	172	157	146
23		190	166	151	141
24		188	164	150	138
25	200	178	154	140	130
26	187	166	143	128	118
27	196	178	152	137	127
28	176	157	136	122	114
29	188	168	146	132	122

Table A-15. Test Data of Air-Cooled Cold Plate No. 3, Manifold Configuration #3

THERMO-COUPLE NO.	TEMPERATURE, °F				
	TEST COND #1	TEST COND #2	TEST COND #3	TEST COND #4	TEST COND #5
1	78	76	73	73	72
2	107	97	88	84	80
3	193	177	158	149	141
4	201	184	165	153	146
5	203	185	168	156	148
6	179	164	146	136	129
7	193	175	157	147	138
8	190	173	155	144	135
9	169	153	136	126	118
10	174	159	142	131	124
11	171	155	138	127	120
12	162	147	129	119	112
13	185	168	150	140	132
14	178	161	143	132	124
15	183	167	148	137	129
16	176	164	147	136	127
17	172	155	136	125	118
18	189	172	154	142	134
19	177	159	142	130	122
20	183	165	146	136	127
21	182	165	147	135	126
22	173	156	139	127	119
23	172	156	138	127	118
24	162	147	129	119	111
25	161	146	128	118	110
26	146	131	114	105	98
27	150	135	118	108	101
28	135	122	108	99	94
29	150	136	118	108	101

Table A-15. Test Data of Air-Cooled Cold Plate No. 3
Manifold Configuration #3 (Cont)

THERMO-COUPLE NO.	TEMPERATURE, °F		
	TEST COND #6	TEST COND #7	TEST COND #8
1	75	76	77
2	87	95	100
3	146	180	215
4	151	187	225
5	151	189	228
6	135	165	195
7	144	178	212
8	141	174	207
9	127	152	178
10	131	159	187
11	128	155	180
12	121	145	167
13	138	169	199
14	132	160	188
15	135	166	197
16	135	164	193
17	127	153	178
18	141	172	205
19	130	158	186
20	131	165	197
21	131	165	194
22	128	154	181
23	128	152	178
24	121	142	165
25	120	141	164
26	110	125	142
27	113	130	147
28	104	116	130
29	112	130	148

Table A-16. Test Data of Air-Cooled Cold Plate No. 4

THERMO-COUPLE NO.	TEMPERATURE, °F			
	TEST COND #1	TEST COND #2	TEST COND #3	TEST COND #4
1	74	76	78	76
2	116	99	94	88
3	130	117	113	110
4	144	126	120	116
5	157	142	137	132
6	137	121	116	112
7	142	125	119	114
8	121	109	106	102
9	136	118	112	107
10	131	116	112	107
11	131	116	111	107
12	140	121	115	111
13	109	97	94	90
14	114	100	97	93
15	114	101	98	94
16	121	106	101	97
17	122	107	102	98
18	124	109	103	99
19	126	110	105	100
20	126	110	105	100
21	125	108	104	98
22	129	111	106	101
23	126	109	104	99
24	125	107	102	98
25	98	89	86	84
26	120	102	97	92

Table A-16. Test Data of Air-Cooled Cold Plate No. 4 (Cont)

THERMO-COUPLE NO.	TEMPERATURE, °F		
	TEST COND #5	TEST COND #6	TEST COND #7
1	77	78	75
2	81	85	86
3	81	85	85
4	83	88	90
5	120	153	182
6	81	86	85
7	83	89	91
8	81	84	85
9	82	87	89
10	94	109	121
11	80	85	86
12	82	88	96
13	82	87	88
14	83	89	91
15	82	87	88
16	82	87	88
17	83	88	89
18	85	94	97
19	86	95	99
20	83	89	90
21	82	87	89
22	84	91	93
23	85	92	95
24	84	91	93
25	80	82	81
26	83	85	88

Table A-17. Test Data of Air-Cooled Cold Plate No. 5, Manifold Configuration #1

THERMO-COUPLE NO.	TEMPERATURE, °F			
	TEST COND #1	TEST COND #2	TEST COND #3	TEST COND #4
1	69	73	75	74
2	100	90	86	105
3	124	114	107	142
4	123	114	111	141
5	118	106	100	130
6	134	121	117	152
7	135	122	115	155
8	125	112	106	138
9	123	111	108	136
10	111	99	93	120
11	115	101	96	122
12	130	118	113	147
13	130	118	112	147
14	104	94	90	110
15	94	86	83	98
16	103	95	92	111
17	103	93	88	109
18	110	99	93	119
19	109	98	92	117
20	107	96	90	114
21	107	96	90	114
22	109	98	93	118
23	110	100	95	120
24	110	99	93	119
25	116	103	97	126
26	110	99	92	119
27	115	103	97	126
28	111	97	93	115
29	110	96	92	114
30	110	100	96	116

Table A-17. Test Data of Air-Cooled Cold Plate No. 5, Manifold Configuration #1 (Cont)

THERMO-COUPLE NO.	TEMPERATURE, °F		
	TEST COND #5	TEST COND #6	TEST COND #7
1	75	75	75
2	116	128	85
3	162	184	84
4	164	185	84
5	147	167	124
6	179	206	89
7	176	204	90
8	158	177	84
9	158	177	84
10	133	149	108
11	136	152	107
12	172	197	89
13	168	193	89
14	122	136	84
15	106	115	84
16	123	136	84
17	120	132	95
18	133	149	86
19	131	147	88
20	126	141	90
21	127	142	97
22	132	147	88
23	134	149	87
24	131	148	100
25	143	161	89
26	132	147	92
27	141	168	89
28	130	143	86
29	126	140	98
30	132	145	86

Table A-18. Test Data of Air-Cooled Cold Plate No. 5, Manifold Configuration #2

THERMO-COUPLE NO.	TEMPERATURE, °F		
	TEST COND #1	TEST COND #2	TEST COND #3
1	73	74	76
2	104	91	87
3	128	118	113
4	128	117	112
5	120	108	102
6	139	124	118
7	136	125	118
8	126	114	111
9	124	113	109
10	113	102	96
11	114	103	97
12	136	121	115
13	132	120	114
14	107	97	94
15	98	89	86
16	107	98	94
17	106	95	90
18	114	102	98
19	113	101	95
20	111	98	93
21	111	99	94
22	112	100	94
23	113	102	97
24	113	100	96
25	120	106	99
26	114	101	95
27	118	105	99
28	112	98	94
29	110	97	92
30	117	105	100

Table A-19. Test Data of Air-Cooled Cold Plate No. 5, Manifold Configuration #3

THERMO-COUPLE NO.	TEMPERATURE, °F			
	TEST COND #1	TEST COND #2	TEST COND #3	TEST COND #4
1	74	75	75	75
2	105	92	87	86
3	126	115	113	83
4	125	114	111	83
5	119	107	103	122
6	138	125	121	88
7	132	120	115	87
8	122	112	110	84
9	120	111	107	82
10	112	100	97	108
11	114	101	98	106
12	135	121	118	88
13	129	116	111	87
14	105	95	93	83
15	95	87	84	83
16	104	94	92	82
17	105	94	91	94
18	113	101	99	87
19	112	101	97	87
20	109	98	95	89
21	109	98	95	95
22	109	97	94	86
23	110	98	95	86
24	111	100	96	99
25	119	106	103	88
26	111	99	95	91
27	115	102	97	88
28	110	99	96	86
29	108	96	93	96
30	114	103	100	85

Table A-20. Test Data of Air-Cooled Cold Plate No. 5, Manifold Configuration #4

THERMO-COUPLE NO.	TEMPERATURE, °F			
	TEST COND #1	TEST COND #2	TEST COND #3	TEST COND #4
1	70	71	74	61
2	101	88	85	73
3	121	117	110	67
4	119	113	107	69
5	114	104	100	108
6	132	119	115	72
7	130	119	115	74
8	118	110	107	70
9	118	108	105	70
10	107	95	92	92
11	110	98	94	93
12	129	116	112	74
13	127	115	111	74
14	100	91	89	68
15	92	84	82	68
16	101	92	90	70
17	100	90	87	80
18	107	95	91	72
19	106	95	91	72
20	104	93	90	75
21	104	93	90	81
22	107	95	91	73
23	108	97	94	73
24	107	96	92	84
25	114	101	95	73
26	107	96	92	77
27	113	100	95	75
28	106	95	92	72
29	104	93	90	84
30	112	101	98	73

Table A-21. Test Data of Air-Cooled Cold Plate No. 6, Manifold Configuration #1

THERMO-COUPLE NO.	TEMPERATURE, °F			
	TEST COND #1	TEST COND #2	TEST COND #3	TEST COND #4
1	68	67	68	69
2	99	84	79	78
3	109	101	98	76
4	117	107	102	130
5	123	107	102	79
6	105	97	94	75
7	106	94	91	74
8	108	98	93	106
9	122	111	106	80
10	118	103	98	78
11	91	82	80	79
12	93	83	80	76
13	102	93	90	78
14	104	94	90	78
15	100	90	87	85
16	101	89	86	84
17	106	91	87	80
18	107	9	90	82
19	105	93	90	86
20	96	84	80	75
21	103	89	85	78
22	99	87	83	78
23	95	85	80	77
24	98	86	84	79
25	102	89	85	78
26	100	88	86	78
27	102	89	86	81
28	103	90	84	80

Table A-22. Test Data of Air-Cooled Cold Plate No. 6, Manifold Configuration #4

THERMO-COUPLE NO.	TEMPERATURE, °F			
	TEST COND #1	TEST COND #2	TEST COND #3	TEST COND #4
1	70	71	71	69
2	100	89	82	78
3	109	101	98	74
4	119	110	105	132
5	122	111	106	78
6	104	97	93	73
7	103	96	92	73
8	109	100	95	107
9	118	109	104	78
10	118	107	102	78
11	92	85	81	78
12	93	86	83	75
13	101	92	88	76
14	102	93	89	77
15	101	92	87	84
16	101	92	87	84
17	104	94	90	79
18	107	96	91	81
19	106	96	92	86
20	95	87	83	75
21	102	92	87	78
22	99	89	84	78
23	94	86	82	75
24	96	89	84	76
25	101	92	88	77
26	100	92	88	78
27	100	91	86	78
28	102	93	88	80

☆ U. S. GOVERNMENT PRINTING OFFICE, 1976 — [illegible]